博　士　論　文

EXPERIMENTAL STUDY ON PARTICLE BREAKAGE UNDER HIGH PRESSURE

（砂粒子の破砕に関する高圧せん断実験）

余 方威

博　士　論　文

EXPERIMENTAL STUDY ON PARTICLE BREAKAGE UNDER HIGH PRESSURE
（砂粒子の破砕に関する高圧せん断実験）

By

Fangwei YU
（余　方威）

A dissertation submitted to
The Department of Civil Engineering

Of

The University of Tokyo

In partial fulfillment of the requirements for the degree of
Doctor of Philosophy

in

Civil Engineering

東京大学大学院工学系研究科
社会基盤学専攻
Department of Civil Engineering
The University of Tokyo, Tokyo, Japan
September 2014

DEDICATED TO MY GREAT PARENTS

MINGYI YU AND ZHENLAN QUE

WHO HAVE RAISED ME TO BE THE PERSON I AM TODAY

AND TO MY FAMILY

HUIHUI WANG, TIANYU YU AND TIANMU YU

WHO I LOVE VERY MUCH

THESIS APPROVAL

Student Name	:	Fangwei YU （余　方威）
Student I.D.	:	37-117315
Institute	:	The University of Tokyo
Department	:	Civil Engineering
Laboratory	:	Geotechnical Engineering Laboratory
Subject	:	EXPERIMENTAL STUDY ON PARTICLE BREAKAGE UNDER HIGH PRESSURE
Submission	:	September 2014

This is to certify that we have read this thesis and that in our opinion it is fully adequate, in scope and quality, as a thesis for the degree of Doctor of Philosophy.

Research Supervisor:

Prof. Dr. Ikuo TOWHATA _____

Advisory Committee Members:

Prof. Dr. Junichi KOSEKI _____

Prof. Dr. Reiko KUWANO _____

Prof. Dr. Noriyuki YASUFUKU _____

Prof. Dr. Masuyuki HYODO _____

Assoc. Prof. Dr. Taro UCHIMURA _____

Department of Civil Engineering
The University of Tokyo, Tokyo, Japan
September 2014

EXPERIMENTAL STUDY ON PARTICLE BREAKAGE UNDER HIGH PRESSURE

Fangwei YU

Ph.D. Dissertation-Civil Engineering
September 2014

Supervisor: Prof. Ikuo TOWHATA

ABSTRACT: Granular materials are comprised of particles which would be crushed under high pressure when the energy imposed on soil particle exceeds its strength. With the increasing height of dam and the high-rise building supported by piles, the force exerted on the soil particles at the bottom of high dam or surrounding the tip of piles results in particle breakage. The weathering or freezing and thawing working on particles for a long time can lead to particle breakage as well. Particle breakage changes the natural grading of soil which affects the soil behavior. In addition, particle breakage challenges the classical soil mechanics which assumes that the soil particle cannot be broken during loading and the deformation of soil just results from the change of void among soil particles and the particle movement that is governed by the theory of friction and slippage of soil particles. To investigate particle breakage in soil behavior becomes a very significant research topic in geotechnical engineering.

For investigating particle breakage in soil behavior, triaxial tests were conducted on high-pressure triaxial apparatus with maximum 3MPa confining pressure.

Ⅰ Study on the characteristics of particle breakage

The characteristics of particle breakage were investigated by triaxial tests under different influence factors to clarify the evolution of particle breakage in identifying the change of grain size distribution curves during shearing. The triaxial tests were conducted to the different designated axial strain levels from 0% to 20% by a 5% increment for detecting the different extents of particle breakage by measuring the grain size distribution curves in sieving the specimens at different designated axial strains, which were quantified by relative breakage proposed by Hardin in 1985 as a single parameter to describe the extent of particle breakage by the difference of grain size distribution curves before and after loading.

Particle breakage was found to increase with increasing axial strain and confining pressure. Slight particle breakage during isotropic consolidation was caused as well. More substantial particle breakage was caused in denser sample. More substantial particle breakage was induced in CD tests than that in CU tests. According to the same mean effective stress to be reached after consolidation, anisotropic consolidation was revealed to result in more particle breakage than isotropic consolidation but during shearing higher confining pressure after isotropic consolidation (σ_c=2.0MPa K_0=1.0) has more influence

on particle breakage than that after anisotropic consolidation (σ_c=1.5MPa K_0=0.5). Unloading-Reloading process during shearing was found to lead to particle crushing. Particle crushing was found to increase with increasing cycle numbers of cyclic loading. A hyperbolic model was established to assess Relative Breakage by plastic work per unit volume. More substantial particle crushing was revealed in Coral sand No.3 than that in Silica sand No.5. In addition, particle breakage of Coral sand No.3 was investigated as well in microscopic views on particles during shearing in intuitionistic observation.

Ⅱ Study on the influence of particle breakage on soil behavior

A series of triaxial tests were run on dense specimens under 3MPa confining pressure to the different designated axial strain from 10% to 50% by a 10% increment for Silica sand No.5 but from 10% to 40% by a 10% increment for Coral sand No.3 for producing the crushed materials, which can be called pre-crushed sand subsequently. The material of specimens after shearing was kept in oven to dry and the grain size distribution curves were obtained by sieve analysis in describing the change of grading of original sand after shearing. The grain size distribution curves were quantified by relative breakage to assess the amount of particle breakage. The pre-crushed sand and original sand were employed to rebuild new specimens for new triaxial tests under same initial conditions to investigate the influence of particle breakage on soil behavior in comparison with the results from pre-crushed sand and original sand.

Particle breakage was also found to increase with increasing axial strain and the slight particle breakage still can be caused during isotropic consolidation. Particle breakage in shear band was found to be slightly more substantial than that outside shear band. Under isotropic consolidation on pre-crushed sands, particle breakage was found to result in more volumetric contractancy with larger residual volumetric change after unloading, which can be regarded as a plastic deformation or subsidence at ground surface in reality. By triaxial test on pre-crushed and original sand under various confining pressures, particle breakage was found to deteriorate stress-stress curve in reduction of peak strength. Particle breakage resulted in loss of dilatancy behavior in increase of more contranctacny of soil. Particle breakage resulted in more substantial development and slower dissipation of excess pore water pressure with higher residual excess pore water pressure in pre-crushed sands. Particle breakage was found to change the stress path in reduction of strength. Particle breakage resulted in reduction of the friction angle and the deformation modulus substantially.

Ⅲ Study on the influence of particle breakage on critical state line

The influence of particle breakage on locations of critical state points was investigated as well in triaxial tests on original sand and pre-crushed sands.

It was found that the initial Critical State Line (CSL) from original sand has nonlinear characteristics with a marked yield stress around 0.7MPa and CSL before yield stress can

be regarded as a linear line being parallel with the NCL on the loosest state. After yield stress, both high pressure and particle breakage have a complex influence effect on CSL during first shearing on original sand. It was found that particle breakage resulted in reduction of dilatancy & strength and intensification of contractancy of soil, which have a significant effect on CSL. It was found that the locations of the critical state points on original sand in CD test under 0.2MPa and 0.5MPa confining pressures were far away from the CSL, which was caused by effect of initial state of the test. In comparison with the locations of critical state points on pre-crushed sands and original sand in CD tests, critical state points moved downwards in e-logp′ plane with the increase of particle breakage but in q-p′ plane they are almost on the CSL linear fitting line. The locations of critical state points on pre-crushed sands in CU tests were found to move to left away in reduction of mean effective stress in e-logp′ plane but in q-p′ plane the critical state points over CSL moved towards the lower left to approach the CSL. With increasing mean effective stress, critical state points at same amount of pre-crushed particle breakage were found to move towards CSL in e-logp′ plane. Considering the locations of all critical state points from original sand and pre-crushed sand, it can be concluded that the locations of critical state points moved to lower left in e-logp′ plane in complex translation and rotation and developed to be nonlinear in increase of M=q/p′ in q-p′ plane with increasing particle breakage.

Key words: Triaxial test, High pressure, Particle breakage, Relative breakage, Grain size distribution curve, Pre-crushed sand, Critical state line, Normal consolidation line, Friction angle, Peak strength, dilatancy, Deformation modulus, Microscopic view, Silica sand, Coral sand

---

Ⅰ-Ⅱ: On Silica sand No.5 and Coral sand No.3
Ⅲ: On Silica sand No.5

ACKNOWLEDGEMENTS

Accomplishing this dissertation for me to gain the Ph.D. degree would be the most remarkable thing I have done so far to enrich my research experience and promote my research ability in the field of Geotechnical Engineering, which should be a very significant milestone in my life.

I would like to express my special wholehearted appreciation and highest esteem to Prof. Ikuo TOWHATA as my Ph.D. research supervisor, who gave me his profound suggestions and creative ideas in pursuing my research during the three years in Geotechnical Engineering Lab at The University of Tokyo with the utmost patience and encouragement to lead me go further in my research. Thank you very much, dear “Sensei” for your persistent support and encouragement.

Many sincere acknowledgements should be expressed to all members of my Academic Advisory Committee Prof. Ikuo TOWHATA, Prof. Junichi KOSEKI, Prof. Reiko KUWANO, Prof. Noriyuki YASUFUKU, Prof. Masayuki HYODO and Associate Prof. Taro UCHIMURA for their enlightening discussions and constructive comments on my research being very helpful to improve my dissertation as well.

Acknowledgements should be extended to Prof. Taro UCHIMURA and Dr. Shigeru GOTO, who provided me many innovative ideas and suggestions during my research with being in supporting me in maintenance of my apparatus and improvement of my research plan, without which it is impossible to complete my research.

The sincerely grateful greetings should be sent to all administrative staff members of Department of Civil Engineering, Foreign Student Officers and Japanese Language Class lecturers in The University of Tokyo for their kindly consistent guidance and assistance during my study in Japan. Single acknowledgement should be expressed to Ms. HIRANO, the secretary of Geotechnical Engineering Laboratory for her continuous assistance in all the academic and administrative matters to me, which always brought me convenience and made me concentrated my mind on this research.

Many thanks should be given to our Lab members, especially Shogo AOYAMA, Masahide OTSUBO, Tsubasa SUZUKI, Bangan LIU, Xuefeng NONG, Wuwei MAO, Yulong CHEN, Ali, Luki, Ghani, Yolanda, Naveed, Rouzbeh, Monoi, who gave me very

precious friendship to enrich my life within the whole three years and any assistance whenever it was required. Special appreciation to all Japanese Lab members for their help to deal with any matters being used in Japanese for me to make me live in Japan comfortably despite without knowing Japanese for me. Sincere acknowledgements should be extended to Prof. Junichi KOSEKI and Prof. Reiko KUWANO including all members of KOSEKI Laboratory and KUWANO Laboratory, IIS, The University of Tokyo, who as a very close relationship with Geotechnical Engineering Laboratory gave me many creative ideas and helpful suggestions being useful to improve my research.

In supporting my study for three years in Geotechnical Engineering laboratory at The University of Tokyo, the CSC Scholarship was awarded by China Scholarship Council (CSC) to me. Hereby many thanks should be given to all members of China Scholarship Council and the Education Branch in Embassy of China in Japan for their kind assistance in administrative matters.

My appreciation should be expressed to my parents (Mingyi YU <余 明义> and Zhenlan QUE <阙 振兰>) for their everlasting love and considerate care with being in eternally unconditional support and understanding for me, notwithstanding which cannot be expressed by all words, with being willing intensively to express that " I love you forever with all my best blessings to you." My sincere acknowledgements should be sent to my wife (Ms. Huihui WANG <王 会会>) who gave me all support whatever decision I made and accompanied me for many years for watching home and nourishing our lovely son (Tianyu YU <余 天域>) and daughter (Tianmu YU <余 天牧>) with giving up her career. To my son and daughter, I really love you with being proud to be a father of you. To my brothers and sisters in my big family and friends, thank all you for accompanying me with giving me the most precious family love, friendship and the wonderful and unforgettable life with sending all my best wishes and blessings to you.

Finally, I would like to express my acknowledgement to everyone who has ever helped and loved me with my best wishes and blessings.

Fangwei YU <余 方威>
September, 2014 in Tokyo, Japan

NOTATION

ABBREVIATIONS

A	Current cross-sectional area of specimen
A/D	Analog signal to Digital signal converter
B	Skempton's value
B_p	Breakage potential
B_r	Relative breakage
B_t	Total breakage
C_c	Coefficient of curvature
C_u	Coefficient of uniformity
CD	Consolidated drained condition
CO_2	Carbon dioxide
CSL	Critical State Line
CU	Consolidated undrained condition
DPT	Differential Pressure Transducer
D/A	Digital signal to Analog signal converter
D_i	Grain diameter at i% passing in sieve analysis $0 \leq i \leq 100$
D_r	Relative density
E_o	Deformation modulus
E/P	Electro-Pneumatic
e	Void ratio
e_0	Initial void ratio
e_{max}	Maximum void ratio
e_{min}	Minimum void ratio
F_v	Axial force
F_c	Fine content
G_s	Specific gravity of soil
GSD	Grain Size Distribution
ΔH	Increment of height of specimen (positive for compression)
H_0	Initial height of specimen
K_0	Consolidated stress ratio
LVDT	Linear Variable Differential Transformer
N	Cycle numbers of cyclic loading
NCL	Norm Consolidation Line

p'	Mean effective stress
P_i	Pressure in chamber
PWP	Pore water pressure
q	Deviator stress
r	Radial direction
t_m	Membrane thickness
ΔV	Increment of volume of specimen (positive of compression)
V_0	Initial volume of specimen
u	Excess pore water pressure
u_i	Excess pore water pressure/back pressure
x, y, z	x, y, z directions in Cartesian coordinate system
1, 2, 3	1, 2, 3 directions in principal stress space

GREEK SYMBOLS

ε	strain
ε_v	Vertical Strain
$\varepsilon_v \; or \; \varepsilon_{vol}$	Volumetric Strain
φ	Friction angle
φ'	Effective friction angle
σ_1	Major principal stress
σ_1'	Major principal effective stress
σ_2	Intermediate principal stress
σ_2'	Intermediate principal effective stress
σ_3	Minor principal stress
σ_3'	Minor principal effective stress
σ_c	Confining stress, herein $\sigma_c = \sigma_2 = \sigma_3$ in triaxial compression
σ_r	Radial stress
σ_r'	Radial effective stress
σ_v	Vertical stress
σ_v'	Vertical effective stress

TABLE OF CONTENT

LIST OF FIGURES

LIST OF TABLES

CHAPTER 1

RESEARCH CURRICULUM

1.1 INTRODUCTION

Granular soils are comprised of particles with the characteristics of good compaction property, fine permeability of water, high filling density, high shearing resistance and capacity, small subsidence deformation, good applicability to terrain, wide distribution in nature and so on, which were used widely in the field of Geotechnical Engineering such in dam, highway, railway, airport, embankment, man-made island, ground improvement and so on where the mechanical characteristics of the soil govern the engineering safety and deformation.

1.2 MOTIVATION AND SIGNIFICANCE

With the development of construction technique and requirement of economy development, more and higher dams and buildings are being in construction nowadays. The tallest earth-fill dam named Nurek Dam was constructed in 1961 and completed in 1980 with the height of 300m in Tajikistan. When completed, the 335m tall Rogun Dam in Tajikistan could be the highest, according to the original design. The 312m tall Shuangjiangkou Dam is being constructed since 2008 in China as well. The tallest building named Burj Khalifa with the height of 828m in Dubai, and the Shanghai Tower can be the second tallest building over the world with the height of 632m being under construction in Shanghai, China when completed in 2014 in plan.

The strength, stiffness and stability of engineering are dominated by soil mechanical characteristics where the grading of soil plays a very significant role in soil properties, which affects the whole engineering function and safety directly. During construction of high dam and high-rise building, the stresses on the soil particles at the bottom of high dam or surrounding the tip of piles sustaining the high-rise buildings are extremely high and complicated, when exceeding the strength of soil particle, the particle breakage occurs and the soil behavior would be changed as well by the change of natural grading of soil induced by particle breakage. In addition, particle breakage challenges the

classical soil mechanics which assumes that the soil particle cannot be broken during loading and the deformation of soil just results from the change of void among soil particles and the particle movement that is governed by the theory of friction and slippage of soil particles. To investigate particle breakage in soil behavior becomes a very significant research topic in geotechnical engineering.

1.3 AIMS AND OBJECTIVES

With an aim to investigate particle breakage under high pressure, the strain-controlled high-pressure triaxial apparatus was used with the maximum 3MPa confining pressure in simulating engineering mechanical process during construction and operating stage of high dams and high-rise buildings. For getting fundamental understanding of evolution of particle breakage under different influence factors and clarifying the mechanism of soil behavior subjected to particle breakage, the main objectives in this research can be outlined in detail as below:

Many triaxial tests were conducted under pressure on original sand to investigate the characteristics of partible breakage under different influence factors for getting fundamental understanding of evolution of particle breakage by
exploring the influence of confining pressure on particle breakage
exploring the influence of initial void ratio on particle breakage
exploring the influence of drainage condition on particle breakage,
exploring the influence of initial stress anisotropy on particle breakage,
exploring the influence of cyclic loading on particle breakage
exploring the influence of unloading-reloading process on particle breakage

Many triaxial tests were conducted on original sand and pre-crushed sand to investigate the influence of particle breakage on soil behavior by
clarifying the influence of particle breakage on stress-strain curve
clarifying the influence of particle breakage on volumetric strain
clarifying the influence of particle breakage on dilatancy behavior
clarifying the influence of particle breakage on excess pore water pressure
clarifying the influence of particle breakage on stress path
clarifying the influence of particle breakage on peak strength
clarifying the influence of particle breakage on friction angle
clarifying the influence of particle breakage on deformation modulus
clarifying the influence of particle breakage on critical state line

By this research on particle breakage, the soil mechanics should be improved with considering the effects of particle breakage on soil behavior in order to assess accurately engineering in safety, deformation, stability and so on.

1.4 SCOPE OF THE WORK AND LIMITATIONS

The scope of this research focuses on the comprehensive study on characteristics of particle breakage by triaxial tests under high pressure to investigate not only influence factors on particle breakage but also the influence of particle breakage on soil behavior, which can be introduced in soil mechanics by considering particle breakage. The silica sand as a kind of common granular material was used in this research to explore its characteristics of particle breakage. Furthermore coral sand with fragility and irregularity was also adopted in this research to clarify its characteristics of particle breakage which has a very significant influence on the engineering relying on the coral sand ground.

As a result of the limitation of time and diversity of specific type of sand, the findings of this research may not be applicable to other type of soil. With regard to the designated type of soil under specific stress path, the characteristics of particle breakage should be reinvestigated on a case-by-case basis. Due to the limitation of the traditional triaxial apparatus, the more complicated stress path has not been employed in this research.

1.5 UNIT SYSTEM

The International System of Units (S.I.) as the modern form of the metric system and the world's most widely used system of measurement was adopted in this research. Following the usual sign and convention in soil mechanics, all mechanical variables and physical variables in soil mechanics are stipulated as positive in compression and negative as in tension.

1.6 DURATION AND PLACE OF THIS RESEARCH

The research and all laboratory tests were conducted in Geotechnical Engineering Laboratory of The University of Tokyo located at 7-3-1 Hongo, Bunkyo-ku, Tokyo 113-8656, Japan. during October 2011-October 2014.

1.7 DISSERTATION ORGANIZATION

On the basis of the expectant objectives and the scope of this research, the dissertation is arranged in six chapters revealing a detailed and comprehensive overview of the work done including the main findings of this research. A comprehensive layout of the dissertation is shown as follows:
Chapter 1 shows an introduction of research curriculum
Chapter 2 shows literature review about particle breakage
Chapter 3 shows apparatus, test procedures and materials tested
Chapter 4 shows study on the characteristics of particle breakage
Chapter 5 shows study on the influence of particle breakage on soil behavior
Chapter 6 shows microscopic view on particle breakage
Chapter 7 shows conclusions and recommendations

CHAPTER 2

LITERATURE REVIEW

2.1 INTRODUCTION

Granular materials are comprised of particles which would be crushed under the pressure exceeding the strength of particle. Particle breakage changes the natural grading of soil which governs soil behavior.

In the classical soil mechanics, soil particles were regarded as being incompressible and uncrushable. In fact, with the increase of stress imposed on soil particles, the force exerted on soil particles exceeding the strength of soil particles results in particle breakage. At the beginning of development of soil mechanics, Terzaghi (1925) and Casagrande (1932) realized that the soil structure had a significant influence on strength of soil and put forward the concept of microstructure of soil which included the arrangement of soil particles, void distribution, particle breakage and connection state of particles. The natural grading of soil as one of the structural characteristics of granular material has an important influence on soil behavior. Particle breakage as a common phenomenon to change the natural grading of soil under high pressure in the field of Geotechnical Engineering should be paid more attention on its influence on soil behavior in this research.

2.2 PARTICLE BREAKAGE ON INIDIVIDUAL GRAIN

Soil is classified primarily into two categories, namely granular materials and cohesive soils. The mechanical properties of granular soils are governed by the grain-to-grain contact as well as friction. Hence, the magnitude of contact force and the geometrical nature of grain packing play major roles. It should be recalled that the magnitude of contact pressure per unit area of soil is called effective stress, which is the most important concept in modern soil mechanics (Towhata, 2008). The deformation of soil particle occurs as the soil particle is subjected to effective stress, and with the increase of the effective stress imposed on soil particle, the micro-cracks in soil particle appear and develop gradually. Particle breakage occurs when the cracks in particle spread through

the whole particle. According Griffith's criterion (Griffith, 1920), the tensile stress occurs along the micro crack edge inside soil particle, being subjecting to the increase of the tensile stress, which is to spread and finally form a through crack inside soil particle. Consequently, it is widely accepted that the failure of a spherical particle under compression is a tensile failure. The tensile strength of rock grains can be measured by diametral compression between flat platens (Jaeger, 1967). For a grain in diameter d under a diameter force F between top and bottom platens, the tensile stress generated inside grain can be defined as

$$\sigma = \frac{F}{d^2} \tag{2.1}$$

by following Jaeger (1967) and Shipway & Hutchings (1993a), which are also consistent with the definition of tensile strength of rock in the Brazilian test.

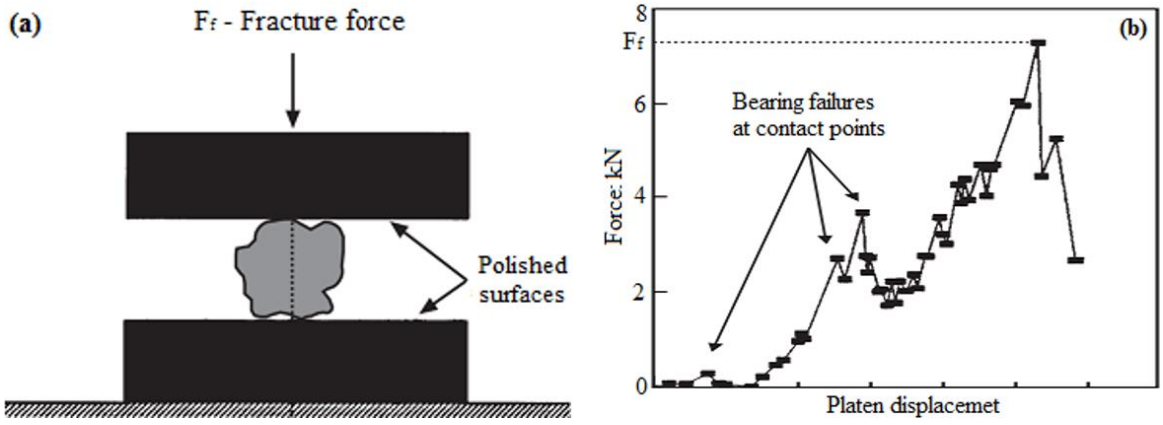

Figure 2.1 Compression test on individual test (Lee, 1992)

Lee (1992) compressed individual grains of Leighton Buzzard sand, Oolitic limestone and Carboniferous limestone as shown in Figure 2.1(a) where according to the equation 2.1, the tensile strength of a grain can be defined by

$$\sigma_f = \frac{F_f}{d^2} \tag{2.2}$$

where F_f represents fracture force in failure of a grain with a diameter of a grain d. Figure 2.1(b) shows a typical testing result of platen load against platen displacement, where it can be seen clearly that several peaks occurred during loading, the initial peak under small platen displacement may cause rounding of particle as small edges and corners were fractured. The force peaks before total failure of a gain can be regards as bearing failures at contact points and the load drops dramatically after fracture failure of a grain. It was also found that the tensile strength of each grain is not a constant but within a standard deviation around a mean value and the mean tensile strength σ_f can be regards as a function of an average particle size d as shown in Figure 2.2, which can be

described by the relation as

$$\sigma_f \propto d^b \tag{2.3}$$

where typical values of b are given by -0.357, -0.343 and -0.420 for Leighton Buzzard sand, Oolitic limestone and Carboniferous limestone respectively. It was found as well that the tensile strength correlated the lithology of grain, weathering degree of grain, grain size and shape and so on. Much less tensile strength existed in large grain with weak lithology and high weathering degree because that the large grain contained more flaws.

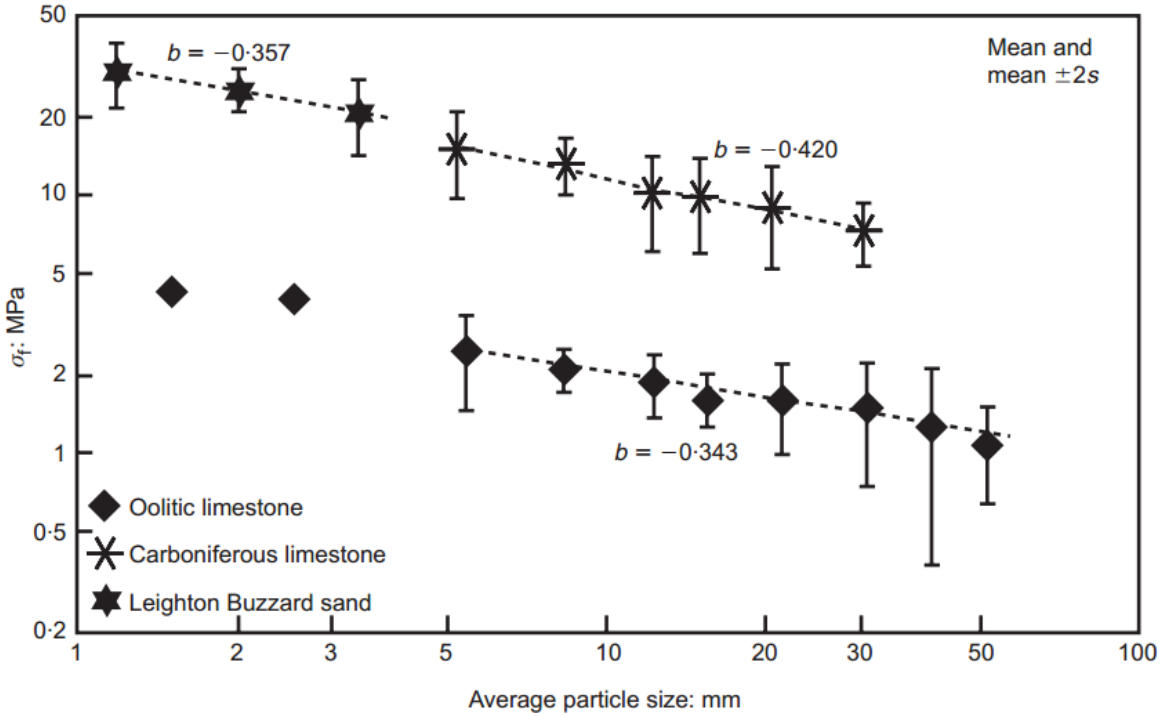

Figure 2.2 Mean tensile strength as a function of particle size (Lee, 1992)

Weibull statistics can be used to describe the tensile strength of fragile grains. Weibull (1951) recognized that the survival of a block of a material under tension is that all its constituent remain intact and stated that for a volume V under an applied tensile stress σ, the $P_s(V)$ as survival probability of block is given by

$$P_s(V) = \exp\left[-\frac{V}{V_0}\left(\frac{\sigma}{\sigma_0}\right)^m\right] \tag{2.4}$$

where V_0 is a reference volume of material such that

$$P_s(V_0) = \exp\left[-\left(\frac{\sigma}{\sigma_0}\right)^m\right] \tag{2.5}$$

where σ_0 is the value of tensile stress σ at 37% ($\sigma = \sigma_0$ in equation 2.5) of the total number of tested blocks survive. The exponent m is the Weibull modulus and decreases with increasing variability in tensile strength. According to the equation 2.5, Figure 2.3 shows Weibull distribution of strengths with the variability in strengths.

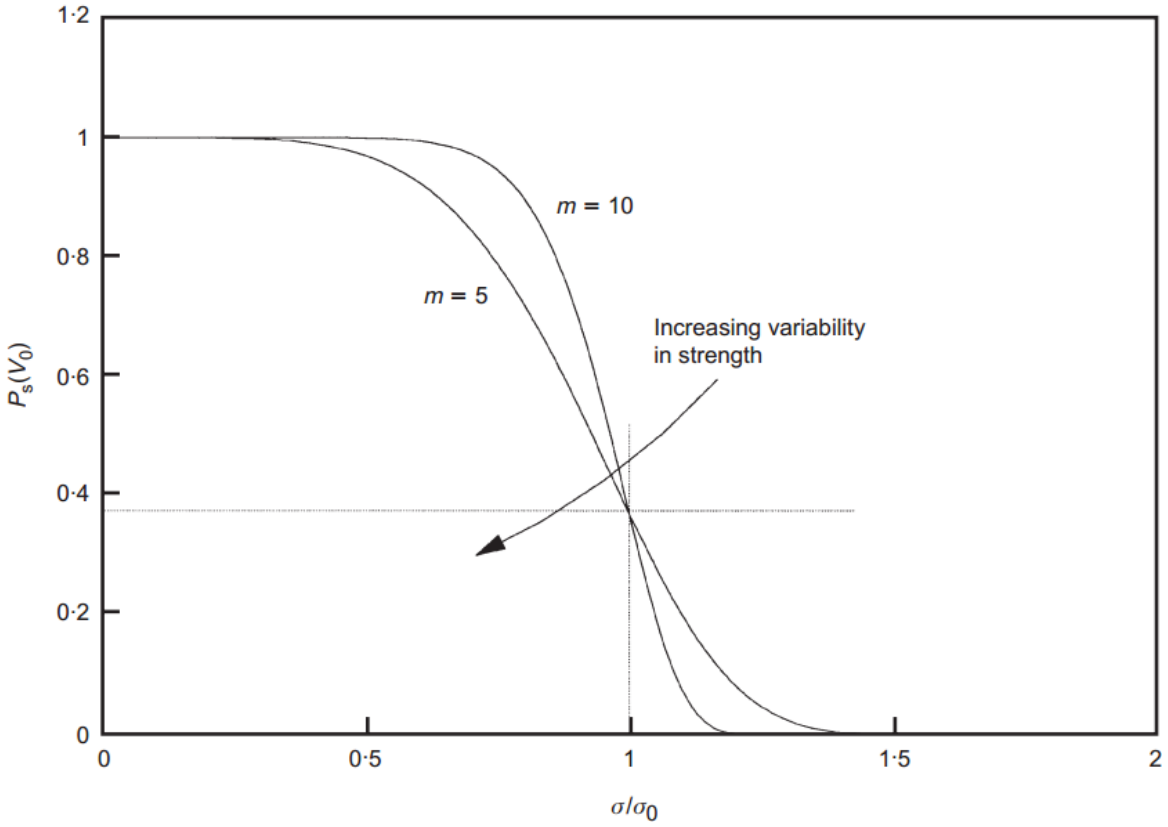

Figure 2.3 Weibull distribution of strengths (McDowell and Bolton, 1998)

By the data in Figure 2.2 to examine the applicability of Weibull as well with assumption of that all particle are similar in size and distribution of contacts and the size of the zones of tensile stress must scale with their volume, the survival probability of a particle size d under diametral compression is therefore given by

$$P_s(d) = \exp\left[-\left(\frac{d}{d_0}\right)^3\left(\frac{\sigma}{\sigma_0}\right)^m\right] \tag{2.6}$$

where σ is the characteristic tensile stress induced in the particle given by equation 2.1 and σ_0 is now the value F/d^2 where 37% of the tested particles survive and is approximately equal to the mean tensile strength of particle size d_0. According to Weibull distribution, the average tensile strength of grains scales with particle size can be

derived as

$$\sigma_0 \propto d^{-3/m} \tag{2.7}$$

which is equivalent to equation 2.3. Apparently, values of m in the range of 5-10 can be used to cover Lee's data in Figure 2.2. It was concluded that the mean value of F/d^2 at fracture for grains compressed dialmetrically between flat platens is a proper statistical meansure of the tensile strength (McDowell and Bolton, 1998).

The volume of solids V_s in a unit volume of soil is given by

$$V_s = \frac{1}{1+e} \tag{2.8}$$

where e is the void ratio. The number of sand particles per unit volume N is then given below in a simplifying assumption of a soil with single size paritcles.

$$N = \frac{V_s}{V_{sp}} \tag{2.9}$$

where V_{sp} is the volume of a single particle. In a unit cubic volume containing N particles, any straight line of unit length cuts through $N^{1/3}$ particles. Thus the number of particles per unit cross sectional area can be then cacluated as $\left(N^{1/3}\right)^2$. The force F_{sp} imposed on a single particle in the specimen is then given by dividing the normal stress σ by the number of across a plane of unit cross section.

$$F_{sp} = \frac{\sigma}{N^{2/3}} \tag{2.10}$$

For calculating particle tensile stress, the average volume of a single particle is given as

$$V_{sp} = \frac{1}{6}\pi \bar{d}^3 \tag{2.11}$$

where $\bar{d}$ is the mean particle dimater. The tensile stress in a sphere of a diameter d subjected to point loads F_{sp} can be shown as

$$\sigma_t = \frac{\chi F_{sp}}{d^2} \tag{2.12}$$

where Hiramatsu and Oka (1966) suggested $\chi = 0.9$.

Following Jaeger (1967), Lee (1992), Shipway and Hutchings (1993a), McDowell et al. (1996), and McDowell and Bolton (1998), the tensile stress was defined by equation 2.2. Substituting equations 2.8, 2.9 and 2.11 into equation 2.10 shows the force on a single particle embedded in a soil matrix

$$F_{sp} = \sigma \left(\sqrt[3]{\frac{(1+e)\pi}{6}} \right)^2 \bar{d}^2 \tag{2.13}$$

And the corresponding characteristic tensile stress

$$\sigma_{sp} = \frac{F_{sp}}{\bar{d}^2} = \sigma \left(\sqrt[3]{\frac{(1+e)\pi}{6}} \right)^2 \tag{2.14}$$

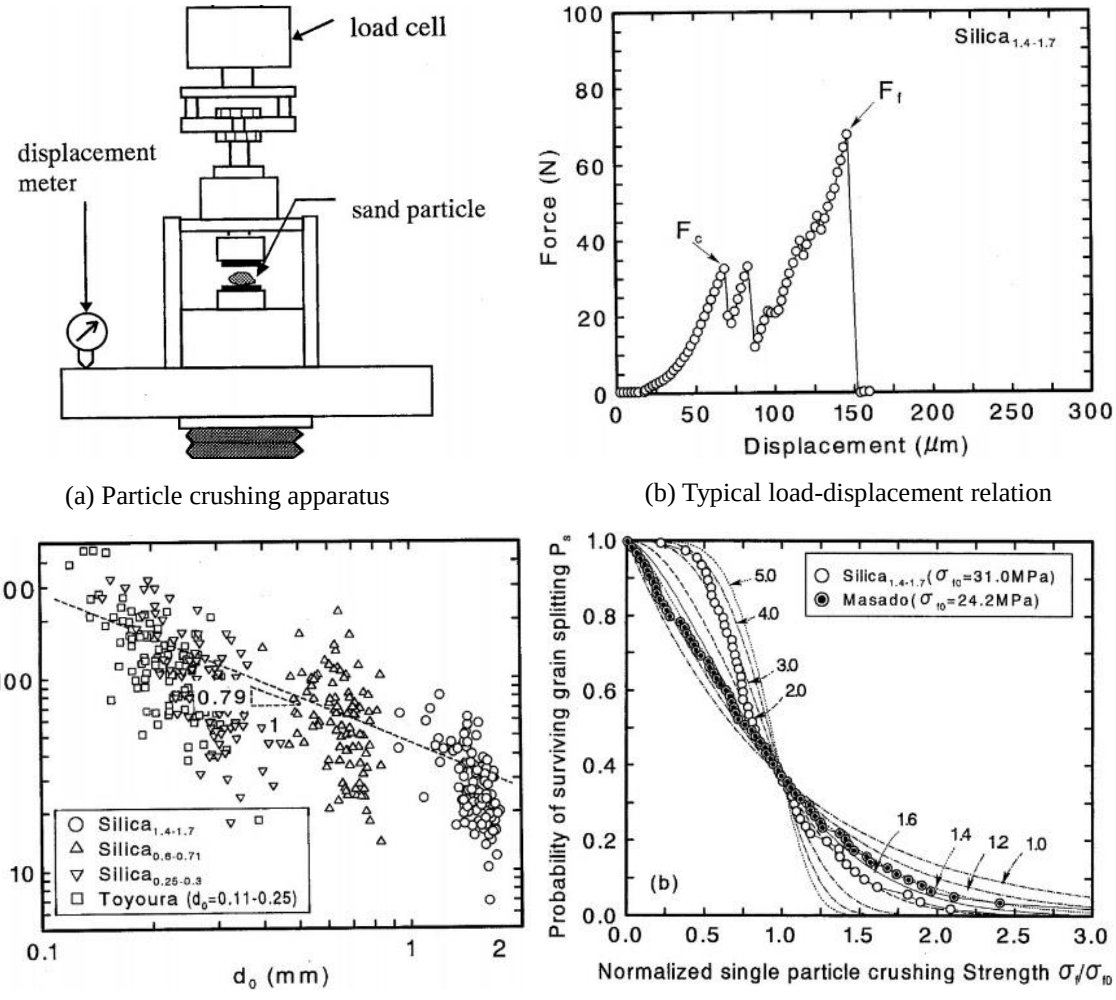

(a) Particle crushing apparatus

(b) Typical load-displacement relation

(c) Particle crushing strength

(d) Normalized survival probability curves

Figure 2.4 Single particle test results (Nakata et al., 2001b)

It can be seen in equation 2.14 that, for a given set of applied stresses, the average characteristic stress is not dependent on the particle size but instead is a function of the void ratio (Nakata et al., 2001b).

The single particle tests were conducted as well to investigate the individual particle crushing characteristics (Nakata, 1999a, 1999b, 2001b). Figure 2.4(a) and (b) show the schematic diagram of particle crushing apparatus and the typical load-displacement relation for a silica particle separately. The relationship between the single particle strength and the initial particle diameter is shown in Figure 2.4(c), where the regression line with as slope -0.79 on a log-log scale. The grain size dependency on strength has already been established by Lee (1992) and Nakata et al. (1999a). Figure 2.4(d) shows the survival probability curves normalized by the appropriate value of stress σ_{f0} at which the probability of grain survival is 37% as shown in the equation 2.5.

2.3 PARTICLE BREAKAGE ON ONE-DIMENSIONAL COMPRESSION

Most of the researches in soil mechanics focused on soil behavior under low pressure, but nowadays the soil in geotechnical engineering is being subjected to higher and higher pressure. Understanding the soil behavior subjected to high pressures is fundamental and significant in soil mechanics. The soil behavior in one-dimensional compression is of significance in soil mechanics. The vertical compression causes the vertical deformation without any lateral strain, which can be regarded as the K_0 consolidation.

Several definitions of the coefficient of lateral earth pressure at rest K_0 have been developed. Understanding the significance of lateral movement of retaining wall in sands and clays, the total vertical stress over horizontal stress was defined as K_0 by Terzaghi (1920) as shown below.

$$K_0 = \frac{\sigma_h}{\sigma_v} \tag{2.15}$$

where σ_h and σ_v represent the total horizontal soil pressure and total vertical soil pressure respectively.

Jaky (1948) developed the well-known semi-empirical relationship between K_0 and the Mohu-Coulomb effective angle of internal friction in understanding earth pressure in piles of granular material.

$$K_0 = 1 - \sin\phi' \tag{2.16}$$

where ϕ' is Mohr-Coulomb effective angle of internal friction angle. It can be concluded in equation 2.16 that K_0 decreases with the increasing friction angle.

Bishop (1958) defined K_0 as a ratio of the lateral effective stress to the vertical effective stress in a confined consolidated soil without any lateral deformation where there were no shear stresses on the principal plane, as displayed below.

$$K_0 = \frac{\sigma_h^{'}}{\sigma_v^{'}} \tag{2.17}$$

where σ_h' and σ_v' represent the effective horizontal soil pressure and effective vertical soil pressure respectively.

The effective stress increments were employed to remove the effect of stress history on soil behavior in definition of K_0 by Andrawes and EI-Sohby (1973) as expressed below.

$$K_0 = \frac{\Delta\sigma_h^{'}}{\Delta\sigma_v^{'}} \tag{2.18}$$

where the $\Delta\sigma_h'$ and $\Delta\sigma_v'$ are the increments of effective soil pressure in horizontal and vertical respectively.

Based on the compression tests under 8.5MPa, Terzaghi (1925) stated that particle crushing was not substantial in natural sands under such stresses and the higher stresses were not likely to be encountered. One-dimensional compression under high pressure was reported by Terzaghi and Peck (1948), where the confined compression tests were performed on sand and sand mica to pressure up to 1000 kg/cm^2. It was found that the displacement was similar with the normal consolidated clay settlement curve but the grain crushing occurred under high pressure. Roberts and De Souza (1958) conducted the confined compression tests on sand and ground quartz up to 1400 kg/cm^2, and observed that larger deformation occurred after a "critical pressure", which mainly caused by particle breakage in conclusion. The confined compression tests were also carried out on four different sands under up to 230 kg/cm^2 by Hendron (1963) who found that the expression of K_0 proposed by Jaky (1948) provided a reasonable estimation of K_0 for most sands and the sands of different initial densities converged onto single loading paths of unique void ratios at high pressure.

Hagerty el al. (1993) conducted one-dimensional compression tests on Ottawa sand, a granulated slag and sode lime glass subjected up to 689MPa to investigate how particle crushing is influenced by initial void ratio, particle size, particle angularity and particle material compositon. It was found that three phases of compression behavior can be regarded as volume contraction in particle arrangement at low stresses; and more intense compression as particles crush and are rearranged extensively under higher stresses; and as the number of contacts between fractured particles increases greatly at very high stresses. All final constrained moduli were in very small variation regardless of the

variation of all specimens in mineralogy, initial void ratio, median grain size, particle shape and initial modulus.

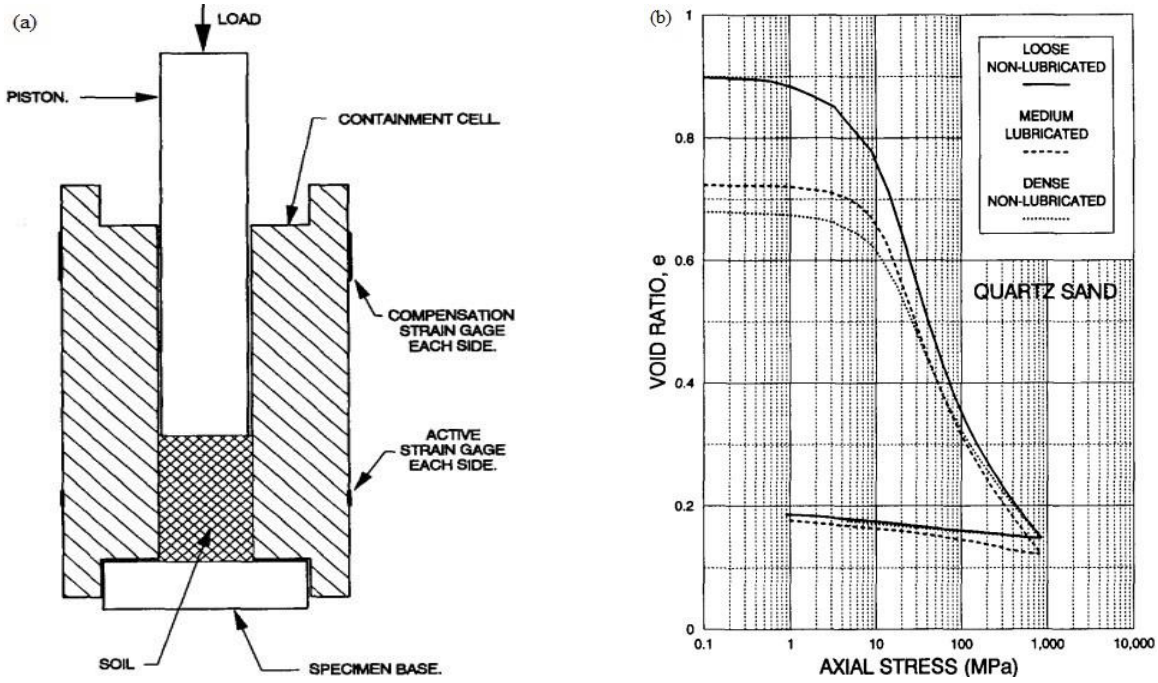

Figure 2.5 One-dimensional compression equipment and compression curve of quartz sand (Yamamuro et al., 1996)

To understand the soil behavior under high pressure, Yamamuro et al. (1996) performed one-dimensional compression tests on three kinds of sands of different mineral hardness subjected up to 800MPa. Figure 2.5 shows the one-dimensional compression equipment and compression curve of quartz sand. It was found that the effect of initial void ratio in sands was eliminated at high pressures, which indicated that the void ratio curves merged together at the high pressure but were related to mineral hardness as shown in Figure 2.5(b). Sand with higher mineral hardness caused a higher stress for the void ratio to merge. K_0 of Cambria sand indicated a constant magnitude (K_0=0.4) at high pressure, which was slightly lower than the K_0 value calculated from Jaky's equation 2.16 (K_0=0.45). The appearance on sand before and after shearing was investigated as well by microscope to find that the quarts sand had extensive crushing and fracturing of the individual grains, initiating crushing of quartz sand over 10MPa suggested by Robert (1996) in the discussion of this research, according to the compression curves of quartz sand.

It is well known that the initiation of marked particle crushing occurred since the yielding stress point during one-dimensional compression. The yield point stress increased with the increase of density of sample. McDowell et al. (1996) developed a mode for crushable aggregates by a statistical function and work equation, and examined the relationship between the statistical parameter and the curvature of the $e - log\sigma_v$ compression line. Nakata et al. (1999a) first examined the statistics of crushing of

individual particles in a soil matrix by seeding marked particles in triaxial samples subjected to compression and shearing. This work was later extended by Nakata et al. (1999b and 2001) who presented more detailed statistical data related to the degree of crushing of individual particles inserted in a silica sand matrix and subjected to one-dimensional compression.

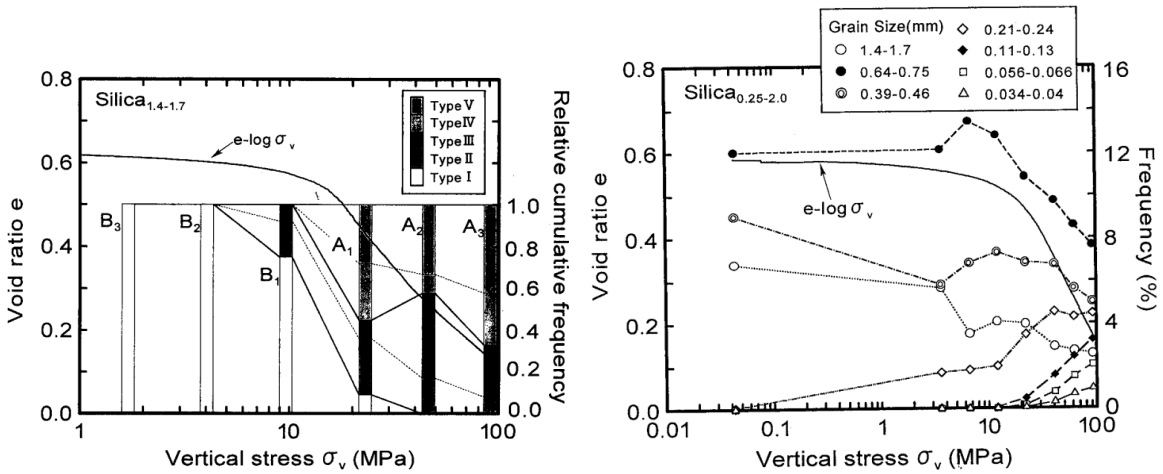

(a) Relative cumulative frequency of damage in uniformly graded sand

(b) Variation with vertical stress of grain size frequency for well graded sand

Figure 2.6 One-dimensional compression results (Nakata et al., 2001a)

Nakata et al. (2001a) carried out high pressure one-dimensional compression tests on silica sand samples seeded with marked particles in order to examine the relationship between the curvature and slope of the compression line and the statistics of individual particle crushing taking into account particle size and overall grading with five levels of particle damage from microscopic observation before and after testing of the 12 particles in each sample. A statistical analysis was carried out on data for the observed levels of damage to investigate the frequency variation with increasing applied stress. Additional one-dimensional compression tests was conducted as well on samples with a wide range of grain size distribution curves ,which were monitored in order to examine the effects of initial void ratio and grain size distribution on soil crushability and consequently the compression behavior. It was found herein that for the same material the yielding characteristics were dependent on the grading curve with much more marked yielding occurring for uniformly graded sands in comparison with well graded sands, and that major splitting of particles occurred mainly between the yield stress and the point at which the compression index C_c reached the maximum from observations of the colored particles inserted in almost uniformly graded sand with 50% of the particles in major splitting after yielding. Figure 2.6 shows the one-dimensional results under high pressure. the relative cumulative frequency of each class has been plotted against the vertical stress as shown in Figure 2.6(a), where particle crushing can be seen to initiate at Point B_2 around 4MPa and 80% of the particles are still undamaged (Type Ⅰ) at Point B_1 around 9.6MPa. However, more than 90% of the particles had some kind of damage with 50% of the particles in splitting when the yield point was passed at Point A_1 around

23MPa, after which the relative cumulative frequency curves began to level out, indicating that particle crushing increase with increasing vertical stress in reduced increment. Figure 2.6(b) reveals that the variation with vertical stress of grain size frequency for well graded sand, where the frequency for the particles of larger than 1.0mm can be found to decrease as the compression progressed. For the 1.4-1.7mm sized particles the frequency gradually reduced from 6% to 3% with a corresponding initial increase in the 0.5-0.8mm particles before yielding. The frequency of the 0.64-0.75mm particles initially increased from about 12% to 13.5% and decreased rapidly to 8% after 6MPa. The growth in the numbers of smaller particles can also be seen in increasing frequency of the 0.21-0.24mm and smaller particles. The frequency of the 0.21-0.24mm particles gradually increased during testing but the frequency of the particles smaller than 0.2mm increased after 20MPa.

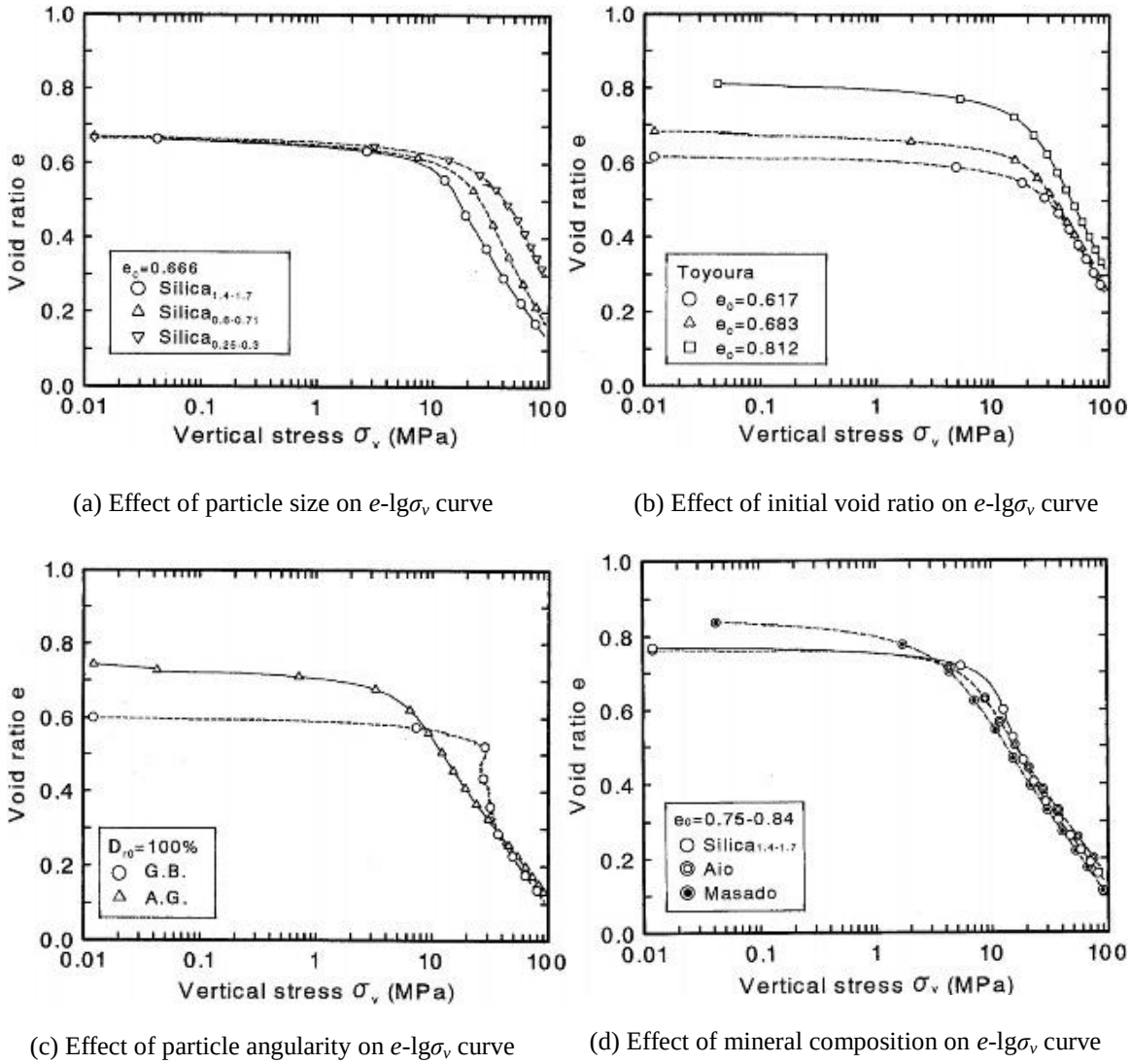

(a) Effect of particle size on e-lgσ_v curve

(b) Effect of initial void ratio on e-lgσ_v curve

(c) Effect of particle angularity on e-lgσ_v curve

(d) Effect of mineral composition on e-lgσ_v curve

Figure 2.7 One-dimensional compression results (Nakata et al., 2001b)

Nakata et al. (2001b) performed as well the one-dimensional compression tests and single particle crushing tests on various granular materials to investigate the influence of

particle size, initial void ratio, angularity and mineralogy on sand crushing and yielding characteristics in one-dimensional compression and to investigate the individual particle crushing characteristics for correlating the one-dimensional compression behavior and single particle crushing behavior. Herein it was found that the one-dimensional compression yield stress was related to the particle size and the single particle crushing strength and the single particle crushing strengths were compared with the characteristic tensile stress for a particle embedded in the soil matrix. The decrease of the vertical yield stress with increasing initial void ratio can be explained by the increase of the particle characteristic stress as the void ratio increased and a corresponding decrease in co-ordination number. Figure 2.7 shows the one-dimensional compression results (Nakata et al., 2001b), where Figure 2.7(a) the yielding stress increases as the particle size decreases. It can be explained that the single particle strength increases as the particle size decreases. As illustrated in Figure 2.7(b), the effect of initial void ratio was investigated to conclude that the yield stress decreased with the increase of initial void ratio as has been found by Hagerty et al. (1993) and Pestana and Whittle (1995). The effect of particle angularity on $e - lg\sigma_v$ curve was discussed as well in Figure 2.7(c) where the samples were prepared to the same relative density of 100% with an initial void ratio 0.74 for the Angular Glass (A.G.) and an initial void ratio 0.6 for the Glass Ballotini (G.B.). It can be seen that the yield stress for Angular Glass (around 6MPa) was less than the yield stress for Glass Ballotini (around 20MPa) by far. And the $e - log\sigma_v$ curve for Angular Glass after yielding becomes smooth but for Glass Ballotini it is discontinuous at the yield stress with a very large curvature. Figure 2.7(d) shows the effect of mineral composition on $e - lg\sigma_v$ curve on three different sands, where the yield stress seems to increase with the increase of quartz content despite the variation in initial void ratio and angularity of each sand. It can be seen as well that the all sands curves merged onto a single post-yield curve, which would seem that there was no influence of mineral composition on the post-yield region.

It is commonly accepted that the onset of particle breakage in sands during compression marked start of yielding. Particle breakage is strongly associated with the tensile strength of a single soil grain. For clarifying the influence of initial density and initial sample grading on the probability of particle breakage, Altuhafi and Coop (2011) performed one-dimensional compression on three sands with distinct mineralogies. It was found that a unique normal compression line is the outcome of a large amount of breakage in poorly graded samples and that a significant reduction in particle breakage is observed by changing the initial grading to a better graded sample with no significant particle breakage measured for very well-graded samples.

2.4 PARTICLE BREAKAGE IN TRIAXIAL TEST

It was early found that the phenomenon of particle crushing has a significant influence on engineering characteristics of soil. Since Terzaghi (1925) proposed the concept of soil microstructure including the particle arrangement, void distribution, connected state of particles and particle crushing, great deal of attention was attracted to the phenomenon of

particle breakage with lots of researches around particle breakage.

Particle crushing depends on particle size distribution, particle shape, state of effective stress, effective stress path, void ratio, particle hardness, water content, mineral composition and so on (Hardin, 1985; Lade et al., 1996; Coop et al., 2004; Donohue et al., 2009; Kikumoto et al., 2010).

Bishop (1966) tested the loose Ham River sand under initial confining pressures of up to 6.8MPa. Lee (1965) preformed undrained triaxial compression tests on Sacramento River sand with various densities at initial confining pressures up to 13.8MPa. Tai (1970) conducted undrained triaxial compression tests on Chattahoochee River sand and Ottawa sand of varying densities under initial confining pressure up to 34.5MPa. It was found herein in these researches that there was significant particle crushing at high consolidation pressures with large positive pore water pressure development as a result of that the high consolidation pressures were sufficient to suppress any dilative tendency in soil.

Triaxial tests under high pressure to investigate the shearing characteristics of rockfill materials were conducted by Marsal (1967) who found that particle crushing was substantial, having a significant influence on the shearing characteristics of rockfill materials and change of stress state in consolidation or shearing results in particle breakage. Figure 2.8 shows the triaxial testing results, where it can be seen in Figure 2.8(a) that particle breakage in materials 2 and 3 increases with the increase of confining pressure, and the principal stress ratio at failure decreases with the increase of particle breakage but converged within a narrow margin as shown in Figure 2.8(b).

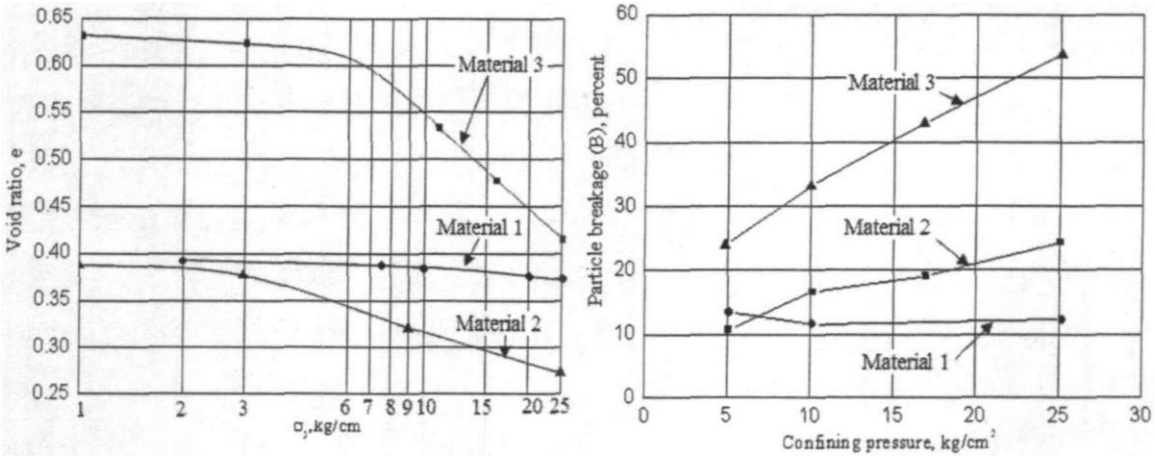

(a) Void ratio and breakage index of three materials at failure of triaxial tests

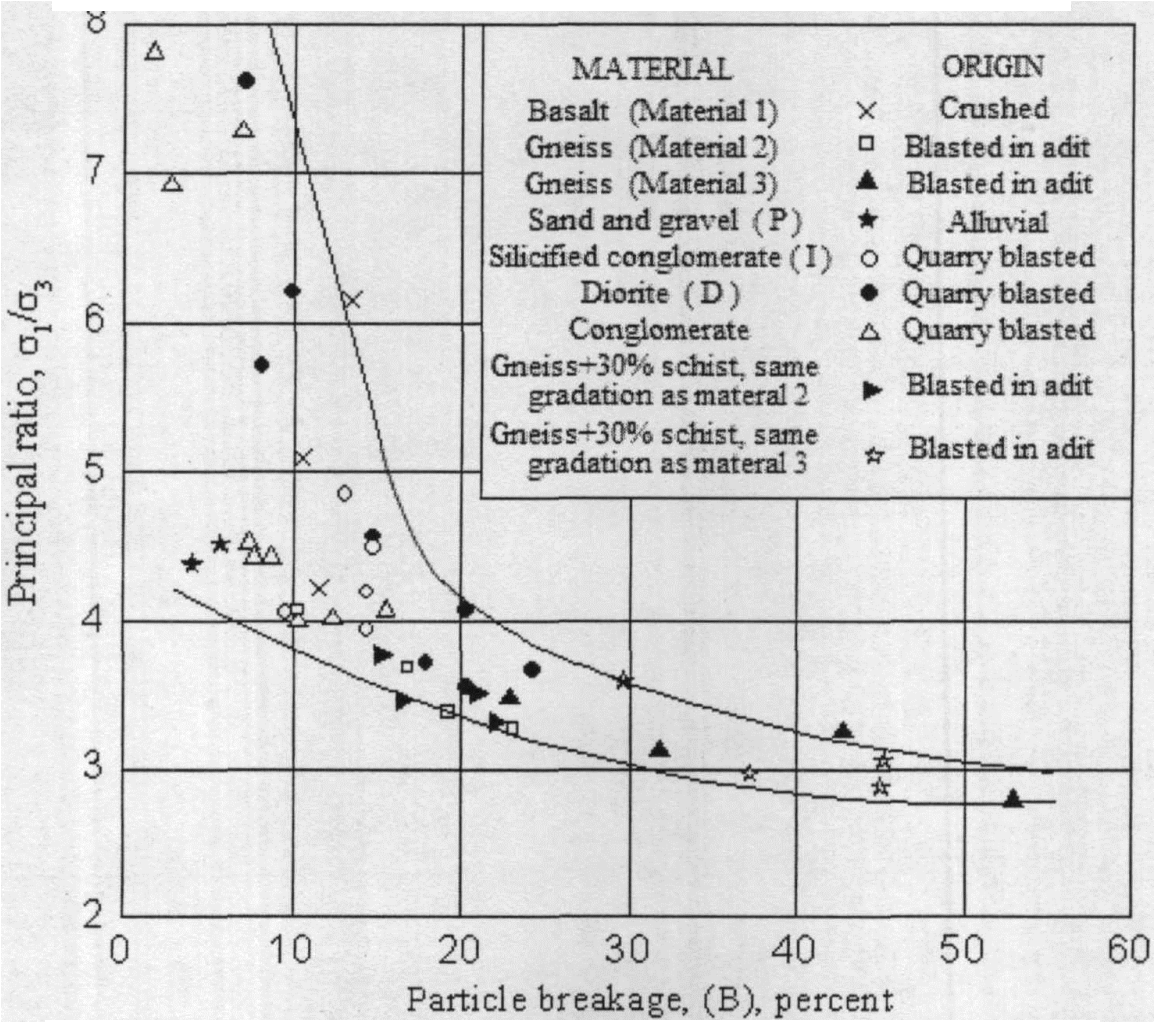

(b) Relationship between principal stress ratio at failure and breakage index Bg

Figure 2.8 Triaxial testing result (Marsal, 1967)

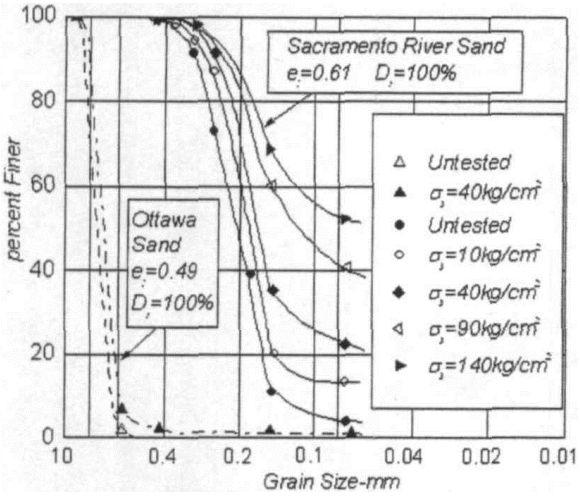

(a) Degradation of sands after drained triaxial tests

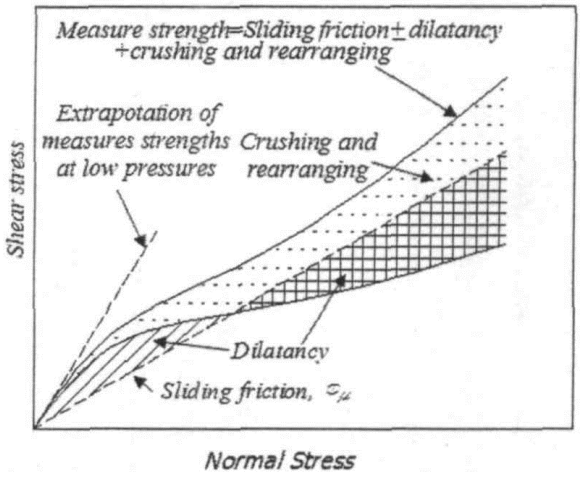

(b) Illustration of contribution of shear strength

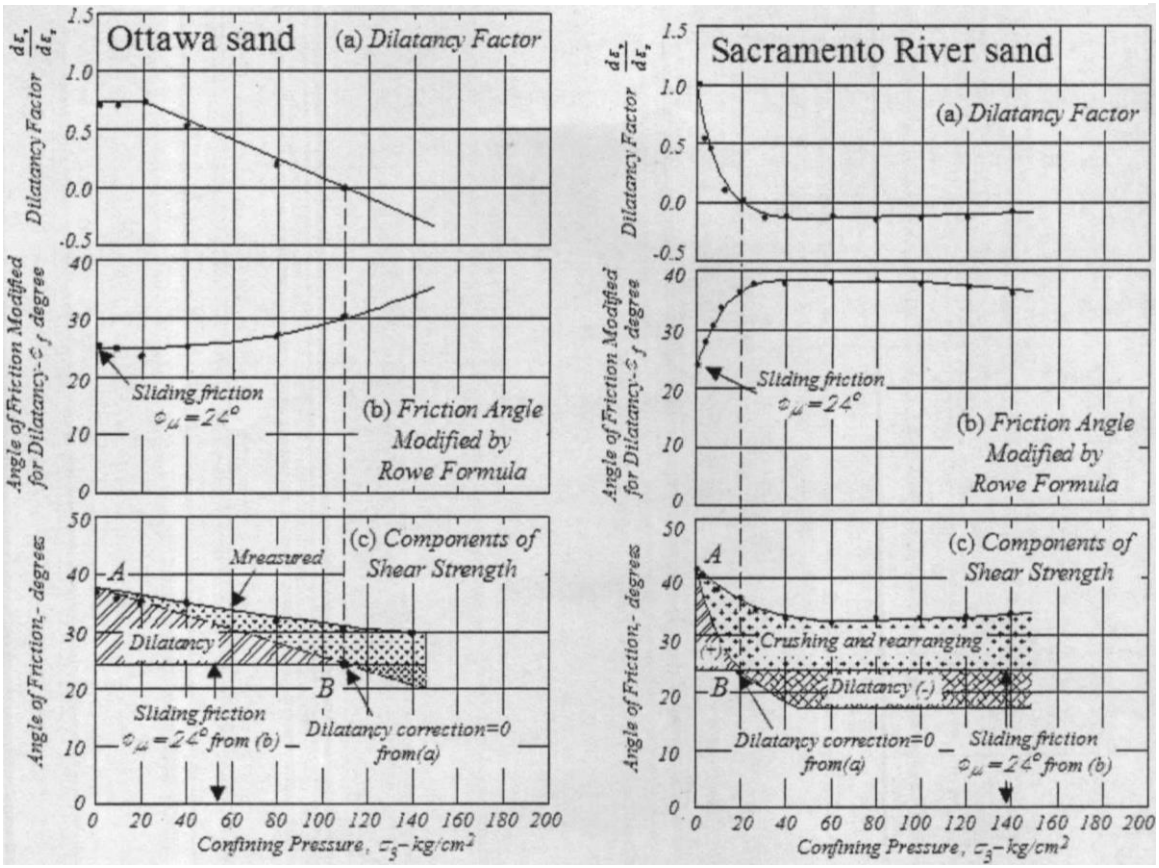

(c) Effect of dilatancy and crushing on measured angle of internal friction of dense sands

Figure 2.9 Drained triaxial compression results (Lee and Seed, 1967)

Lee and Seed (1967) performed drained triaxial compression tests with volume change measurements on Ottawa sand and Sacramento River sand up to 140kg/cm^2 confining pressure. Sliding friction, dilation and particle breakage & rearrangement were regarded as three components of shearing strength in this study. Figure 2.9 shows the drained triaxial compression results. Figure 2.9(a) shows the evolution of grain size distribution curves with increasing confining pressure, where particle breakage was caused at high

pressure particularly on Sacremento River sand. Lee and Seed (1967) accepted herein that the effect of particle breakage on stress-strain curve of sand was similar as the effect of rearrangement of particles in loose sample. Under high confining pressure, particle crushing consuming the energy weakens the contribution of dilatancy to friction angle so as to make real friction angle higher than sliding friction angle. Schematic illustration of contribution of shear strength is shown in Figure 2.9(b), where shear strength is comprised of sliding friction, dilatancy and crushing & rearranging of soil with regarding dilatancy as positive in expansion. And the sliding friction was almost independent of confining pressure but dilatancy contributed to shear strength substantially for dense samples at low pressure with a negative contribution under high pressure. Particle breakage and rearranging increased from an insignificant value at low pressures to make a substantial contribution to the overall shearing resistance at high pressures. Figure 2.9(c) shows the effect of dilatancy and crushing on measured angle of internal friction of dense sands at various confining pressures.

The dilatancy factors on Ottawa sand and Sacramento River sand were calculated at failure under different confining pressure as shown in part (a) of Figure 2.9(c), where the dilatancy factor on Ottawa sand decreased linearly with increasing confining pressure except an almost constant value under 20kg/cm^2 but the dilatancy factors on Sacramento River sand decreased sharply at low pressure to reach a constant value at high pressure, which may be caused by particle crushing. In the part (b) of Figure 2.9(c), according to Rowe's stress-dilatancy equation (Rowe, 1962), friction angles were calculated under various confining pressure but started by a sliding friction angle obtained at low pressure and assumed to a constant. The components of shear strength were drawn in part (c) of Figure 2.9(c), where it can be seen that the friction angle at A point was the peak friction angle at low pressure but the friction angle at B point was obtained under the dilatancy factor of zero. According to the Rowe's theory (Rowe, 1962), there is no any effect of dilatancy on friction angle at zero dilatancy factor. Lee regarded the linear connection from A point to B point as a simple evaluation of effect of dilatancy on shear strength on Ottawa sand but on Sacramento River sand the nonlinear relation of effect of dilatancy was used under large amount of particle breakage. In fact, the effect of dilatancy on shear strength with considering particle breakage is rather complicated. It can be seen that on Sacramento River sand with large amount of particle crushing in part (c) of Figure 2.9(c), particle crushing and rearranging have a very significant influence on shear strength, and effect of dilatancy on shear strength decreased with increasing particle breakage.

Vesic and Clough (1968) performed triaxial compression tests on Chattahooochee River sand under maximum 663kg/cm^2 confining pressure. It was found that few particle crushing occurred at low pressure being less than 0.1MPa, under which the dilatancy has a very significant effect on shearing characteristics of soil. But under elevated pressures there was intense crushing until the breakdown pressure which was defined as the stress with eliminating the effect of initial void ratio as a linearly deformable solid with modulus of deformation E proportional to mean effective stress q. It was found herein that friction angle of sand was larger than the friction angle among particles before

breakdown pressure, and with increasing particle breakage the friction angle of sand was reduced to friction angle among particles until the breakdown pressure with the depressing dilatancy.

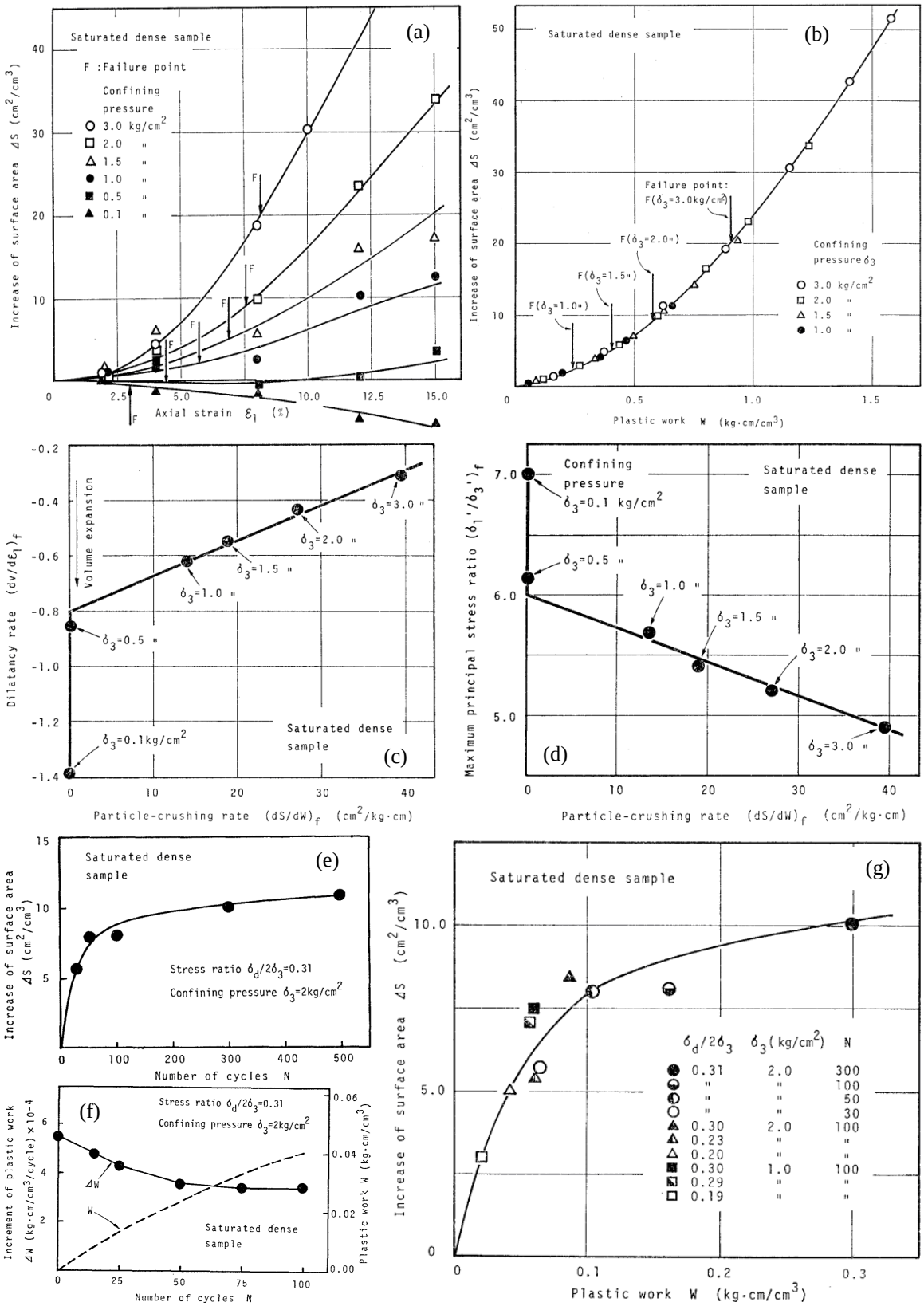

Figure 2.10 Results of triaxial tests and repeated triaxial tests (Miura and Ohara, 1979)

Miura and Ohara (1979) conducted triaxial compression tests and cyclic triaxial tests on a decomposed granite soil to investigate the effect of particle crushing on the shear characteristics of the soil. Here the increase in surface area, ΔS is used in measurement of the amount of particle crushing, and it was shown that the amount of particle crushing ΔS induced by the shear stresses has a close relation with the plastic work done W. The particle crushing property of the sample under shear stresses is defined by the rate of increase of the surface area S to the plastic work done W (dS/dW), which was called "particle-crushing rate" in this study.

The particle-crushing property was investigated in adoption of surface area increase as the measure of the amount of particle-crushing. Figure 2.10(a) indicates the change in surface area increase ΔS with increasing the axial strain in CD tests at various confining pressure. It can be seen herein that the surface area increase of a sample sheared under 0.1kgf/cm^2 confining pressure decreases with increasing axial strain as a result of the marked expansion in volume causing a decrease of dry density during shearing, which can be understood by that under the initial specific surface area S_w (cm^2/g) and dry density γ_d (g/cm3), the surface area increase ΔS decreases as the decrease in γ_d overcomes the increase in S_w during shearing. It is noted as well that the value of ΔS continues to increase with increasing the axial strain even after the failure point, where the stress increment is zero or negative, which means that the surface area increase may be a function of the magnitude of stress. Consequently the surface area increase ΔS is a function of plastics work W done to specimen, which should be applicable here. The $\Delta S - W$ curve shown in Figure 2.10(b) may be an initial part of the "S" type curve, namely which would be developed into an "S" type curve with increasing plastic work done. Herein the slope of the $\Delta S - W$ curve, dS/dW called "particle-crushing rate", was introduced to assess the particle-crushing property of a sample under triaxial compression stresses, which can be employed to investigate the effect of particle-crushing on shear characteristics.

The relation between the particle-crushing rate at failure and the dilatancy rate is illustrated in Figure 2.10(c), which shows a linear relation. It is notable herein that at the confining pressure lower than 0.65kgf/cm^2, the relevant value of particle-crushing ratio is substantially zero, meaning that no particles are crushed at failure. Under the confining pressure larger than 0.65kgf/cm^2, both particle-crushing rate and dilatancy rate increase with increasing confining pressure. In other words, particle crushing resulted in larger particle-crushing rate and less dilatancy. Figure 2.10(d) shows the relation between maximum principal stress ratio and particle-crushing rate in drained compression tests, where a linear relation exists between them. It can be seen herein that with increasing of particle-crushing rate, the maximum principal stress ratio decreases linearly except that the maximum principal stress ratio decreases vertically at the zero particle-crushing ratio. The cyclic triaxial tests were performed as well to investigate the effect of particle crushing on shear characteristics. The relations between surface area increase & plastic work and number of cycles are shown separately in Figure 2.10(e) and (f), where both surface area increase and plastic work increase with increasing number of cycles in

reduced increment. Figure 2.10(g) shows the relation between the surface area increase ΔS and plastic work done W, where the shape of $\Delta S - W$ curve is convex, being different from the shape of $\Delta S - W$ curve in triaxial compression tests as shown in Figure 2.10(b). It can be concluded that the particle crushing mechanism between triaxial compression tests and cyclic triaxial tests may be different under static and dynamic loading, which may cause different particle-crushing properties.

Fragaszy and Voss (1986) conducted high-pressure undrained isotropic compression tests on Monterey No.0 sand and Eniwetok sand to verify a theory proposed to explain the mechanism of blast-induced liquefaction. It was found that the sand can be liquefied by a single cycle of isotropic compressive stress applied under quasi-static undrained condition. And the Eniwetok sand was found to be much easier to liquefy than Monterey sand. Initial dry density was not a significant factor in generation of residual excess pore water pressure for both sands. The plastic volume changes causing residual excess pore water pressure under compressive loading appear to come from the crushing of individual particles. In addition, the compressive loading was regarded as a dominant factor in causing blast-induced liquefaction. Yasufuku and Hyde (1995) employed the spherical cavity expansion method to predict pile end-bearing capacity in considering the soil crushability and the decreased friction angle with increasing mean normal stress.

Yamamuro and Lade (1996) performed drained triaxial tests on dense Cambria sand at high pressure up to 52MPa. As the confining pressure is increased, it was found that the stress-strain curve, volumetric strain and axial strain to failure increased rapidly at a certain stress magnitude, which was shown to be related directly to a marked increase in particle crushing. Beyond a certain higher value of stress magnitude, the stress-strain curves steepen with the decrease of the volumetric and axial strains to failure, which was directly related to the cessation of particle crushing. And the Mohr-Coulomb secant friction angle was found to be related to the rate of volume change at failure regardless of the soil was dilatant or highly contractive and subjected to large amounts of particle crushing. Figure 2.11 shows the drained triaxial tests results. Figure 2.11 (a1) and (a2) show the major principal strain at failure and volumetric strain at failure versus effective main normal stress at failure, where major principal strain at failure and volumetric strain at failure increase gradually with increasing confining pressure at low mean principal stress at failure but after 4MPa mean normal stress, the major principal strain at failure and the volumetric strain at failure increase dramatically particularly in compression tests to reach peaks between 20MPa and 30MPa mean normal stresses at failure. Increasing mean normal stress, the smaller major principal strain to failure was produced in extension but before 4MPa effective mean normal stress the volumetric strain at failure almost converged into one line in compression and extension. Figure 2.11(b1) shows the relative breakage under various effective mean normal stress at failure, where it can be seen clearly that the particle crushing increases with increasing effective mean normal stress at low pressure exactly to 4MPa, after which particle crushing increase dramatically to reach a peak between 20MPa and 30MPa effective mean normal stress. Considering the evolution of particle crushing during loading, it was concluded that the

development of major principal stain at failure and volumetric strain at failure were related directly to particle crushing. Figure 2.11(b2) shows the void ratio at failure against the effective mean normal stress at failure in compression and extension tests, where one point should be notable that with increasing confining pressure at high pressure, the void ratio at failure decreases in reduced increment. The volume change rate at failure and secant friction angle against effective mean normal stress were discussed as well in Figure 2.11 (c1) and (c2), where the secant friction angle was found to be related to the volume change rate at failure.

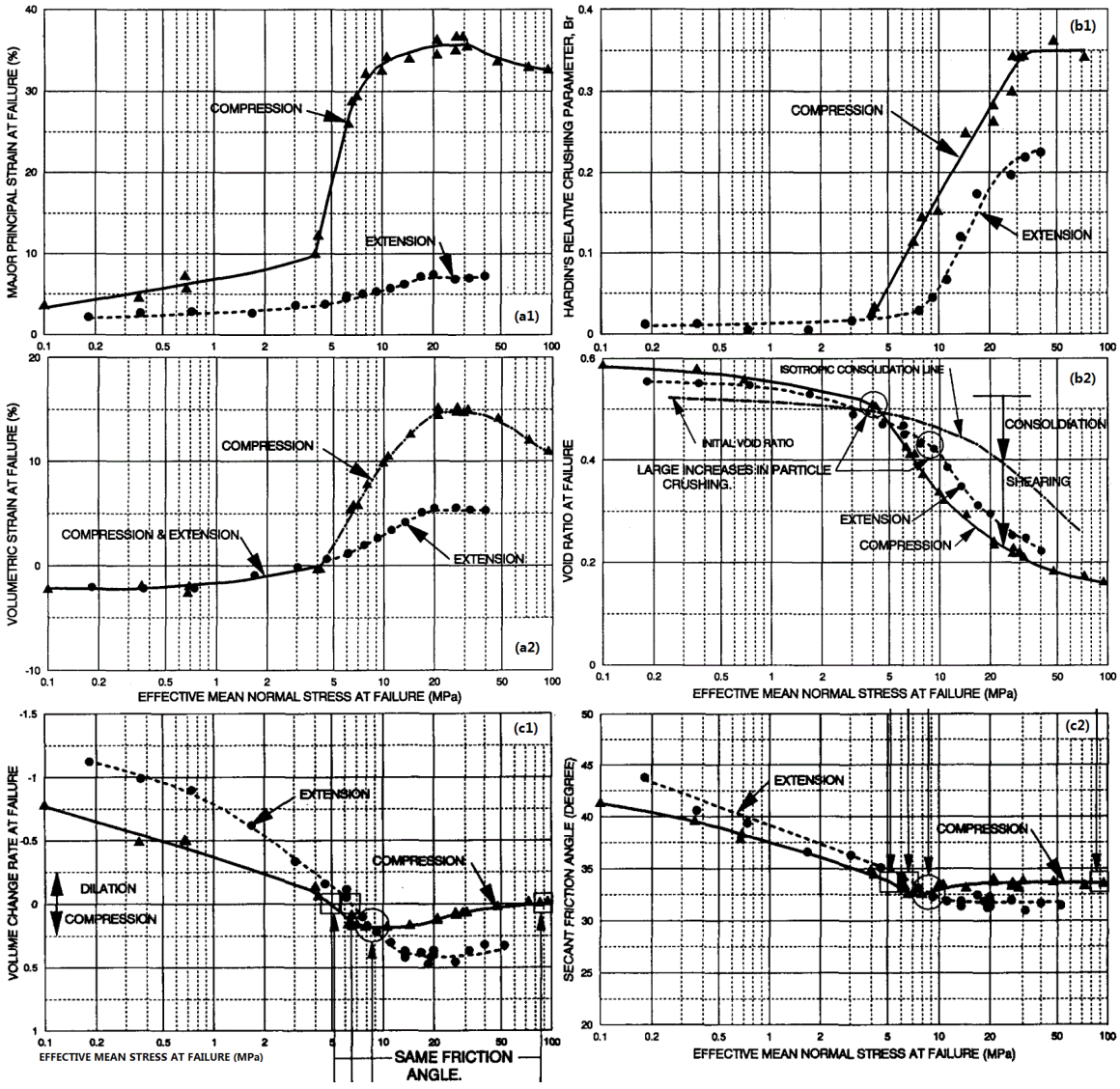

Figure 2.11 Drained triaxial tests results (Yamamuro and Lade, 1996)

Lade and Yamamuro (1996) performed as well undrained triaxial tests at high pressure up to 68.9MPa on dense Cambria sand. It was found herein that the higher confining pressures cause larger amounts of particle crushing to occur, which in turn results in the development of higher positive pore pressures, leading to the effective stress path to move rapidly toward the effective stress failure envelope. The applicability of critical

state soil mechanics at high pressure is explored. Figure 2.12 shows the typical triaxial results. Grain size distribution curves were determined from the sheared soil recovered from the undrained test specimens and Hardin's (1985) relative breakage parameter B_r was calculated. Figure 2.12(a) shows the Hardin's relative breakage against the effective mean normal stress at failure, where it can be seen clearly that there is more particle crushing in undrained compression than in extension at high confining pressure. The undrained triaxial compression tests caused larger increment of the particle crushing to move to peak quickly but in drained triaxial tests at high pressure, the particle crushing increases gradually in reduced increment to converge a stable value, which means that the particle breakage could cease at some stress. The comparisons of undrained friction angle with the friction angles obtained from drained compression and extension tests is shown in Figure 2.12(b), which indicates that the friction angles from undrained tests appear to cross the drained friction angle lines near the stress magnitudes that coincide with a rate of volume change at failure of zero in drained tests as illustrated in Figure 2.11(c1). The confluence of these friction angles near the mean normal stress of 5MPa seems to be related to the amount of particle crushing, which was approximately the same in drained and undrained tests for both compression and extension as shown in Figure 2.12(a). However, at higher stress magnitudes, the undrained compression and extension friction angles are higher than the drained friction angle. As drained test specimens are sheared at constant effective confining pressure, the void ratio s should move from the isotropic consolidation line toward the critical state line defined by the undrained tests as shown in Figure 2.12(c).

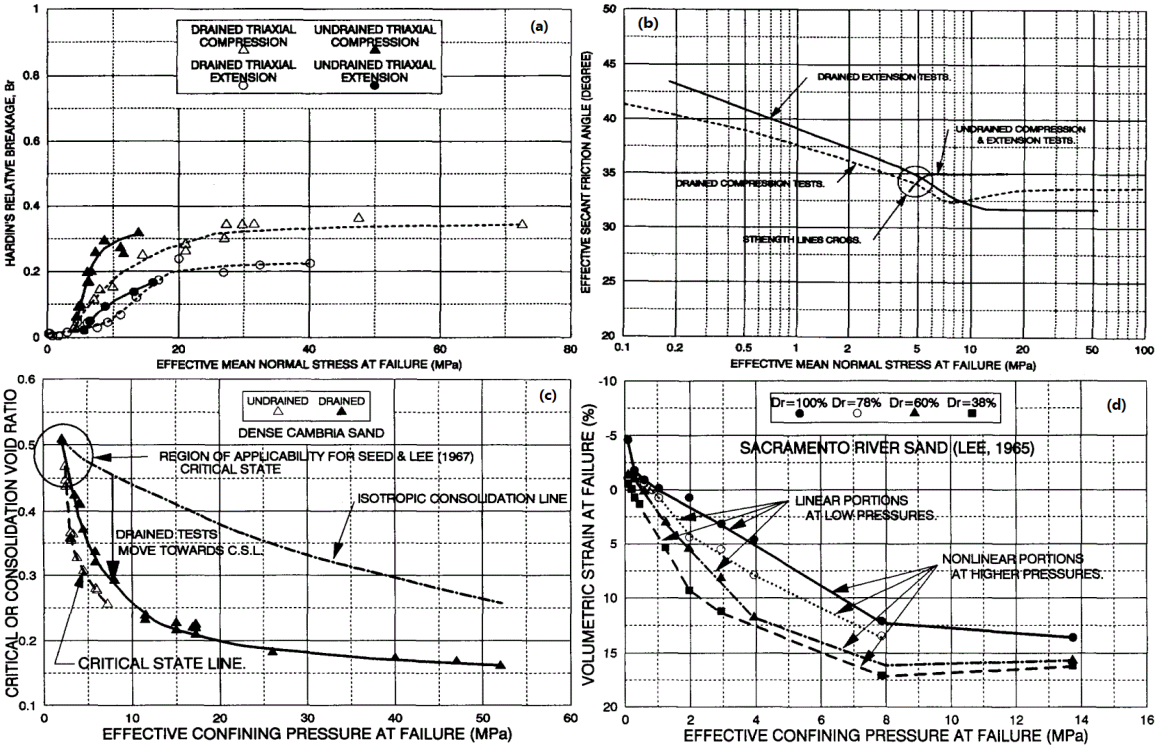

Figure 2.12 Triaxial results (Lade and Yamamuro, 1996)

However, the results of high-pressure drained tests indicate that the lines don't coincide at the maximum principal stress ratio or even at larger strain. Due to the elimination of effect of initial void ratio at high pressure, compression from any initial void ratio results in always a unique relation between void ratio and compressive stress. Subsequent shearing at high pressures results in only large contractive volumetric strains at failure caused by large amount of particle crushing. Therefore, at high pressures, regardless of the variation of initial void ratio or confining pressure magnitude, a volumetric strain of zero at failure as required by the definition of critical state condition is not possible. At high pressure the volumetric strain at failure is not linear as shown in Figure 2.12(d), where the failure volumetric strains from four different densities of Sacramento River sand are shown plotted against confining pressure (Lee, 1965). It can be seen here, the linear portion occurs only at low pressures. Since at high pressure, the volume change at failure actually decreases with increasing confining pressure, it is possible to achieve any critical confining pressure. Thus, the determination of a unique critical confining pressure at a critical void ratio for drained tests is not possible.

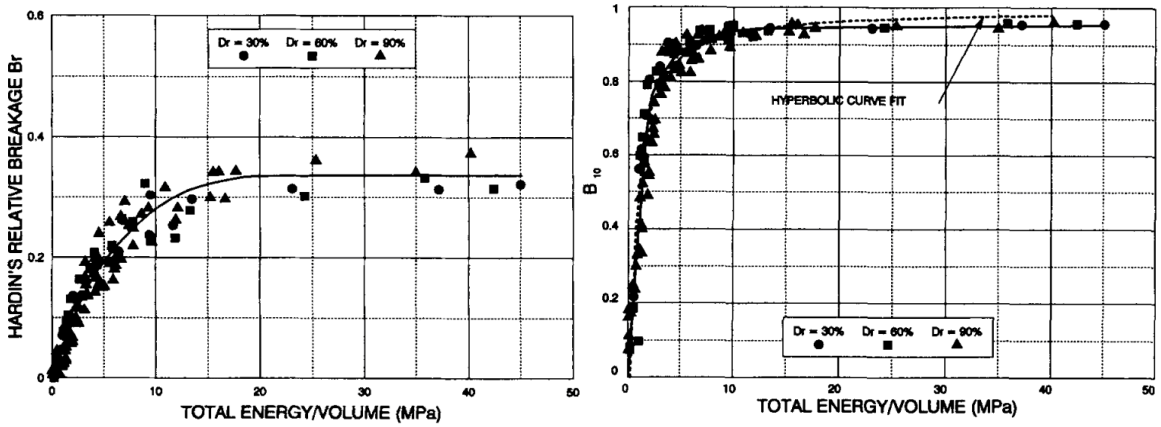

(a) Hardin's (1985) particle breakage factor B_r related to total input energy

(b) Proposed particle breakage factor B_{10} related to total input energy

Figure 2.13 Particle breakage factors related to total input energy (Lade, et al., 1996)

Lade et al. (1996) performed many drained and undrained triaxial compression and extension tests on dense Cambria sand under various confining pressures up to 68.9MPa. Under high pressure the significant particle breakage occurred. Many particle breakage factors were discussed to quantify the extent of particle breakage. To produce a unique correlation with all particle breakage factors, the total energy input into tests was proposed to describe a particle factor in hyperbolic curve as a combined factor which can be used to estimate the permeability of soil, from which to prove that the particle breakage could affect pore pressure distribution and seepage quantities. Figure 2.13 shows the Hardin's particle breakage factor B_r and proposed particle breakage factor B_{10} related to total input energy for drained and undrained triaxial compression and extension tests on three different densities of Cambria sand, where both correlations of crushing parameters with the total input energy can be acceptable with being related to all type of tests in one unique curve but the scatter is substantially reduced in the formulation

of the proposed particle breakage factor B_{10} in comparison with the Hardin's particle breakage factor B_r.

By means of triaxial testing over an extended range of pressures, Coop and Lee (1993) concluded that there was a unique relationship between the amount of particle breakage that occurred on shearing to a critical state and the value of mean normal effective stress for a variety of sands of various mineralogies. Luzzani and Coop (2002) carried out ring shear tests on carbonate sand and quartz sand to investigate the relationship between volume change and particle breakage during shearing. The carbonate sand was sheared at high confining pressures to examine whether, in the region of compressive shearing behavior due to particle breakage, the breakage would ever cease and the soil would reach a stable grading, and the quartz sand was sheared under low confining pressures to investigate whether a dilatant sand would also be subjected to particle breakage. It was found that the particle breakage continued to very large strains in both sands with no evidence of a stable grading being reached within the range of strains used. While the particle breakage was small for quartz sand it was large for the carbonate sand, emphasizing that any definition of a critical state by means of conventional triaxial or shear box testing would be approximate only as a result of the limited strains allowed.

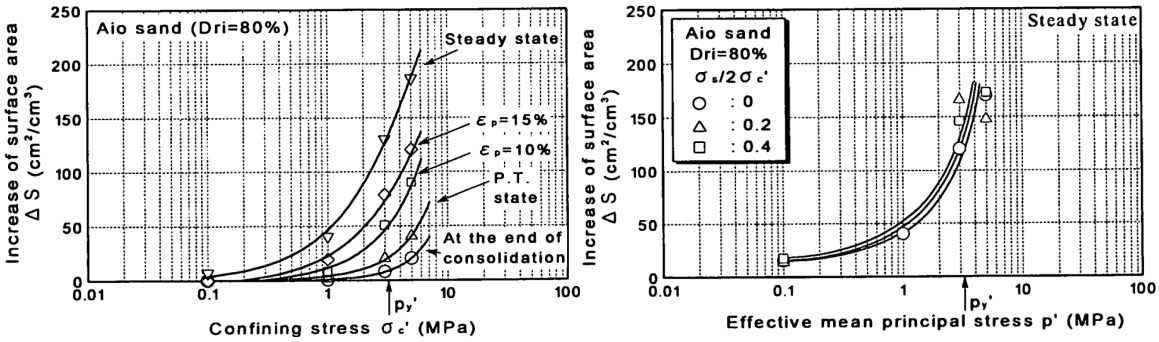

(a) Development of surface area for isotropically consolidated undrained shear tests

(b) Development of surface area at steady state

Figure 2.14 Development of surface area of undrained shear tests (Hyodo et al., 2002)

Hyodo et al. (2002) carried out monotonic and cyclic loading tests on silica sand over a wide range of stresses for comparing non-crushing and crushing behavior with sieving the samples at several stages to determine the increase in particle surface area and degree of particle crushing. Samples consolidated to 0.1MPa demonstrated strong dilative behavior but the dilation was found to be suppressed with considerable particle crushing by shearing above the yield stress of 3MPa. Shearing after the phase transformation point resulted in a marked increase in particle crushing with similar particle crushing at steady state for isotropic and anisotropic consolidated sands. Crushing was seen to increase rapidly after the phase transformation point, where particle rotation and translation contributed to the crushing process with development of high strains. The development of surface area of undrained shear tests is shown in Figure 2.14, where a marked increase in surface area can be seen in Figure 2.14(a) after the phase transformation state with more

increase of surface area in larger axial strain, and the particle crushing continued to increase up to the steady state. As shown in Figure 2.14(b), the surface area was also found to increase rapidly after the phase transformation state but there was no big difference in increase of surface area at steady state for isotropic and anisotropic consolidated sand.

Indraratna and Salim (2002) performed the large-scale triaxial tests on Latite basalt under from 10kPa to 300kPa, which were terminated at specific axial strain levels from 0% to 20% by a 5% increment for getting the grain size distribution curves after shearing, and found that particle breakage increases with increasing axial strain and confining pressure with reduced increments of particle breakage, and particle breakage still increases during shearing after failure. And axial strain at peak strength increases with increasing axial strain.

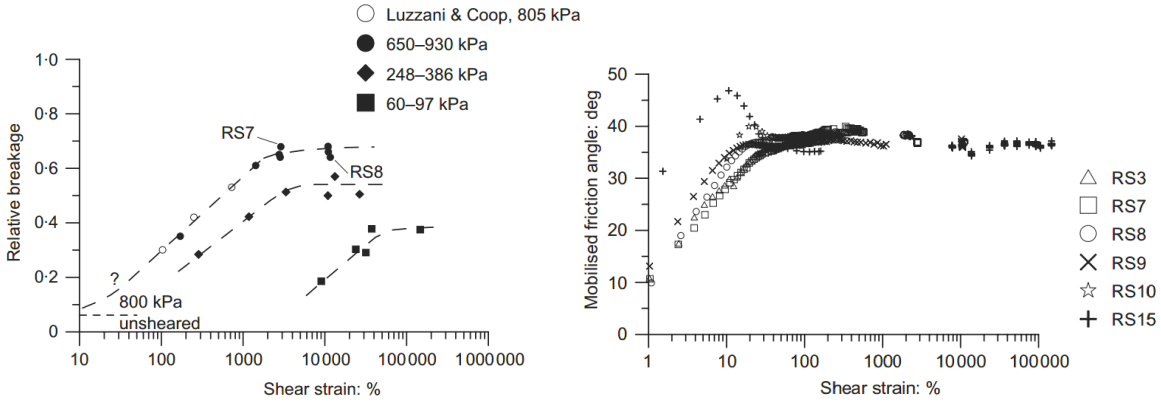

(a) Relative breakage vs. shear strain (b) Evolution of mobilised angle

Figure 2.15 Typical results of ring shear tests on carbonate sand (Coop et al., 2004)

Coop et al. (2004) conducted also a series of ring shear tests to investigate the development of particle breakage with shear strain for a carbonate sand. It was found herein that the soil reached a stable grading at very large strain but the final grading depended on both applied normal stress and the initial grading. And the particle breakage causing a volumetric compression ceased at stable grading, emphasizing that the critical state as observed at much smaller strains in triaxial tests are not rigorously defined. The mobilized angle of shearing resistance was found not to change significantly despite of the severe degradation of the soil. Figure 2.15 shows the typical results of ring shear tests on carbonate sand, where it can be seen clearly herein that the relative breakage B_r reached a stable value at very large shear strain but final value of relative breakage B_r increases with increasing the applied vertical stress as shown in Figure 2.15(a), whereas the mobilised friction angle of shearing resistance converged to a constant value at very large shear strain despite of different extent of particle breakage in soil but the mobilised friction angle was related to initial density and stress level at the low shear strain as illustrated in Figure 2.15(b).

The traditional Cam-Clay model was modified by introducing crushing energy to consider the effect of particle breakage on soil behavior (Mcdowell et al., 1996). The energy consumption induced by particle breakage among particles was introduced to traditional stress-dilatancy equation proposed by Rowe (1962) for developing new modified stress-dilatancy equation considering effect of particle breakage, which can be used to assess the friction angle under particle breakage (Ueng and Chen, 2000). Based on the modified stress-dilatancy equation considering particle breakage developed by Ueng and Chen (2000), Salim and Indraratna (2004) proposed a new elastoplastic stress-strain constitutive model incorporating the degradation of particles for granular coarse aggregates subjected to breakage during triaxial shearing by developing a plastic flow rule incorporating the energy consumption due to particle breakage during shearing, which can accurately predict stress-strain curve, volume change and amount of particle breakage at any stage of shear deformation.

A new constitutive model considering sand crushing with adoption of a new hardening parameter with the crushing stress was developed to be able to predict the tri-axial compression test results well (Yao et al., 2008). Grain size distribution as a weight function of the stored energy in the different grain fractions was introduced to continuum model for considering the effect of breakage, which assumes that the larger particle stores more energy than the smaller one to explain that the particle will became smaller with time in accordance with the principle of energy minimization. Then Continuum Breakage Mechanics models were developed by the concept of breakage as a thermomechanical internal variable (Einav, 2007a). Additionally, the new theory of Continuum Breakage Mechanics was developed further by combination of the two dissipative mechanisms of breakage and plasticity (Einav, 2007b).

Since the critical void ratio was discussed by Casagrande (1936) and critical state soil mechanics was put forward by Roscoe et al. (1958), considering the grading of soil is changed by particle breakage, the effect of particle breakage on the locations of Critical State Line (CSL for short subsequently) has been paid more attention. Many researches have been done about the characteristics of CSL on the plane of void ratio e against logarithm of mean effective stress p' (Been and Jefferies, 1985; Been et al., 1991; Coop and Lee, 1993; Verdugo and Ishihala, 1996; Konrad, 1998). CSL was shown to be nonlinear with a marked increase in slope as the stress level greater than around 1MPa. It was suggested that the critical friction angle in sands may be a function of the critical state void ratio and the effect of initial state of each test on the location of CSL was discussed as well (Been et al., 1991). CSL was a unique line in $e - lnp'$ plane with a threshold high pressure as the onset of particle breakage (Verdugo and Ishihala, 1996; Konrad, 1998). Coop and Lee (1993) found that the larger plastic volumetric change during compression was caused by particle crushing for granular soils and a unique relationship between the degree of breakage and the stresses applied was identified. The grain strength governed the strength and dilatancy of crushable soil and particle breakage resulted in a flattening of the grading curve satisfied the Weibull statistics (McDowell and Bolton, 1998), it was found as well that the dilatational component of the angle of

internal friction was proportional to the logarithm of mean effective stress at a given relative density. However, Coop et al. (2004) conducted ring shear tests to investigate the development of particle breakage, and it was found that the soil reached a stable grading at very large displacement where the volumetric compression ceased.

Wood (2008) proposed a constitutive model for sands in using a series of critical state lines in e-logp′ plane which are related to the current grading of soil. It is thereby assumed that the current critical state moves downwards toward a limiting critical state line at the limiting gradation of soil with on change of gradient. The family of those critical state lines was also regarded as being parallel with the initial critical state line at lower pressure (Verdugo and Ishihara, 1996; Konrad, 1998).

For the influence of particle breakage on the locations of the critical state line in $e - lnp'$ plane, the locations of critical state line moved downward in $e - lnp'$ plane with the increase of particle breakage or finer content (Fourie and Papageorgiou, 2001; Murthy et al., 2007). But with the further increase of fine content, the locations of CSL may move back to upward in $e - lnp'$ plane (Thevanayagam et al., 2002; Carrera et al., 2011).

Particle breakage occurs in granular materials with various engineering application and the influence of particle breakage on the mechanical behavior of soils should be given proper consideration in a constitutive model for soils. Particle breakage results in increase in the number of fine particle and broadens the grading of particle sizes. And the primary effect of broadening the grading is to lower the critical state line and other characteristics of the compression of soil. The effect of particle breakage on soil behavior is adopted into the Severn-Trent sand model as a frictional hardening Mohr-Coulomb model in kinematic hardening and bounding surface framework with regarding the critical state lime as the locus of asymptotic states, where the strength is regarded as a variable quantity being dependent on the current value of the state parameter (volumetric distance from the critical state line). The state parameter tends to increase with loosening soil if the critical state line falls as a result of particle breakage (Kikumoto et al, 2010).

Dynamic loading of embankment, foundation and pavement structures results in particle breakage as well when the stresses imposed on their particles exceed their strength. Donohue et al. (2009) conducted drained cyclic triaxial tests on loose, uniformly graded samples of Dogs Bay carbonate sand. It was observed that particle breakage depends on stress level, cyclic stress ratio, and creep, being directly related to volumetric strain. And more breakage occurs with increasing numbers of cyclic loading as a results of more contractive volumetric stain induced by gradually increased drained cycling, which indicates that even through particle may not be loaded to their full capacity in a given cycle, particles were found to be able to be crushed in subsequent cycles without any variation in the amplitude of cyclic loading.

Sadrekarimi and Olson (2010) performed stress-displacement response measured ring shear tests on three sands with different mineralogical compositions with examining

particle shape changes by scanning electron microscope. Particle damage was found to produce a wider particle size distribution and continue until the normal stress was small in constant volume ring shear tests. And the dominant particle damage mechanism (typically either particle abrasion and shear-off asperities or particle splitting) depended on strongly on the soil response (i.e. contraction or dilation), particle hardness, and particle size distribution, being producing more angular and rougher post-shear particles than the original sand particles. Particle crushing resulting in increase of fines content led to increased contraction and liquefaction susceptibility when undrained condition prevailed. The mobilized friction angle was found to decrease as dilation was compensated by particle-crushing-induced contraction.

Karimpour and Lade (2010) performed triaxial compression tests on Virginia Beach sand at high pressures, where grain crushing is prevalent to study effects of initial loading strain rates on subsequent amounts of creep and stress relaxation. Particle crushing was found to have a significant contribution to axial and volumetric strains but rearrangement and frictional sliding among intact grains play much smaller roles in the stress-strain and volume change behavior of granular materials at high stresses and shear strains because that particle breakage is a time-dependent phenomenon described as static fatigue or delayed fracture, based on which, the close relationship between time effects and crushing in granular materials is established as well. Lade and Karimpour (2010) presented that the phenomenon of static fatigue of individual particles seems to be at the root of time effects in sand with grain crushing related to the observed time effects, and that the effect of water is demonstrated in support of static fatigue mechanism with effects of time to crushing in glass beads from additional triaxial tests.

Friction angle is the most important parameter in soil strength. Sadrekarimi and Olson (2011) conducted triaxial tests and ring shear tests to investigate the yield friction angle and the critical state friction angle. The yield friction angle was found to be affected by initial sand fabric and decrease with increasing the pre-shear void ratio but the critical state friction angle from ring shear tests was independent of stress path and initial sand fabric and dependent of particle mineralogy and shape. Particle breakage induced in the ring shear tests resulted in increase of the critical state friction angle by a few degree with producing a wider range of particle sizes and more angular particles.

Recent constitutive models for sands incorporating the effects of particle breakage have emphasized the change of location of the critical state line in the void ratio and logarithm of the mean effective stress plane as the grading changes (Kikumoto et al, 2010). Bandini and Coop (2011) carried out a series of triaxial tests to investigate the effect of particle breakage on the current location of the critical state line. It was found that the critical state line does move with particle breakage and large amount of particle breakage results in a significant shift of the critical state line with a vertical movement and a rotation induced by the change of grading. Figure 2.16 shows the effect of particle breakage induced in first shearing stages on the critical state line, where the fitting lines are not obtained from a regression analysis but proposing three lines being consistent with

breakage are distinctly different from the original critical state line. As shown in Figure 2.16(a), the lines are not parallel but in reduction of gradient with increasing relative breakage B_r, indicating that the larger particle breakage has much more significant effect on the location of critical state line. Reconstituted samples with grading of soil equivalent to those at the end of the first shearing stages were isotropically compressed to different mean effective stress but then sheared just one time. It was clearly revealed in Figure 2.16(b) that the relative breakage B_r is too low to produce any significant movement of the critical state line of the reconstituted soil. However, it is also clear that the critical state line from reconstituted soil is not same as that from the second shearing stage of the original soil, which demonstrates that the effect of change of grading induced by particle crushing results in translation and rotation of the critical state line.

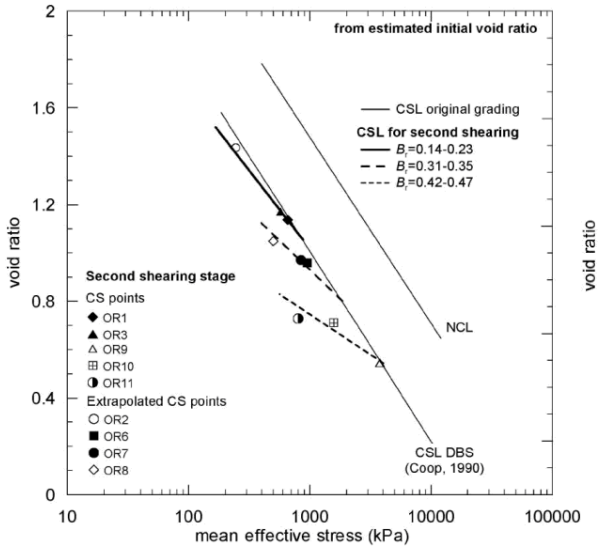

(a) Critical state line for second shearing stages

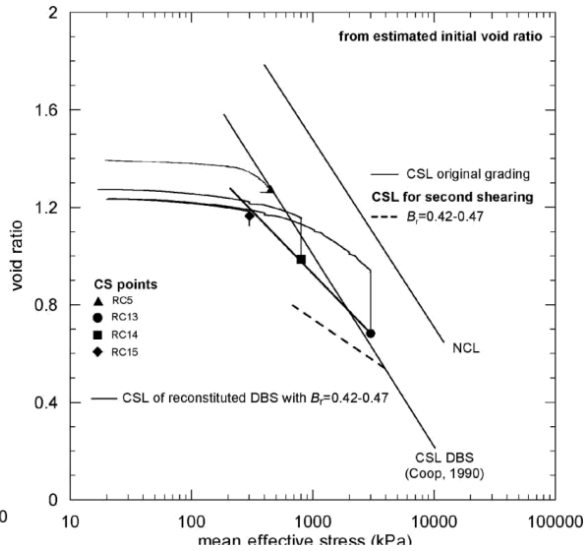

(b) Critical state line for reconstituted samples

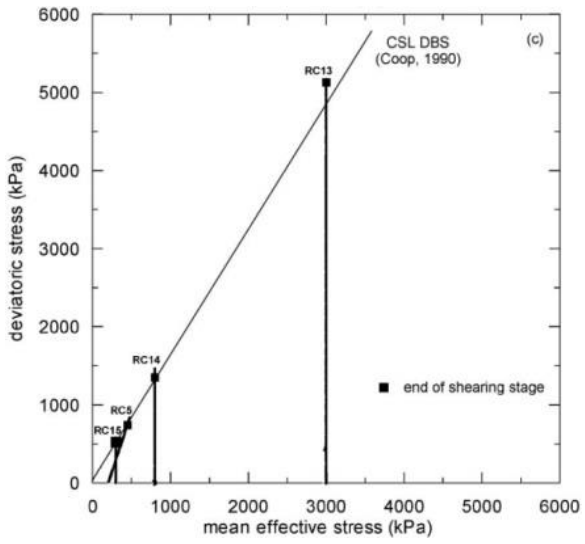

(c) Critical state points for reconstituted samples

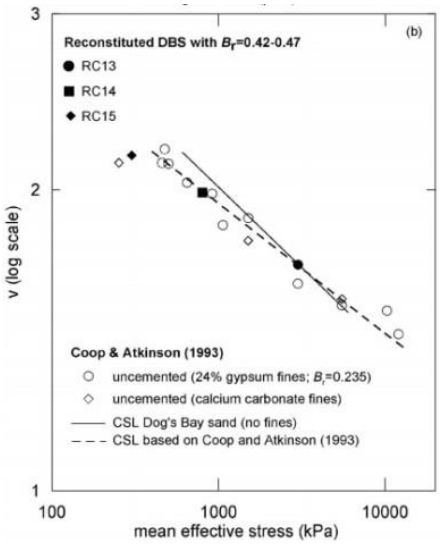

(d) Critical states for reconstituted samples

Figure 2.16 Effect of particle breakage on critical state line (Bandini and Coop, 2011)

Figure 2.16 (c) shows the critical state points for reconstituted samples, which indicates that under low pressures the critical state points are almost on the critical state line but under high pressure the critical state point under larger amount of particle breakage is over the critical state line, which may be caused by the combined effects of high pressure and particle breakage. Figure 2.16 (d) shows that the major effect of a flattening of the gradation curve caused by particle breakage of reconstituted samples is rotate the critical state line to a lower gradient.

2.5 MEASUREMENT OF PARTICLE BREAKAGE

Particle crushing results in change of original grain size distribution. The amount of particle breakage during loading of a soil can be defined by the grain size distribution curves measured before and after loading. But grain size distribution curve is a multi-parametric variable, which is inconvenient to be used in comparison with others. Consequently many particle breakage factors as a single parameter variable have been proposed with an aim to quantify the amount of particle breakage induced during loading. The most widely used particle breakage factors were developed by Marsal (1967), Lee & Farhoomand (1967) and Hardin (1985) as shown in Figure 2.17.

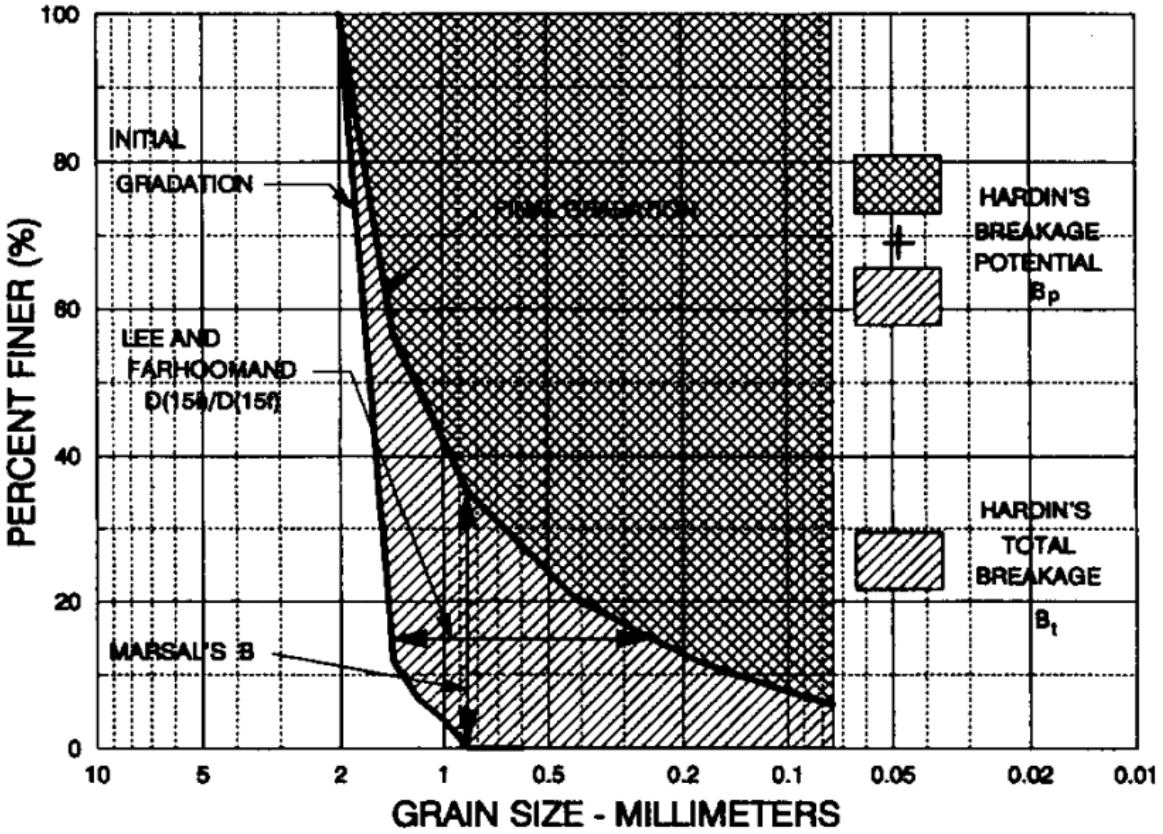

Figure 2.17 Definitions of particle breakage factors proposed by Marsal (1967), Lee and Farhoomand (1967) and Hardin (1985) (Lade et al., 1996)

Marsal (1967) performed large-scale triaxial compression tests in connection with the design and construction of earth and rockfill dam and found that significant amount of

particle breakage occurred. Consequently a breakage index B was developed to quantify the particle breakage, involving the change in individual particle sizes between the initial grain size distribution and final grain sized distribution. Marsal's breakage factor B is the sum of all same-signed differences in percentage retained at each sieve size with a limited range from 0% to 100%, which falls in the category of increase in percent passing.

The particle crushing measure can be also related to the particle size scale instead of the percent finer scale. Lee and Farhoomand (1967) developed a measure of particle crushing while investigating the particle crushing in the earth dam filter materials whether to effectively plug dam filters by conducting a series of isotropic and proportional loading tests on sands. Herein, a particle breakage factor representing the change in a single particle diameter that related to 15% finer on the grain size distribution curves before and after testing was proposed as a result of that this grain size was chosen on the base of gravel filter drainage requirement. This particle breakage factor was defined as a ratio $D_{15(initial)}/D_{15(final)}$ where the $D_{15(initial)}$ and $D_{15(final)}$ are the grain size diameters at where there is 15% finer in initial and final grain size distribution curves respectively with a range from unity to infinite.

Considering the facts that the increase of the normal contact forces in a soil element among larger-size particles and the higher probability of a defect in larger size particles, Hardin (1985) proposed a particle breakage factor, relative breakage: B_r, as a ratio of two parts: B_t/B_p as shown in Figure 2.17 where the breakage potential B_p, is defined as the area between the original grain size distribution curves and the 0.074mm sieve size in semi-logarithmic coordinate, which represents total possible particle breakage in change of gradation of soil without considering the particle crushing on the particles less than 0.074mm as a result of that the very small particle crushing occurs on the particles less than 0.074mm, and the total breakage B_t, is defined as the area between the original grain size distribution curve and the grain size distribution curve after loading.

Miura and Yamanouchi (1977) suggested that the increase in surface area ΔS (in cm^2/cm^3) is a reasonable measure for describing the amount of particle-crushing quantitatively. ΔS is the increase in surface of sample after and before test. The surface area S is given by $S_w * \gamma_d$, where γ_d (g/cm^3) is the current value of dry density of specimen being tested, and S_w is the specific surface area (cm^2/g). The value of a specific surface area of the sample finer than 74μm is measured by the Blaine method, which is widely used for measuring the specific surface area of a cement powder. Miura and Ohara (1979) suggested the increase in surface area, ΔS is used in measurement of the amount of particle crushing, and it was also found that the amount of particle crushing ΔS induced by the shear stresses has a close relation to the plastic work done W.

Based on the Weibull statistics of fracture (Weibull, 1951), McDowell et al. (1996) introduced the concept of probability into the study of grain crushing by developing a

fractal theory of crushing, with the premise that grains split probabilistically with the likelihood increasing with an increase in applied stress and number of flaws but reducing with an increase in the number of particle contacts or a reduction in particle size.

Most of particle breakage factor are employed to quantify particle crushing by the change of grain size distribution before and after loading without considering any correlation with the mechanical properties of soil as a result of the variation of soil physical properties induced by particle crushing. However the permeability characteristics of soil are closely related to the grain size distribution. Consequently taking into account the soil permeability related to grain size (Taylor, 1948; Duncan et al., 1972), based on the grain size diameter D_{10} related to the characteristics of soil permeability, Lade et al. (1996) proposed a new particle breakage factor $B_{10} = 1 - D_{10f}/D_{10i}$ in which D_{10i} and D_{10f} represent the effective grain size of the initial gradation and the effective grain size of the final gradation respectively, with being a range from 0 to infinite.

An index that shows the quantity of particle crushing is indispensable to quantitatively grasp the effect of particle crushing on mechanical property (Miura et al., 2003). Miura and Yagi (1997) presented that the degree of particle crushing for volcanic coarse-grained soils can be estimated by increment of fines content ΔF_c (75μm or less) induced during consolidation and shear process. It was reported as well thereby that there is a unique relation between ΔF_c and the indices proposed by Marsal (1967), Lee and Farhoomand (1967) and Lade et al. (1996).

2.6 SUMMARY

Particle breakage changes the original gradation of soil, which has a very significant influence on soil behavior. The fundamental and comprehensive understandings about previous main studies on the significance of particle breakage in soil mechanics are introduced in this chapter which is categorized into four fields: particle breakage on individual grain, particle breakage on one-dimensional compression, particle breakage in triaxial test and measurement of particle breakage.

Most of the previous researches about particle breakage mainly focused on the characteristics of particle breakage and particle breakage mechanism in compression or shearing. The influence of particle breakage on soil behavior is not yet clarified well especially in the direct influence mechanism of particle breakage on soil behavior, which would be investigated in this research. In addition, as well known that the original grain size distribution curve and basic properties of sand have a significant influence on characteristics of particle breakage, consequently the findings from the comprehensive research on other designated various kinds of sand (herein Silica sand No.5 and Coral sand No.3) are still meaningful and constructive as a complement in getting fundamental understanding of particle breakage mechanism and its influence mechanism on soil behavior even though the some similar works have been done.

CHAPTER 3

APPARATUS, TEST PRECEDURES AND MATERIALS TESTED

3.1 INTRODUCTION

In 1930, Casagrande investigated compression test on cylindrical sample under stress boundary instead of direct shearing test for determining the strength parameters of soil. Thereafter many investigations and improvements have been done by many researchers on cylindrical sample so that the triaxial test being used comprehensively later in study of soil mechanics was developed. The whole procedure from deformation to failure of soil can be simulated in triaxial test. The stress-strain relation curve can be obtained under different drained conditions with measuring the volumetric strain or excess pore water pressure. So, the triaxial test becomes an indispensable manner in studying soil mechanics.

Hereafter, many triaxial apparatuses were invented for specific testing aim, such as dynamic triaxial apparatus for dynamic behavior of soil, high pressure triaxial apparatus for particle breakage, large-scale triaxial apparatus for gravel material, unsaturated soil triaxial apparatus, true triaxial apparatus for arbitrary stress path and so on. With improving precision of transducers and integrating of new technologies, the full automatization operation in triaxial apparatus is being developed as well.

3.2 BACKGROUND OF HIGH-PRESSURE TRIAXIAL APPARATUS

Historically, most researches in the field of soil mechanics have focused on soil behavior under low pressure, where most geotechnical engineering problems tend to arise. However, more and more practical geotechnical problems are falling into the category of high pressure considering that more and higher dams and buildings are being in construction nowadays.

The triaxial equipment with maximum confining pressure less than 1MPa can be regards

as the low-pressure triaxial apparatus (Verdugo and Ishihara, 1996). In isotropic consolidation curve or critical state line, a yield stress occurs after the stress level is greater than 1MPa, which can be as an onset of particle breakage affecting the soil behavior (Been et al. 1991). Consequently, herein the high pressure can be defined as the pressure no less than 1MPa. In addition, the stress range up to 3MPa used in this research covers most of cases in practice.

The soil behavior subjected to high pressure has attracted more attention in the field of geotechnical engineering. Understanding the soil behavior under high pressure is fundamental to assist in the solution to geotechnical engineering and geological problems being subjected to high pressure. The triaxial test as a very important manner to simulate the loading process in laboratory test to investigate the soil behavior under high pressure are popular to be conducted by high-pressure triaxial apparatus, especially for the study on particle breakage in my research. Herein the shearing procedure to crush soil particles can be simulated by the high-pressure triaxial apparatus.

This high-pressure triaxial apparatus still falls into the category of traditional triaxial apparatus with the $\sigma_2 = \sigma_3$ in triaxial compression or $\sigma_1 = \sigma_2$ in triaxial extension. In comparison with the true triaxial apparatus, it is impossible to reach a true generalized stress state: $\sigma_2 \neq \sigma_2 \neq \sigma_3$ and it cannot conduct continuous rotation of principal stresses but a sudden $90\,^\circ$ rotation. However it still has some advantages such as the simplicity of drainage control and measurement of PWP & axial strain & volumetric strain, the explicit application of principal stresses and convenience of testing procedure and preparation of specimen.

3.3 DESCRIPTION OF HIGH-PRESSURE TRIAXIAL APPARATUS

The general description of high-pressure triaxial testing system will be introduced in detail in succeeding sections. The general layout and schematic diagram of the high-pressure triaxial apparatus are shown in Figure 3.1 and Figure 3.2. The main features of the high-pressure triaxial apparatus are listed in Table 3.1.

The main components of high-pressure triaxial testing system used in this research are outlined as follows:

a. Loading system including axial loading by a computer-controlled motor and a high-pressure supply system with Electro-Pneumatic (E/P) transducer
b. Measuring system including the measurements of cell pressure & axial loading & PWP & axial strain & volumetric strain
c. Recording system with a microcomputer incorporating a data acquisition software to record the basic variables and calculated variables after being in using amplifier to amplify the outputs to get a better resolution in measurement of mechanical variables
d. Control and feedback system by a macro-computer with the A/D and D/A converters which are used to convert analog signal (digital signal) to digital signal

(analog signal) to be fed back to recording unit (control unit)

e. Reaction system including reaction frame and triaxial steel-cell which contains the water and specimen
f. Software system: a data acquisition software (Digitshow Basic) used to perform testing procedure setting, sampling frequency setting, initial dimension setting of specimen, A/D & D/A boards parameters setting, calibration factors setting, sampling frequency setting and the files to save the data.

Table 3.1 Main features of the high-pressure triaxial apparatus

No.	ITEM	VALUE
1	Max. axial loading	100kN
2	Max. cell pressure	3.5MPa
3	Max. black pressure	1.0MPa
4	Specimen dimension	D*H=100mm*200mm & 75mm*160mm
5	Membrane thickness	1mm

3.3.1 Loading System

The loading system is mainly comprised of axial loading by a computer-controlled motor, the confining pressure loading by a high-pressure compressor with Electro-Pneumatic transducer and a negative pressure generated by a CONVUM. The axial loading is applied by a motor whose speed can be controlled by computer to adjust the displacement rate. Loading piston connected with top cap of specimen is driven by the motor to produce the force on specimen by exerting the vertical displacement rate on specimen in compression. The load cell was installed on loading piston to measure the force. The pressure chamber sealed by a steel shell is separated by a membrane covering the specimen into two compartments: the compartment outside the membrane can be regarded as a confining pressure cell and the compartment inside the membrane between the top cap and pedestal is full of the soil material as a specimen as shown in Figure 3.2. The confining pressure is supplied by a terminal compressor with Electro-Pneumatic (E/P) transducer which obtains the relative pressure from an air pressure tank. The air pressure as the confining pressure was exerted into the steel cell filled with water, by which the uniform water pressure can be imposed on the specimen. For removing the air between the membrane and the mould to stretch the membrane during preparation of specimen or keeping the specimen standing stably on the pedestal after removing the split mould or For reaching a specific Skempton's B value during the saturation of specimen, a negative pressure is required. This negative pressure was applied by a CONVUM which generated a partial vacuum through a fast air flow.

(Motor information: Nippon Gear Co. LTD. Japan, Type:J3GLIK, Serial No.0610173148)

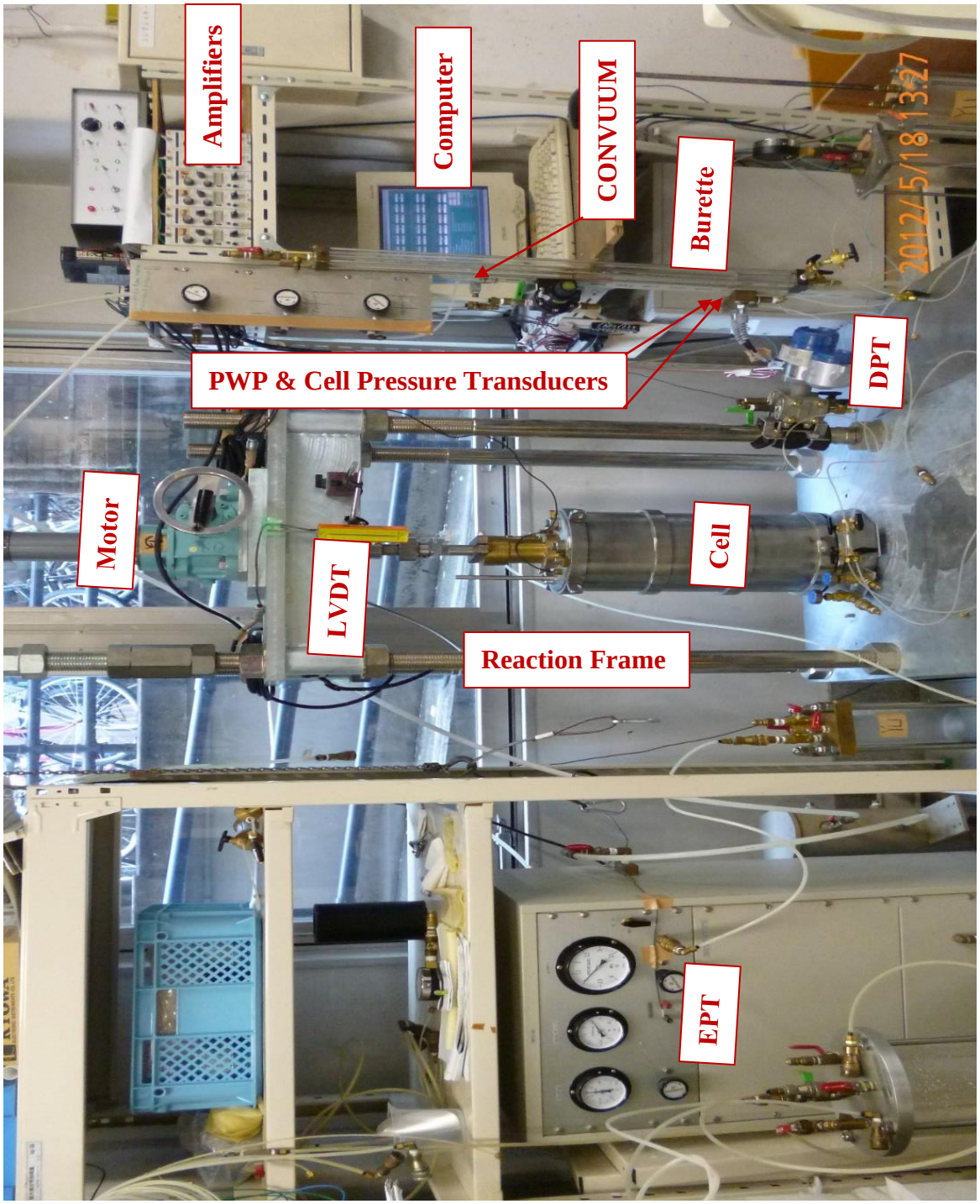

Figure 3.1 General layout of the high-pressure triaxial apparatus

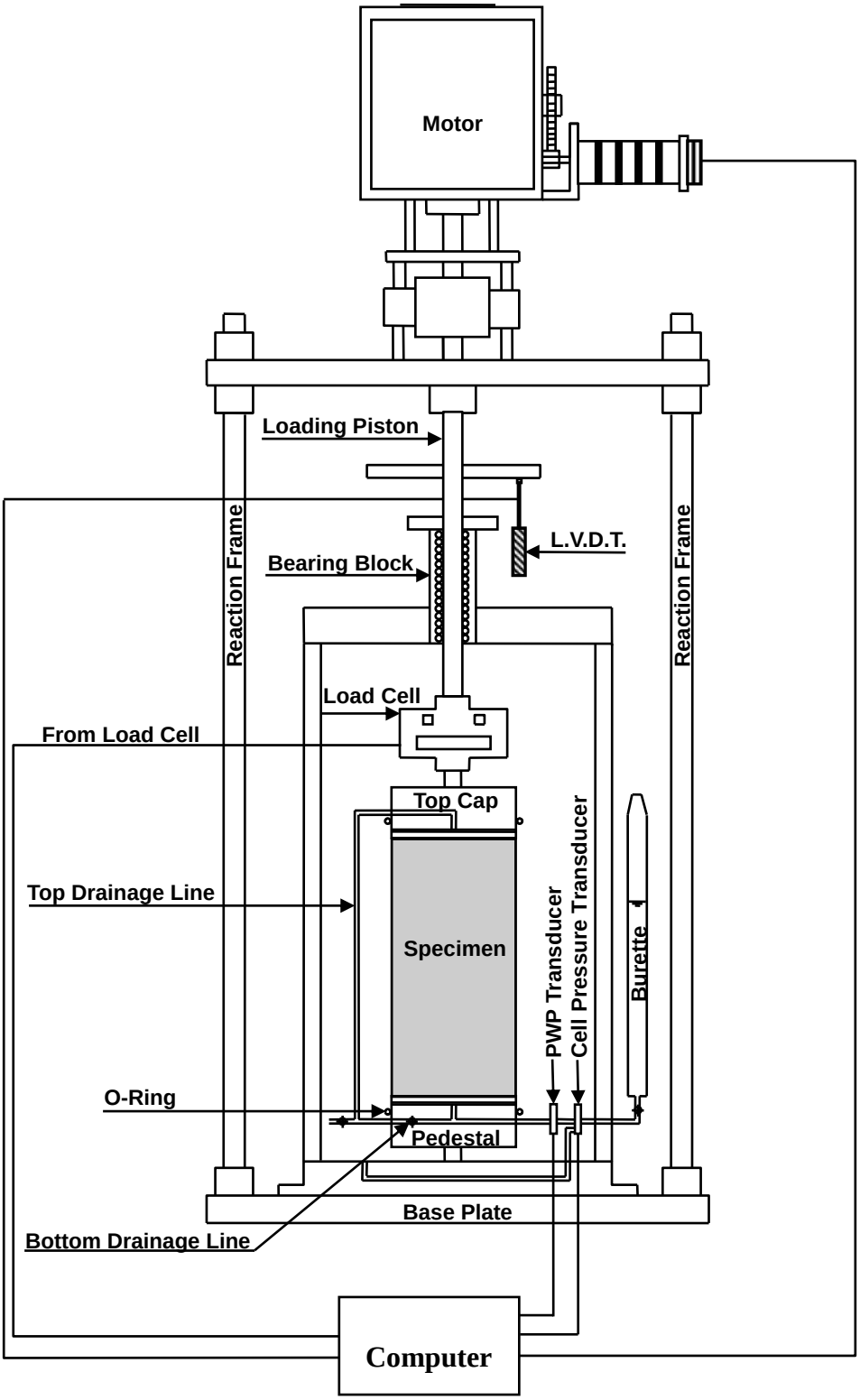

Figure 3.2 Schematic diagram of strain-controlled high-pressure triaxial apparatus

3.3.2 Measuring System

Most of the transducers used in measuring fall into the electronic-resistant strain gauge type of transducer with a Wheatstone bridge, which is used to convert a force into an electrical signal. The strain gauge measures the strain as an electrical signal by changing the effective electrical resistance of wheatstone bridge on the gauge. Generally the electrical signal output as a few millivolts is too weak to measure. The electrical signal output of the strain gauge can be recorded after amplifying the real weak electrical signal of the strain gauge by an amplifier. The electrical signal of the transducer can be scaled to calculate the relevant force applied to the transducer by the calibration factor.

3.3.2.1 Load cell

Load cell is classified to electronic-resistance strain gauge type of transducer. The load cell was screwed into the loading piston bar, which is connected with the motor and the top cap of a specimen, being placed inside the triaxial pressure chamber to measure the net force exerted on load cell by removing the effect of friction force between loading piston and the bearing block. For obtaining the calibration factor of load cell, a series of known dead forces were used to establish the relationship of applied force and the relevant micro-strain related to relative response voltage proportionally. The calibration characteristics of load cell are shown in Figure 3.3.

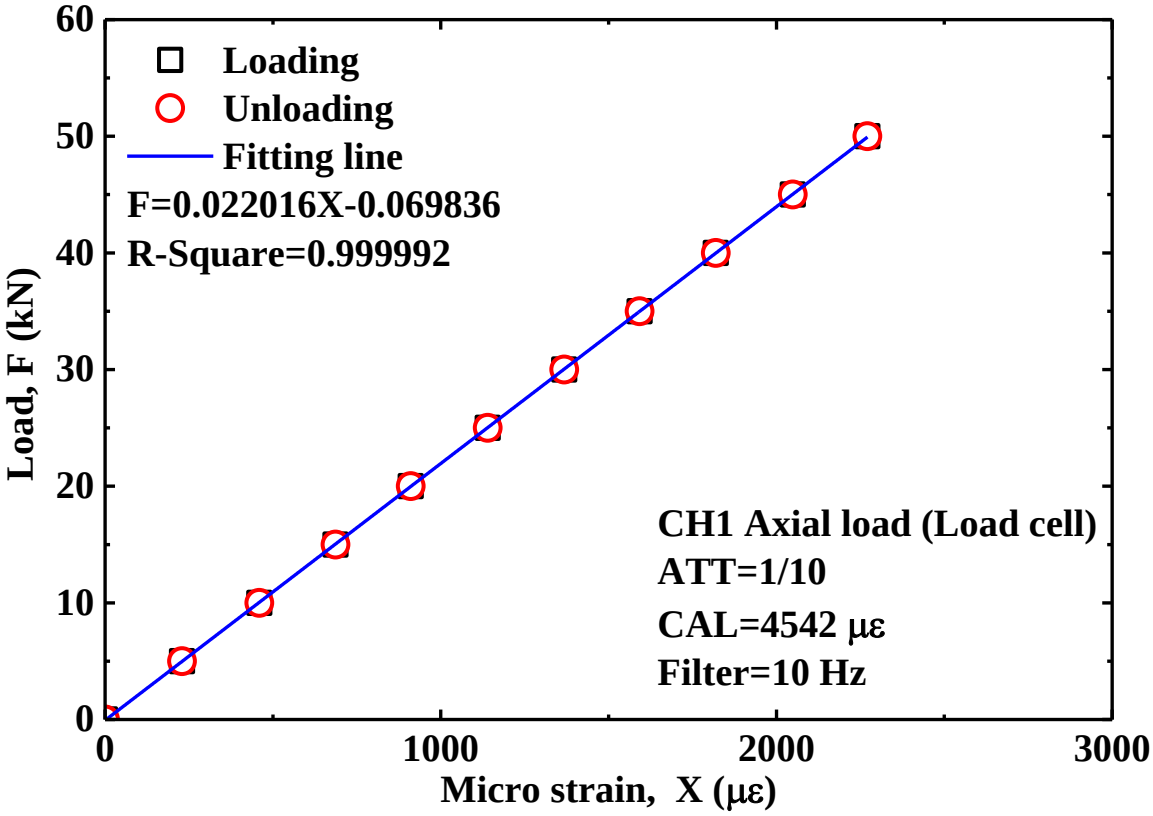

Figure 3.3 Calibration characteristics of load cell

3.3.2.2 Pressure transducers

In order to measure confining pressure and the pore water pressure, the two transducers connected with the triaxial cell and the specimen separately were installed outside the triaxial pressure chamber. By establishing the relationship between the applied pressure and relevant micro-strain to obtain the calibration factor, the transducers can be used to convert the relevant voltage to physical value. The calibration characteristics of these two transducers are shown in Figure 3.4 and Figure 3.5.

3.3.2.3 Strain transducers

The vertical deformation of the specimen was measured by a LVDT with a range of 100mm, which was fixed vertically on the reaction frame to move together with the vertical displacement of specimen. Liner Variable Differential Transformer (abbreviated as LVDT subsequently) is a type of electrical transformer used for measuring linear displacement. The LVDT converts a linear displacement from a mechanical reference into a proportional electrical signal, by which it is possible to measure a linear displacement. The calibration factor of LVDT was obtained in establishment of the relationship between the known displacement and the relevant micro strain related to voltage in using block gauge setup as shown in Figure 3.6.

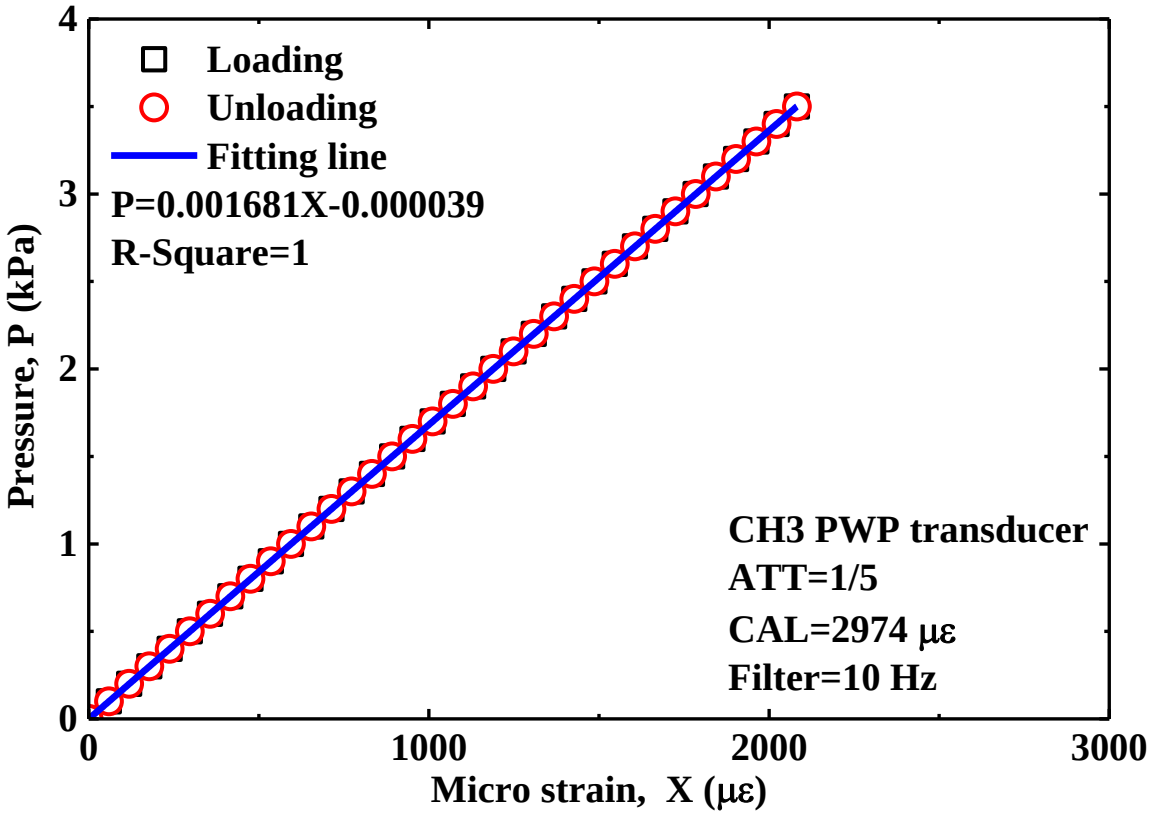

Figure 3.4 Calibration characteristics of PWP transducer

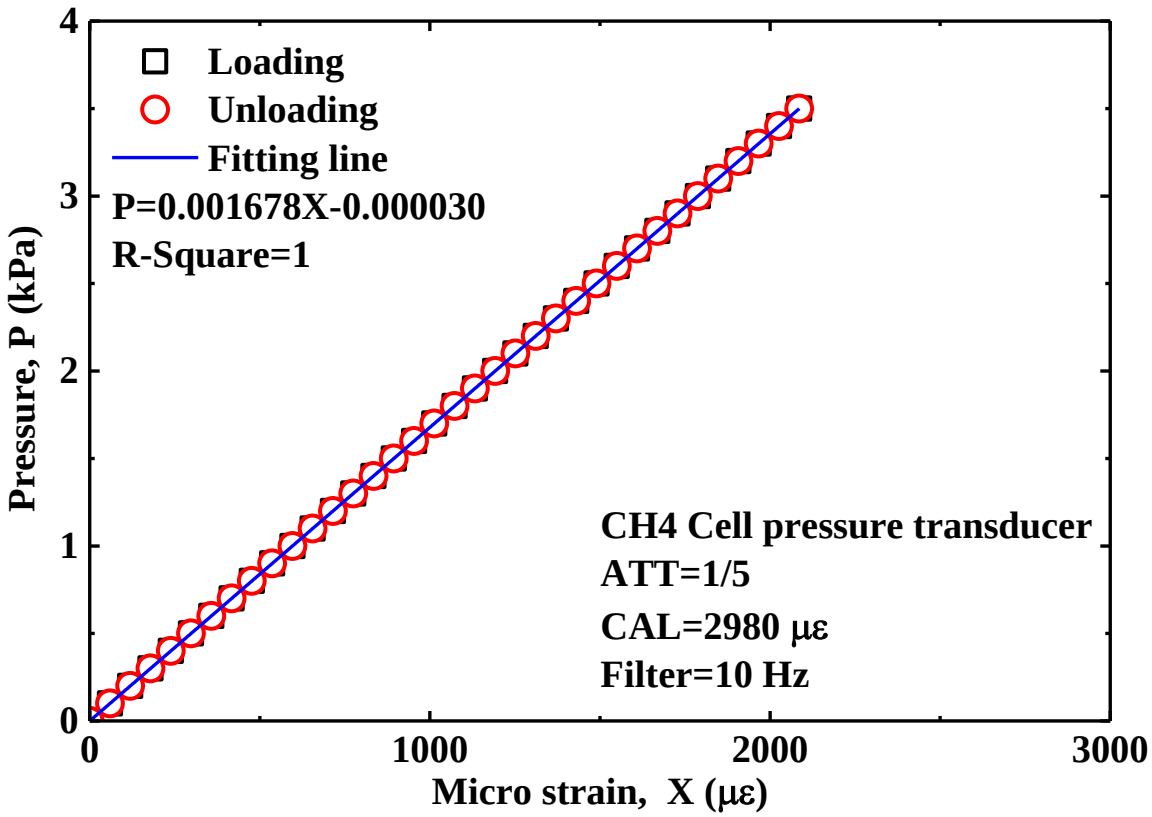

Figure 3.5 Calibration characteristics of cell pressure transducer

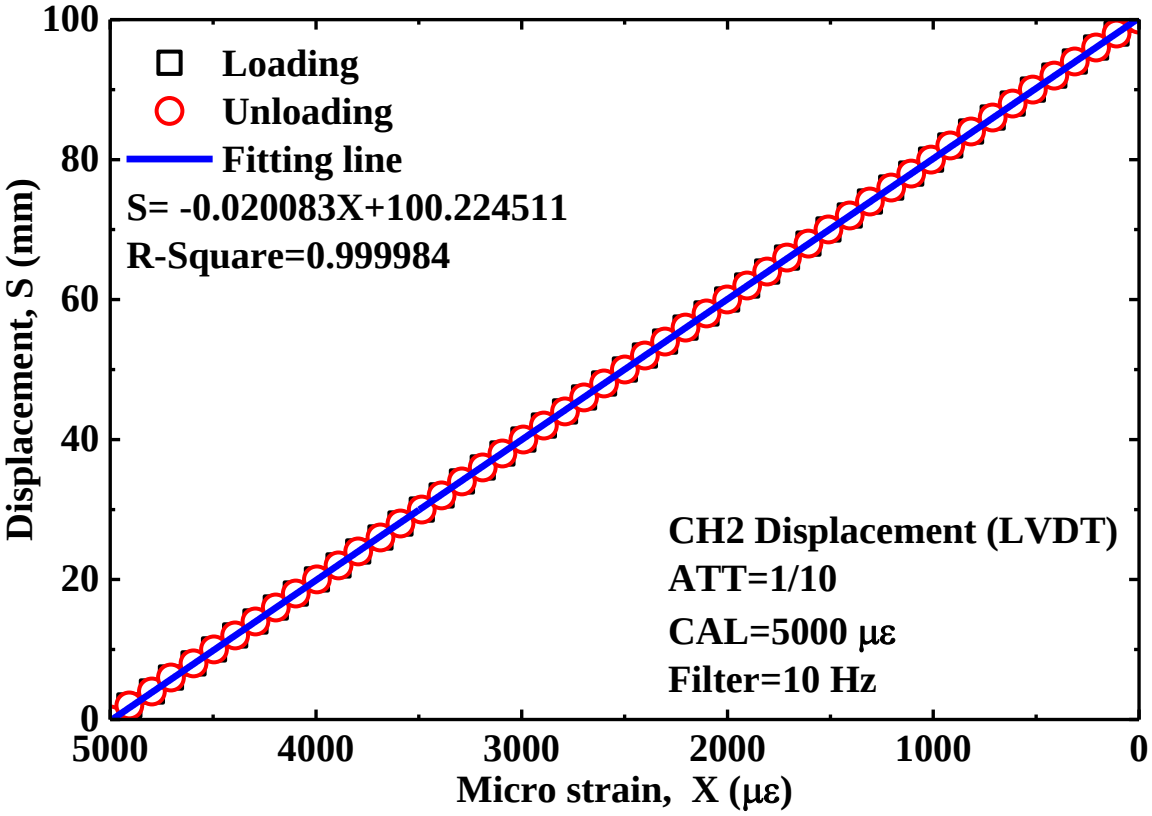

Figure 3.6 Calibration characteristics of LVDT

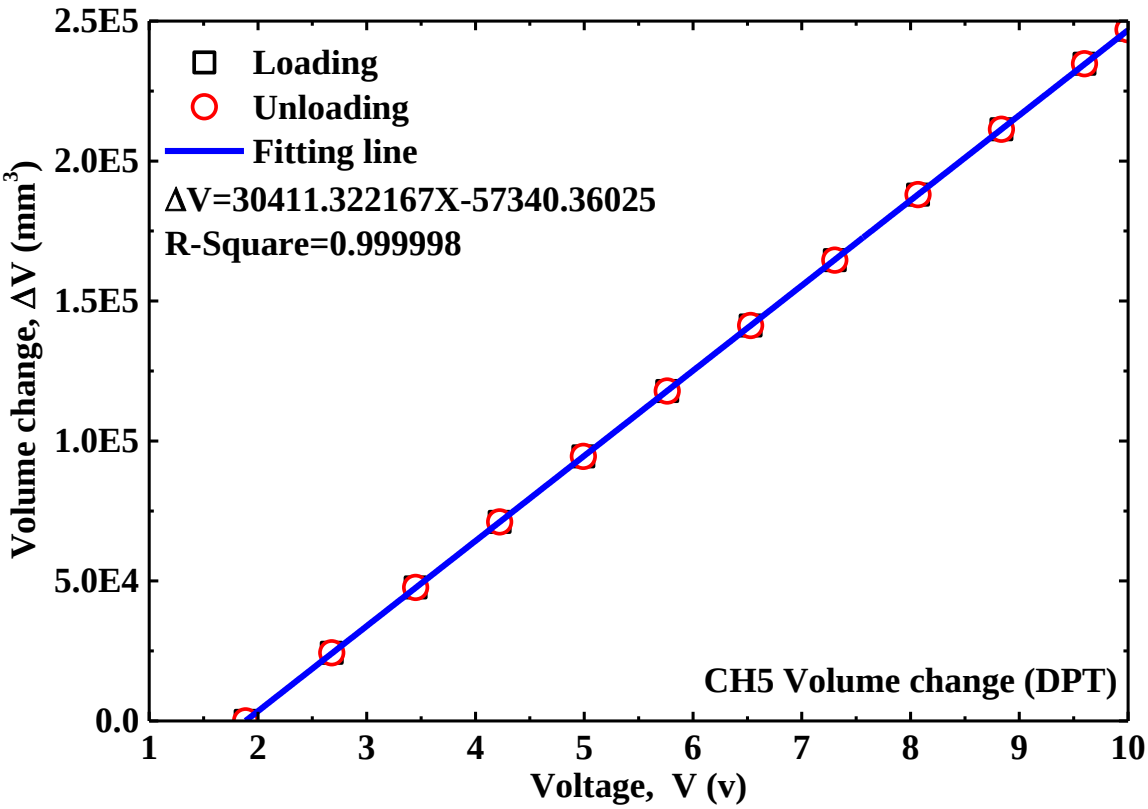

Figure 3.7 Calibration characteristics of DPT

The measurement of deformation in volume of specimen was done as well. In saturated soil, the total volume change of soil specimen can be assumed to be equal to the volume change of drained water from the soil specimen (water is regarded as an incompressible material), which was measured by a Differential Pressure Transducer (abbreviated as DPT) as a kind of volume change gauge. DPT consists of two transducers on both sides of a gauge in measuring the difference between two transducers, which is useful and effective to measure the volume change of soil specimen precisely even under using negative pressure inside the soil specimen to meet the expectant Skempton's B value in saturation. Figure 3.7 shows the calibration characteristics of DPT. The summary of information of transducers in measuring system is shown in Table 3.2.

Table 3.2 Summary of information of transducers in measuring systems

No.	Transducer Type	Serial No.	Max. Capacity	Calibration Factor	Micro-Strain
0	Load Cell	—	100 kN	22.017 N/με	4542 με
1	LVDT	SDP-1000R No.031811	100 mm	0.0200 mm/με	5000 με
2	PWP	FD2950014	5MPa	1.681 kPa/με	2974 με
3	Cell Pressure	FD2950015	5MPa	1.678 kPa/με	2980 με
4	DPT	A1B3273T	10kPa	—	—
5	E/P		3.5MPa		

3.3.3 Recording System

The analog signals of electronic transducers are detected and amplified by a set of strain amplifiers, then converted by an A/D converter board to digital signals, which can be recorded by the computer with a data acquisition software (DigitShow Basic) in specific sampling frequency. The function of A/D converter board is to convert the analog signal to digital signal, which can be quantified to be relevant physical values by using the calibration factors. Herein one A/D differential converter board with 16 bit and maximum 8 channels embedded into CPU by PCI slot was used in this research. The channel arrangement adopted in this research is shown as below:

a. CH1 Axial load (Load cell)
b. CH2 Displacement (LVDT)
c. CH3 Pore water pressure (Pressure transducer)
d. CH4 Cell pressure (Pressure transducer)
e. CH5 Volume change (DPT)

The schematic diagram of recording system of triaxial apparatus is shown in Figure 3.8.

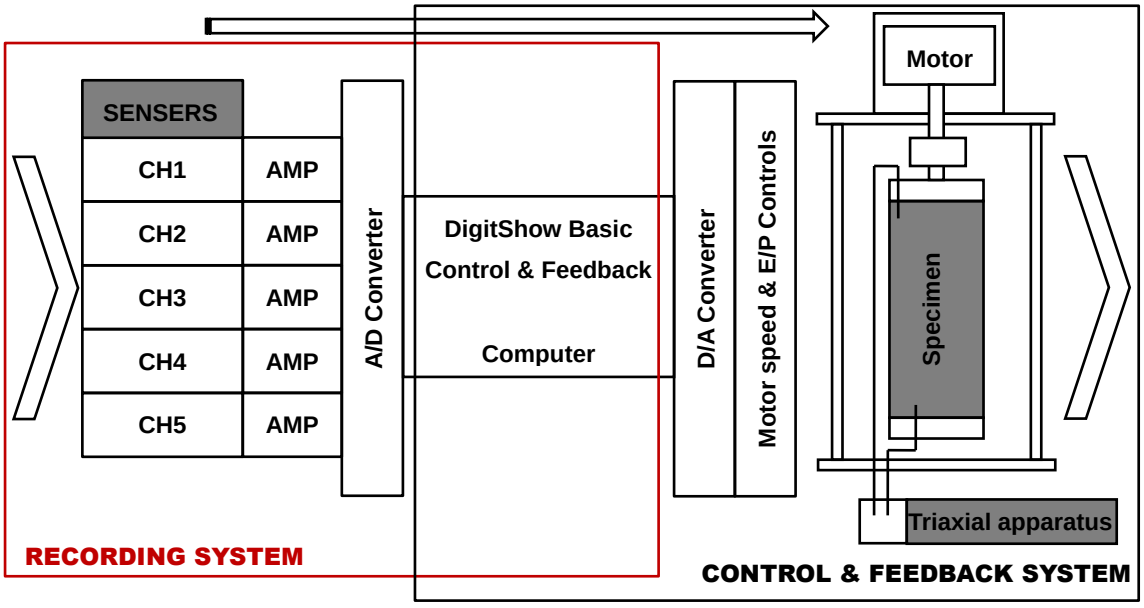

Figure 3.8 Schematic diagram of recording and control & feedback systems

3.3.4 Control and Feedback System

The computer with the data acquisition software would be initialized by settings of initial dimension of specimen, A/D & D/A boards configurations, testing procedures setting, sampling frequency setting and the files to save the data, which govern the whole triaxial testing process automatically. According to the pre-set testing procedures, the recorded digital signals in measuring system are recorded and judged to determine whether or how to convert the digital signal to analog signal by D/A converter in controlling triaxial

apparatus, which can be regarded as the control and feedback system as a continuous cycle of cause-and-effect with successive controls as shown in Figure 3.8. In strain-controlled high-pressure triaxial apparatus, the motor (Switch, Clutch and Speed) and air volume booster with E/P transducer are herein controlled in the feedback system with using a D/A converter board of 12 bit and maximum 8 channels. The channel settings of D/A converter board is shown as below:

a. CH1 Motor switch (On/Off)
b. CH2 Motor clutch (Loading/Unloading)
c. CH3 Motor speed (Loading speed/Unloading speed)
d. CH4 EP transducer (Cell pressure)

Electro-Pneumatic Transducer (abbreviated as EP Transducer) herein is designed to convert an electrical input signal into a pressure output with a linear relationship in using a force balance with moving coil system. Electro-Pneumatic transducer with an air compressor connected with the terminal air pressure source tank was used in triaxial apparatus to provide high confining pressure exerted on specimen in this research. The calibration characteristics of Electro-Pneumatic transducer are shown in Figure 3.9.

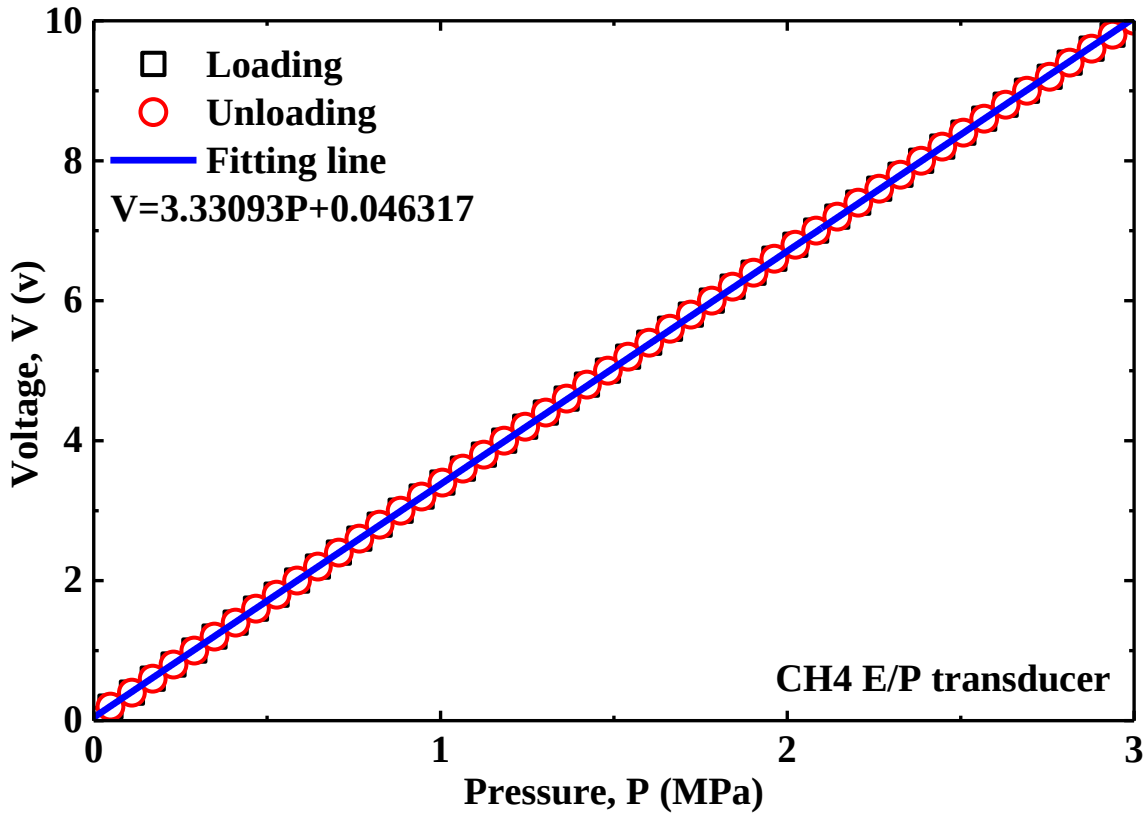

Figure 3.9 Calibration characteristics of Electro-Pneumatic transducer

3.3.5 Reaction System

Reaction system consists of hard wares in triaxial apparatus, mainly including the

reaction frame and the steel shell sealing the high-pressure chamber as shown in Figure 3.2. The reaction frame provides necessary reacted force against axial loading exerted by the motor on specimen. The steel shell of the high-pressure chamber is indispensable to resist high confining pressure up to 3MPa.

3.4 DERIVATION OF STRESS AND STRAIN IN TRIAXIAL APPARATUS

Triaxial apparatus as a common and versatile apparatus is employed for soil element testing, being able to exert some certain stress path on soil specimen and reproduce the stress process undergone in the field. The derivation of stress and strain in triaxial apparatus is of fundamental significance in understanding data to be processed and discussed in the way of geotechnical engineering.

The loading state on specimen and the stress element are shown in Figure 3.10, where the specimen is subjected to an axial load P_v and a confining pressure P_r and the stress state with σ_v in vertical direction and σ_r in transverse direction are exerted on the soil element. The stress state in terms of principal stresses directions are various and generally categorized by triaxial compression and triaxial extension as shown in Figure 3.10(b).

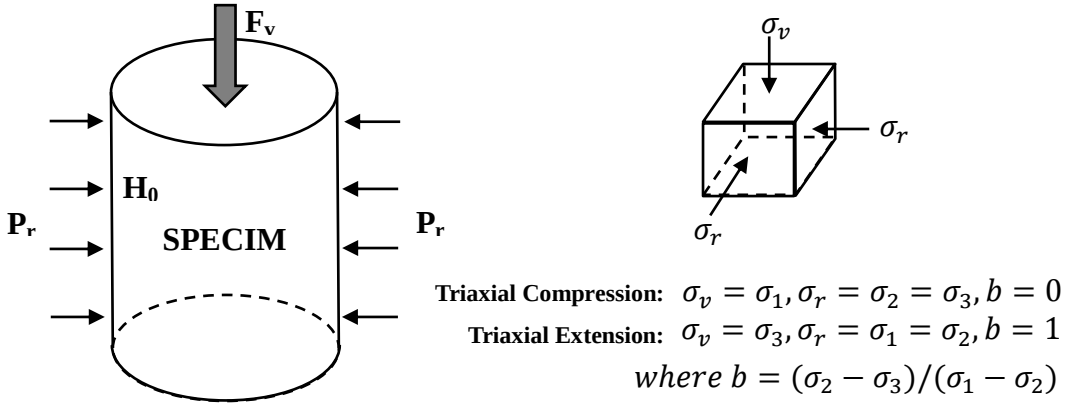

(a) loading state on specimen (b) stress state on soil element

Figure 3.10 Schema of loading state on specimen and stress state on soil element

The derivation of stress components in triaxial apparatus are given as below.
The vertical stress can be calculated by

$$\sigma_v = \frac{F_v}{A} + P_r \tag{3.1}$$

The confining pressure is equal to the cell pressure as below:

$$\sigma_r = P_r \tag{3.2}$$

According to the effective stress principle, the radical effective stress can be derived by

$$\sigma_r' = \sigma_r - u \tag{3.3}$$

$$\sigma_v' = \sigma_v - u \tag{3.4}$$

The deviator stress and mean effective stress would be calculated by

$$q = \sigma_v - \sigma_r = \sigma_v' - \sigma_r' \tag{3.5}$$

$$q = \frac{\sigma_v' + 2\sigma_r'}{3} \tag{3.6}$$

The axial strain and volumetric strain can be derived by

$$\varepsilon_v = -\frac{\Delta H}{H_0} \tag{3.7}$$

$$\varepsilon_{vol} = -\frac{\Delta V}{V_0} \tag{3.8}$$

3.5 TRIAXIAL TEST PROCEDURE

The main purposes of this research are to investigate the characteristics of particle crushing and the influence of particle breakage on soil behavior. A series of triaxial test were conducted on silica sand No.5 and coral sand No.3. The triaxial test procedures are introduced step-by-step herein in detail, including the introduction of tested materials, specimen preparation and triaxial test steps.

3.5.1 Tested Materials

Sand is a natural granular material composed of residual weathered rock and mineral particles, being variable in composition but mostly being kinds of silica in inland and calcium carbonate created in coastal and marine area. Silica sand as a kind of very common sand is popular to be used in engineering and researches in the field of geotechnical engineering. Nowadays more and more man-made engineering activities are being extended to the coastal and marine area involving substantial amount of coral sand originating in tropical and sub-tropical marine environments from bio-erosion of limestone skeletal material of marine organisms with the characteristics of particle shape irregularity, particle fragility and porosity inside particle. The silica sand No.5 and coral sand No.3 were employed herein to investigate their characteristics of particle crushing under high pressure and their influences on soil behavior. Table 3.3 shows the physical

properties of silica sand No.5 and coral sand No.3. Relevant grain size distribution curves of silica sand No.5 and coral sand No.3 are shown in Figure 3.11.

Table 3.3 Physical properties of silica sand No.5 and coral sand No.3

Property	**Silica sand No.5**	**Coral sand No.3**
Specific gravity, G_s	2.761	2.803
Minimum void ratio, e_{min}	0.766	0.904
Maximum void ratio, e_{max}	1.215	1.176
Fine content, F_c	0.02%	0.02%
D_{50}	0.564 mm	1.306 mm
Coefficient of uniformity, C_u	1.647	1.561
Coefficient of curvature, C_c	0.378	0.837

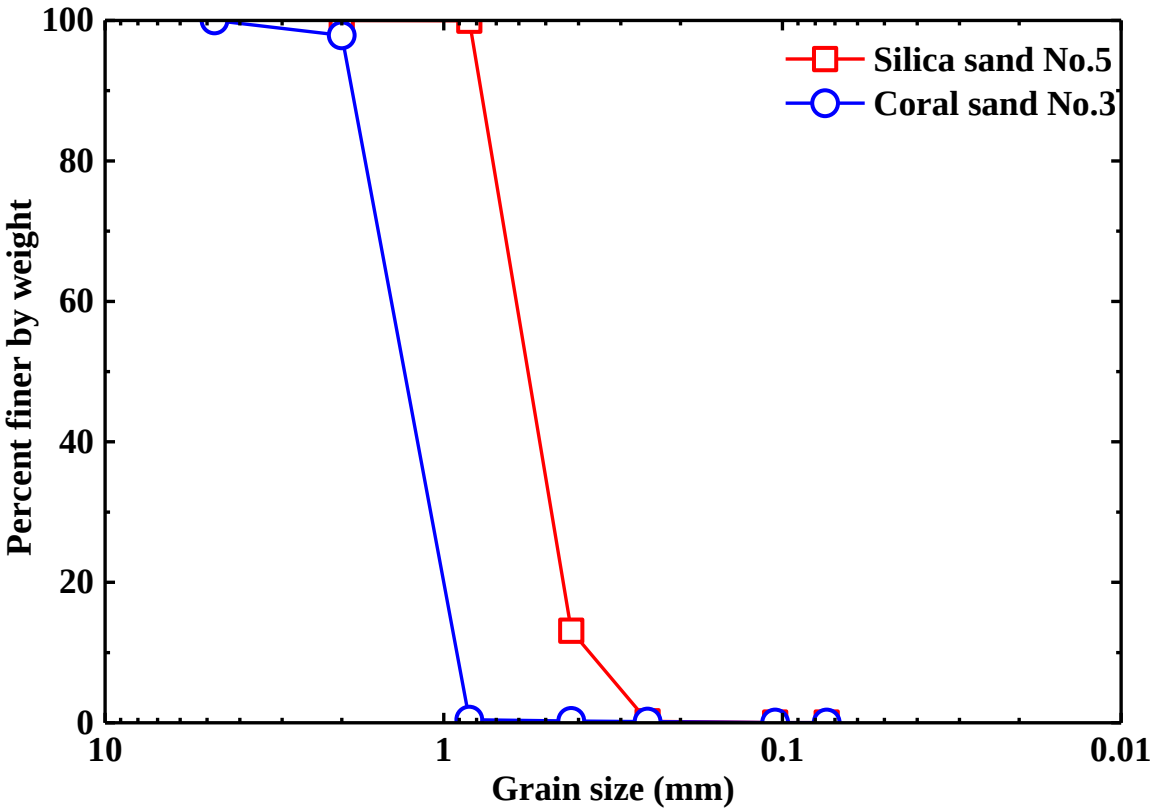

Figure 3.11 Grain size distribution curves of silica sand No.5 and coral sand No.3

3.5.2 Specimen Preparation Method

For trying to eliminate non-uniformity of tested materials, sand from several bags was thoroughly mixed together and then oven-dried. In this study all specimens were prepared by air pluviation into a mould with a membrane in ten lays for the specimens in dimension of diameter 100mm and height 200mm and in eight layers for the specimens in dimension of diameter 75mm and height 160mm with necessarily tamping to meet expected relative density or void ratio of specimen in creating the relatively uniform samples for triaxial testing. Figure 3.12 shows the procedures of preparation of specimen.

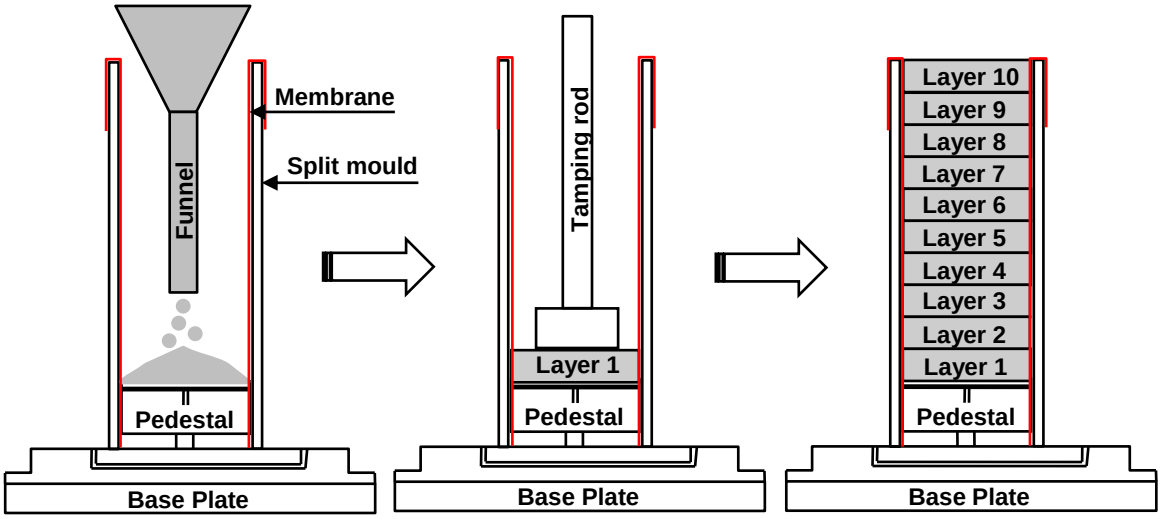

Figure 3.12 Illustration of specimen preparation method

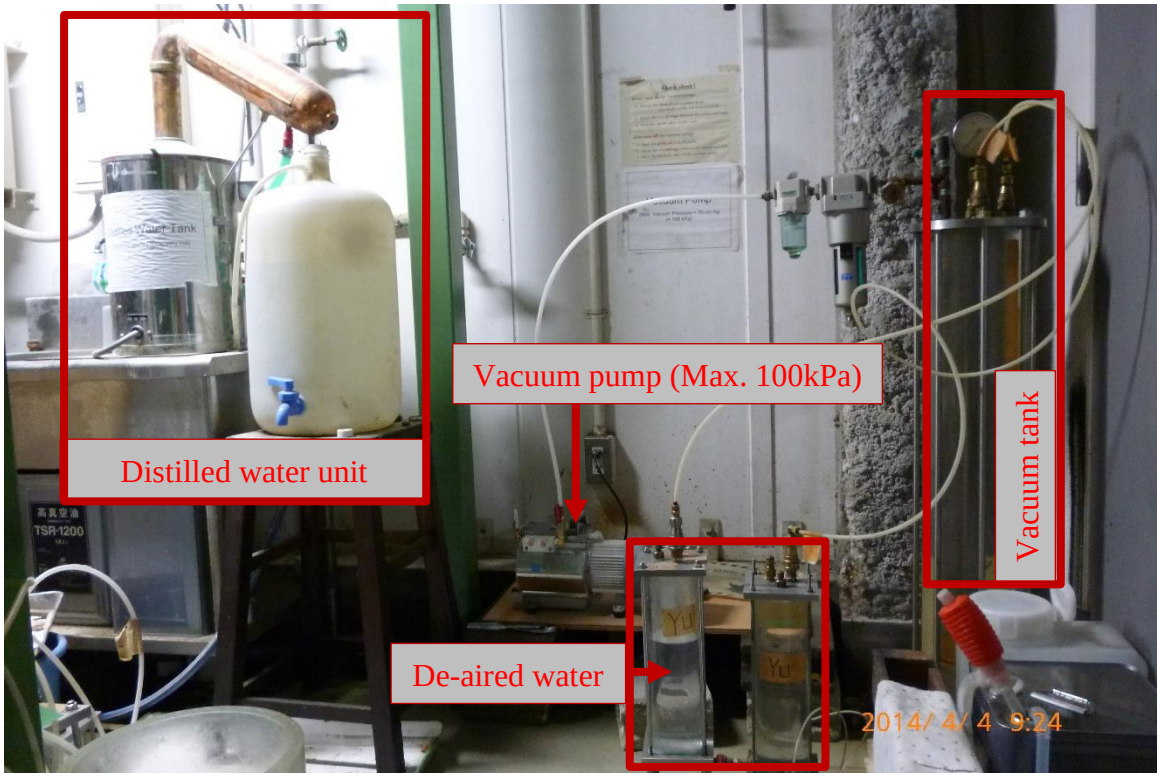

Figure 3.13 Vacuum system for de-aired water

3.5.3 Triaxial Test Steps

3.5.3.1 Before specimen preparation

a. De-aired water preparation: the distilled water tanks (Four tanks are used in this research, two of them can be standby) were kept for being de-aired in vacuum pump over 12 hours considering so many connections of distilled water tanks to vacuum pump. The de-airing apparatus is shown in Figure 3.13.

b. Tested material preparation: the tested materials were kept to dry in oven over 24 hours. It should be air-cooled before preparing the specimen.
c. Apparatus check: To check state of the machine to ensure that it can be working well mainly including the pressure source check, motor running check and strain amplifiers check.
d. Configuration of the data acquisition software: set the calibration factors of all transducers, testing procedures, sampling frequency and so on.

3.5.3.2 Specimen preparation

As illustrated in Figure 3.12, the specimens tested in this study were prepared by air-pluviation tamping method, which is introduced step-by-step in detail as below.

a. Clean the top cap and pedestal of triaxial apparatus and ensure the connection pipe unobstructed to top cap and pedestal.
b. Apply grease to rigid ends of the top cap and pedestal in laying two layers of membranes with grease between two layers of membranes for each end to lubricate the ends of them just for the specimens in dimension of diameter 100mm and height 200mm. For the specimens in dimension of diameter 75mm and height 160mm, it didn't use the two layers membranes on top cap and pedestal.
c. Fasten a membrane on pedestal by a rubber band.
d. Place the split mould on base plate to cover the pedestal and membrane and ensure the gap among split moulds not to clip membrane and then fasten the split mould tightly by a fastener so that the membrane gets stuck on the mould during application of vacuum pressure.
e. Stretch up the membrane over the mould top and tie it by a rubber band. Herein the length of membrane stretched up should be recorded to set same length for all tests to eliminate the effect of difference of membrane setting.
f. Apply vacuum (-20kPa) through two openings of mould by CONVUM to the room between the membrane and mould for a firm fitting of the membrane against the mould.
g. A funnel was used to collect the materials and pour the materials into the mould by a small nozzle of the funnel in ten equal layers for the specimens in dimension of diameter 100mm and height 200mm or eight equal layers for the specimens in dimension of diameter 75mm and height 160mm.
h. Pour pre-calculated weight of uniformly mixed oven-dried sand in a layer-wise pattern tamping by a rod to a fixed height for meeting relevant density of the material. Herein the top surface of each layer tamped by rod should be scratched by a small brush to avoid the discontinuity between the successive layers.
i. On filling up the mould with material, level the top surface of the specimen by a smoother.
j. As all layers of specimen are in place, screw on the all four steel pillars supporting the top part of pressure chamber to base plate and fasten the top part of pressure chamber on four pillars tightly with screws. Then put on the top cap gently on the top of specimen and fix the load cell frame rod to hold the top cap

and fasten the membrane to top cap.

k. Connect the cap-to-base line.
l. Apply vacuum (-20kPa) inside specimen to maintain specimen standing alone without the restraint of mould and then remove the spit mould. During this stage, the leakage condition of membrane can be checked by the state of current pore pressure.
m. Measure the diameter of specimen at top, middle and bottom of specimen by Pi tape and the height of specimen in four direction vertically by vernier caliper or steel rule, and then the mean dimension of specimen in diameter and height would be calculated.
n. The steel shell of pressure chamber was lifted up by a crane and put down along the frame of the pressure chamber to seal the chamber and fixed as well by three screws. Then the water was injected from bottom to top to fill the whole chamber.
o. Move the whole triaxial pressure chamber back to right place with load cell frame rod in alignment with loading piston rod connected with motor. Rotate down the loading piston rod just to the top of the load cell frame rod and fix them by screw cap.
p. Fix LVDT in measuring vertical displacement of specimen. And connect the load cell cable to relevant strain amplifier.
q. Connect the line to top of triaxial pressure chamber for vaccumizing or pressurizing later.

3.5.3.3 Vacuumizing

The volume change of specimen can be measured by the volume of drained water into the burette with a DPT in full saturation of specimen. Consequently the most of tests are expected to be conducted on saturated specimen. For obtaining the full saturated material to measure the volume change and pore water pressure, the methods to dissolve the entrapped air into the water are adopted in geotechnical laboratory test by the flushing of CO_2-deaired water through specimen or the double vacuum method to saturate the specimen. Herein the double vacuum method in vacuumizing-flushing-back pressurizing process was used in this research to saturate the specimen as shown in Figure 3.14. The vacuumizing procedures are herein described in detail as below.

a. A CONVUM was connected previously to the bottom of specimen with pressurizing -20kPa.
b. Connect other CONVUM to the top of pressure chamber.
c. Raising back pressures of both CONVUMs connected to specimen and pressure chamber separately gradually simultaneously by increment of -10kPa until that the back pressure connected to specimen reaches -100kPa and the back pressure connected to pressure chamber reaches -80kPa as shown in Figure 3.14 for maintaining the original difference of effective stress of 20kPa.

3.5.3.4 De-aired water flushing

Flushing was done through the specimen by two tanks of de-aired water as shown in Figure 3.14, where the elevated de-aired water tank placed on the top of reaction frame of triaxial apparatus was connected to the bottom of specimen but the other tank connected to the top of specimen was used to collect the flushed water, being placed on the base plate of triaxial apparatus. Both tanks were maintained under vacuum -100kPa as mentioned above. The elevation around 1.5m between two tanks was used to flush the de-aired water from the bottom to top of specimen by gravity. The flushing was completed up to two times of void volume of material flushed out.

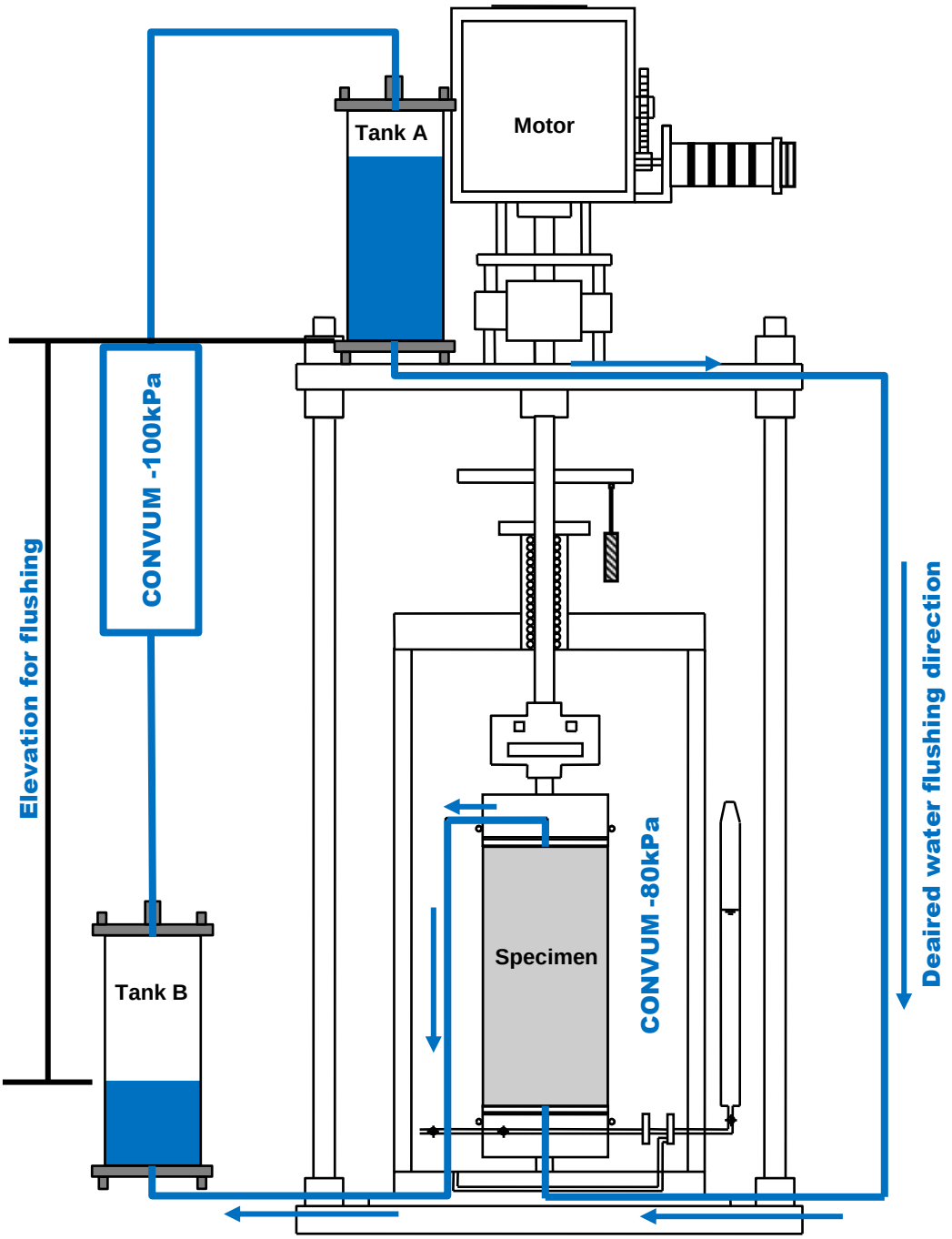

Figure 3.14 Illustration of saturation process of specimen

3.5.3.5 Back pressurization and B-value check

The saturation condition of specimen was determined by B-value check (Skempton, 1954) as shown in equation 3.9.

$$B = \frac{u_{i+1} - u_i}{P_{i+1} - P_i} = \frac{\Delta u_{i+1}}{\Delta P_{i+1}} \tag{3.9}$$

Back pressurization and B-value check were conducted subsequently after saturation of specimen as stated below.

a. Decrease gradually the vacuum of pressure chamber from -80kPa to 20kPa and the back pressure from -100kPa to 0kPa simultaneously by increment of -10kPa.
b. To check B-value with closed the valve connected to burette, the cell pressure was raised by 50kPa with recording the corresponding increment of pore water pressure. Then the B-value can be calculated according to the equation 3.9.
c. If the B-value is less than the expected value (B>0.98), the back pressure should increase up to 50kPa with closed drainage valve to burette. Then the back pressure was dissipated into the specimen by opening the drainage valve connected to specimen. The cell pressure increases up to 100kPa subsequently under closed valve to burette with recording the increment of pore water pressure for calculating the B-value. Repeat those procedures until and unless the B-value is more than 0.98 as shown in Figure 3.15.

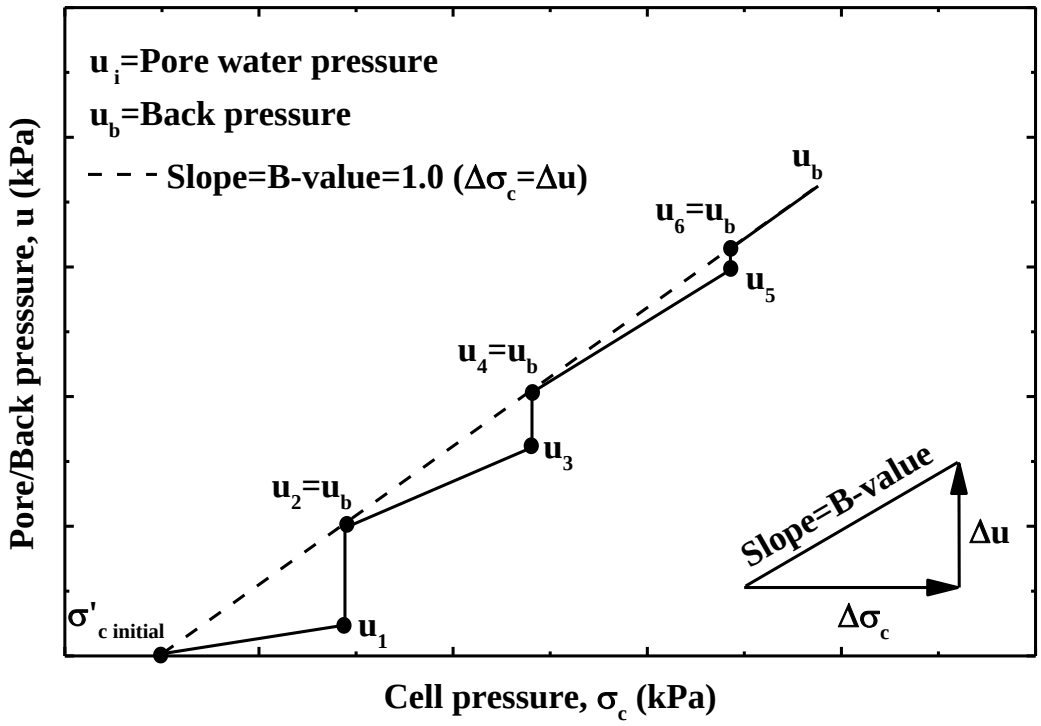

Figure 3.15 Illustration of B-value check

3.5.3.6 Consolidation

Triaxial tests procedures generally are composed of consolidation and load application. Herein the detailed introduction of consolidation is given as below.

a. The pre-consolidation should be performed automatically by *Pre-Consolidation* setting in computer before consolidation for removing the initial deviator stress on specimen back to isotropic stress state (20kPa) with opened valve connected to burette, where the volume change was stabilized and recorded by computer.
b. The current dimension of specimen was updated by the function of *Before-Consolidation* in *Digitshow Basic* (a data acquisition and control software) in using the recorded volume change produced during pre-consolidation and initial dimension of specimen.
c. The consolidation can be conducted according to the relevant settings of consolidation in Digitshow Basic including the target axial stress, back pressure, K_0, rate of cell pressure and motor speed. The testing data was recorded and saved in specific files automatically in set sampling frequency.
d. The consolidation is completed as the volume change is stabilized. The volume change induced during consolidation was used to update the dimension of specimen to be present dimension by the functions for *After-Consolidation* and *Present* on the *Digitshow Basic*.
e. The B-value can be also reverified again in this stage.

3.5.3.7 Load application

After consolidation of specimen, the loading application should be performed on specimen to investigate the soil behavior of soil, being explained as below.

a. Due to that the triaxial apparatus is strain-controlled, the loading or shearing is governed by setting the target axial strain in *Digitshow Basic*.
b. All testing procedures of loading are controlled in settings in the *Digitshow Basic*, where the *Control_ID 15* was used in this study.
c. The triaxial apparatus was detached, cleaned and maintained in specific period in releasing all loading after completion of tests. And the materials of specimen after shearing herein were kept for determination of grain size distribution.

3.6 SUMMARY

The funtional description and fundamental principles of the high-pressure triaxial apparatus as well as the tested materials & testing procedures employed in this research have been elaborated in this chapter.

CHAPTER 4

STUDY ON THE CHARACTERISTICS OF PARTICLE BREAKAGE

4.1 INTRODUCTION

This chapter presents the study on the characteristics of particle breakage induced by high-pressure triaxial tests. The tested condition, tested procedures and stress paths herein were elaborated in successive sections. All tested results were shown as well in comparison with different tested condition to investigate the characteristics of particle breakage subjected to various influence factors such as the confining pressure, void ratio, drainage condition, cycle number, dry & saturated sand and unloading process during shearing. The grain size distribution of tested materials after shearing were obtained and used to identify the extent of particle breakage directly perceived through the senses, being quantified by a single-parameter particle breakage factor: Relative Breakage for being able to be in direct application in comparison. The conclusions were summarized in discussion to facilitate the fundamental understanding of the characteristics of particle breakage under high pressure.

4.2 METHODOLOGY

Triaxial tests on silica sand No.5 and coral sand No.3 separately were terminated at designated axial strain from 0% to 20% by a 5% increment. The whole material of the specimen after shearing was kept in an oven to dry and then all sand were mixed and laid open uniformly as a thin cylinder on a big tray, which was divided into four parts uniformly to remove diagonal two of them until around 200g left by repeating this method, with an aim to get few amount of uniform material of specimen to sieve. Hereafter the around 200g of tested material was collected to obtain the grain size distribution curve by sieve analysis, which can be regarded as grain size distribution curve of the specimen after shearing. And then the sieve analyses of tested materials of each test after shearing were performed to obtain the relevant grain size distribution (abbreviated as GSD subsequently) curves at each specific axial strain of each test with

identifying the extent of progressive particle breakage by the difference of grain size distribution curves before and after shearing. A single-parameter particle breakage factor: Relative Breakage B_r was adopted in this study to quantify the extent of particle breakage by using the grain size distribution curves before and after shearing, being used in discussion against different stress variables (Note: All sieve analyses were done in this way in this research). Finally the characteristics of particle breakage were investigated against the various influence factors. Figure 4.1 shows the illustration of tested methodology.

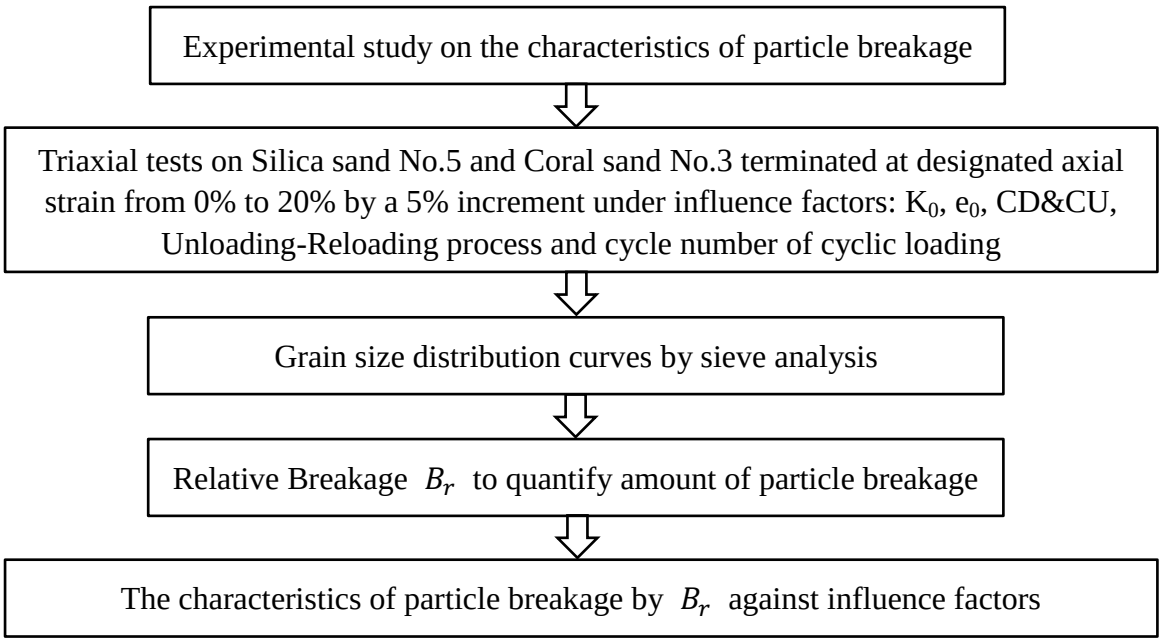

Figure 4.1 Illustration of tested methodology

4.3 ILLUSTRATION OF TEST CONDITION

All triaxial cylindrical specimens of silica sand No.5 and coral sand No.3 herein were prepared in pluviation into a mould in dimension of diameter 100mm and height 200mm with 1mm-thick membrane, which avoided to be pierced by sharp edge of particles under high pressure and minimized the penetration of specimen surface. The double-layer membranes separated by the silicon grease have been employed on upper and lower plates to lubricate the surfaces of the plates to make the deformation of the specimen on the plates develop easily for minimizing the friction of the plates in order to get the uniform stress inside specimen. This method to be able to reduce the plate friction angle less than 1 degree at minimum was proposed by Tatsuoka and his co-workers (Tatsuoka et al., 1984, 1985). Figure 4.2 shows the detailed illustration of lubrication method on top cap and pedestal of specimen, where the deformation of specimen with lubrication can be seen to be relatively uniform.

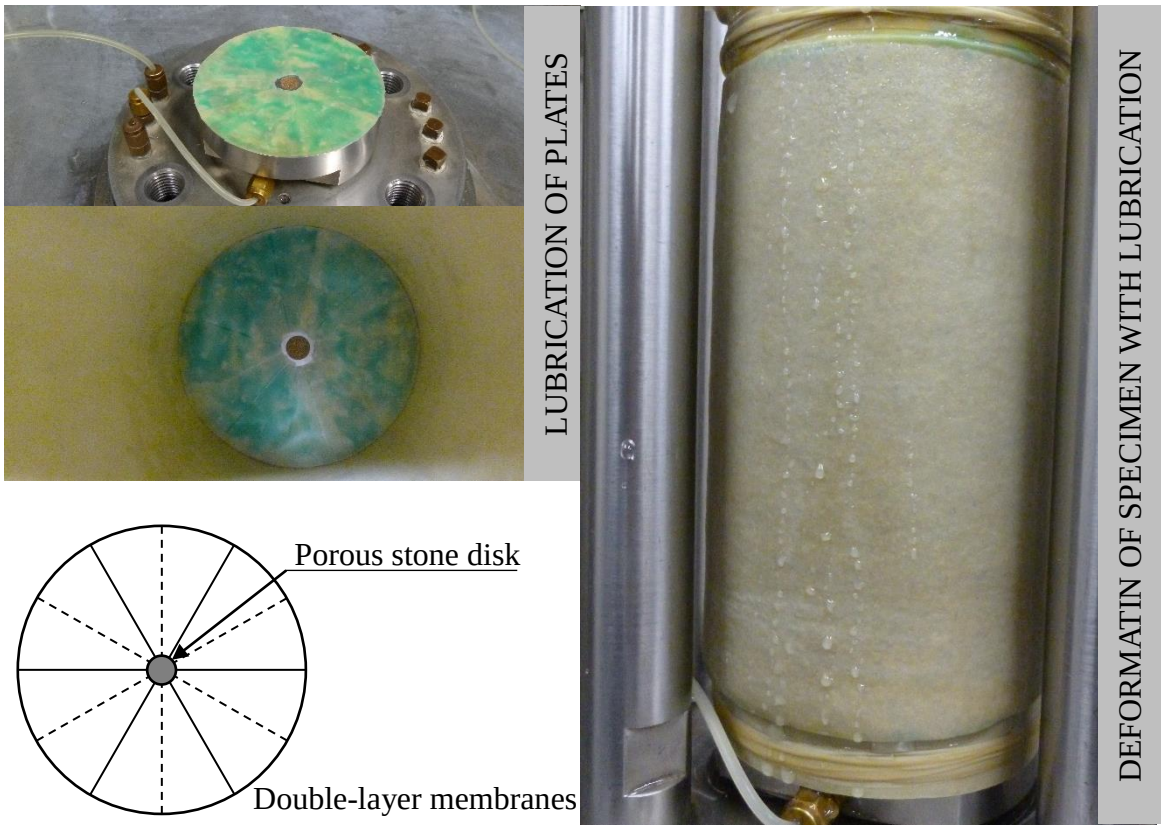

Figure 4.2 Illustration of lubrication method on top cap and pedestal of specimen

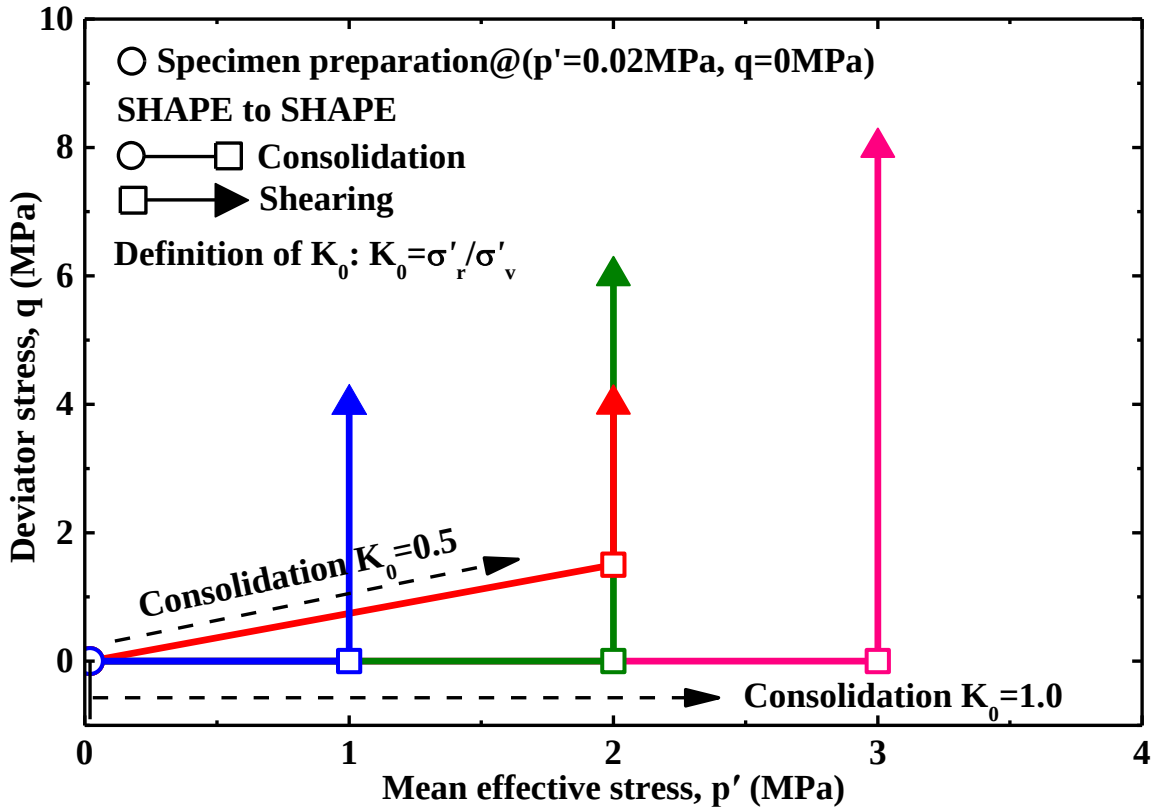

Figure 4.3 Schematic illustration of stress paths in triaxial compression

The traditional standard procedures of triaxial test on cylindrical soil specimen are mainly comprised of consolidation and shearing on saturated specimens. Herein the general stress paths of consolidation and shearing in triaxial tests were performed as shown in Figure 4.3, where it can be seen that the specimens after preparation were consolidated to different mean effective stresses under K_0=1.0 and K_0=0.5 and then sheared in triaxial compression to designated axial strain. The specimens under K_0=1.0 and K_0=0.5 were consolidated to same mean effective stresses (p′=2MPa) to investigate the effect of initial consolidation stress ratio on particle breakage.

4.4 QUANTIFICATION OF PARTICLE BREAKAGE

In the present research, the Relative Breakage (abbreviated as B_r subsequently) developed by Hardin (1985) is introduced to assess the extent of particle breakage, where the area between the initial grain size distribution curve and the grain size distribution curve after loading can be called the total breakage B_t, and the area between initial grain size distribution curve and the vertical line of 0.074mm sieve size can be regarded as the breakage potential B_p. The relative breakage B_r is defined as a ratio of the total breakage B_t over the breakage potential B_p as illustrated in Figure 4.4.

Relative breakage B_r does not take into account the differences in shape of the grain size distribution curves but it has an important advantage of representing all change of gradation of soil in all sieve sizes as a single parameter, consequently the relative breakage factor B_r is stable and robus to quantify particle breakage with removing small variation in individual measurements.

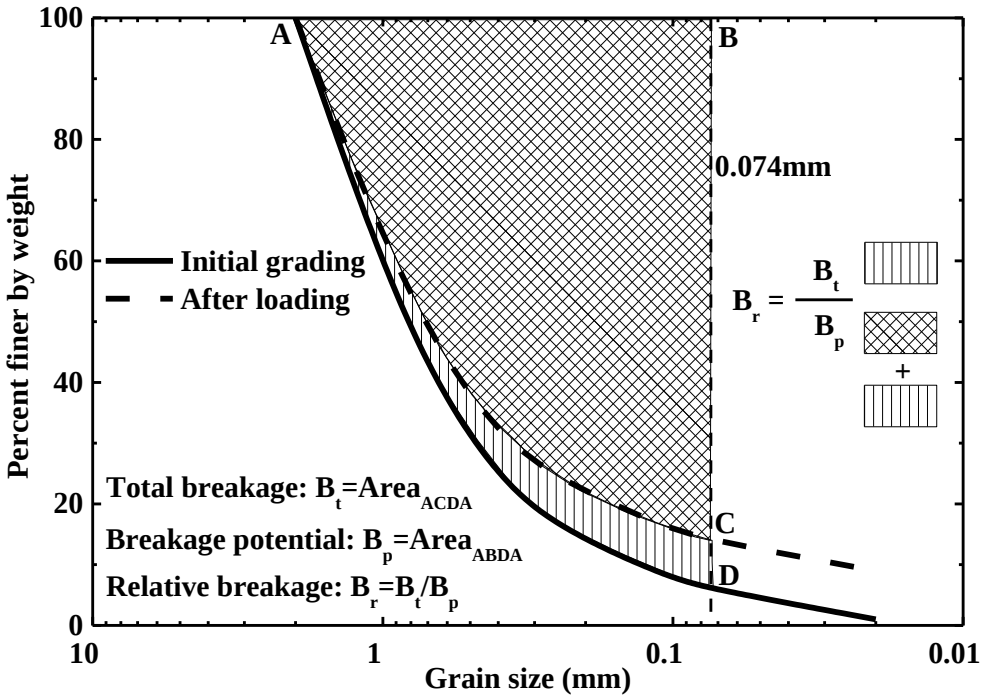

Figure 4.4 Definition of relative breakage B_r (after Hardin, 1985)

A series of triaxial tests were conducted by strain-controlled high-pressure triaxial apparatus on silica sand No.5 and coral sand No.3 to investigate the characteristics of particle breakage by analyzing the various influence factors on particle breakage. All detailed test data in investigation of the characteristics of particle breakage are shown in successive sections. Herein all grain size distribution curves after consolidation and shearing were quantified by relative breakage as shown in Figure 4.4, which was employed to investigate the characteristics of particle breakage in interpretation. The characteristics of particle breakage could be manifested self-evidently by the progressive evolution of relevant grain size distribution curves in increasing particle breakage.

4.5 EXPERIMENTAL RESULTS ON SILICA SAND NO.5

4.5.1 The Influence of Confining Pressure on Particle Breakage

Confining pressure as a very important parameter in triaxial tests has a significant influence on soil behavior, especially under high pressure. Herein many triaxial tests were carried out after isotropic consolidation under different confining pressures as 1MPa, 2MPa and 3MPa in order to investigate the influence of confining pressure on the characteristics of particle breakage. As mentioned above, the tests were conducted up to specific axial strain levels as 0%, 5%, 10%, 15% and 20% in order to obtain the relevant grain size distribution curves by means of sieve analysis after testing.

Figure 4.5 shows CD test results under different confining pressures. It can be seen in Figure 4.5(a) that the deviator stresses increase typically with the increase of axial strain and the higher confining pressure resulted in larger deviator stress. In addition, the stress-strain curve tended to soften slightly with the development of axial strain under 1MPa confining pressure but 2MPa and 3MPa confining pressures just hardened the strain-strain curves without any softening phases. The relevant volume change of the specimens during the triaxial compression was measured as shown in Figure 4.5(b), where the higher confining pressure was found to result in larger volume change and depressed the dilatancy behavior of soil, and the dilatancy behavior of soil occurred in relatively larger axial strain under 1MPa confining pressure but the contractancy of specimen were just caused under 2MPa and 3MPa confining pressures. The grain size distribution curves were obtained by sieving the specimen after testing to analyze the characteristics of particle breakage induced by high pressure.

The relevant grain size distribution curves from the CD tests in Figure 4.5 are shown in Figure 4.6, Figure 4.7 and Figure 4.8, where it can be revealed that particle breakage increases with the increase of axial strain, and the particle breakage occurred during isotropic consolidation despite that it was rather few. From the evolution of the grain size distribution at each sieve size, it is notable that the fine content increases slightly in comparison with the relatively evident increase of finer particles in weight at mediate sieve size. Particle breakage herein may be caused by the combination of attrition and split to reduce the original particle size. In Figure 4.8, the D_{50} of grain size distribution

curves was changed, which means that the split of particles plays important role in particle breakage. The gain size distribution curves were employed to quantify the extent of particle breakage by relative breakage. As shown in Figure 4.9, particle breakage in relative breakage increases with increasing axial strain, which is consistent with the findings (Indraratna and Salim, 2002). The relationship of relative breakage and axial strain in Figure 4.9 can be approximately regarded as being linear with steeper slope under higher confining pressure, which means that particle breakage increases more sharply under higher pressure, which is consistent with the findings (Lade et al., 1996). The relative breakage at axial strain $\varepsilon_1 = 0$ was found to be not zero but increase with the increase of confining pressure, which means that particle breakage occurred after isotropic consolidation to high confining pressure and increased with increasing consolidated confining pressure that are consistent with the findings (Marsal, 1967; Lade et al. 1996).

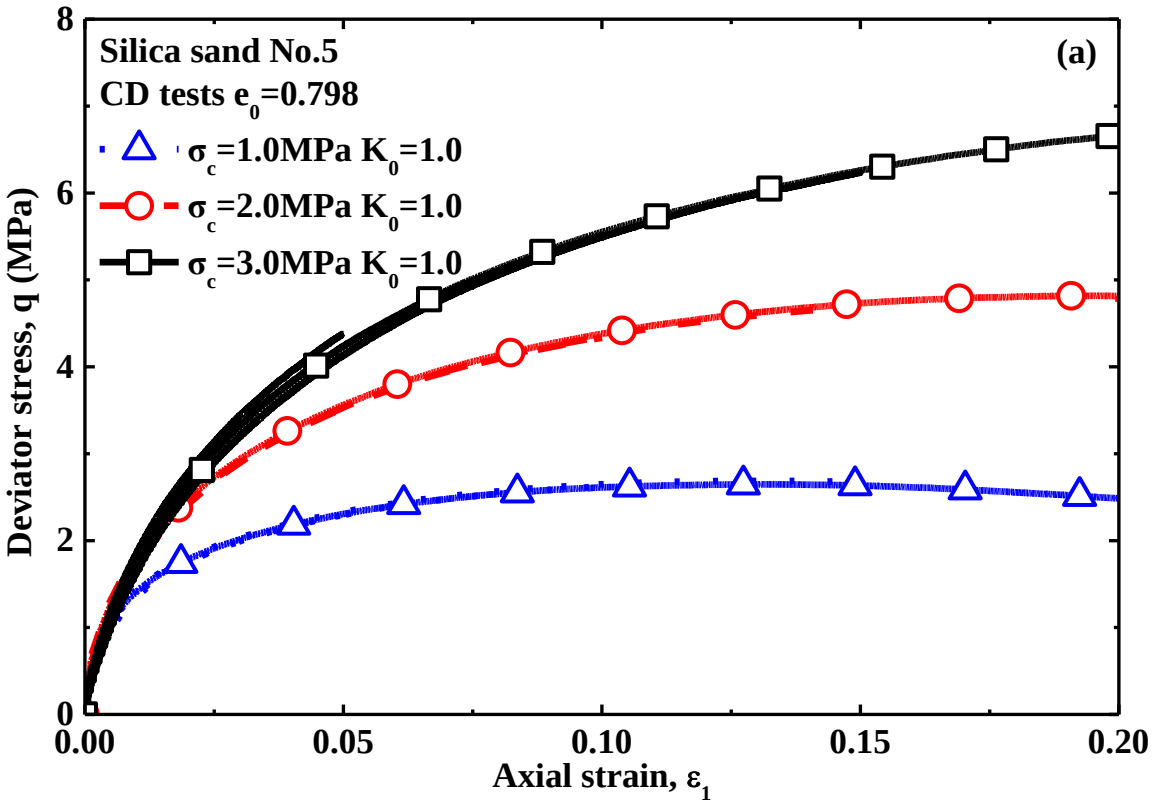

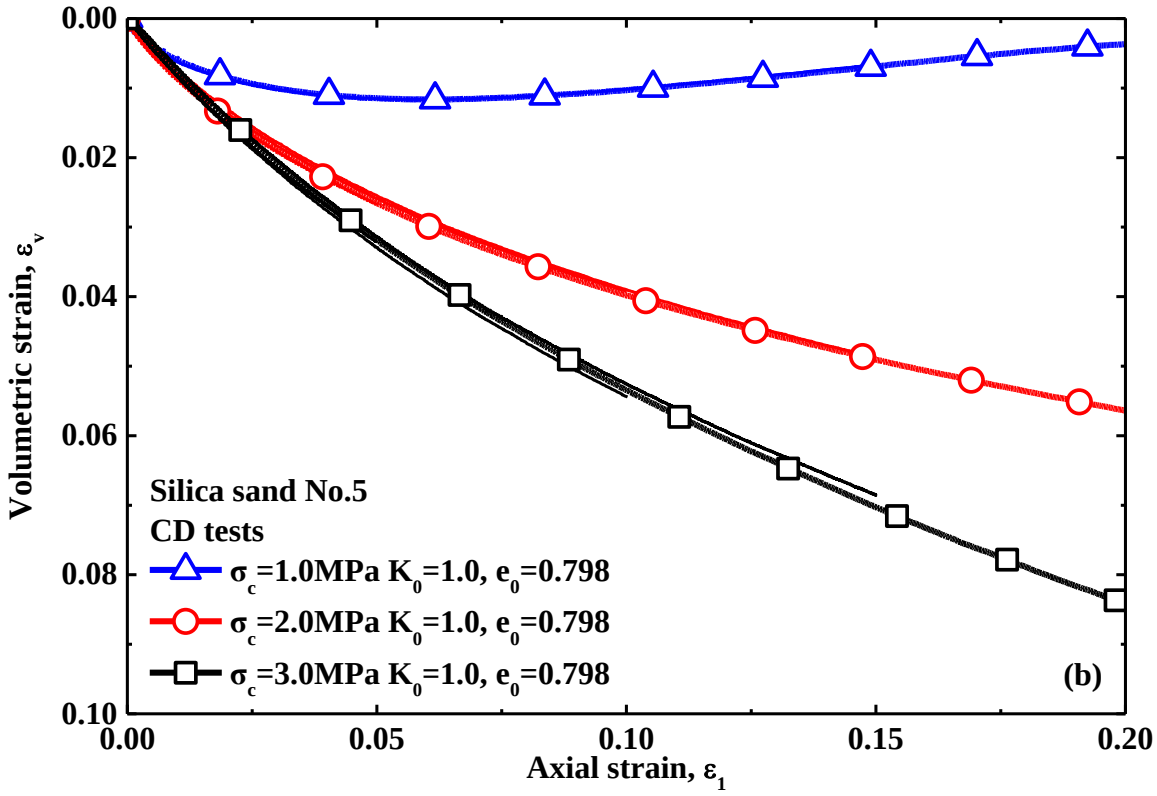

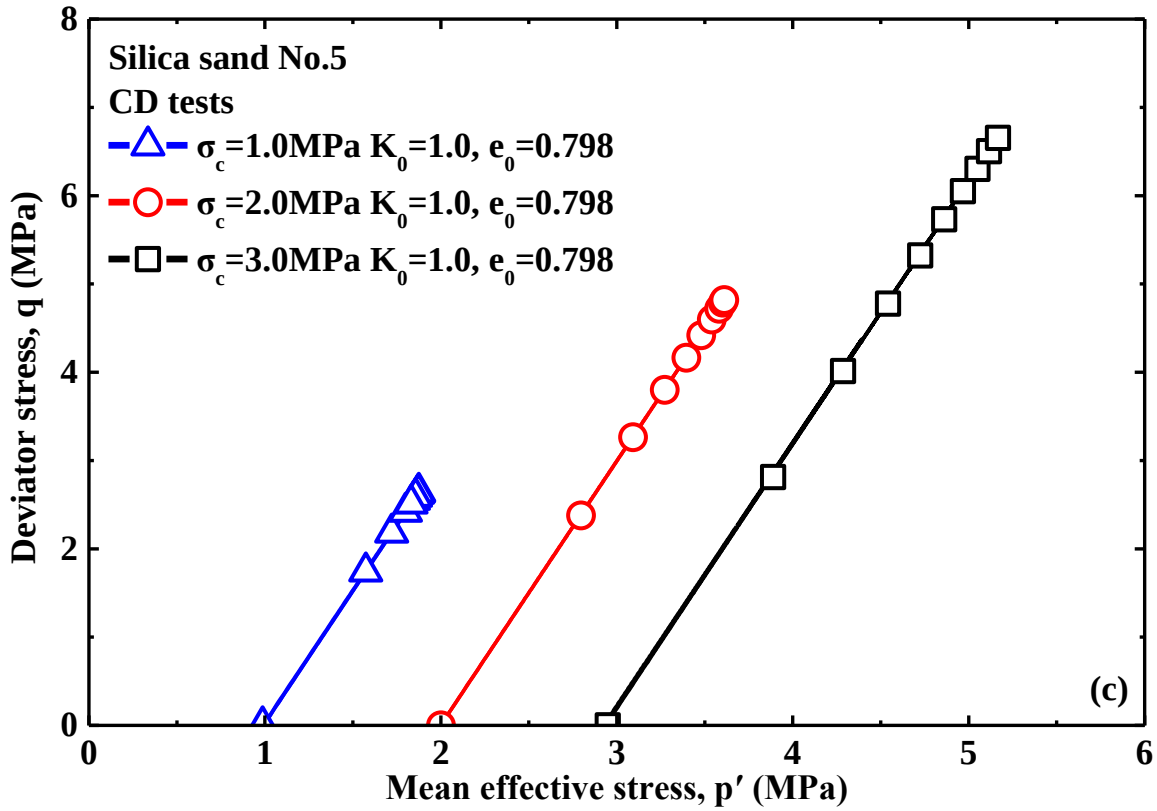

Figure 4.5 CD test results (σ_c=1.0MPa, 2.0MPa & 3.0MPa K_0=1.0, e_0=0.798)

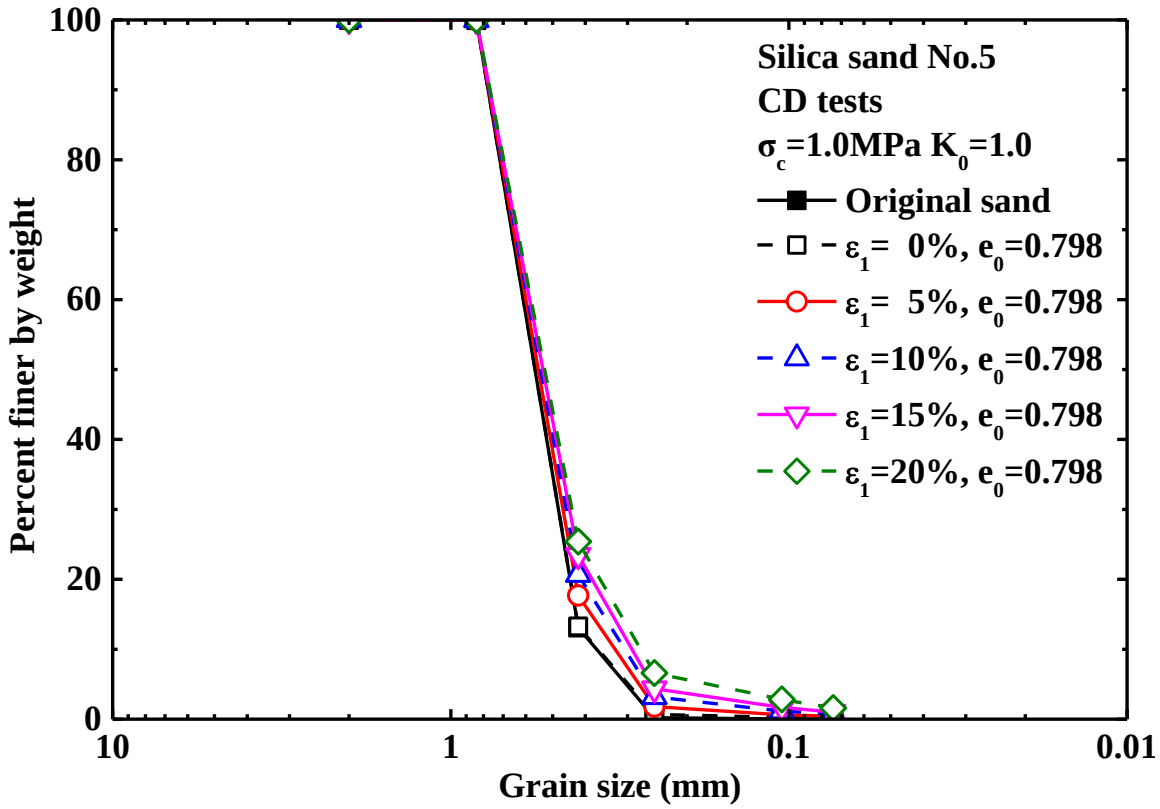

Figure 4.6 Grain size distribution curves from CD tests (σ_c=1.0MPa K_0=1.0, e_0=0.798)

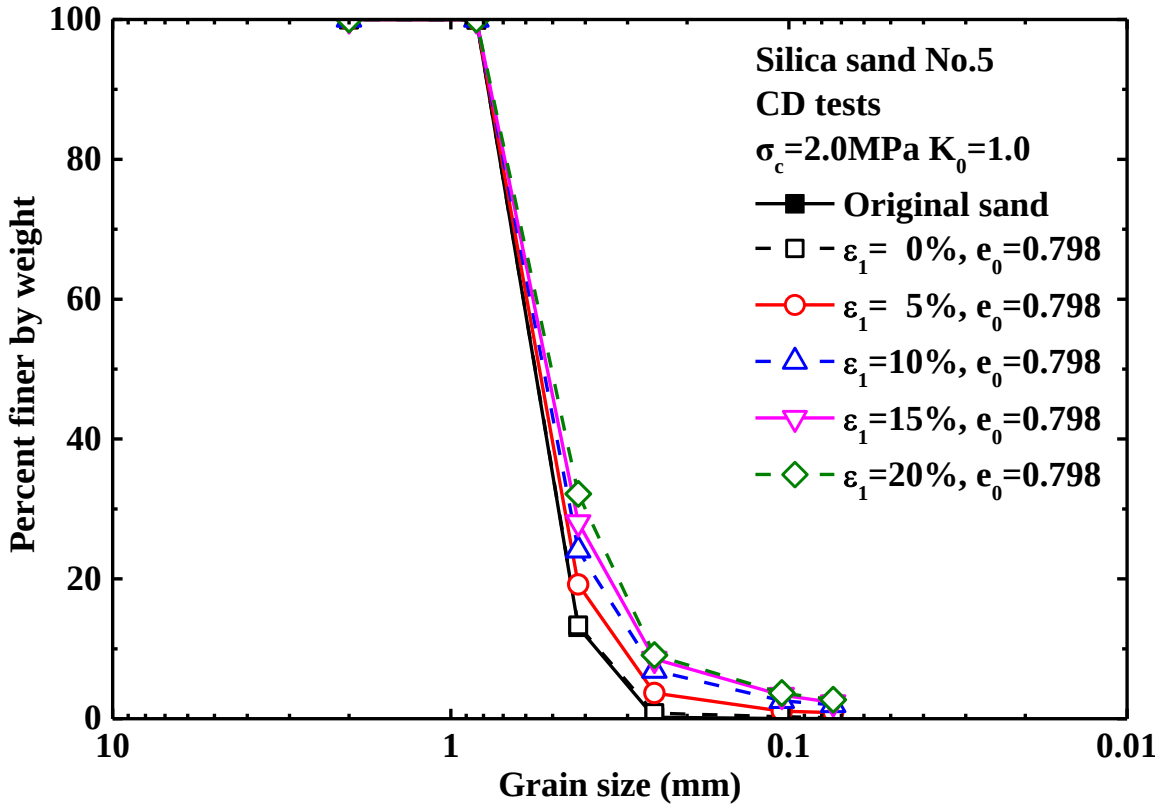

Figure 4.7 Grain size distribution curves from CD tests (σ_c=2.0MPa K_0=1.0, e_0=0.798)

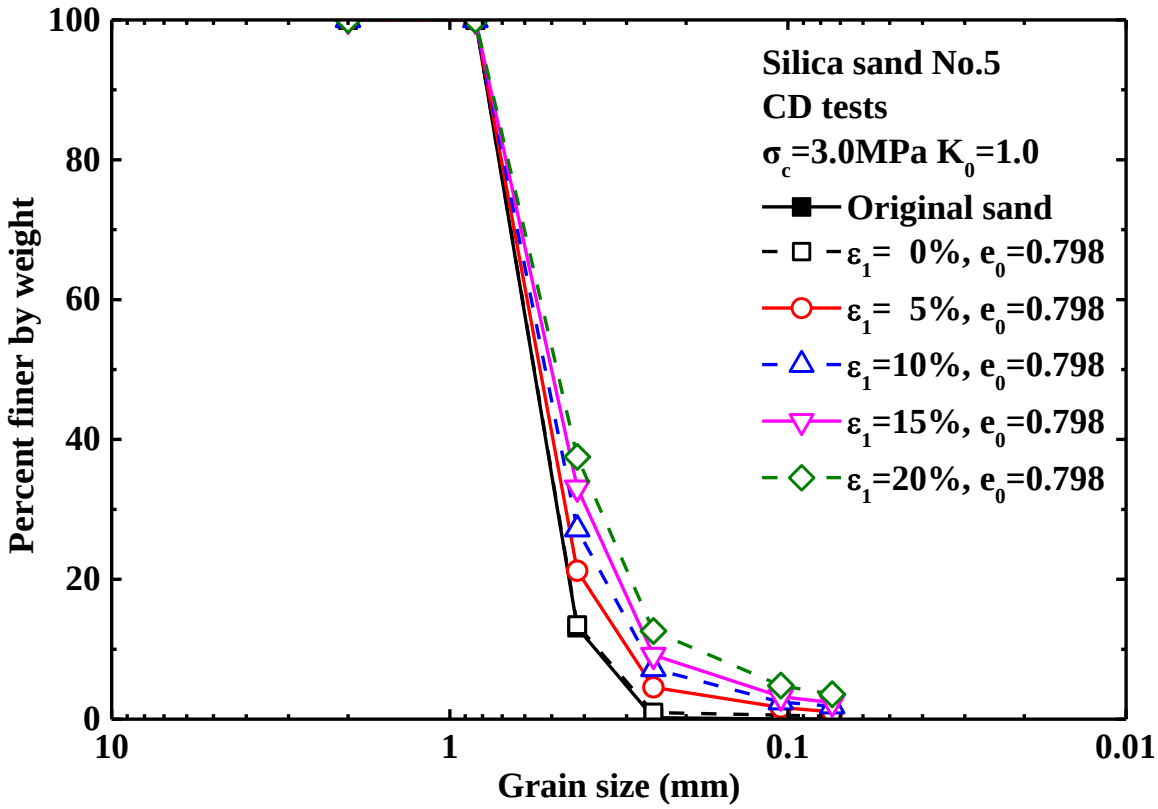

Figure 4.8 Grain size distribution curves from CD tests (σ_c=3.0MPa K_0=1.0, e_0=0.798)

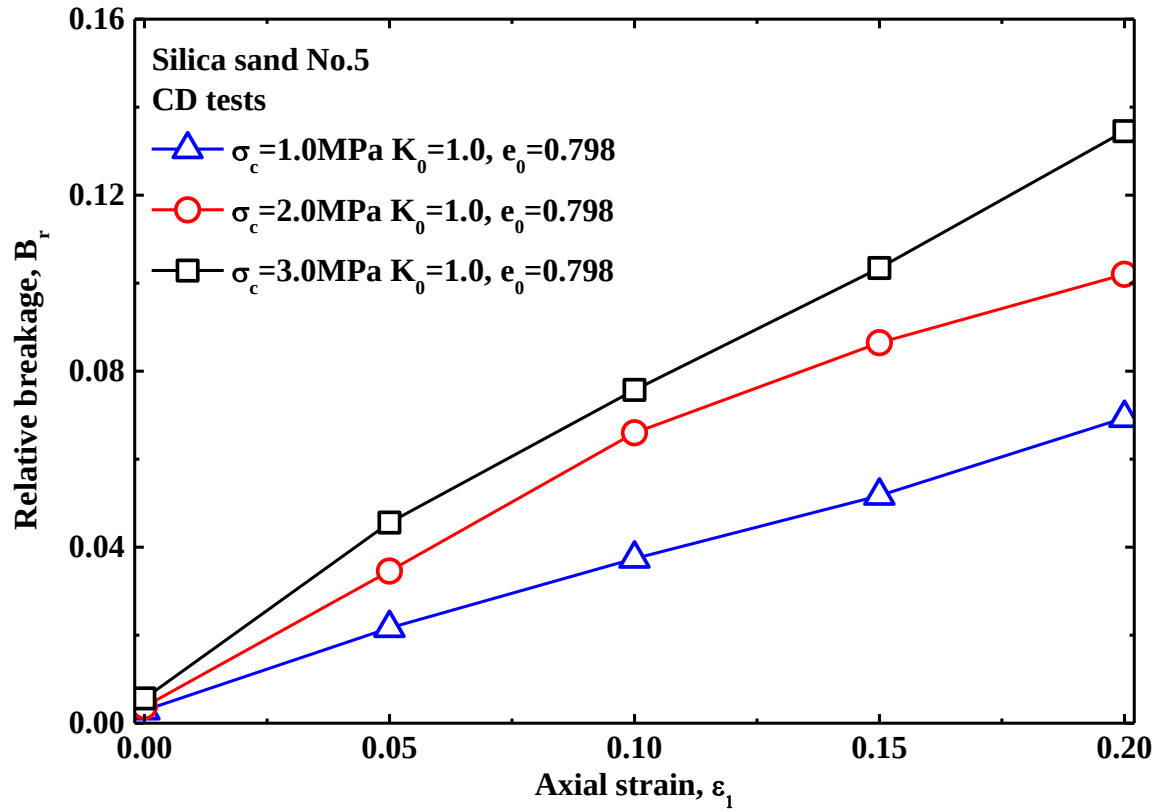

Figure 4.9 B_r-ε_1 relation from CD tests (σ_c=1.0, 2.0 & 3.0MPa K_0=1.0, e_0=0.798)

The corresponding triaxial tests were conducted as well in Consolidated Undrained (CU) condition to investigate the characteristics of particle breakage under CU condition. It can also show indirectly the influence of excess PWP on particle breakage. Figure 4.10 shows the CU test results under different confining pressures, where at onset of shearing, the deviator stresses increases sharply because the excess pore pressures doesn't ascend so much in time yet as shown in Figure 4.10(a). Due to the constant volume of specimen in CU tests, the provisional shear contraction of soil particle results in the sharp development of excess PWP up to summit. With increasing axial strain, the evident dilatancy among soil particles in damage of soil particles arrangement resulted in increase of void among particles which transfers more stress gradually on soil particles. Consequently it can be seen clearly that the deviator stresses increases gradually with increasing axial strain after the summit of excess PWP with the gradual reduction of excess PWP. During shearing, particle breakage occurred, which resulted in depression of dilatancy of soil, namely particle breakage led to faster development and slower dissolution of excess PWP as well. Consequently it can be concluded that particle breakage has a significant influence on permeability and dilatancy behavior of soil. In view of overall data, it can be revealed in Figure 4.10 that both deviator stresses and excess PWPs were elevated with the increase of confining pressure. And the more predominant dilatancy behavior among soil particles under 1MPa confining pressure resulted in slower development and faster dissolution of excess PWP in comparison with those under 2MPa and 3MPa confining pressures.

The corresponding grain size distribution curves from the CU tests in Figure 4.10 are shown in Figure 4.11, Figure 4.12 and Figure 4.13, where the evolution of grain size distribution of soil moves towards the increase of finer particles with the increase of axial strain, that is to say, particle breakage increases with the increase of axial strain. From the evolution characteristics of grain size distribution at each sieve size, it was found as well that the mediate-size particle increased evidently. These grain size distribution curves were quantified by relative breakage which is used in detailed interpretation quantitatively. The relationship between relative breakage and axial strain is shown in Figure 4.14 where at the beginning of shearing there is a slower increase stage of particle breakage that may be caused by relative lower effective stresses on soil particles as a result of higher excess PWP. Thereafter particle breakage has a relatively faster increase with increasing axial strain related to the higher deviator stresses on soil particles. Considering the influence of confining pressure on particle breakage, higher confining pressure resulted in more particle breakage in a steeper slope of increase of particle breakage with increasing axial strain.

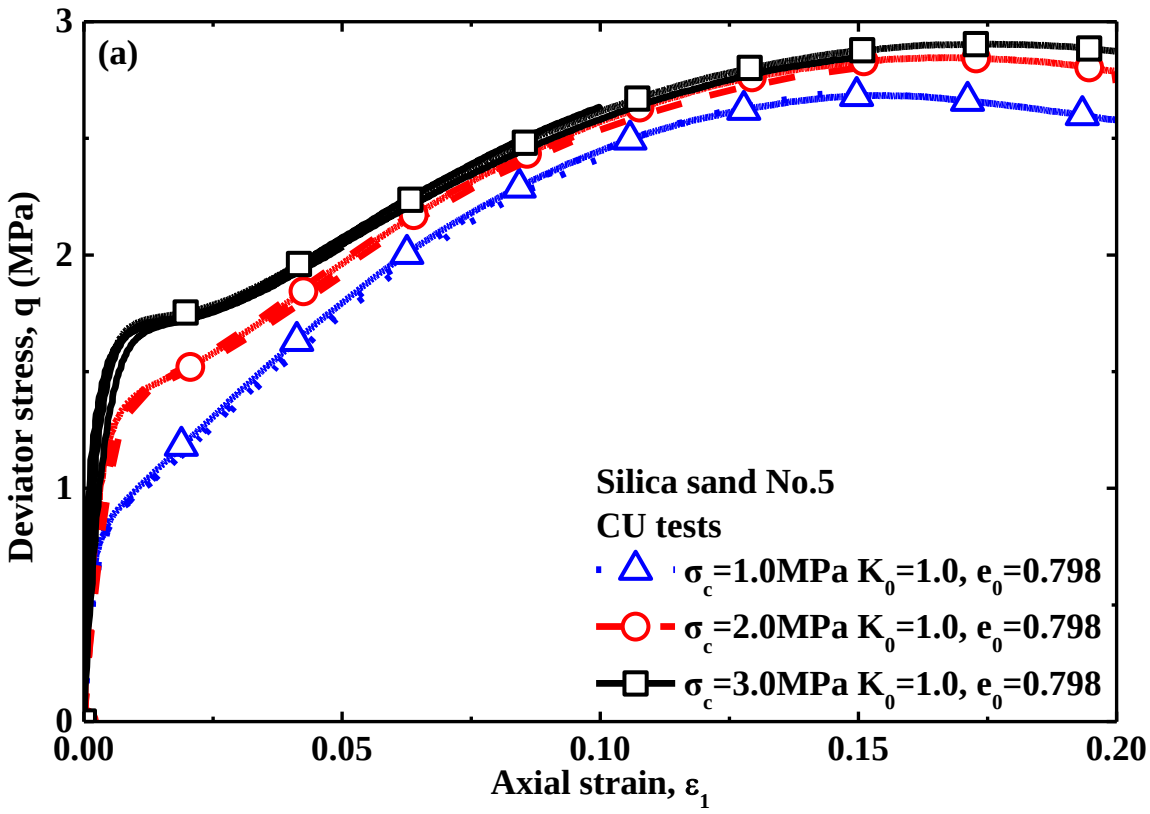
(a)
Deviator stress, q (MPa)
Axial strain, ε1
Silica sand No.5
CU tests
σc=1.0MPa K0=1.0, e0=0.798
σc=2.0MPa K0=1.0, e0=0.798
σc=3.0MPa K0=1.0, e0=0.798

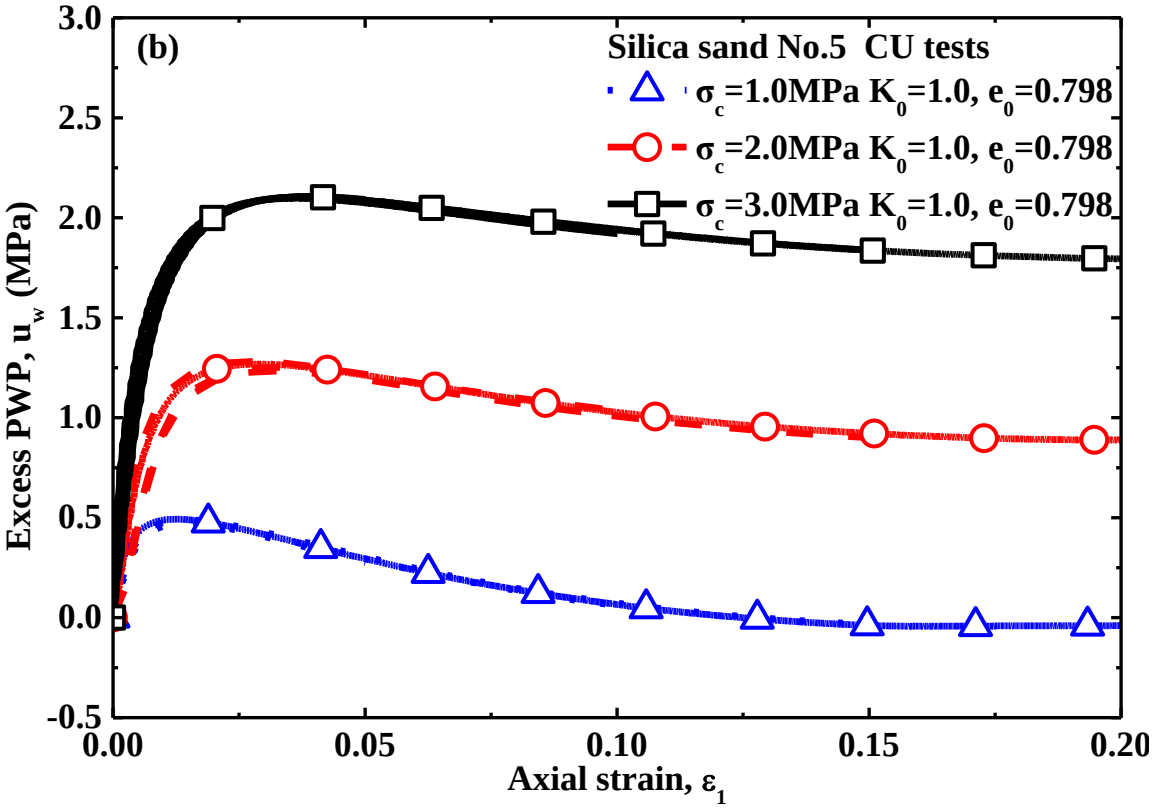
(b)
Silica sand No.5 CU tests
Excess PWP, uw (MPa)
Axial strain, ε1
σc=1.0MPa K0=1.0, e0=0.798
σc=2.0MPa K0=1.0, e0=0.798
σc=3.0MPa K0=1.0, e0=0.798

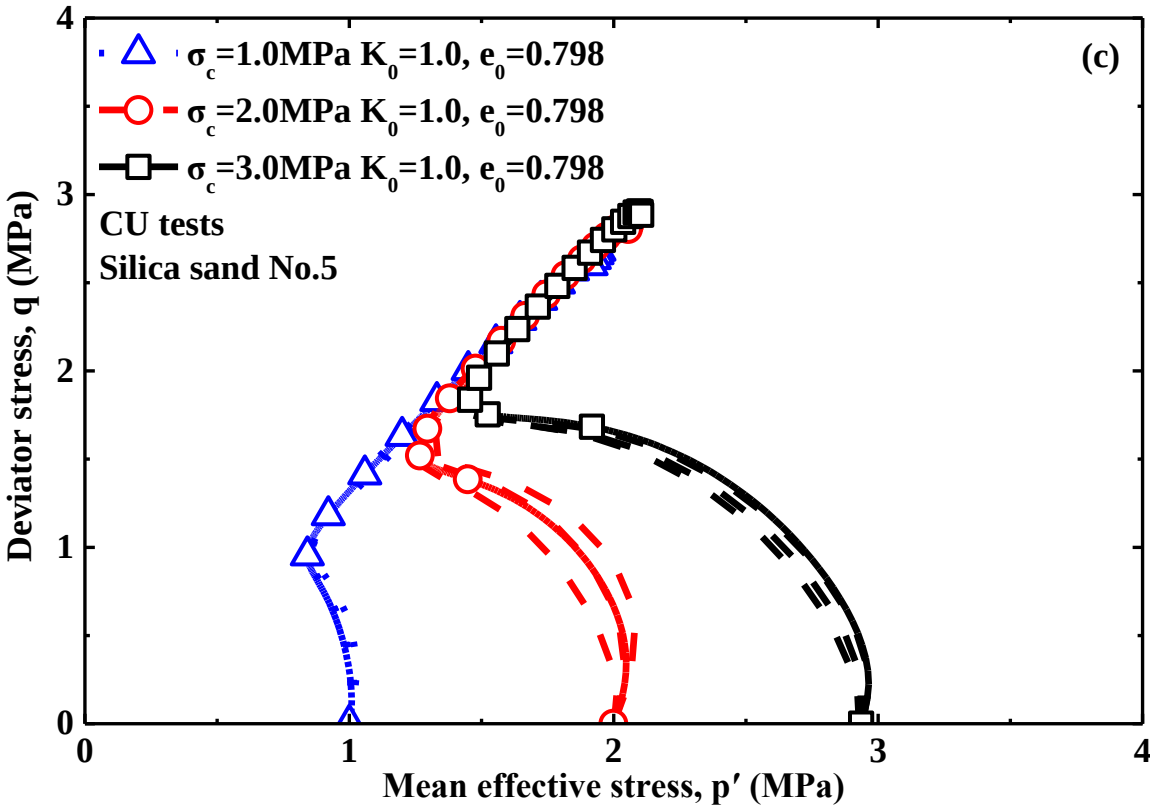

Figure 4.10 CU test results (σ_c=1.0MPa, 2.0MPa & 3.0MPa K_0=1.0 e_0=0.798)

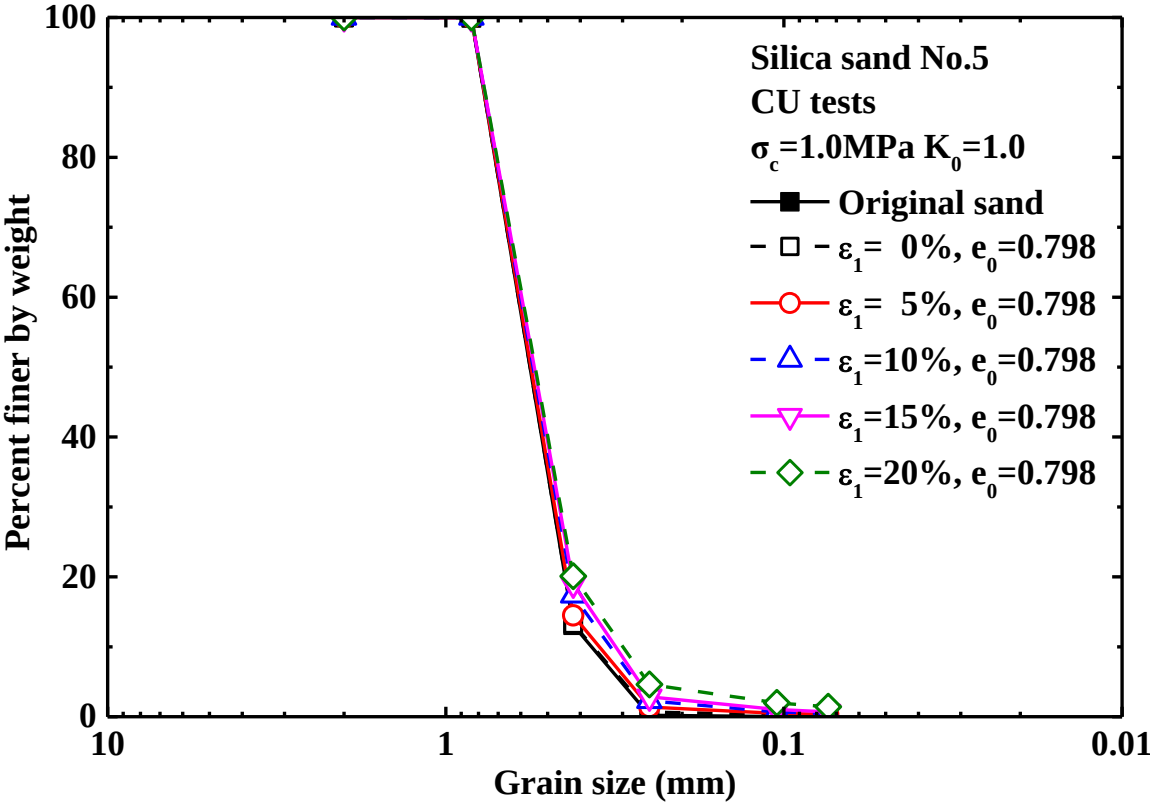

Figure 4.11 Grain size distribution curves from CU tests (σ_c=1.0MPa K_0=1.0, e0=0.798)

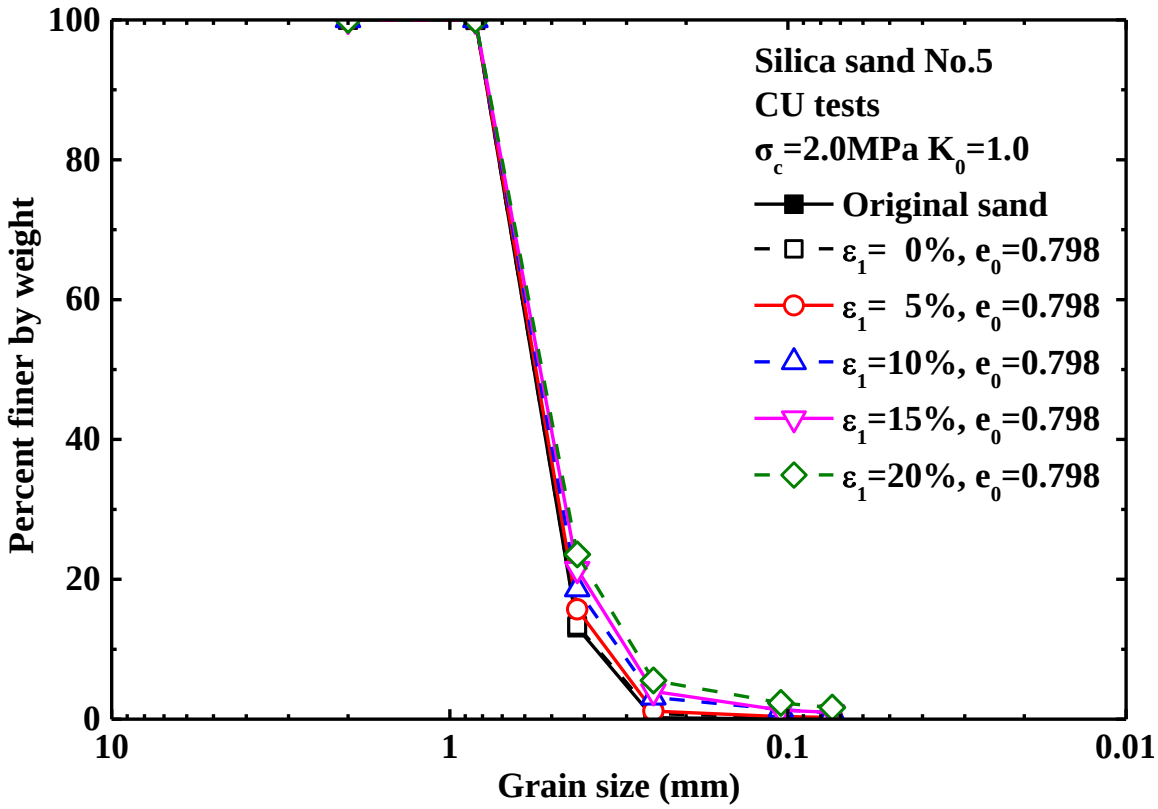

Figure 4.12 Grain size distribution curves from CU tests (σ_c=2.0MPa K_0=1.0, e_0=0.798)

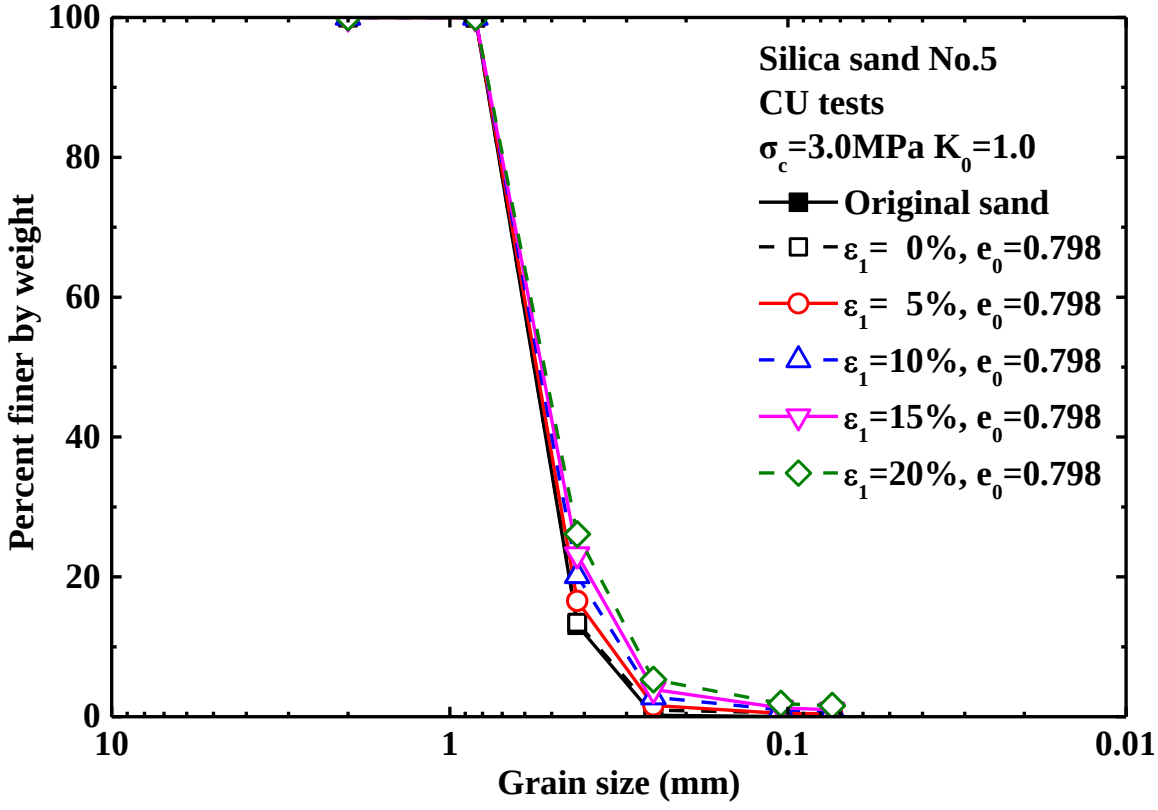

Figure 4.13 Grain size distribution curves from CU tests (σ_c=3.0MPa K_0=1.0, e_0=0.798)

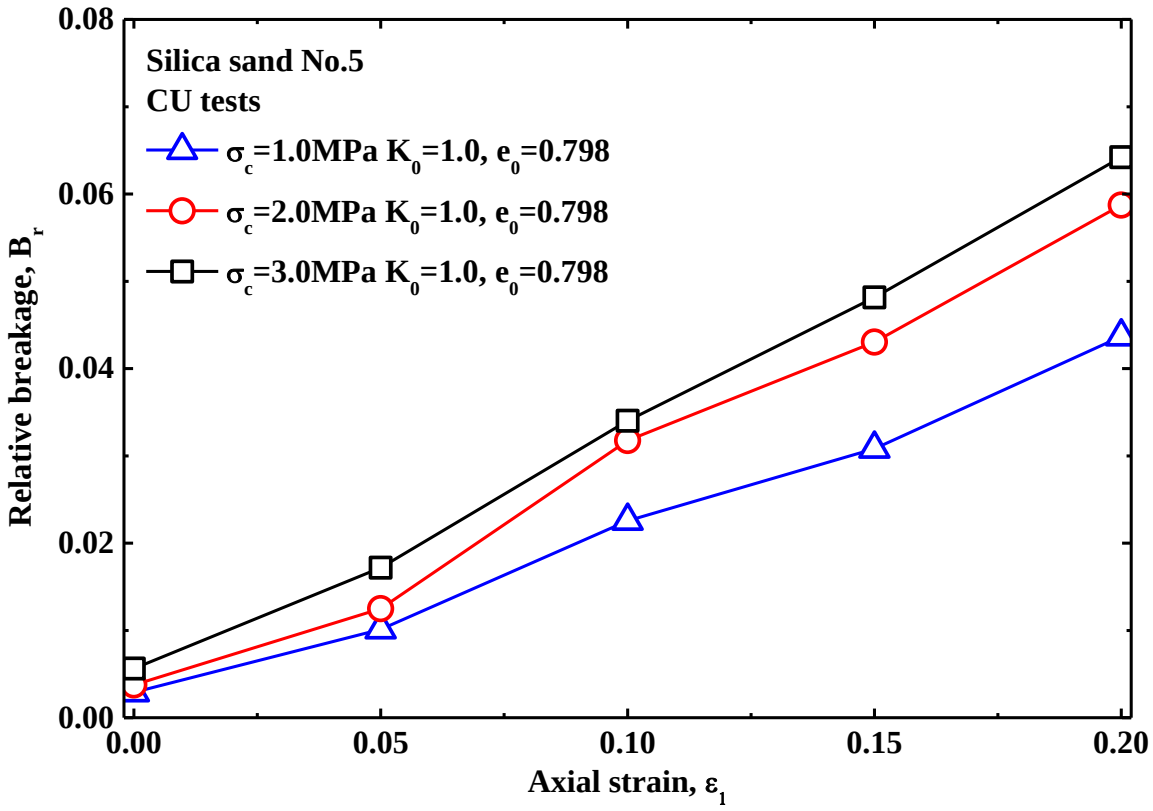

Figure 4.14 B_r-ε_1 relation from CU tests (σ_c=1.0, 2.0 & 3.0MPa K_0=1.0, e_0=0.798)

4.5.2 The Influence of Initial Void Ratio on Particle Breakage

Void ratio as a very important physical parameter of soil has a significant influence on soil mechanics. Many tests were performed under same confining pressure with various initial void ratio of the specimens to clarify the effect of void ratio on particle breakage. The triaxial tested results under 1.0MPa confining pressure with two initial void ratios are shown in Figure 4.15, where the deviator stresses on denser specimens were found to be higher in CD tests or CU tests especially at the beginning of shearing with larger deformation modulus. The deviator stresses are higher in CD tests than that in CU tests as a result of excess PWP occurred in CU tests. As illustrated in Figure 4.15(b), the volume change in denser samples was found to be smaller than that in looser samples. Both volume changes in CD tests tended to dilatancy after a stage of contractancy but there is much more dilative on denser samples. Figure 4.15(c) shows the development of excess PWP against axial strain. The excess PWP was found to be faster and larger in looser samples with a larger residual excess PWP at the end of shearing.

During shearing on specimens, particle breakage occurred and was measured by grain size distribution curves by sieve analyses of specimen. The relevant grain size distribution curves measured in CD tests and CU tests with initial void ratio e_0=0.825 under 1.0MPa confining pressure are shown in Figure 4.16 and Figure 4.17 separately, where evolution of grain size distribution moved toward the increase of smaller-size particles especially in larger amount increase of mediate-size particles in weight. Figure

4.6 and Figure 4.11 show the grain size distribution curves in the CD tests and CU tests with initial void ratio e_0=0.798 under 1.0MPa confining pressure.

All grain size distribution curves were quantified by relative breakage in Figure 4.18 to investigate particle breakage against axial strain. It can be seen clearly herein that particle breakage increases with the increase of axial strain. In the CD tests, the relative breakage against axial strain was regarded approximately as a linear relationship with a steeper slope on denser samples. In the CU tests, particle breakage increases in an increased increment with increasing axial strain. The difference of relative breakage between dense samples and loose samples increases with the increase of axial strain. It was concluded herein that the void ratio of specimen has a significant influence on particle breakage and it resulted in more particle breakage in denser samples.

The confining pressure was elevated to 2.0MPa to investigate the characteristics of particle breakage subjected to effect of various void ratios as well. Another triaxial tests were performed under 2.0MPa confining pressure. Triaxial test results under 2.0MPa confining pressure are shown in Figure 4.19. It can be seen herein that the denser samples resulted in higher deviator stresses in CD tests and CU tests. There is larger contractancy caused in looser samples in CD tests and higher excess PWP was caused in looser samples. The relevant grain size distribution curves were obtained after sieving the samples after shearing.

The grain size distribution curves under 2.0MPa confining pressure at initial void ratio e_0=0.811 in CD tests and CU tests are shown in Figure 4.20 and Figure 4.21 separately, which describe the characteristics of grain size distribution of soil after being tested. From the evolution of grain size distribution curves, it can be proved that particle breakage results in the increase of finer particles in Figure 4.20 and Figure 4.21. All grain size distribution curves herein were quantified as well by relative breakage as shown in Figure 4.22. It was illustrated that particle breakage increases with increasing axial strain, and in CD tests the relative breakage increases with increasing axial strain in reduced increments especially at the larger axial strain but in CU tests the particle breakage increases with increasing axial strain in increased increments. More particle breakage was caused in denser samples, which may be interpreted by that in denser sample under high pressure, particle breakage (split or abrasion) would play a very significant role in contribution of volume change for squeezing crushed particles into the voids among soil particles. The opposite mention (Lade et al., 1996) was given as that looser sample raises particle breakage as a result of that looser sample yields fewer contact points among particles producing larger stress concentration. Particle breakage should be a function of void ratio.

Figure 4.18 and Figure 4.22 show relationship between relative breakage and axial strain under 1MPa confining pressure and 2MPa confining pressure separately, where the particle breakage in relative breakage is found to be more substantial in CD tests than that in CU tests and the difference of particle breakage in relative breakage between CD tests

and CU tests is shown to increase with increasing axial strain, which are related to the increased difference of deviator stress between CD tests and CU tests with the increase of axial strain. The difference of particle breakage between CD tests and CU tests is slightly more substantial in dense samples than in loose samples.

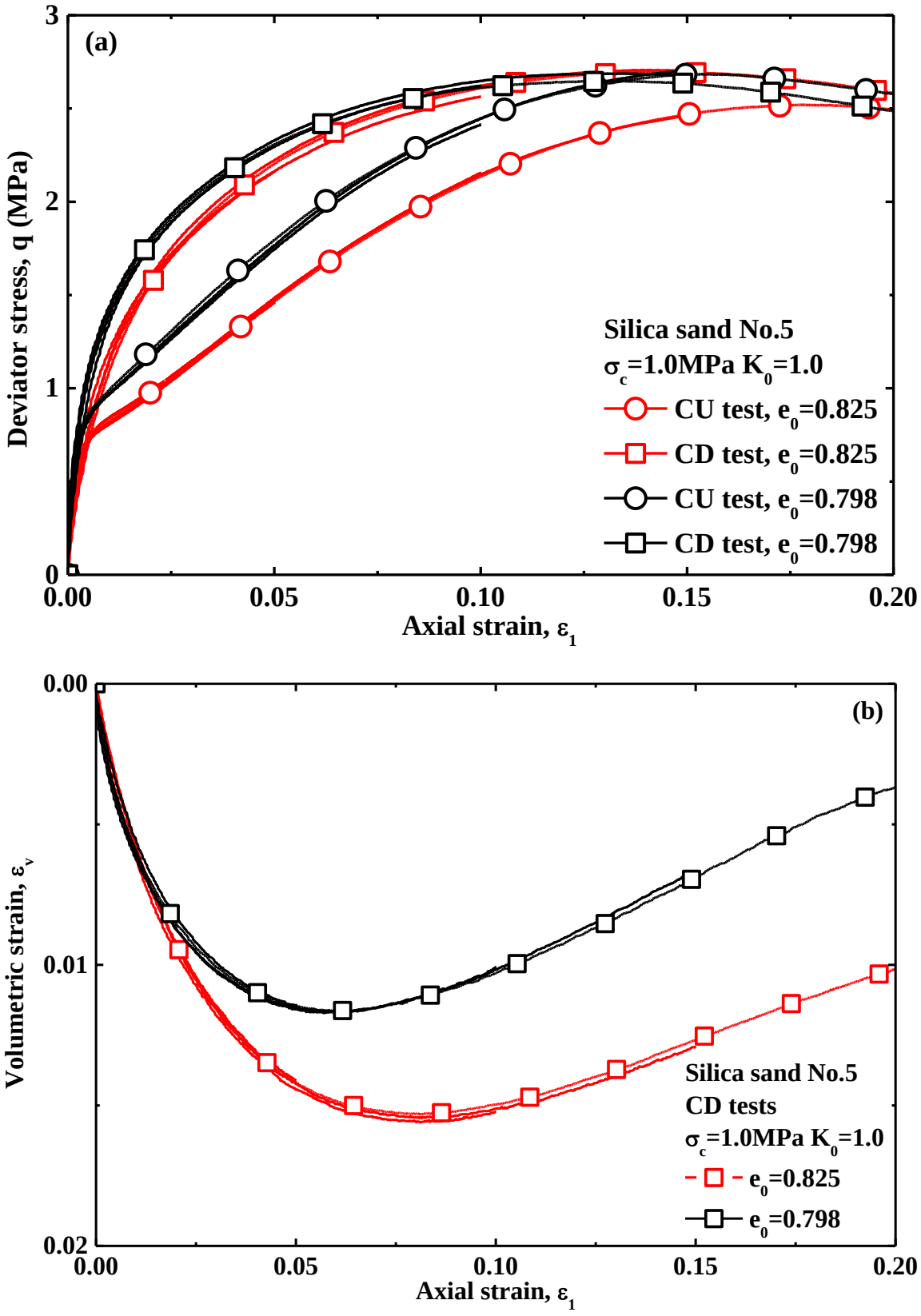

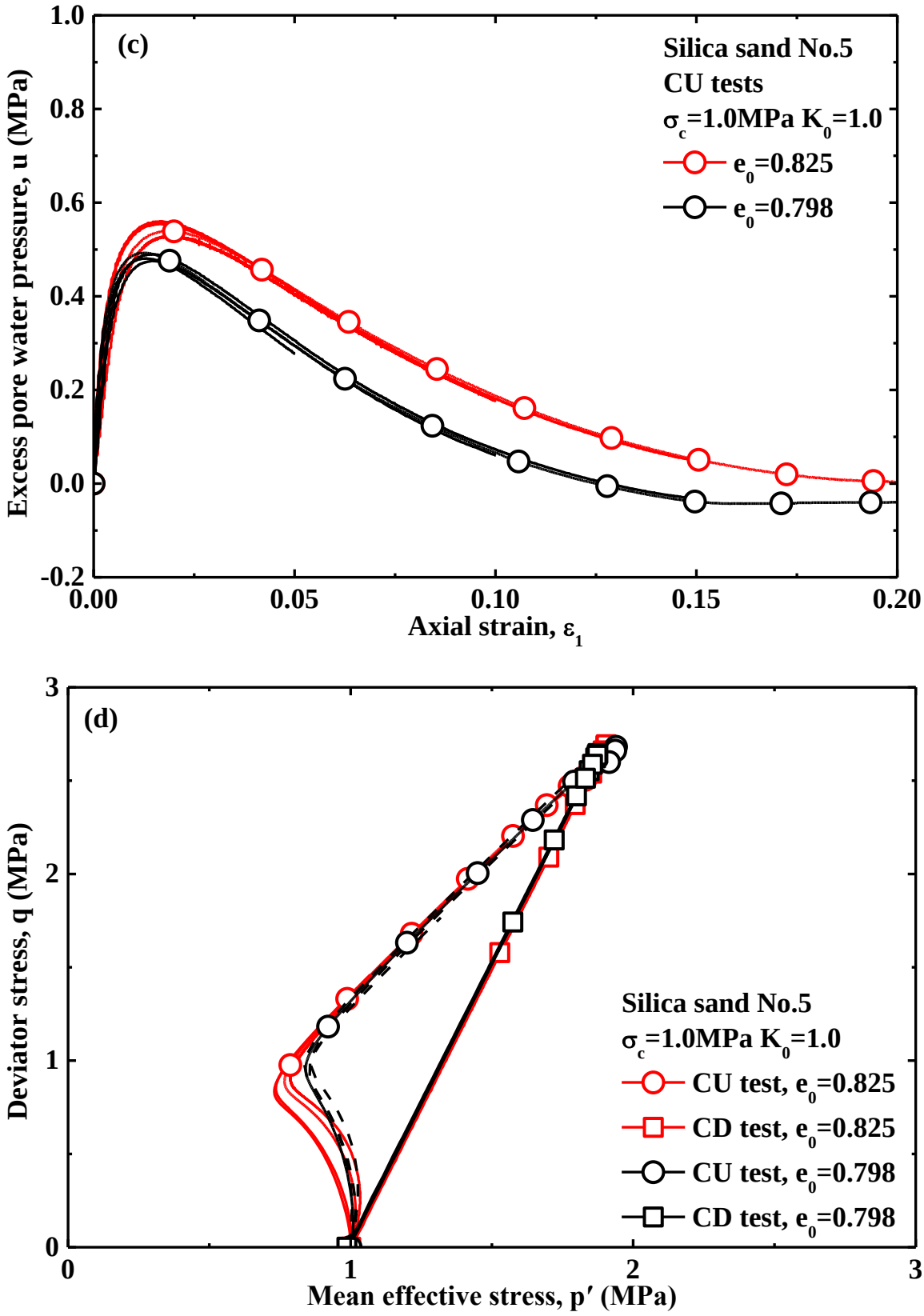

Figure 4.15 Triaxial test results (σ_c=1.0MPa K_0=1.0, e_0=0.798 & 0.825)

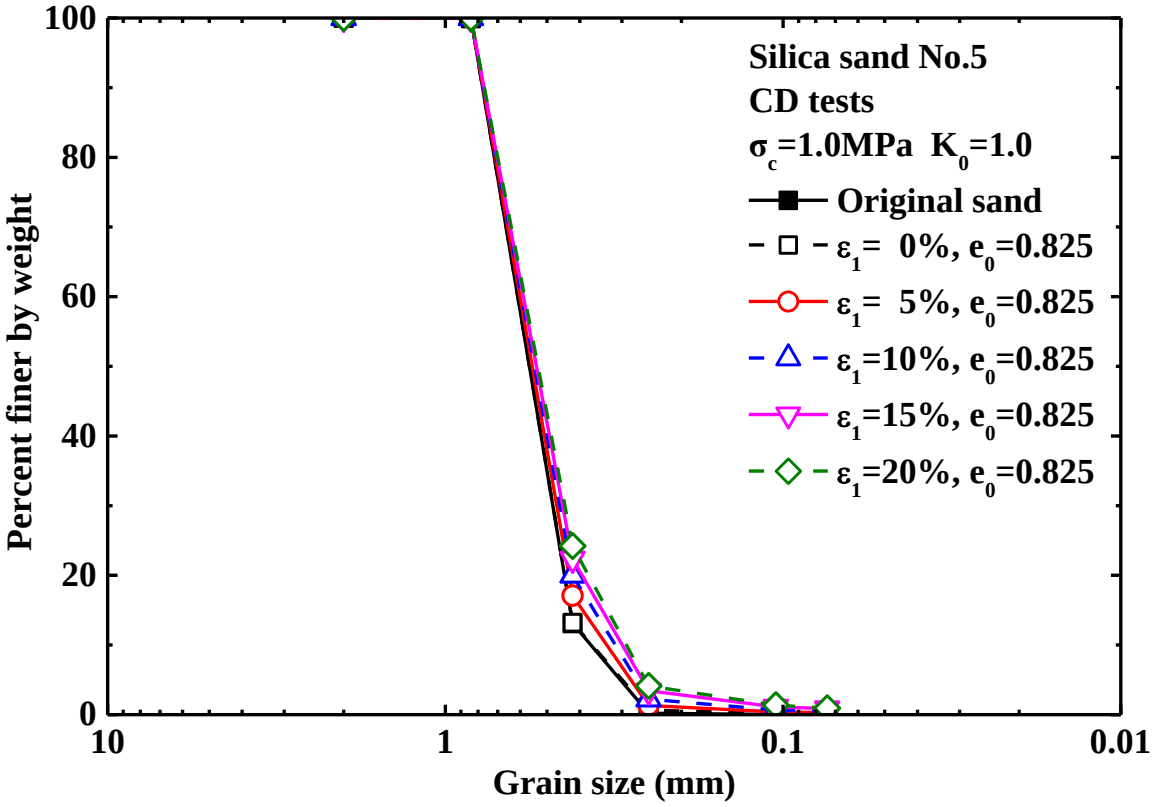

Figure 4.16 Grain size distribution curves from CD tests (σ_c=1.0MPa K_0=1.0, e_0=0.825)

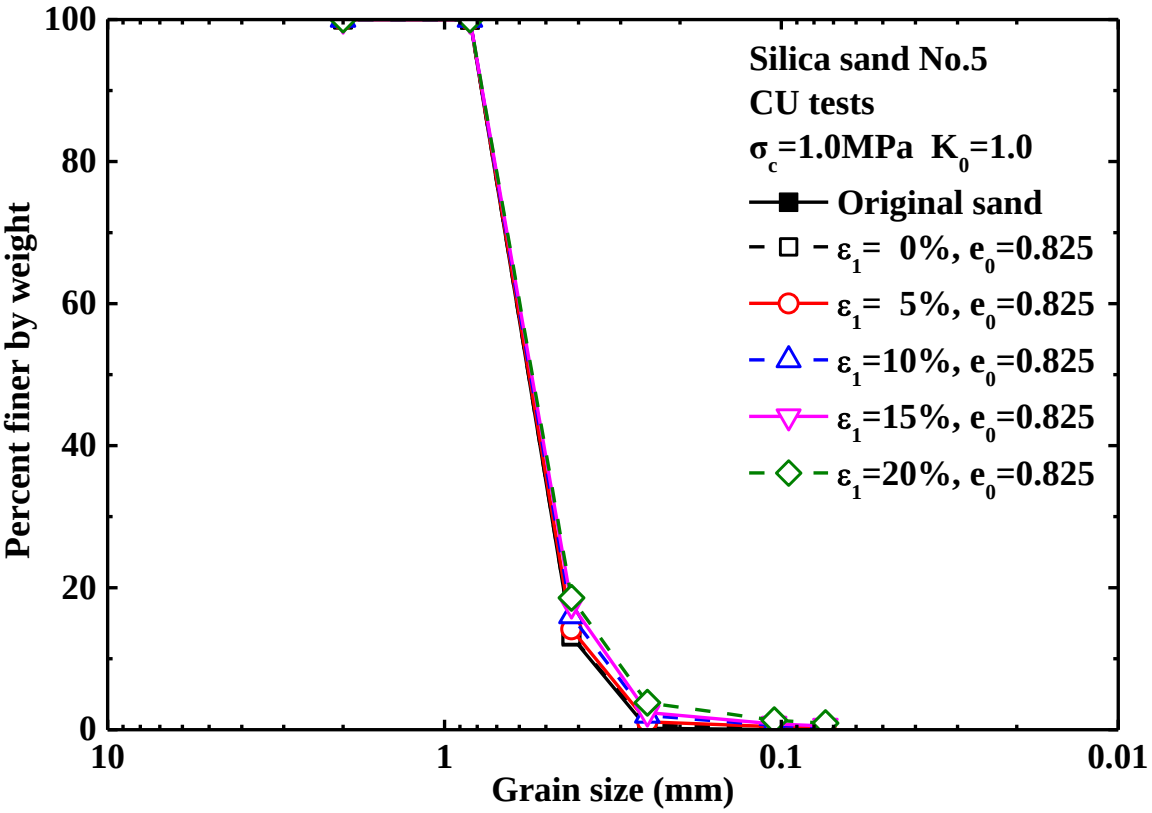

Figure 4.17 Grain size distribution curves from CU tests (σ_c=1.0MPa K_0=1.0, e_0=0.825)

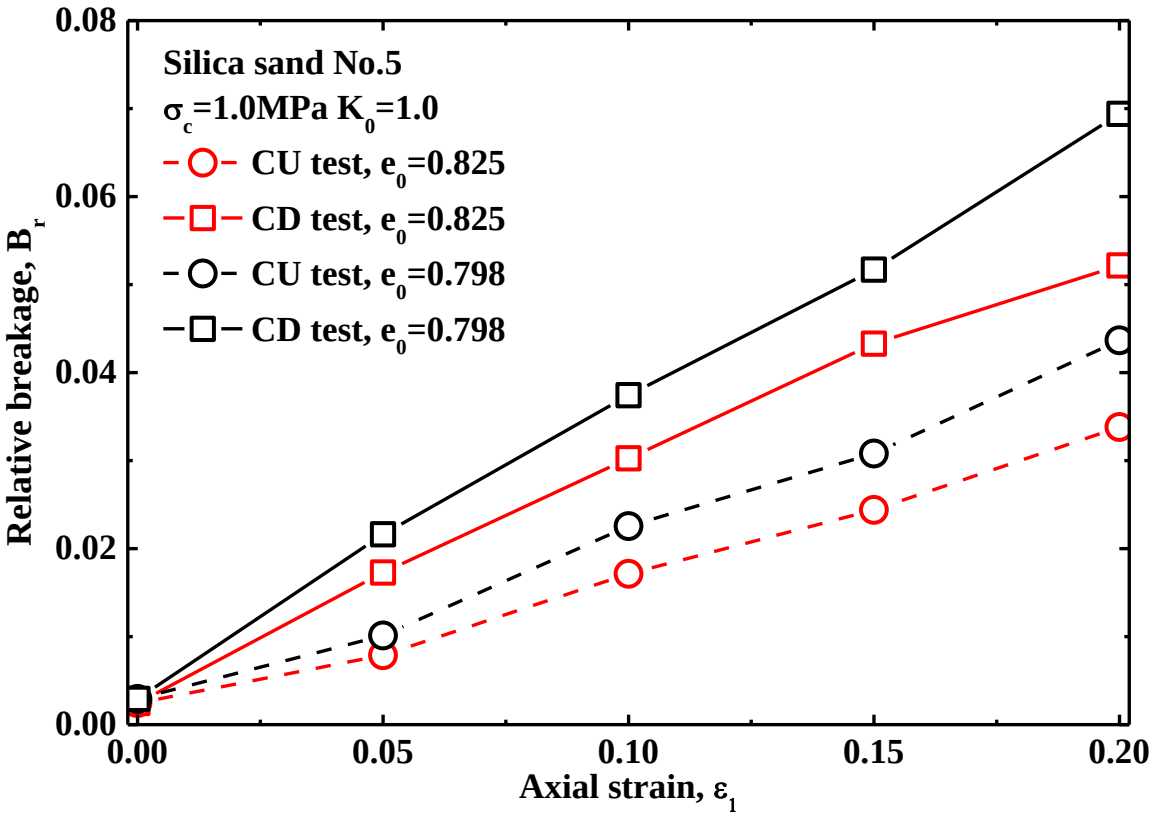

Figure 4.18 B_r-ε_1 relation from CU tests (σ_c=1.0MPa K_0=1.0, e_0=0.798 & 0.825)

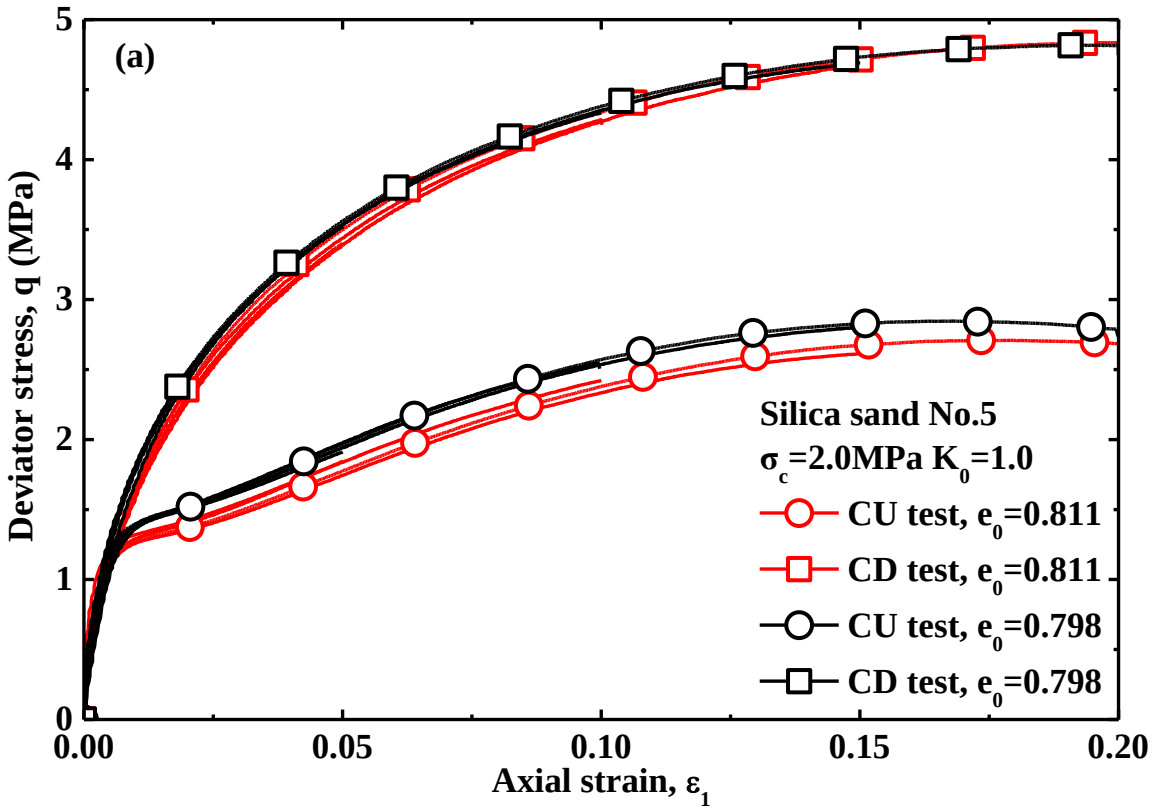

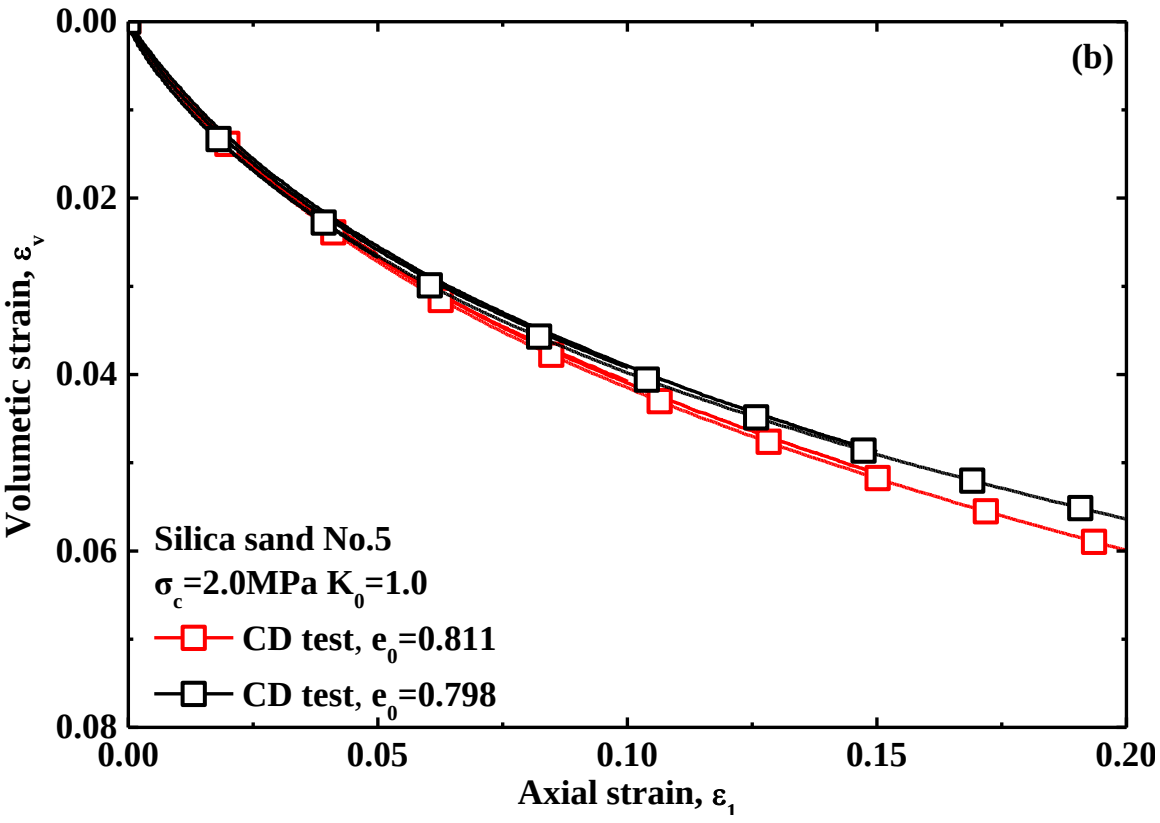
(b)
Volumetic strain, ε_v
Axial strain, ε_1
0.00
0.02
0.04
0.06
0.08
0.00
0.05
0.10
0.15
0.20
Silica sand No.5
σ_c=2.0MPa K_0=1.0
CD test, e_0=0.811
CD test, e_0=0.798

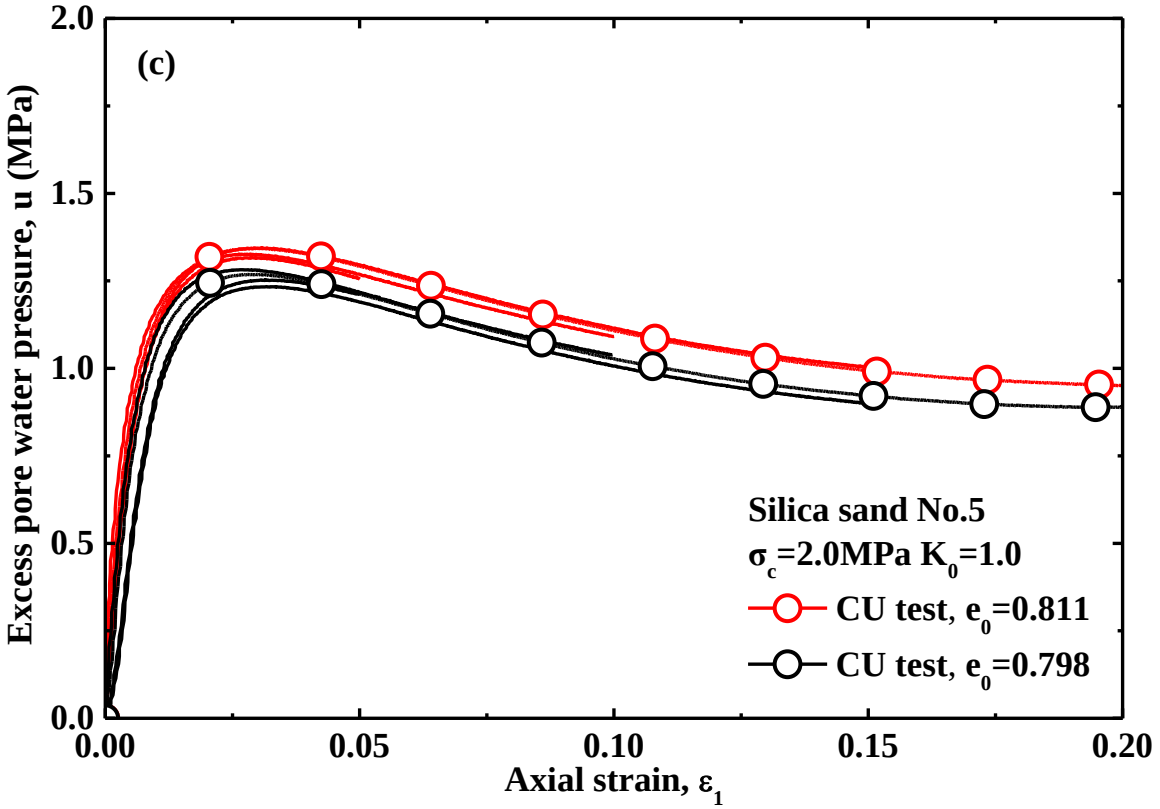
(c)
Excess pore water pressure, u (MPa)
Axial strain, ε_1
2.0
1.5
1.0
0.5
0.0
0.00
0.05
0.10
0.15
0.20
Silica sand No.5
σ_c=2.0MPa K_0=1.0
CU test, e_0=0.811
CU test, e_0=0.798

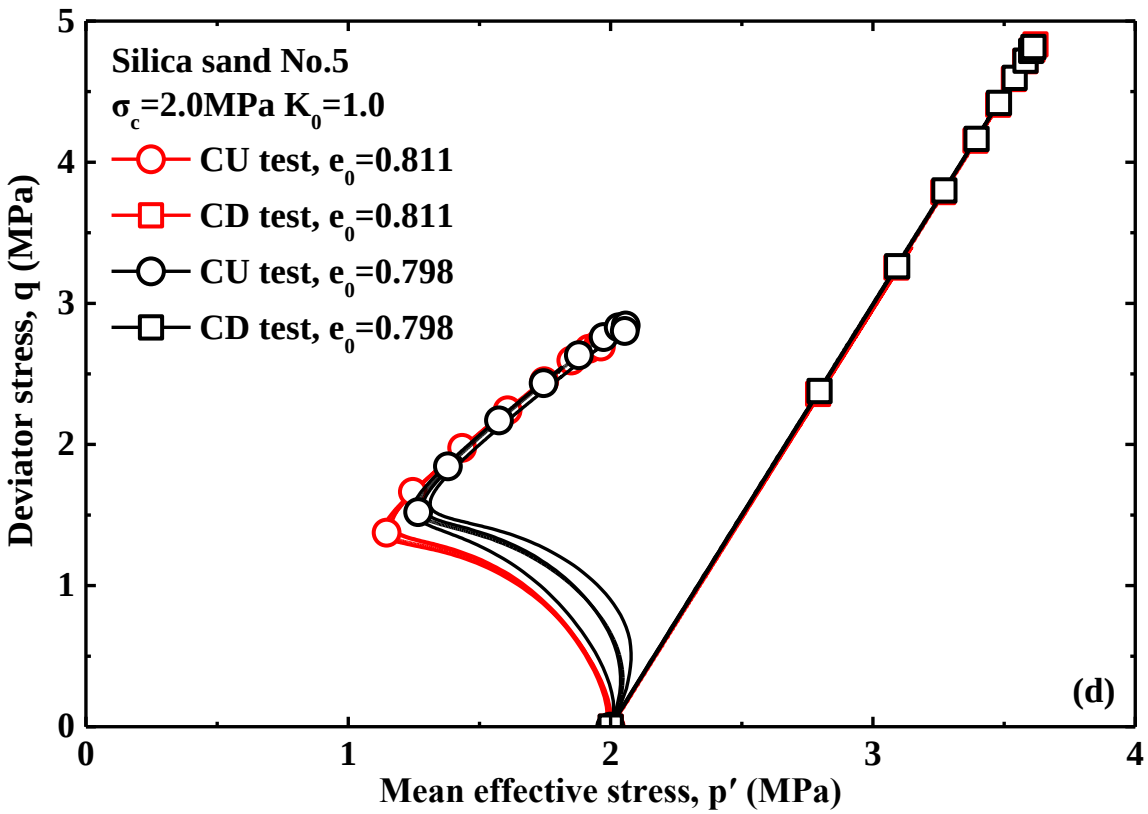

Figure 4.19 Triaxial test results (σ_c=2.0MPa K_0=1.0, e_0=0.798 & 0.811)

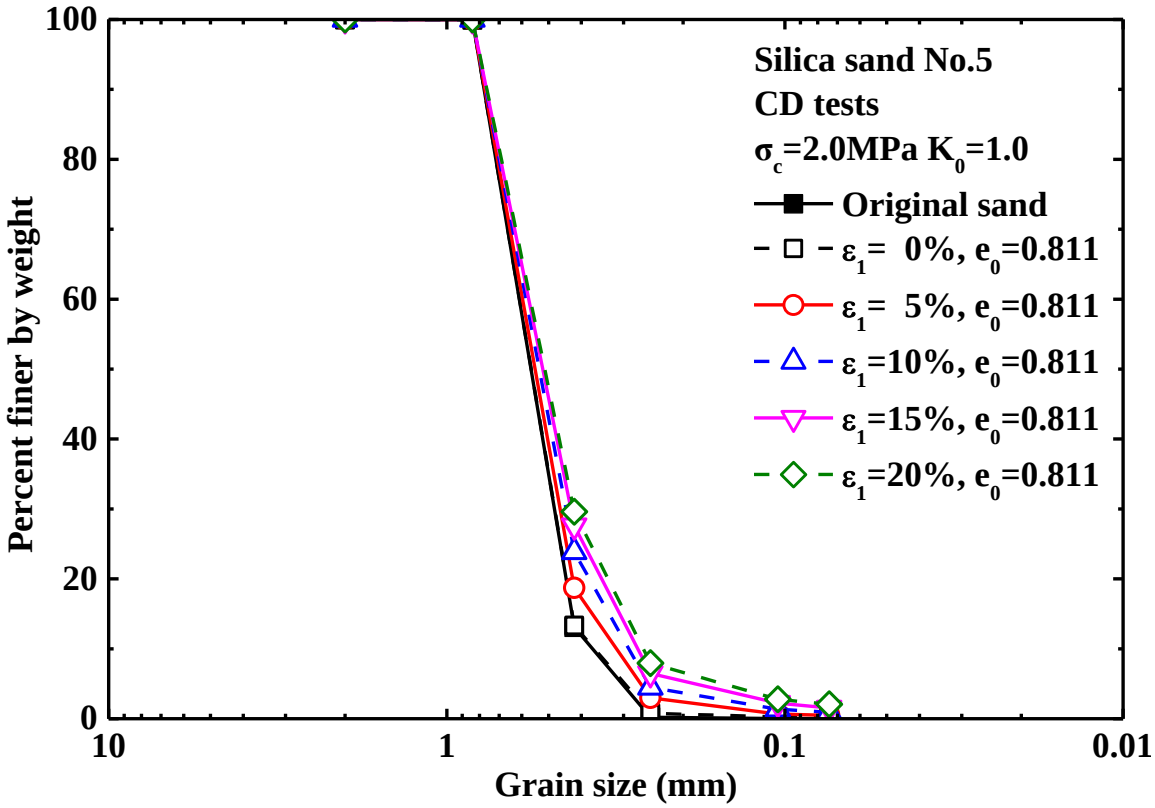

Figure 4.20 Grain size distribution curves from CD tests (σ_c=2.0MPa K_0=1.0, e_0=0.811)

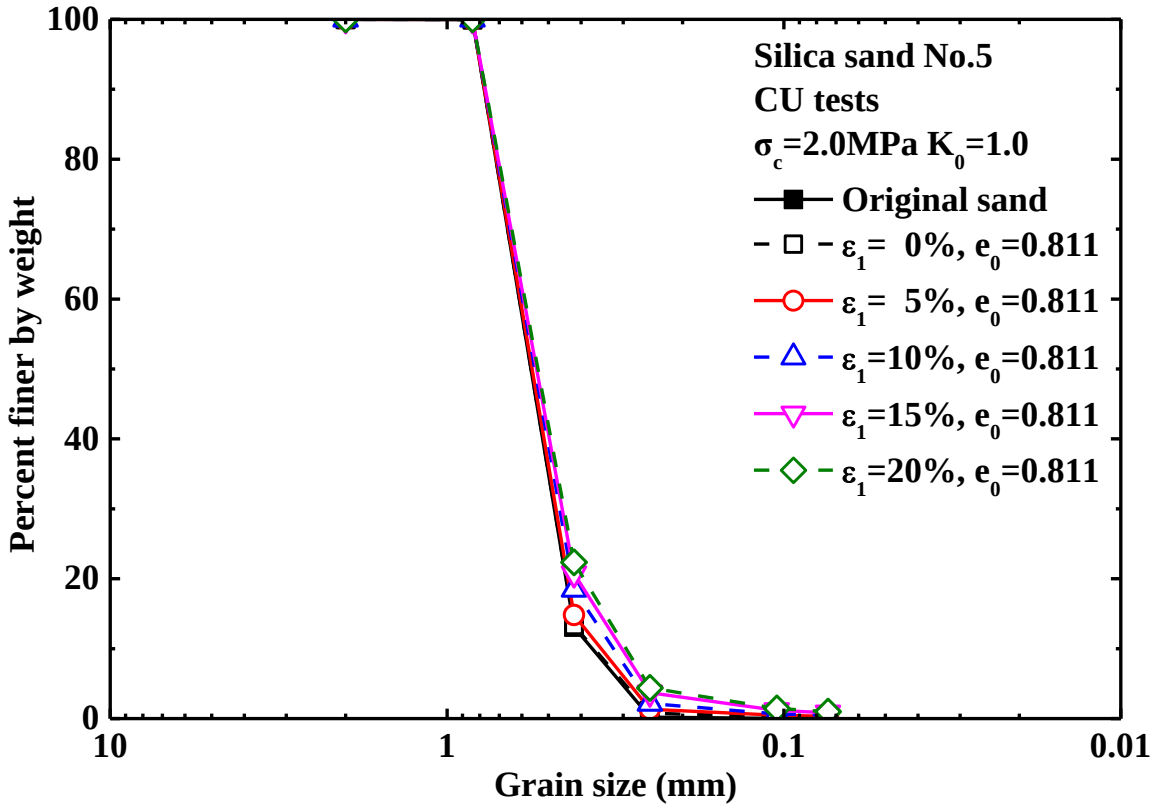

Figure 4.21 Grain size distribution curves from CU tests (σ_c=2.0MPa K_0=1.0, e_0=0.811)

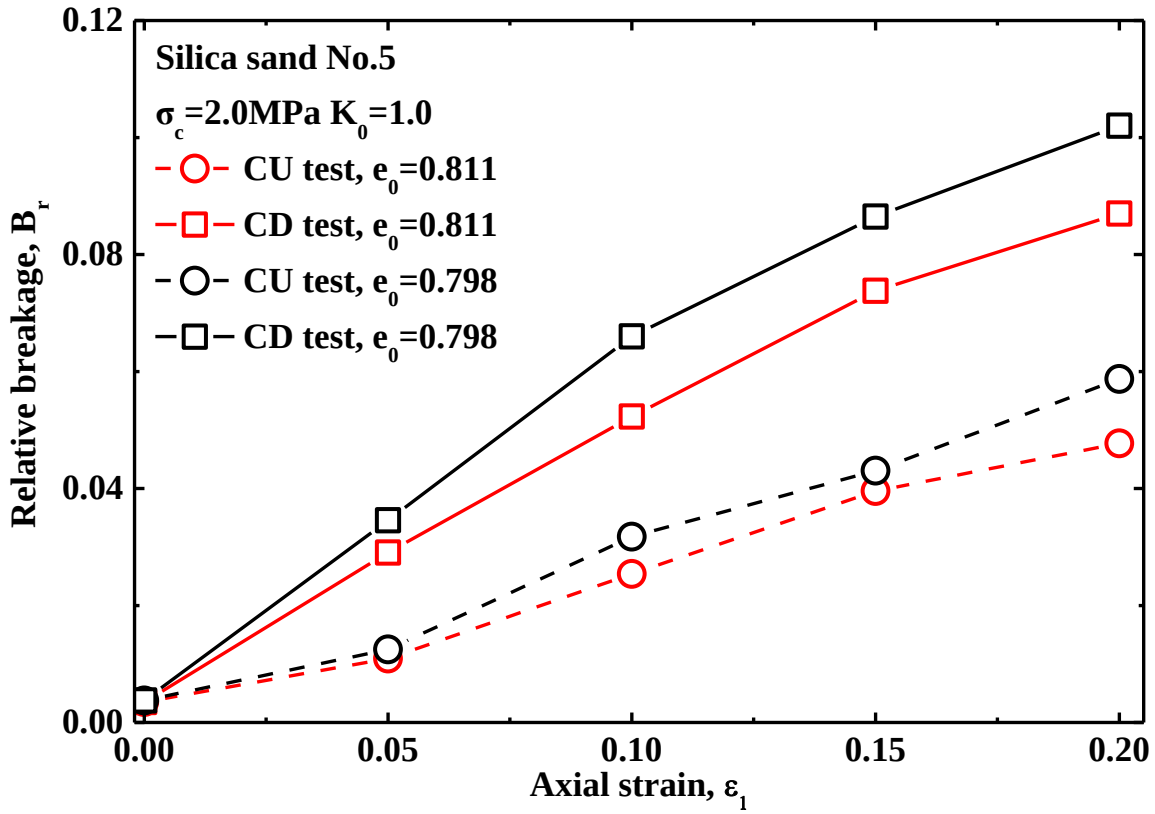

Figure 4.22 B_r-ε_1 relation from CU tests (σ_c=2.0MPa K_0=1.0, e_0=0.798 & 0.811)

4.5.3 The Influence of Initial Stress Anisotropy on Particle Breakage

Considering the effect of initial consolidation stress ratio ($K_0 \neq 1.0$ as stress anisotropy) on particle breakage, many tests with two different initial consolidated stress ratios under same mean effective stress (p'=2MPa) after consolidation were carried out to investigate the characteristics of particle breakage subjected to two different initial consolidated stress ratios. One kind of specimens was consolidated to confining pressure σ_c=1.5MPa in K_0=0.5 where at the end of consolidation the stress state reached the mean effective stress p'=2MPa and deviator stress q=1.5MPa existed but the other kind of specimens was isotropically consolidated up to 2MPa (K_0=1.0) where the stress state reached the mean effective stress p'=2MPa and deviator stress q=0MPa as shown in Figure 4.3. Both kinds of specimens were sheared under confining pressure σ_c=1.5MPa in K_0=0.5 and under confining pressure σ_c=2MPa in K_0=1.0 separately, where the two kinds of initial consolidation stress states on specimens have an influence on particle breakage.

The triaxial tested results under confining pressure σ_c=1.5MPa in K_0=0.5 and confining pressure σ_c=2MPa in K_0=1.0 are shown in Figure 4.23, where the shearing on specimens under σ_c=1.5MPa in K_0=0.5 was seen to start from the initial deviator stress q=1.5MPa, and shearing was to start after isotropic consolidation under confining pressure σ_c=2.0MPa (K_0=1.0), being up to same mean effective stress at the end of consolidation in both cases. The deviator stress on specimens with initial stress anisotropy (σ_c=1.5MPa K_0=0.5) is found to increase almost up to be constant with increasing axial strain but on the specimens without initial stress anisotropy (σ_c=2.0MPa K_0=1.0) the deviator stress tends to increase much more sharply in comparison with the deviator stresses on the specimens with initial stress anisotropy (σ_c=1.5MPa K_0=0.5). The deviator stress under stress isotropy (σ_c=2.0MPa K_0=1.0) is seen in CD tests to be higher than those under stress anisotropy (σ_c=1.5MPa K_0=0.5) expect a short stage at the beginning of shearing with an initial deviator. However, in CU tests the initial stress anisotropy on specimens has an important influence on development of deviator stress which is larger than those on specimens with initial stress isotropy within very large range of axial stress. The volume changes of the specimens with initial stress isotropy (σ_c=2.0MPa K_0=1.0) are found to be much more substantial in comparison with the volume changes of the specimens with initial stress anisotropy (σ_c=1.5MPa K_0=0.5) as shown in Figure 4.23(b). The higher excess PWPs were generated in the specimens with initial stress isotropy (σ_c=2.0MPa K_0=1.0) in comparison with the excess PWPs in the initial stress anisotropic specimens (σ_c=1.5MPa K_0=0.5) as shown in Figure 4.23(c). It may be caused by the combined influence of confining pressure and stress isotropy on soil behavior, which can be illustrated by that the dilatancy behavior was to be depressed more substantially during shearing under 2MPa confining pressure than 1.5MPa confining pressure on specimens with an initial stress anisotropy. Figure 4.23(d) shows the stress paths during shearing with initial stress anisotropy (σ_c=1.5MPa K_0=0.5) and initial stress isotropy (σ_c=2.0MPa K_0=1.0).

The grain size distribution curves with initial stress anisotropy (σ_c=1.5MPa K_0=0.5) are

shown in Figure 4.24 for CD tests and Figure 4.25 for CU tests, where particle breakage increases with increasing axial strain in evolution of grain size distribution curves. It is notable that particle breakage occurred just during anisotropic consolidation in an initial consolidation stress ratio K_0=0.5 as well. The grain size distribution curves under confining pressure σ_c=2.0MPa subjected to isotropic consolidation K_0=1.0 are shown in Figure 4.7 for CD tests and Figure 4.12 for CU tests.

Herein all grain size distribution curves were quantified by relative breakage as well as shown in Figure 4.24 and Figure 4.25. Figure 4.26 shows the relative breakage under initial stress anisotropy and isotropy. Figure 4.26(a) show relationship between relative breakage and axial strain under confining pressure σ_c=1.5MPa in K_0=0.5 and confining pressure σ_c=2.0MPa in K_0=1.0, where it is notable that particle breakage occurred during consolidation (same finding from Lade et al., 1996) and increases with increasing axial strain . Herein the initial stresses anisotropically consolidated to confining pressure σ_c=1.5MPa in K_0=0.5 resulted in more substantial particle breakage than that under the stresses isotropically consolidated to confining pressure σ_c=2.0MPa (K_0=1.0), which means that the initial deviator stress (σ_c=1.5MPa K_0=0.5) exerted on specimen has a more significant influence on particle breakage than the isotropic consolidation to a relatively higher confining pressure (σ_c=2.0MPa K_0=1.0). Shearing is much more important in causing particle breakage than isotropic consolidation, which was also found by Yamamuro and Lade (1996).

In CD tests, particle breakage is found to increase in reduced increments approximately. And particle breakage is found to be more substantial in increment on specimens with initial stress isotropic consolidation (σ_c=2.0MPa K_0=1.0) in comparison with that on specimens with initial stress anisotropic consolidation (σ_c=1.5MPa K_0=0.5) expect the particle breakage induced just during consolidation, which is related to the mechanical behavior in development of stress-strain as shown in Figure 4.23(a). The difference of particle breakage during shearing between the initial stress anisotropic consolidation (σ_c=1.5MPa K_0=0.5) and the initial stress isotropic consolidation (σ_c=2.0MPa K_0=1.0) is shown to increase with increasing axial strain, which means that the higher confining pressure in isotropic consolidation (σ_c=2.0MPa K_0=1.0) has a more substantial and effective influence on particle breakage than the initial stress anisotropy with lower confining pressure (σ_c=1.5MPa K_0=0.5).

In CU tests, it is found that particle breakage increases approximately in increased increments with increasing axial strain. Particle breakage is seen clearly to be more substantial in increment on specimens with initial stress isotropy (σ_c=2.0MPa K_0=1.0) than that on specimens with initial stress anisotropy (σ_c=1.5MPa K_0=0.5) in addition to the particle breakage induced just during consolidation.

As shown in Figure 4.26(a), particle breakage in relative breakage is found to be more substantial in CD tests than that in CU tests and the difference of particle breakage in relative breakage between CD tests and CU tests is shown to increase with increasing

axial strain, which are related to the increased difference of deviator stress between CD tests and CU tests with the increase of axial strain. The difference of particle breakage in relative breakage between CD tests and CU tests is slightly more substantial under confining pressure σ_c =2.0MPa in K_0 =1.0 than that under confining pressure σ_c=1.5MPa in K_0=0.5.

Figure 4.26(b) shows the relationship of relative breakage and mean effective stress under initial stress anisotropy and isotropy, where more particle breakage is found clearly to be caused during anisotropic consolidation than isotropic consolidation. Figure 4.26(c) shows the evolution of particle breakage in relative breakage against effective stress obliquity ratio under initial stress anisotropy and isotropy.

It can be concluded that based on consolidation to same mean effective stress (herein p'=2MPa), the anisotropic consolidation to confining pressure σ_c=1.5MPa in K_0=0.5 results in more particle breakage than the isotropic consolidation to confining pressure σ_c=2.0MPa. However, during shearing the higher confining pressure after isotropic consolidation (σ_c=2.0MPa K_0=1.0) has more significant influence on particle breakage than initial stress anisotropy with a relatively lower confining pressure (σ_c=1.5MPa K_0=0.5).

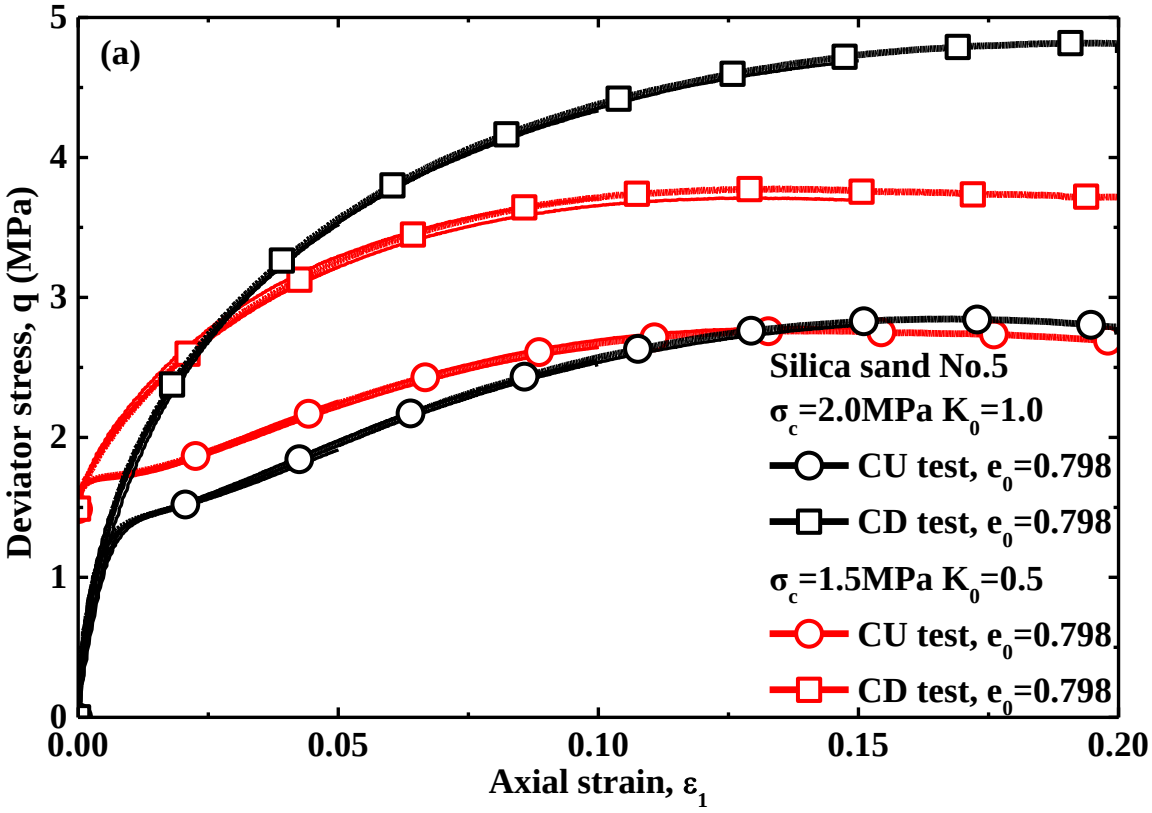

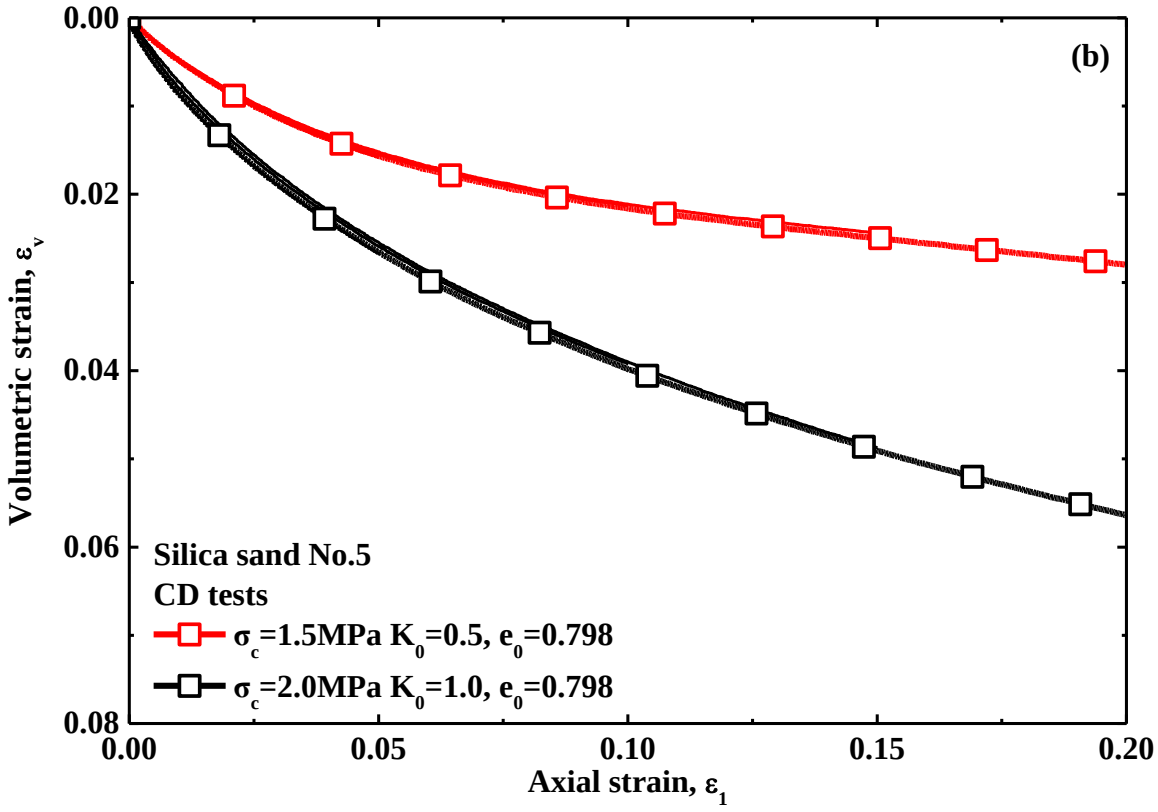
(b)
Volumetric strain, ε_v
Axial strain, ε_1
0.00
0.02
0.04
0.06
0.08
0.00
0.05
0.10
0.15
0.20
Silica sand No.5
CD tests
σ_c=1.5MPa K_0=0.5, e_0=0.798
σ_c=2.0MPa K_0=1.0, e_0=0.798

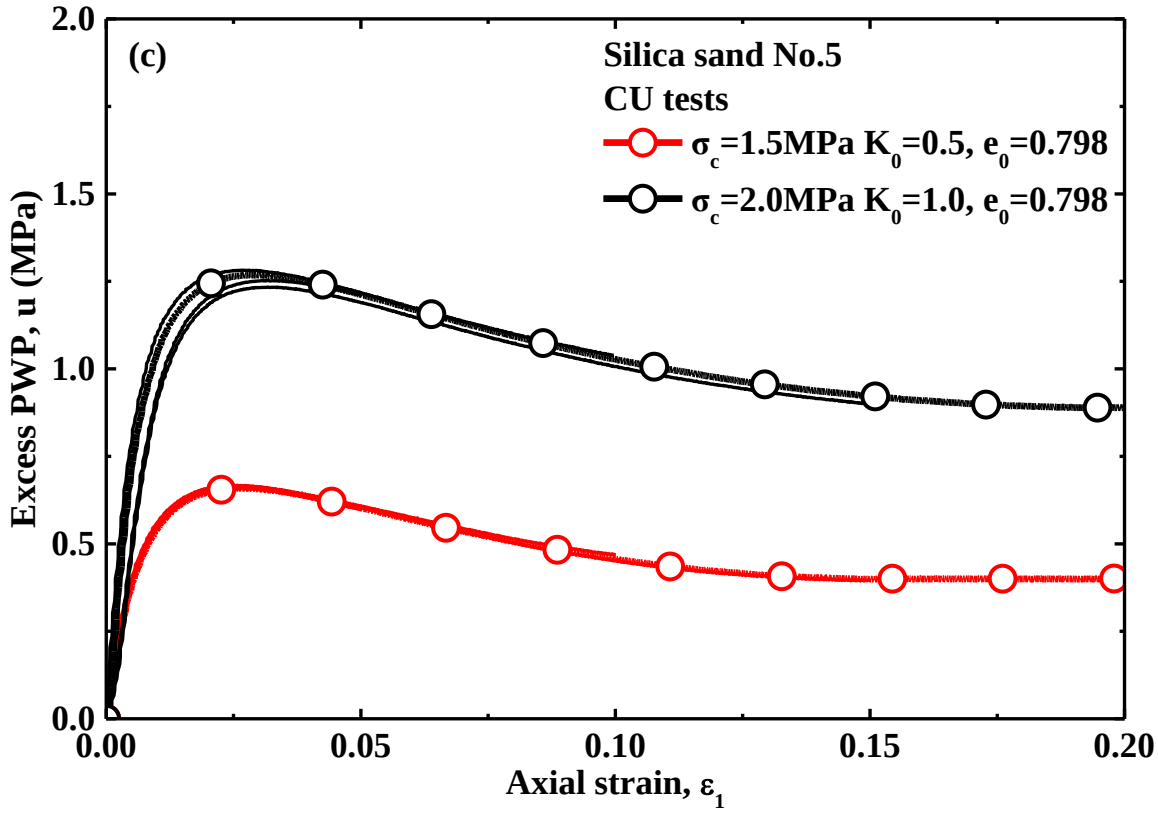
(c)
Excess PWP, u (MPa)
Axial strain, ε_1
0.0
0.5
1.0
1.5
2.0
0.00
0.05
0.10
0.15
0.20
Silica sand No.5
CU tests
σ_c=1.5MPa K_0=0.5, e_0=0.798
σ_c=2.0MPa K_0=1.0, e_0=0.798

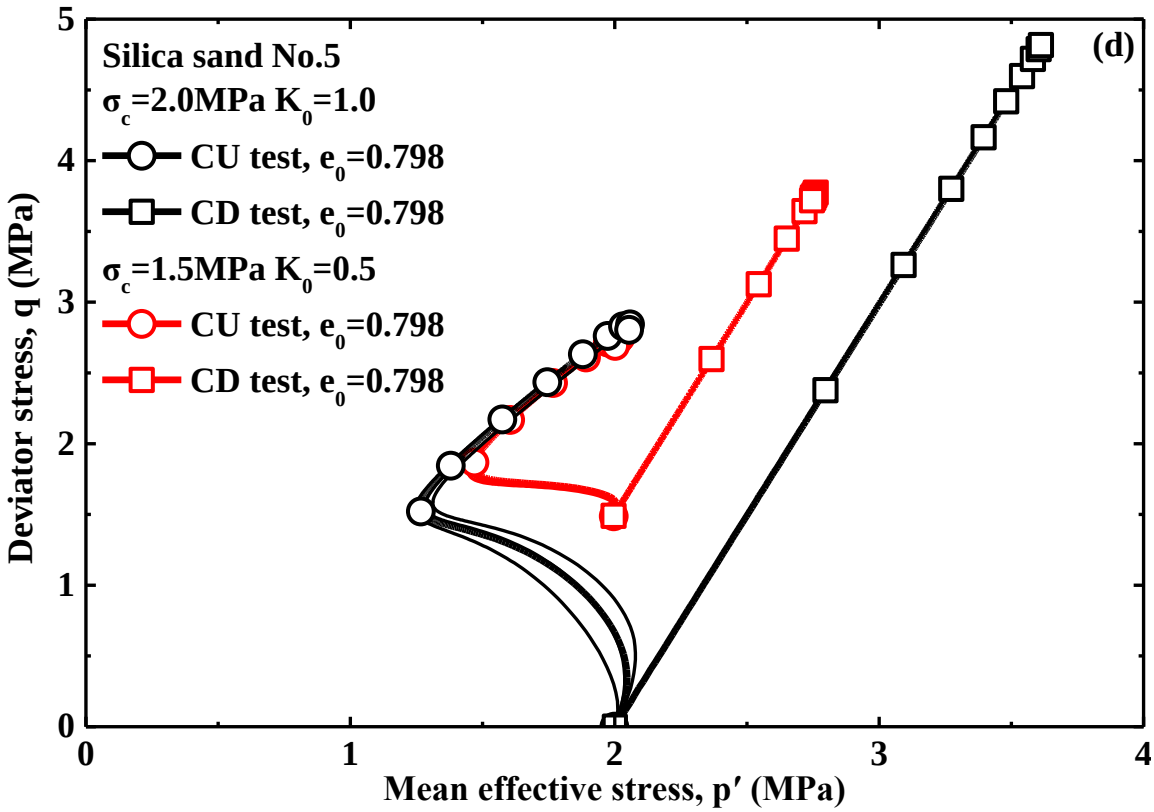

Figure 4.23 Triaxial test results (σ_c=1.5MPa K_0=0.5 & σ_c=2.0MPa K_0=1.0)

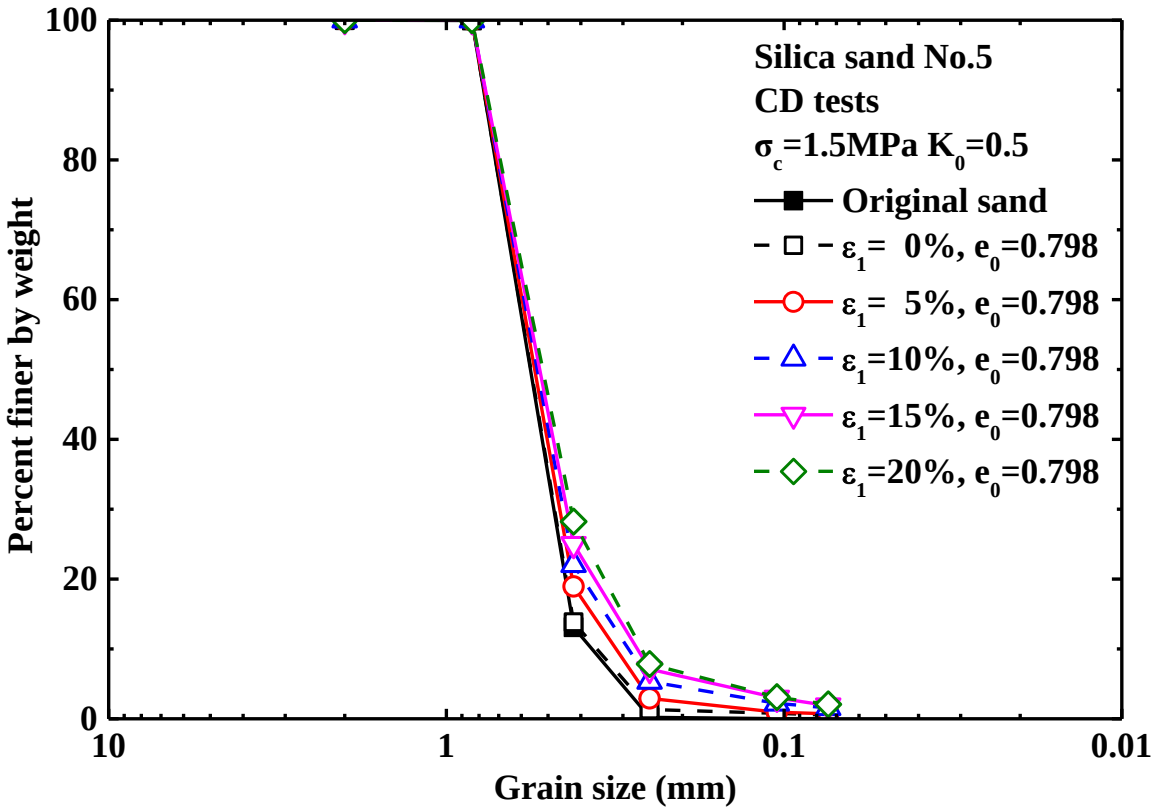

Figure 4.24 Grain size distribution curves from CD tests (σ_c=1.5MPa K_0=0.5, e_0=0.798)

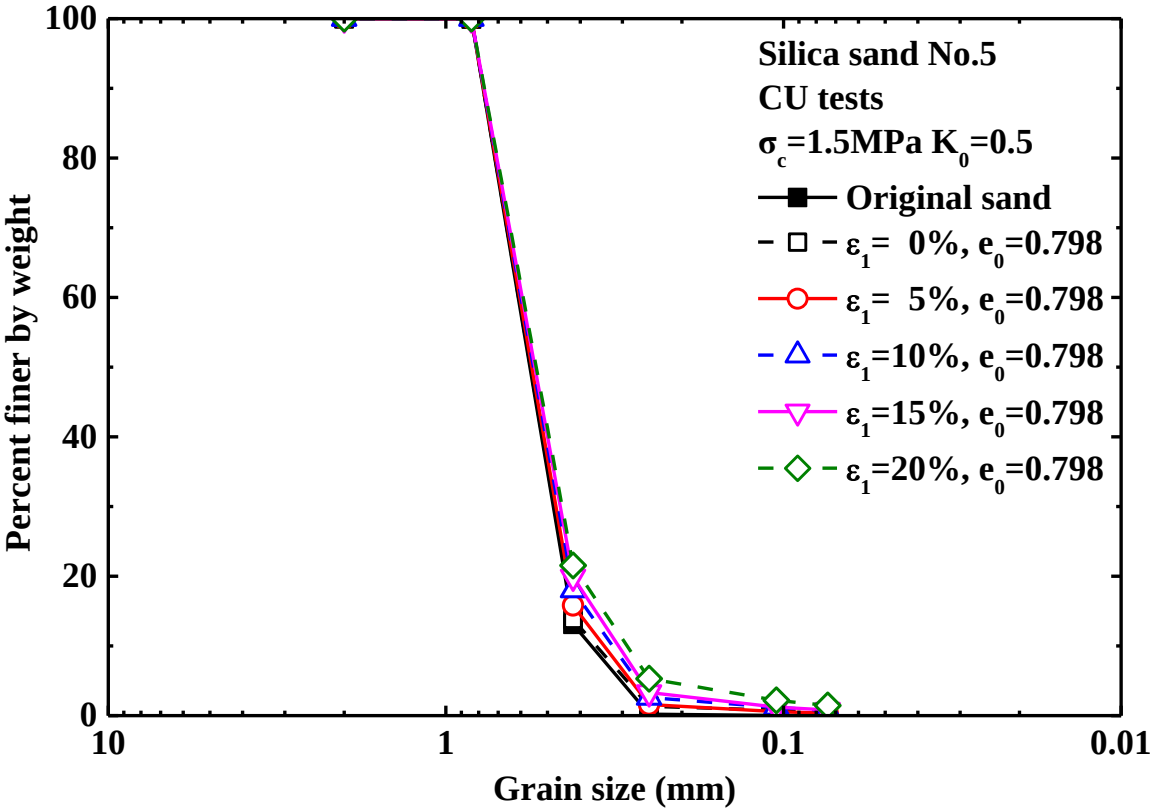

Figure 4.25 Grain size distribution curves from CU tests (σ_c=1.5MPa K_0=0.5, e_0=0.798)

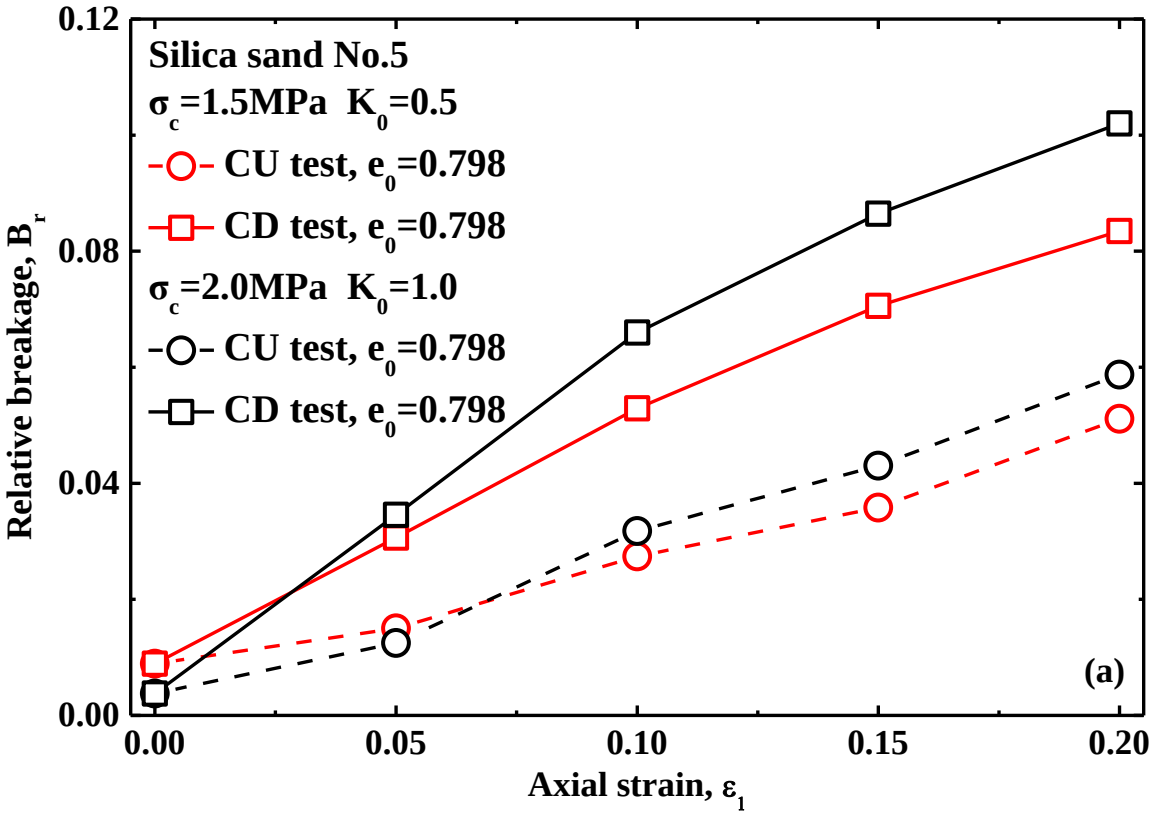

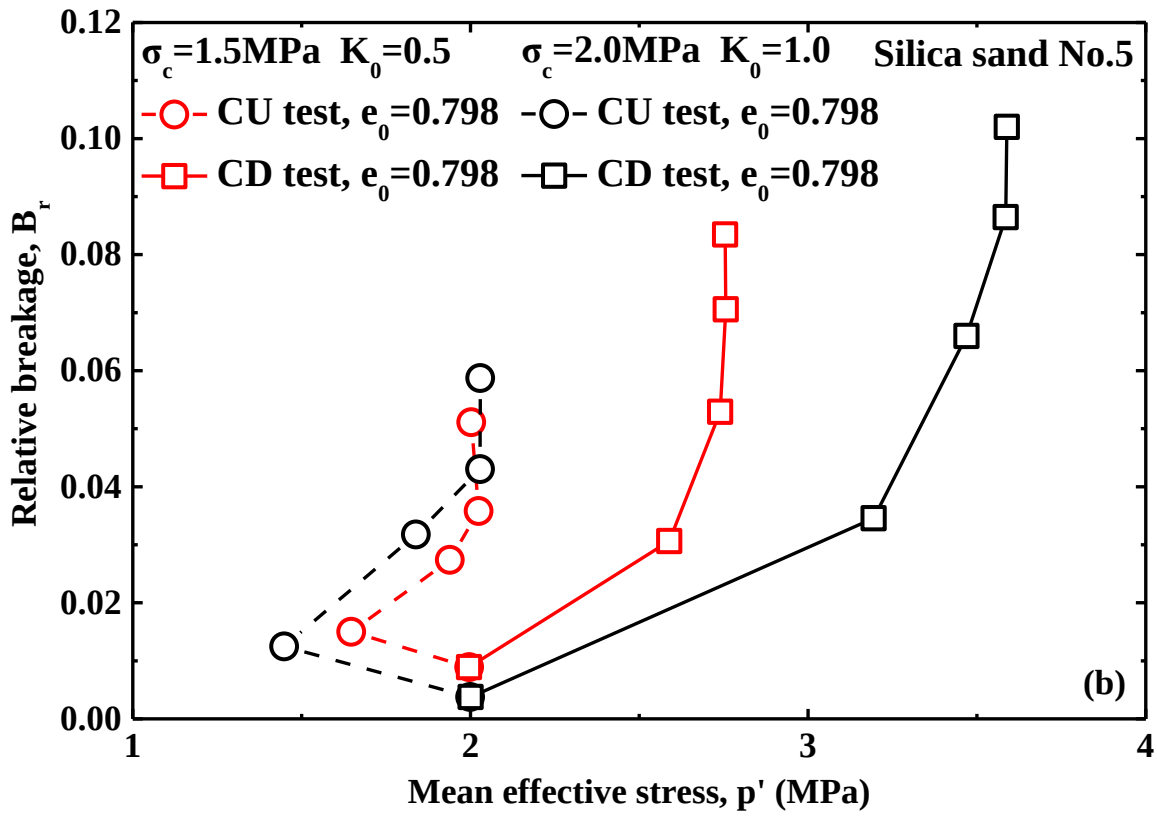

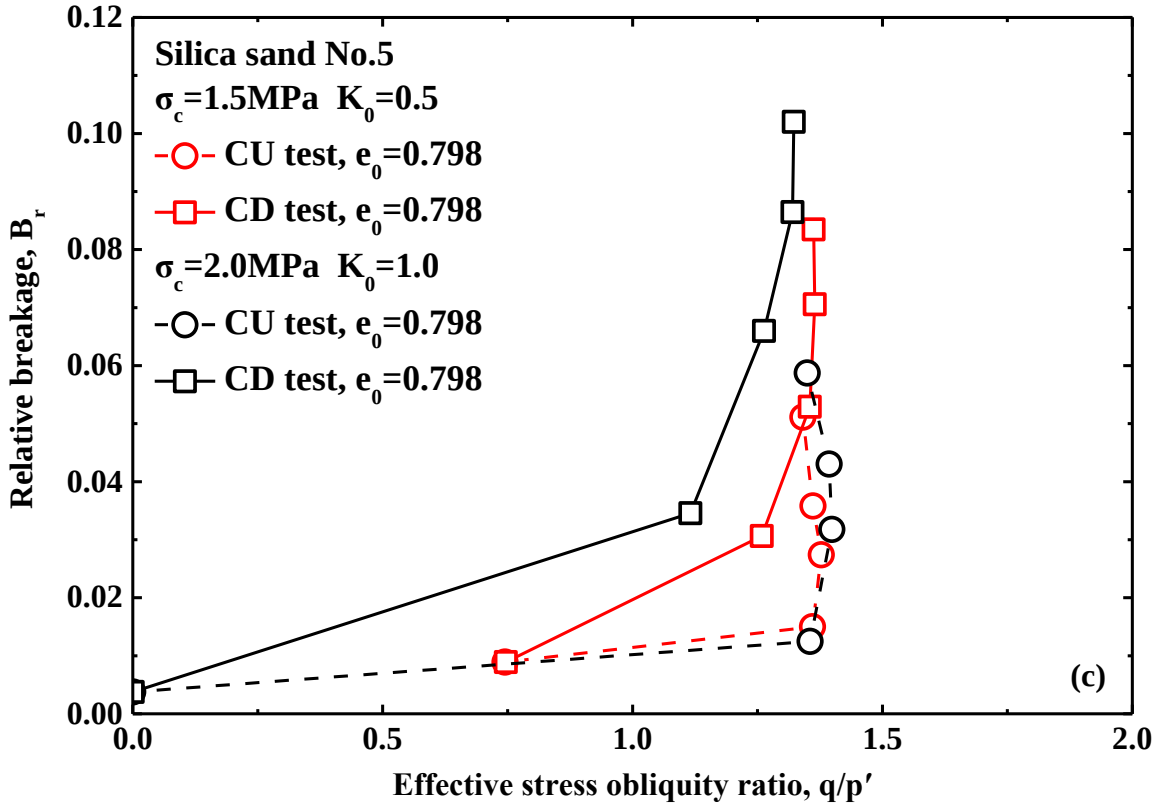

Figure 4.26 Relative breakage under initial stress anisotropy and isotropy

4.5.4 The Influence of Cyclic Loading on Particle Breakage

The loading on the materials of dam can be regarded as a cyclic loading as water table in reservoir behind a dam changes up and down slowly in an elevation. The cyclic loading on specimens was employed in triaxial tests to investigate its influence on the characteristics of particle breakage. Herein the triaxial tests were carried out to axial strain 20% and then terminated under designated cycle numbers of cyclic loading such as 0, 2, 5, 10 and 20 times in order. All specimens after shearing were kept in an oven to dry and the relevant grain size distribution curves were obtained by sieve analysis of oven-dried material. The relative breakage was used to quantify the extent of particle breakage according to relevant grain size distribution curves.

Figure 4.27 shows the triaxial tests subjected to cyclic loading, where the cyclic loading was performed in various cycle numbers as the axial strain reached 20% in triaxial tests. It is found that additional axial strains were produced simultaneously during cyclic loading under high pressure, which has a significant influence on particle breakage. And the volume change during cyclic loading is found to be more substantial than that during monotonic loading, which may be related to particle breakage induced by cyclic loading.

The grain size distribution curves subjected to cyclic loading are shown in Figure 4.28, where it can be seen that the grain size distribution curves evolved towards the increase of fines content with increasing cycle numbers of cyclic loading. All grain size distribution curves were quantified by relative breakage in description of extent of particle breakage. Figure 4.29 shows the $B_r - N$ relationship under cyclic loading, where particle breakage in relative breakage is found to increase in down concavity with increasing cycle number of cyclic loading. Particle breakage is found to increase in up concavity with increasing axial strain but particle breakage has a very dramatic increase after cycle numbers N=5 with increasing axial strain.

Under cyclic loading even without any change of amplitude of cyclic loading, particle breakage was found to increase with increasing cycle numbers of cyclic loading and to be related to additional axial strain or volume change induced during cyclic loading, which are consistent with the finding from Donohue et al. (2009). The mechanism of particle breakage caused by cyclic loading may be that during cyclic loading the contact force network among soil particles would be changed by the progressive rearrangement of soil particles including damage, rotation and attrition, which would cause more particle breakage.

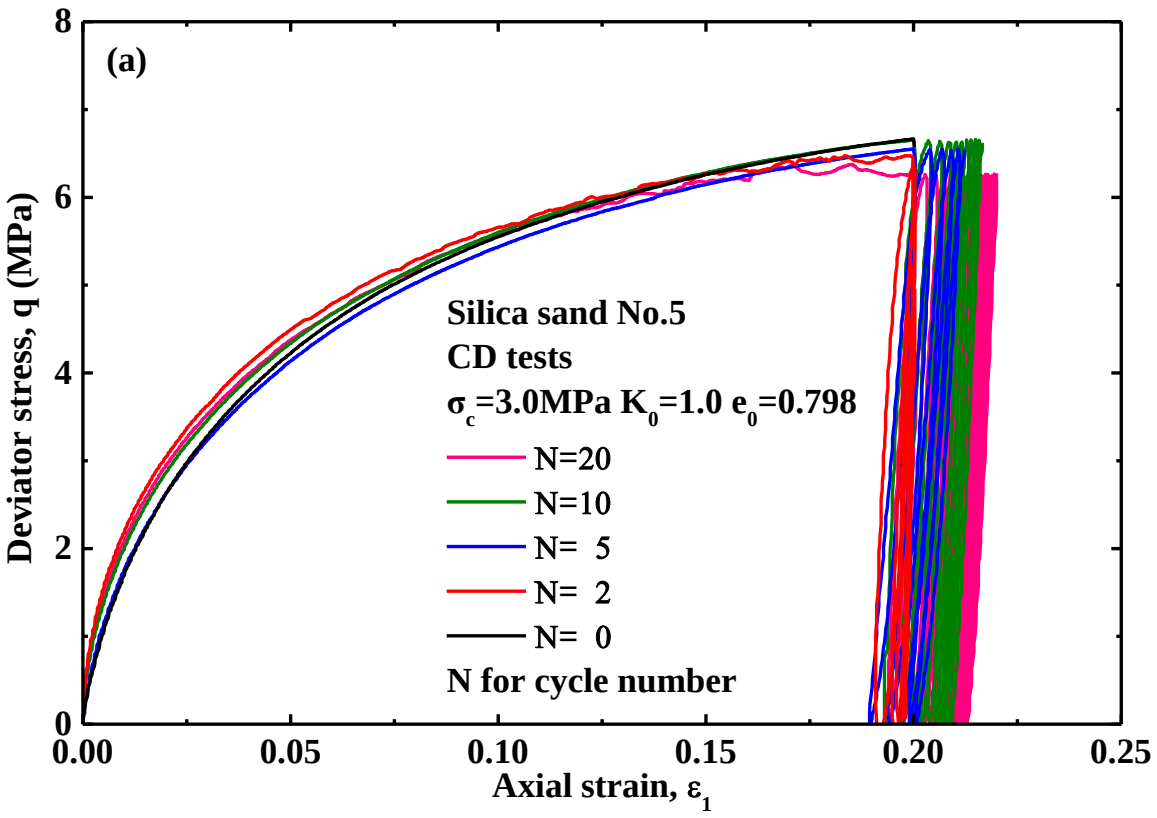
(a)
Deviator stress, q (MPa)
Axial strain, ε1
Silica sand No.5
CD tests
σc=3.0MPa K0=1.0 e0=0.798
N=20
N=10
N= 5
N= 2
N= 0
N for cycle number

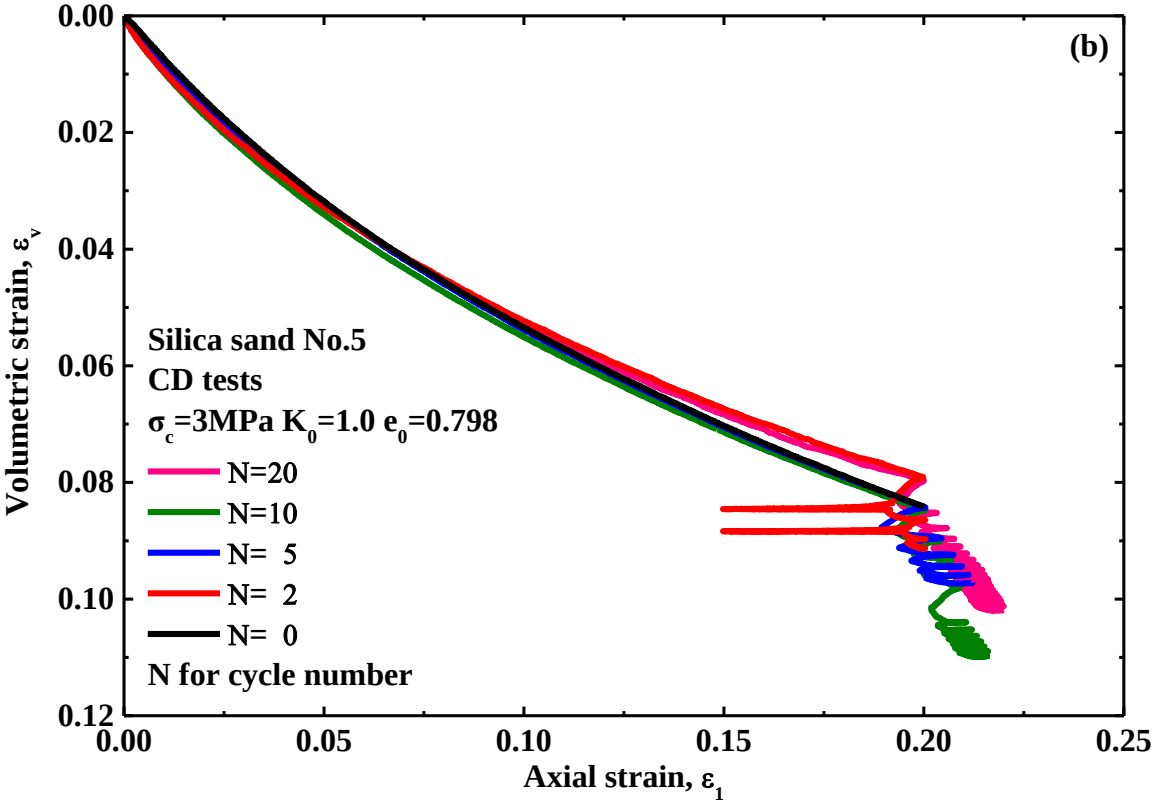
(b)
Volumetric strain, εv
Axial strain, ε1
Silica sand No.5
CD tests
σc=3MPa K0=1.0 e0=0.798
N=20
N=10
N= 5
N= 2
N= 0
N for cycle number

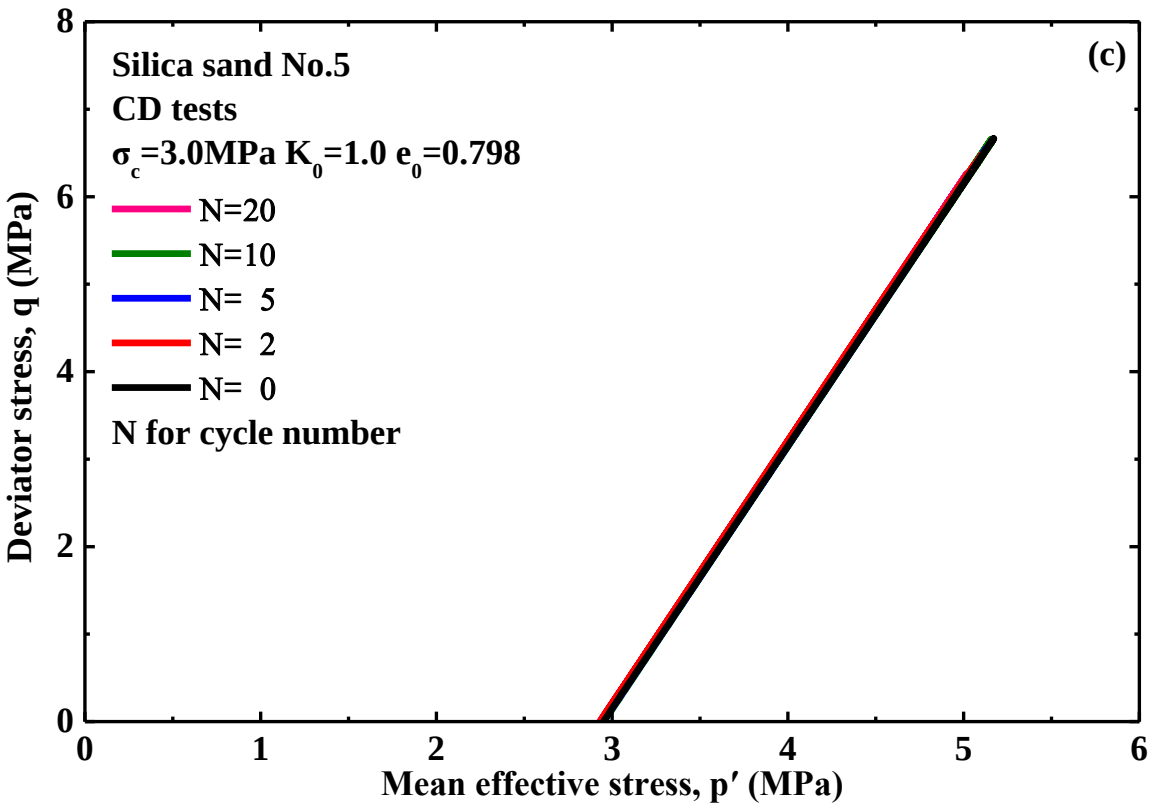

Figure 4.27 Triaxial test results under cyclic loading (σ_c=3.0MPa K_0=1.0, e_0=0.798)

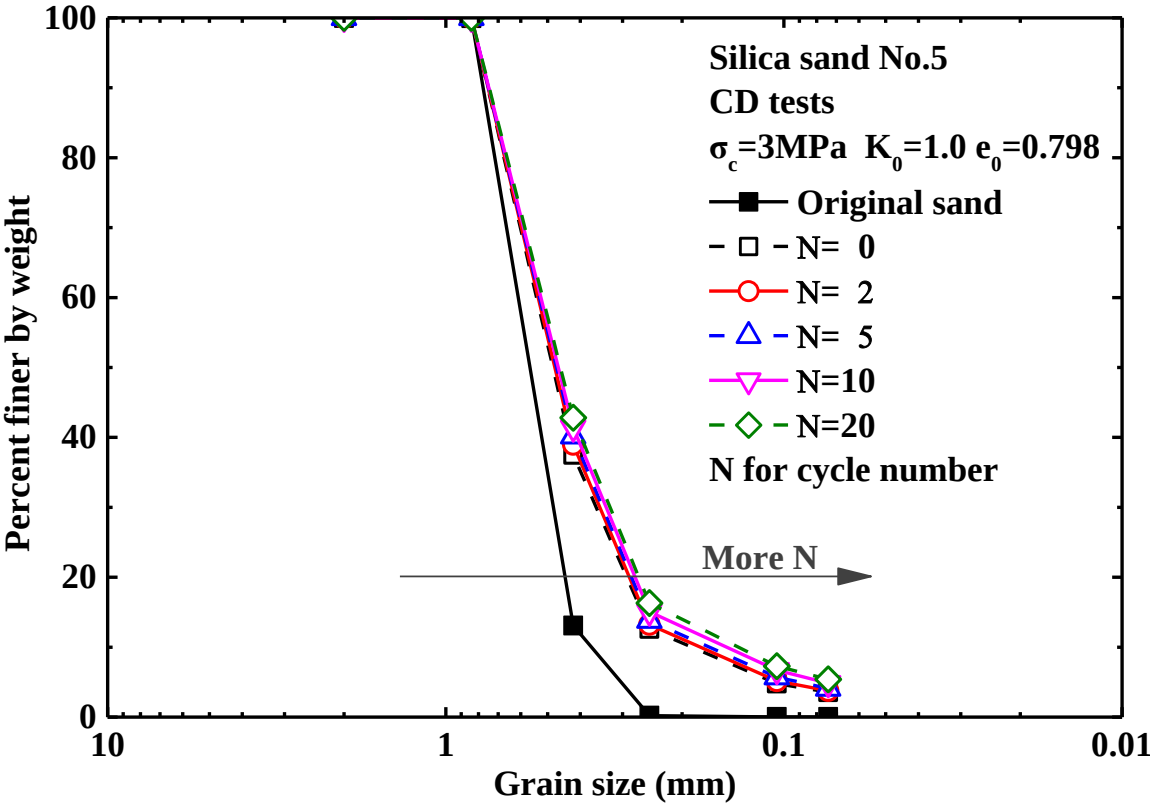

Figure 4.28 Grain size distribution curves under cyclic loading (σ_c=3.0MPa K_0=1.0, e_0=0.798)

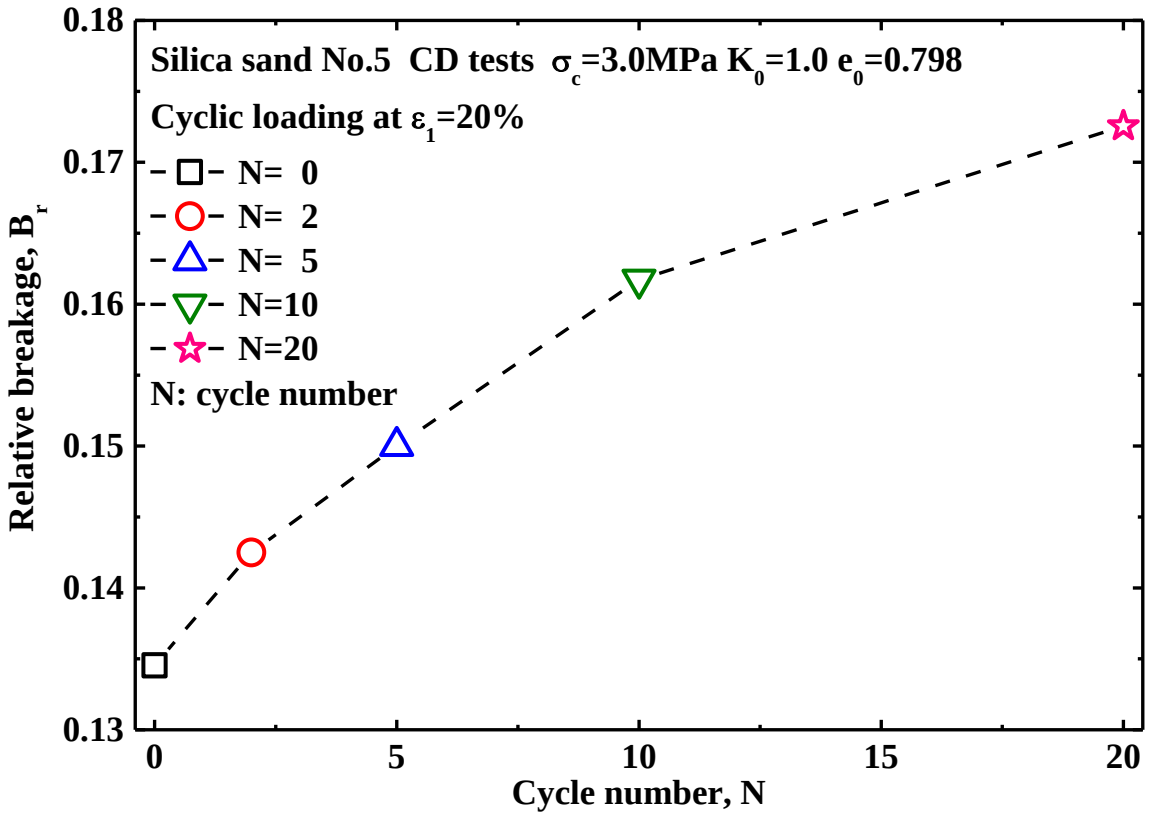

Figure 4.29 Br-N relation under cyclic loading (σ_c=3.0MPa K_0=1.0, e_0=0.798)

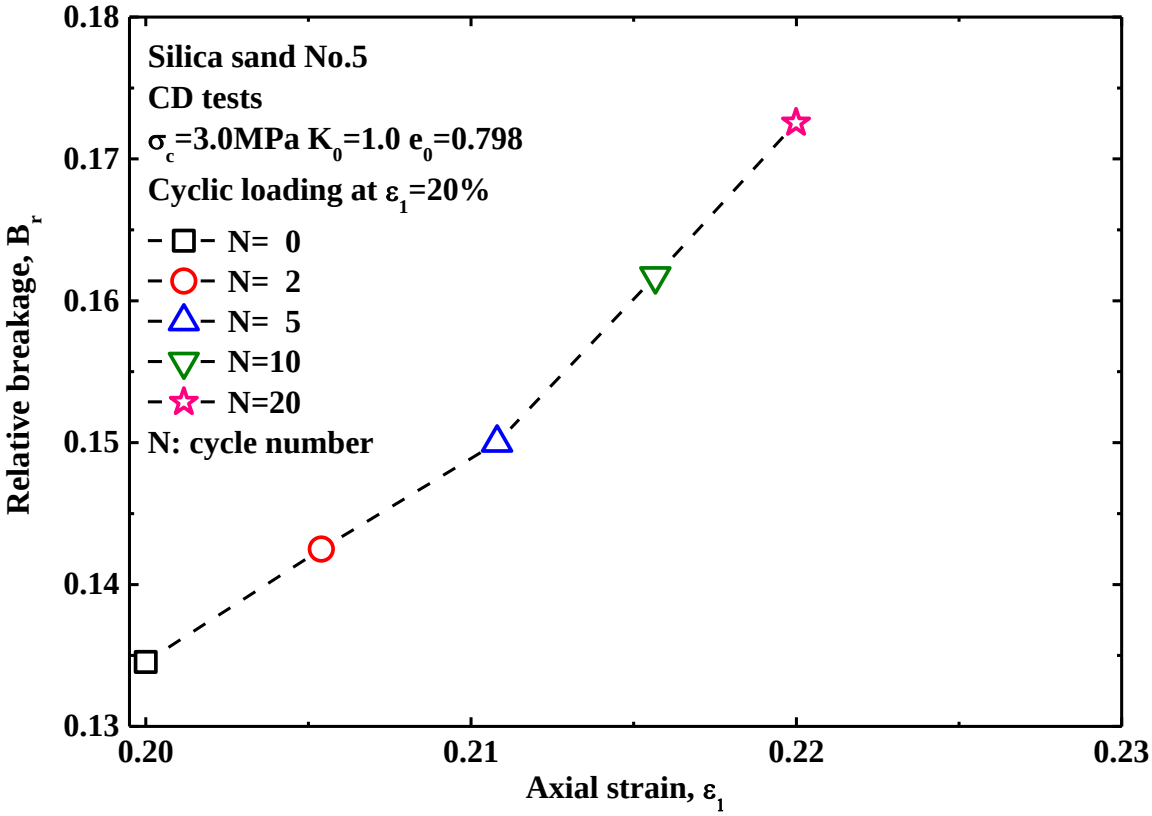

Figure 4.30 B_r-ε_1 relation under cyclic loading (σ_c=3.0MPa K_0=1.0, e_0=0.798)

4.5.5 The Influence of Unloading-reloading Process on Particle Breakage

The unloading-reloading process during shearing has an important influence on soil behavior especially under high pressure. The unloading-reloading process during shearing was employed in triaxial tests under high pressure to investigate the characteristics of particle breakage. All triaxial tests under high pressure were terminated at axial strain 20% with one time unloading-reloading process at designated axial strain from 5%, 10% and 15% separately or three times unloading-reloadings process at 5%, 10% and 15%.

The CD tested results under unloading-reloading process during shearing are shown in Figure 4.31, where stress-strain curves and volume change during unloading-reloading process are given during shearing. The stress-strain curves with unloading-reloading during shearing at different axial strains are found to be consistent approximately but the unloading-reloading during shearing is found to result in more contractancy in volume change in comparison with the volume change without unloading-reloading during shearing. More contractive behavior under unloading-reloading condition may be caused by particle breakage induced during unloading-reloading process in shearing. However, the resilience moduli are seen to be different especially the resilience moduli under one time unloading-reloading condition and three times unloading-reloadings condition.

All grain size distribution curves were measured after testing by sieving the materials of specimen after shearing. Figure 4.32 shows the grain size distribution curves under unloading-reloading conditions, which were quantified by relative breakage as shown in Figure 4.33. It can be seen clearly herein that the unloading-reloading process during shearing results in slight particle breakage. Particle breakage is found to increase with increasing axial strain where unloading-reloading was performed, which means herein that particle breakage with unloading-reloading at larger axial strain is more substantial. It may be related to the relatively higher deviator stress state during unloading-reloading at larger axial strain in shearing. However the increment of relative breakage for one time unloading-reloading process during shearing was found to decrease with increasing axial strain of one-time unloading-reloading, which means that particle breakage increases in reduced increments with increasing axial strain of one-time unloading-reloading. The particle breakage under three times unloading-reloadings at 5%, 10% and 15% during shearing is seen to be the most substantial as shown in Figure 4.33, consequently it can be concluded that the more times unloading-reloadings results in more particle breakage.

Unloading-reloading process during shearing was employed as well in triaxial tests under Consolidated Undrained (CU) condition to investigate its influence on characteristics of particle breakage. All CU tests were terminated at axial strain 20% with one time unloading-reloading at 5%, 10% and 15% separately or three times unloading-reloadings process at 5%, 10% and 15%.

Figure 4.34 shows the CU tests results subjected to unloading-reloading during shearing,

where the stress strain curves and excess PWPs are given herein. It is found herein that the one-time unloading-reloading at relatively small axial such 5% and 10% during shearing has some influence on stress-strain curves. The three-time unloading-reloadings process during shearing has a significant influence on stress-strain curves in reduction especially at larger axial strain. However the unloading-reloading process during shearing has a very significant influence on excess pore water pressure, which is found to increase clearly during and after unloading-reloading process in comparison with the excess pore water pressure without unloading-reloading process during shearing. The development of excess pore water pressure under three-time unloading-reloading process during shearing is seen to be same approximately as those under one-time unloading-reloading process during shearing.

The relevant grain size distribution curves related to CU tests were acquired by sieving the materials of specimens after shearing as shown in Figure 4.35. The relative breakage was introduced to quantify all grain size distribution curves in description of extent of particle breakage. The relationship between relative breakage and axial strain related to unloading-reloading process during shearing in CU tests is shown in Figure 4.36. It is revealed clearly herein that particle breakage increases in linearity approximately with increasing axial strain related to one-time unloading-reloading process during shearing, which is related to the development of deviator stresses with relative unloading-reloading process. The three-time unloading-reloading process during shearing is found to result in the most substantial particle breakage.

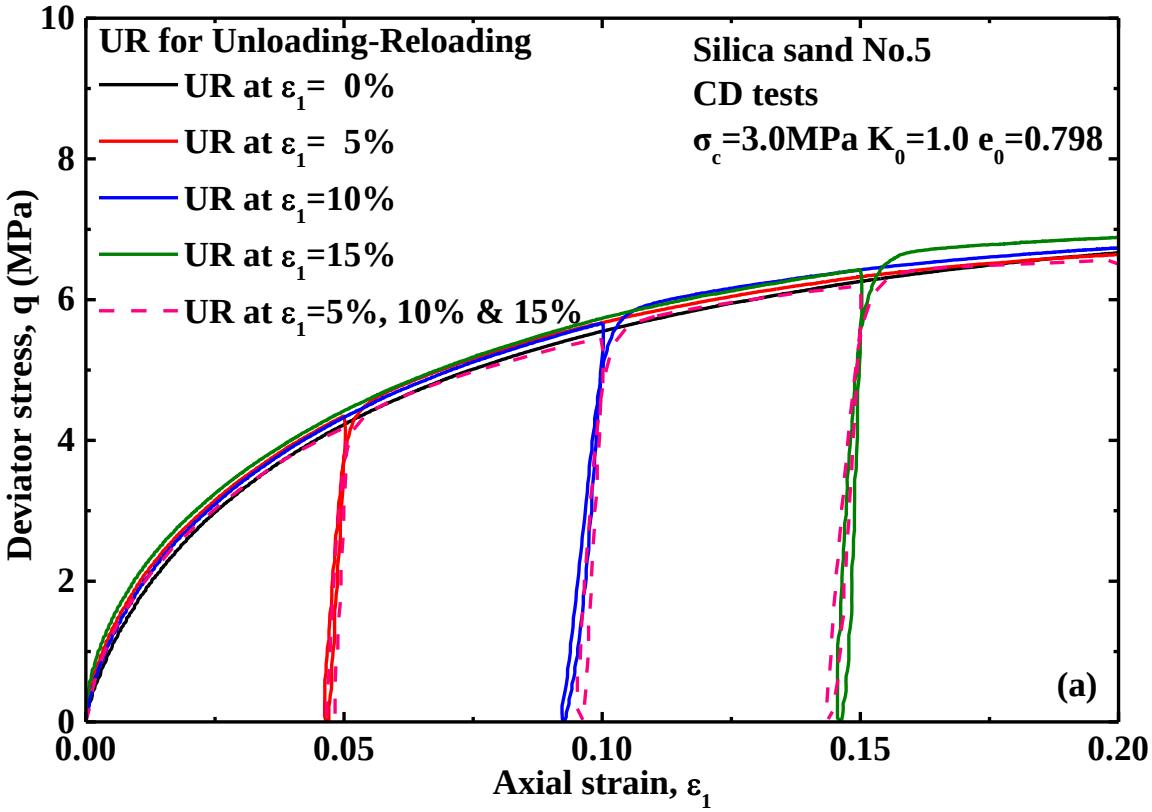

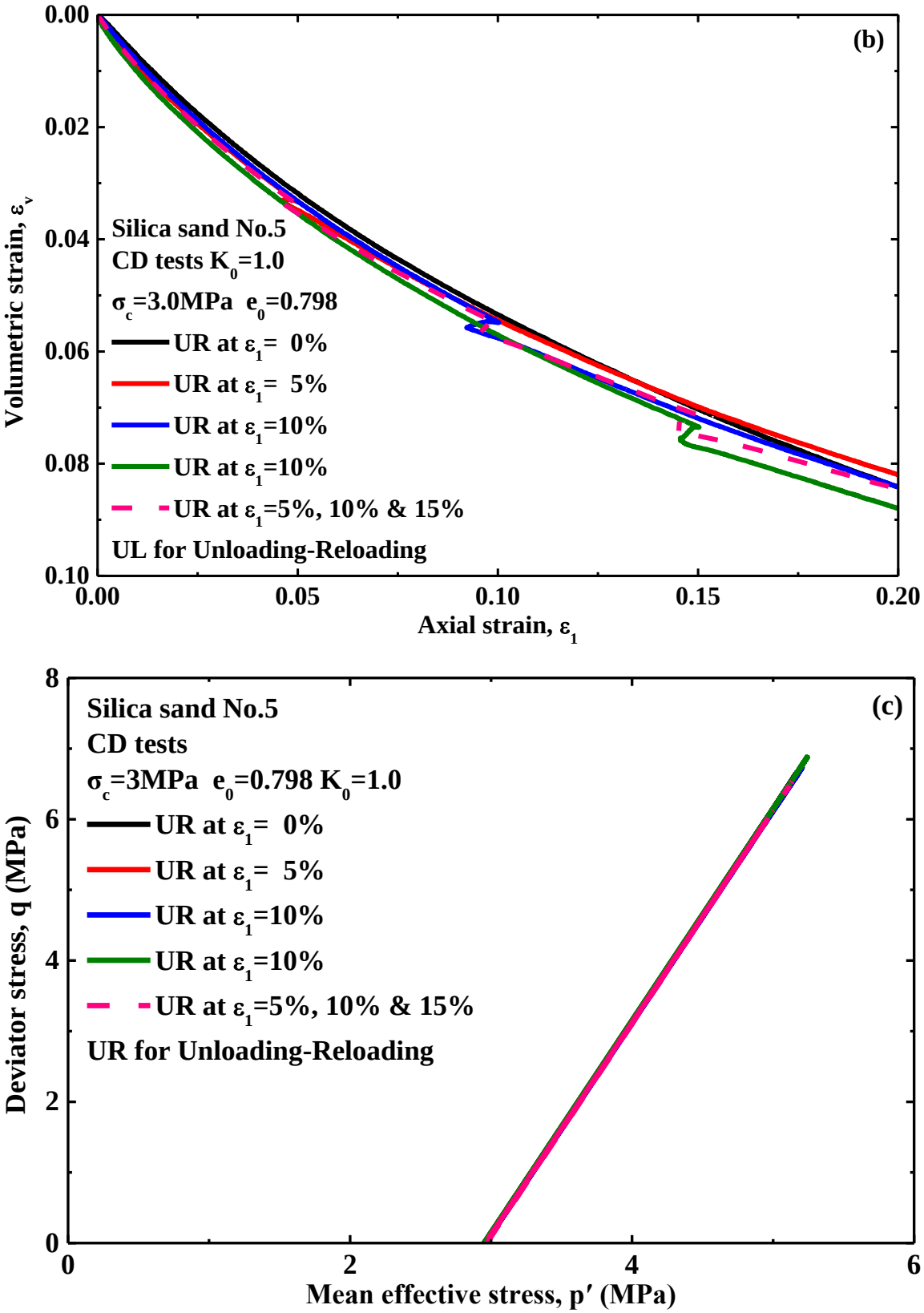

Figure 4.31 CD test results under unloading-reloading (σ_c=3.0MPa K_0=1.0, e_0=0.798)

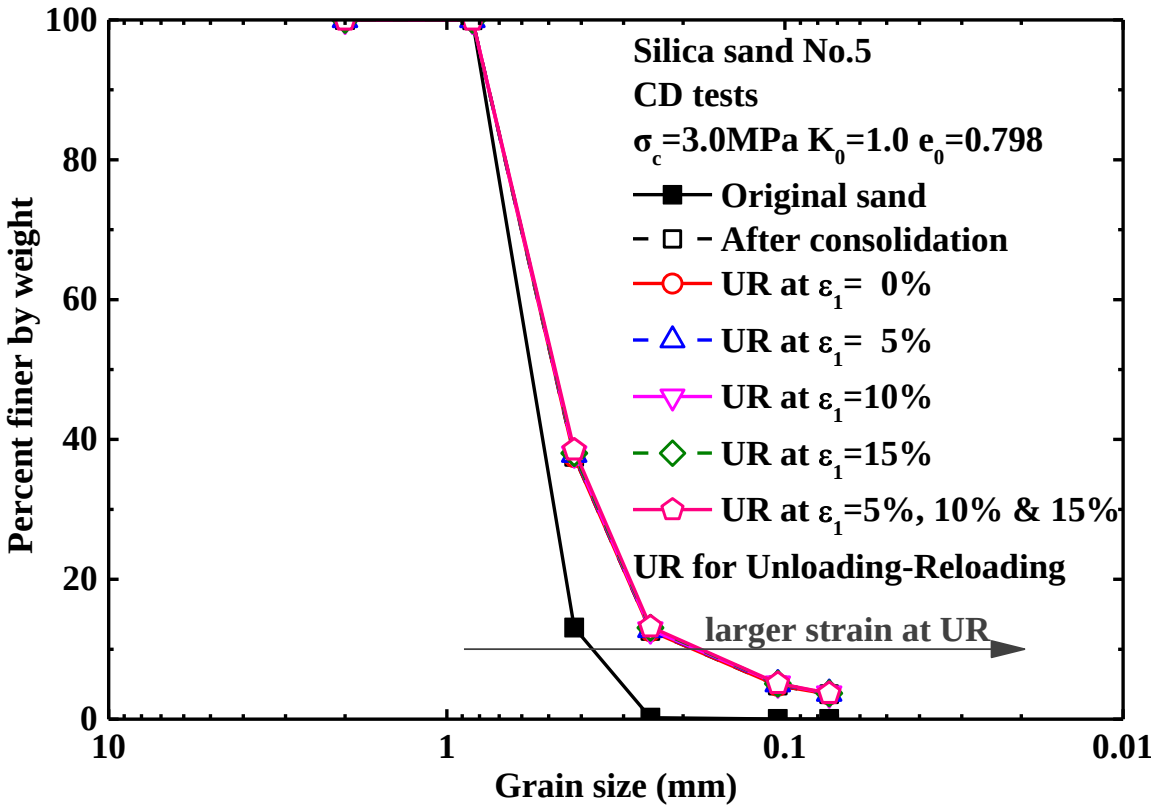

Figure 4.32 Grain size distribution curves from CD tests under unloading-reloading (σ_c=3.0MPa K_0=1.0, e_0=0.798)

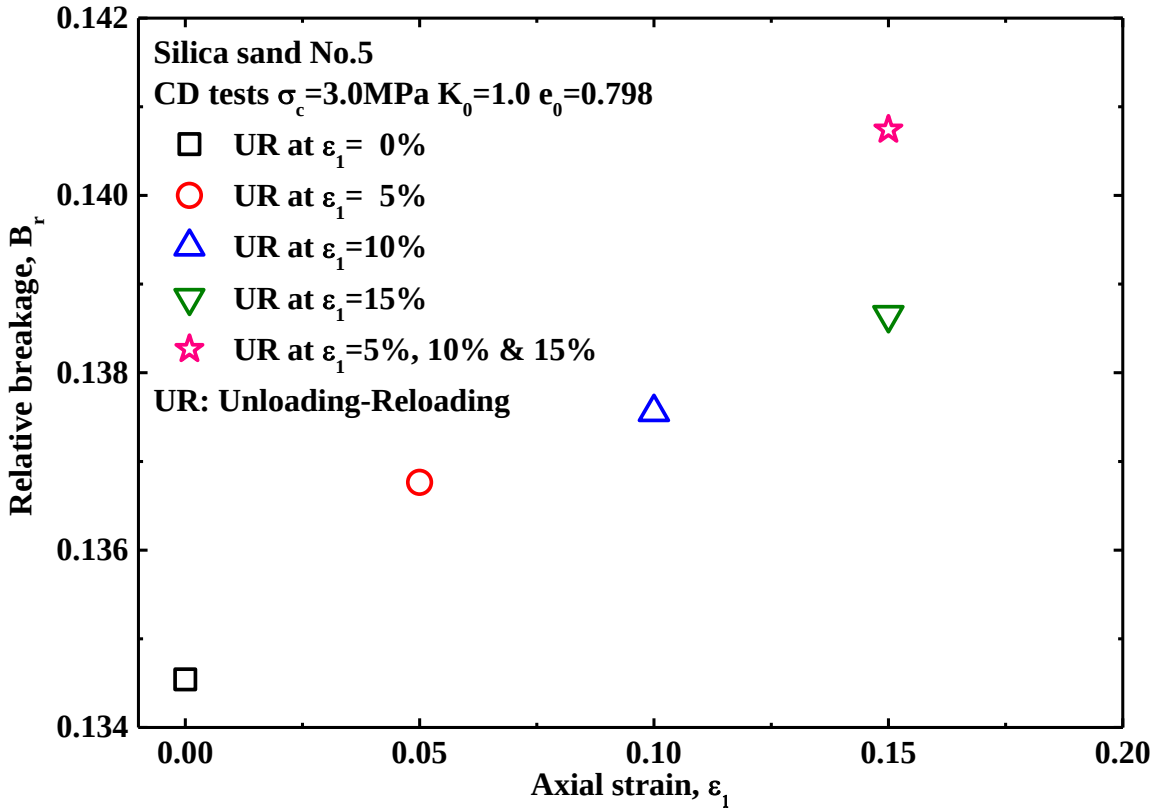

Figure 4.33 B_r-ε_1 relation from CD tests under unloading-reloading(σ_c=3.0MPa K_0=1.0, e_0=0.798)

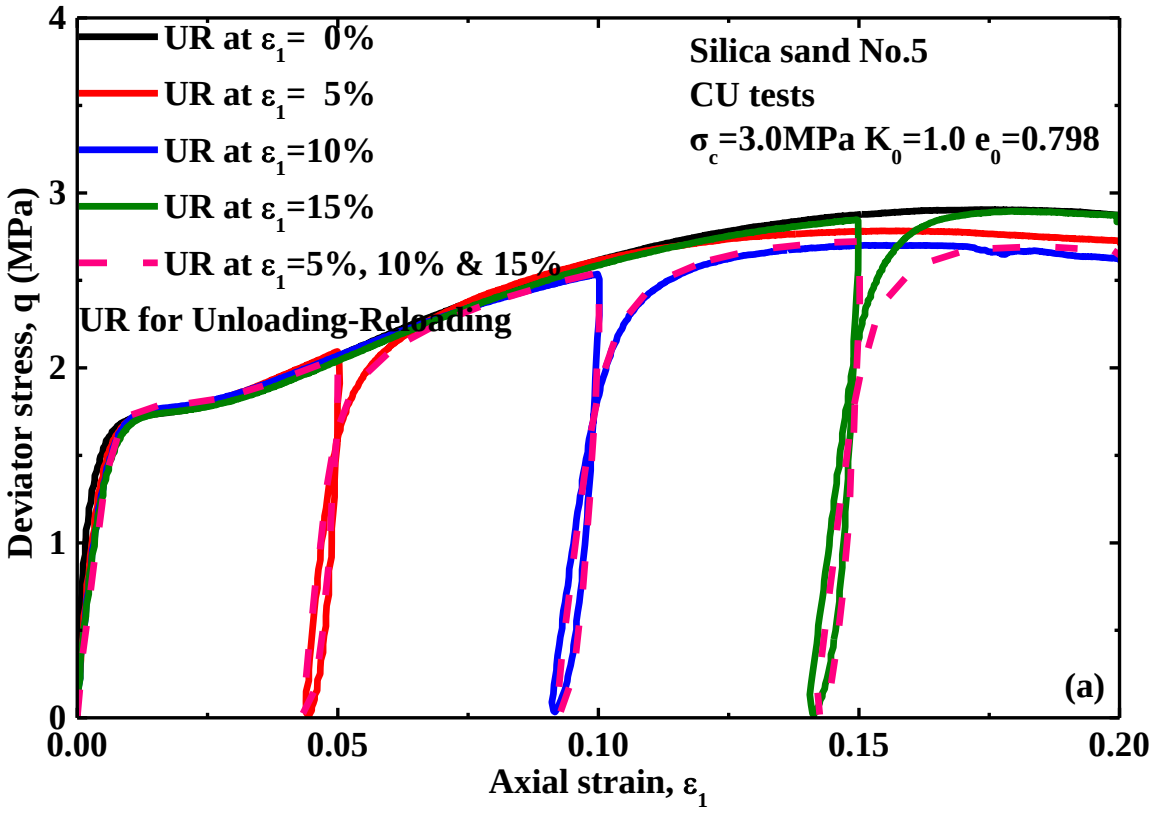
UR at ε1= 0%
UR at ε1= 5%
UR at ε1=10%
UR at ε1=15%
UR at ε1=5%, 10% & 15%
UR for Unloading-Reloading
Silica sand No.5
CU tests
σc=3.0MPa K0=1.0 e0=0.798
(a)
Deviator stress, q (MPa)
Axial strain, ε1
0
1
2
3
4
0.00
0.05
0.10
0.15
0.20

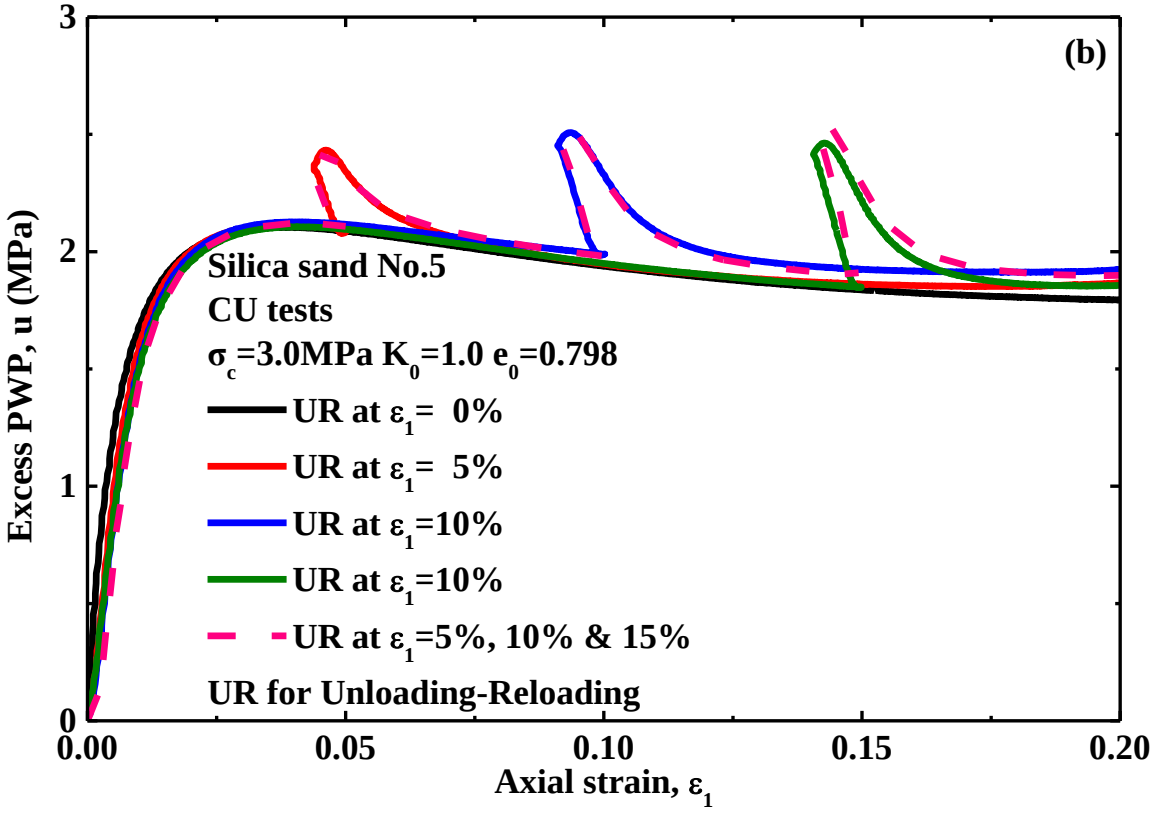
(b)
Silica sand No.5
CU tests
σc=3.0MPa K0=1.0 e0=0.798
UR at ε1= 0%
UR at ε1= 5%
UR at ε1=10%
UR at ε1=10%
UR at ε1=5%, 10% & 15%
UR for Unloading-Reloading
Excess PWP, u (MPa)
Axial strain, ε1
0
1
2
3
0.00
0.05
0.10
0.15
0.20

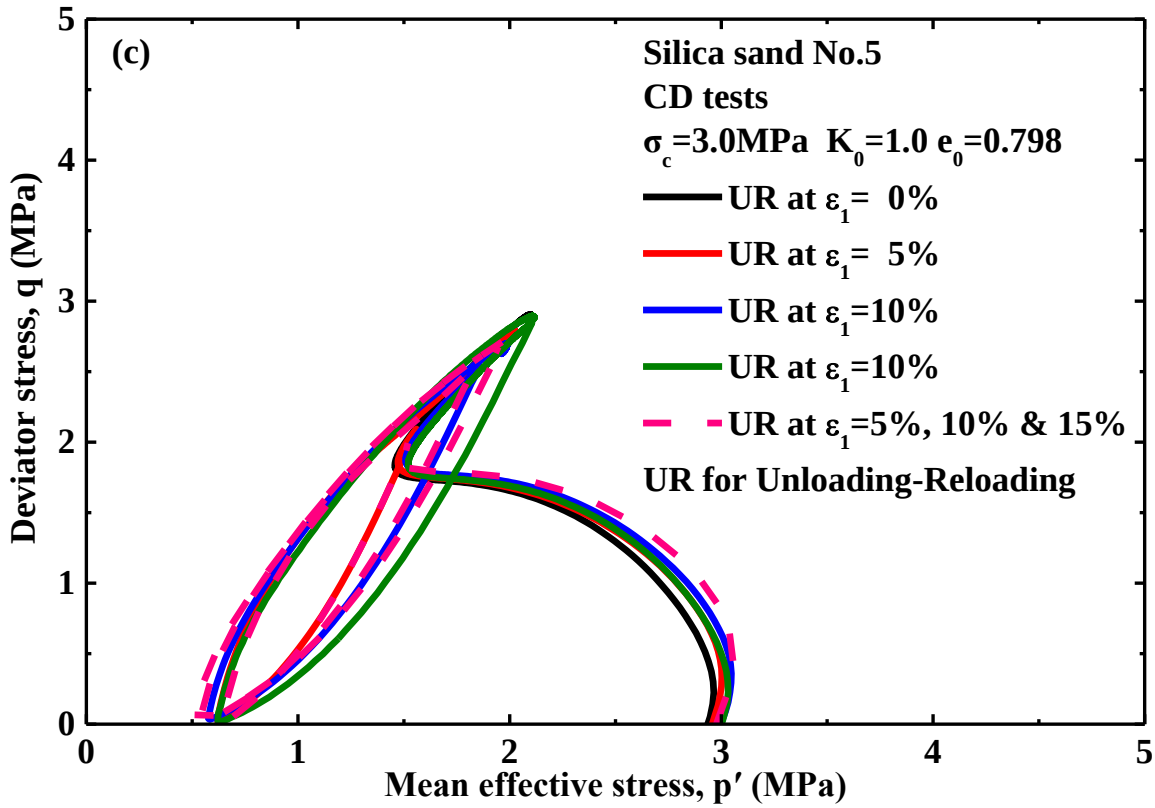

Figure 4.34 CU test results under unloading-reloading (σ_c=3.0MPa K_0=1.0, e_0=0.798)

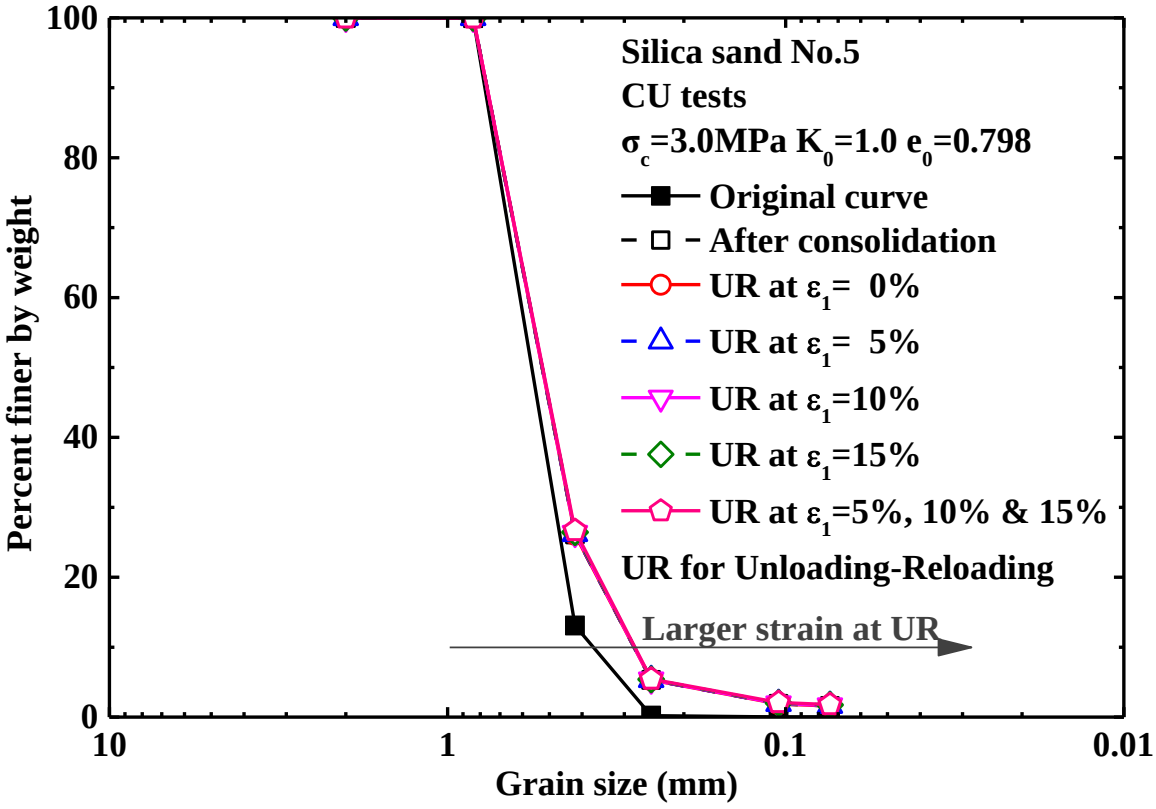

Figure 4.35 Grain size distribution curves from CU tests under unloading-reloading (σ_c=3.0MPa K_0=1.0, e_0=0.798)

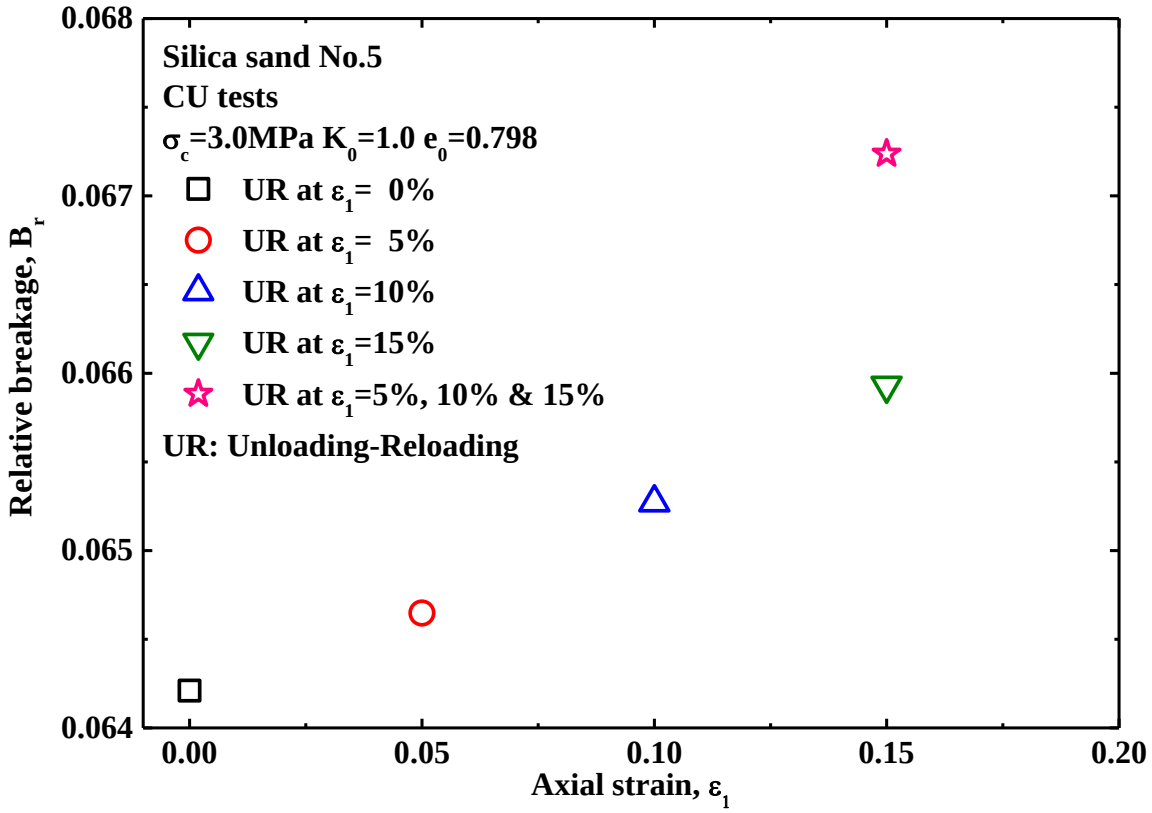

Figure 4.36 B_r-ε_1 relation from CU tests under unloading-reloading (σ_c=3.0MPa K_0=1.0, e_0=0.798)

4.5.6 The Influence of Drainage Condition on Particle Breakage

The drainage condition has a significant influence on soil behavior. The Consolidated Drained condition (CD) and Consolidated Undrained (CU) condition are adopted widely in triaxial test for investigating the soil behavior of soil. Herein the characteristics of particle breakage subjected to CD condition or CU condition were investigated as well. Most triaxial tests herein were carried out under both CD and CU condition to obtain the relevant grain size distribution curves which were quantified by relative breakage. By combining the Figure 4.5(a) and Figure 4.10(a) into one figure for comparing the deviator stresses in CD and CU conditions, Figure 4.37 shows the triaxial results in CD and CU condition with same initial void ratio under various confining pressure, which shows that CD tests have much higher strength in deviator stress curves than CU tests as a result of that the development of excess pore water pressure under high confining pressure resulted in reduction of strength of soil in deviator stress. The relationship between relative breakage and axial strain is shown in Figure 4.38 as a combination of Figure 4.9 and Figure 4.14. It can be seen clearly herein that the relative breakage in CD tests is higher than that in CU tests, namely the particle breakage is much more substantial in CD tests than in CU tests, which is related to the higher deviator stress in CD tests than in CU tests under high confining pressure as shown in Figure 4.37. As shown in Figure 4.38, the difference of particle breakage in relative breakage between CD tests and CU tests is found to increase with increasing axial strain for each confining pressure and the

difference of particle breakage in relative breakage between CD tests and CU tests is seen to increase with increasing confining pressure as well, which all are related to the findings as shown in Figure 4.37.

The characteristics of particle breakage in relative breakage subjected to the shearing under various initial void ratio under 1MPa and 2MPa confining pressure have been discussed above according to the CD and CU condition, where those findings are consistent with the findings as shown in Figure 4.38. Combining Figure 4.33 and Figure 4.36 into one figure as shown in Figure 4.39 to investigate the particle breakage under CD and CU conditions, it is found herein that in CD tests subjected to unloading-reloading process the particle breakage in relative breakage increases with increasing axial strain to unloading-reloading in reduced increments but in CU tests subjected to one-time unloading-reloading particle breakage in relative breakage increases linearly approximately with increasing axial strain to unloading-reloading. Particle breakage in relative breakage in CD tests is larger than that in CU tests.

It can be concluded that the drainage condition in triaxial test has a significant influence on particle breakage. Particle breakage in CD tests is much more substantial than that in CU tests because of higher effective stress imposed on soil particles. And the difference of particle breakage in relative breakage between CD tests and CU tests was found to increase with increasing axial strain.

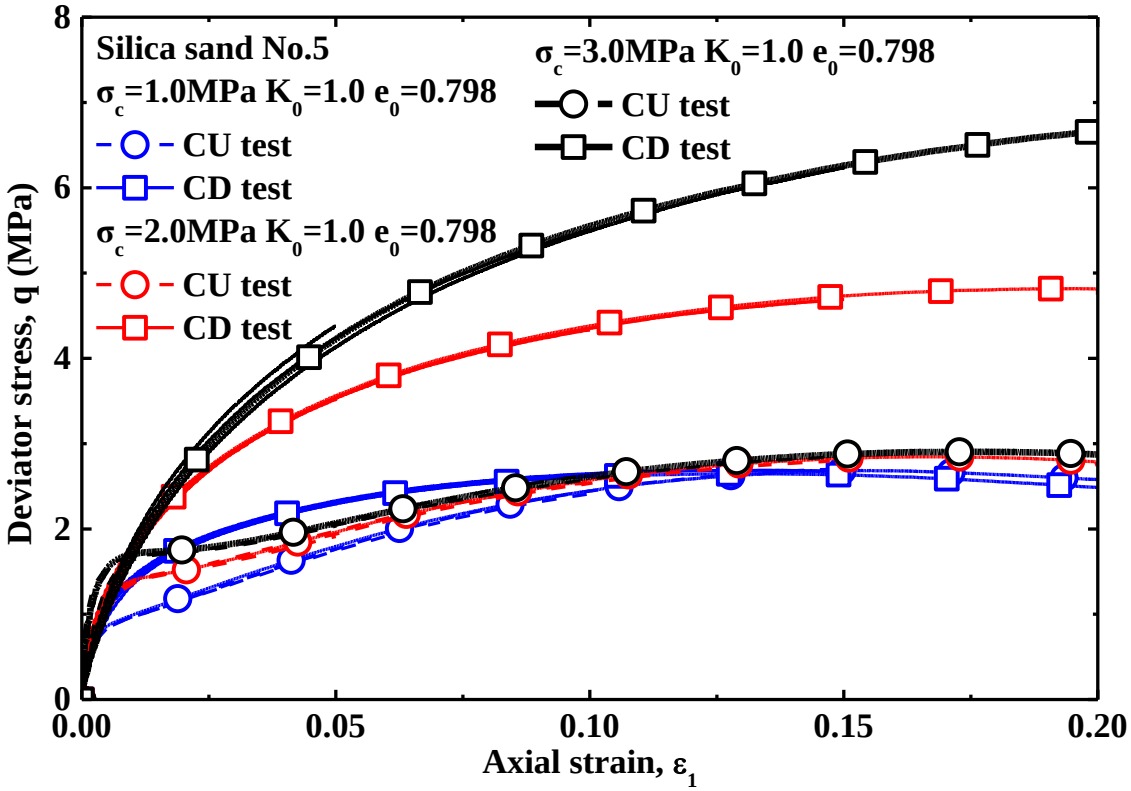

Figure 4.37 Triaxial results in CD and CU conditions (σ_c=1MPa, 2MPa & 3MPa K_0=1.0, e_0=0.798)

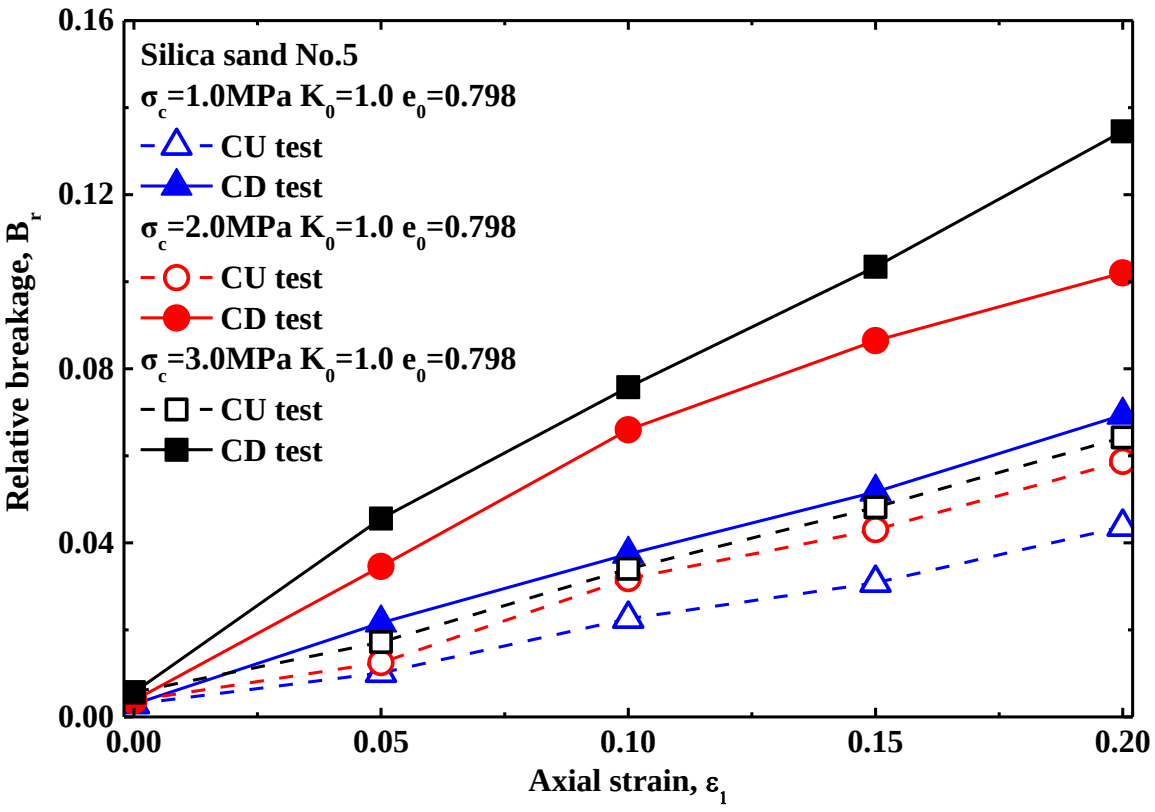

Figure 4.38 B_r-ε_1 relation from CD and CU tests (σ_c=1MPa, 2MPa & 3MPa K_0=1.0, e_0=0.798)

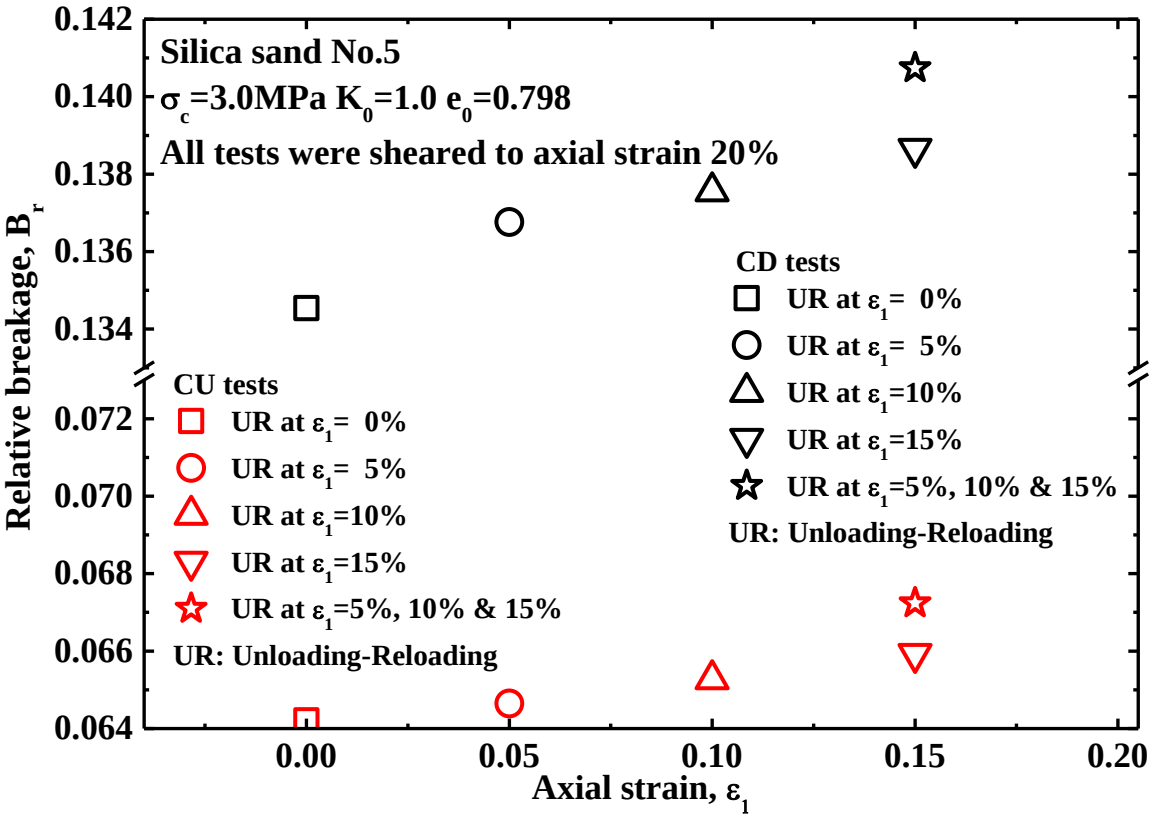

Figure 4.39 B_r-ε_1 relation from CD and CU tests subjected to unloading-reloading

4.5.7 A Model to Assess Relative Breakage of Silica Sand No.5

Crushability of the granular materials depends on initial grain size distribution, particle shape, state of effective stress, effective stress path, void ratio, particle hardness and the presence or absence of water and so on (Hardin, 1985; Lade et al., 1996; McDowell and Bolton, 1998). It is rather difficult or impossible to find a unique rule to depict the relative breakage considering all of the influence factors. In an attempt to establish a rule to express the relative breakage which can be used in practice, the relationship between relative breakage and plastic work per unit volume were reanalyzed further under different conditions.

As derived in detail in APPENDIX Ⅰ, plastic work per unit volume can be obtained by triaxial results directly after each test was unloaded back to initial consolidation state after shearing for removing the elastic work per unit volume from total work per unit volume. Figure 4.40 shows the relationship between relative breakage and plastic work per unit volume. It is notable herein that the relative breakage increases gradually with the increase of plastic work per unit volume in triaxial tests in reduced increments, which is consistent with the characteristics of a hyperbola. In addition, plastic work per unit volume can be regarded as a comprehensive index including the effect of confining pressure, dilatancy behavior, contractive behavior, shearing behavior and so on which are related to particle breakage. Consequently, a hyperbola can be used to approximate the relatively convergent relationship between relative breakage and plastic work per unit volume regardless of different confining pressure, different initial void ratio, different consolidation stress ratio etc. Consequently, the hyperbola model should be established as follows:

$$B_r = \frac{w^p}{a + bw^p} \tag{4.1}$$

where w^p represents plastic work per unit volume, B_r is relative breakage (Hardin, 1985), and a and b are the model parameters.

The hyperbola model is very convenient to use in practice with just two model parameters which can be determined easily by the experimental data from the traditional triaxial tests or by fitting. Here, the general method to determine the parameters of this hyperbola model will be given as below:

$$\frac{1}{a} = \frac{dB_r}{dw^p} = \lim_{w^p \to 0} \frac{1}{a + bw^p} \overset{\Delta}{=} E_{B_{ri}} \tag{4.2}$$

$$\frac{1}{b} = \lim_{w^p \to \infty} \frac{w^p}{a + bw^p} \overset{\Delta}{=} B_{rult} \tag{4.3}$$

where $E_{B_{ri}}$ represents initial tangent modulus in B_r-Plastic work per unit volume plane and B_{rult} is the ultimate relative breakage.

Based on the relation of relative breakage and plastic work per unit volume, $E_{B_{ri}}$ can be calculated by the initial tangent modulus in B_r-Plastic work per unit volume plane but B_{rult} as an ultimate relative breakage can be substituted sometimes by the relative breakage obtained after the triaxial tests up to critical state in which the further shear strain can occur without any change in deviator stress, mean effective stress and specific volume i.e. $\partial q/\partial \varepsilon_s = \partial p'/\partial \varepsilon_s = \partial v/\partial \varepsilon_s = 0$. Under the condition that the tests don't reach the critical state or it is rather different to obtain $E_{B_{ri}}$ and B_{rult} , the two model parameters can be obtained directly by fitting as shown in Figure 4.40(a). Figure 4.40(a) can be redrawn in semi-logarithmic coordinate in B_r-Plastic work per unit volume plane for more detailed information of the data and fitting line as shown in Figure 4.40(b).

As shown in Figure 4.40(a), many influence factors on relationship of relative breakage and plastic work per unit volume can be discussed as well. It is herein found that according to same plastic work per unit volume, more particle breakage in relative breakage was caused in CD tests than in CU tests especially under low pressure on loose samples. And same plastic work per unit volume results in more particle breakage in denser sample. In addition, same plastic work causes more particle breakage during shearing on samples under (σ_c=2.0MPa, K_0=1.0) than that during shearing on samples under (σ_c=1.5MPa, K_0=0.5). In fact, the initial state and conditions of tests have significant influences on the relationship of relative breakage and plastic work per unit volume. Consequently, the relationship of relative breakage and plastic per unit volume should be considered and investigated on the case-by-case basis.

Miura and Ohara (1979) correlated the surface area increase with plastic work per unit volume, and found that for drained triaxial compression tests a unique concave line was represented which should be developed into "S" shape but for cyclic loading tests a hyperbolic curve was expressed approximately in correlation of surface area increase and plastic work per unit volume. However, Lade et al. (1996) employed a hyperbolic mode to correlate the relative breakage and total input energy per unit volume. Herein a hyperbolic model was established to correlate relative breakage and plastic work per unit volume, which is different from the findings in triaxial compression tests but is similar as findings in cyclic loading tests (Miura and Ohara, 1979). Those may be caused by different particle breakage factor used to quantify particle breakage. In addition, herein the plastic work per unit volume was employed instead of the total input energy which was used to be correlated with relative breakage (Lade et al., 1996).

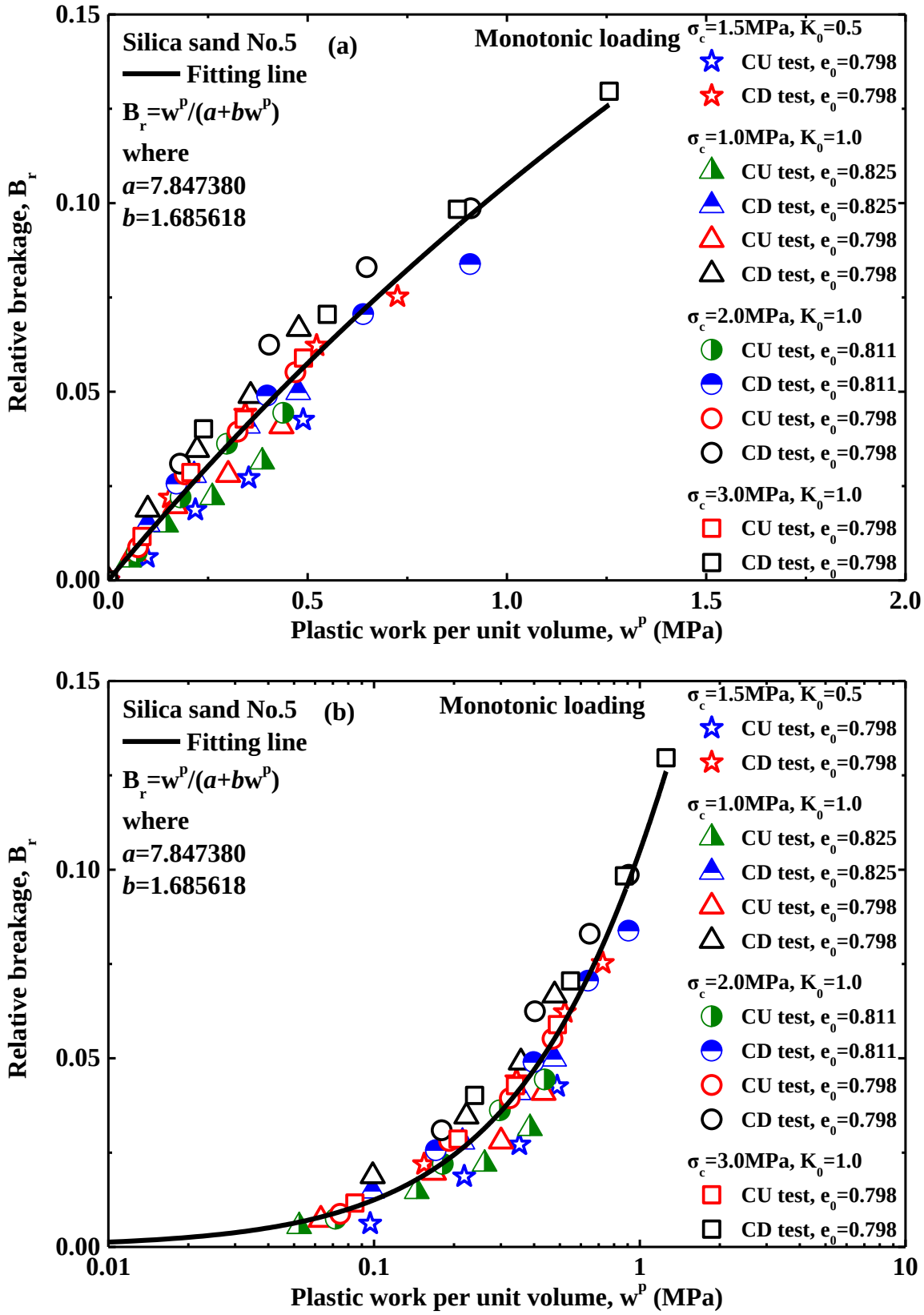

Figure 4.40 Relationship between relative breakage and plastic work per unit volume of Silica sand No.5 in monotonic loading

4.6 EXPERIMENTAL RESUTLS ON CORAL SAND NO.3

4.6.1 The Influence of Confining Pressure on Particle Breakage

A specimen is usually consolidated to a specific confining pressure prior to shear in triaxial test. Consequently the confining pressure has an important effect on soil behavior. For getting fundamental understanding of the characteristics of particle breakage especially under high pressure, the influences of confining pressure were investigated by many triaxial tests on coral sand No.3. Herein the triaxial tests were conducted under various confining pressure as 2MPa and 3MPa separately and terminated at a series of designated axial strain levels from 0% to 20% by 5% increment to obtain the relevant grain size distribution curves after testing by sieve analysis.

Figure 4.41 shows that triaxial tests results under 2MPa and 3MPa confining pressures, where it is found that higher confining pressure results in higher strength in deviator stress and the deviator stresses in CD tests is higher than that in CU tests except at the beginning shearing as a result of the excess pore water pressure occurred during shearing in CU tests. It is notable that the difference of deviator stresses between CD tests and CU tests under 3MPa confining pressure or 2MPa confining pressure is getting increasing approximately with increasing axial strain, which would be related to the characteristics of particle breakage in difference between CD tests and CU tests. In CD tests, the deviator stresses are found to increase typically with increasing axial strain and the difference of deviator stresses between 3MPa and 2MPa confining pressures are shown to increase with increasing axial strain, which may be related to the characteristics of particle breakage. It can be seen clearly in Figure 4.41(b) that the contractive volume change under 3MPa confining pressure is more substantial than that in 2MPa confining pressure, which is related to the specimens subjected to higher deviator stresses under 3MPa confining pressure. In CU tests, the deviator stresses has a relatively level development with increasing axial strain except a dramatically increase at the beginning stage of shearing as shown in Figure 4.41(a) and the higher excess pore water pressures was produced in the specimens subjected to the higher confining pressure. The stress paths of CD tests and CU tests are shown in Figure 4.41(d).

The grain size distribution curves of all tests herein were obtained by sieving the materials (around 200g) from the specimens subjected to relevant shearing. The relevant grain size distribution curves are shown in Figure 4.42 for CU test under 2MPa confining pressure, Figure 4.43 for CD tests under 2MPa confining pressure, Figure 4.44 for CU tests under 3MPa confining pressure and Figure 4.45 for CD tests under 3MPa confining pressure, where all grain size distribution curves evolved toward the increase of fines content with increasing axial strain especially the increase of moderate-size particles. In other words, particle breakage is revealed to increase with increasing axial strain. All grain size distribution curves were quantified by relative breakage as well.

Figure 4.46 shows the relationship between relative breakage and axial strain under

2MPa and 3MPa confining pressures. It can be seen herein that particle breakage in relative breakage increases with increasing axial strain. Particle breakage in relative breakage under 3MPa confining pressure is found to increase approximately in linearity after a relatively larger increment at the beginning stage of shearing but under 2MPa confining pressure particle breakage in relative breakage is found to increase in linearity with increasing axial strain. Particle breakage in relative breakage under 3MPa confining pressure is more substantial than that 2MPa confining pressure, which is related to the higher shear stress in triaxial tests under 3MPa confining pressure. For each confining pressure (2MPa or 3MPa confining pressure), particle breakage in relative breakage in CD tests is more substantial than that in CU tests. Meanwhile the difference of particle breakage in relative breakage between CD tests and CU tests is found to increase with increasing axial strain, which is also related to development of difference of deviator stresses between CD tests and CU tests as shown in Figure 4.41(a).

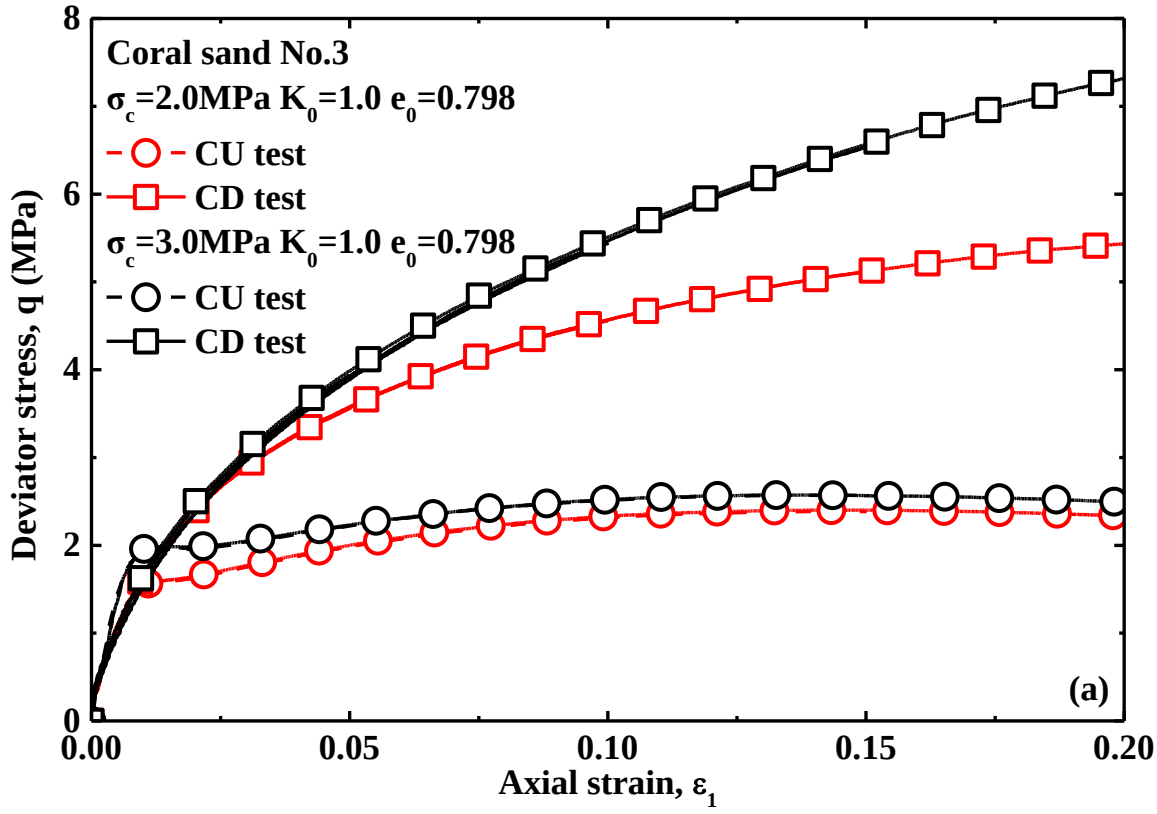

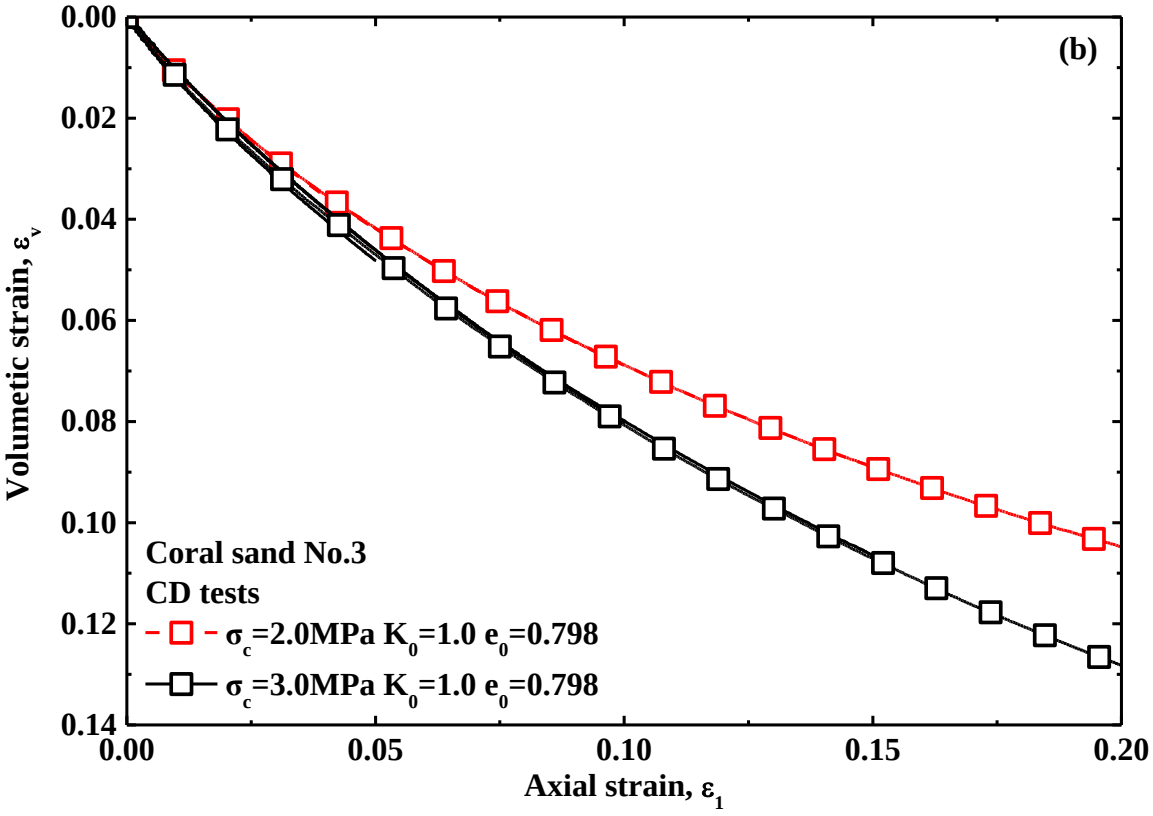
(b)
Volumetic strain, ε_v
0.00
0.02
0.04
0.06
0.08
0.10
0.12
0.14
0.00
0.05
0.10
0.15
0.20
Axial strain, ε_1
Coral sand No.3
CD tests
σ_c=2.0MPa K_0=1.0 e_0=0.798
σ_c=3.0MPa K_0=1.0 e_0=0.798

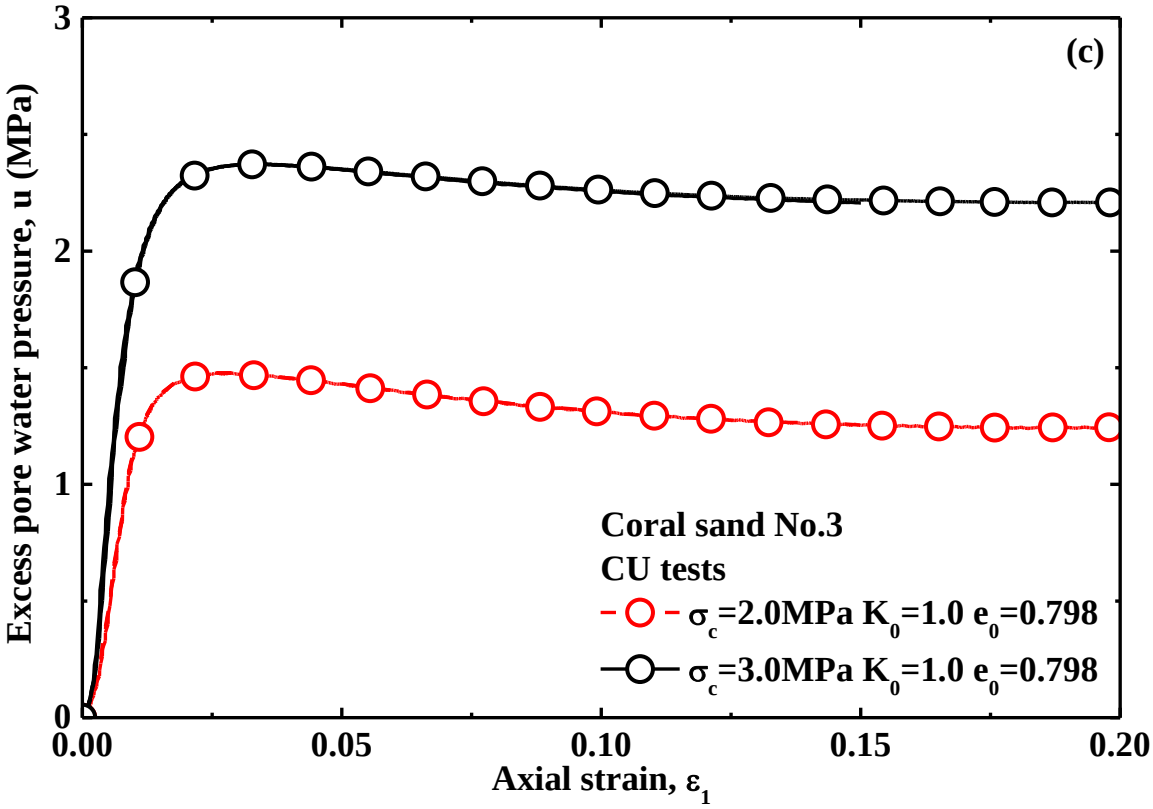
(c)
Excess pore water pressure, u (MPa)
0
1
2
3
0.00
0.05
0.10
0.15
0.20
Axial strain, ε_1
Coral sand No.3
CU tests
σ_c=2.0MPa K_0=1.0 e_0=0.798
σ_c=3.0MPa K_0=1.0 e_0=0.798

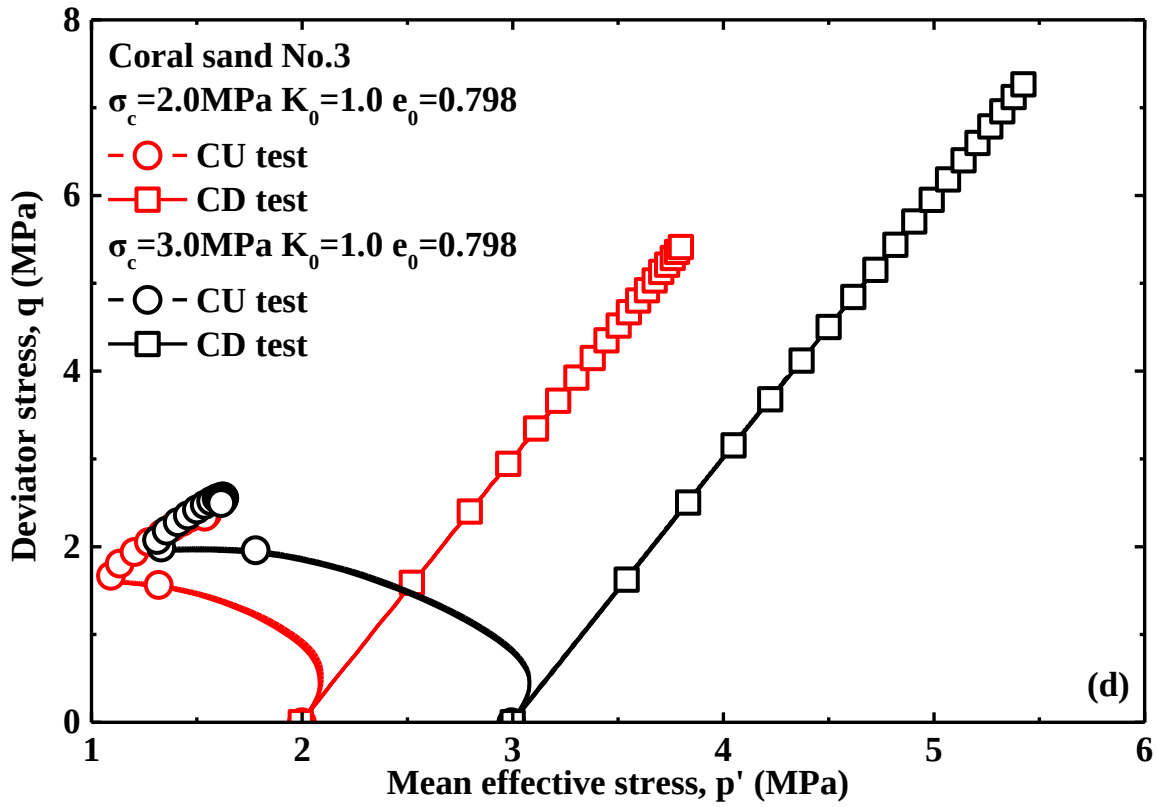

Figure 4.41 Triaxial test results (σ_c=2.0MPa & 3.0MPa K_0=1.0, e_0=0.798)

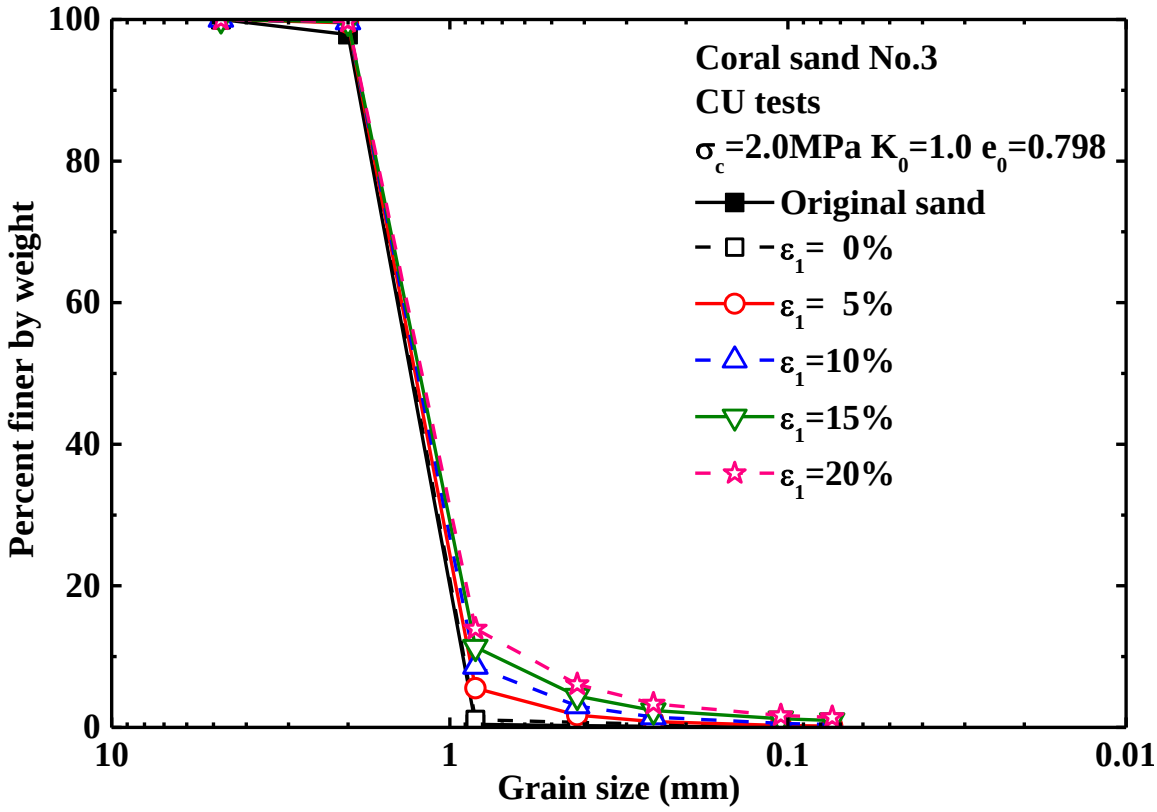

Figure 4.42 Grain size distribution curves from CU tests (σ_c=2.0MPa K_0=1.0, e_0=0.798)

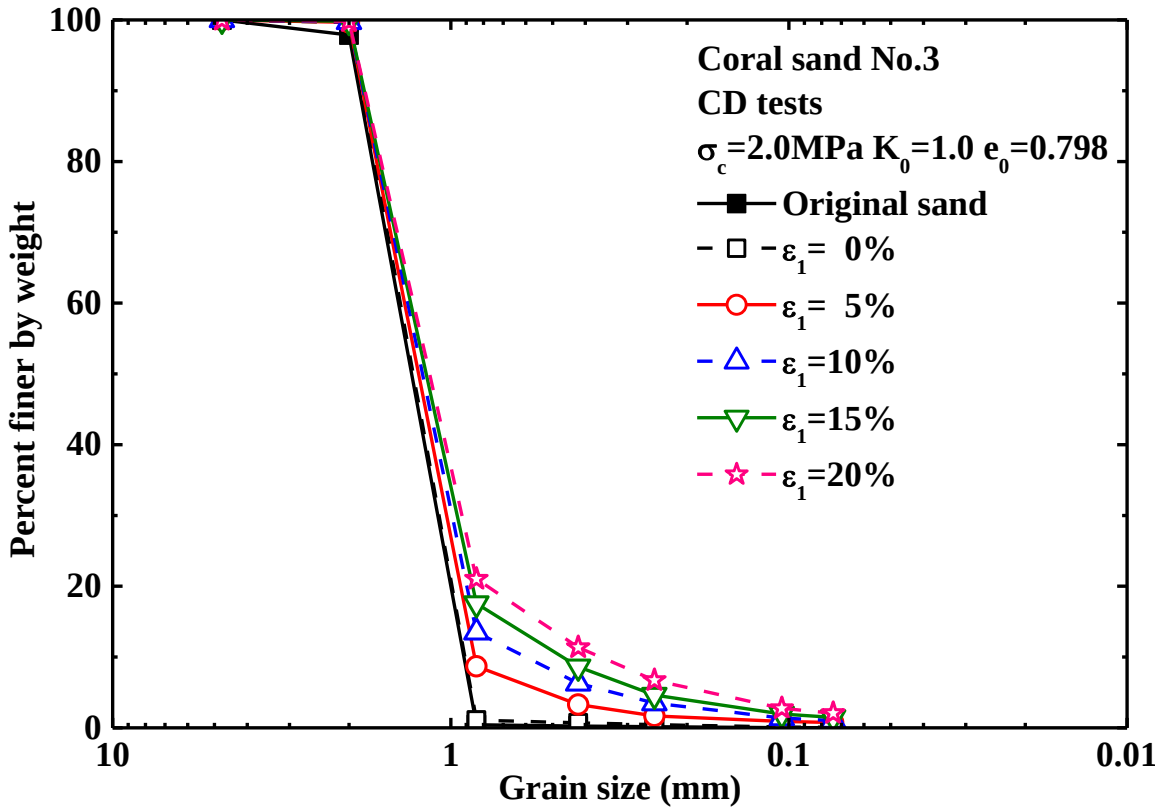

Figure 4.43 Grain size distribution curves from CD tests (σ_c=2.0MPa K_0=1.0, e_0=0.798)

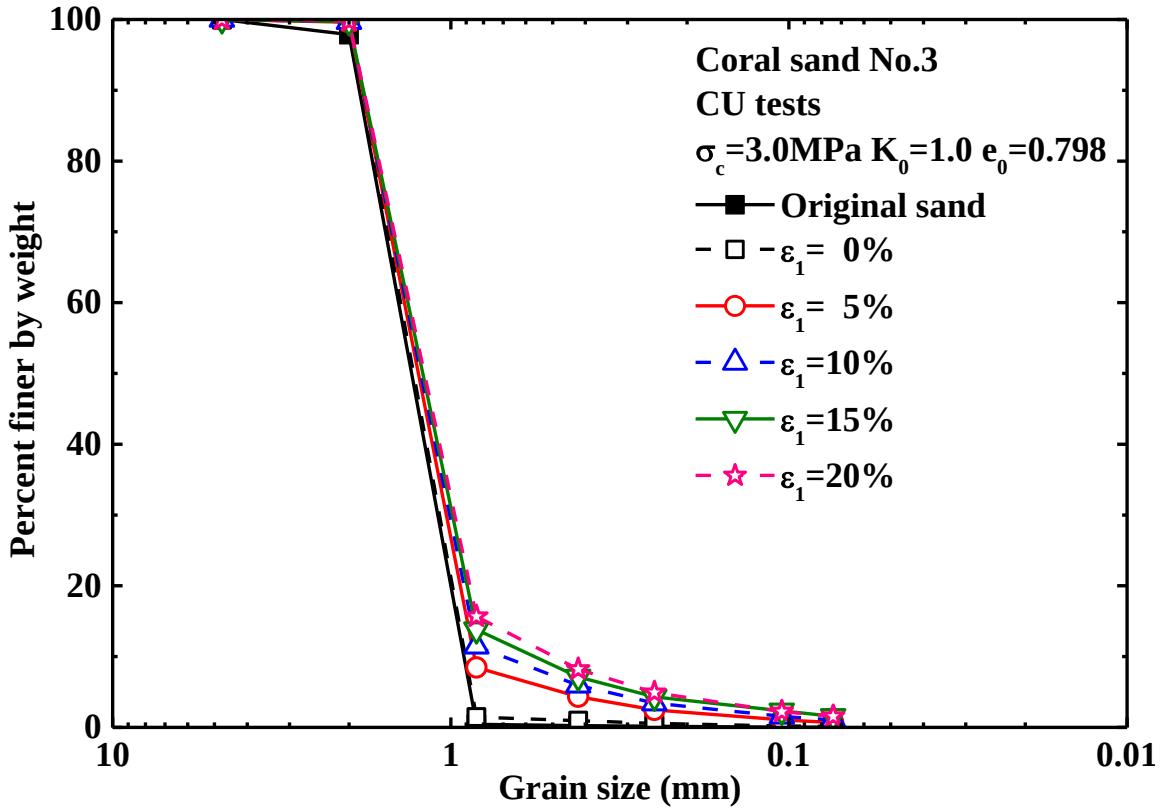

Figure 4.44 Grain size distribution curves from CU tests (σ_c=3.0MPa K_0=1.0, e_0=0.798)

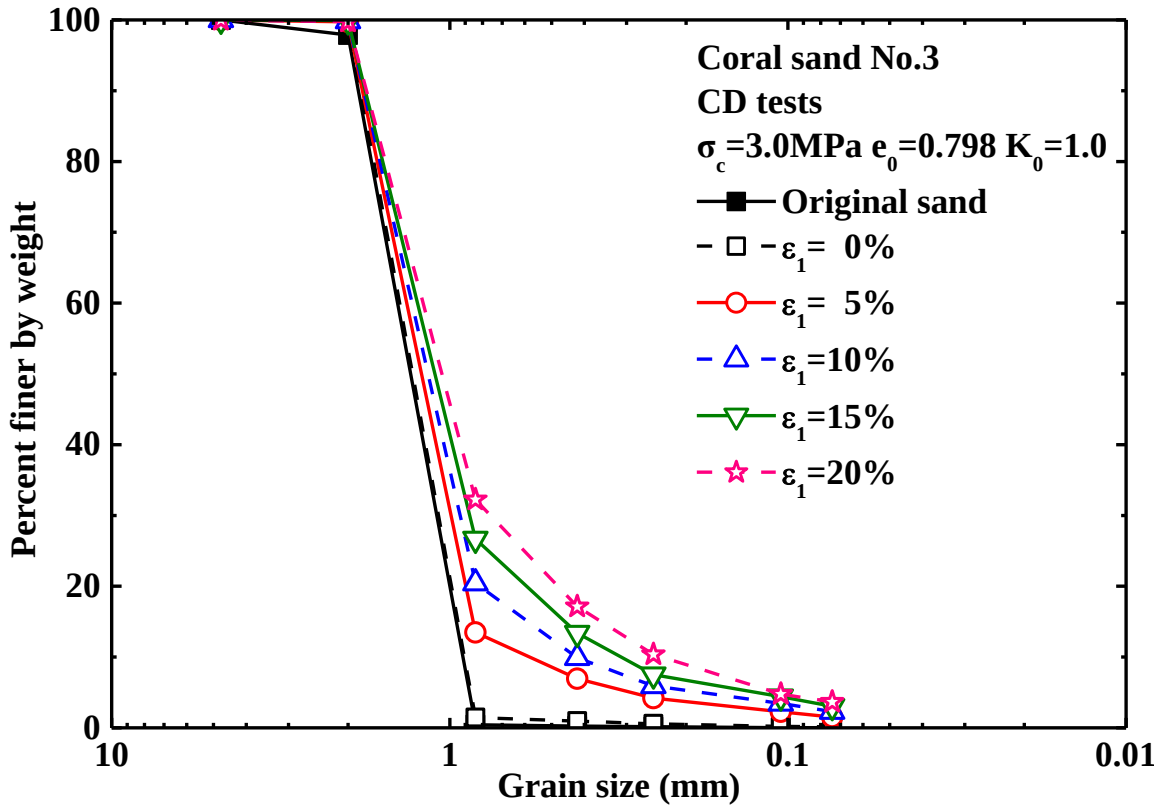

Figure 4.45 Grain size distribution curves from CD tests (σ_c=3.0MPa K_0=1.0, e_0=0.798)

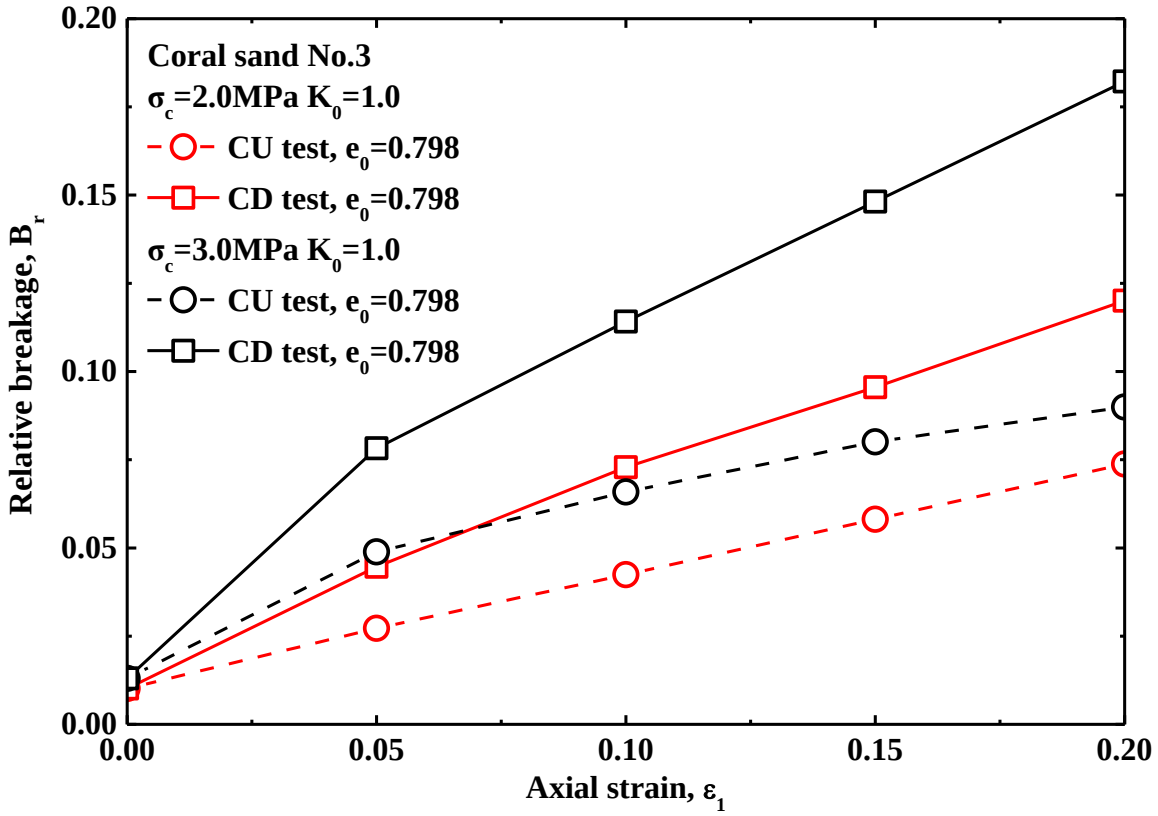

Figure 4.46 B_r-ε_1 relation from CD and CU tests (σ_c=2.0MPa & 3.0MPa K_0=1.0, e_0=0.798)

4.6.2 The Influence of Initial Void Ratio on Particle Breakage

Initial void ratio adopted in specimen has a direct influence on soil behavior. Various initial void ratios were adopted herein in specimens under 3MPa confining pressure to investigate their influence on particle breakage. Figure 4.47 shows the triaxial tests results under 3MPa confining pressure with various initial void ratios. It is found herein that the deviator stresses in CD tests increase typically with increasing axial strain but in CU tests the deviator stresses has a dramatic increase at the beginning stage of shearing and then develop gradually with relatively reduced increments up to peak strength. And there is a higher deviator stress in denser sample. In CD tests, more volume change was caused in looser sample as shown in Figure 4.47(b) but in CU tests higher excess pore water pressure was produced in looser sample as shown in Figure 4.47(c). Figure 4.47(d) shows the stress paths of triaxial tests under 3MPa pressure with various initial void ratios.

The grain size distribution curves of the sands of the specimens after shearing were measured by sieve analysis in order to identify the characteristics of particle breakage. The relevant grain size distribution curves are shown in Figure 4.48 for CU tests with initial void ratio e_0=0.924, Figure 4.49 for CD tests with initial void ratio e_0=0.924, Figure 4.50 for CU tests with initial void ratio e_0=0.870 and Figure 4.51 for CD tests with initial void ratio e_0=0.870. The grain size distribution curves under 3MPa confining pressure with initial void ratio e_0=0.798 have been shown above in Figure 4.44 for CU tests and Figure 4.45 for CD tests. From these grain size distribution curves, it can be seen that grain size distributions developed towards the increase of fines content with increasing axial strain, which means that particle breakage increases with increasing axial strain. In comparison with evolution of the grain size distribution curves from CU tests, there is a more substantial evolution of the grain size distribution curves toward the increase of fines content at same axial strain, which are related to the difference of triaxial tests results between CU tests and CD tests.

All grain size distribution curves herein were quantified by relative breakage to investigate the characteristics of particle breakage. Figure 4.52 shows the relationship between relative breakage and axial strain for the triaxial tests results under 3MPa confining with various initial void ratios, where particle breakage in relative breakage is much more substantial in denser samples, namely particle breakage in relative breakage increases with decreasing initial void ratio of the specimens. It can be seen clearly that particle breakage in relative breakage increases with increasing axial strain in a larger increment of particle breakage at beginning stage of shearing such as the increment of particle breakage up to 5% axial strain. And particle breakage in relative breakage is found to be larger in CD test than that in CU tests, which is related to the higher deviator stress in denser samples in comparison with that in CU tests. The difference of particle breakages in relative breakage between CD tests and CU tests with same initial void ratio is found to increase with increasing axial strain, which is related to the development of difference of deviator stresses between CD tests and CU tests.

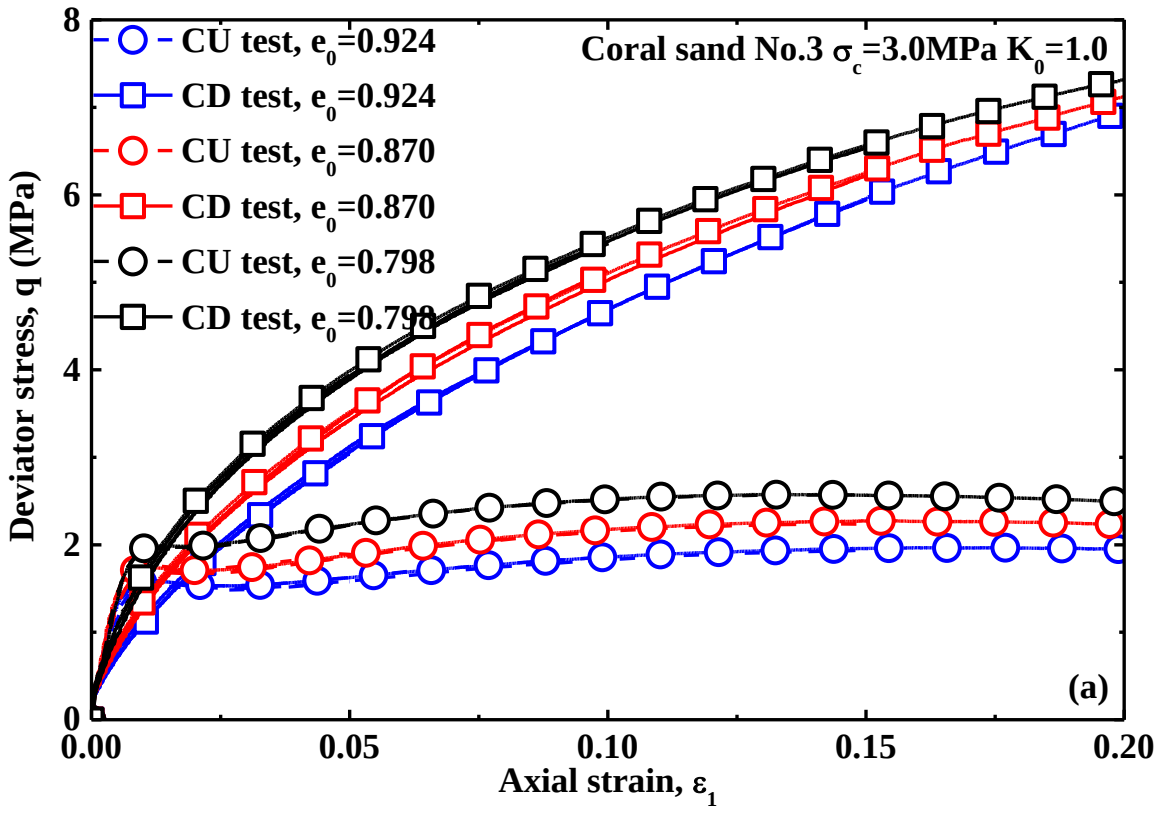
CU test, e0=0.924
CD test, e0=0.924
CU test, e0=0.870
CD test, e0=0.870
CU test, e0=0.798
CD test, e0=0.798
Coral sand No.3 σc=3.0MPa K0=1.0
(a)
Deviator stress, q (MPa)
Axial strain, ε1
0
2
4
6
8
0.00
0.05
0.10
0.15
0.20

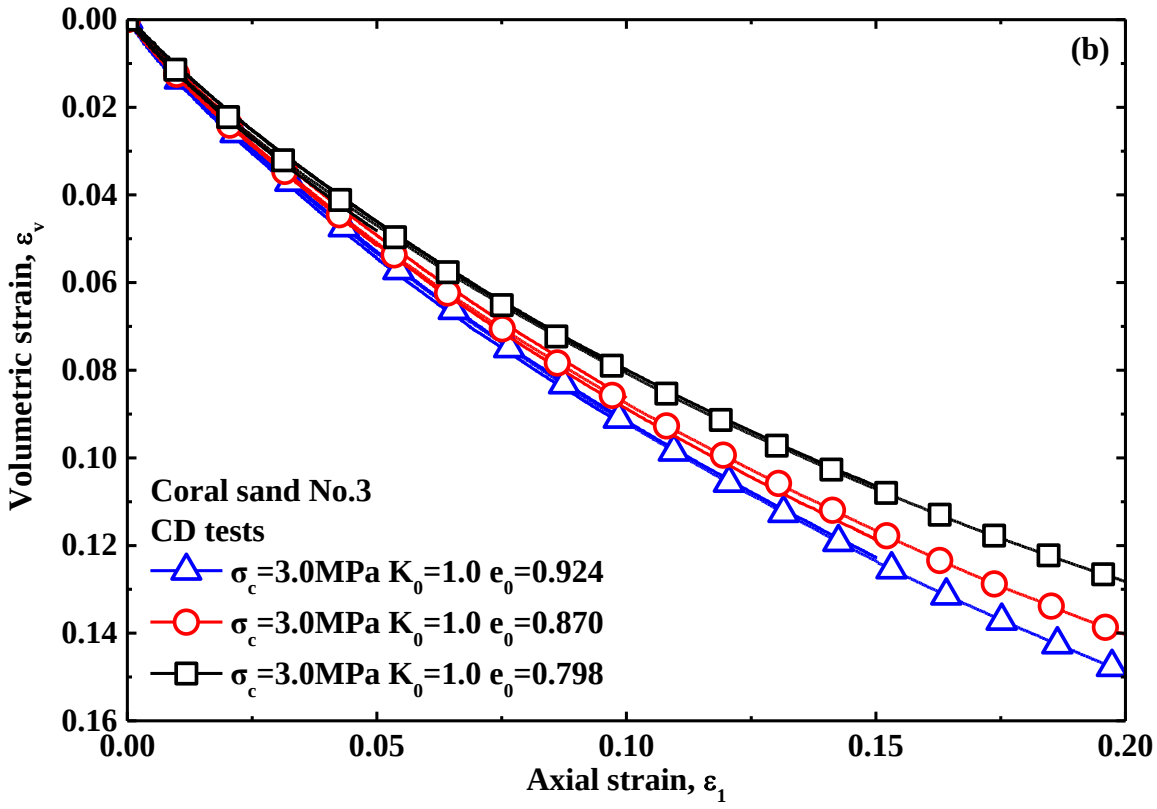
(b)
Coral sand No.3
CD tests
σc=3.0MPa K0=1.0 e0=0.924
σc=3.0MPa K0=1.0 e0=0.870
σc=3.0MPa K0=1.0 e0=0.798
Volumetric strain, εv
Axial strain, ε1
0.00
0.02
0.04
0.06
0.08
0.10
0.12
0.14
0.16
0.00
0.05
0.10
0.15
0.20

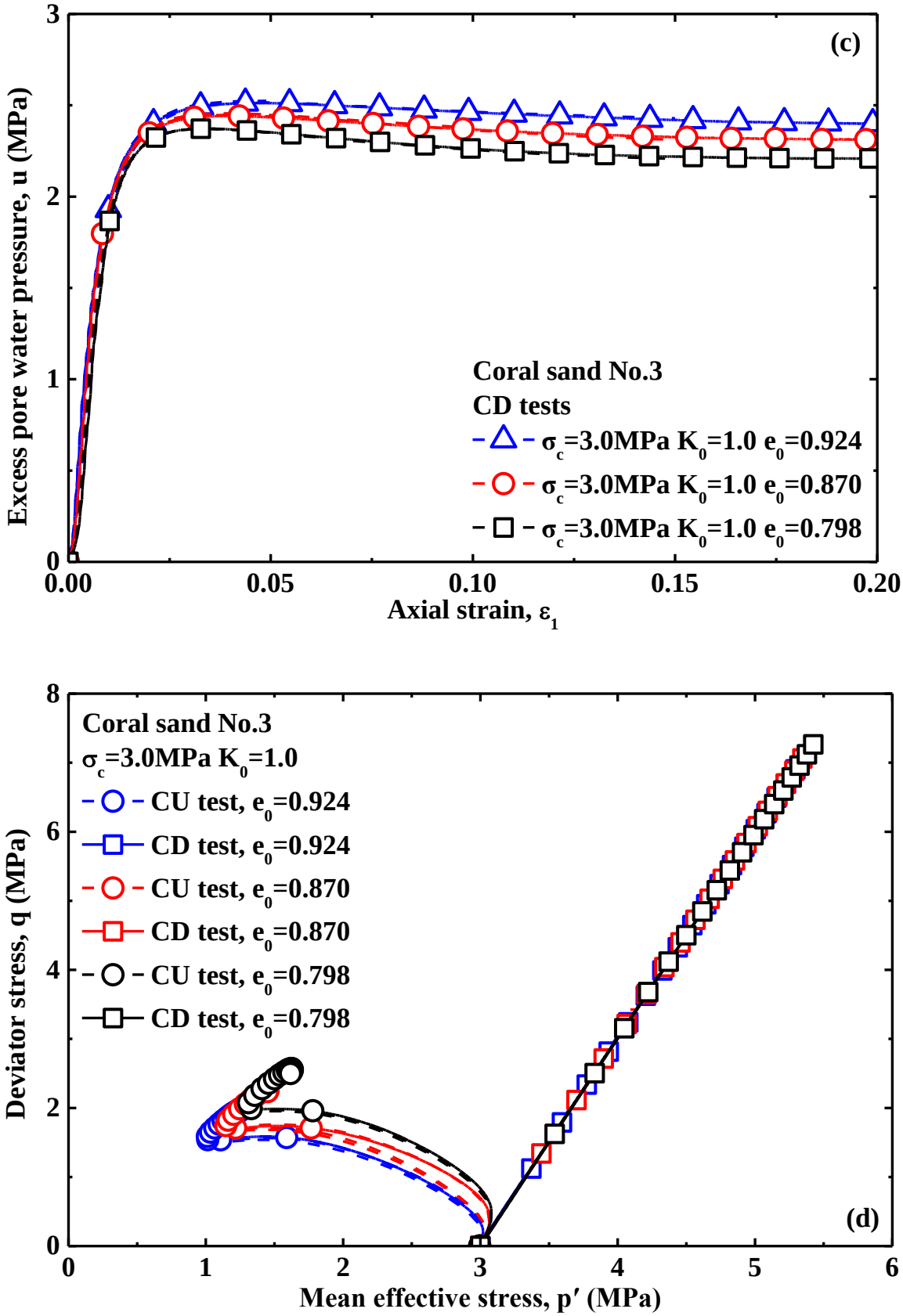

Figure 4.47 Triaxial test results (σ_c=3.0MPa K_0=1.0 e_0=0.798, 0.870 & 0.924)

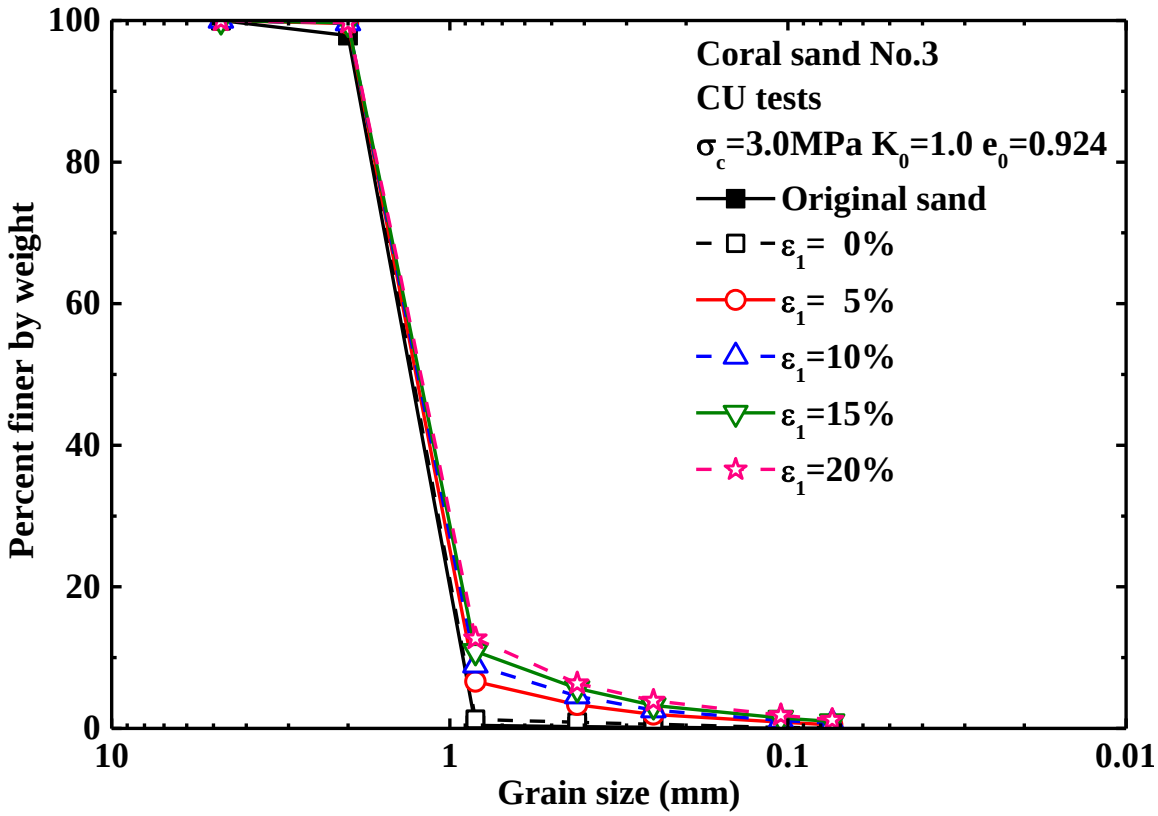

Figure 4.48 Grain size distribution curves from CU tests (σ_c=3.0MPa K_0=1.0 e_0=0.924)

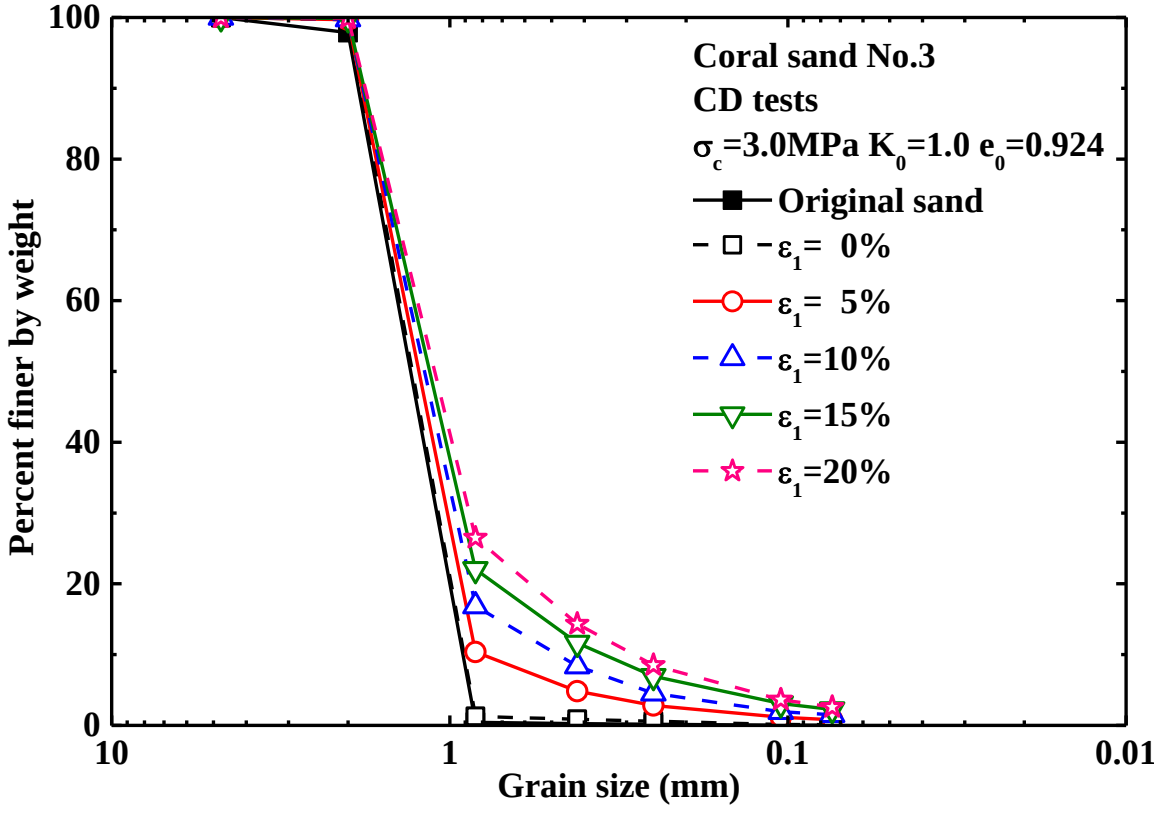

Figure 4.49 Grain size distribution curves from CD tests (σ_c=3.0MPa K_0=1.0 e_0=0.924)

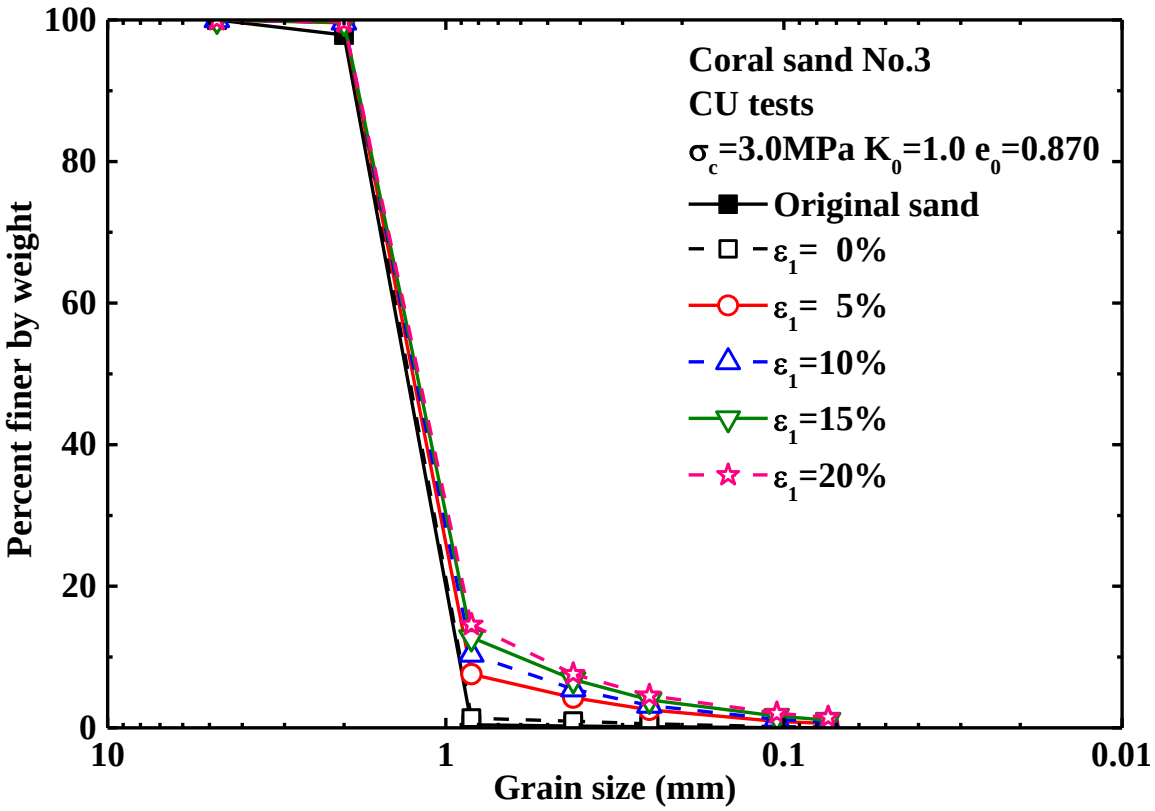

Figure 4.50 Grain size distribution curves from CU tests (σ_c=3.0MPa K_0=1.0 e_0=0.870)

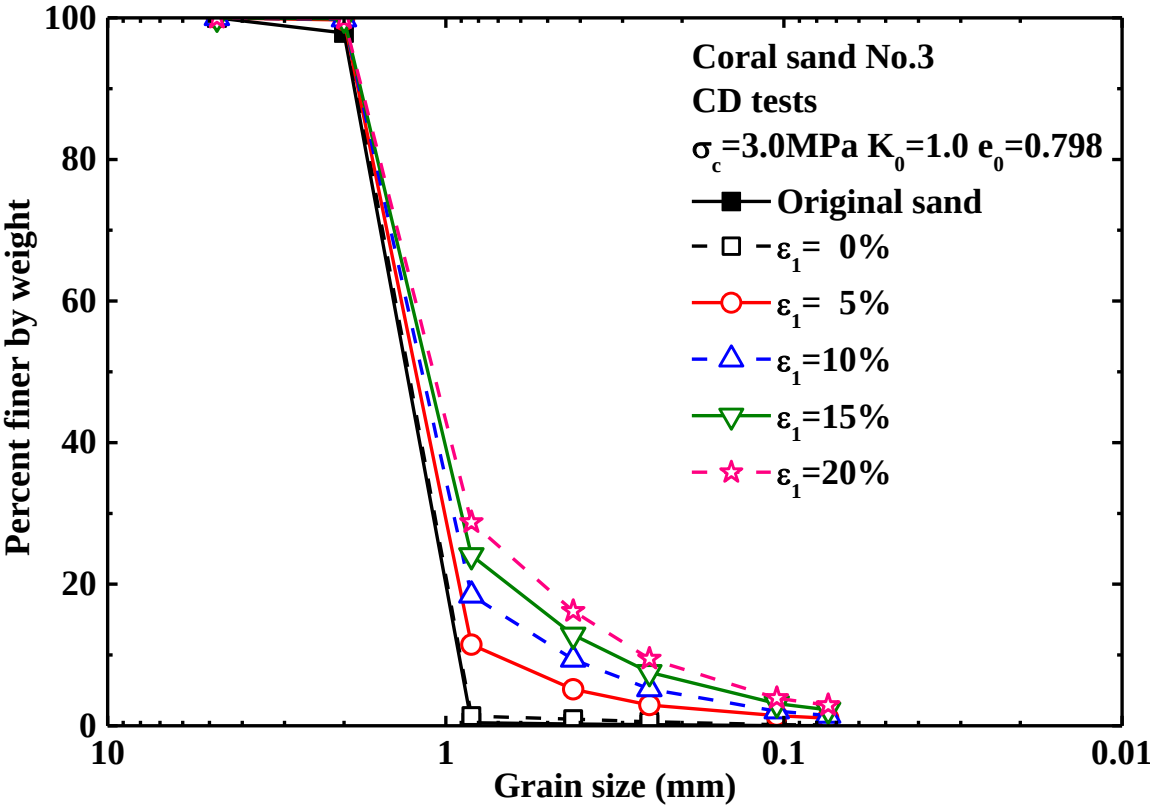

Figure 4.51 Grain size distribution curves from CD tests (σ_c=3.0MPa K_0=1.0 e_0=0.870)

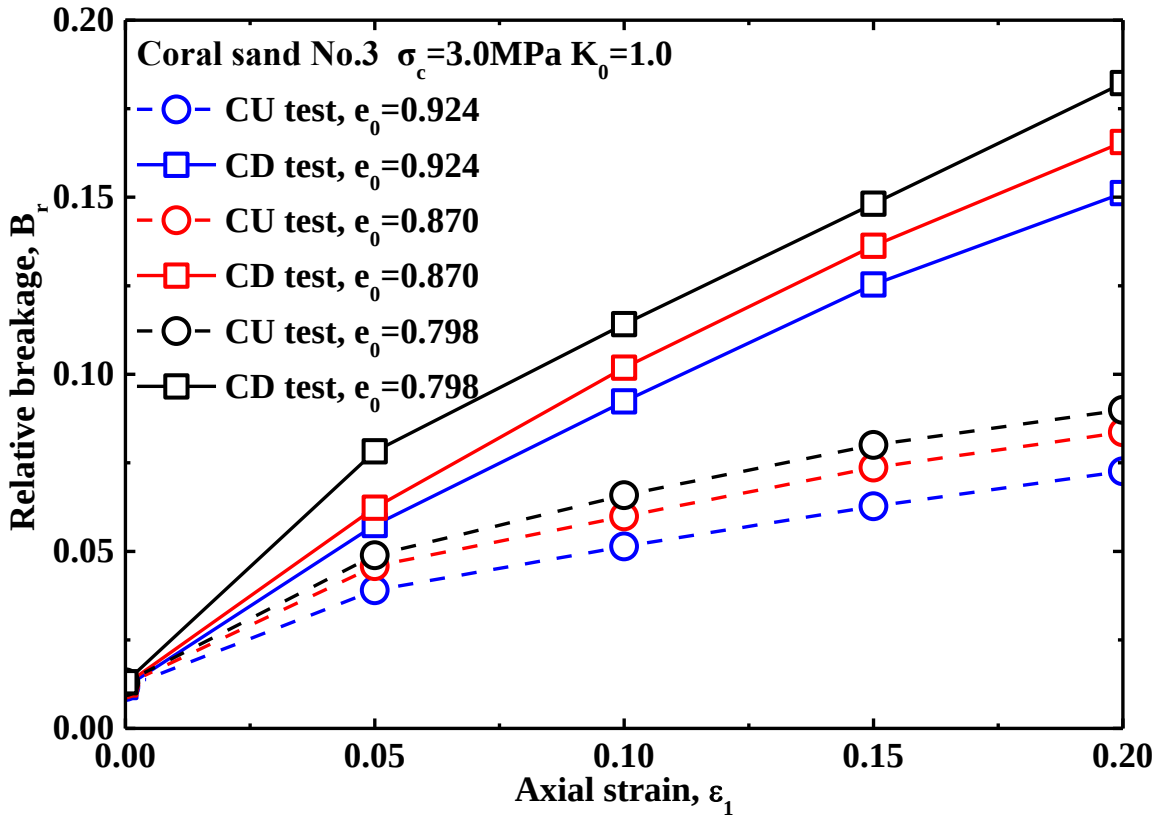

Figure 4.52 B_r-ε_1 relation from CD and CU tests (σ_c=3.0MPa K_0=1.0 e_0=0.798, 0.870 & 0.924)

4.6.3 The Influence of Initial Stress Anisotropy on Particle Breakage

Corresponding to initial stress isotropy on soil specimen, the initial stress anisotropy on specimen is much more widespread in geotechnical engineering in reality. The initial stress anisotropy has an important influence on soil behavior. Consequently the influence of initial stress anisotropy on the characteristics of particle breakage was herein investigated by many triaxial tests under high pressure in comparison with the initial stress isotropy. The specimens were consolidated linearly to confining pressure σ_c=1.5MPa in an initial consolidation stress ratio K_0=0.5 for producing an initial stress anisotropy (q=1.5MPa) on specimens after consolidation, and other kind of specimens were consolidated isotropically to confining pressure σ_c=2.0MPa (K_0=1.0) without stress anisotropy (q=0MPa) on specimens during consolidation. Both kinds of specimens were to reach same mean effective stress (p′=2MPa) after consolidation but two different initial deviator stresses (q=1.5MPa under σ_c=1.5MPa & K_0=0.5 and q=0 under σ_c=2.0MPa & K_0=1.0) as shown in Figure 4.3. All specimens were herein terminated at specific axial strain from 0% to 20% by 5% increment for obtaining grain size distribution curves by sieving the crushed materials of the specimens.

Figure 4.53 shows the triaxial tests results under initial stress anisotropy (σ_c=1.5MP K_0=0.5) and initial stress isotropy (σ_c=2.0MPa K_0=1.0), where there is an initial deviator stress (q=1.5MPa as stress anisotropy on specimen) on specimens before shearing in the

tests under stress anisotropy (σ_c=1.5MP K_0=0.5) and the stress isotropic specimens were to shear from zero initial deviator stress as shown in Figure 4.53(a). It can be seen clearly that all deviator stresses in CD tests are found to increase with increasing axial strain in down concavity but the deviator stresses in CU tests are seen to have a sharp increase at beginning of shearing and then develop to peak strength gradually with a softening stage at the end stage of shearing. And the difference of deviator stresses between CD tests and CU tests are found to increase with increasing axial strain, which may be related to the characteristics of difference of particle breakage between CD tests and CU tests. The deviator stresses on specimens with initial stress isotropy (σ_c=2.0MPa K_0=1.0) are found to be larger than those under stress anisotropy (σ_c=1.5MPa K_0=0.5) except at beginning stage of shearing, where the deviator stresses developed from the initial deviator stress (q=1.5MPa) was caused before shearing under initial stress anisotropy (σ_c=1.5MPa K_0=0.5). The volume change of the specimens under initial stress isotropy (σ_c=2.0MPa K_0=1.0) is found to be much more substantial in comparison with the volume change of specimen under initial stress anisotropy (σ_c=1.5MPa K_0=0.5) as shown in Figure 4.53(b), and the development of excess pore water pressure in Figure 4.53(c) is displayed to be more substantial under initial stress isotropy (σ_c=2.0MPa K_0=1.0) than that under initial stress anisotropy (σ_c=1.5MPa K_0=0.5), which are influenced by the combination of confining pressure and initial consolidated stress ratio. Figure 4.53(d) shows all stress paths under initial stress anisotropy (σ_c=1.5MPa K_0=0.5) and initial stress isotropy (σ_c=2.0MPa K_0=1.0).

Grain size distribution curves were obtained by sieving the materials of specimens after shearing. The relevant grain size distribution curves under initial stress anisotropy (σ_c=1.5MPa K_0=0.5) are shown in Figure 4.54 for CU tests and Figure 4.55 for CD tests, where the evolution of grain size distribution curves moved toward the increase of finer particles passing in weight in each sieve size with increasing axial strain, namely particle breakage was proved to increase with increasing axial strain. It is notable that particle breakage occurred just during anisotropic consolidation in an initial consolidation stress ratio K_0 =0.5 to consolidate to confining pressure σ_c =1.5MPa and axial stress σ_c=3.0MPa. The grain size distribution curves under confining pressure σ_c=2.0MPa subjected to isotropic consolidation (K_0=1.0) are shown in Figure 4.42 for CU tests and Figure 4.43 for CD tests.

Herein all grain size distribution curves were quantified by relative breakage, which is adopted to interpret the characteristics of particle breakage. Figure 4.56 shows the relative breakage under initial stress anisotropy and isotropy. Figure 4.56(a) shows $B_r - \varepsilon_1$ relationship under initial stress anisotropy (σ_c=1.5MPa K_0=0.5) and initial stress isotropy (σ_c=2.0MPa K_0=1.0), where particle breakage is found to increase linearly approximately with increasing axial strain. It is notable that the particle breakage in relative breakage induced during anisotropic consolidation to confining pressure σ_c =1.5MPa in K_0 =0.5 is more substantial than that induced during isotropic consolidation to confining pressure σ_c=2.0MPa in K_0=1.0 as a result of that the deviator stress imposed on specimens increased from 0 to 1.5MPa during anisotropic

consolidation (σ_c=1.5MPa K_0=0.5) but the deviator stress imposed on specimens was not produced during isotropic consolidation (σ_c=2.0MPa K_0=1.0). Particle breakage in relative breakage in increment from particle breakage in relative breakage induced just during consolidation is found to be more substantial under initial stress isotropy (σ_c=2.0MPa K_0=1.0) than that under initial stress anisotropy (σ_c=1.5MPa K_0=0.5). However according to particle breakage in relative breakage as an absolute value from original grain size distribution curve, the initial stress anisotropy has a more influence on particle breakage in relative breakage at the beginning stage of shearing but with increasing axial strain the higher confining pressure under initial stress isotropy (σ_c=2.0MPa K_0=1.0) has a more influence on particle breakage than that under initial stress anisotropy (σ_c=1.5MPa K_0=0.5) with the influence of initial stress anisotropy. In addition, during shearing, the increment of particle breakage under initial stress isotropy (σ_c=2.0MPa K_0=1.0) is found to be larger than that under initial stress anisotropy (σ_c=1.5MPa K_0=0.5). As seen clearly in Figure 4.56(a), the particle breakage in relative breakage is more substantial in the tests with initial stress anisotropy (σ_c=1.5MPa K_0=0.5) than that in the tests with initial stress isotropy (σ_c=2.0MPa K_0=1.0) but with increasing axial strain particle breakage in relative breakage becomes larger in the tests with initial stress isotropy (σ_c=2.0MPa K_0=1.0) than that in the tests with initial stress anisotropy (σ_c=1.5MPa K_0=0.5). The difference of particle breakage in relative breakage between CD tests and CU tests with the initial stress anisotropy or initial stress isotropy is found to increase with increasing axial strain, which is related to the increasing difference of deviator stresses between CD tests and CU tests with increasing axial strain.

Figure 4.56(b) shows the relationship of relative breakage and mean effective stress under initial stress anisotropy and isotropy, where more particle breakage is found clearly to be caused during anisotropic consolidation than isotropic consolidation. Figure 4.56(c) shows the evolution of particle breakage in relative breakage against effective stress obliquity ratio under initial stress anisotropy and isotropy.

It can be concluded herein that during consolidation the initial stress anisotropy (σ_c=1.5MPa K_0=0.5) results in more particle breakage than the initial stress isotropy (σ_c=2.0MPa K_0=1.0) and during shearing the higher confining pressure (σ_c=2.0MPa K_0=1.0) has a much more influence on particle breakage in comparison with the initial stress anisotropy (σ_c=1.5MPa K_0=0.5).

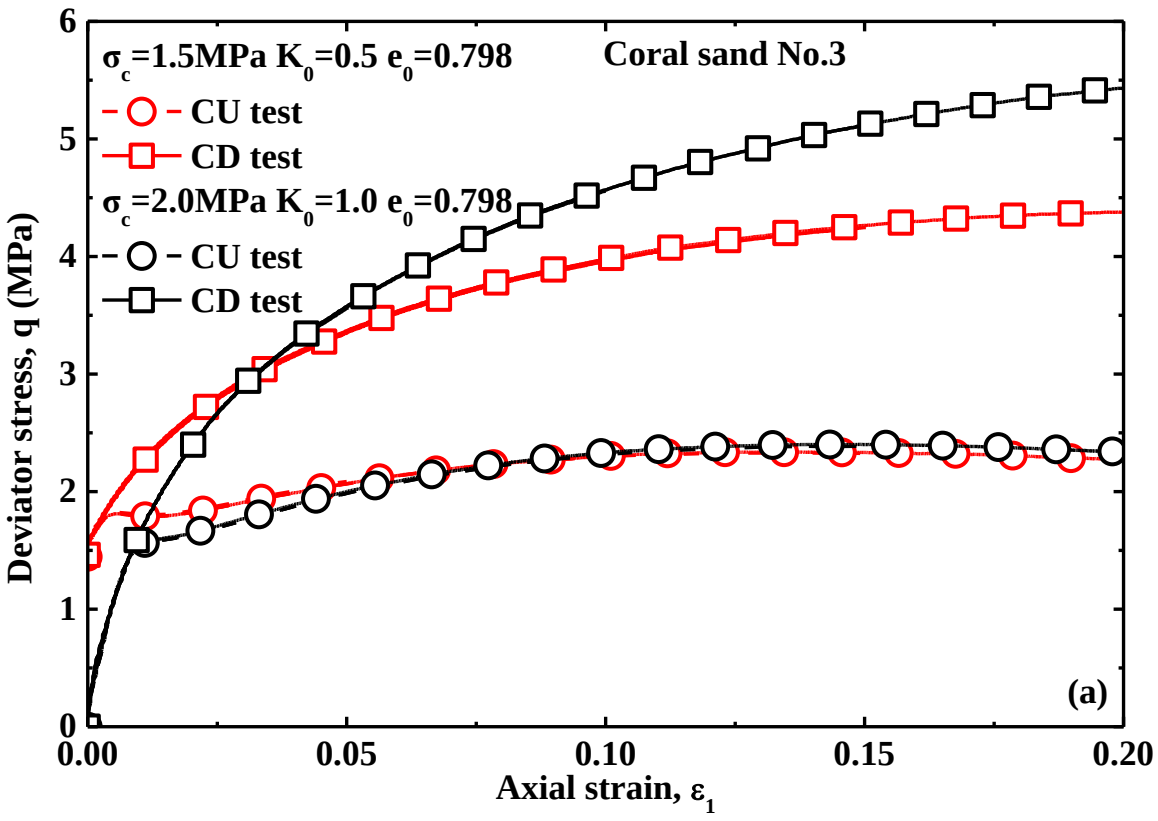
σc=1.5MPa K0=0.5 e0=0.798
Coral sand No.3
CU test
CD test
σc=2.0MPa K0=1.0 e0=0.798
CU test
CD test
Deviator stress, q (MPa)
Axial strain, ε1
(a)
0
1
2
3
4
5
6
0.00
0.05
0.10
0.15
0.20

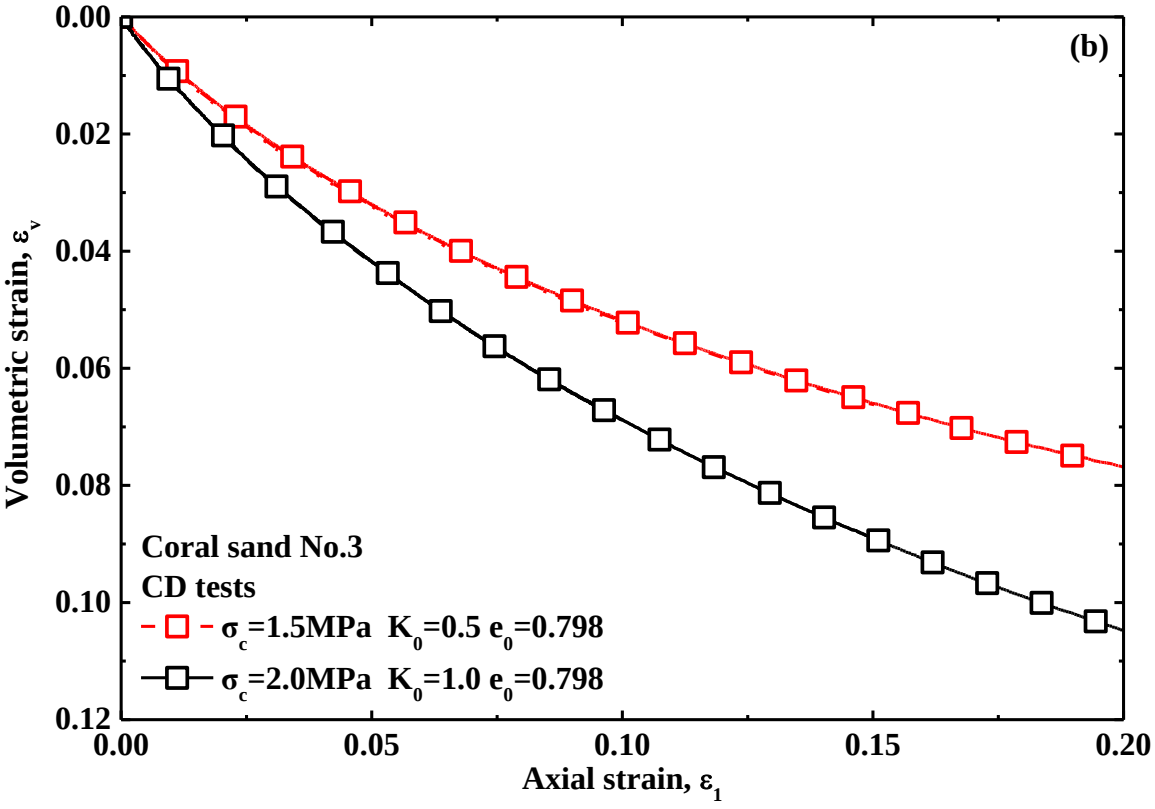
(b)
Volumetric strain, εv
Coral sand No.3
CD tests
σc=1.5MPa K0=0.5 e0=0.798
σc=2.0MPa K0=1.0 e0=0.798
Axial strain, ε1
0.00
0.02
0.04
0.06
0.08
0.10
0.12
0.00
0.05
0.10
0.15
0.20

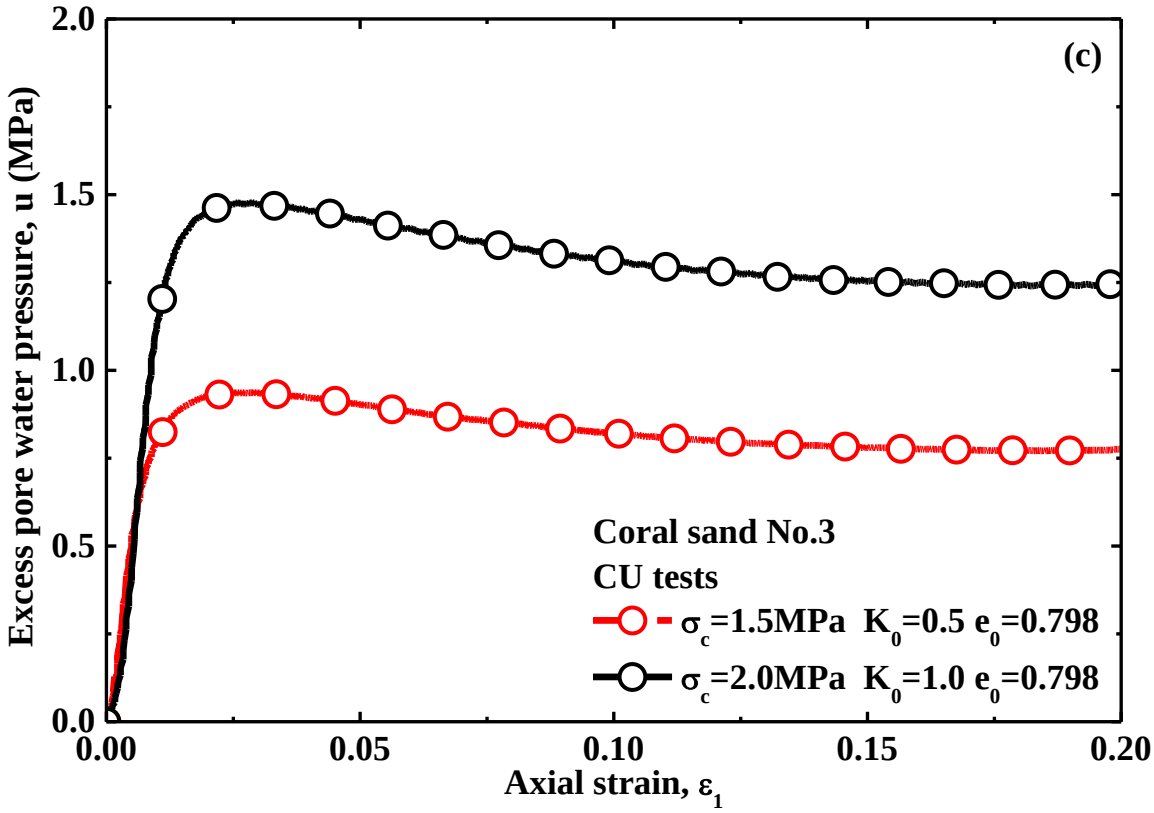

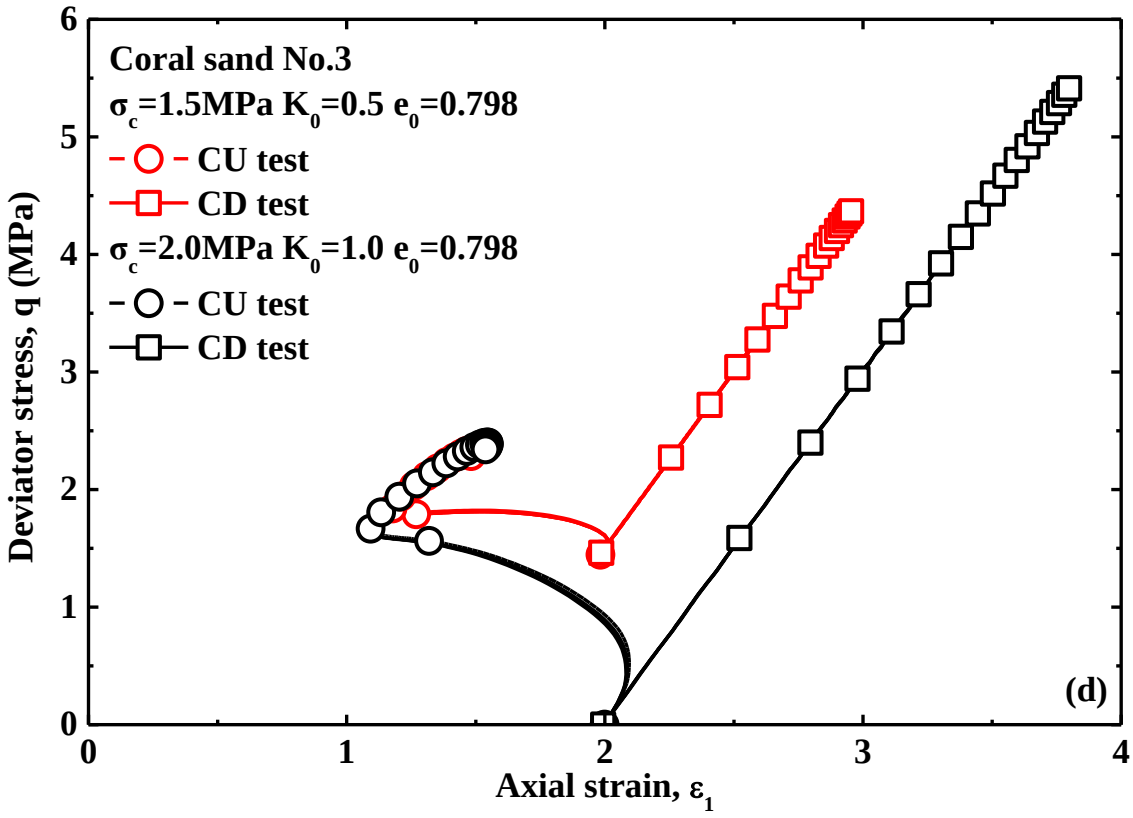

Figure 4.53 Triaxial test results (σ_c=1.5MPa K_0=0.5 & σ_c=2.0MPa K_0=1.0)

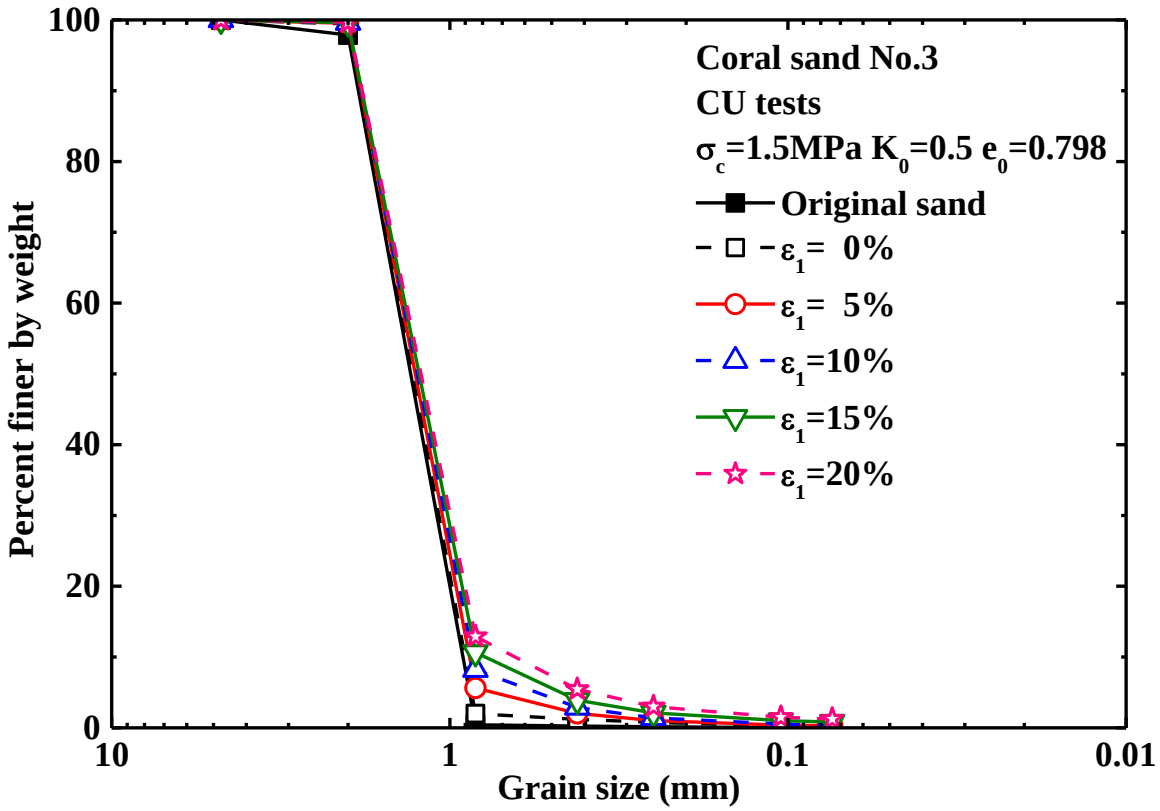

Figure 4.54 Grain size distribution curves from CU tests (σ_c=1.5MPa K_0=0.5 e_0=0.798)

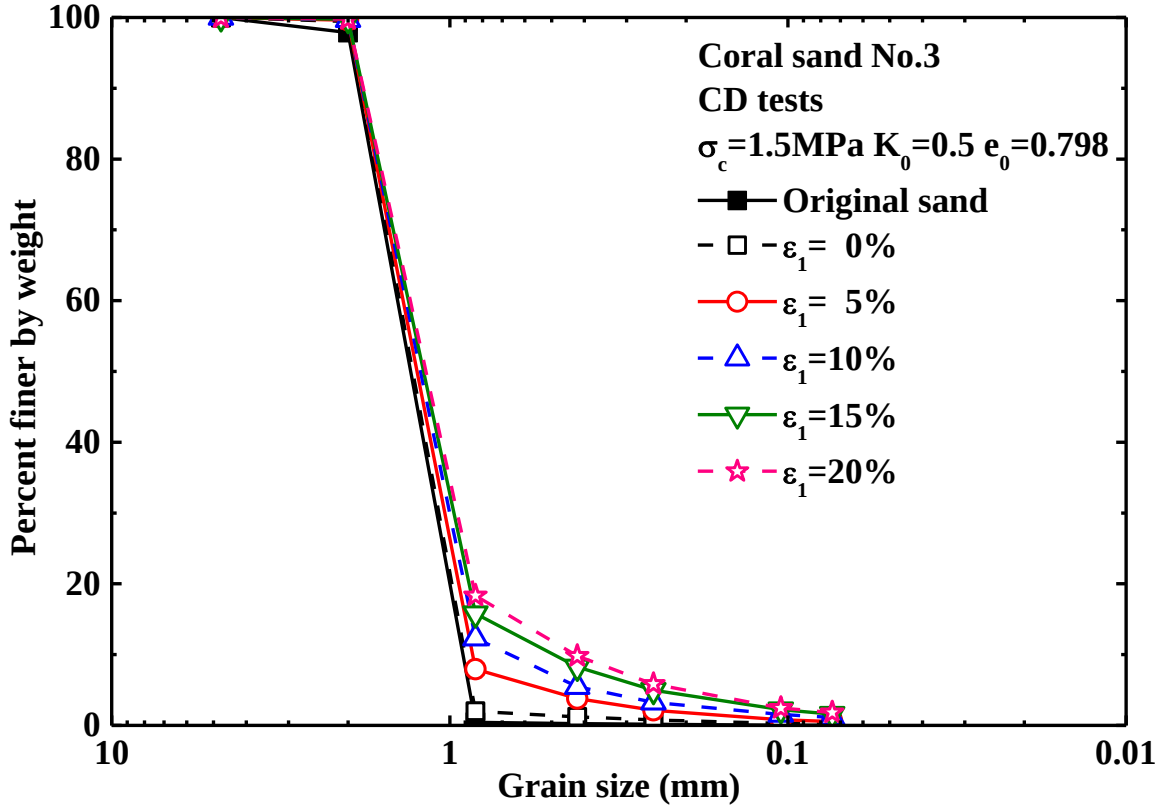

Figure 4.55 Grain size distribution curves from CD tests (σ_c=1.5MPa K_0=0.5 e_0=0.798)

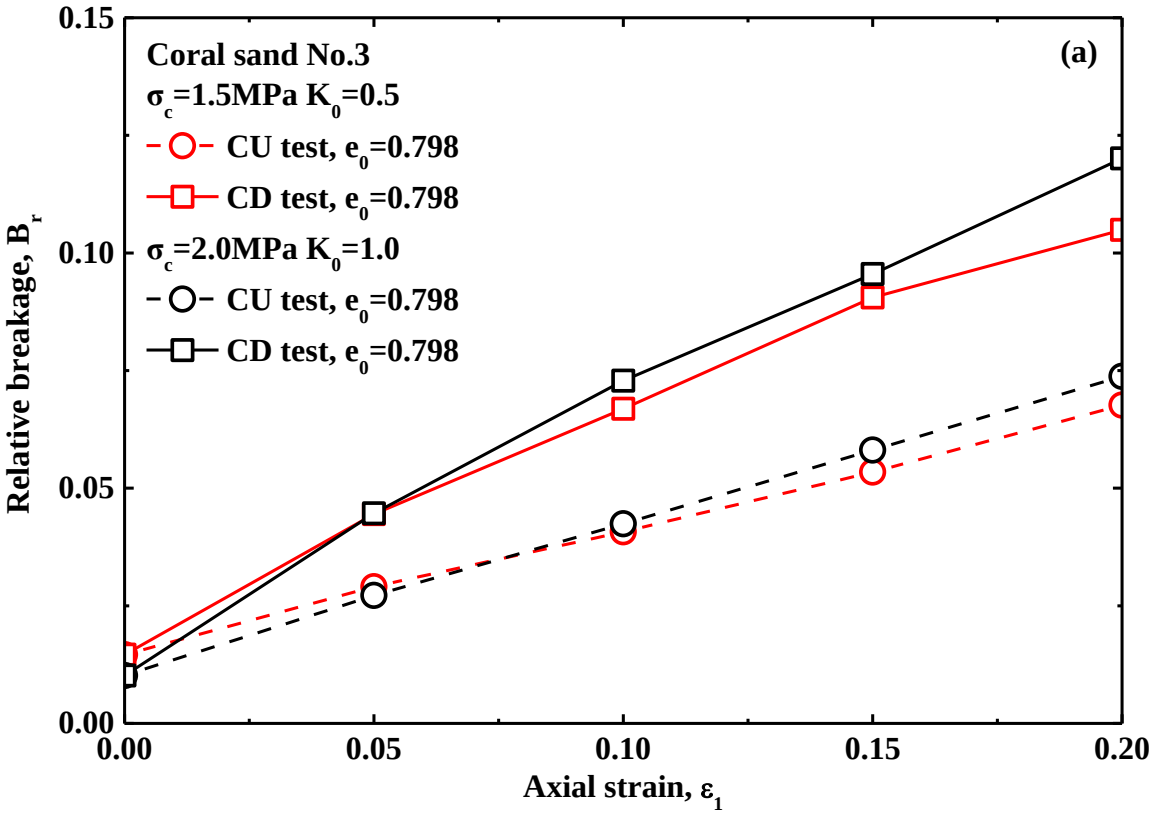
Coral sand No.3
(a)
σc=1.5MPa K0=0.5
CU test, e0=0.798
CD test, e0=0.798
σc=2.0MPa K0=1.0
CU test, e0=0.798
CD test, e0=0.798
Relative breakage, Br
Axial strain, ε1
0.00
0.05
0.10
0.15
0.20

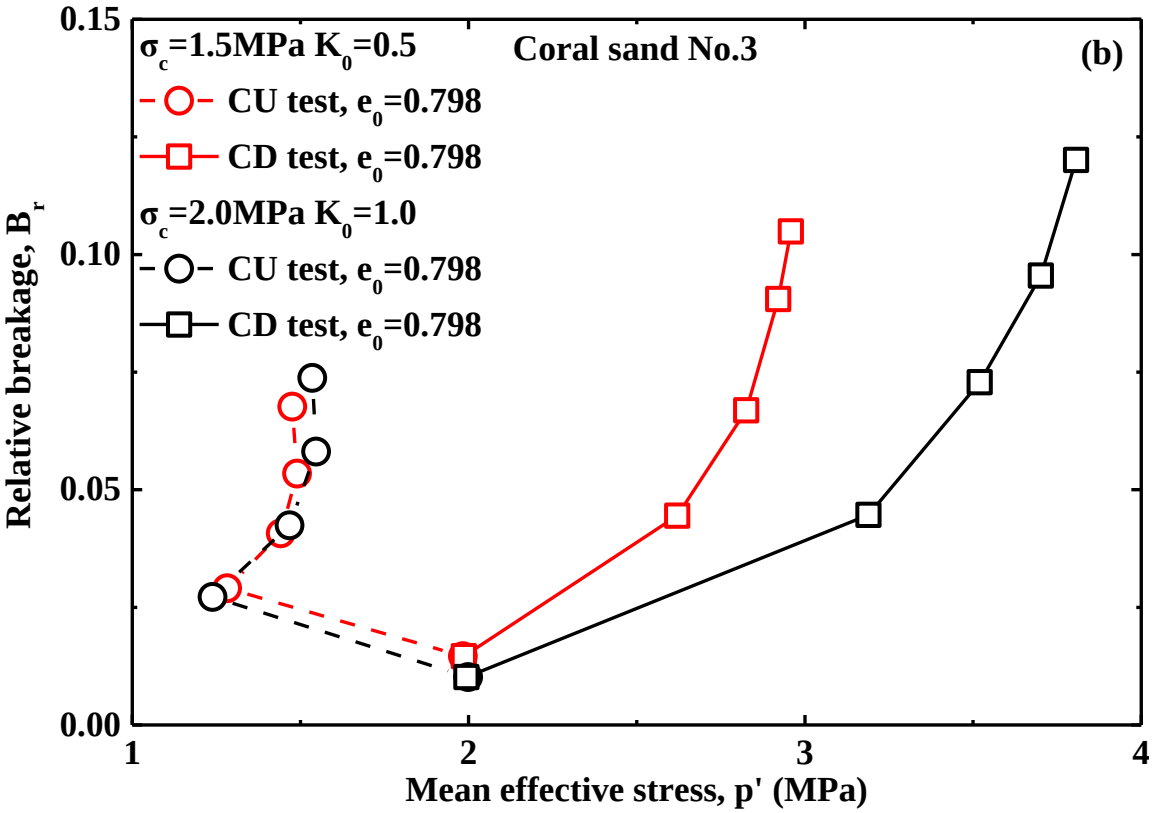
Coral sand No.3
(b)
σc=1.5MPa K0=0.5
CU test, e0=0.798
CD test, e0=0.798
σc=2.0MPa K0=1.0
CU test, e0=0.798
CD test, e0=0.798
Relative breakage, Br
Mean effective stress, p' (MPa)
1
2
3
4

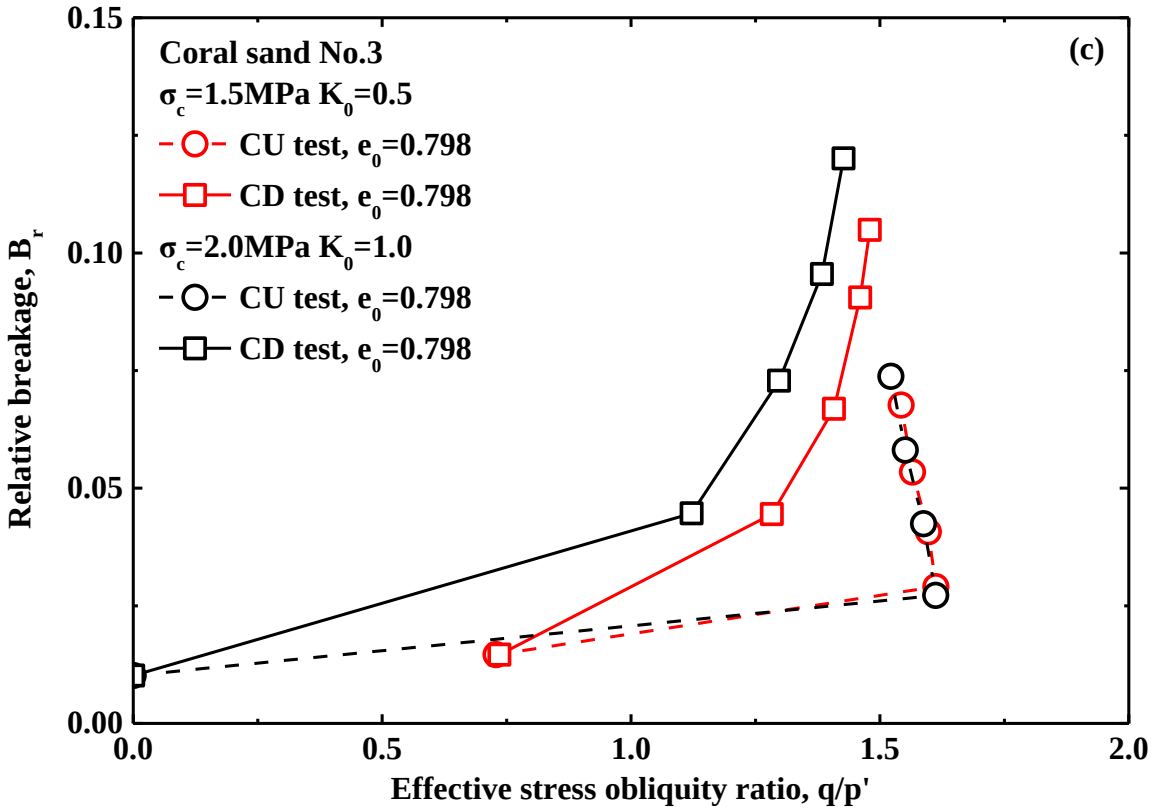

Figure 4.56 Relative breakage under initial stress anisotropy and isotropy

4.6.4 The Influence of Cyclic Loading on Particle Breakage

Cyclic loading has a significant influence on soil behavior. The cyclic loading imposed on specimen was adopted in triaxial tests under high pressure to investigate its influence on the characteristics of particle breakage. All triaxial tests were sheared to 20% axial strain and then terminated after the designated cycle numbers of cyclic loading such as 0, 2, 5, 10 and 20 times in order.

Figure 4.57 shows the triaxial tests results subjected to cyclic loading, where the cyclic loading is found to result in increase of additional axial strain and volume change with increasing cycle numbers of cyclic loading as shown in Figure 4.57(a) and (b). It can be seen in Figure 4.57(b) that the cyclic loading results in a dramatic increase of volume change in comparison with the development trend of volume change during monotonic loading, which may be related to the particle breakage. Figure 4.57(c) shows the stress paths of triaxial tests subjected to cyclic loading.

All specimens after shearing were kept to dry for getting the relevant grain size distribution curves by sieve analysis. The relevant grain size distribution curves from the triaxial tests subjected to cyclic loading are shown in Figure 4.58, where it can be seen that the grain size distribution curves evolved toward the increase of fines content with increasing cycle numbers of cyclic loading. All grain size distribution curves were quantified by relative breakage in description of extent of particle breakage. Figure 4.59

shows the $B_r - N$ relationship under cyclic loading, where particle breakage in relative breakage is found to increase in reduced increments with increasing cycle numbers of cyclic loading, which are related to the additional axial strain and volume change during cyclic loading. The relationship between relative breakage and axial strain would be also investigated as shown in Figure 4.60, where particle breakage in relative breakage is found to increase in increased increments with increasing axial strain.

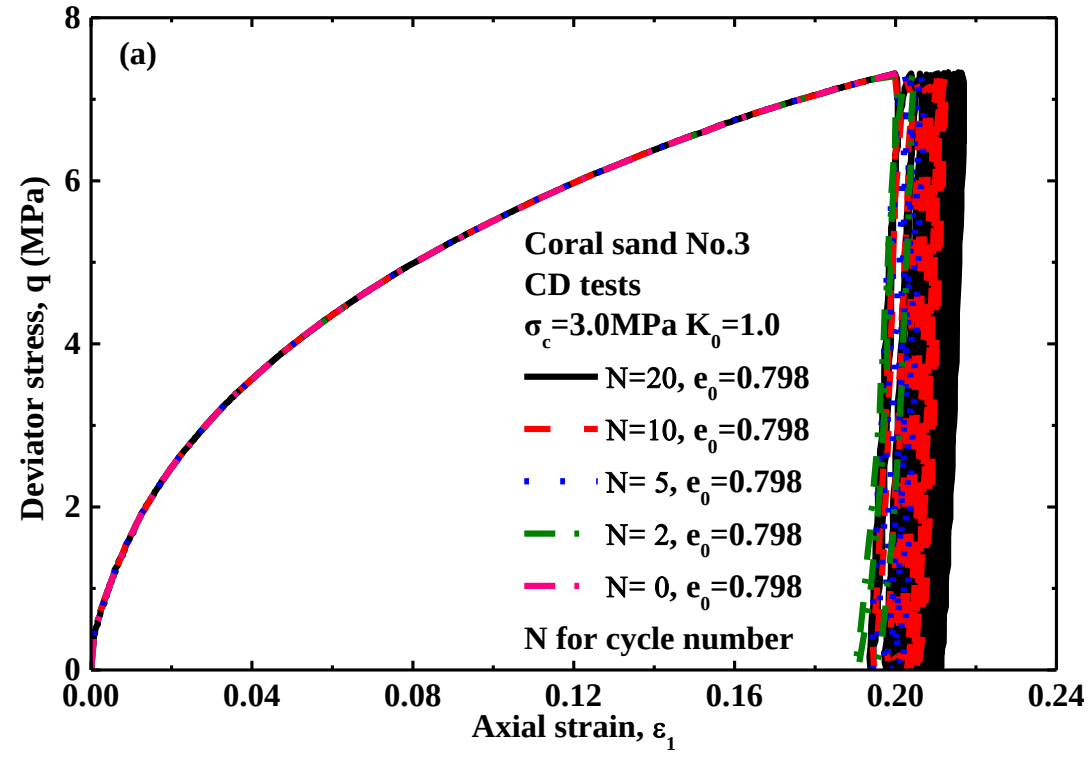

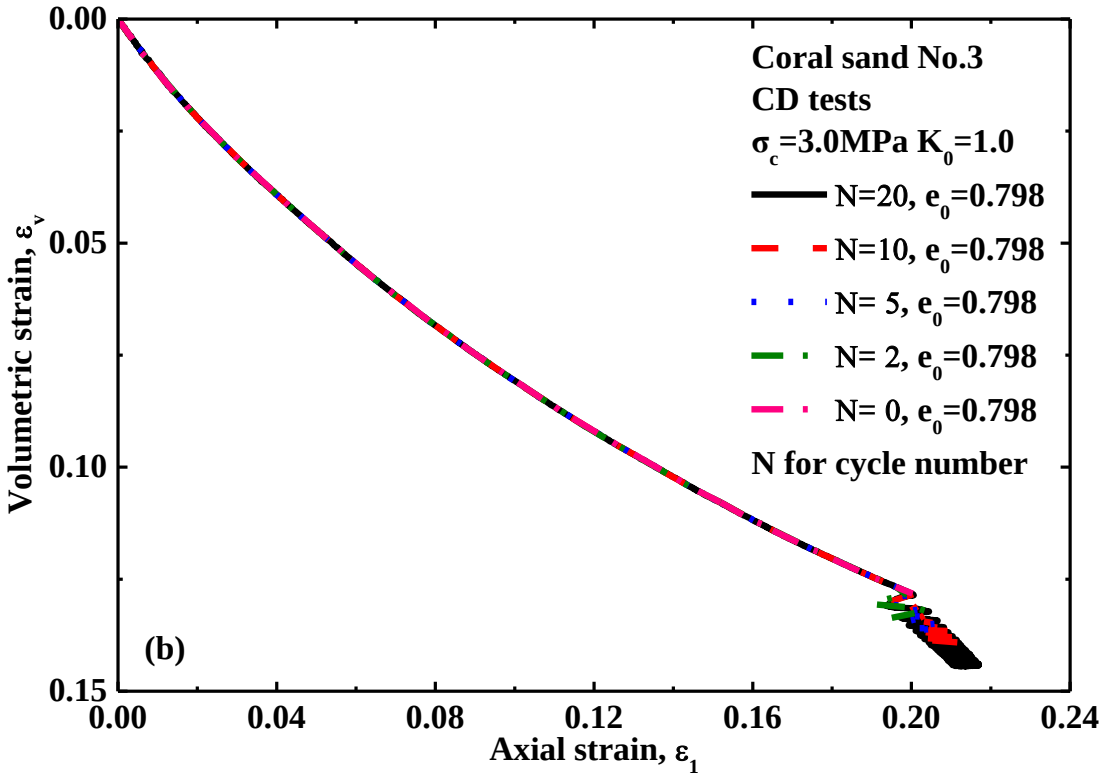

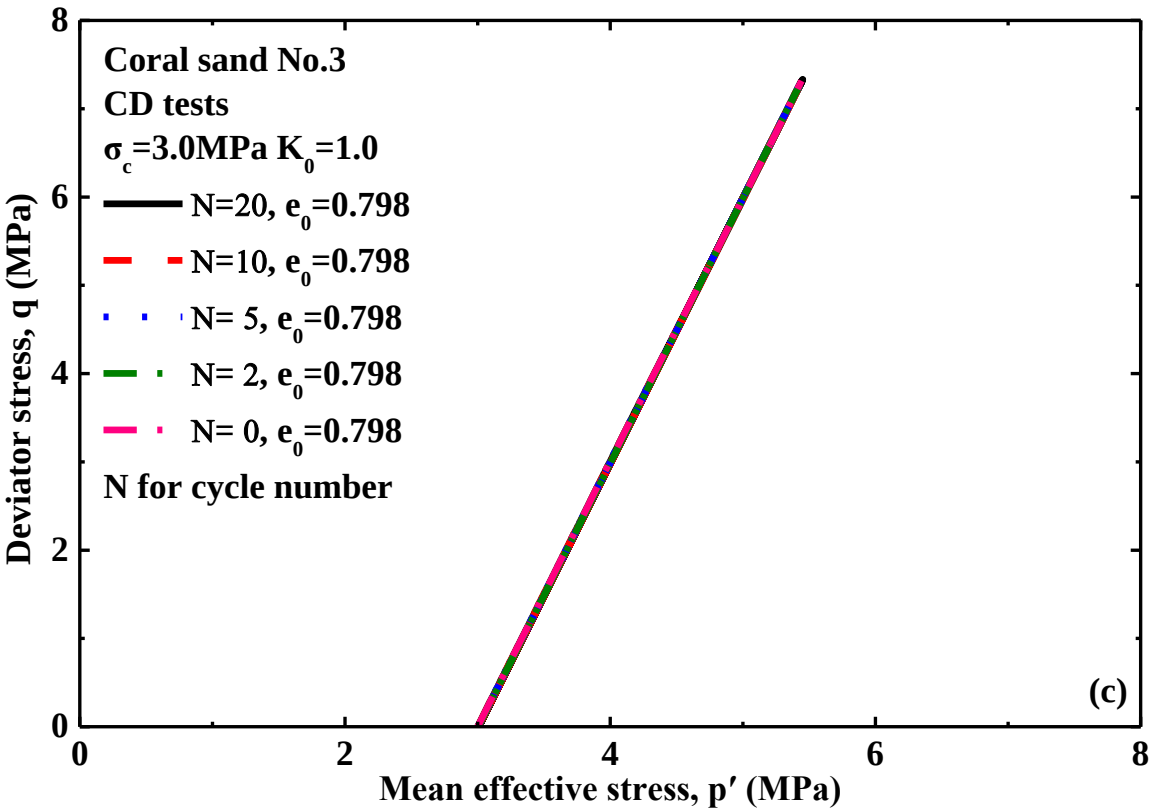

Figure 4.57 Triaxial test results under cyclic loading (σ_c=3.0MPa K_0=1.0 e_0=0.798)

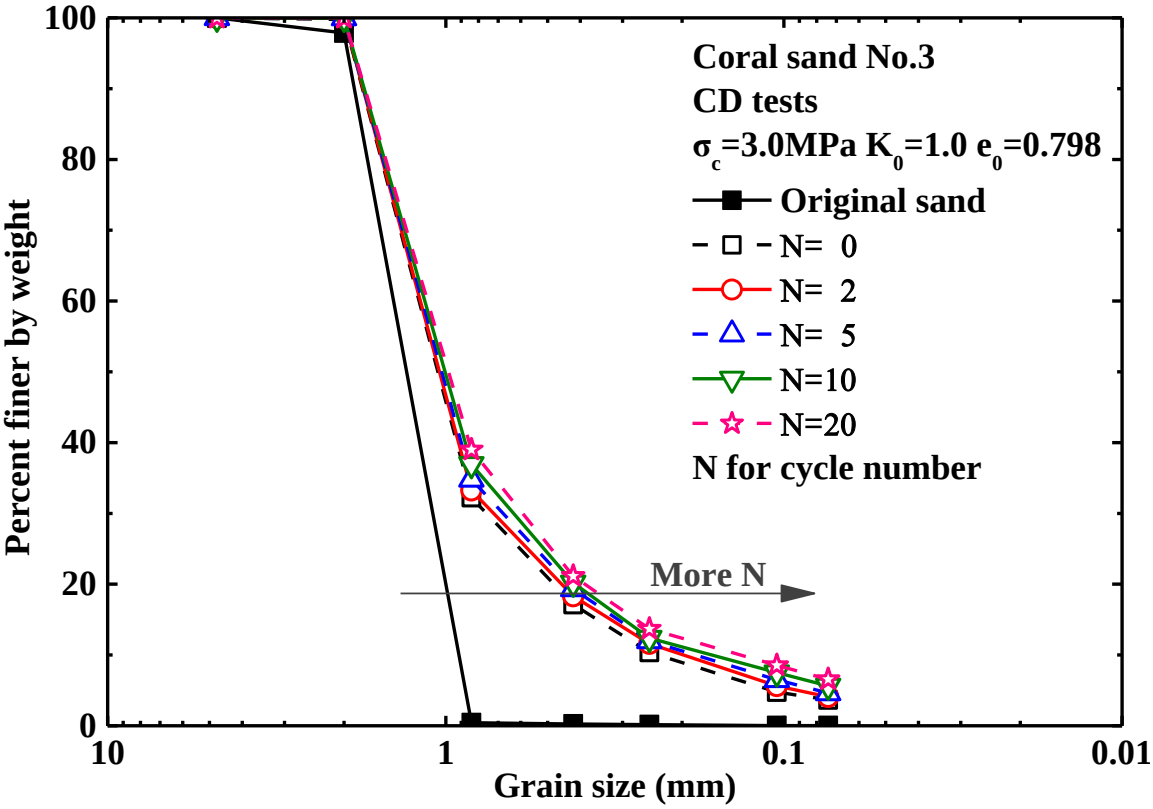

Figure 4.58 Grain size distribution curves under cyclic loading (σ_c=3.0MPa K_0=1.0 e_0=0.798)

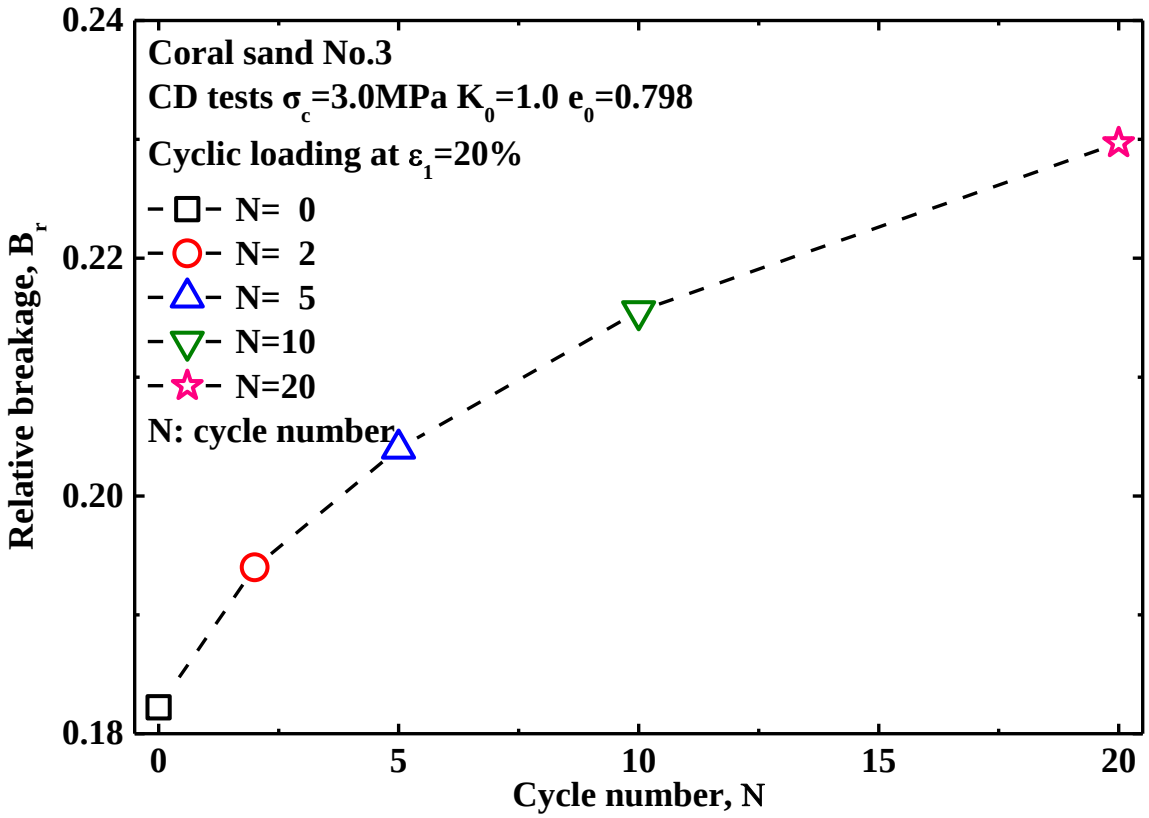

Figure 4.59 B_r-N relation under cyclic loading (σ_c=3.0MPa K_0=1.0 e_0=0.798)

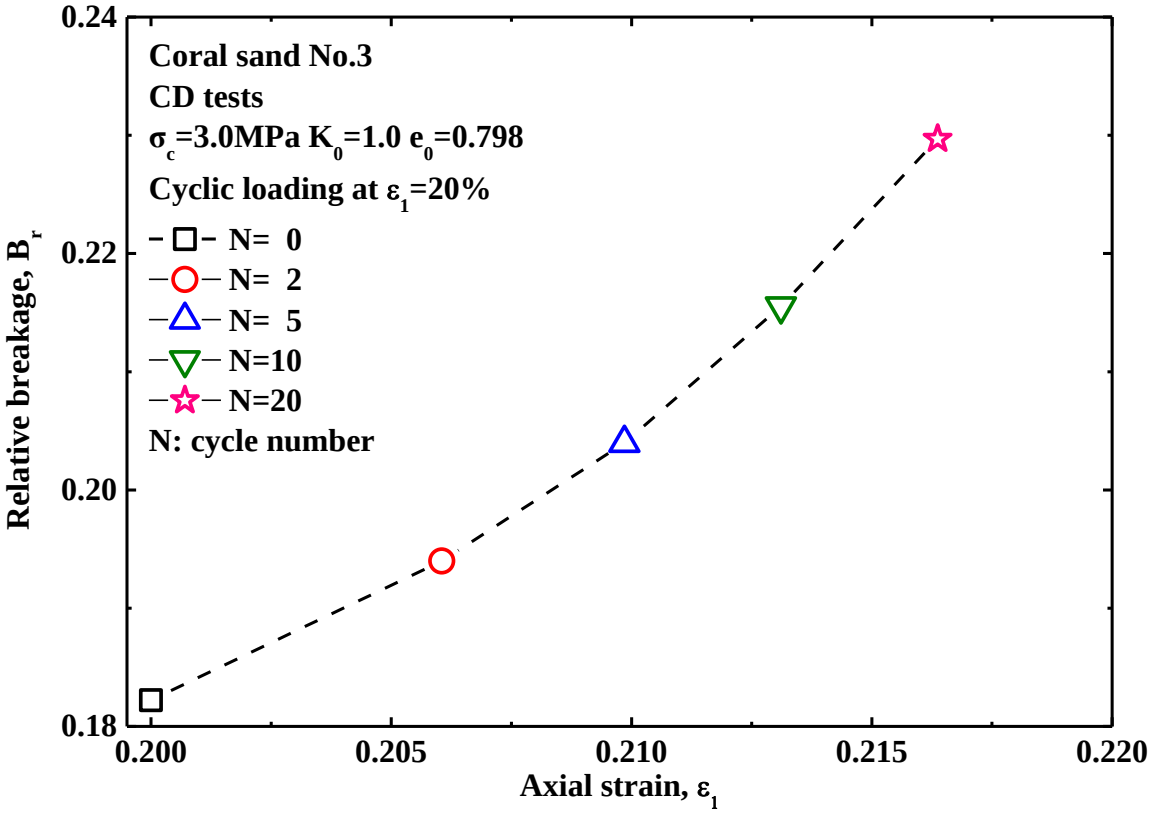

Figure 4.60 B_r-ε_1 relation under cyclic loading (σ_c=3.0MPa K_0=1.0 e_0=0.798)

4.6.5 The Influence of Drainage Condition on Particle Breakage

Most of triaxial tests were conducted under Consolidated Drained (CD) condition and Consolidated Undrained (CU) condition to investigate the influence of drainage condition on characteristics of particle breakage. The influences of drainage condition on soil behavior and particle breakage have been discussed above in relevant sections. It can be summarized herein that the deviator stresses are much larger in CD tests than that in CU tests as a result of the generation of excess pore water pressure and the difference of deviator stresses between CD tests and CU tests was found to increase with increasing axial strain as shown in Figure 4.41(a), Figure 4.47(a) and Figure 4.53(a). In addition, particle breakage in relative breakage was found to be more substantial in CD tests than that in CU tests and the difference of particle breakage in relative breakage between CD tests and CU tests was found to increase with increasing axial strain, which are related to the findings in development of deviator stress between CD tests and CU tests, as shown in Figure 4.46, Figure 4.52 and Figure 4.56(a).

4.6.6 A Model to Assess Relative Breakage of Coral Sand No.3

Characteristics of Particle breakage are influenced by many factors such as particle shape, particle hardness, stress paths, initial void ratio, initial grain size distribution, and so on, which have a significant cross-jointed influence on relative breakage. In laboratory tests, the grain size distribution curves after shearing can be obtained by sieve analysis but the laboratory tests is not always effective to simulate the mechanical process especially in complex stress paths. In this case, the relevant grain size distribution curves after shearing cannot be obtained. With an attempt to establish a model to express relative breakage, the relationship between relative breakage and plastic work per unit volume were reanalyzed further under various conditions. In addition, the plastic work per unit volume can be regarded as a comprehensive index to consider characteristics of material such as initial grain size distribution, particle shape, state of effective stress, etc.

As derived in detail in APPENDIX Ⅰ, plastic work per unit volume can be obtained by triaxial results directly after that each test was unloaded back to initial consolidation state after shearing for removing the elastic work per unit volume from total work per unit volume. In addition, plastic work per unit volume can be regarded as a comprehensive index including the effects of confining pressure, initial void ratio of specimen, initial stress anisotropy, drainage conditions during shearing, shearing behavior and so on, which influence the characteristics of particle breakage. The relationship between relative breakage and plastic work per unit volume is shown in Figure 4.61, where the relative breakage is found to increase gradually in reduced increments with increasing plastic work per unit volume, being consistent with the characteristics of a hyperbola. Consequently, the hyperbola model should be established as shown in equation 4.1. The two model parameters were determinated by data fitting as shown in Figure 4.61(a), which was redrawn in semi-logarithmic coordinates to see the detailed data as shown in Figure 4.61(b).

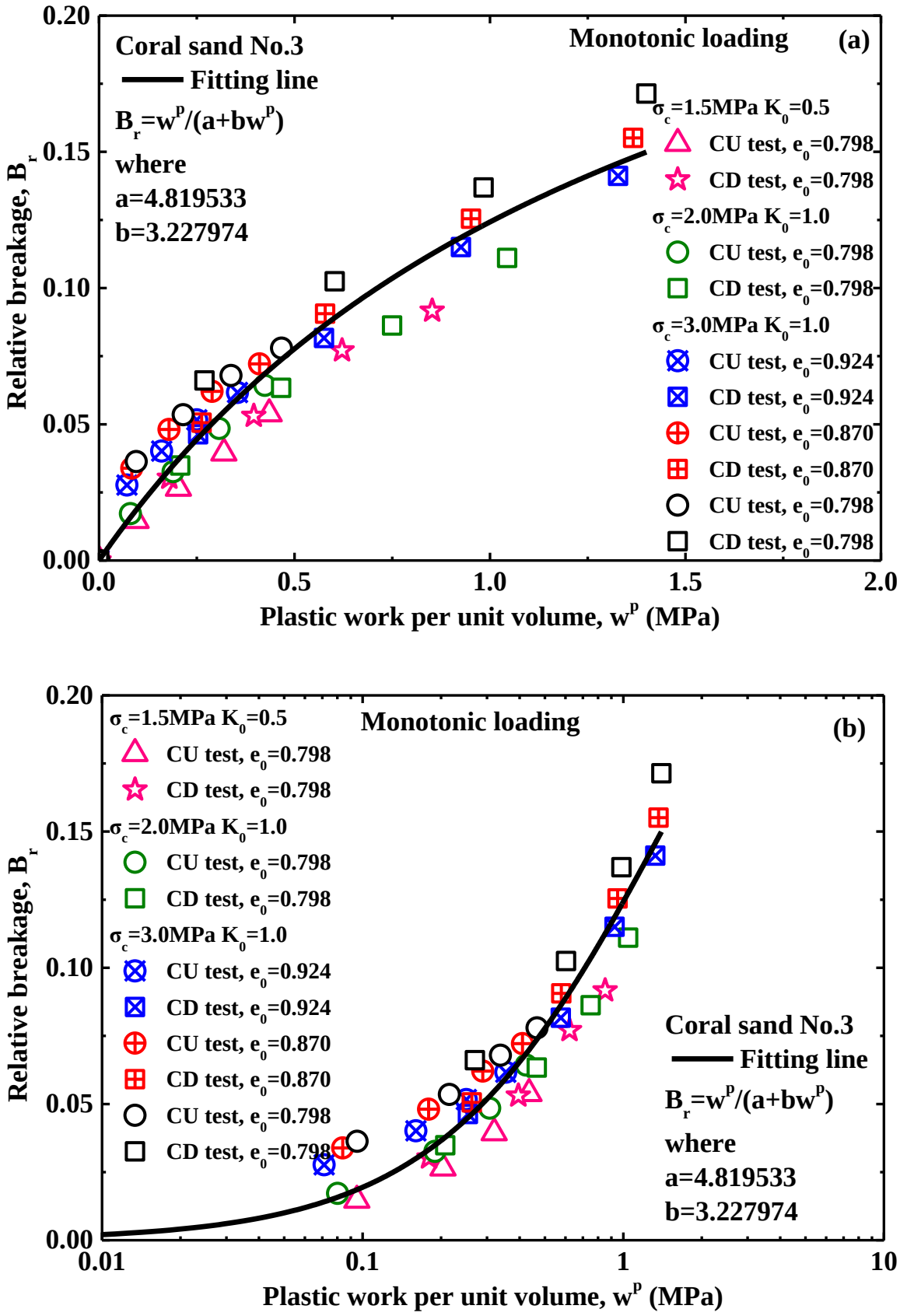

Figure 4.61 Relationship between relative breakage and plastic work per unit volume of Coral sand No.3 in monotonic loading

The influence of the initial state of tests and tested conditions can be investigated as well. Under same plastic work per unit volume, more particle breakage was caused in denser samples and CD tests results in more particle breakage. In addition, more particle breakage against same plastic work per unit volume was caused on samples under (σ_c=2.0MPa, K_0=1.0) than that under (σ_c=1.5MPa, K_0=0.5). However, the data of relative breakage and plastic work per unit volume falls into an approximately parallel margin following a hyperbolic relationship, which has a different type with the relationship of relative breakage and plastic work per unit volume from Silica sand No.5. This may be caused by different characteristics of particle breakage during monotonic loading.

4.7 COMPARISON ON SILICA SAND NO.5 AND CORAL SAND NO.3

The experimental results from Silica sand No.5 and Coral sand No.3 were compared to investigate the characteristics of particle breakage by two completely different types of sand.

4.7.1 Comparison Under Same Initial Void Ratio

Initial void ratio on specimen has a significant influence on soil behavior. The specimens were prepared by Silica sand No.5 and Coral sand No.3 separately to reach same initial void ratio after consolidation.

Figure 4.62 shows the compared results between Silica sand No.5 and Coral sand No.3 under 3MPa confining pressure with same initial void ratio. It can be seen herein that in CD tests the deviator stress of Coral sand No.3 has much steeper development with increasing axial strain than that of Silica sand No.5, and exceeds the deviator stress of Silica sand No.5 at the latter half part of shearing as shown in Figure 4.62(a). Even though there is no big difference of the deviator stresses between Silica sand No.5 and Coral sand No.3 in CD tests, the volume change in contractancy on Coral sand No.3 is much more substantial than that of Silica sand No.5 as shown in Figure 4.62(b) which may be related to particle breakage during shearing. The deviator stress of Silica sand No.5 is seen in CU tests to exceed that of Coral sand No.3 after a slightly lower stage in first half shearing as displayed in Figure 4.62(a) but the excess pore water pressure is found to much more substantial in Coral sand No.3 than that in Silica sand No.5 as shown in Figure 4.62(c).

Figure 4.62(d) shows the relationship between relative breakage and axial strain for comparison of Silica sand No.5 and Coral sand No.3 under 3MPa confining pressure. It is seen clearly that particle breakage increases with increasing axial strain but the particle breakage of Coral sand No.3 is much more substantial than that of Silica sand No.5 in CD tests, which may be related to more crushability causing the more volume change in contractancy in Coral sand No.3. However in CU tests particle breakage in relative breakage of Coral sand No.3 is more substantial than that of Silica sand No.5 but the increment of particle breakage of Coral sand No.3 is gradually reduced in comparison

with the increased increments in Silica sand No.5, which may be caused by that the more substantial particle breakage elevated the development of larger excess pore water pressure so as to reduce the deviator stresses of Coral sand No.3. It is notable that the particle breakage during cyclic loading has sharper increase than that during monotonic loading, which should be caused by different characteristics and mechanism of particle breakage induced by different loading mode (herein monotonic loading and cyclic loading). This proved that loading mode may result in different tendency of particle breakage (Miura and Ohara, 1979). In addition, the increase rate of particle breakage of Silica sand No.5 is slightly lower than that of Coral sand No.3 which is more crushable.

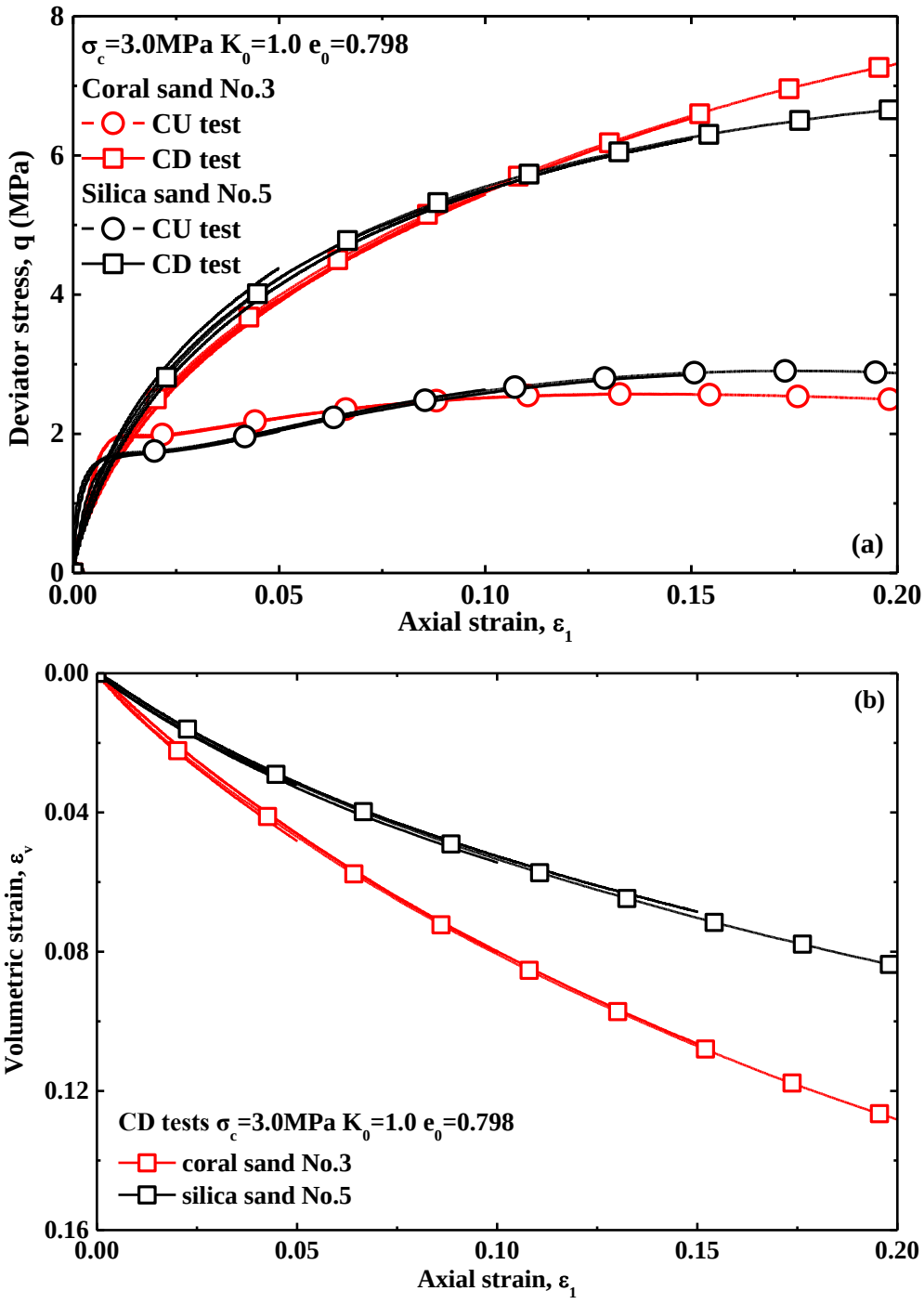

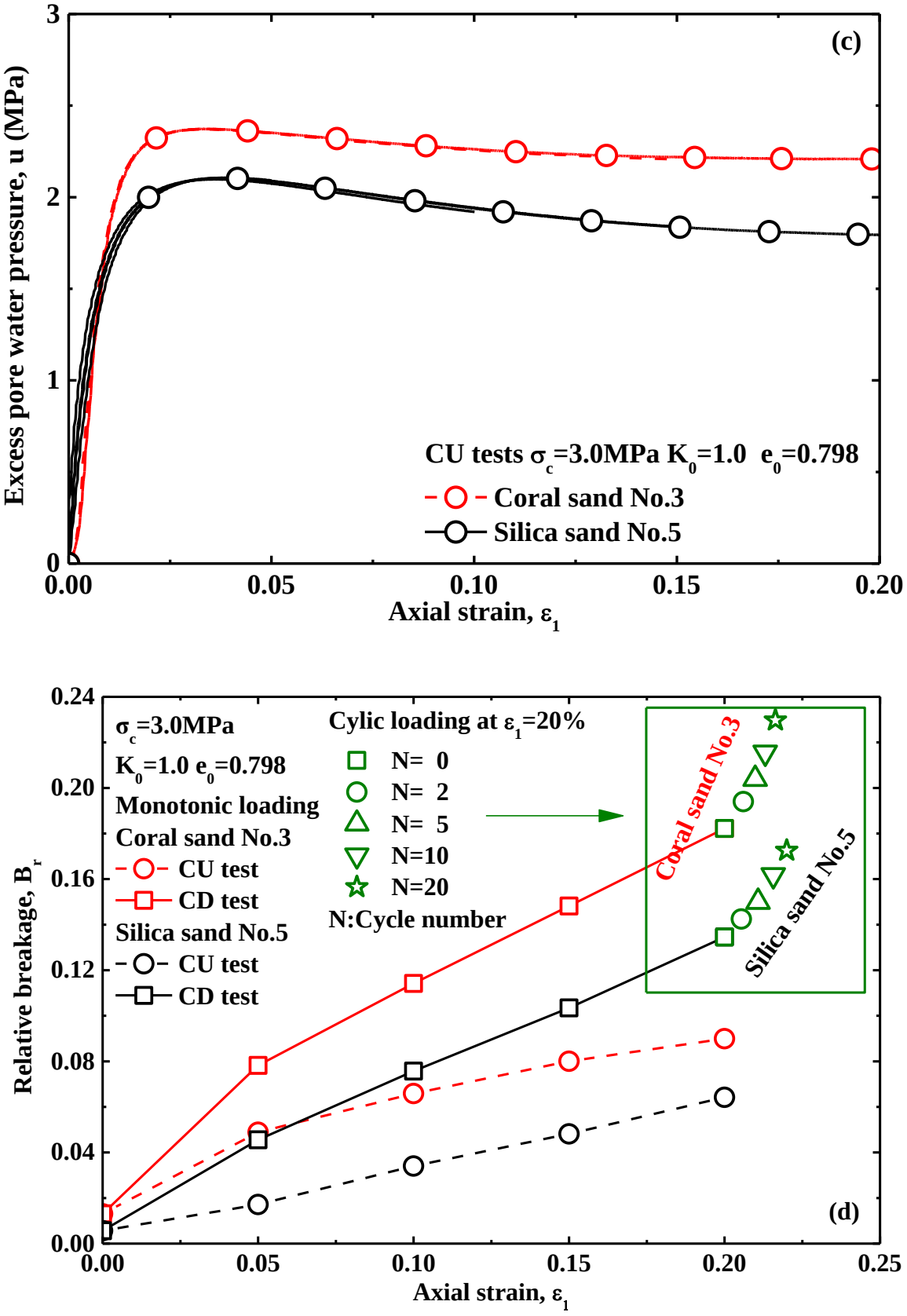

Figure 4.62 Comparison between Silica sand No.5 and Coral sand No.3 (σ_c=3.0MPa K_0=1.0 e_0=0.798)

The triaxial tests on specimens of Silica sand No.5 and Coral sand No.3 with same initial void ratio were also conducted under 2MPa confining pressure to investigate the characteristics of particle breakage. Figure 4.63 shows the compared results from Silica sand No.5 and Coral sand No.3 under same initial void ratio and 2MPa confining pressure. It is seen clearly herein that in CD tests the deviator stress of Coral sand No.3 is similar with that of Silica sand No.5 at the beginning stage of shearing and then getting larger than that of Silica sand No.5 at the latter stage of shearing as shown in Figure 4.63. However the volume change in contractancy of Coral sand No.3 is much more substantial than that of Silica sand No.5 as shown in Figure 4.63(b), which may be related to the particle breakage. The deviator stress of Coral sand No.3 in CU tests is found to have a faster development at the beginning stage of shearing than that of Silica sand No.5 but the deviator stress of Silica sand No.5 is getting larger with bigger increments to peak strength than that of Coral sand No.3 with increasing axial strain as shown in Figure 4.63(a). As shown in Figure 4.63(c), the excess pore water pressure has a more substantial development in Coral sand No.3 than Silica sand No.5.

All grain size distribution curves were obtained after each test to identify the evolution of particle size. The relative breakage was adopted to quantify the extent of particle breakage. Figure 4.63(d) shows the relationship between Coral sand No.3 and Silica sand No.5 under 2MPa confining pressure. It is found herein that particle breakage in relative breakage of Coral sand No.3 is more substantial than that of Silica sand No.5, which means that Coral sand No.3 is much more crushable than Silica sand No.5.

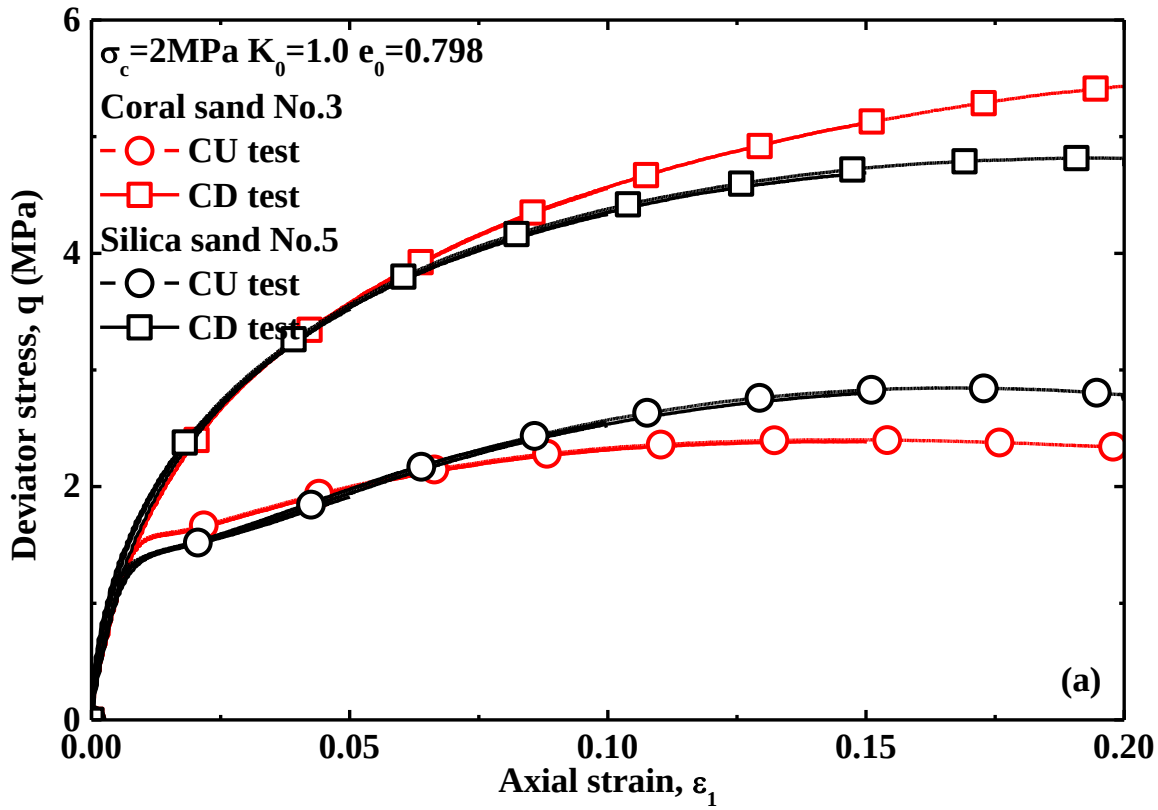

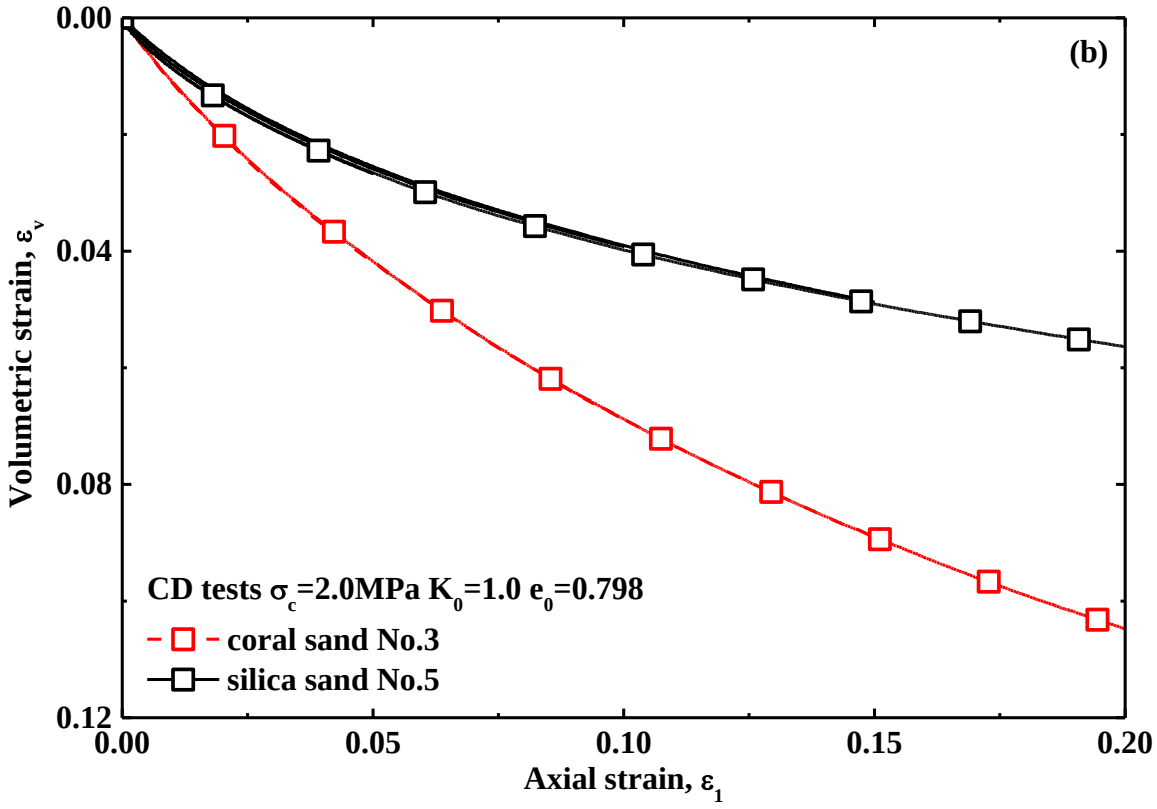
(b)
Volumetric strain, ε_v
0.00
0.04
0.08
0.12
0.00
0.05
0.10
0.15
0.20
Axial strain, ε_1
CD tests σ_c=2.0MPa K_0=1.0 e_0=0.798
coral sand No.3
silica sand No.5

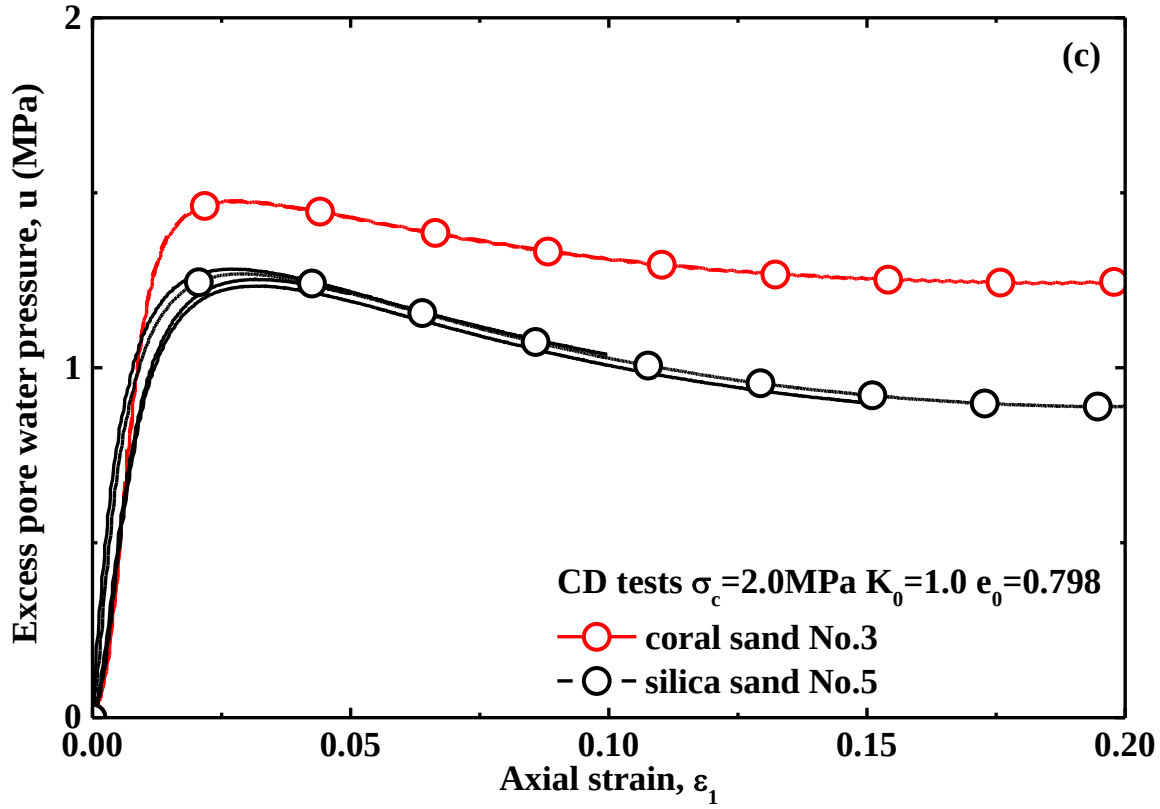
(c)
Excess pore water pressure, u (MPa)
0
1
2
0.00
0.05
0.10
0.15
0.20
Axial strain, ε_1
CD tests σ_c=2.0MPa K_0=1.0 e_0=0.798
coral sand No.3
silica sand No.5

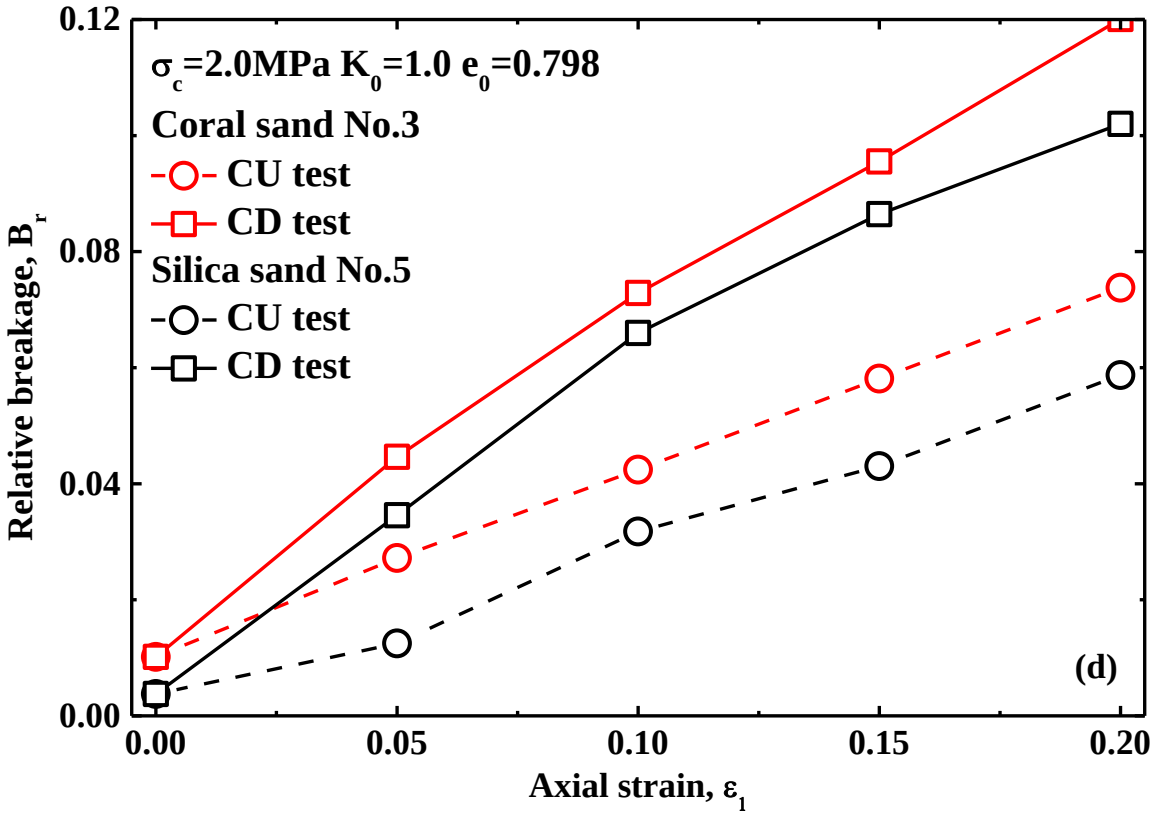

Figure 4.63 Comparison between Silica sand No.5 and Coral sand No.3 (σ_c=2.0MPa K_0=1.0 e_0=0.798)

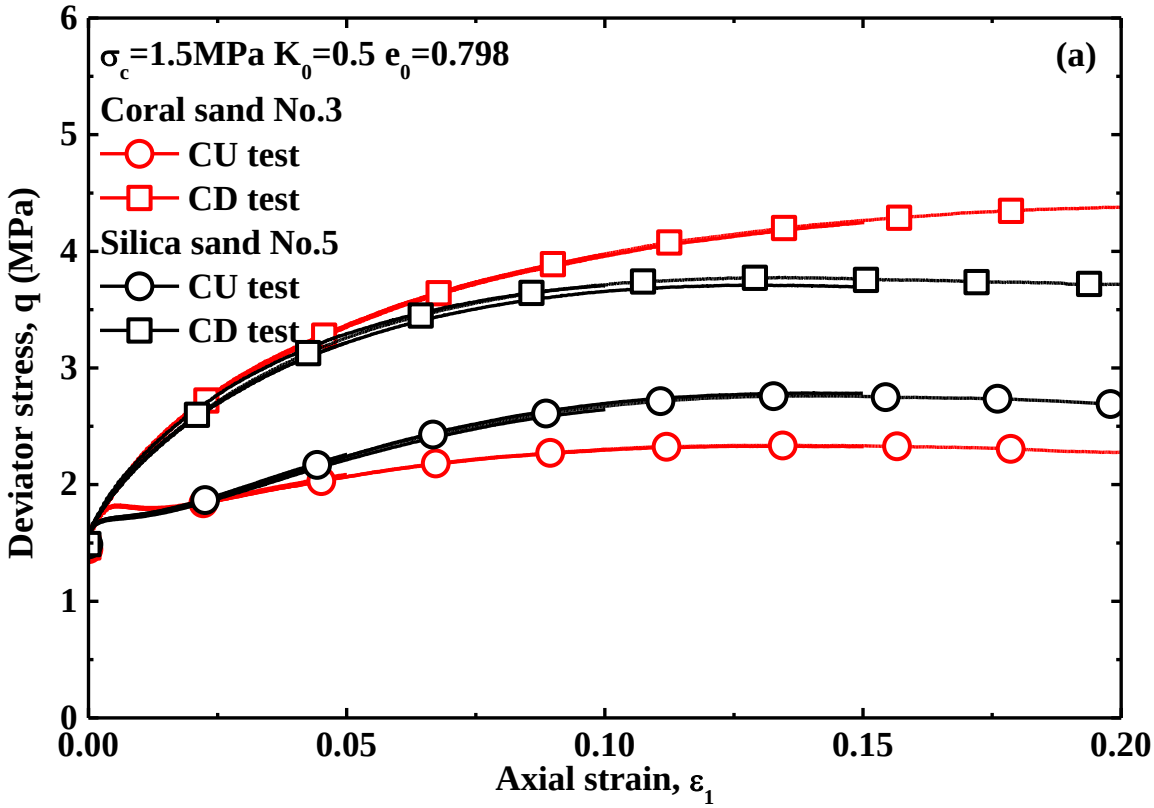

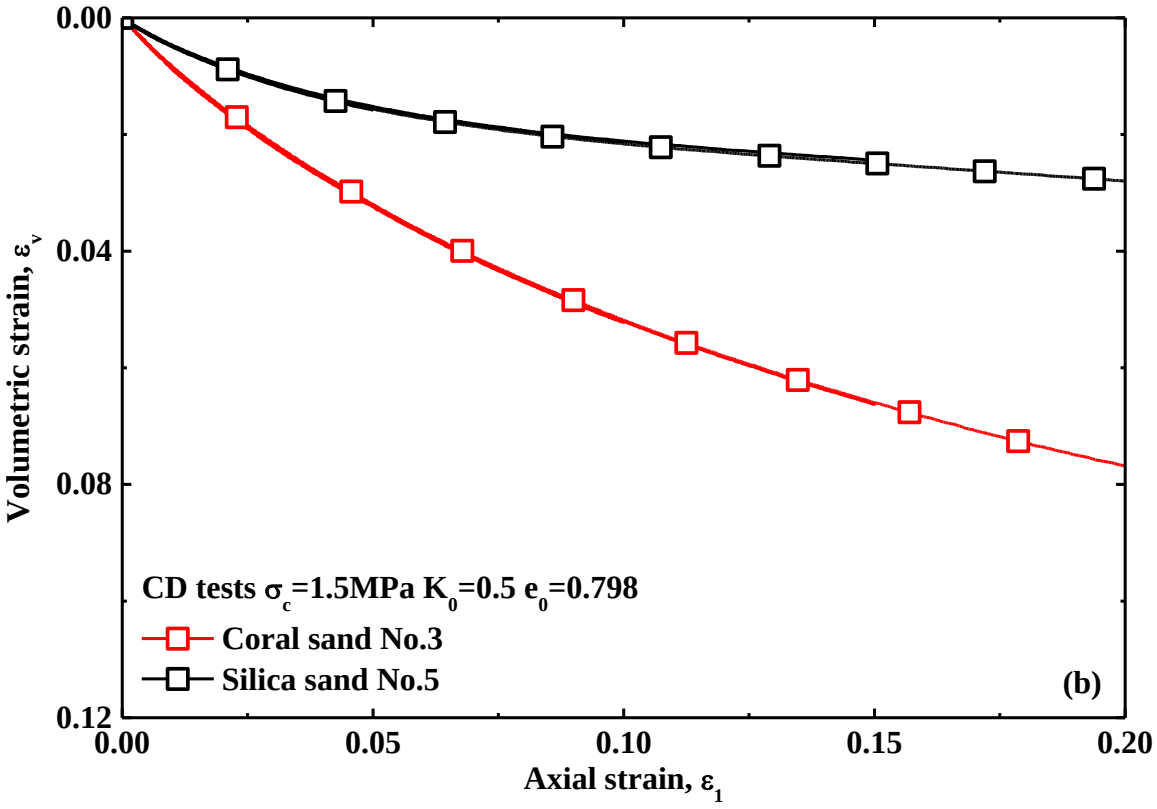
0.00
0.04
0.08
0.12
Volumetric strain, ε_v
CD tests σ_c=1.5MPa K_0=0.5 e_0=0.798
Coral sand No.3
Silica sand No.5
(b)
0.00
0.05
0.10
0.15
0.20
Axial strain, ε_1

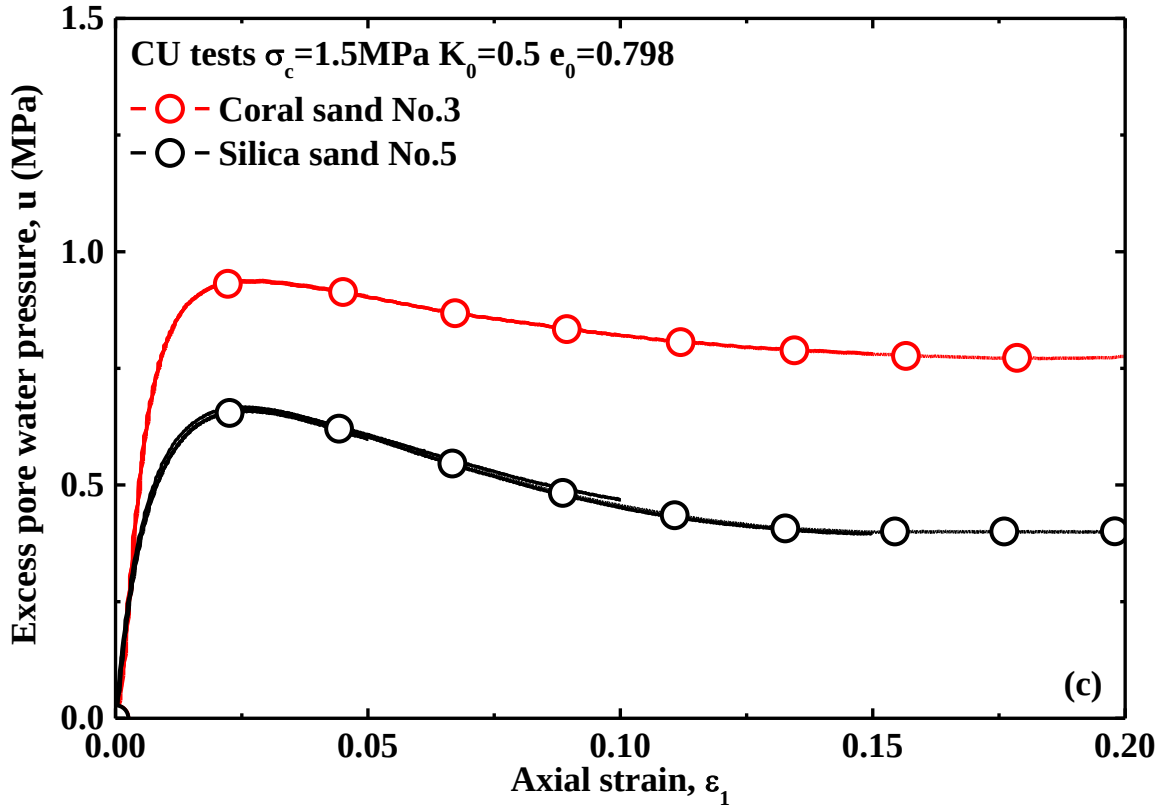
1.5
1.0
0.5
0.0
Excess pore water pressure, u (MPa)
CU tests σ_c=1.5MPa K_0=0.5 e_0=0.798
Coral sand No.3
Silica sand No.5
(c)
0.00
0.05
0.10
0.15
0.20
Axial strain, ε_1

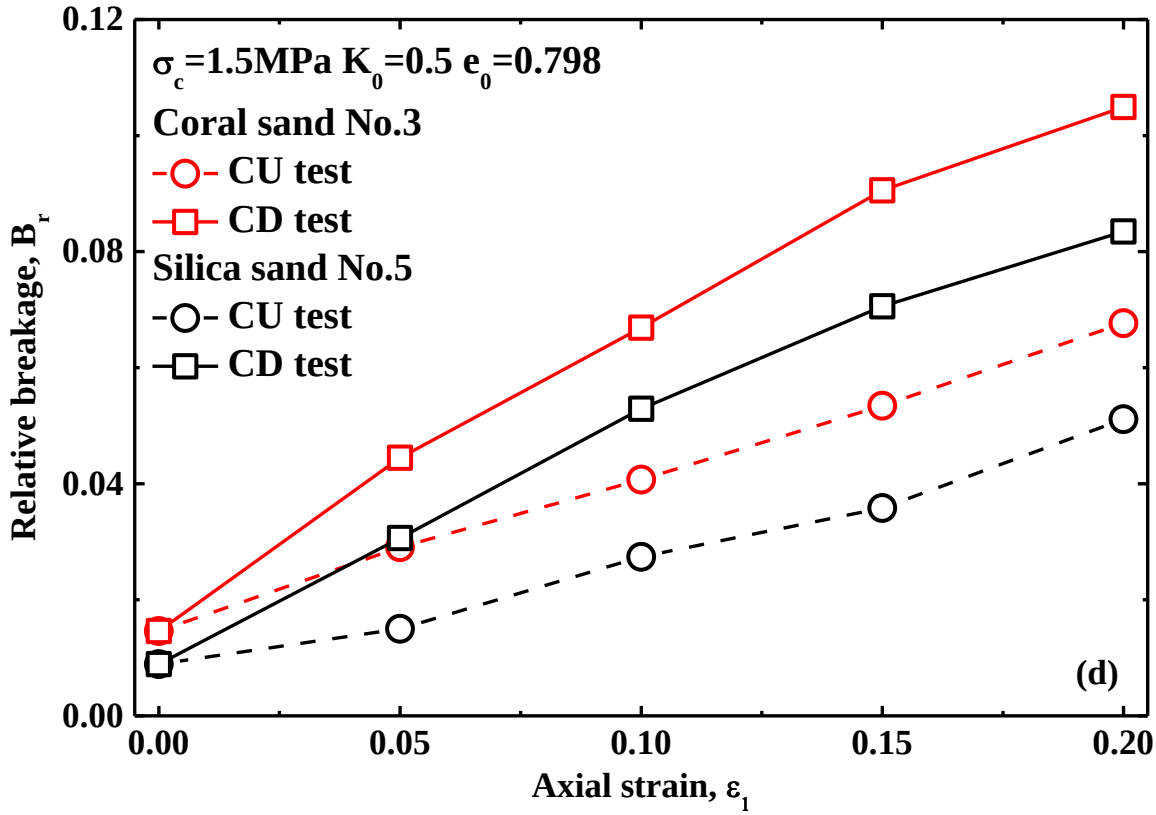

Figure 4.64 Comparison between Silica sand No.5 and Coral sand No.3 (σ_c=1.5MPa K_0=0.5 e_0=0.798)

Another results under initial stress anisotropy from Silica sand No.5 and Coral sand No.3 were combined into one figure to investigate the characteristics of particle breakage on two different types of sand as shown in Figure 4.64. It can be seen herein that the deviator stress of Coral sand No.3 is getting larger than that of Silica sand with increasing axial strain in CD tests but in CU tests the deviator stress of Coral sand No.3 is getting smaller than that of Silica sand No.5. However there is more substantial volume change in contractancy caused in Coral sand No.3 than that in Silica sand No.5 as shown in Figure 4.64(b). As illustrated in Figure 4.64(c), the more substantial excess pore water pressure is found to be caused in Coral sand No.3 than that in Silica sand No.5. The relative breakage was adopted to quantify the extent of particle breakage. Figure 4.64(d) shows the relationship between relative breakage and axial strain of Silica sand No.5 and Coral sand No.3. It is found herein that the particle breakage in relative breakage of Coral sand No.3 is more substantial than that of Silica sand No.5 with the similar increments in development of relative breakage.

4.7.2 Comparison Under Same Initial Relative Density

Considering the difference of Silica sand No.5 and Coral sand No.3, the specimens were prepared by Silica sand No.5 and Coral sand No.3 under same initial relative density after isotropic consolidation to investigate the characteristics of particle breakage.

Figure 4.65 shows the compared results from Silica sand No.5 and Coral sand No.3 under same initial relative density. It is shown herein that the deviator stresses of Silica sand No.5 is much higher than that of Coral sand No.3 as shown in Figure 4.65(a) but the more volume change in contractancy and more substantial development of excess pore water pressure in Coral sand No.3 was caused that that in Silica sand No.5 as shown in Figure 4.65(b) and Figure 4.65(c) separately.

All grain size distribution curves of these tests have been shown above. The relative breakage was calculated according to the grain size distribution curves and the relationship of relative breakage of Silica sand No.5 and Coral sand No.3 is shown in Figure 4.65(d). Particle breakage in relative breakage is found to be slightly more substantial in Coral sand No.3 and that in Silica sand No.5 as a result of more crushability of Coral sand No.3. It is seen that in CU tests the particle breakage in relative breakage in Coral sand No.3 has a relatively bigger increment at beginning stage of shearing than that in Silica sand No.5.

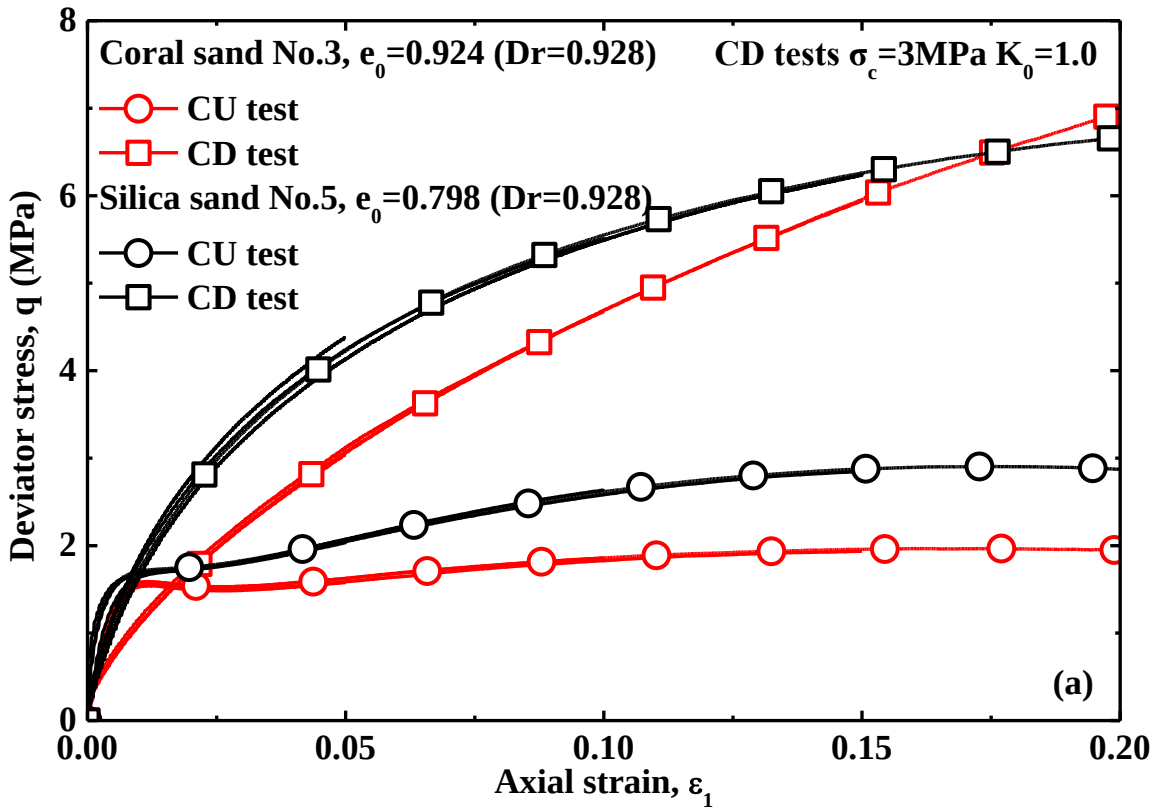

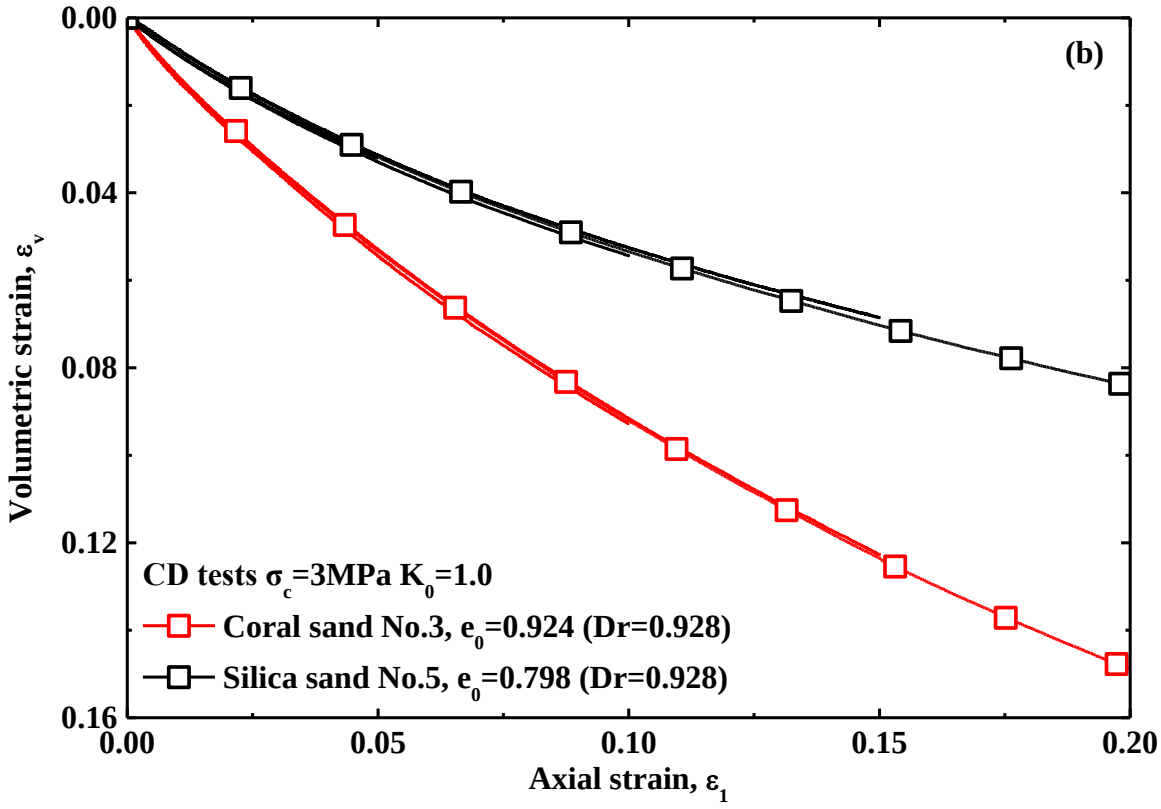
(b)
Volumetric strain, ε_v
0.00
0.04
0.08
0.12
0.16
0.00
0.05
0.10
0.15
0.20
Axial strain, ε_1
CD tests σ_c=3MPa K_0=1.0
Coral sand No.3, e_0=0.924 (Dr=0.928)
Silica sand No.5, e_0=0.798 (Dr=0.928)

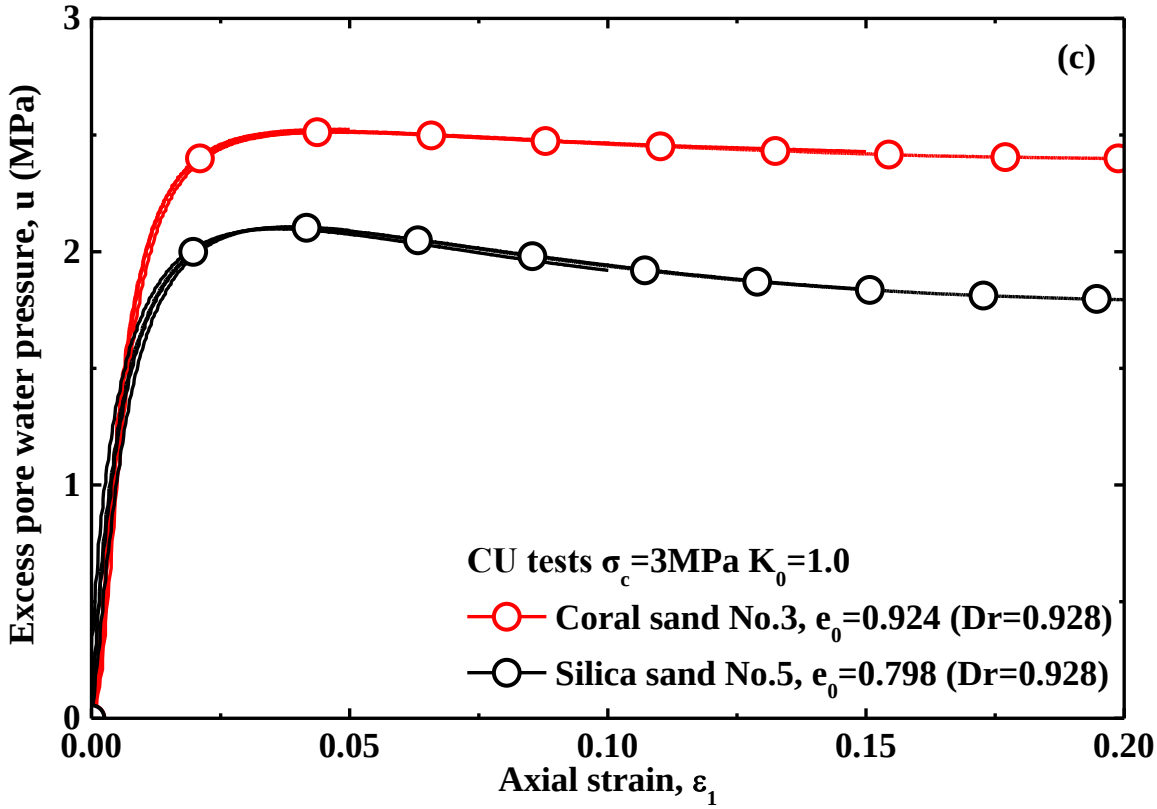
(c)
Excess pore water pressure, u (MPa)
0
1
2
3
0.00
0.05
0.10
0.15
0.20
Axial strain, ε_1
CU tests σ_c=3MPa K_0=1.0
Coral sand No.3, e_0=0.924 (Dr=0.928)
Silica sand No.5, e_0=0.798 (Dr=0.928)

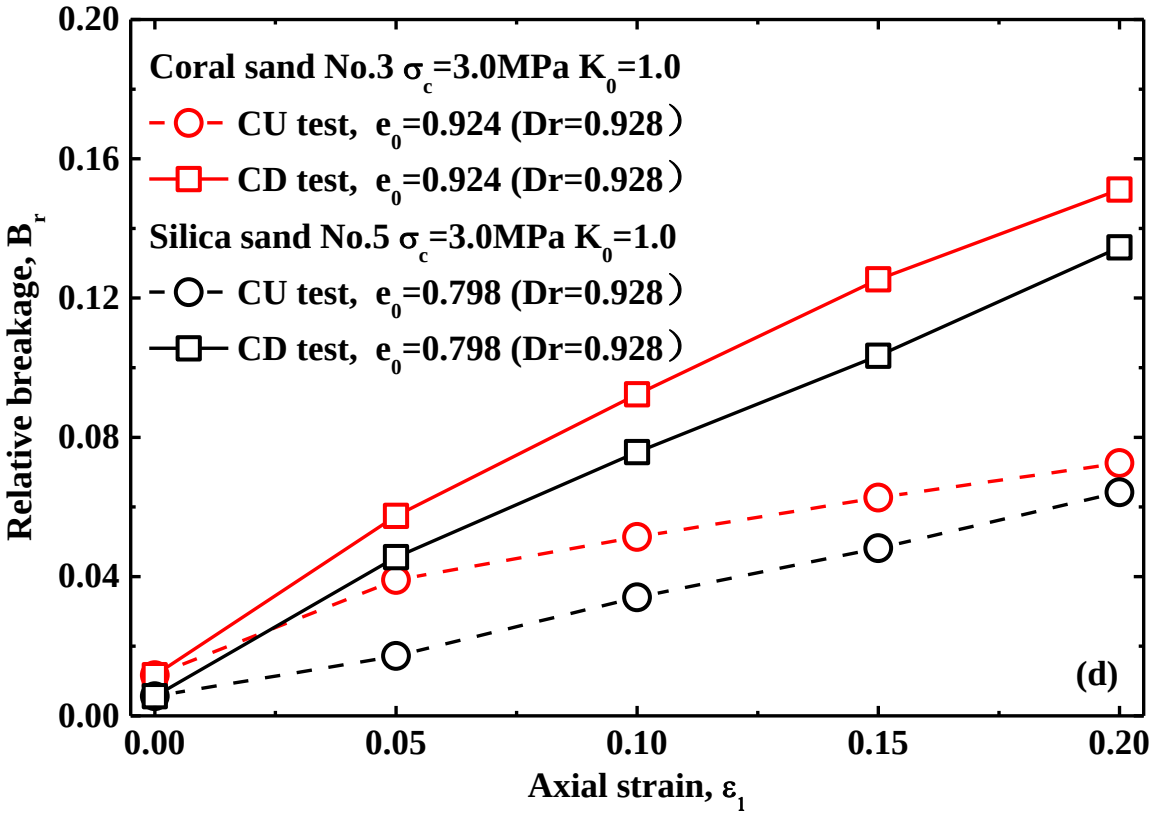

Figure 4.65 Comparison between Silica sand No.5 and Coral sand No.3 (σ_c=3.0MPa K_0=1.0 D_r=0.928)

4.7.3 Comparison Under Cyclic Loading

Cyclic loading was imposed on specimens of Silica sand No.5 and Coral sand No.3 to investigate the characteristics of particle breakage. Figure 4.66 shows the compared results from Silica sand No.5 and Coral sand No.3 subjected to cyclic loading. It is seen herein that the amplitude of cyclic loading on specimens of Coral sand No.3 is larger than that of Silica sand No.5 as shown in Figure 4.66(a). The more volume change in contractancy of Coral sand No.3 was caused than that of Silica sand No.5 as shown in Figure 4.66(b). As shown in Figure 4.66(c), particle breakage increases with increasing cycle number of cyclic loading with more substantial particle breakage in Coral sand No.3 than that in Silica sand No.5 (Donohue et al., 2009). However the particle breakage in relative breakage of Coral sand No.3 has much bigger increments than that of Silica sand No.5. The additional axial strain was caused during cyclic loading. Figure 4.66(d) shows that relationship between relative breakage and additional axial strain of Silica sand No.5 and Coral sand No.3, where the particle breakage in relative breakage is found to increase in increased increments with increasing additional axial strain induced during cyclic loading (Coop et al., 2004; Agung et al, 2004). Particle breakage in relative breakage of Coral sand No.3 is found to be larger than that of Silica sand No.5 with slightly larger increments in Coral sand No.3 as a result of more crushability of Coral sand No.3.

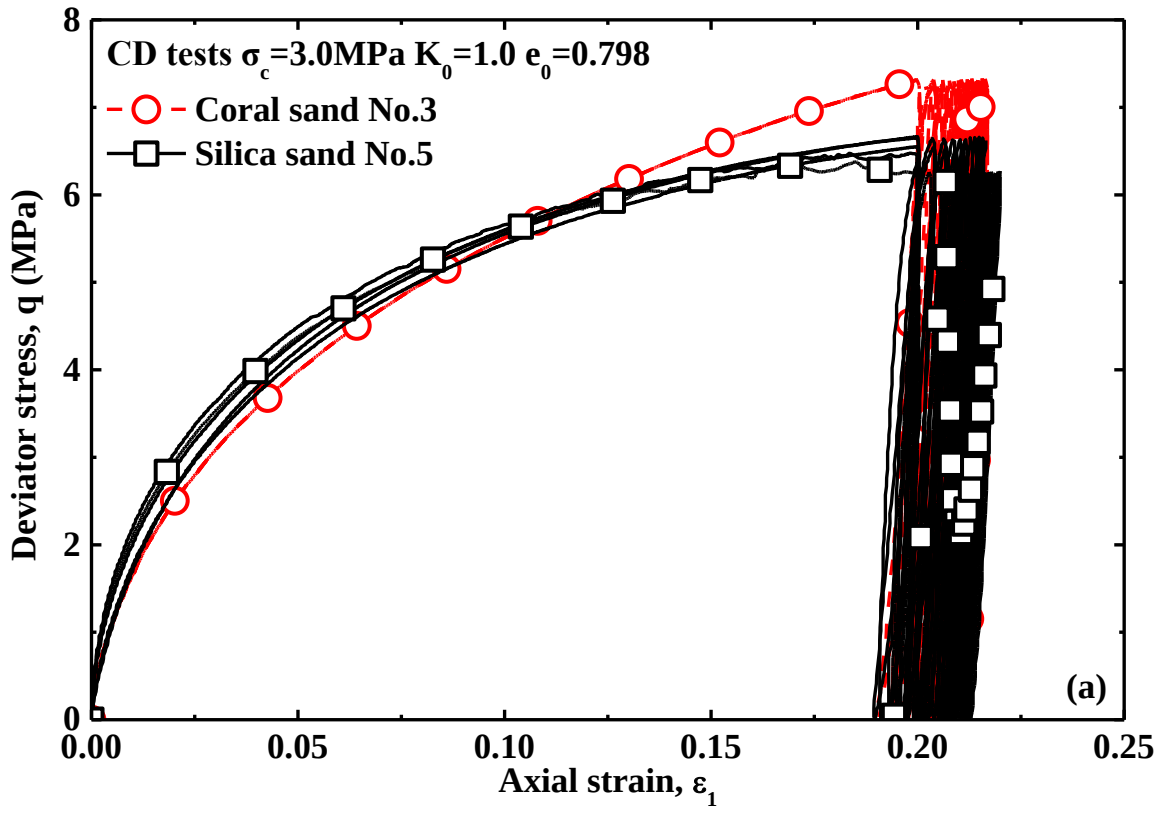
CD tests σc=3.0MPa K0=1.0 e0=0.798
Coral sand No.3
Silica sand No.5
Deviator stress, q (MPa)
Axial strain, ε1
(a)
0
2
4
6
8
0.00
0.05
0.10
0.15
0.20
0.25

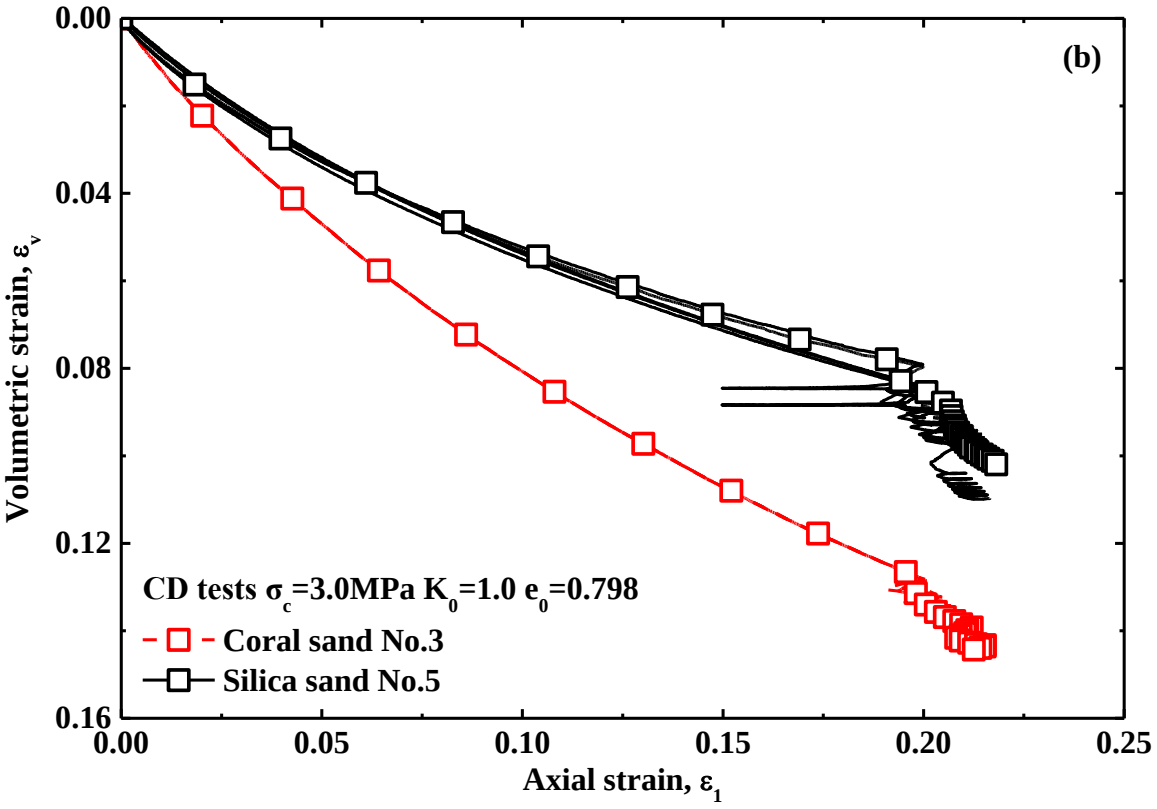
(b)
CD tests σc=3.0MPa K0=1.0 e0=0.798
Coral sand No.3
Silica sand No.5
Volumetric strain, εv
Axial strain, ε1
0.00
0.04
0.08
0.12
0.16
0.00
0.05
0.10
0.15
0.20
0.25

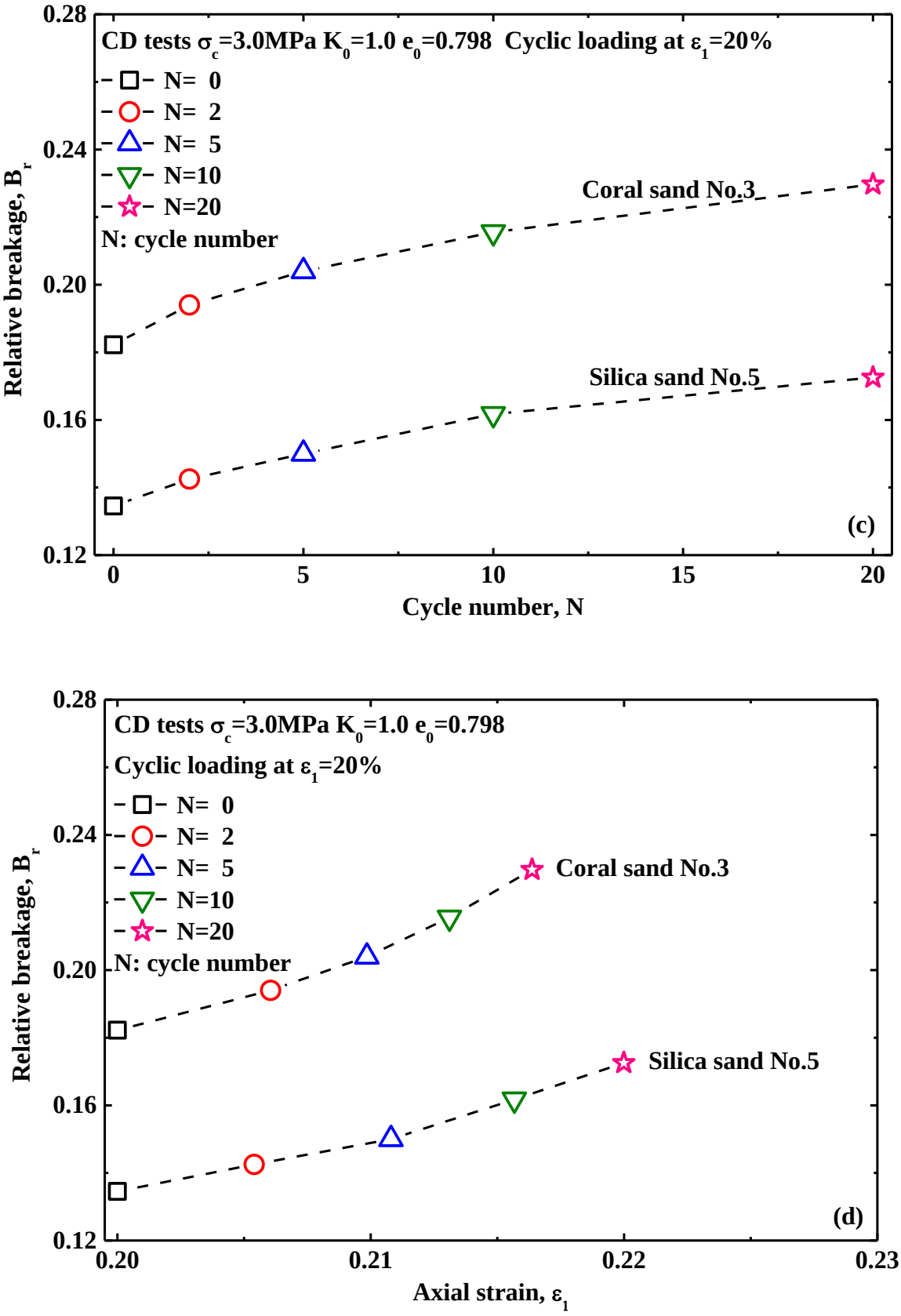

Figure 4.66 Comparison from Silica sand No.5 and Coral sand No.3 subjected to cyclic loading (σ_c=3.0MPa K_0=1.0 e_0=0.798)

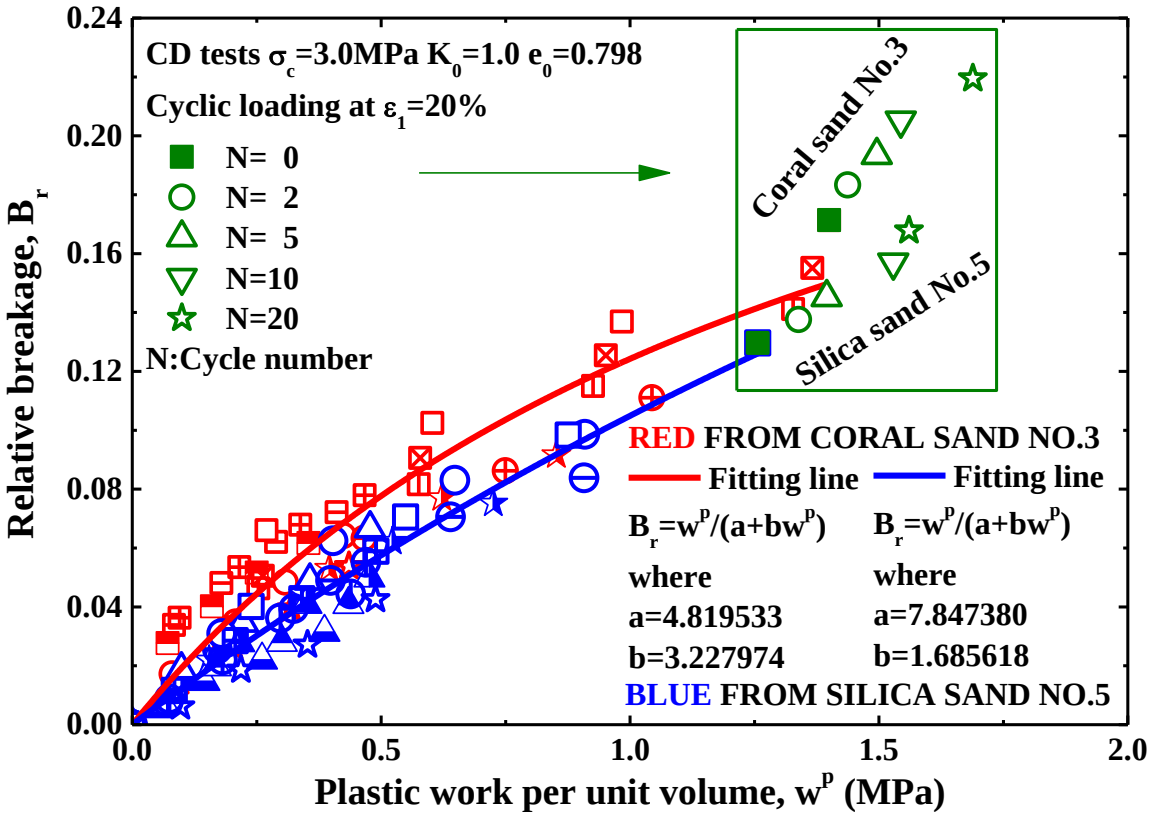

Figure 4.67 Relationship between relative breakage and plastic work per unit volume of Silica sand No.5 and Coral sand No.3 considering the effect of loading mode

4.7.4 Comparison in A Hyperbolic Model

A hyperbolic model can be used to assess relative breakage by plastic work per unit volume. Combining Figure 4.40 and Figure 4.61 into Figure 4.67 from monotonic loading, it is shown herein that the fitting line of Coral sand No.3 is over the fitting line of Silica sand No.5, namely the same plastic work per unit volume results in more particle breakage in relative breakage of Coral sand No.3 than that of Silica sand No.5. For being able to check the more detailed information under low pressure, data in Figure 4.67(a) can be redrawn in semi-logarithmic coordinate as shown in Figure 4.67(b).

The data from cyclic loading on Silica sand No.5 and Coral sand No.3 were appended as well to investigate the influence of loading type on relationship of relative breakage and plastic work per unit volume as shown in Figure 4.67(a). Considering the evolution of relative breakage against plastic work per unit volume caused during monotonic loading and cyclic loading, the relative breakage during cyclic loading has a more evident increase in different way with increasing plastic work per unit volume that that during monotonic loading especially for Coral sand No.3, which means that under high pressure cyclic loading results in more substantial particle breakage than monotonic loading and loading mode (herein monotonic loading and cyclic loading) has also a significant effect on property and mechanism of particle breakage. With increasing plastic work per unit volume during cyclic loading, the particle breakage of Silica sand No.5 during cyclic

loading is found to increase approximately linearly but the particle breakage of Coral sand No.3 has an increase in down concavity, which means that initial cyclic loading results in more particle breakage, being related to the properties of Coral sand No.3. It is notable that during cyclic loading more particle breakage against same plastic work per unit volume was caused on Coral sand No.3 than that on Silica sand No.5, which still is related to the more crushable property of Coral sand No.3.

Considering the development of relative breakage against plastic work per unit volume from monotonic loading and cyclic loading, a significant influence of loading mode on mechanism & evolution of particle breakage would be found clearly, which is proved that loading mode may result in different tendency of particle breakage (Miura and Ohara, 1979). Various particle contact network was being formed and developed during monotonic loading and cyclic loading. Consequently, the influences of loading mode and material properties on the characteristics and mechanism of particle breakage should be investigated on the case-by-case basis in reality.

Coral sand has physical characteristics of larger particle, irregularity & angularity, mineral fragility, porosity inside particle in comparison with Silica sand. Larger particle contains more flaws which have higher probability to crush and smaller particles are generally created from larger particles by fracturing these flaws (Lade et al., 1996). Easier stress concentration at irregular angular contact points of soil particles fractures sharp edges and corners of particle (Hardin, 1985). And porosity inside particles reduces the strength of particle to be fractured easier. In addition, mineral fragility of Coral sand raises the possibility of fracture. Such characteristics results in more crushable of Coral sand than Silica sand. Consequently, it is reasonably understood that more particle breakage was caused on Coral sand No.3 than that on Silica sand No.5.

4.8 SUMMARY

Many triaxial tests were conducted on Silica sand No.5 and Coral sand No.3 for investigating the characteristics of particle breakage subjected to various influence factors. Overall experimental results were shown herein in fundamental interpretation of evolution of particle breakage during shearing. The major findings in characteristics of particle breakage are shown as follows:

(a) Particle breakage was found to increase with increasing axial strain. However, more increment of particle breakage was caused during cyclic loading than that during monotonic loading.
(b) Particle breakage was caused as well during consolidation.
(c) Higher confining pressure was found to result in more substantial particle breakage.
(d) More particle breakage was caused in denser samples.
(e) More particle breakage was induced in CD tests than that in CU tests.
(f) Initial stress anisotropy was found to result in more particle breakage during anisotropic consolidation than that during isotropic consolidation but during shearing higher confining pressure (σ_c=2.0MPa K_0=1.0) has more influence on particle

breakage than initial stress anisotropy with a relatively lower confining pressure (σ_c=1.5MPa K_0=0.5).

(g) Unloading-reloading process during shearing was found to lead to particle breakage. More times unloading-reloading results in more particle breakage.

(h) Particle breakage was found to increase with increasing cycle numbers of cyclic loading.

(i) A hyperbolic model was established to assess Relative Breakage by plastic work per unit volume in monotonic loading. Cyclic loading results in different development tendency of relative breakage against plastic work per unit volume in comparison with monotonic loading. Loading mode has an influence on the characteristics and mechanism of particle breakage.

(j) More substantial particle breakage was revealed in Coral sand No.3 than that in Silica sand No.5.

CHAPTER 5

STUDY ON THE INFLUENCE OF PARTICLE BREAKAGE ON SOIL BEHAVIOR

5.1 INTRODUCTION

This chapter presents the study on the influence of particle breakage on soil behavior. The stresses at the bottom of high dam or around the tip of piles supporting high-rise buildings are high enough exceeding the strength of particles so that particle breakage is very significant in influence on soil behavior. During high-speed train moving on tracks supported by gravel materials, particle breakage can be induced by dynamic loading from high-speed train. The impact force during deep-driven pile can result in particle breakage as well. In addition, particle breakage can be caused by the high shear force existed in slopes which can develop landslides with increasing shear particle breakage gradually and rainfall injection. Nowadays, the stresses encountered in geotechnical engineering are getting higher and higher. The changed gradation of soil subjected to considerable particle breakage has a significant influence on soil behavior, which has a significant influence on the strength, stiffness and stability of engineering. Consequently the influence of particle breakage on soil behavior should be clarified by this research.

5.2 METHODOLOGY

Triaxial tests were carried out by a strain-controlled high-pressure triaxial apparatus with maximum 3MPa confining pressure with measuring axial displacement in LVDT mounted outside cell pressure chamber and volume change in DPT. All specimens in dimension of diameter 75mm and height 160mm were prepared by dry rodding method in air pluviation into a mound with a 1mm-thick membrane in eight layers with necessarily tamping to reach relative density or void ratio. Herein the 1mm-thick membrane was used to avoid being pierced by sharp edge of soil particles under high effective pressure and minimize membrane penetration under high effective stress. The triaxial tests were consolidated isotropically to designated confining pressure and then sheared to specific axial strain. All triaxial tests were conducted on saturated specimens with Skempton’s B

value over 0.98 by using de-aired water to flush the specimens under around -100kPa vacuum. The initial void ratio of specimen e_0 was herein calculated before shearing by the value of void ratio just after preparation of specimen and volume change after consolidation.

Triaxial tests on dense specimens of original sand were conducted after consolidation in Consolidated Drained (CD) condition under 3MPa confining pressure for producing crushing sand. Therein the axial compression for each test was terminated at specified axial strain from 10% and 50% with a 10% increment for Silica sand No.5 or from 10% and 40% with a 10% increment for Coral sand No.3 for producing different extents of crushed sand, and all crushed sand was collected for each test after shearing. It is called pre-crushed sand subsequently.

The whole material of specimen after shearing was kept in an oven to dry and then all sand were mixed and laid open uniformly as a thin cylinder on a big tray, which was divided into four parts uniformly to remove diagonal two of them until around 200g left by repeating this method, with an aim to get few amount of uniform material of specimen to sieve. Hereafter the around 200g of specimen was collected to obtain the grain size distribution curve by sieve analysis, which can be regarded as grain size distribution curve of the specimen after shearing. Silica sand No.5 and Coral sand No.3 herein were employed in this research. The physical properties of Silica sand No.5 and Coral sand No.3 are shown in Table 3.3.

For getting fundamental understanding on the influence of particle breakage on soil behavior, the pre-crushed sand and original sand were employed separately in triaxial tests in comparison with the results from pre-crushed sand and original sand. All triaxial tests herein were sheared after isotropic consolidation to a designated confining pressure. The illustration of tested conditions is shown in Table 5.1.

Table 5.1 Illustration of tested conditions

SAND	TESTED CONDITION		REMARK
Silica sand No.5	O	σ_c=3.0MPa CD tests	For producing pre-crushed sand
	O & P	σ_c=0.2MPa CD & CU tests	In comparison
	O & P	σ_c=0.5MPa CD & CU tests	
	O & P	σ_c=1.0MPa CU tests	
	O & P	σ_c=3.0MPa CU tests	
Coral sand No.3	O	σ_c=3.0MPa CD tests	For producing pre-crushed sand
	O & P	σ_c=0.2MPa CD & CU tests	In comparison

O: Original sand P:Pre-crushed sand

5.3 EXPERIMENTAL RESULTS ON SILICA SAND NO.5

5.3.1 Generation of Pre-crushed Sand

For producing pre-crushed materials with various extents of particle breakage, a series of CD tests were sheared on original sand under 3MPa confining pressure after isotropic consolidation to designated axial strain such as from 10% to 50% by a 10% increment.

The triaxial tests results under 3MPa confining pressure for producing pre-crushed sand are shown in Figure 5.1. It can be seen herein that the deviator stresses have a evident softening stage after reaching peak strength but the volume change in contractancy continues increasing even during softening stage of shearing, which is related to particle breakage during shearing. The materials of specimens after shearing were kept in an oven to dry and the grain size distribution curves of pre-crushed sands were obtained by sieve analysis as shown in Figure 5.2. Figure 5.2(a) shows the grain size distribution curves of the tests shown in Figure 5.1. The changed D_{50} of grain size distribution curves proves that the split of soil particles during shearing plays an important role in particle breakage. These grain size distribution curves were quantified by Relative Breakage (B_r) to assess the amount of particle breakage as illustrated in Figure 5.2(a), where according to the evolution of grain size distribution curves during shearing, particle breakage increases in reduced increments with increasing axial strain. It should be noted as well that particle breakage occurred during isotropic consolidation but the amount of particle breakage was not so much as shown in Figure 5.2(a). These pre-crushed sands with various extent of particle breakage and original sand were employed to prepare new specimens for new triaxial tests to investigate the effect of particle breakage on soil behavior.

The shear band in specimen was formed as the axial strains reached 50%. Particle breakage in shear band was investigated as well in comparison with the particle breakage outside shear band. Herein, three parts of the specimen, namely top, middle and bottom as shown in Figure 5.2(b), were picked out about 200g separately to get the grain size distribution curves, where the 200g at the top or bottom parts in specimen was picked up along the center axis of the specimen but at the middle part of the specimen it was picked up along the shear band. Figure 5.2(b) shows the grain size distribution curves in shear band and at top & bottom parts of the specimen. It can be seen herein that the particle breakage in shear band is slightly more substantial than that at top or bottom parts of the specimen but there is no big difference about the particle breakage between top part and bottom part of specimen.

The shearing on original sand to produce pre-crushed sand was employed in simulating the mechanical process during construction of high dam and high-rise building, and the pre-crushed sand represents the crushed soil particles with various extent of pre-crushed particle breakage existed in different area in dam or around the tip of group pile. The soil behavior of the pre-crushed materials should be investigated to clarify the effect of particle breakage on soil behavior.

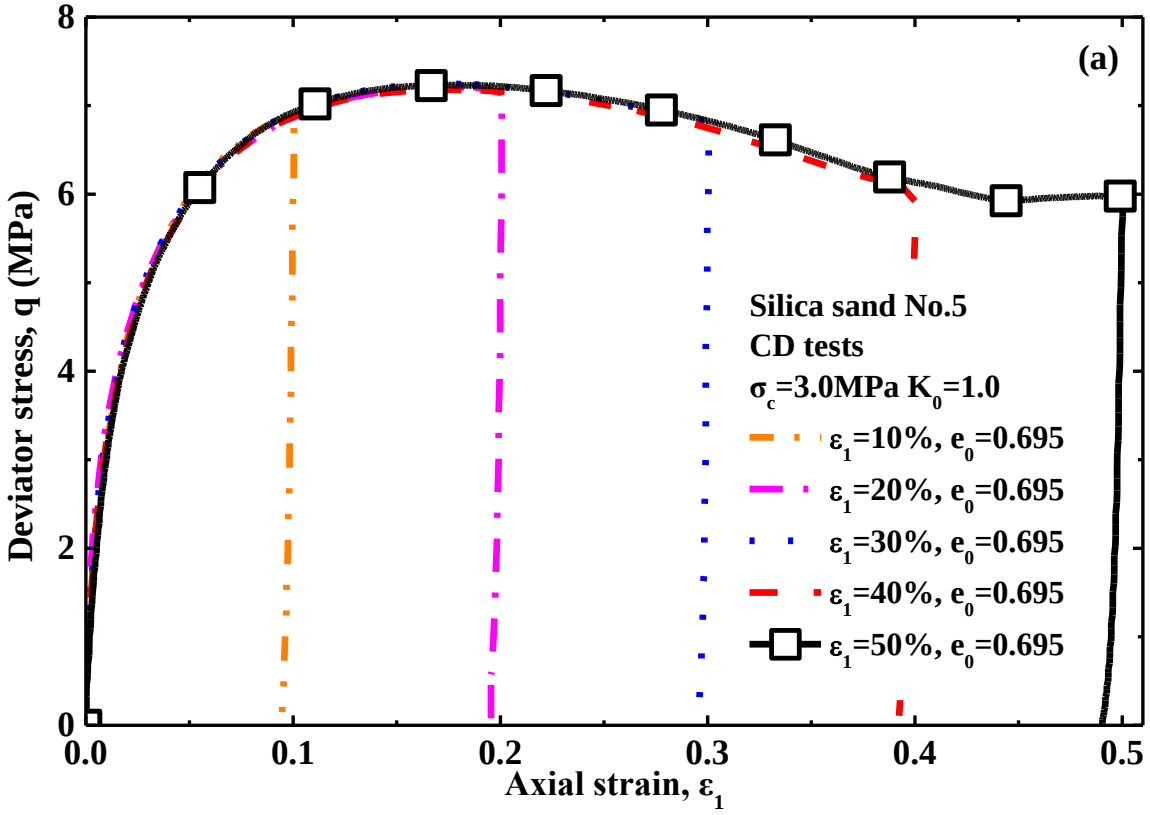
(a)
Deviator stress, q (MPa)
Axial strain, ε1
Silica sand No.5
CD tests
σc=3.0MPa K0=1.0
ε1=10%, e0=0.695
ε1=20%, e0=0.695
ε1=30%, e0=0.695
ε1=40%, e0=0.695
ε1=50%, e0=0.695

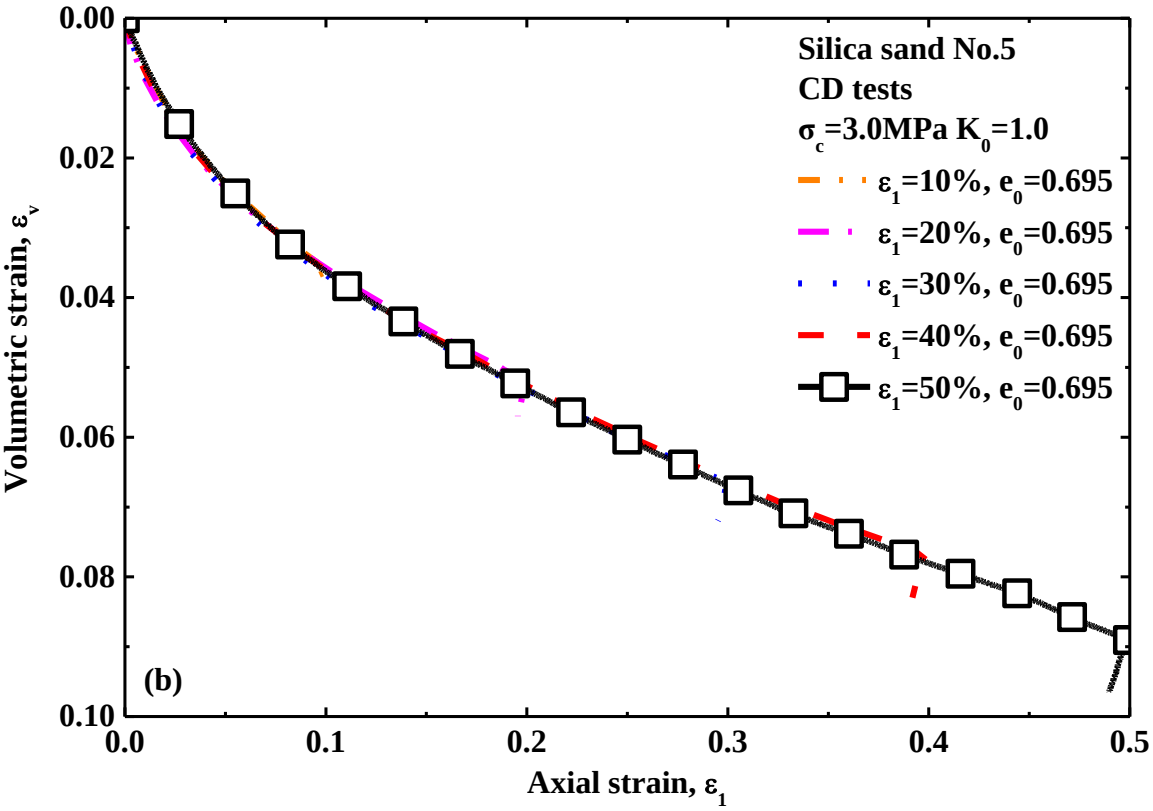
(b)
Volumetric strain, εv
Axial strain, ε1
Silica sand No.5
CD tests
σc=3.0MPa K0=1.0
ε1=10%, e0=0.695
ε1=20%, e0=0.695
ε1=30%, e0=0.695
ε1=40%, e0=0.695
ε1=50%, e0=0.695

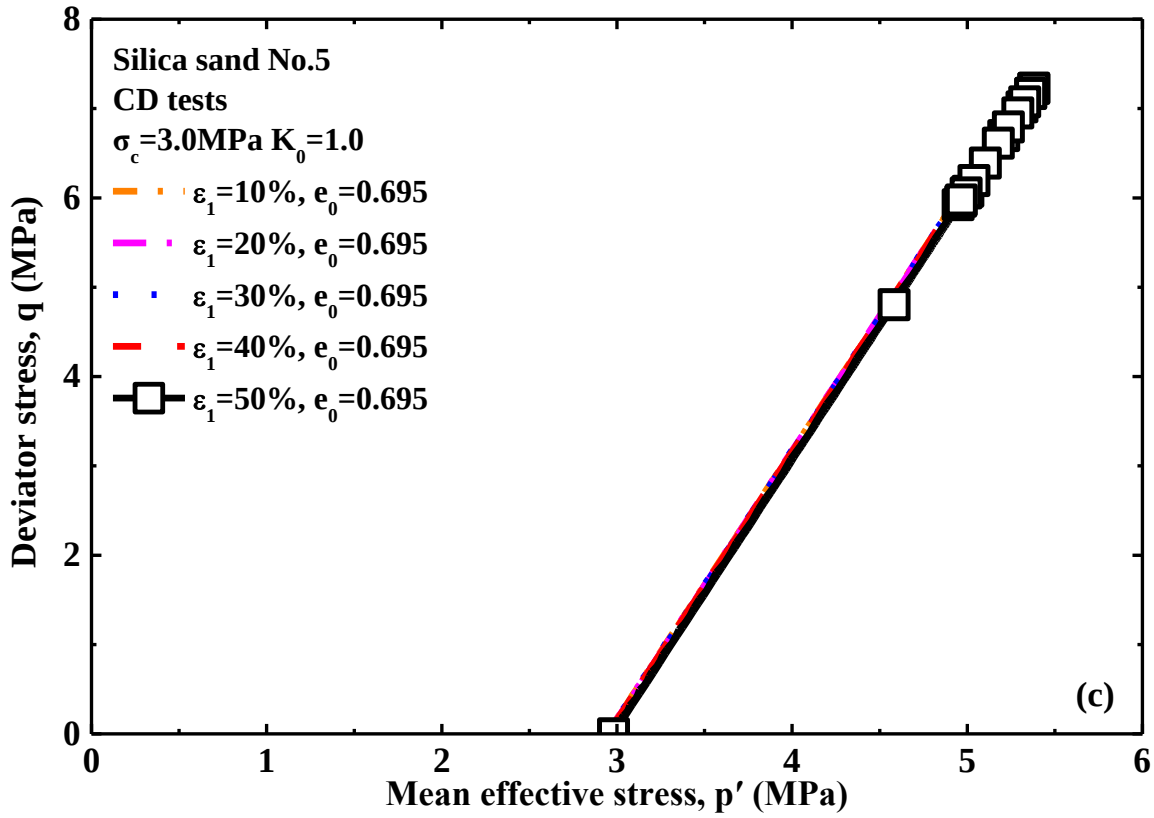

Figure 5.1 Triaxial test results on original sand for producing pre-crushed sand

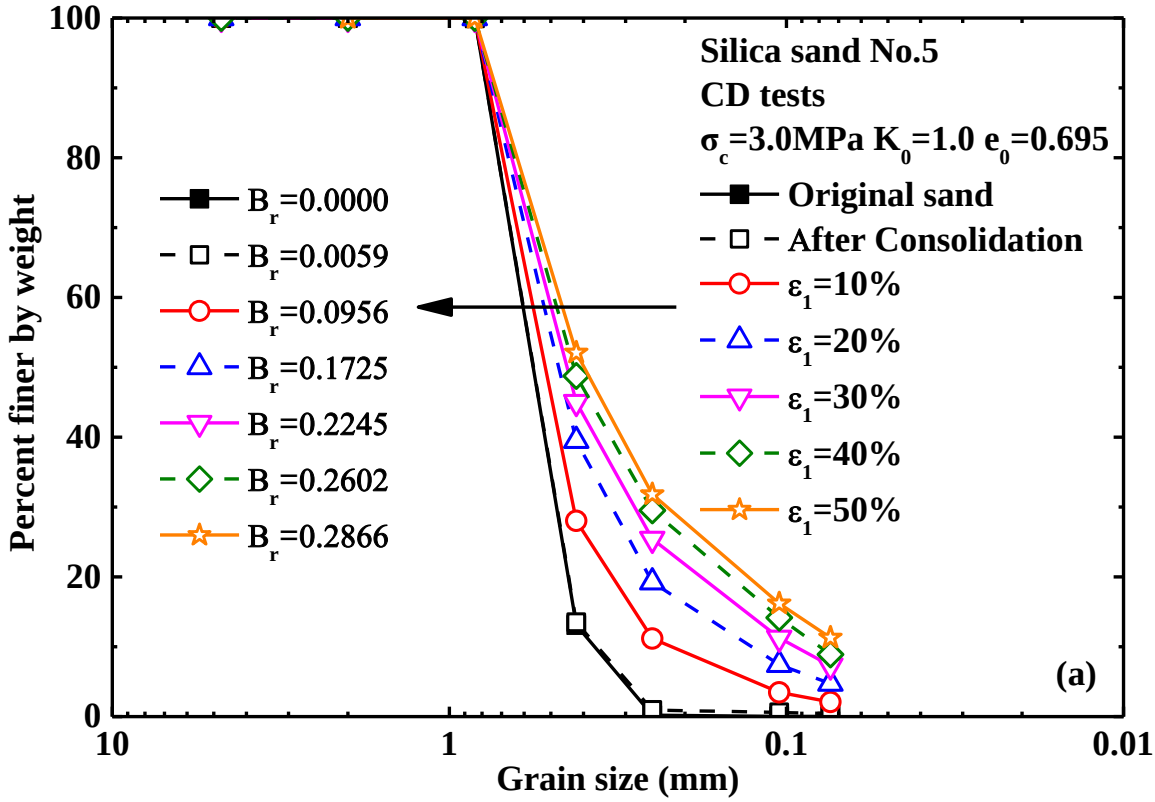

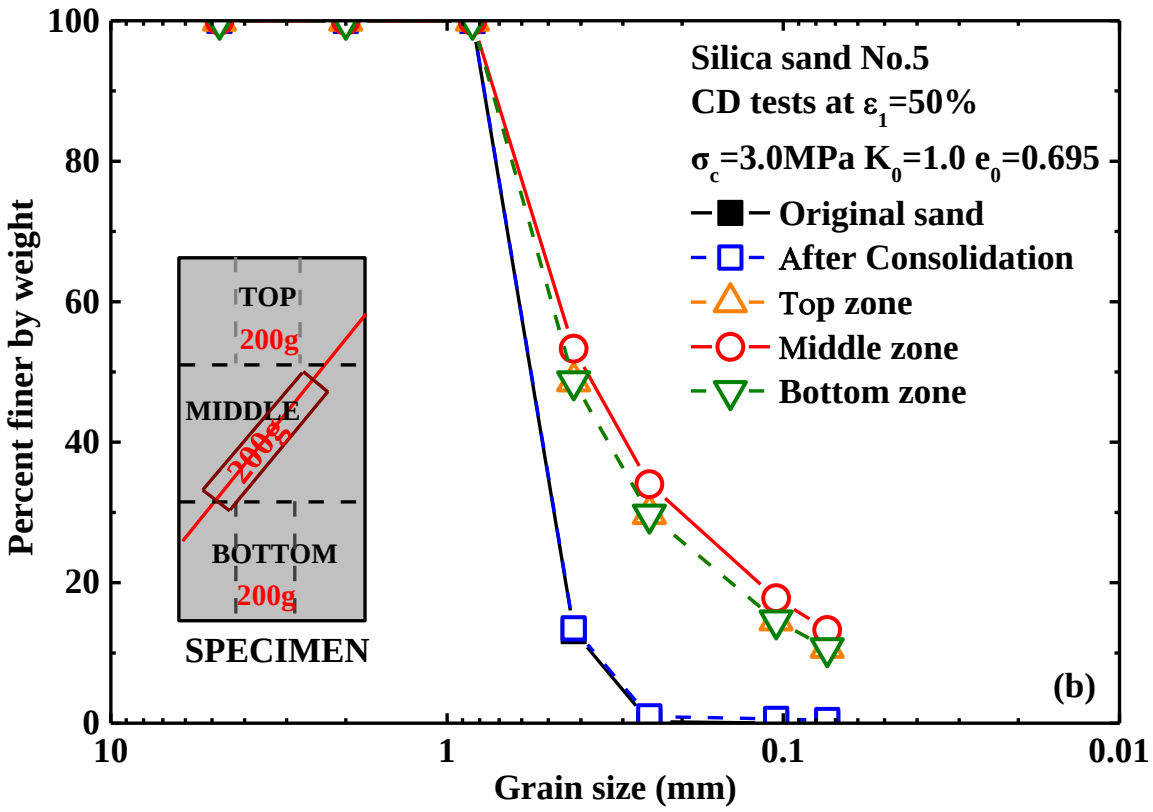

Figure 5.2 Grain size distribution curves during shearing and in shear band

Table 5.2 Physical properties of pre-crushed sand from Silica sand No.5

Item	Relative breakage B_r	D_{50} (mm)	$C_u=D_{60}/D_{10}$	$C_c=(D_{30})^2/(D_{10}*D_{60})$
Original sand	0.0000	0.564	1.647	1.021
After consolidation	0.0059	0.563	1.676	1.038
ε_1=0.10	0.0956	0.519	2.612	1.462
ε_1=0.20	0.1725	0.474	4.181	1.605
ε_1=0.30	0.2245	0.447	5.394	1.669
ε_1=0.40	0.2602	0.427	6.113	1.636
ε_1=0.50	0.2866	0.398	–	–

Note: D_i is the grain diameter at i% passing. D_{10} <0.074mm is not available at ε_1=0.50.

The physical properties of pre-crushed sand from Silica sand No.5 are shown in Table 5.2, which particle breakage is shown clearly to reduce $D_{50,}$ but to result in increase of coefficient of uniformity, namely the coefficient of uniformity in gradation of soil is found to increase with increasing particle breakage. For a sand to be classified as well graded, the $C_u \geq 6$ & $1<C_c<3$ should be met. The gradation of soil is herein found to be changed with increasing particle breakage and to become well graded as the particle breakage reached B_r=0.2602.

5.3.2 The Influence of Particle Breakage on Soil Behavior

5.3.2.1 Isotropic consolidation behavior subjected to particle breakage

Isotropic consolidations to 3.0MPa confining pressure were conducted on pre-crushed sand and original sand to clarify the effect of particle breakage on e-logp′ curve under isotropic consolidation. Figure 5.3 shows e-logp′ curves of pre-crushed sand and original sand under isotropic consolidation. It can be seen therein that more volumetric contraction was induced in pre-crushed sand and particle breakage resulted in increase of compressibility of soil. In reality, particle breakage causes more volumetric contractancy or subsidence at ground surface. At beginning of loading stage of isotropic consolidation, the nonlinearity of e-logp′ curve becomes much more evident with the increase of particle breakage. Particle breakage is found to result in as well the larger residual volume contraction after unloading as shown in Figure 5.3.

It can be concluded that the particle breakage has a very significant effect on the compression characteristics of soil in being more contractive, especially under high pressure. Consequently it is indispensable to consider permanent subsidence or deformation induced by particle breakage in reality.

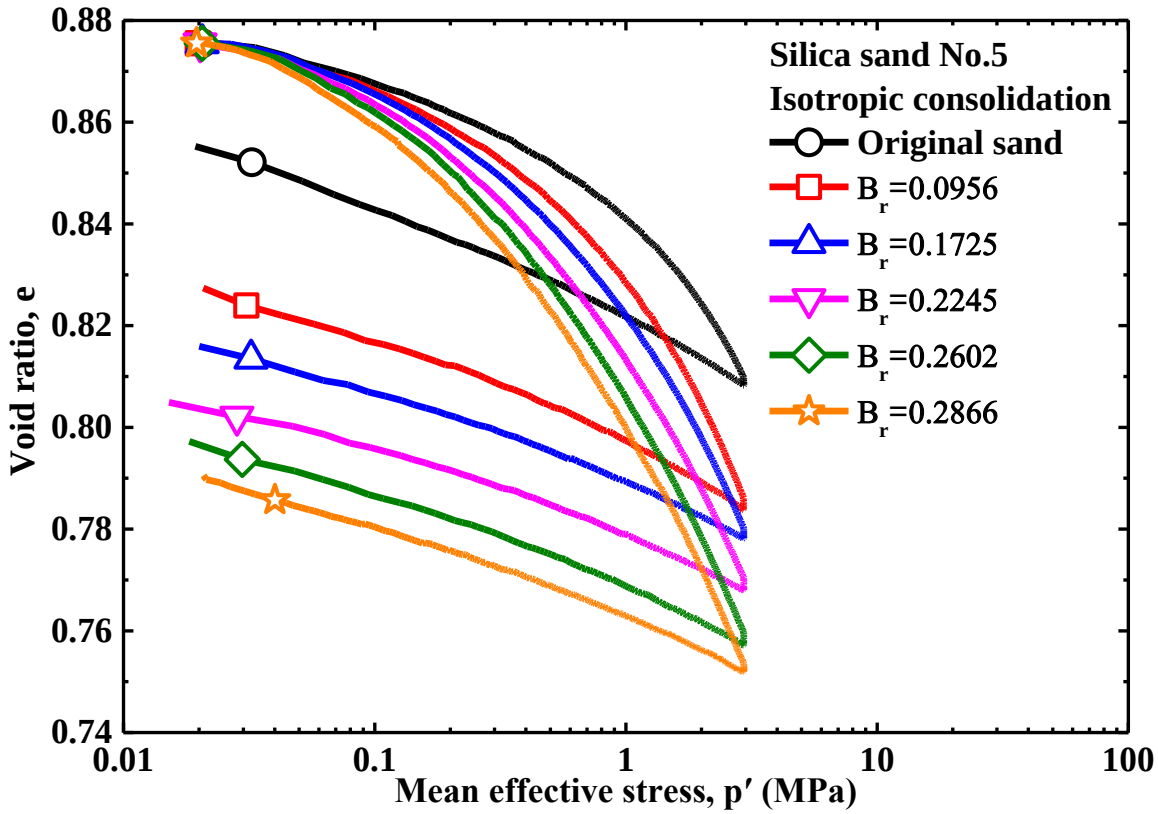

Figure 5.3 Isotropic consolidation on original sand and pre-crushed sand

5.3.2.2 Shearing behavior subjected to particle breakage under 0.2MPa confining pressure

The new specimens on pre-crushed sand and original sand were prepared separately in air pluviation into a mould with a membrane in eight subsegments. The triaxial tests were sheared after isotropic consolidation under Consolidated Drained condition (CD) and Consolidated Undrained condition (CU) on pre-crushed sand and original sand under 0.2MPa confining pressure to examine the effect of particle breakage on soil behavior. Herein the 0.2MPa confining pressure as a relatively low confining pressure was used in triaxial tests for trying not to crush the sand any more. Consequently it can find out the differences of soil behavior between pre-crushed sand and original sand by these tests.

Figure 5.4 shows the CD tests results of original sand and pre-crushed sand under 0.2MPa confining pressure. As shown in Figure 5.4(a), it can be seen herein that particle breakage deteriorates the stress-strain curves in reduction of peak strength with the highest peak strength in specimen of original sand. As displayed in Figure 5.4(b), the volumetric strain changed quickly to dilatancy after very small contractancy at the beginning of shearing of original sand, but the volumetric strain of pre-crushed sand is revealed to become more contractive, which means that particle breakage impaired the dilatancy behavior of soil to intensify the compressibility of soil correspondingly. There is no big difference about the residual strengths between original sand and pre-crushed sand but they have evidently different volumetric changes at the residual stage.

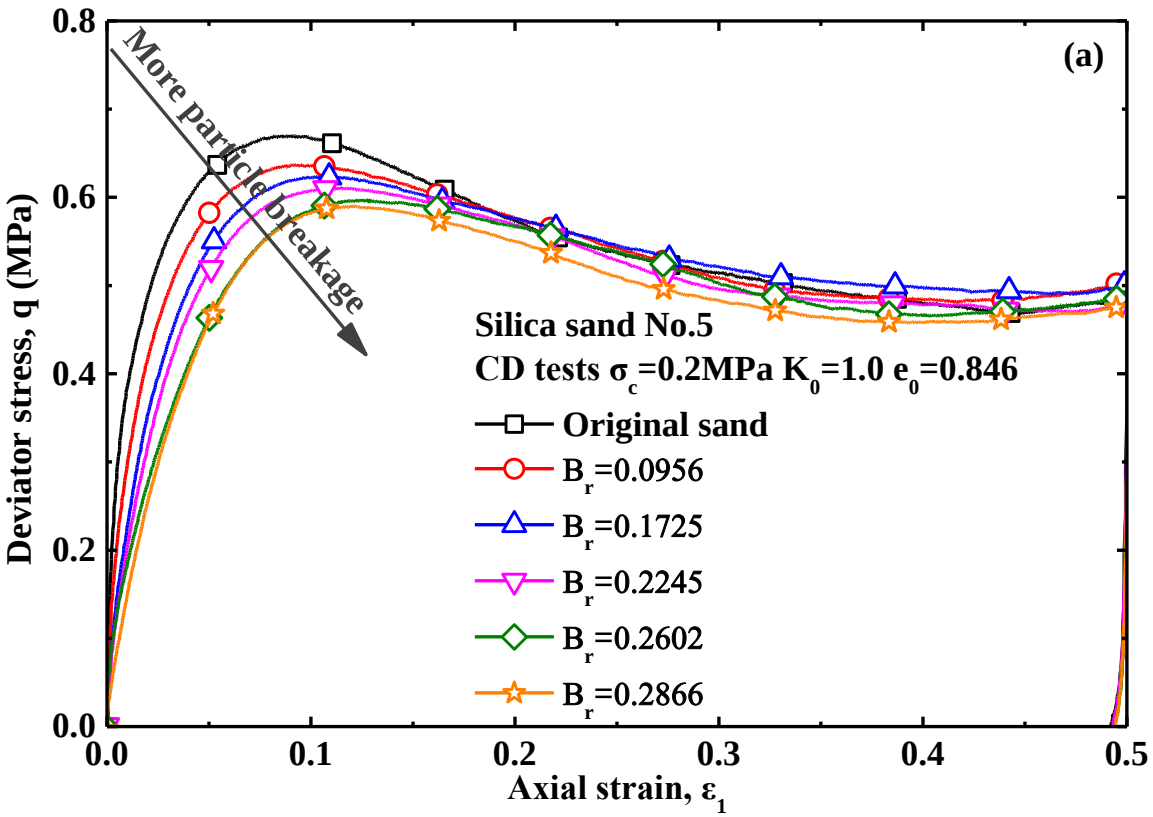

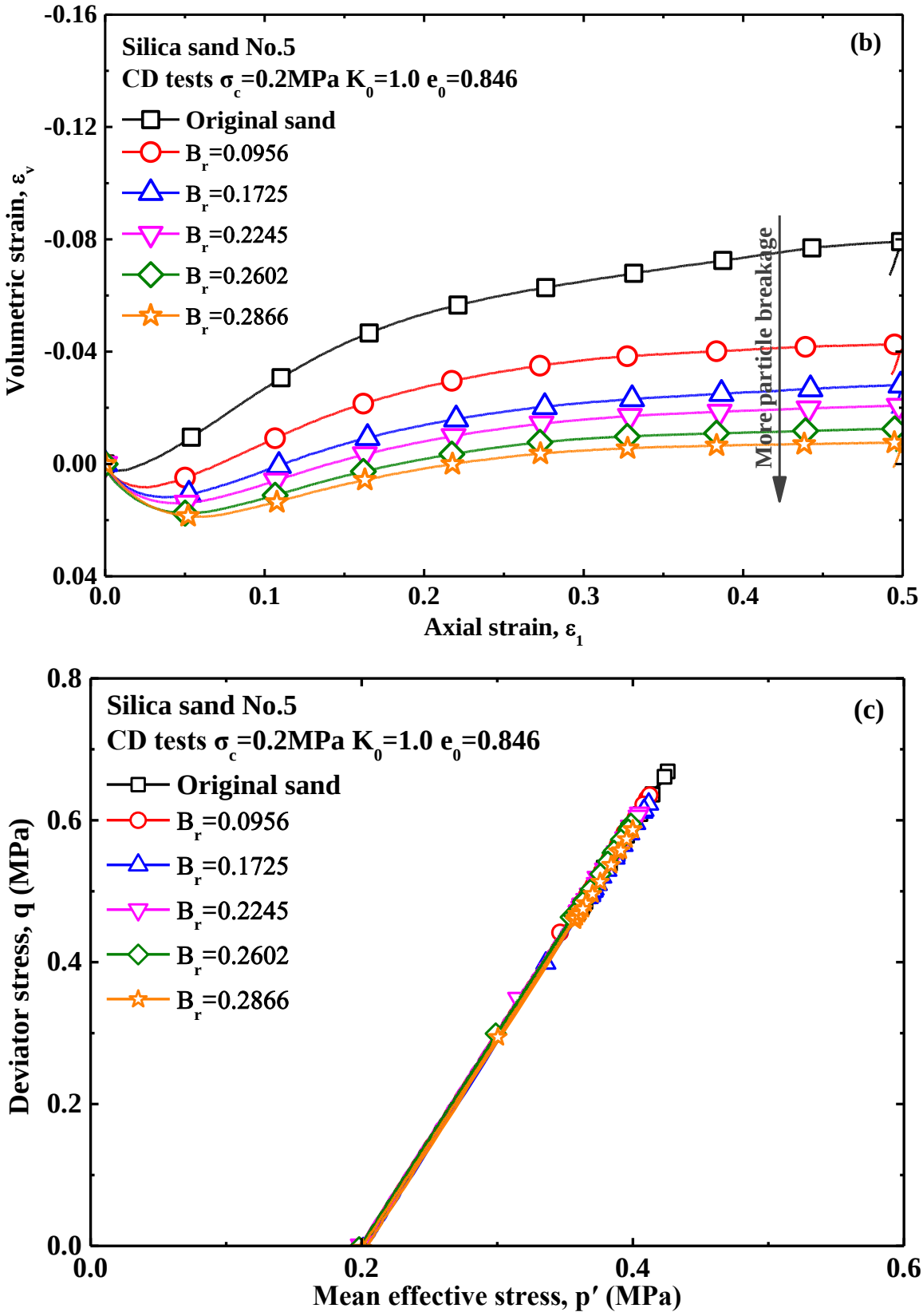

Figure 5.4 CD test results of original sand and pre-crushed sand under 0.2MPa confining pressure

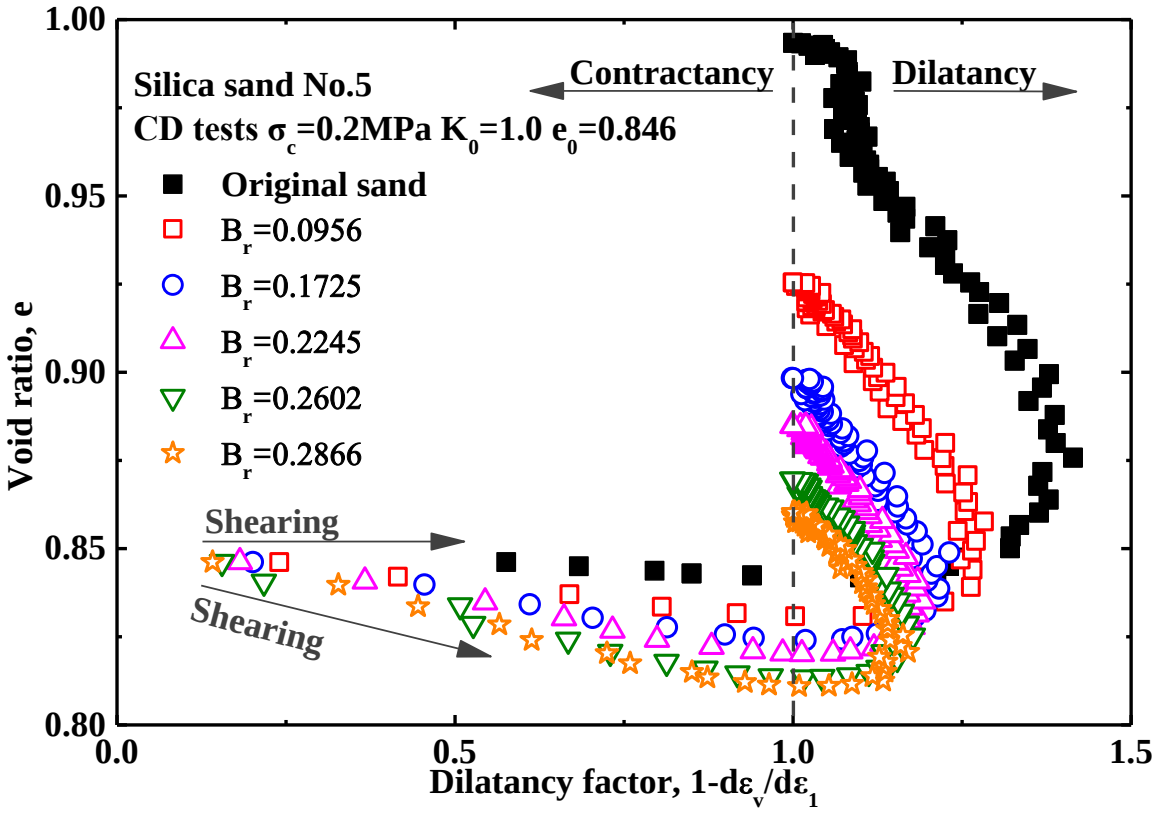

Figure 5.5 Dilatancy behavior on pre-crushed sand and original sand under 0.2MPa confining pressure

The dilatancy behavior of soil has a very important influence on soil behavior. For clearly investigating the effect of particle breakage on the dilatancy behavior of soil, the data of CD tests in Figure 5.4 was redrawn in Figure 5.5 where the original sand is found to be more dilatant than the pre-crushed sand in spite of the same void ratio at the beginning of shearing. It can be concluded that particle breakage has a significant influence on dilatancy behavior of soil with resulting in reduction of dilatancy or increase of contractancy, which are consistent with findings from Lee and Seed (1967), Miura and Ohara (1979) and Feda (2002).

CU tests on original sand and pre-crushed sand were carried out as well under 0.2MPa confining pressure to study the effect of particle breakage on stress-strain curves and the development of excess pore water pressure (abbreviated as PWP subsequently). The CU tests results of original sand and pre-crushed sand under 0.2MPa confining pressure are shown in Figure 5.6 where particle breakage is seen to substantially deteriorate the stress-strain curves in reduction of peak strengths as shown in Figure 5.6(a) and excess pore water pressure in pre-crushed sands increases with the increase of particle breakage with higher residual excess pore water pressure as shown in Figure 5.6(b). The stress-strain curve on original sand in Figure 5.6(a) has the highest peak strength with the lowest development of excess pore water pressure, which is related to the most dilatant behavior existed in original sand in comparison with pre-crushed sands. Moreover the axial strain at the peak strength of soil is found to increase with the increase of particle

breakage, which means that pre-crushed sand needs to be larger axial strain to exert its peak strength with increasing particle breakage. Figure 5.6(b) shows that the influence of particle breakage on development and dissolution of the excess pore water pressure, which is related to the more contractive behavior induced in pre-crushed sand than that in original sand. Stress paths of CU tests are shown in Figure 5.6(c) in which particle breakage affects the whole stress path in reduction of strength.

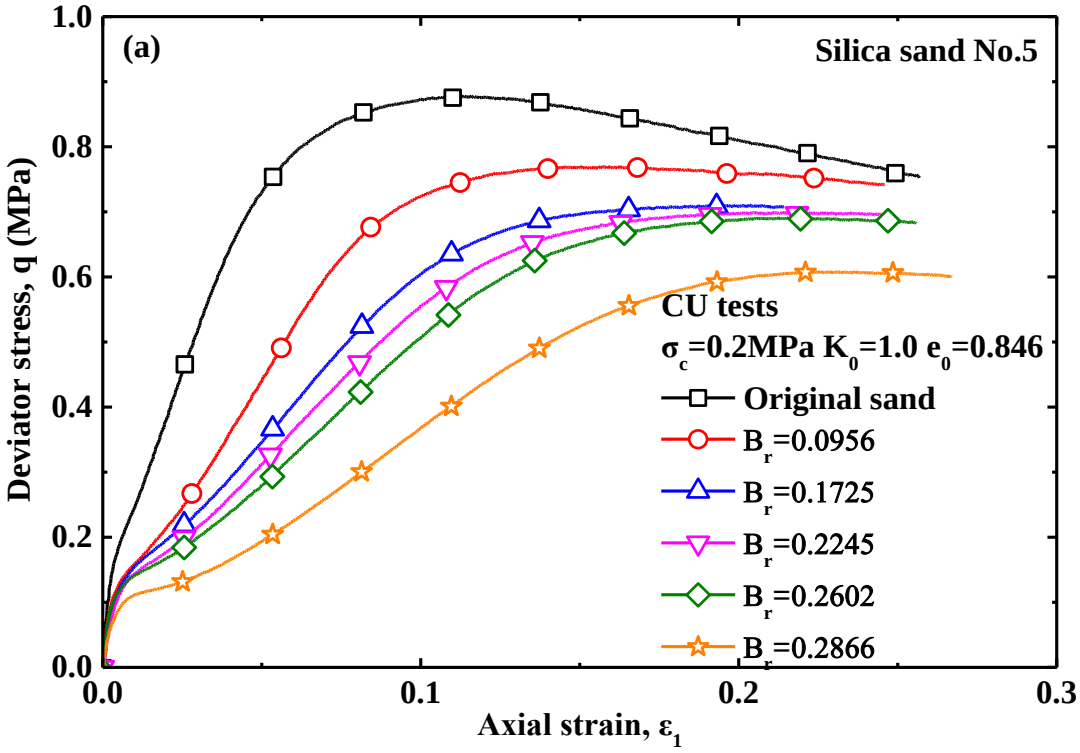

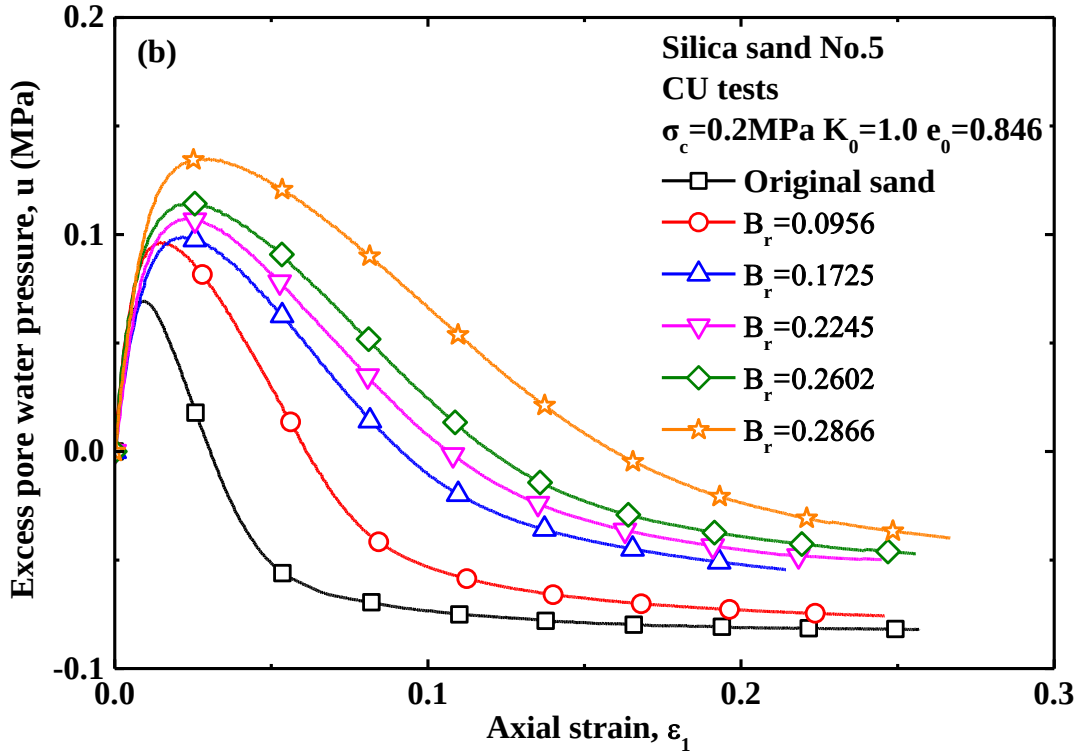

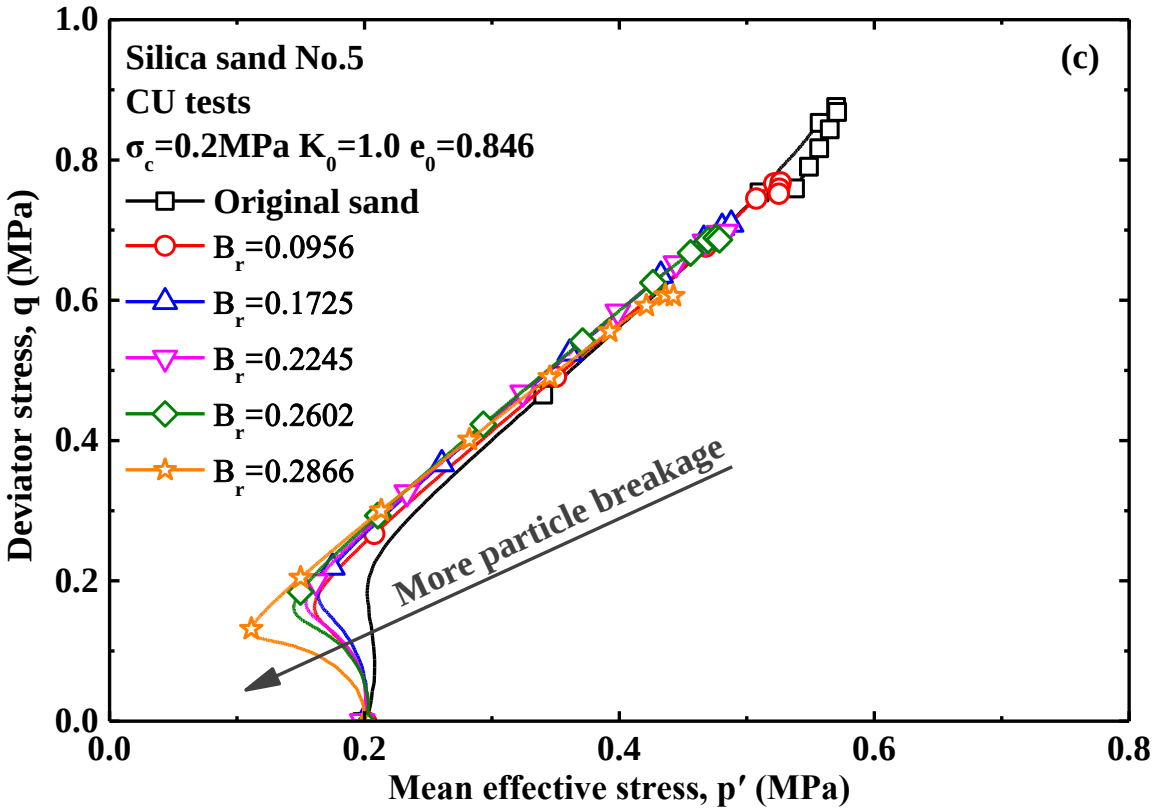

Figure 5.6 CU test results of original sand and pre-crushed sand under 0.2MPa confining pressure

As shown in Figure 5.4 and Figure 5.6, peak strengths and residual strengths were reached except a residual strength of original sand in CU test as shown in Figure 5.6(a). Herein the peak strengths and residual strengths were picked out and investigated considering the influence of particle breakage. Figure 5.7 shows the peak strengths and residual strengths against relative breakage under 0.2MPa confining pressure. It is found clearly in Figure 5.7(a) that the peak strengths from CU tests is larger than that from CD tests as a results of that under low confining pressure (0.2MPa) herein the dilatancy of soil in CU condition has much more substantial contribution on peak strength than that in CD condition. As a result of the softening of stress-strain curves in CD tests, it is understood reasonably that the residual strengths are lower than the relevant peak strength as shown in Figure 5.7(a). It is found in Figure 5.7 that peak strengths decrease with increasing particle breakage in relative breakage. However particle breakage in relative breakage has a more influence on reduction rate of peak strengths in CU tests than in CD tests. With increasing particle breakage in relative breakage, the difference of peak strengths between CU tests and CD tests is found to reduce and under particle breakage in B_r=0.2866 the peak strength in CU test is seen to be same as that in CD test approximately. The residual strength in CD tests has a slight increase at beginning of increase of particle breakage but with increasing amount of particle breakage the residual strengths tends to decrease as shown in Figure 5.7(a). However the difference between peak strengths and residual strengths are found to decrease approximately with increasing particle breakage, which means that particle breakage results in reduction of variation of

peak strength and residual strength. The peak strengths or residual strengths were normalized by the relevant strength on original sand as shown in Figure 5.7(b), where peak strengths are found to reduce to 88% of peak strength of original sand in CD test and 69% of peak strength of original sand in CU test in maximum but residual strengths in CD tests reduce to 95% of residual strength of original sand in maximum, which shown be paid more attention in practice.

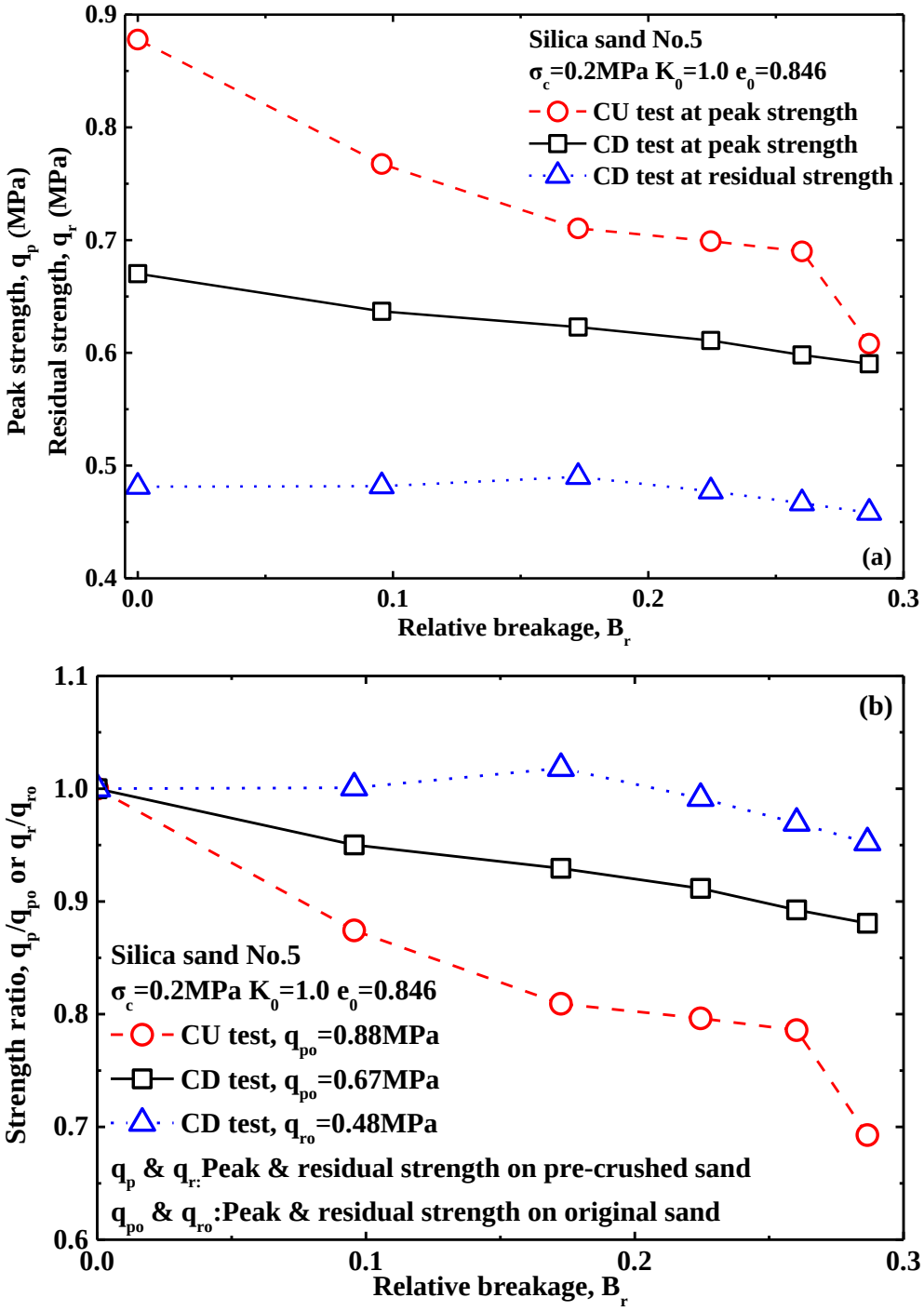

Figure 5.7 Peak strength and residual strength against relative breakage under 0.2MPa confining pressure

Shear strength of soil depends on many factors such as void ratio, stress path, effective stress, friction angle, deformation modulus and so on. Friction angle is an important mechanical parameter in silica sand as a kind of cohesionless material. Consequently the friction angles of pre-crushed sand and original sand were investigated by using the friction angle at peak strength and residual strength. The friction angle was calculated by Mohr-Coulomb theory as follows:

$$\varphi' = \sin^{-1}\left(\frac{3M}{6+M}\right) \tag{5.1}$$

where M is the axisymmetric principal stress ratio $3(\sigma_1' - \sigma_3')/(\sigma_1' + 2\sigma_3')$. σ_1' and σ_3' are major and minor effective principal stresses respectively.

Figure 5.8(a) shows the friction angle against relative breakage under 0.2MPa confining pressure. It is seen herein that the friction angles in CD tests and CU tests at peak strengths decrease with the increasing particle breakage but the friction angles in CD tests is larger than that in CU tests. However the friction angles in CD tests at residual strengths have little increase before slightly decreasing monotonically with increasing particle breakage, which is consistent with the trend of residual strengths as shown in Figure 5.7.

The fiction angles were normalized by that of original sand at peak strength or residual strength as shown in Figure 5.8(b), where the friction angles at peak strengths under 0.2MPa confining pressure are found to decrease with increasing particle breakage being in characteristics of sharp reduction, trending to slight reduction and then dramatic reduction with monotonic increase of particle breakage, where is consistent with the findings (Ghanbari et al., 2013). In fact the critical state was reached in residual strength. However it is found in residual strength (critical state) herein that friction angle has little increase before slightly decreasing with increasing particle breakage according to the friction angle at residual strength (critical state) of original sand, which is different from that particle breakage induced in ring shear tests resulted in increase of the critical state friction angle by a few degrees (Sadrekarimi and Olson, 2011). The friction angle at peak strength was reduced up to 93% and 90% of friction angle of original sand in maximum in CD tests and CU tests separately. Residual friction angle reduced up to 97% of friction angle of original sand in maximum.

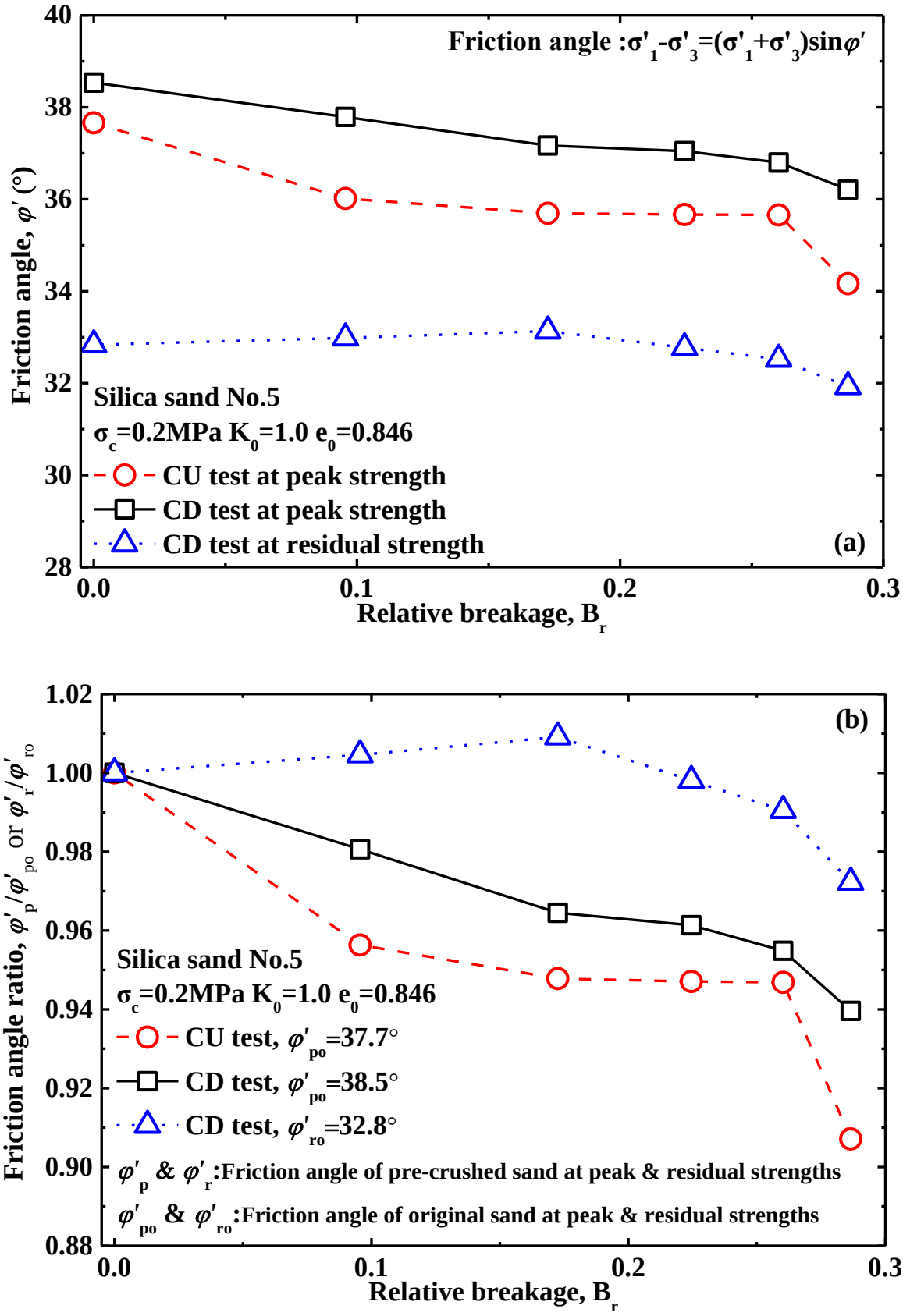

Figure 5.8 Relationship between friction angle and relative breakage under 0.2MPa confining pressure

The deformation modulus is another the significant parameter of soil behavior. The deformation modulus was calculated at ε_1=0.002 for each test as follows:

$$E_o = \left.\frac{\sigma_1^{'} - \sigma_3^{'}}{\varepsilon_1}\right|_{\varepsilon 1=0.002} \tag{5.2}$$

where σ_1' is major principal effective stress, σ_3' is minor principal effective stress and ε_1 is axial strain.

Figure 5.9 shows the relationship between deformation modulus and relative breakage, where the deformation modulus is found to decrease with increasing particle breakage in relative breakage. As illustrated in Figure 5.9(a), the initial modulus in CD tests herein is found to be larger with sharper reduction in comparison with that in CU tests but with increasing particle breakage in relative breakage the difference of deformation moduli between CD tests and CU tests is seen to decrease and be consistent at relatively large amount of particle breakage. The deformation modulus of pre-crushed sands was normalized by that of the original sand as shown in Figure 5.9(b) where the more substantial reduction of initial modulus occurred in CD tests than that in CU tests with increase particle breakage in relative breakage, which is consistent with the finding that the particle breakage softens the stress-strain curve, herein including the deformation modulus. It is revealed clearly in Figure 5.9(b) that the deformation modulus reduces up to 26% of the deformation modulus of original sand in CD tests in maximum and up to 47% of the deformation modulus of original sand in CU tests in maximum, which should be considered in practice.

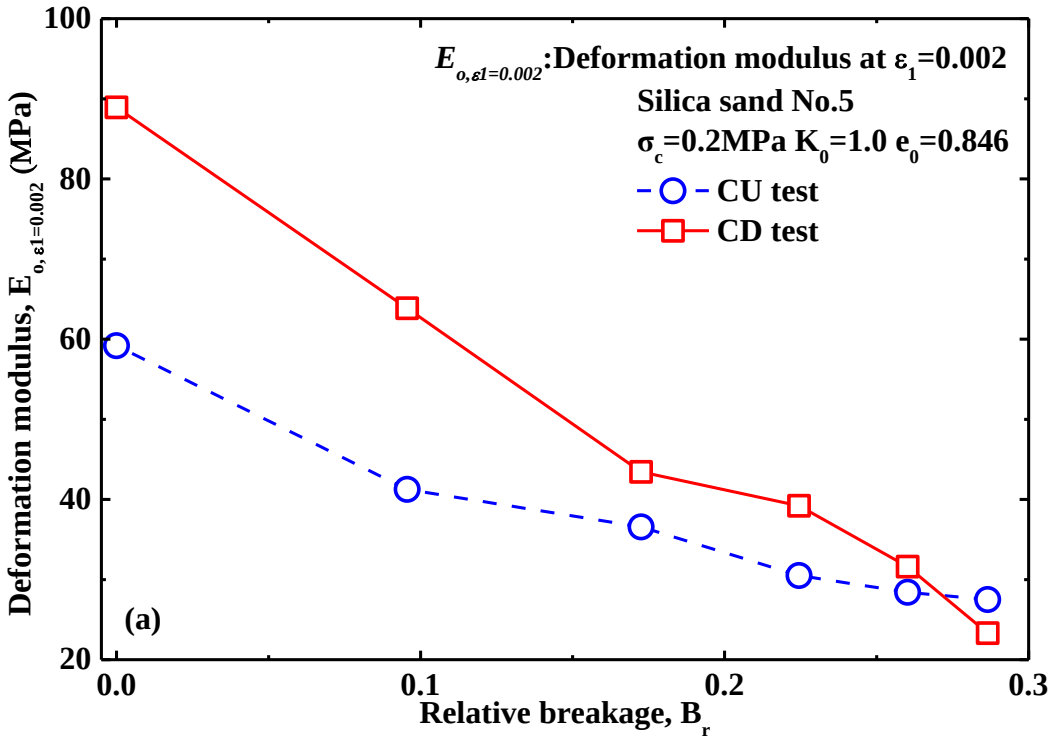

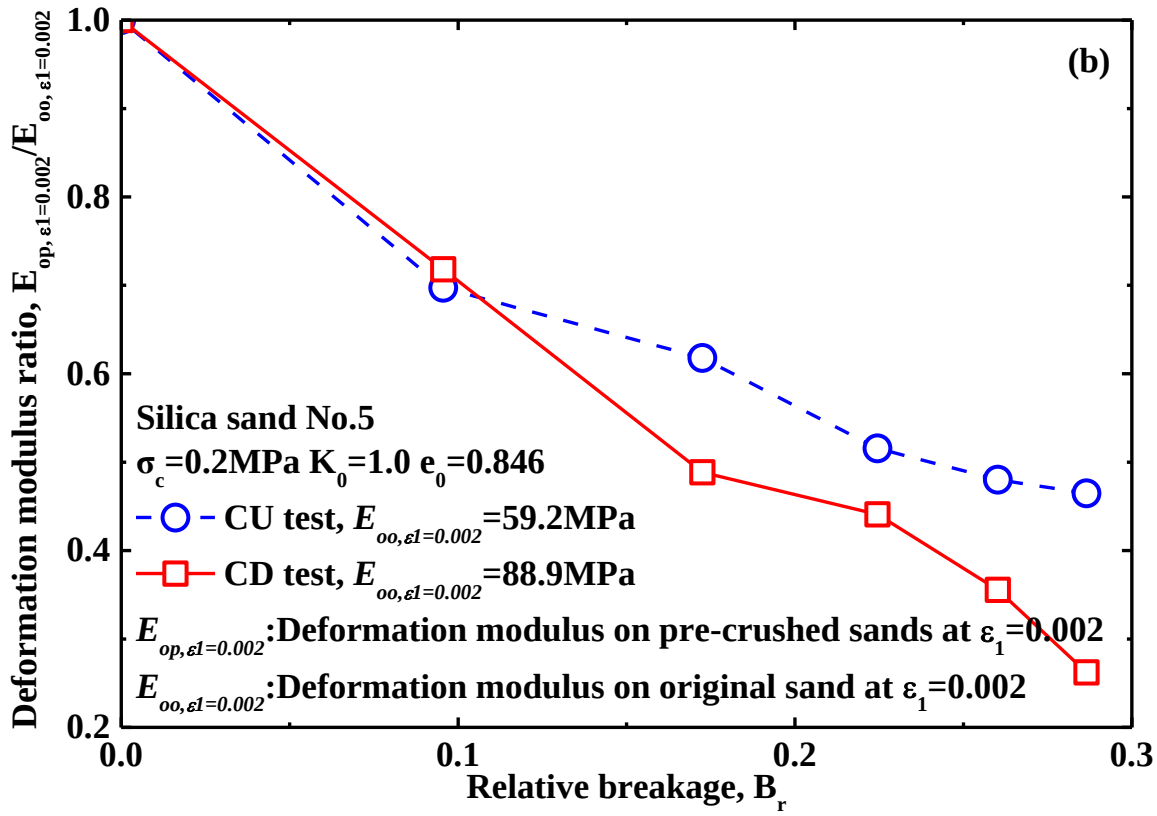

Figure 5.9 Relationship between deformation modulus and relative breakage under 0.2MPa confining pressure

5.3.2.3 Shearing behavior subjected to particle breakage under 0.5MPa confining pressure

Many triaxial tests on original sand and pre-crushed sand were conducted in CD and CU conditions under 0.5MPa confining pressure as well to investigate the influence of particle breakage on soil behavior subjected to relatively higher confining pressure in comparison with the 0.2MPa confining pressure. Figure 5.10 shows the CD tests results of original sand and pre-crushed sand under 0.5MPa confining pressure. It is found herein that the particle breakage deteriorates the stress-strain curves in reduction of peak strength as well but the original sand has the lowest residual strength as shown in Figure 5.10(a). The volume changes of original sand and pre-crushed sand during shearing under 0.5MPa confining pressure are shown in Figure 5.10(b), where the volume changes tend to dilatancy after a short contractancy at beginning stage of shearing but with increasing particle breakage it is getting more contractive in depression of dilatancy. Figure 5.10(c) shows the relevant stress paths of CD tests under 0.5MPa confining pressure.

For clearly understanding the influence of particle breakage on dilatancy behavior of soil, Figure 5.11 shows the void ratio change against dilatancy factor subjected to the influence of particle breakage where the original sand is seen to be most dilatant than the pre-crushed sands under the same initial void ratios of original sand and pre-crushed sand. particle breakage results in being more contractive before tending to dilatancy, and then

particle breakage results in depression of dilatancy, which are consistent with findings from Lee and Seed (1967), Miura and Ohara (1979) and Feda (2002).

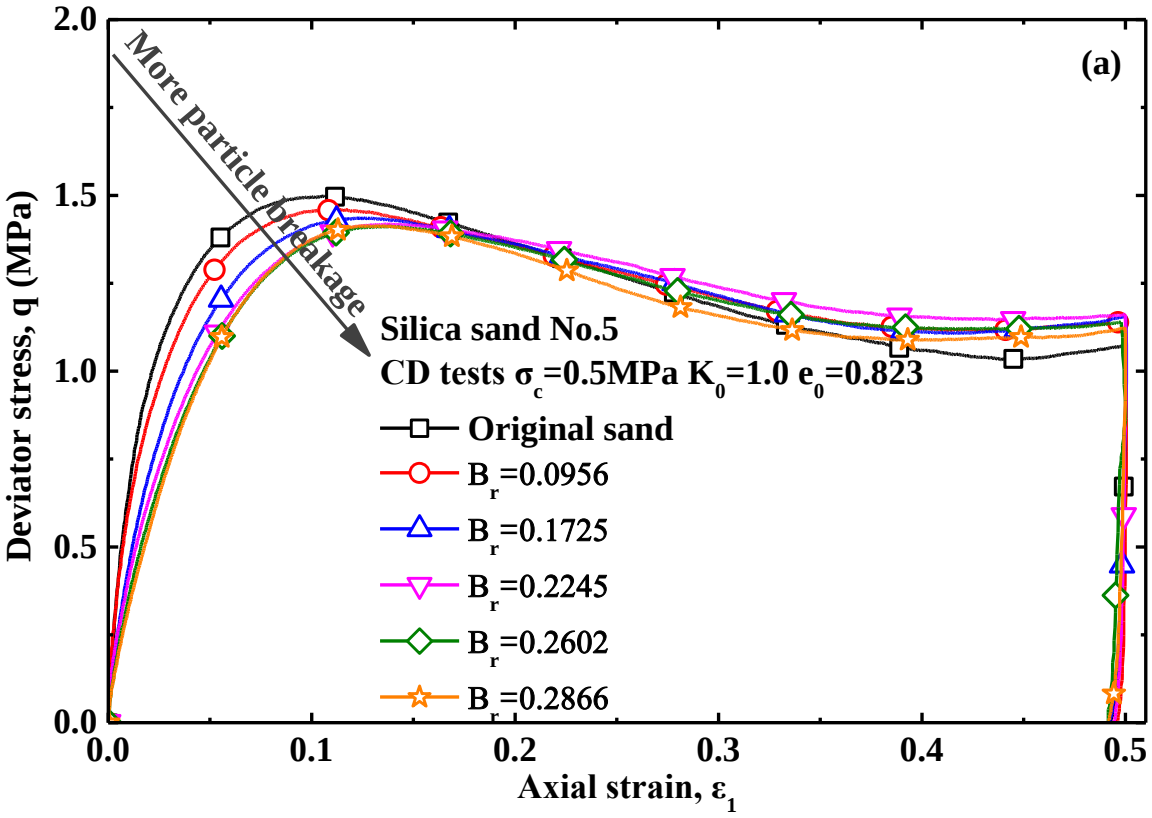

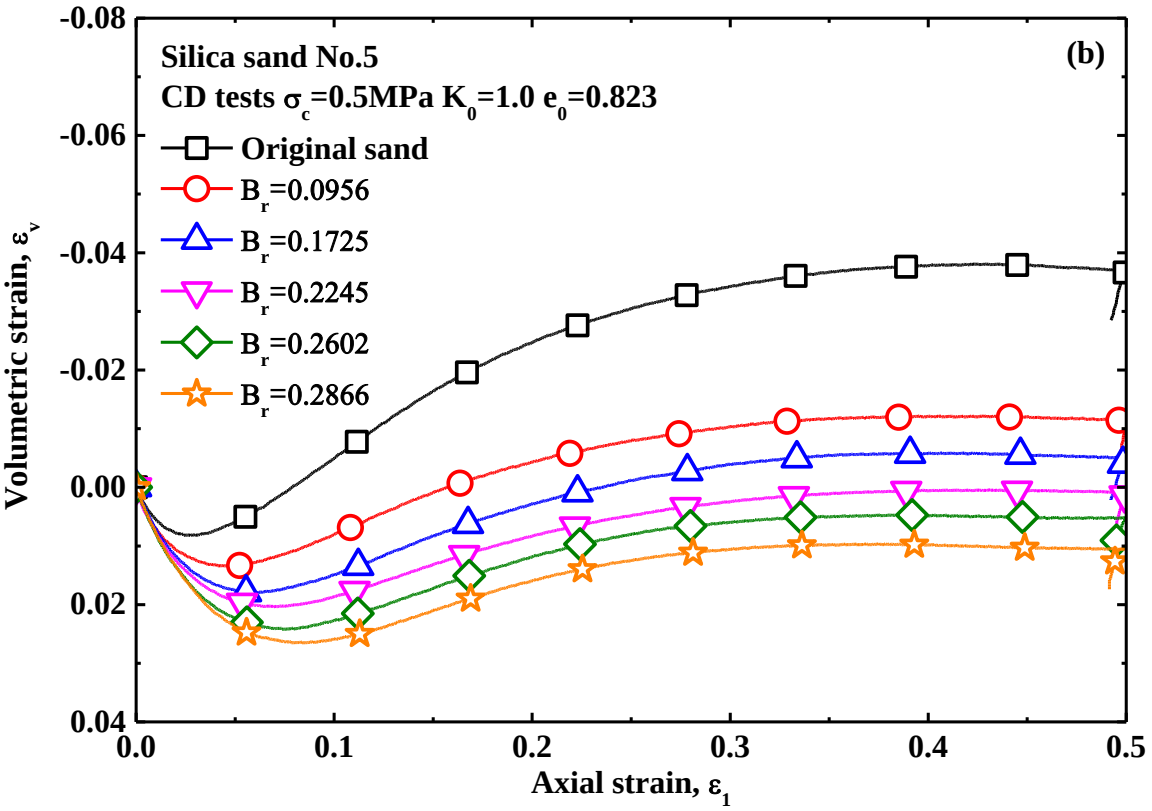

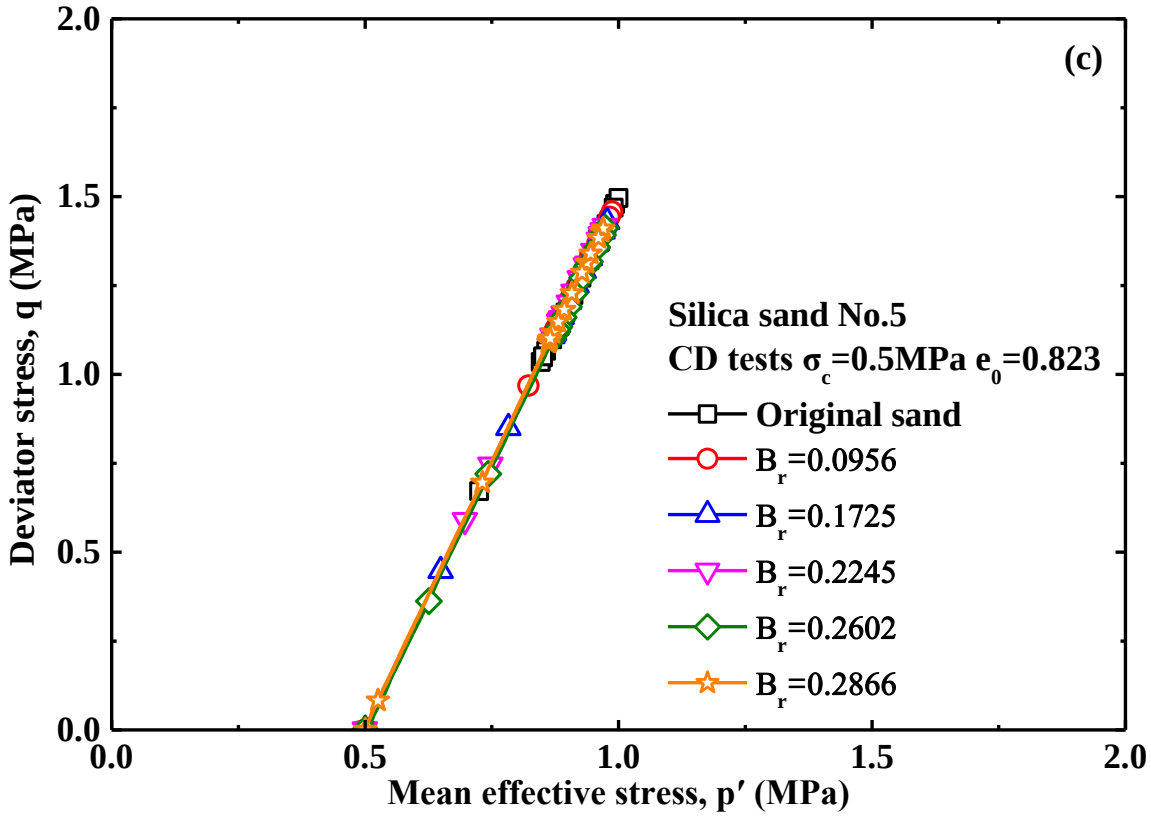

Figure 5.10 CD test results of original sand and pre-crushed sand under 0.5MPa confining pressure

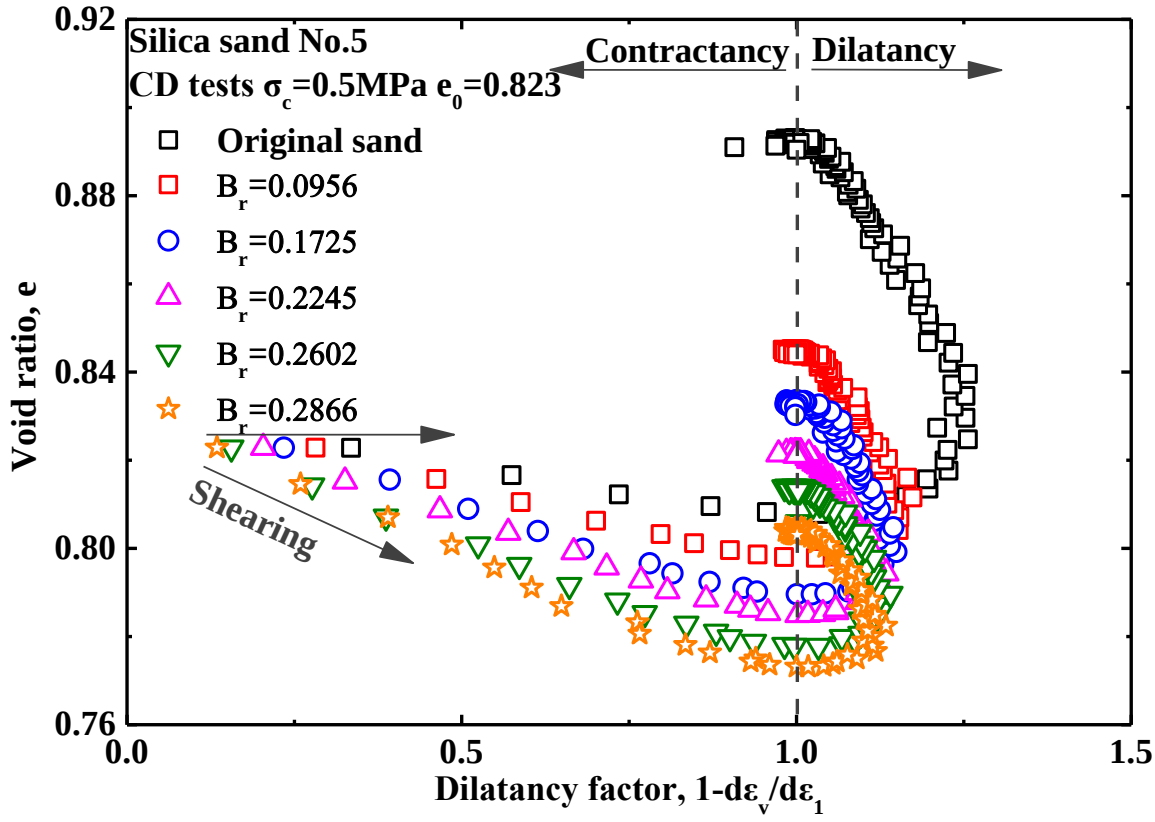

Figure 5.11 Dilatancy behavior on pre-crushed sand and original sand under 0.5MPa confining pressure

Triaxial tests on original sand and pre-crushed sand were performed in CU condition under 0.5MPa confining pressure for investigating the influence of particle on soil behavior including development of excess pore water pressure. Figure 5.12 shows the CU tests results of original sand and pre-crushed sand under 0.5MPa confining pressure. It is found herein that the deviator stress curves are weakened in gradual reduction of peak strengths by increasing particle breakage in relative breakage as shown in Figure 5.12(a). In comparison with the results from original sand and the pre-crushed sand with most pre-crushed breakage, it is concluded that particle breakage has a very important influence on strength of soil. The development of excess pore water pressure subjected to particle breakage under 0.5MPa confining pressure is shown in Figure 5.12(b), where particle breakage is found to result in higher development and slower dissolution of excess pore water pressure with higher residual excess pore water pressure in pre-crushed sand as a result of the increased contraction behavior induced by particle breakage. The stress paths of CU tests under 0.5MPa confining pressure is shown in Figure 5.12(c), which proves that particle breakage has a very significant influence on stress paths with being in reduction of peak strength.

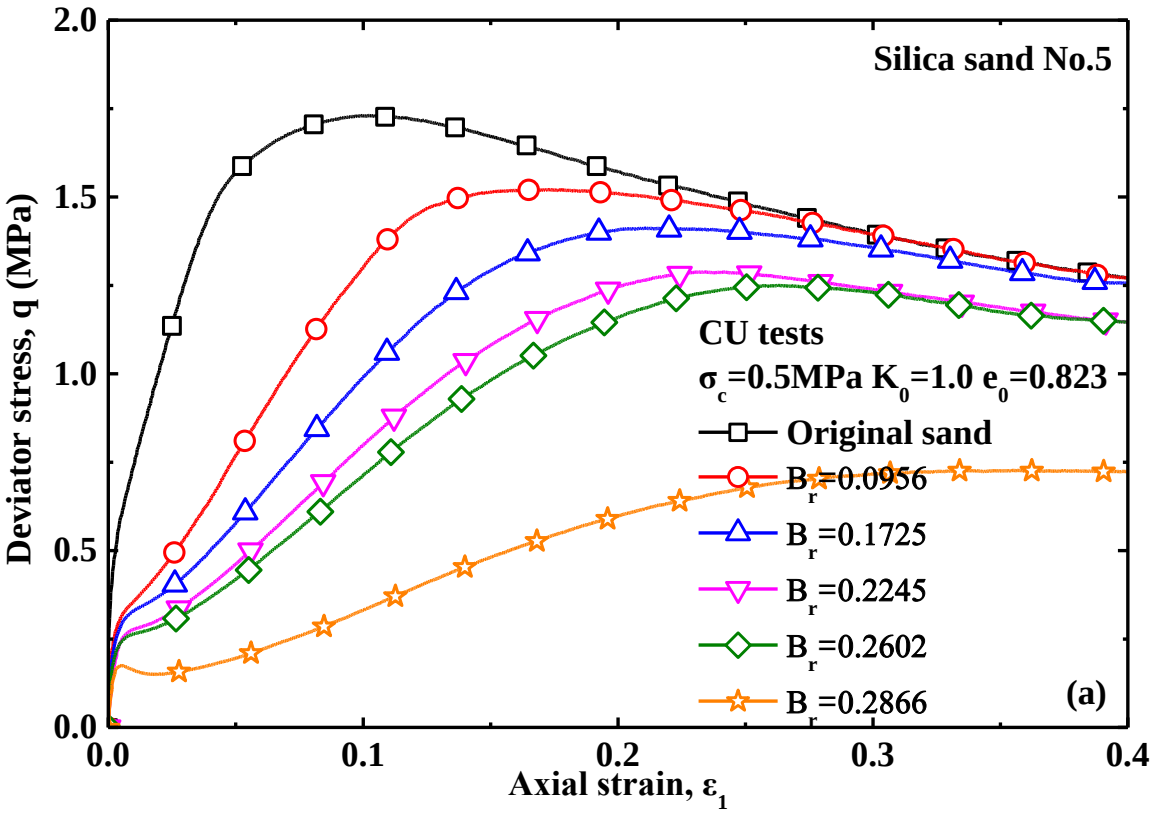

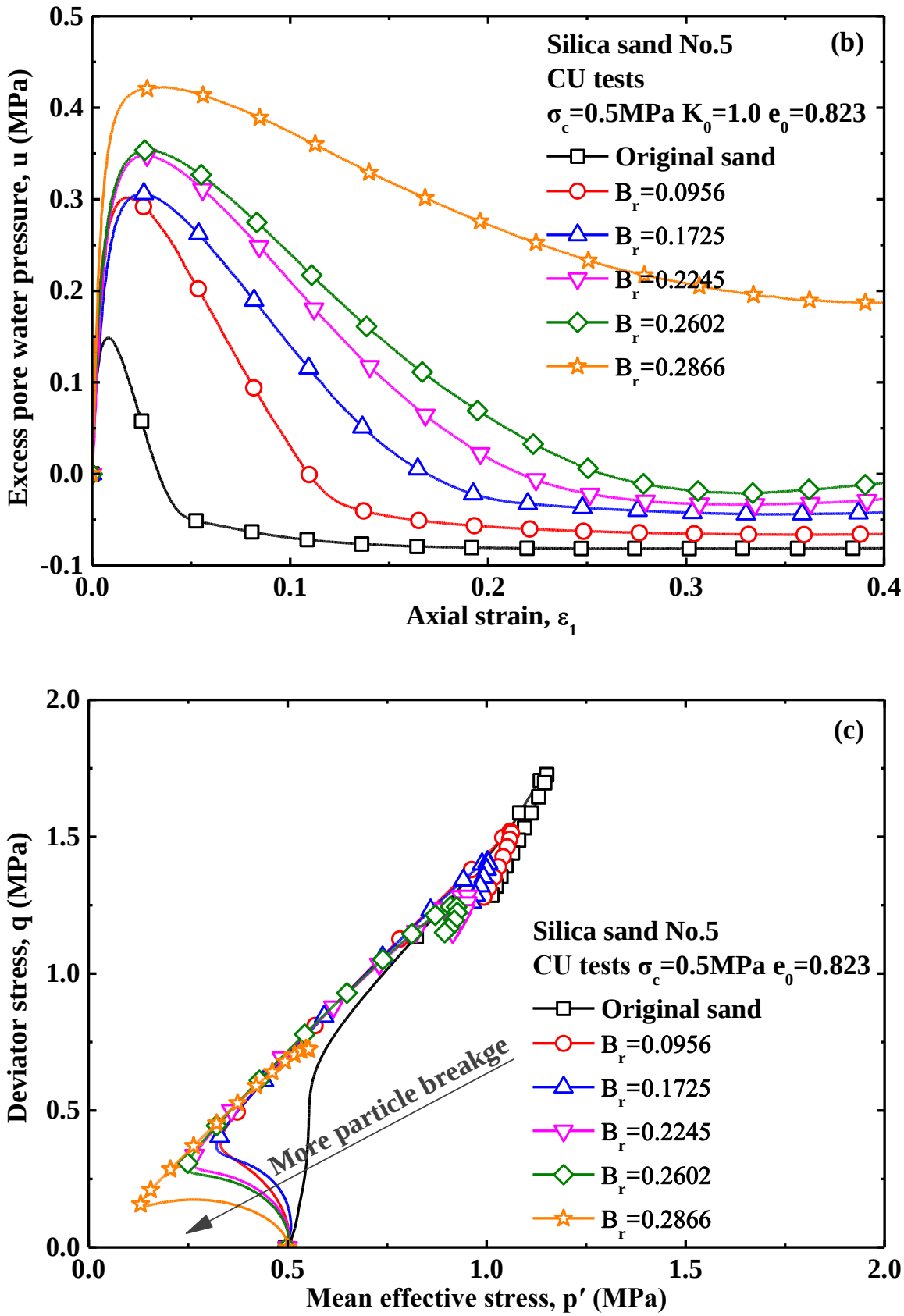

Figure 5.12 CU test results of original sand and pre-crushed sand under 0.5MPa confining pressure

The peak strengths and residual strengths of all triaxial tests under 0.5MPa confining pressure were picked out and combined into Figure 5.13, where the peak strengths are found to decrease with increasing particle breakage and residual strengths in CD tests have slight increase in vibration based on residual strength of original sand may as a result of the increased relative density related to the residual strengths. Peak strengths in CD tests are found to decrease linearly with increasing particle breakage but in CU tests it has more severe reduction of peak strength with a higher initial strength of original sand and a more dramatic reduction in the most amount of pre-crushed sand as shown in Figure 5.13(a). It is notable that the peak strengths in CD tests are lower than that in CU tests in first half of relative breakage but with continuing increasing particle breakage the peak strength in CU tests becomes smaller, which herein means more dilatancy contributed to initial peak strengths in CU tests was to be weakened more sharply than that in CD tests with increasing particle breakage, namely particle breakage has more influence on reduction of peak strength in CU tests than that in CD tests. Peak strengths and residual strengths were normalized by the relevant strength of original sand to investigate the corresponding change of peak strengths or residual strengths subjected to particle breakage as illustrated in Figure 5.13(b), where according to the peak strength of original sand peak strengths of pre-crushed sand has more substantial reduction in CU tests than that in CD tests with increasing particle breakage but residual strengths in CD tests have a vibrated increase as a results of smaller void ratio existed in pre-crushed sand.

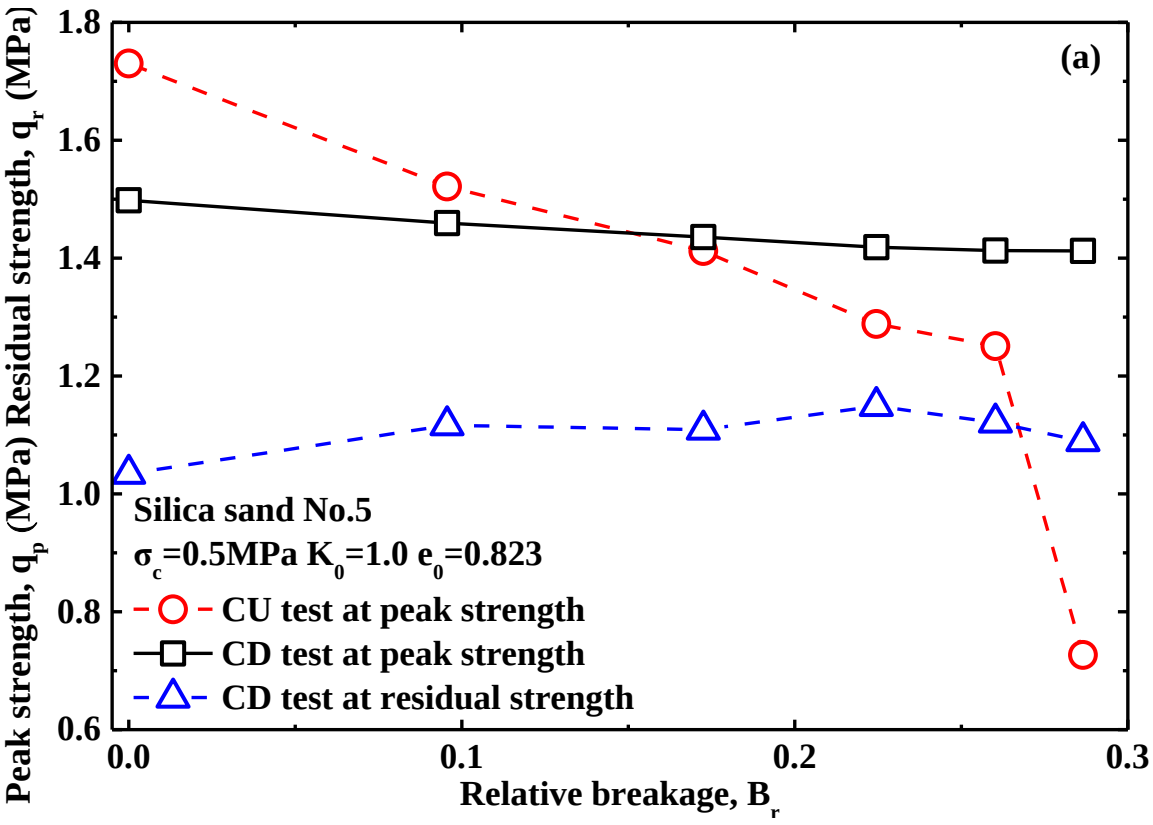

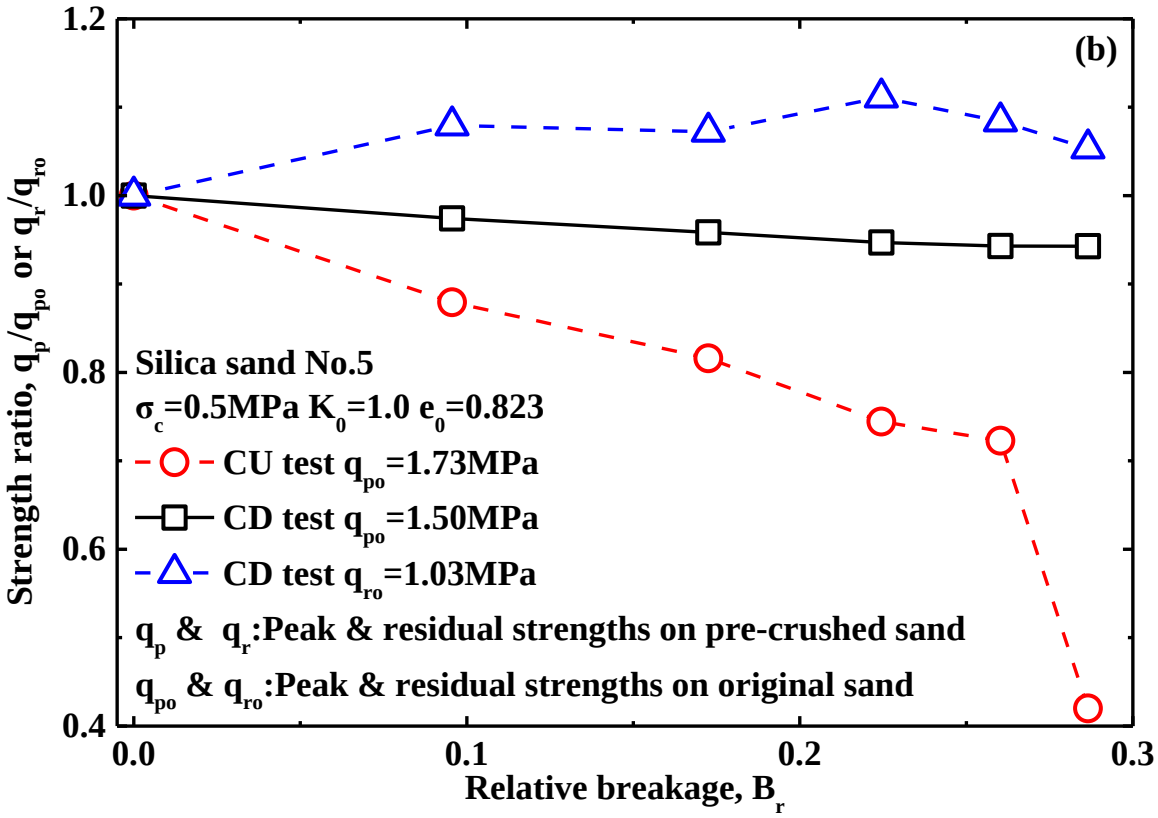

Figure 5.13 Peak strength and residual strength against relative breakage under 0.5MPa confining pressure

The friction angles at peak strengths and residual strengths of triaxial tests under 0.5MPa confining pressure were calculated for investigating the development of friction angle against particle breakage in relative breakage. Figure 5.14 indicates the relationship between friction angle and relative breakage under 0.5MPa confining pressure, where the friction angles at peak strengths are found to decrease linearly approximately with increasing particle breakage in relative breakage, which is consistent with finding (Ghanbari et al., 2013). However, the friction angles at residual strengths of CD tests are found to increase in fluctuation with increasing particle breakage. It can be seen in Figure 5.14(a) that it has a faster reduction of friction angles at peak strengths in CU tests than that in CD tests with almost same friction angle at peak strength of original sand in CD and CU tests. The friction angles were normalized by the relevant friction angle of original sand to investigate the change of friction angles in percentage of friction angle of original sand as shown in Figure 5.14(b). It is seen herein that friction angle at peak strengths in CD tests is in slight reduction with increasing particle breakage but in CU tests the maximum reduction of peak strength is up to around 11% of friction angle of original sand, which should be notable in practice. In fact, critical state was reached in residual state. The friction angle in residual strength (critical state) is found to increase, which is consistent with the finding (Sadrekarimi and Olson, 2011). Been et al. (1991) concluded that critical state friction angle in sands may be a function of critical state void ratio. Considering the evolution of friction angle at residual state (critical state) against particle breakage under 0.2MPa confining pressure in Figure 5.8 and 0.5MPa confining

pressure in Figure 5.14, the influence of particle breakage on the evolution of friction angle at critical state depends on the current critical state.

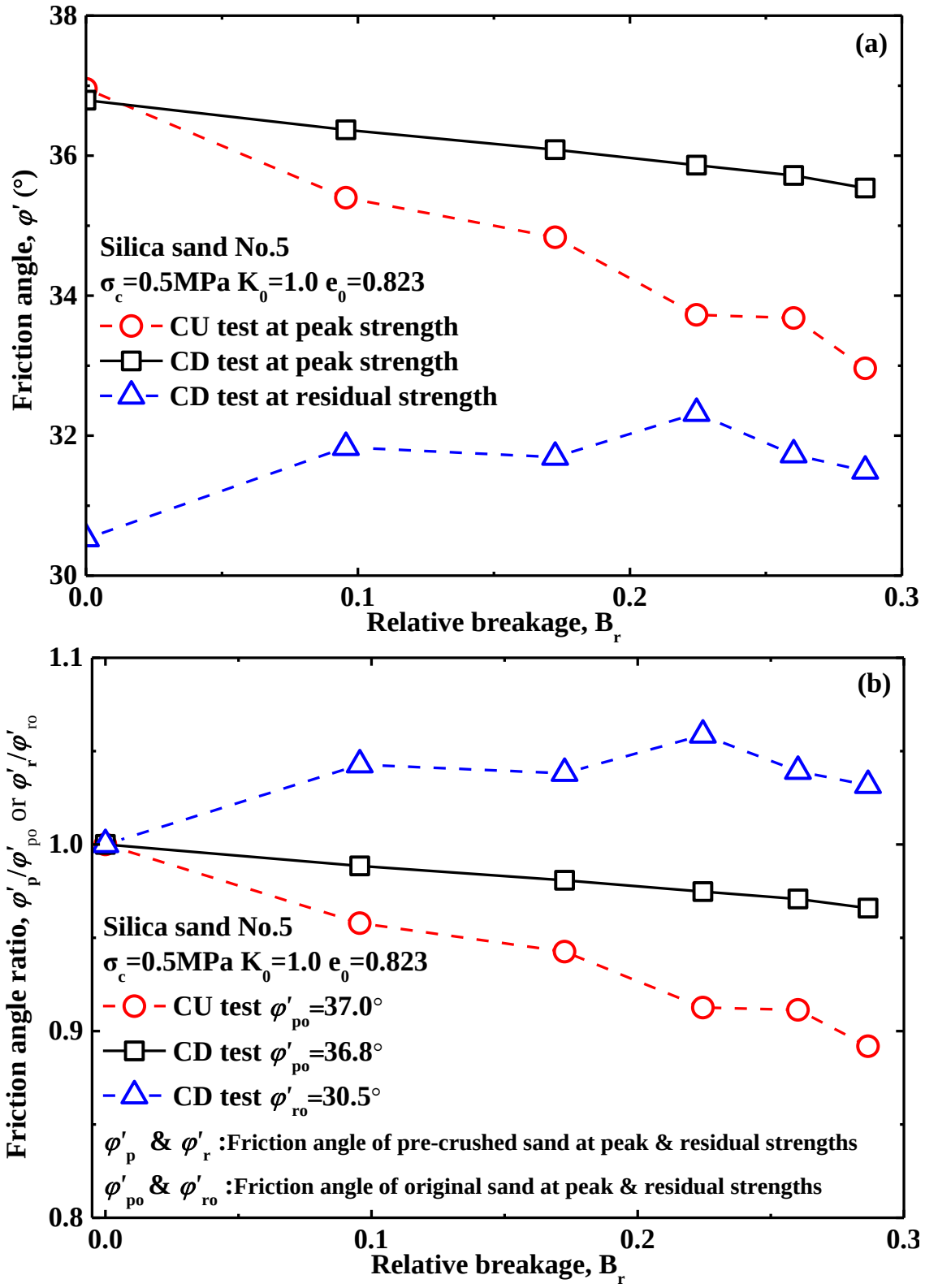

Figure 5.14 Relationship between friction angle and relative breakage under 0.5MPa confining pressure

For getting fundamental understanding of the influence of particle breakage on deformation modulus, the deformation modulus of all triaxial tests under 0.5MPa confining pressure were calculated at 0.002 axial strain. Figure 5.15 shows the deformation modulus against particle breakage in relative breakage under 0.5MPa confining pressure, where deformation moduli are found to decrease with increasing particle breakage in relative breakage but the initial modulus of original sand in CU test is larger by far than that in CD test may because of the contribution of elastic modulus of water at the beginning of shearing. It is notable that deformation moduli in CD and CU tests are getting closer with increasing particle breakage as shown in Figure 5.15(a). All deformation moduli were normalized by the relevant initial modulus of original sand as shown in Figure 5.15(b), where the deformation moduli decrease gradually up to 30% of deformation modulus of original sand in CU test and 40% of deformation modulus of original sand in CD test.

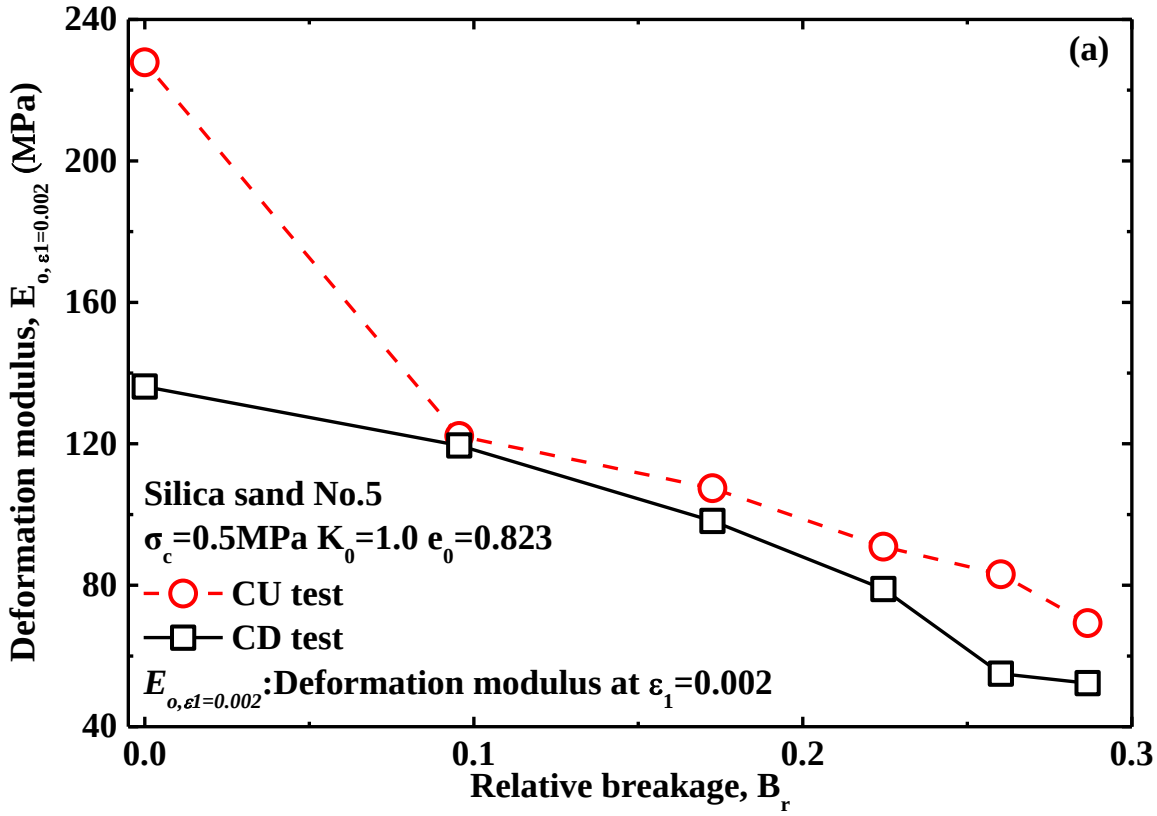

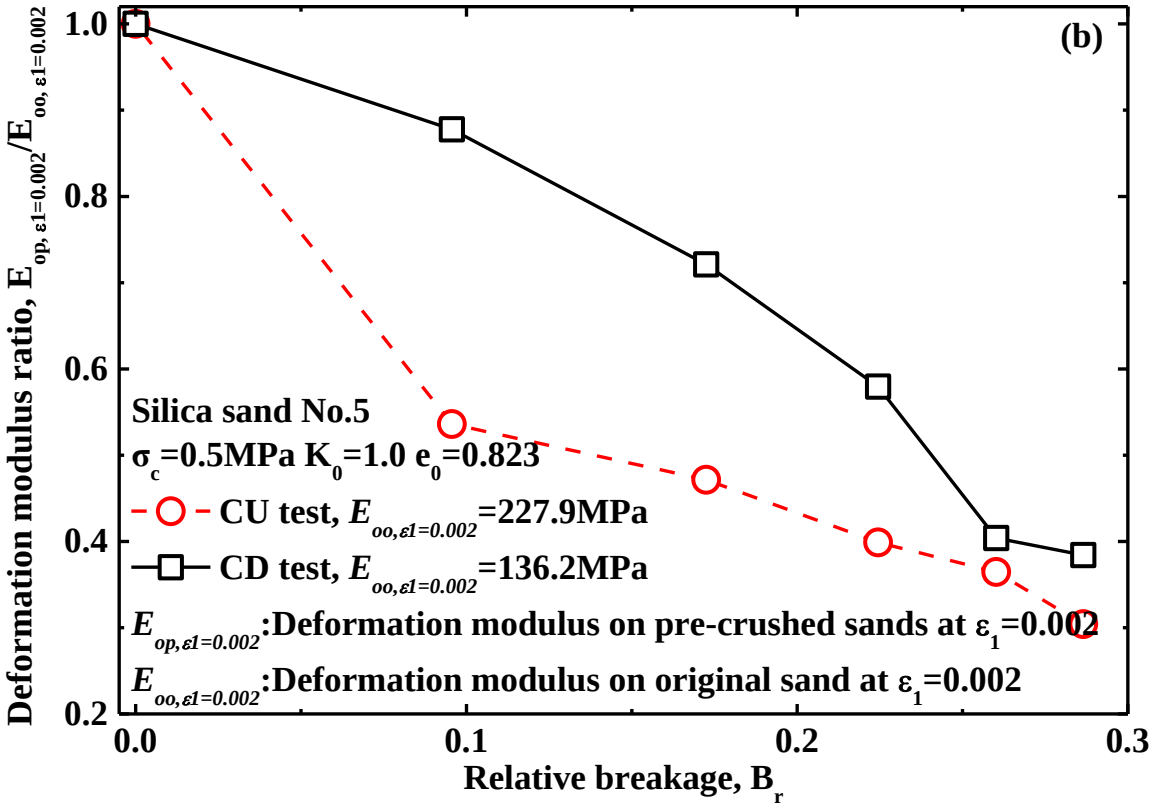

Figure 5.15 Relationship between deformation modulus and relative breakage under 0.5MPa confining pressure

5.3.2.4 Shearing behavior subjected to particle breakage under 1.0MPa confining pressure

The influence of particle breakage on soil behavior should be investigated as well under relatively higher pressure causing some amount of particle breakage again during shearing which would not be measured in this research. Another triaxial tests on original sand and pre-crushed sand were conducted in CU condition under 1.0MPa confining pressure for investigate the influence of particle breakage on soil behavior. Figure 5.16 shows the CU tests results of original sand and pre-crushed sand under 1.0MPa confining pressure, where particle breakage is found to deteriorate whole stress-strain curves in reduction with higher development and slower dissolution of excess pore water pressure. It is notable that the original sand has the lowest axial strain to reach the highest peak strength and with increasing particle breakage pre-crushed sands need larger axial strain to reach the relatively lower peak strengths, which means that particle breakage depresses the exertion extent of dilatancy contributing to the peak strength in some extent. The stress paths of CU tests under 1.0MPa confining pressure subjected to particle breakage is shown in Figure 5.16(c), where particle breakage changed completely the whole stress paths in reduction of peak strength.

Figure 5.17 show the peak strengths against particle breakage in relative breakage under 1.0MPa confining pressure. It is seen clearly that the peak strengths decrease in up

concavity with increasing particle breakage in relative breakage as shown in Figure 5.17(a). The peak strengths were normalized by the peak strength of original sand as shown in Figure 5.17(b) where maximum loss of peak strength induced by pre-crushed sand with most amount of pre-crushed breakage is up to around 50% of peak strength of original sand, which should be paid more attention in practice.

Friction angle at peak strength of each test under 1.0MPa confining pressure was calculated and normalized by the friction angle of original sand for investigating the evolution of friction angles subjected to particle breakage. The relationship between friction angle and relative breakage under 1.0MPa confining pressure is shown in Figure 5.18 where the friction angles are found to experience sharp decrease first, then tend to slight reduction and finally dramatic decrease with increasing particle breakage in relative breakage. And the friction angle of the pre-crushed sand with most amount of pre-crushed breakage is reduced to around 94% of friction angle of original sand as shown in Figure 5.18(b).

Deformation modulus of each test under 1.0MPa confining pressure was calculated at 0.002 axial strain and normalized by the deformation modulus of original sand for investigating the development of deformation modulus against particle breakage in relative breakage. The relationship between deformation modulus and relative breakage under 1.0MPa confining pressure is shown in Figure 5.19 where the deformation modulus is found to decrease in up-concave bilinearity and the deformation modulus of pre-crushed sand with most amount of pre-crushed breakage is reduced to 32% of deformation modulus of original sand.

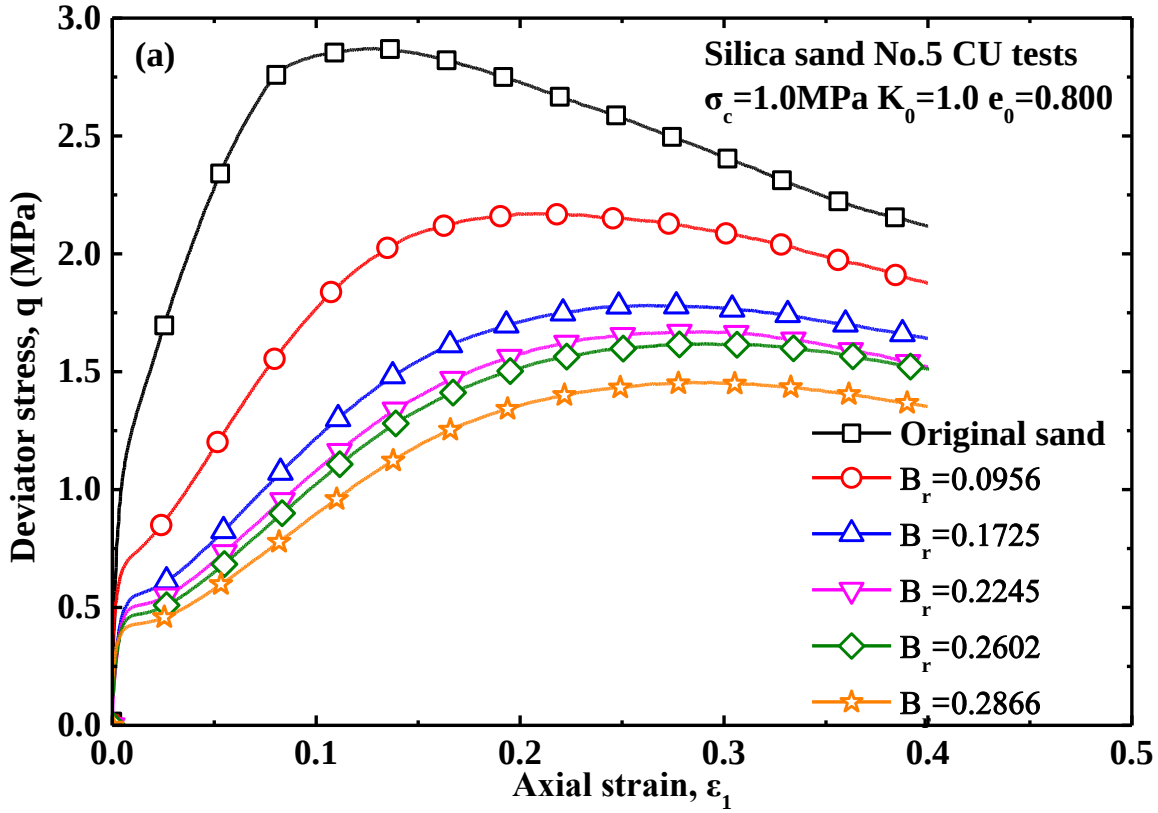

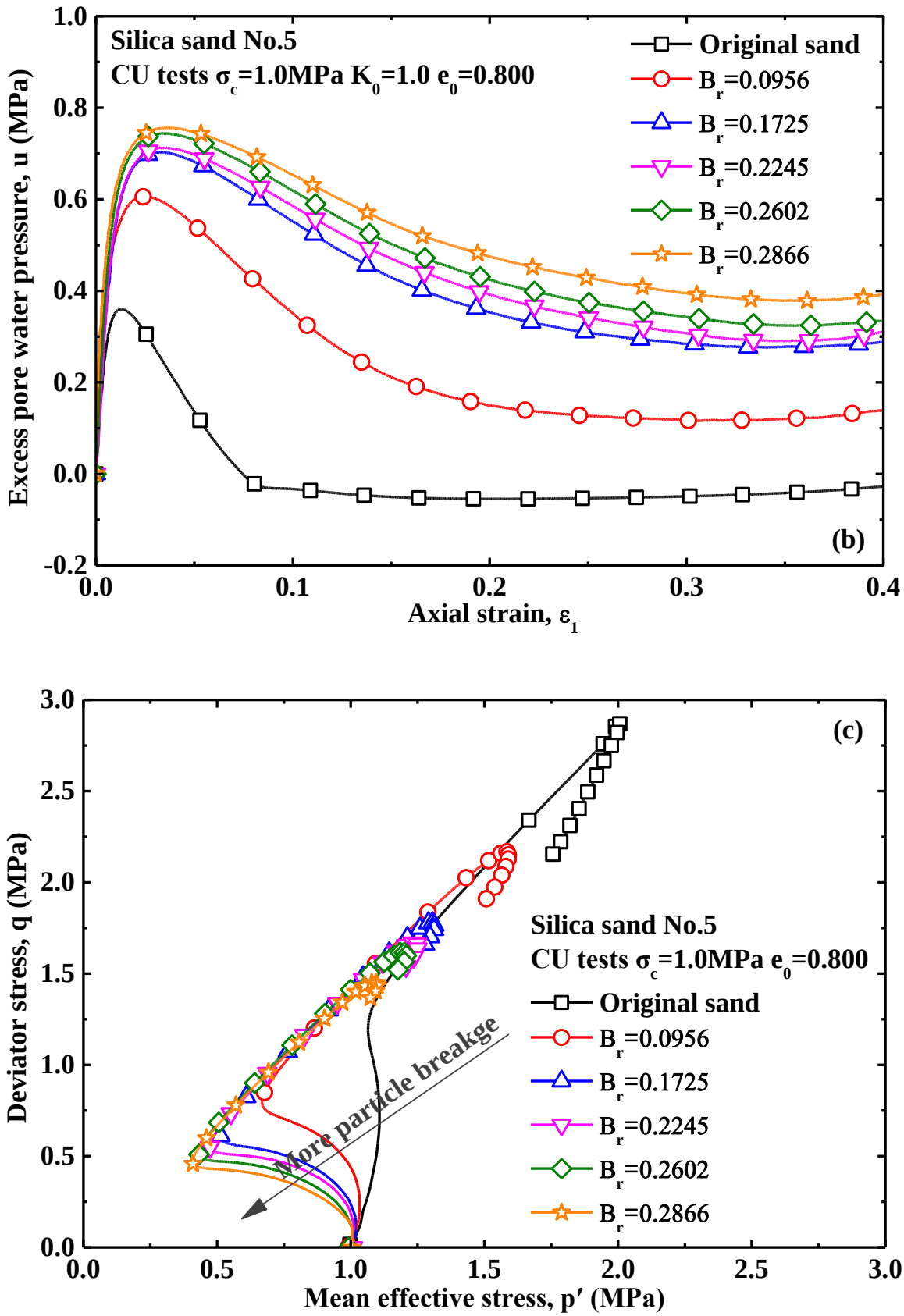

Figure 5.16 CU test results of original sand and pre-crushed sand under 1.0MPa confining pressure

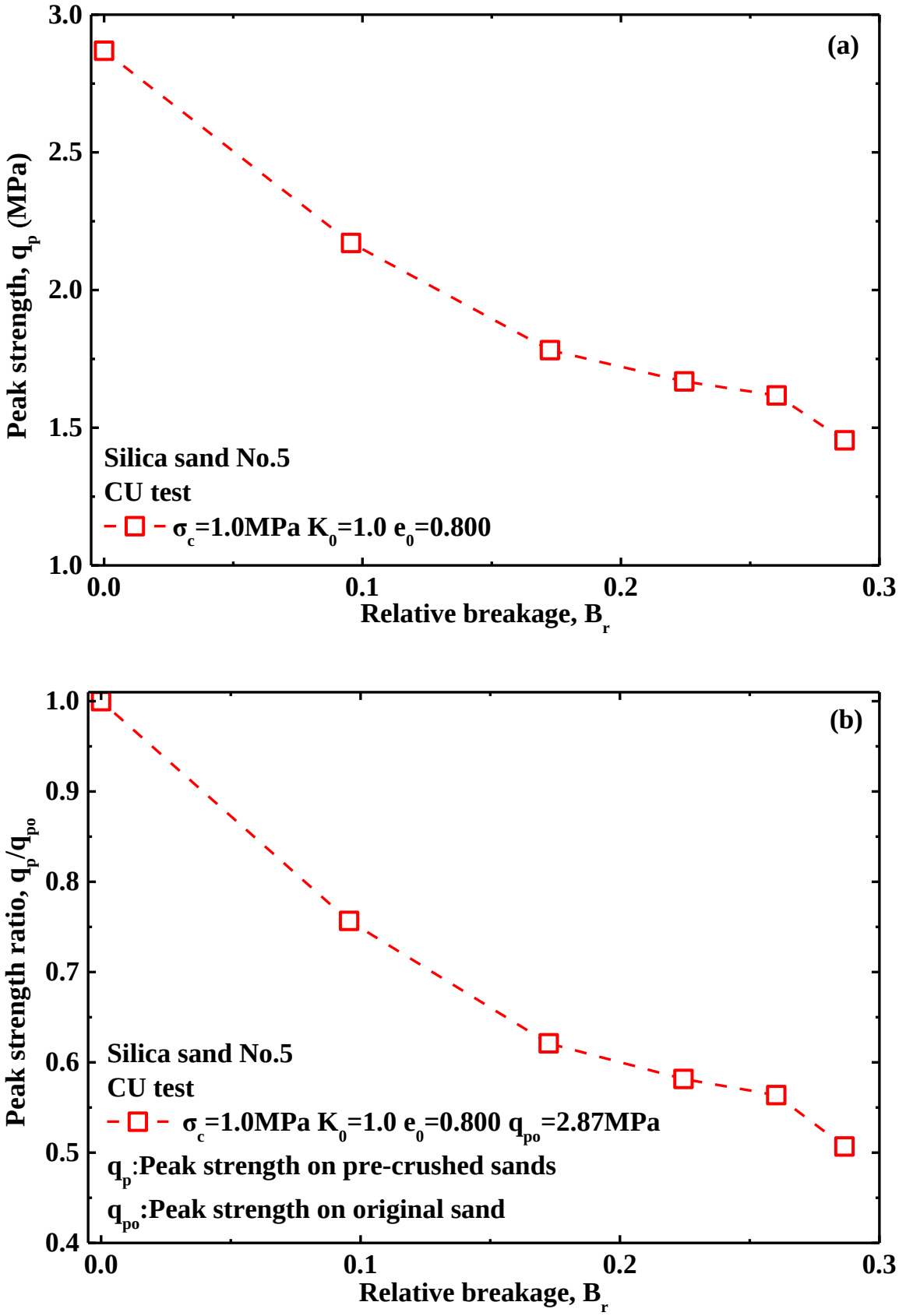

Figure 5.17 Peak strength against relative breakage under 1.0MPa confining pressure

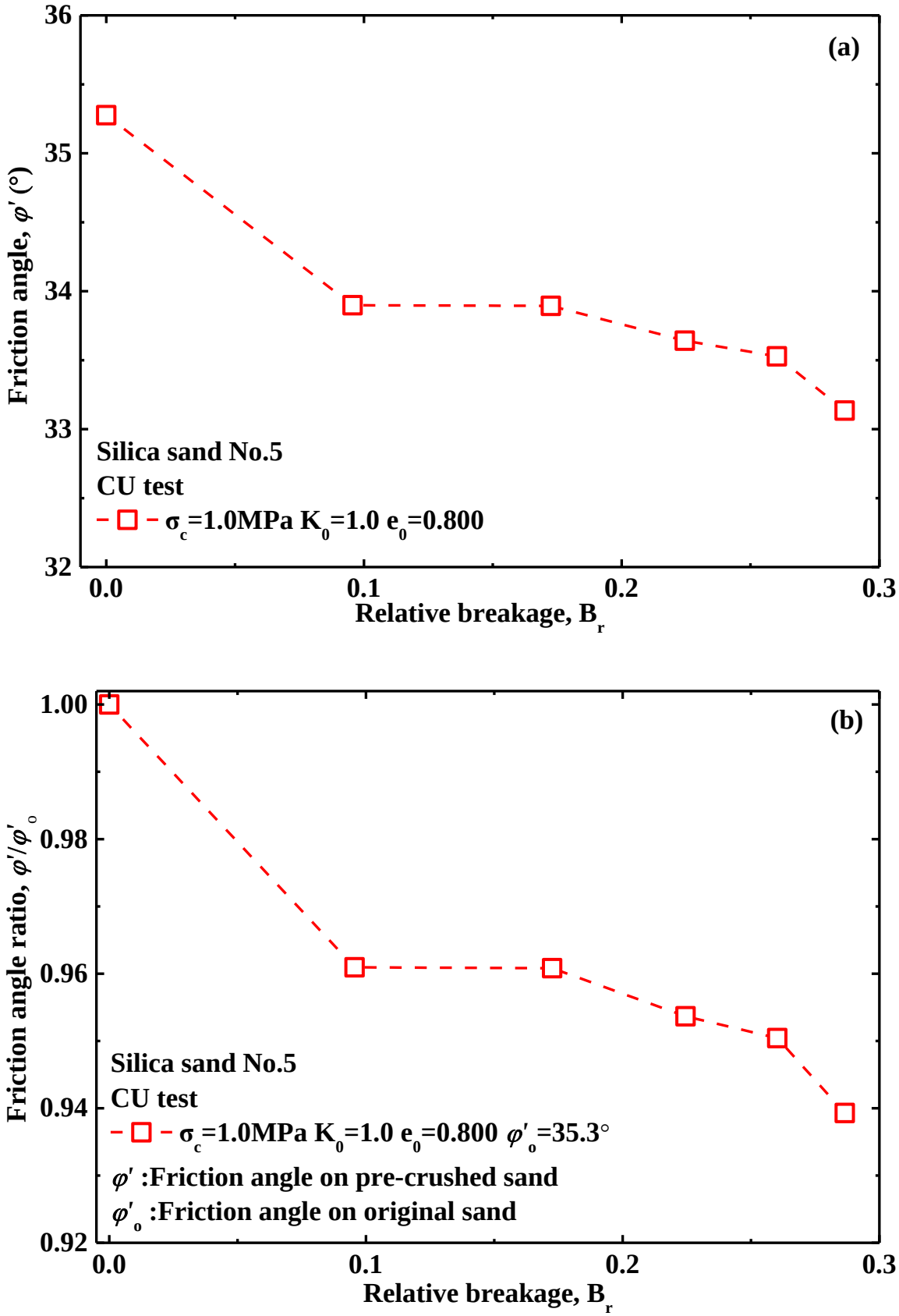

Figure 5.18 Relationship between friction angle and relative breakage under 1.0MPa confining pressure

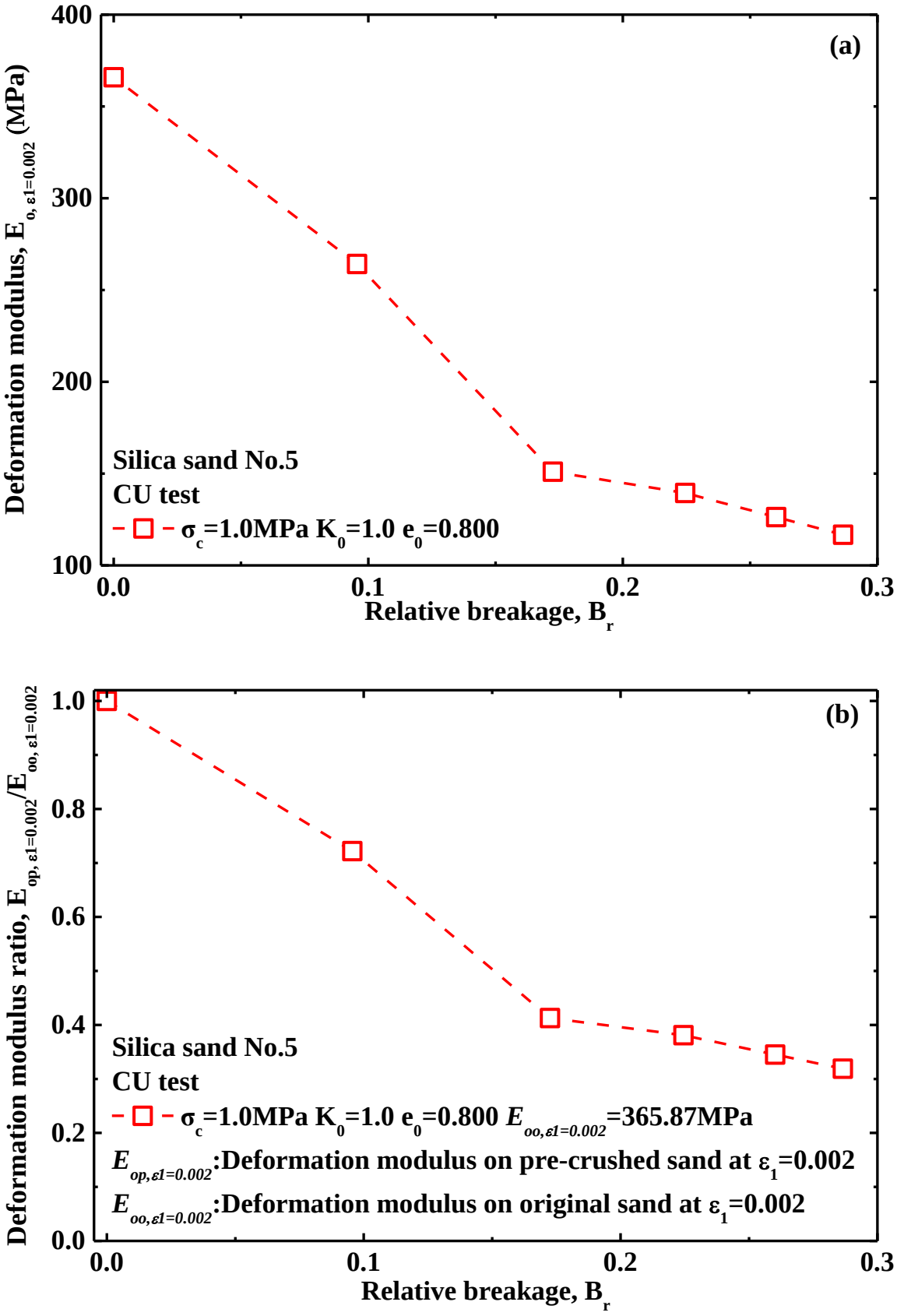

Figure 5.19 Relationship between deformation modulus and relative breakage under 1.0MPa confining pressure

5.3.2.5 Shearing behavior subjected to particle breakage under 3.0MPa confining pressure

Another CU triaxial tests on original sand and pre-crushed sand were carried out under 3MPa confining pressure to investigate the influence of particle breakage on soil behavior. Figure 5.20 shows the CU tests results of original sand and pre-crushed sand under 3MPa confining pressure, where particle breakage is found to deteriorate the stress-strain curves in reduction of peak strength and result in higher development of excess pore water pressure. However particle breakage has a monotonic influence on deterioration of whole stress-strain curves of pre-crushed sands and increase of excess pore water pressure of pre-crushed sands with increasing particle breakage as shown in Figure 5.20 (a) and (b). Note herein that the deviator stress curve of original sand has the highest peak strength but a steeper dropping softening stage after peak strength in comparison with that of pre-crushed sands as shown in Figure 5.20(a). However the excess pore water pressure of original sand has a more evident increase during the softening stage of deviator stress after peak strength as displayed in Figure 5.20(b). It is notable that the original sand has the lowest axial strain to reach the highest peak strength and with increasing particle breakage pre-crushed sands need larger axial strain to reach the relatively lower peak strengths, which means larger shear deformation is needed in pre-crushed sand to reach maximum dilatancy contributing to the peak strength with increasing particle breakage. Figure 5.20(c) shows the stress paths of CU tests under 3MPa confining pressure subjected to particle breakage. It is notable herein that particle breakage influenced thoroughly the whole stress paths in reduction of peak strength.

The peak strength of each test was picked up against particle breakage for investigating the influence of particle breakage in quantity. Figure 5.21 shows the peak strengths against particle breakage in relative breakage in CU tests under 3MPa confining pressure. It is found clearly that particle breakage results in reduction of peak strength in linearity approximately as shown in Figure 5.21(a). The peak strengths were normalized by the peak strength of original sand as shown in Figure 5.21(b), where the peak strength of pre-crushed sand with most amount of pre-crushed breakage is seen to decrease to around 72% of peak strength of original sand which should be considered during engineering design in practice.

Fiction angle at peak strength of each CU test under 3MPa confining pressure was calculated and normalized by the friction angle of original sand for investigating the development of friction angles subjected to particle breakage. Figure 5.22 shows the friction angles against particle breakage in relative breakage, where friction angle is found to decrease in down-concave bilinearity with intercept point around B_r=0.1 and the friction angle of pre-crushed sand with most amount of pre-crushed breakage is seen to decrease to around 98.4% of friction angle of original sand as shown in Figure 5.22(b).

Deformation modulus of each test under 3MPa confining pressure was calculated at 0.002 axial strain and normalized by the deformation modulus of original sand for

investigating the evolution of deformation modulus against particle breakage in relative breakage. Figure 5.23 indicates the deformation modulus subjected to particle breakage in relative breakage in CU tests under 3MPa confining pressure, where deformation modulus is found to undergo dramatic decrease, gentle decrease and dramatic decrease again with increasing particle breakage in relative breakage and the deformation modulus of pre-crushed sand with most amount of pre-crushed breakage is reduced up to 59% of deformation modulus of original sand.

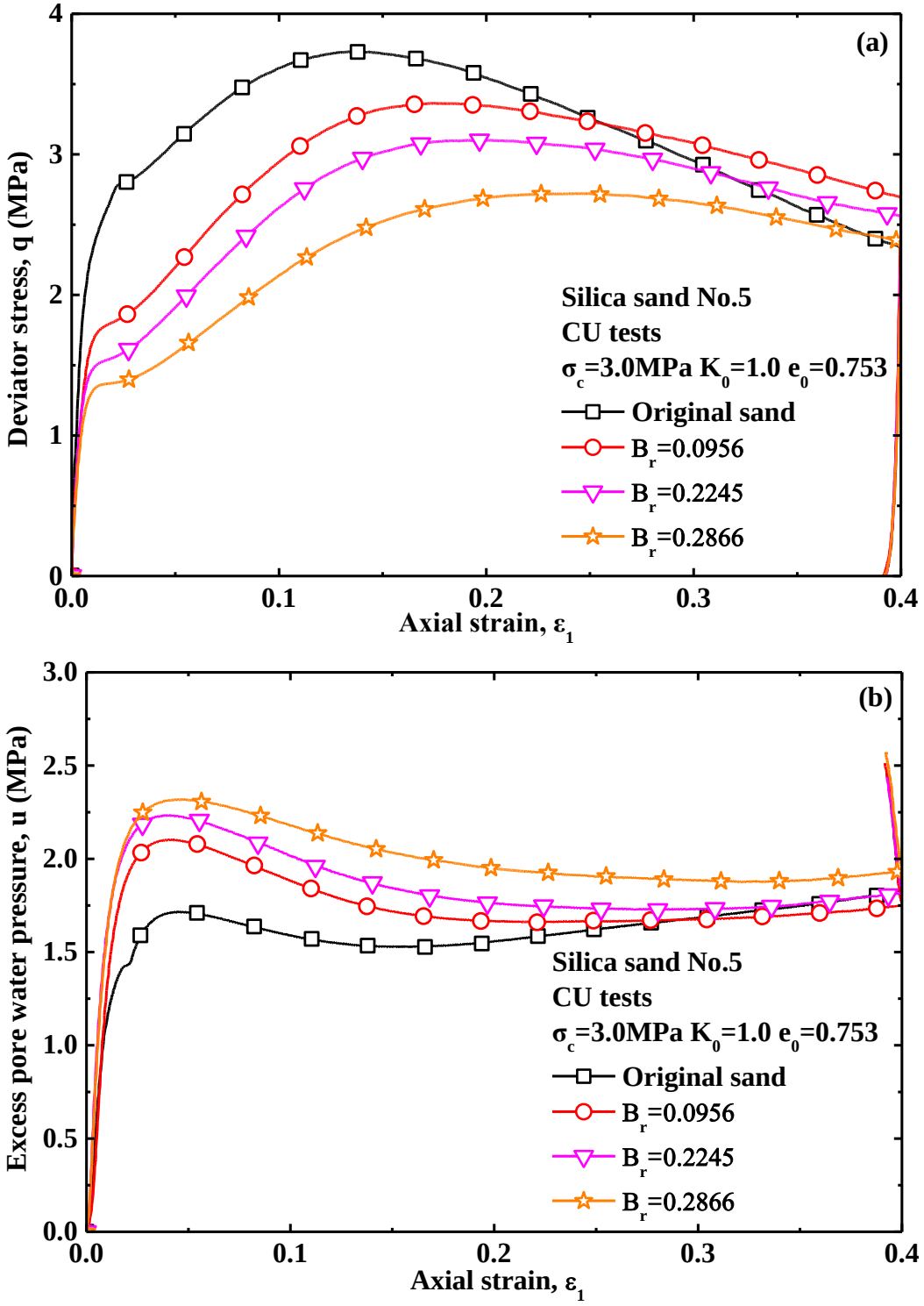

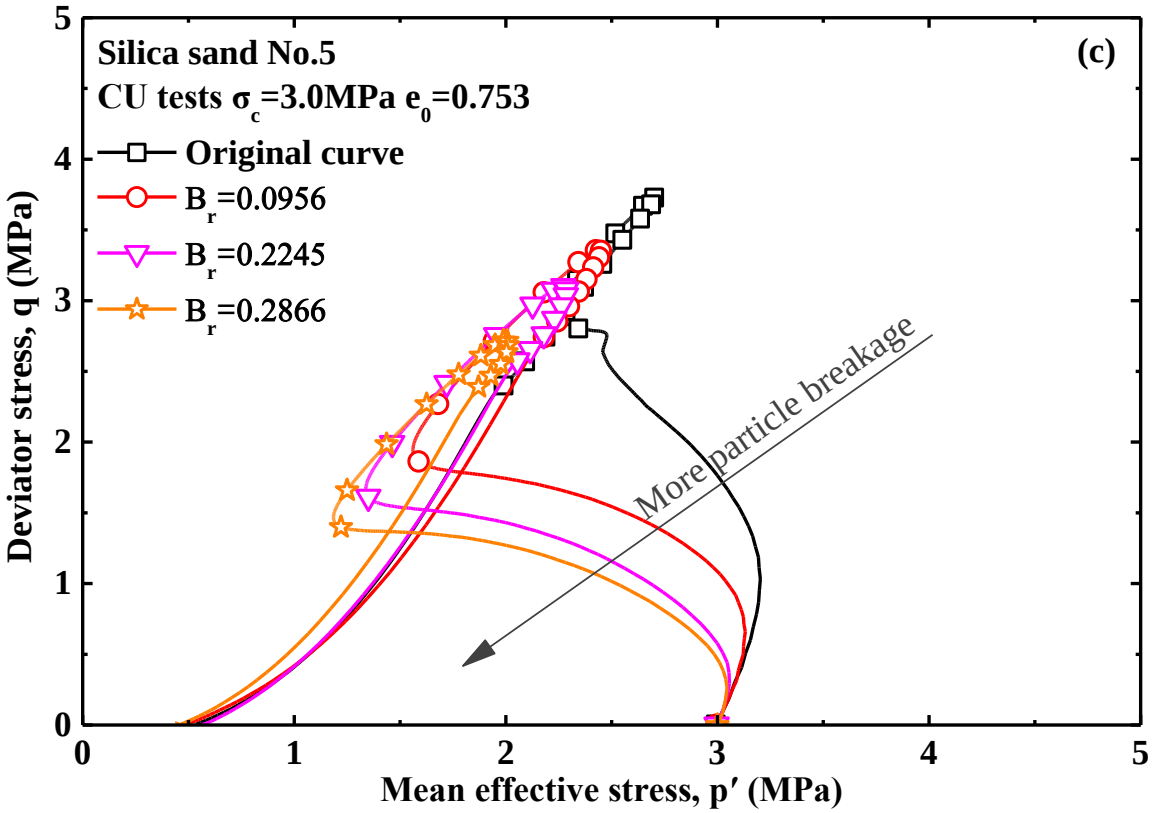

Figure 5.20 CU test results of original sand and pre-crushed sand under 3.0MPa confining pressure

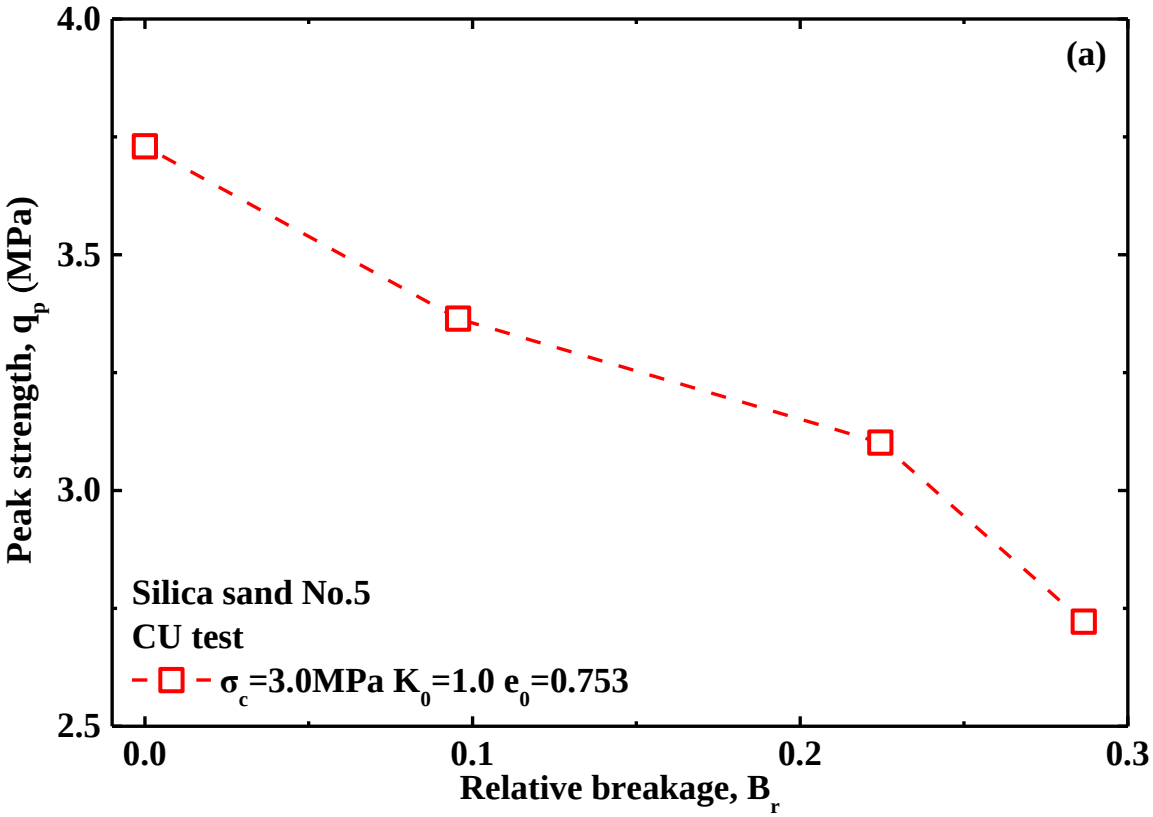

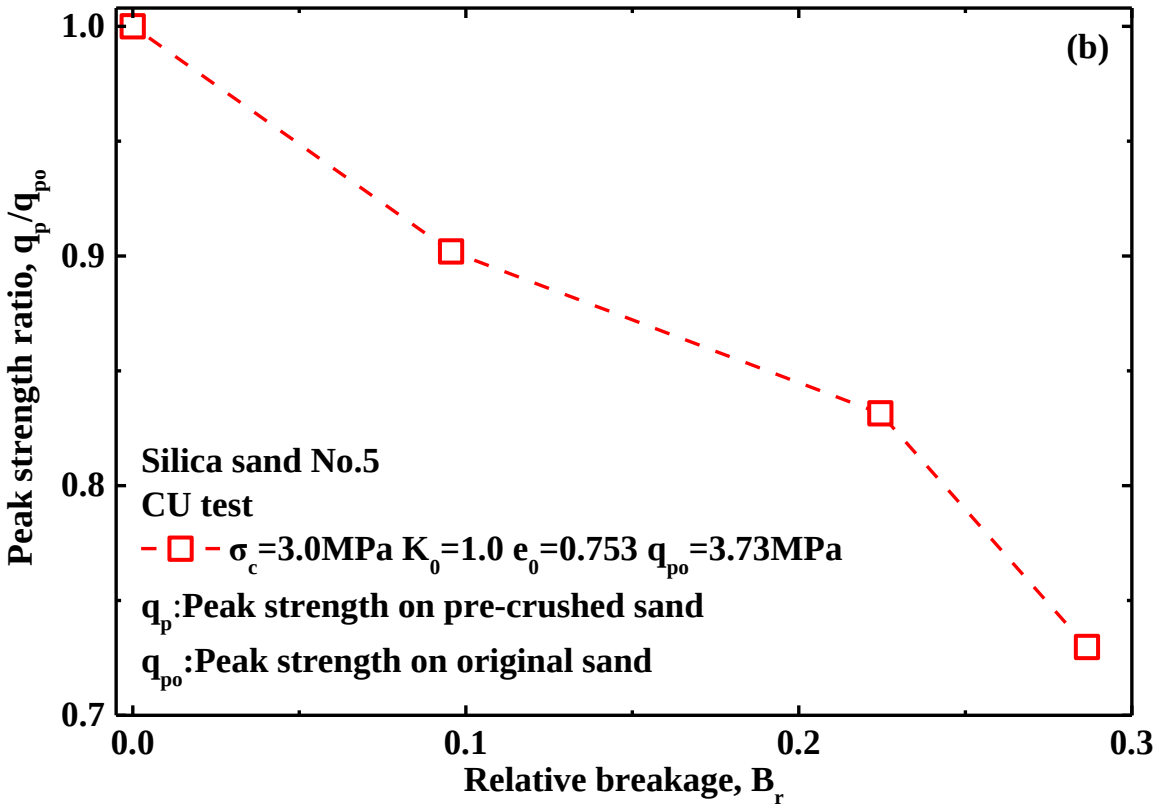

Figure 5.21 Peak strength against relative breakage under 3.0MPa confining pressure

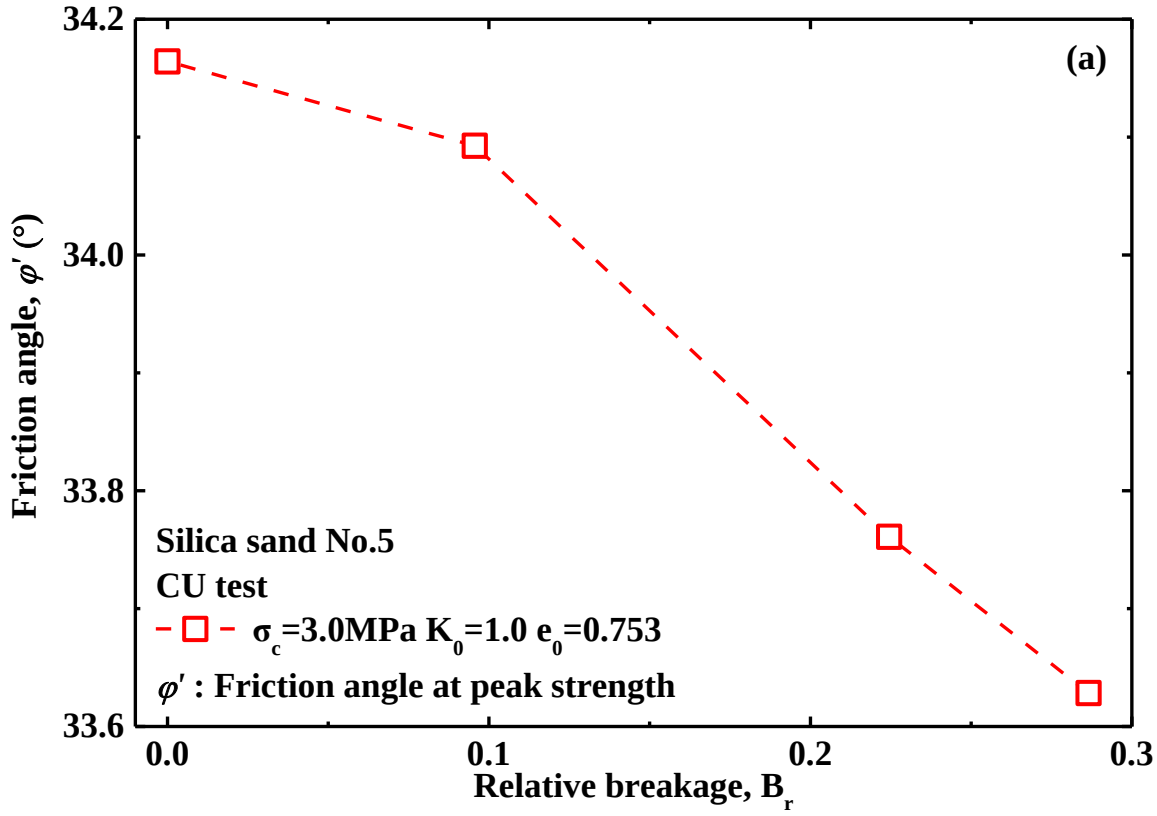

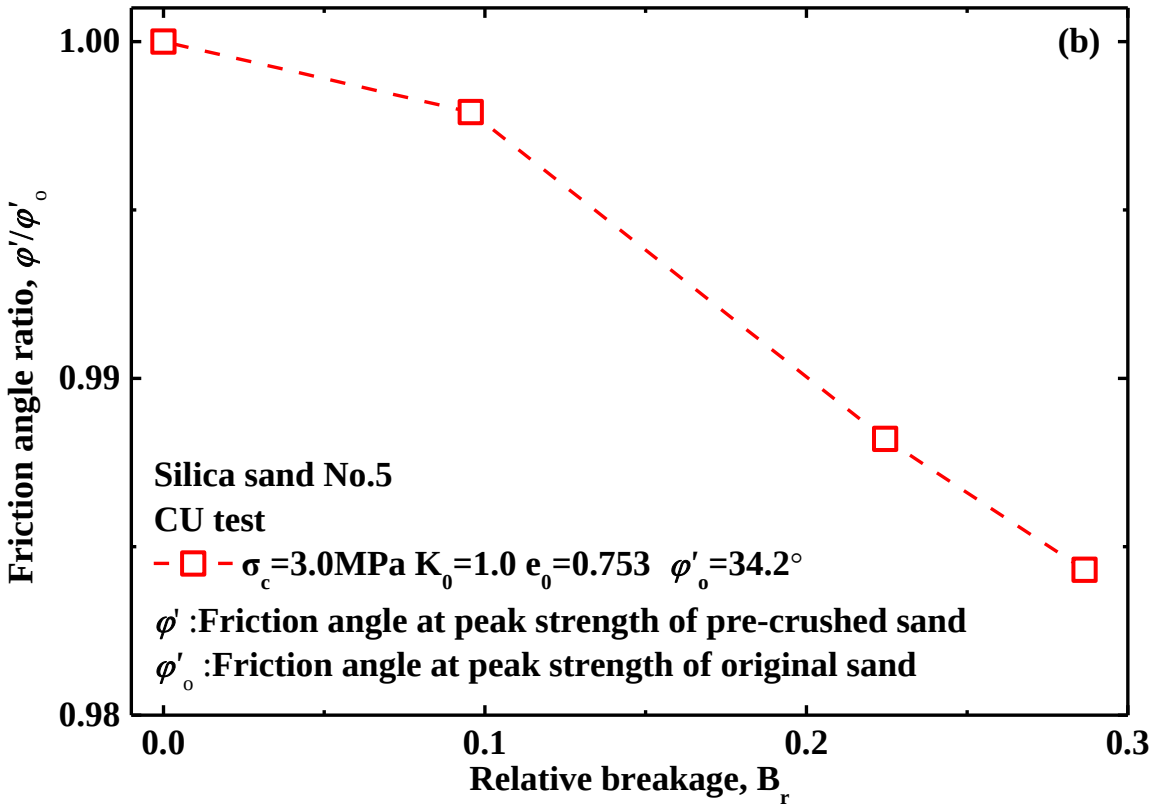

Figure 5.22 Relationship between friction angle and relative breakage under 1.0MPa confining pressure

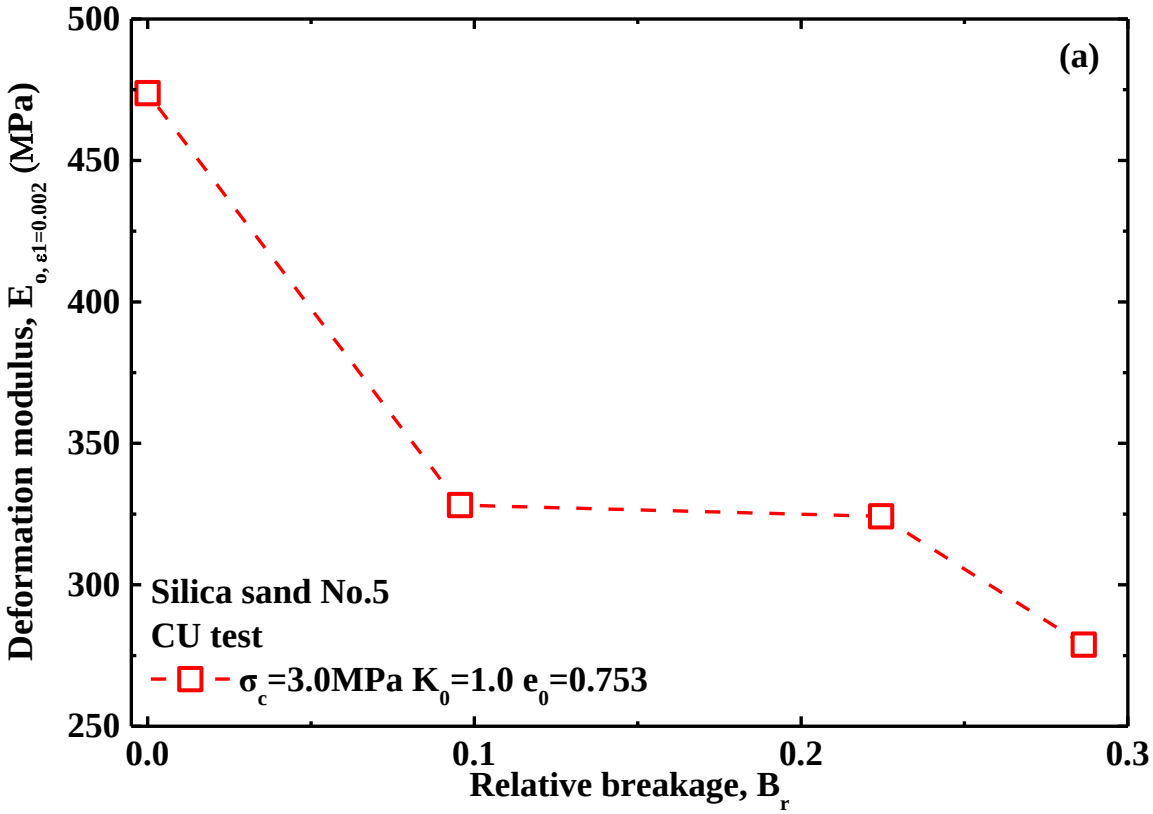

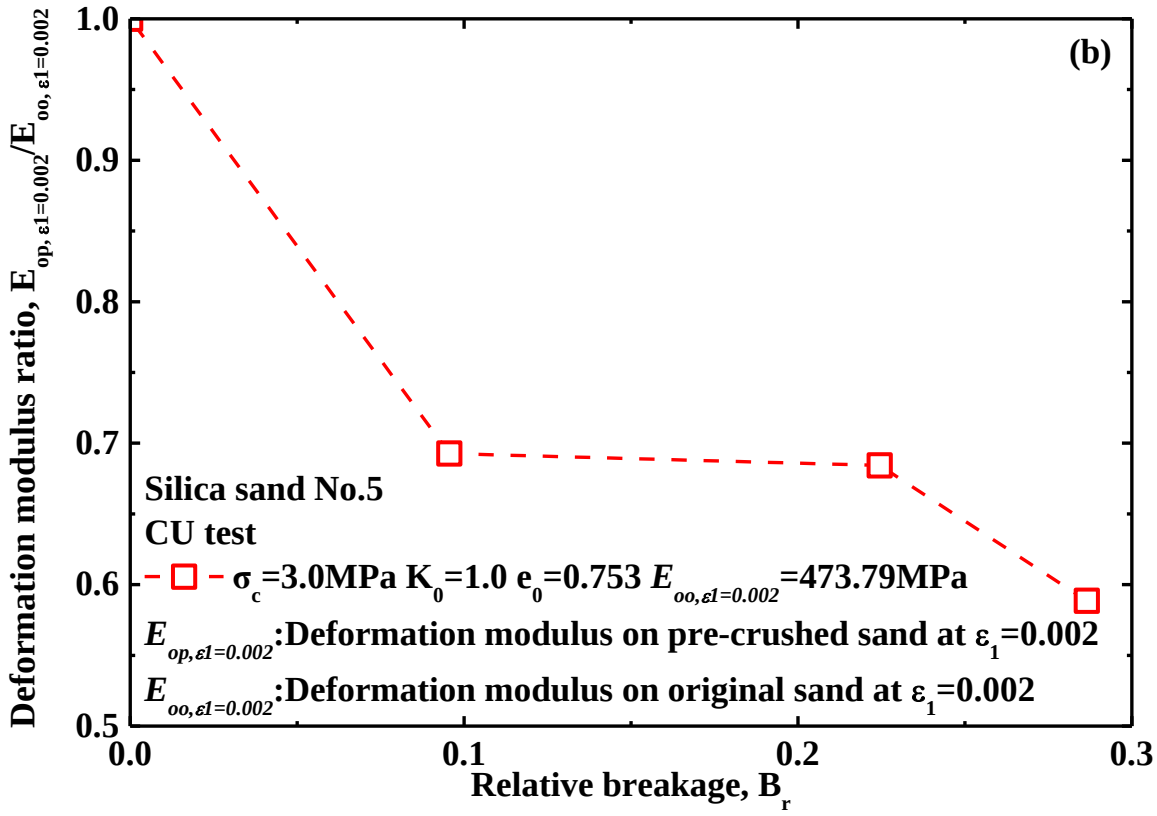

Figure 5.23 Relationship between deformation modulus and relative breakage under 3.0MPa confining pressure

5.3.2.6 Shearing behavior subjected to particle breakage in comparison

Peak strengths of all tests under various confining pressures were combined into one figure to investigate the influence of particle breakage on peak strengths under various confining pressure. Figure 5.24 shows the peak strengths subjected to particle breakage in relative breakage, where peak strengths subjected to particle breakage are found to increase with increasing confining pressure but particle breakage is seen to result in more substantial reduction of peak strength under higher confining pressure than that under lower pressure (<1.0MPa) as shown in Figure 5.24(a). There is no big difference of reduction of peak strengths subjected to particle breakage in relative breakage in CD tests under 0.2MPa and 0.5MPa confining pressures. It is notable that particle breakage has a more significant influence on reduction of peak strengths in CU tests than that in CD tests under 0.2MPa or 0.5MPa confining pressure with higher peak strength of original sand in CU tests, which means that depression of dilatancy induced by particle breakage has a much more influence on reduction of peak strength in CU tests than that in CD tests under lower confining pressures. However Note herein that particle breakage results in more substantial reduction of peak strength under 1MPa confining pressure and that under 3MPa confining pressure, which means that the influence of particle breakage on soil behavior is not monotonic with increasing confining pressure. Figure 5.24(b) shows the normalized peak strengths by the peak strength of original sand under corresponding confining pressure, where in CD tests particle breakage is found to result in more

substantial reduction in percentage of peak strength of original sand under 0.2MPa confining pressure than that in 0.5MPa confining pressure, which means that the reduction of dilatancy induced by particle breakage has more significant influence on contribution to reduction of peak strength under lower confining pressure. However it is notable in CU tests that peak strength ratio is found to decrease with increasing particle breakage but with increasing confining pressure it has no evident trend to be found. All peak strength ratios under 0.2MPa or 0.5MPa confining pressure are larger in CD tests than in CU tests, which means that particle breakage results in more substantial reduction of peak strength in CU tests than that in CD tests.

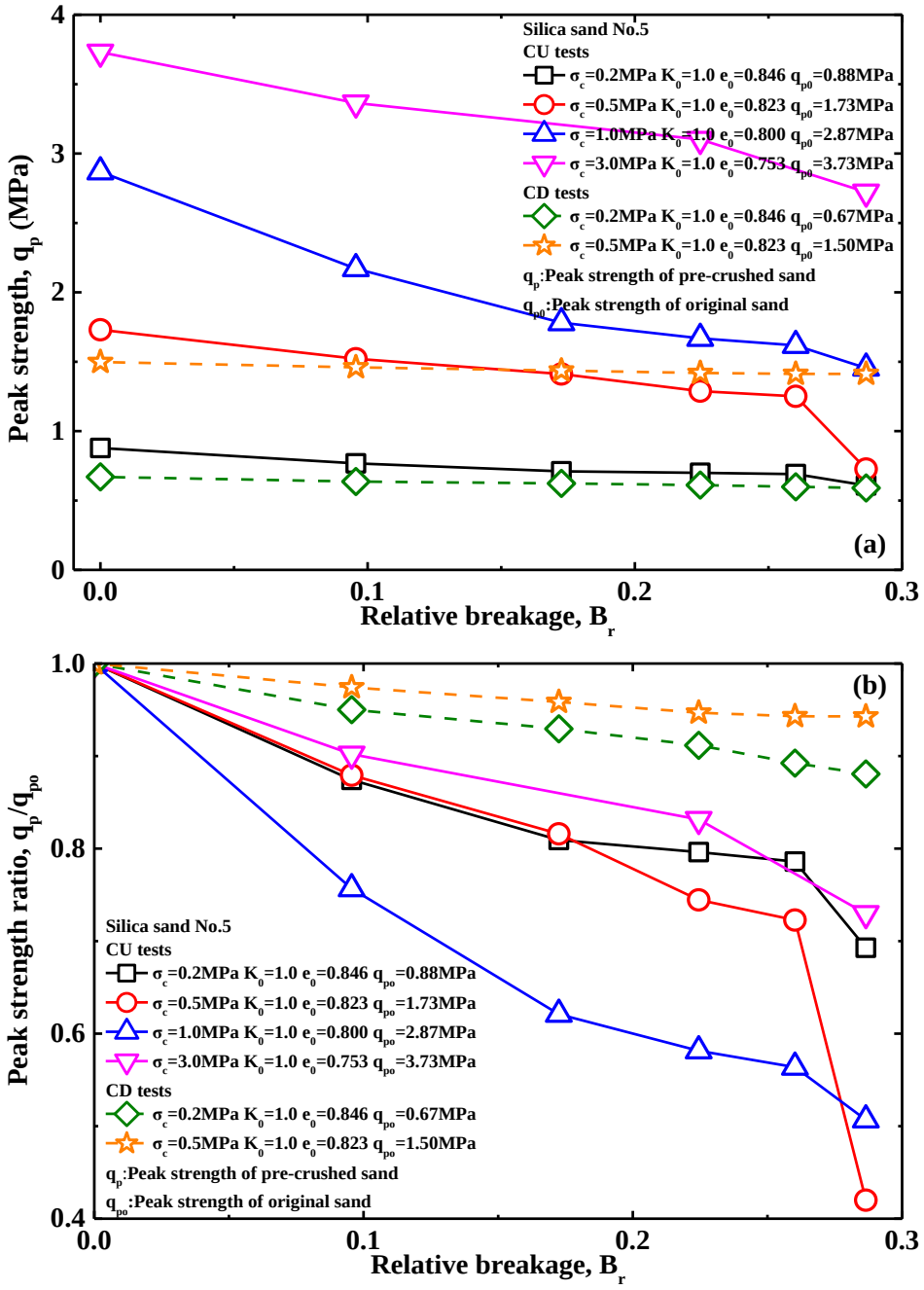

Figure 5.24 Peak strength against relative breakage under various confining pressures

Friction angles at peak strengths of all tests under various confining pressures were combined into one figure to investigate the influence of particle breakage on evolution of friction angle under various confining pressure. Figure 5.25 shows friction angles at peak strengths against particle breakage in relative breakage under various confining pressures. It is found in Figure 5.25(a) that the friction angle of original sand decreases with increasing confining pressure and friction angles decreases with increasing particle breakage. In CD tests, friction angles are seen to be larger in more substantial reduction under 0.2MPa confining pressure than that under 0.5MPa confining pressure, which means that the dilatancy has a more positive contribution to the friction angles under lower confining pressure and impairment of dilatancy induced by particle breakage has a more influence on reduction of friction angles of pre-crushed sands under 0.2MPa confining pressure than that under 0.5MPa confining pressure. In CU tests friction angles are found to decrease more substantially with increasing particle breakage under lower confining pressures (0.2MPa and 0.5MPa) especially under 0.5MPa confining pressure, but under higher confining pressures (1MPa and 3MPa), the friction angles are seen to be same approximately except the friction angle of original sand with increasing particle breakage. Figure 5.25(b) shows the normalized friction angle against particle breakage in relative breakage under various confining pressures, where friction angle ratio is found to decrease with increasing particle breakage. Consequently particle breakage is found to result in reduction of friction angle at peak strength, which is consistent with finding (Ghanbari et al., 2013). The friction angle ratio in CD tests decreases with increasing confining pressure. However in CU tests friction angle ratios are found to increase approximately with increasing confining pressure except that friction angle ratios under 0.2MPa confining pressure are over that under 0.5MPa confining pressure. It can be concluded herein that the influence of particle breakage on friction angle is found to decrease with increasing confining pressure, which may be caused by the depression of dilatancy and additional particle breakage under high pressure.

All deformation moduli were combined into Figure 5.26 for investigating deformation modulus subjected to particle breakage under various confining pressures. Figure 5.26 shows deformation modulus against particle breakage in relative breakage under various confining pressures, where deformation moduli are found to decrease with increasing particle breakage and to increase with increasing confining pressures. It is seen in Figure 5.26(a) that under 0.2MPa confining pressure the deformation moduli are larger in CD tests than that in CU tests but under 0.5MPa confining pressure it is getting smaller in CD tests than that in CU tests. It is found herein that particle breakage has an increased influence in reduction of deformation moduli with increasing confining pressure approximately. All deformation moduli were normalized by the deformation modulus of original sand to investigate the change of deformation modulus against particle breakage as shown in Figure 5.26(b), where deformation modulus ratios are found to decrease with increasing particle breakage and deformation moduli subjected to maximum amount of pre-crushed breakage are found to reduce into a range of 20% to 60% of the deformation modulus of original sand, which should be paid more attention in practice.

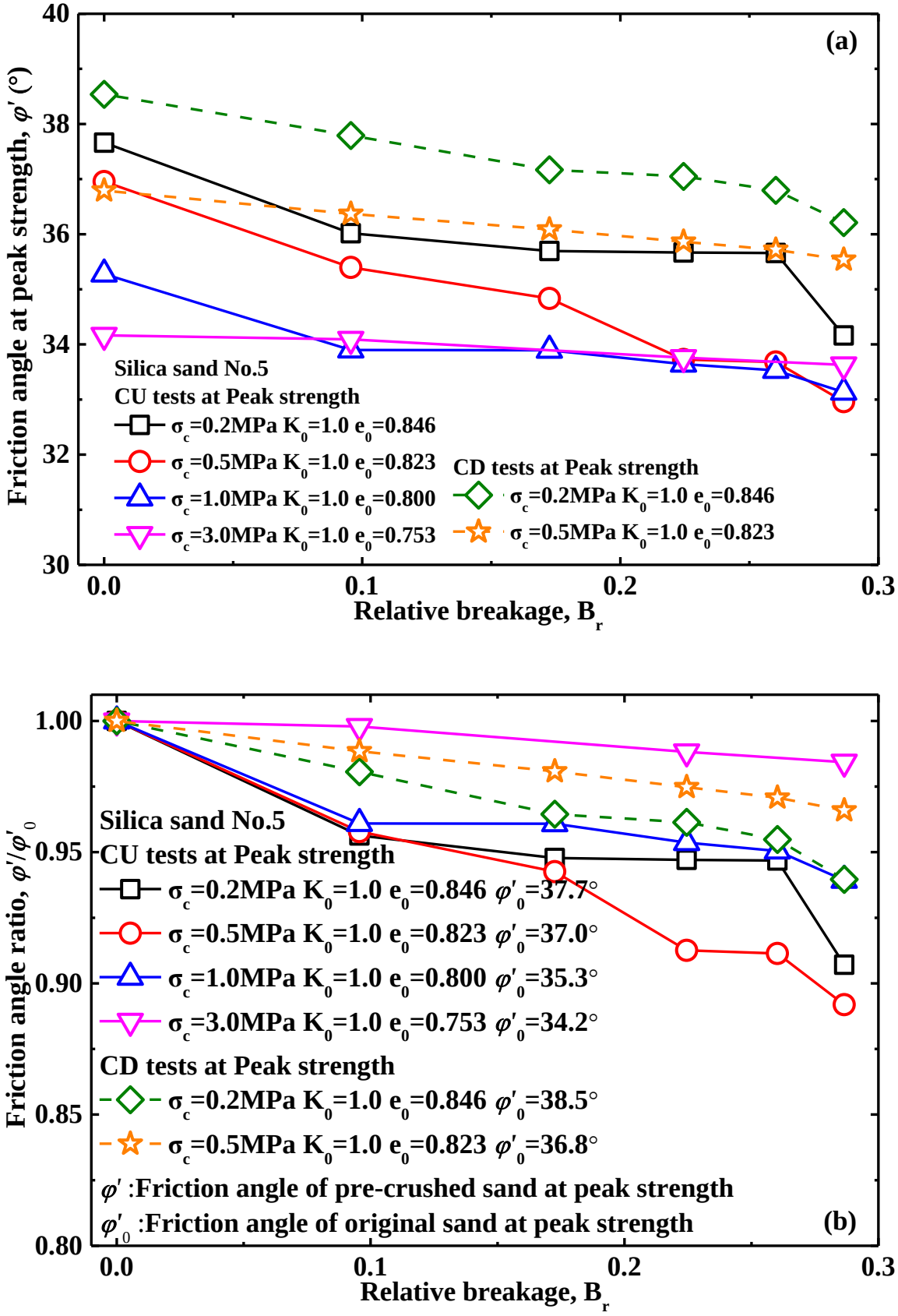

Figure 5.25 Friction angle at peak strengths against relative breakage under various confining pressures

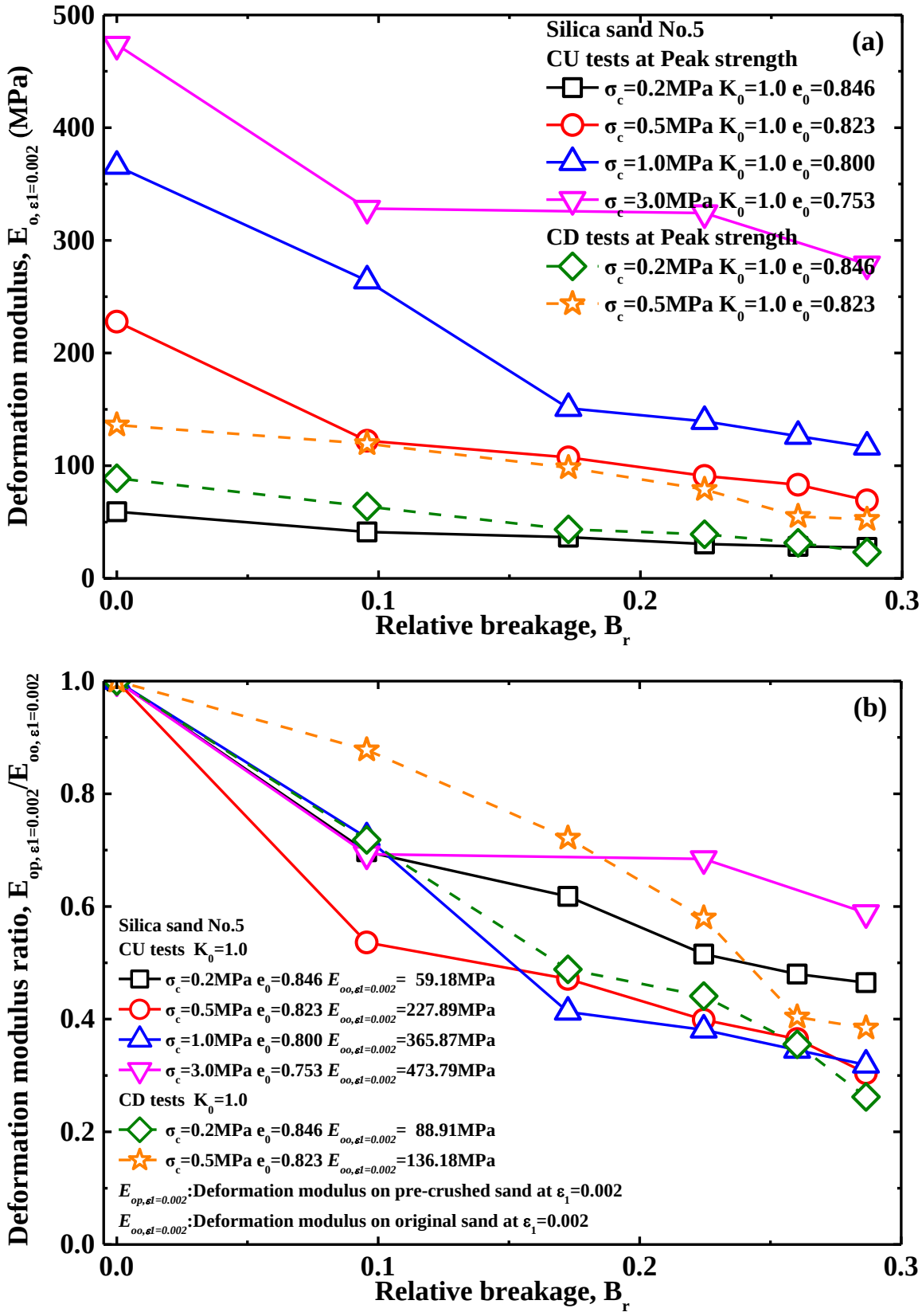

Figure 5.26 Deformation modulus against relative breakage under various confining pressures

5.3.3 The Influence of Particle Breakage on Critical State Line

5.3.3.1 Normal Consolidation Line (NCL) on The Loosest State

The Critical State Line (CSL) can be investigated in e-logp′ plane, and it may be useful and helpful to define boundaries in characterizing and understanding the soil response in e-logp′ plane. For sandy soils, it is possible conceptually to define an upper boundary by the isotropic consolidation line on the loosest state, which is equivalent to the normal consolidation line for clays (Verdugo and Ishihara, 1996). Note that the sample preparation procedure has a significant effect on the isotropic consolidation line of sandy soils (Ishihara, 1993). All samples were prepared by air pluviation with necessary tamping. For consistency, herein the air pluviation method was employed as well to obtain the isotropic consolidation line on the loosest sample, which would be called normal consolidation line for keeping consistent with the same technical term in the theory for clays.

Normal Consolidation Line (abbreviated as NCL subsequently) on the loosest state was obtained by isotropic consolidation on the loosest sample created by slowly pluviating the original sand into a mould in a long funnel with a small mouth such as the preparation method to get the maximum void ratio. Herein the 10kPa vacuum pressure was employed to stabilize the sample for trying not to disturb the sample in compression. Figure 5.27 shows the normal consolidation line on the loosest state of Silica sand No.5, where the normal consolidation line before yield stress (around 0.7MPa) can be regarded as being linear and with increasing mean effective stress up to high pressure normal consolidation line is getting nonlinear especially after yield stress. It is concluded herein that the nonlinear characteristics of normal consolidation line should be considered under high pressure especially after yield stress in practice. In classic soil mechanics, the normal consolidation line is just considered as a linear line in e-logp′ plane, which is not adaptable any more under high pressure.

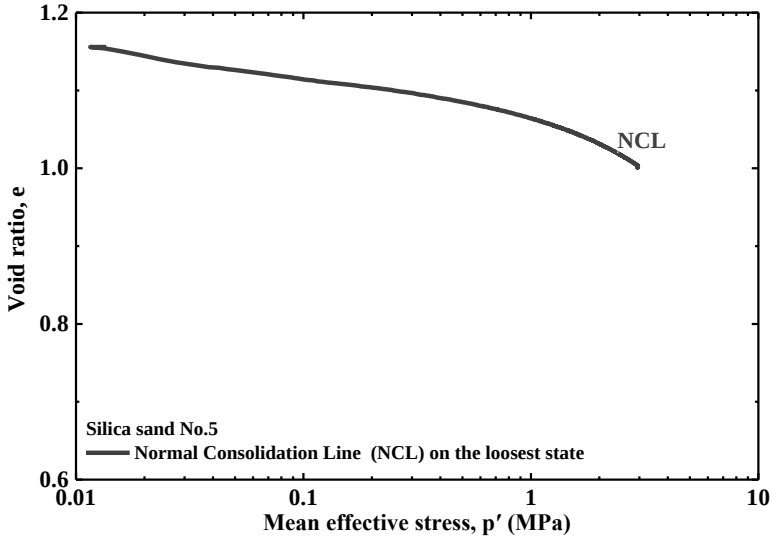

Figure 5.27 Normal Consolidation Line on the loosest state of Silica sand No.5

5.3.3.2 Generation of critical state points subjected to first shearing

For getting a whole critical state line of original sand, many tests were carried out to reach the critical state under different void ratios and mean effective stresses. Many tests were conducted on loose samples which were prepared by slowly pluviating original sand into a mould for trying not to crush the original sand during shearing to obtain the locations of relevant critical state points with the negligible particle breakage. Figure 5.28 shows the triaxial tests on loose samples of original sand to obtain critical state points, where all tests were to shear to critical state after isotropic consolidation under CU condition in an exception of one CD test under 0.5MPa confining pressure. Considering the relatively low deviator stresses and loose samples during shearing, grain size distribution curves were not obtained for these tests with neglecting the effect of particle breakage on the location of critical state line in an assumption.

The critical state points of all tests in Figure 5.28 were appended to Figure 5.27 for investigating evolution of locations of critical state points in comparison with the NCL. Figure 5.29 shows the critical state points on loose samples of original sand with relevant stress paths from initial state to critical state points in e-logp′ plane and q-p′ plane, where the critical state points in q-p′ plane was fitted by a linear line with an interception of zero as a traditional linear relationship with an assumption of neglecting the effect of particle breakage as illustrated in Figure 5.29(b) but in in e-logp′ plane as shown in Figure 5.29(a), it is notable that the critical state points are getting nonlinear with the increase of mean effective stress with having a marked yield stress point around 0.7 MPa which is almost consistent with the yield stress of NCL. Yield stress herein is defined as the stress at the point of the maximum curvature on the e-logp′ curve. This yield stress can be regarded as being related to the onset of particle breakage (Been et al., 1991; McDowell et al., 1996). It is found herein that the critical state points before yield stress can be considered as a linear relationship which can be assumed to be approximately parallel with NCL before the yield stress of NCL but after yield stress both NCL and CSL are getting nonlinear and not parallel any more. In classical theory of NCL and CSL, NCL and CSL are linear and parallel in e-logp′ plane, but in fact both NCL and CSL are getting nonlinear and not parallel any more with the increase of mean effective stress in e-logp′ plane, which should be paid more attention in practice.

As shown in Figure 5.29(b), CSL as a fitting line of critical state points can be regarded as a linear relation in q-p′ plane, which would be hereafter employed as a basis in comparison with locations of critical state points subjected to higher pressure or pre-crushed sand.

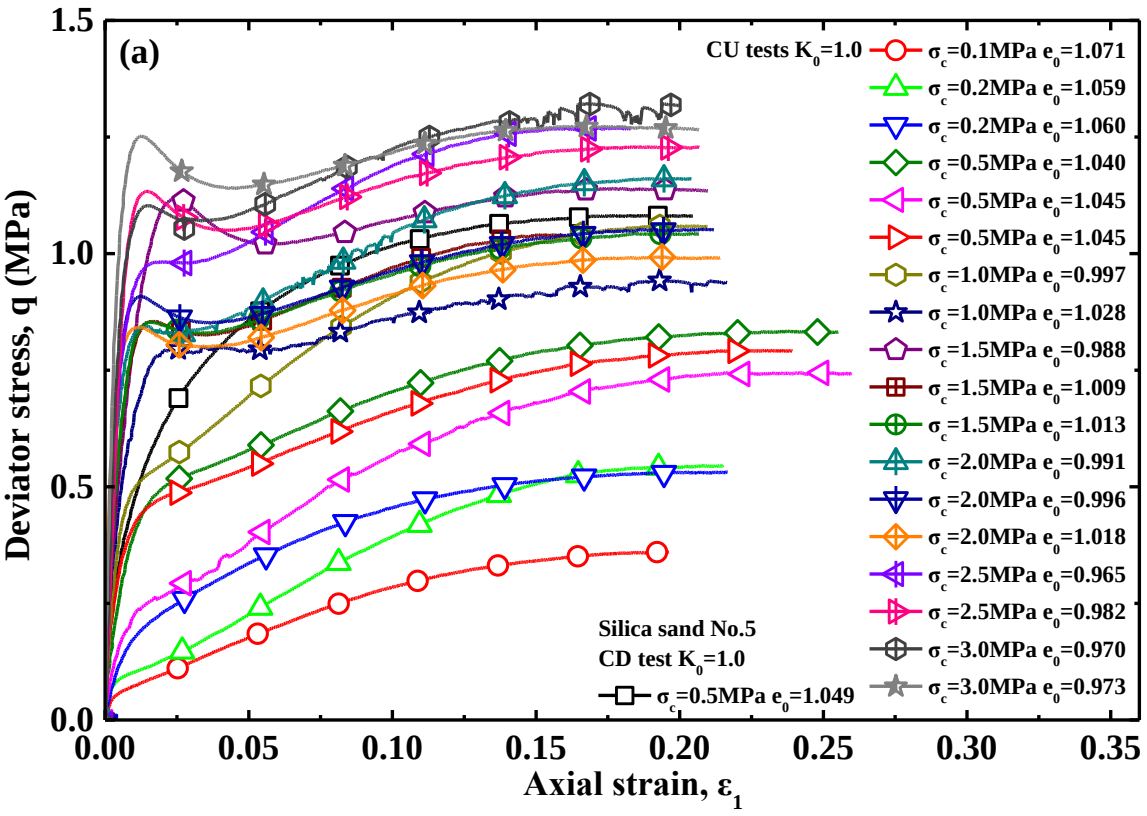
(a)
CU tests K0=1.0
σc=0.1MPa e0=1.071
σc=0.2MPa e0=1.059
σc=0.2MPa e0=1.060
σc=0.5MPa e0=1.040
σc=0.5MPa e0=1.045
σc=0.5MPa e0=1.045
σc=1.0MPa e0=0.997
σc=1.0MPa e0=1.028
σc=1.5MPa e0=0.988
σc=1.5MPa e0=1.009
σc=1.5MPa e0=1.013
σc=2.0MPa e0=0.991
σc=2.0MPa e0=0.996
σc=2.0MPa e0=1.018
σc=2.5MPa e0=0.965
σc=2.5MPa e0=0.982
σc=3.0MPa e0=0.970
σc=3.0MPa e0=0.973
Silica sand No.5
CD test K0=1.0
σc=0.5MPa e0=1.049
Deviator stress, q (MPa)
Axial strain, ε1
0.0
0.5
1.0
1.5
0.00
0.05
0.10
0.15
0.20
0.25
0.30
0.35

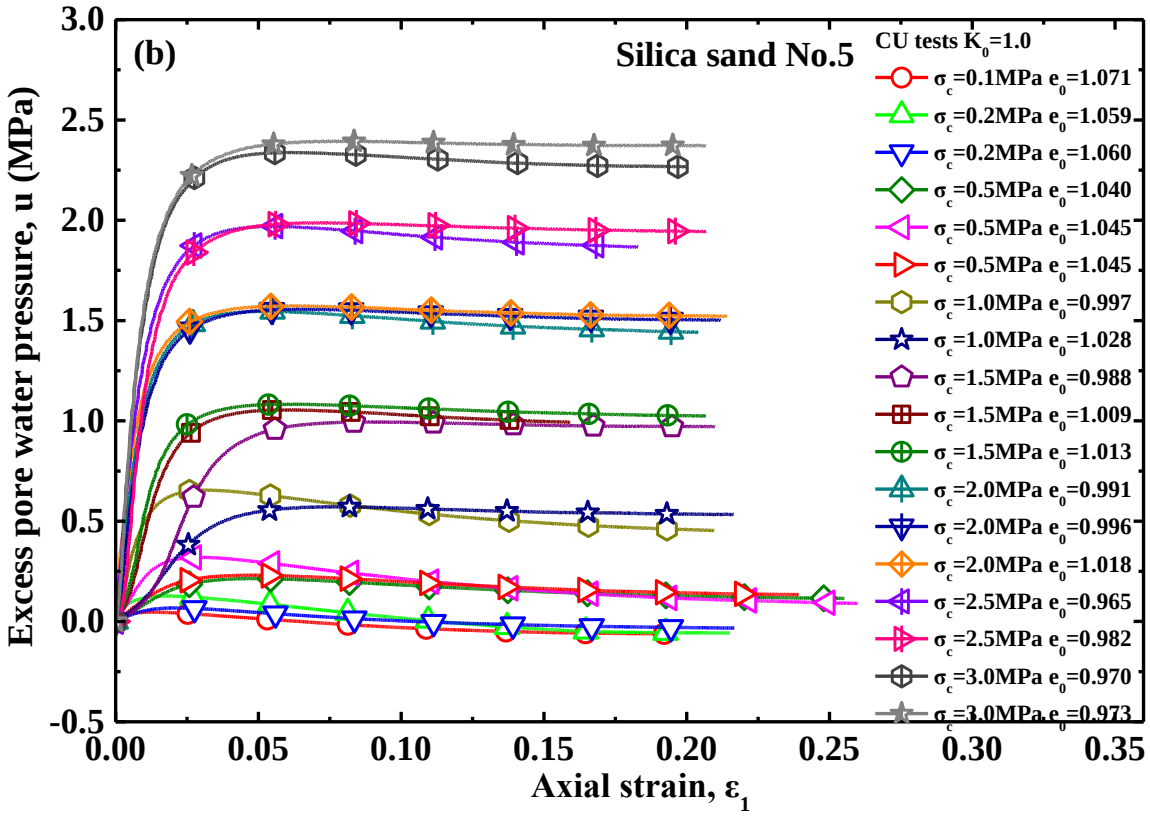
(b)
Silica sand No.5
CU tests K0=1.0
σc=0.1MPa e0=1.071
σc=0.2MPa e0=1.059
σc=0.2MPa e0=1.060
σc=0.5MPa e0=1.040
σc=0.5MPa e0=1.045
σc=0.5MPa e0=1.045
σc=1.0MPa e0=0.997
σc=1.0MPa e0=1.028
σc=1.5MPa e0=0.988
σc=1.5MPa e0=1.009
σc=1.5MPa e0=1.013
σc=2.0MPa e0=0.991
σc=2.0MPa e0=0.996
σc=2.0MPa e0=1.018
σc=2.5MPa e0=0.965
σc=2.5MPa e0=0.982
σc=3.0MPa e0=0.970
σc=3.0MPa e0=0.973
Excess pore water pressure, u (MPa)
Axial strain, ε1
-0.5
0.0
0.5
1.0
1.5
2.0
2.5
3.0
0.00
0.05
0.10
0.15
0.20
0.25
0.30
0.35

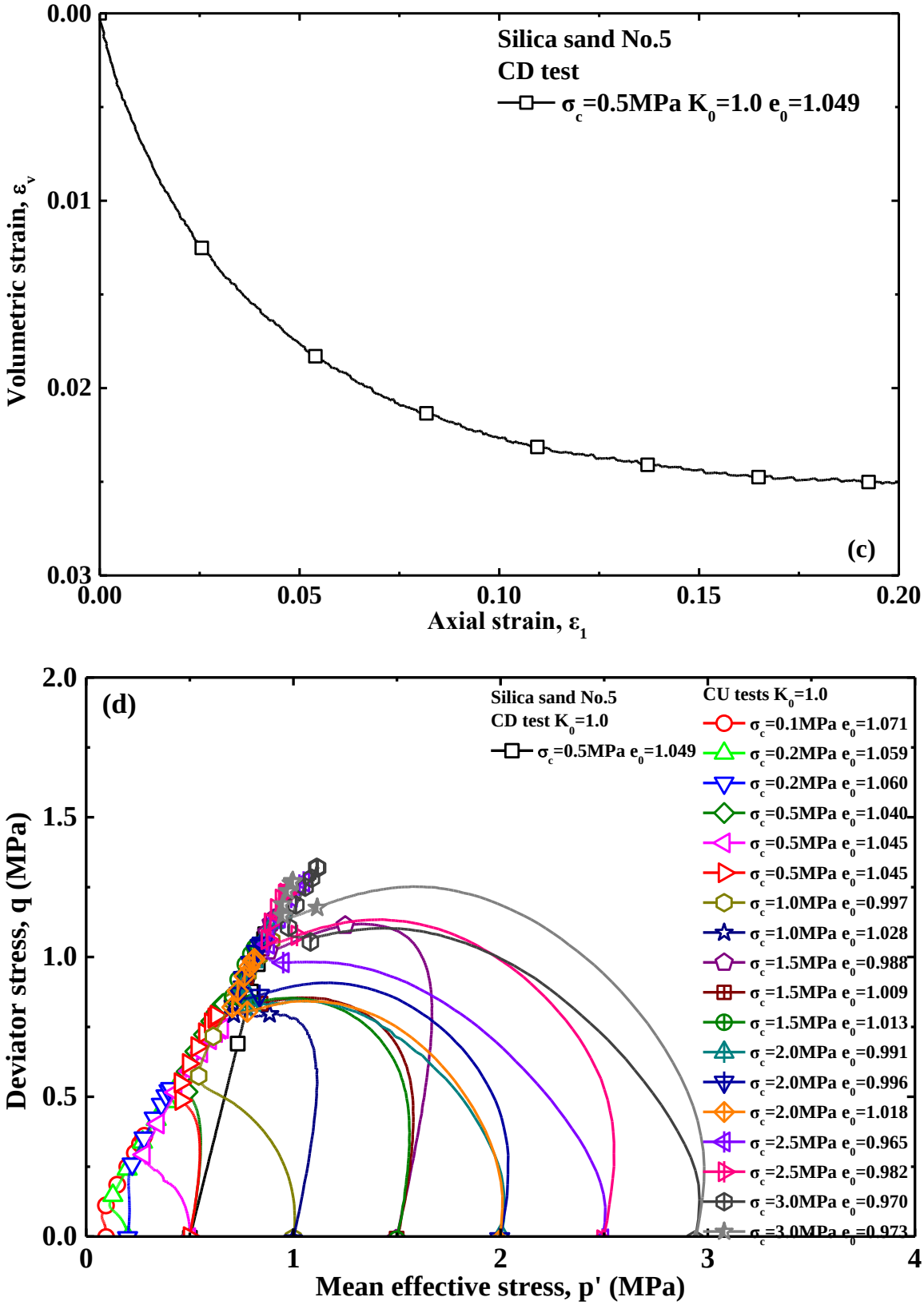

Figure 5.28 Triaxial tests on loose samples of original sand to obtain critical state points

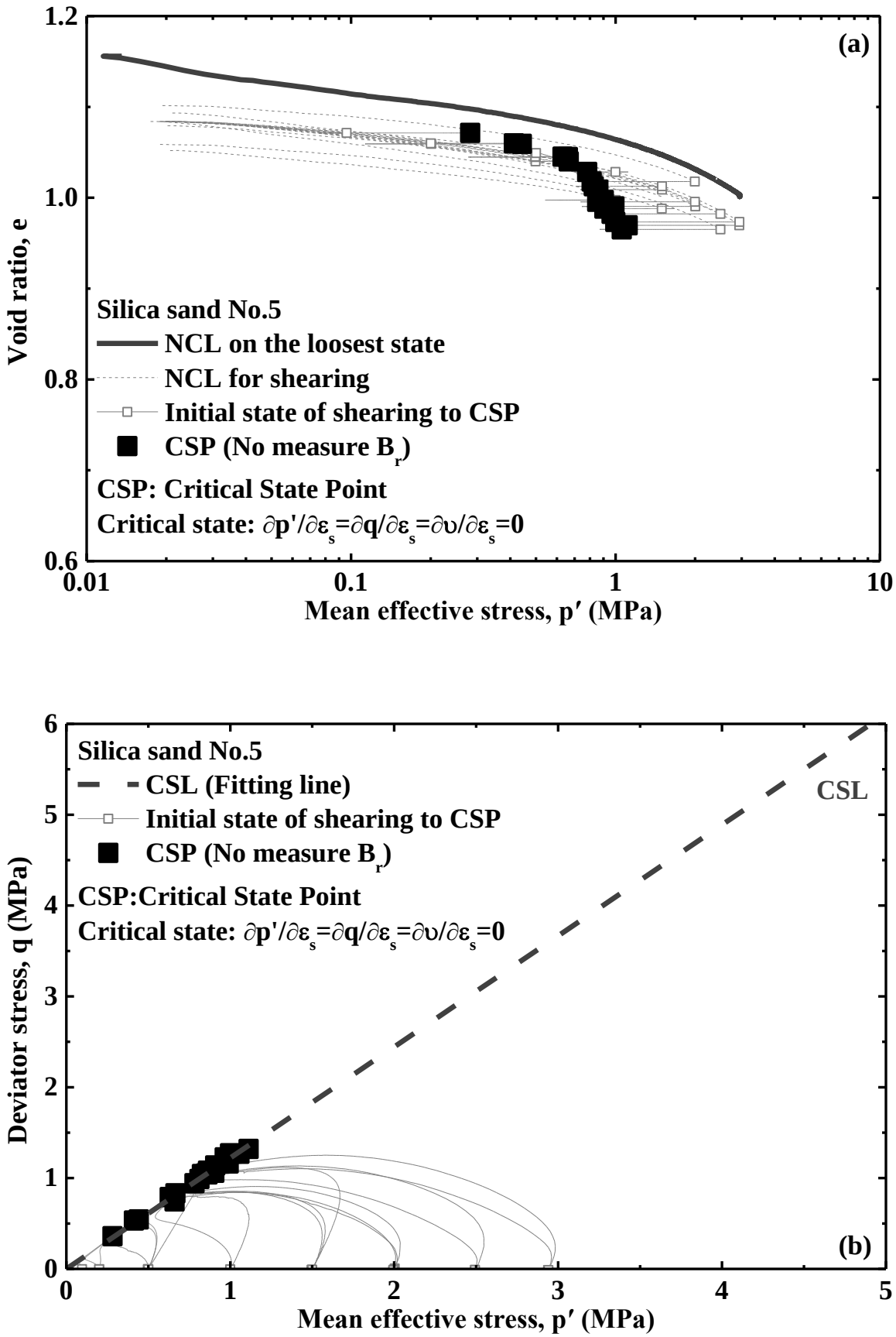

Figure 5.29 Critical state points on loose samples of original sand

New triaxial tests were carried out on relatively dense samples of original sand under high pressure to investigate the location of CSL subjected to high pressure and particle breakage. As a result of that particle breakage was caused during shearing in triaxial tests on dense samples under high pressure to reach critical states with small void ratios and high mean effective stress, the grain size distribution curves after shearing to critical state were obtained by sieve analysis to be quantified by relative breakage. The triaxial tests on original sand to obtain critical state points under high pressure are shown in Figure 5.30. Figure 5.31 shows the relevant grain size distribution curves which were quantified by relative breakage as well.

Critical state points of all tests in Figure 5.30 were added to e-logp′ plane and q-p′ plane as shown in Figure 5.32, where all critical state points in e-logp′ plane can be fitted by a nonlinear line (CSL) with a marked yield stress around 0.7MPa as shown in Figure 5.32(a) but as shown in Figure 5.32(b) the critical state points in q-p′ plane are seen clearly to be over the initial CSL, which indicates that the CSL in q-p′ plane has a nonlinear characteristics under high pressure resulting in particle breakage as well. It can be concluded herein that the characteristics of CSL are influenced by high pressure and particle breakage (e.g. Been et al., 1991). As known that particle breakage changes the original grading of soil which affects the soil behavior, it is also reliable to understand that particle breakage affects the characteristics of CSL. However, so far, the locations of critical state points were obtained on original sand, where the particle breakage has a progressive effect on the locations of critical state points as a result of that particle breakage occurred simultaneously with shearing. Consequently it is rather difficult to separate the sole effect of particle breakage on location of CSL from the complex effects of both high pressure and particle breakage resulting in depression of dilatancy of soil.

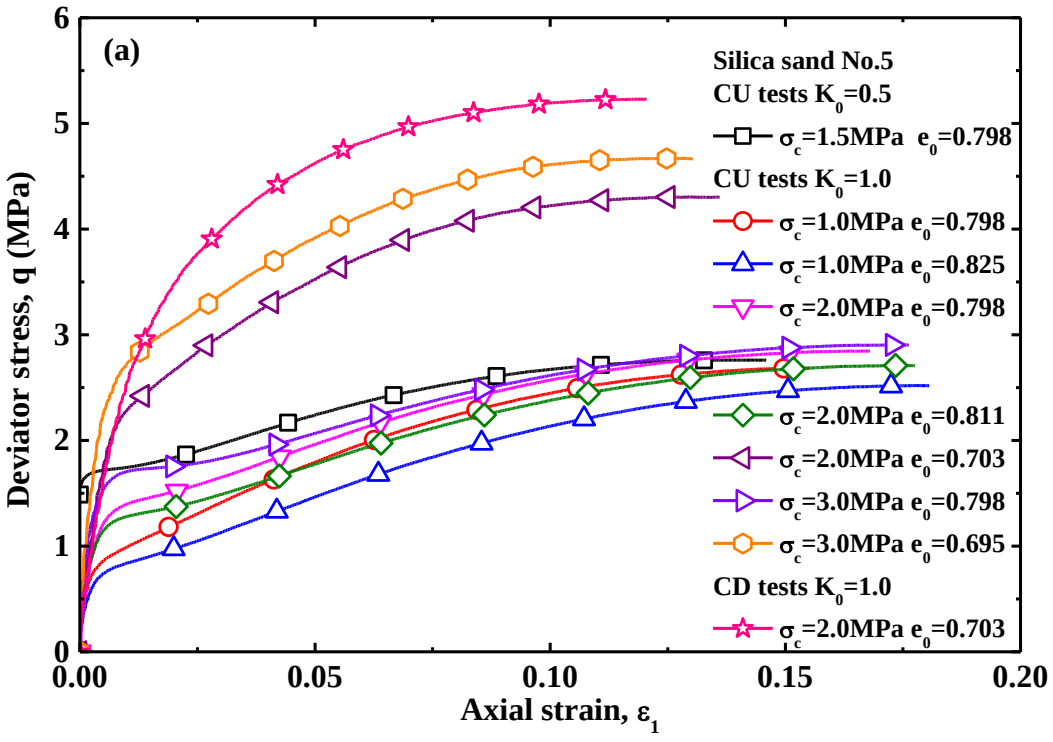

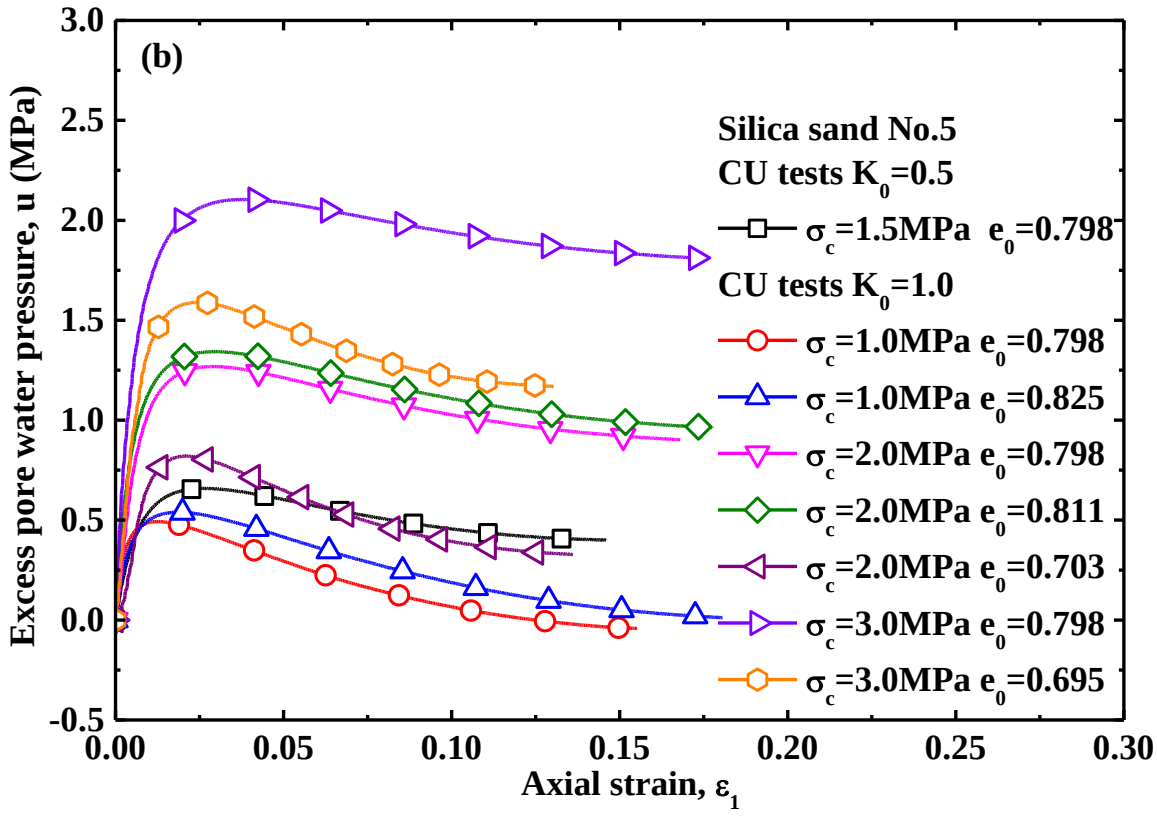
(b)
Silica sand No.5
CU tests K0=0.5
σc=1.5MPa e0=0.798
CU tests K0=1.0
σc=1.0MPa e0=0.798
σc=1.0MPa e0=0.825
σc=2.0MPa e0=0.798
σc=2.0MPa e0=0.811
σc=2.0MPa e0=0.703
σc=3.0MPa e0=0.798
σc=3.0MPa e0=0.695
Excess pore water pressure, u (MPa)
Axial strain, ε1
3.0
2.5
2.0
1.5
1.0
0.5
0.0
-0.5
0.00
0.05
0.10
0.15
0.20
0.25
0.30

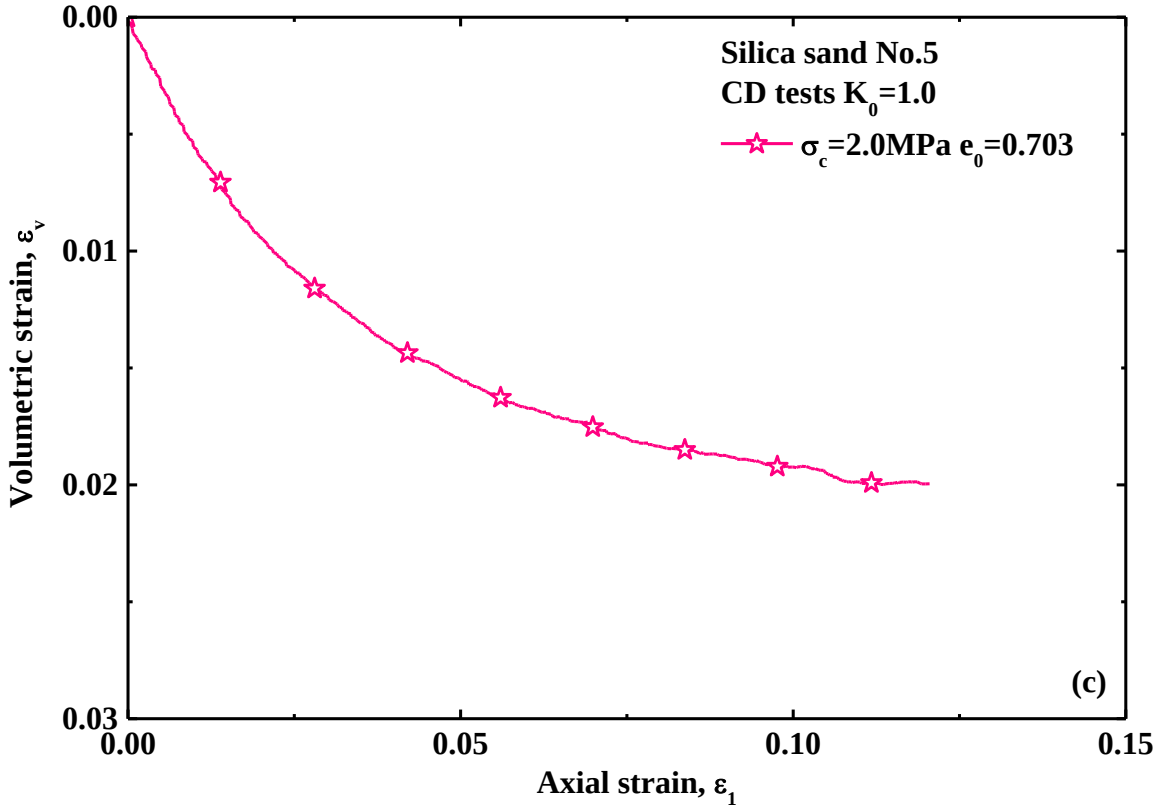
Silica sand No.5
CD tests K0=1.0
σc=2.0MPa e0=0.703
(c)
Volumetric strain, εv
Axial strain, ε1
0.00
0.01
0.02
0.03
0.00
0.05
0.10
0.15

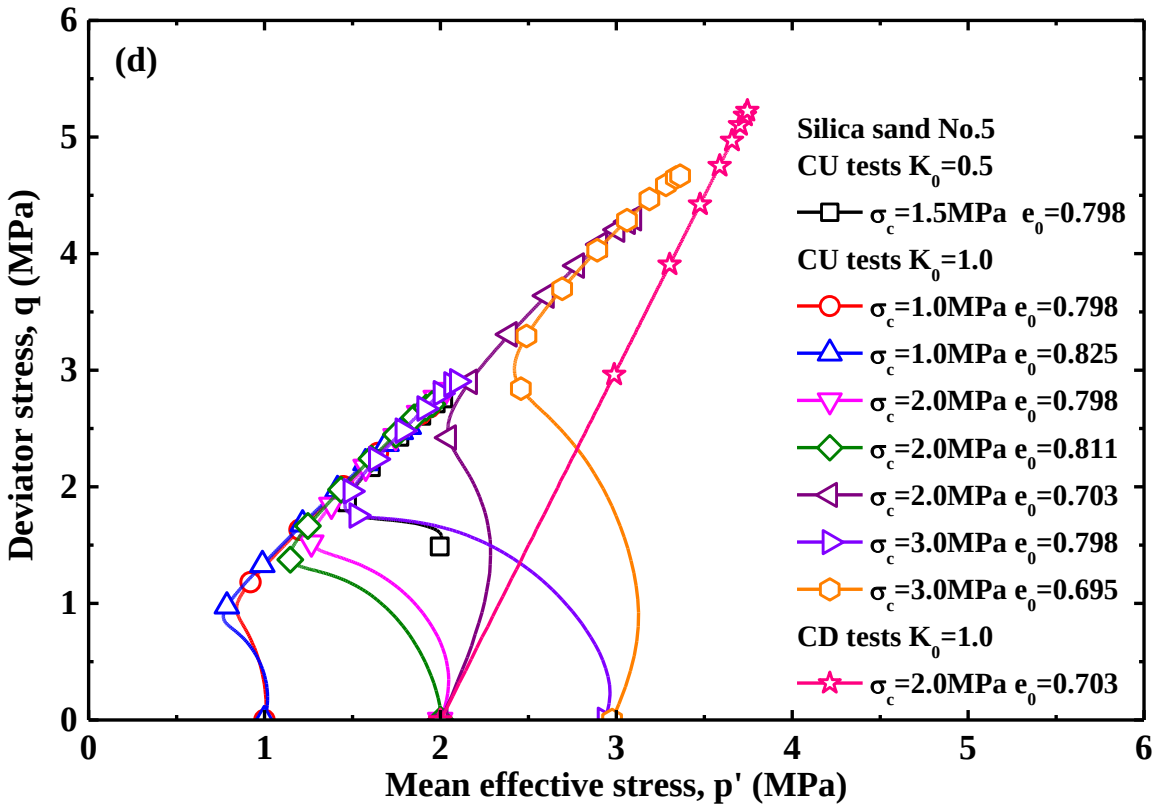

Figure 5.30 Triaxial tests on original sand to obtain critical state points under high pressure

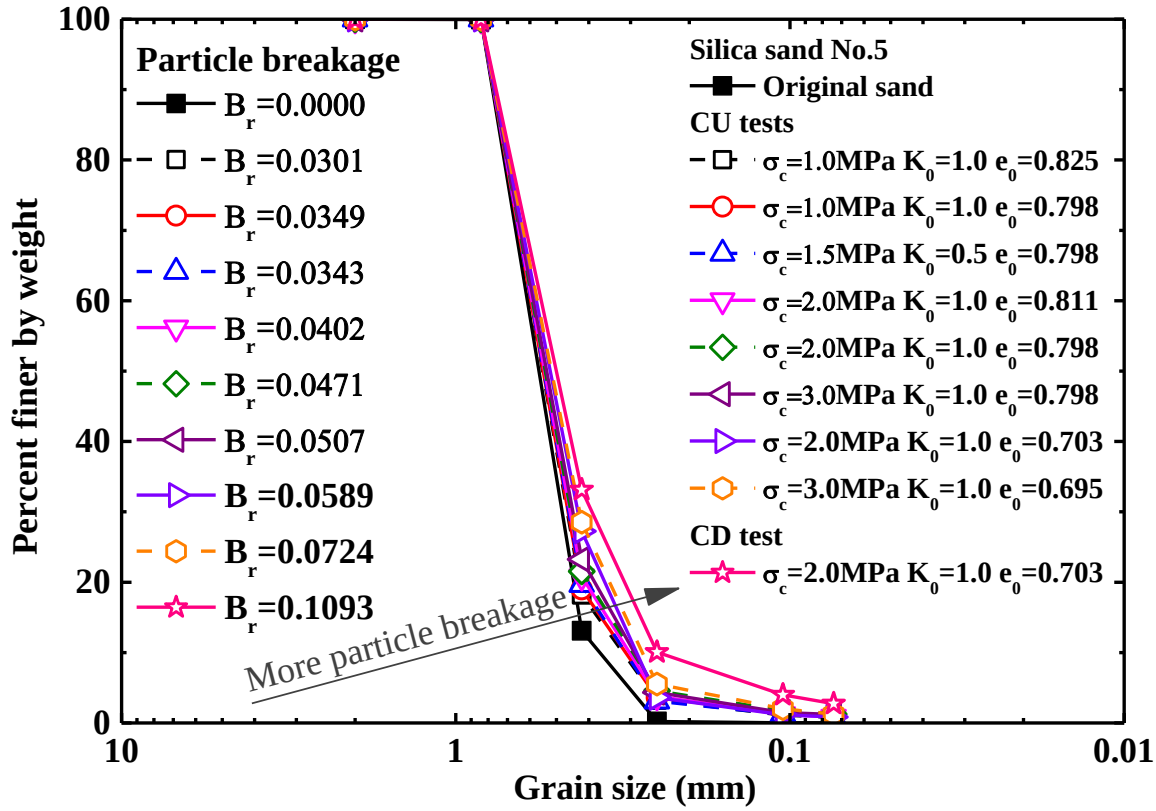

Figure 5.31 Grain size distribution curves at critical state points under high pressure

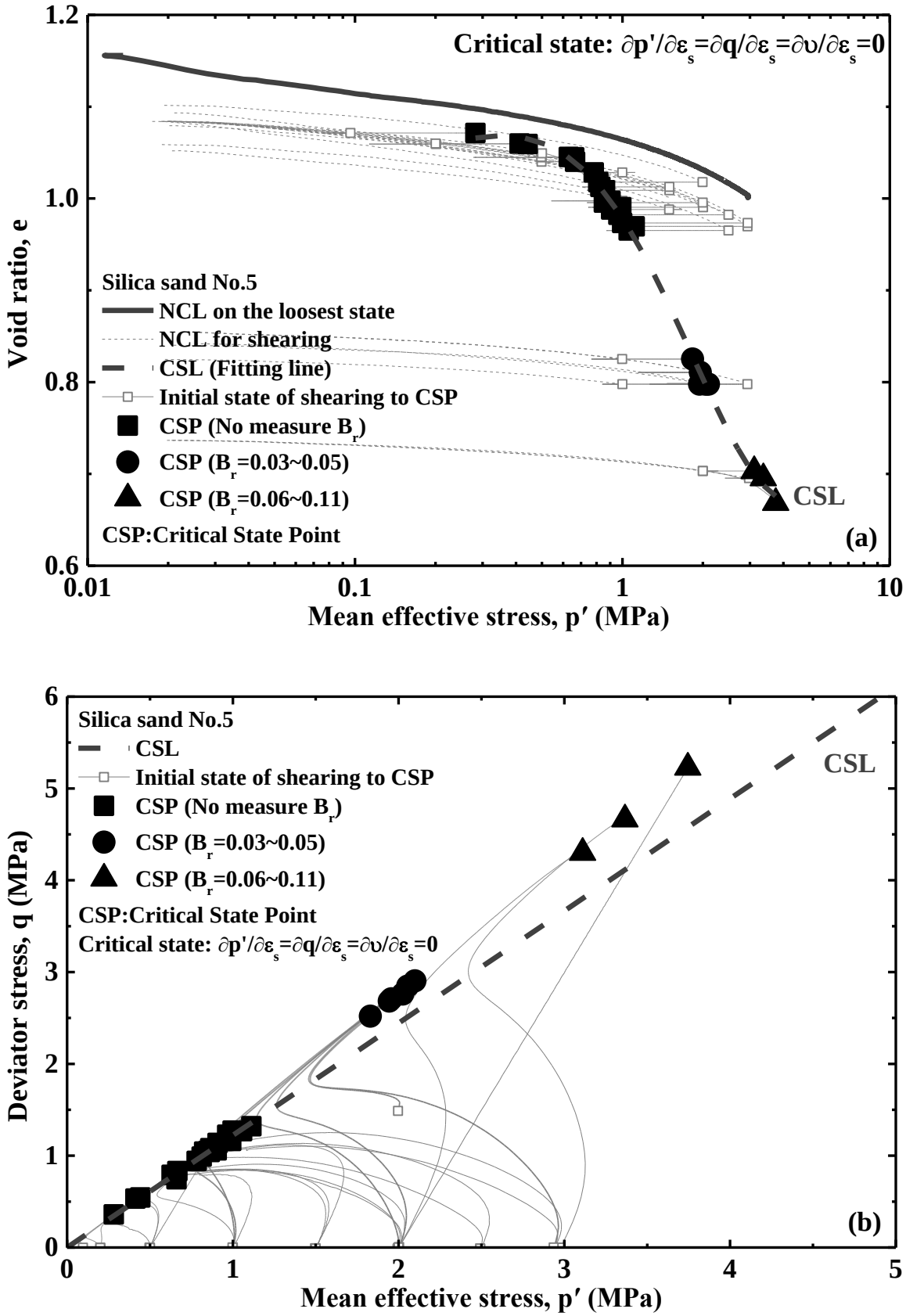

Figure 5.32 Critical state points subjected to particle breakage during shearing

5.3.3.3 Location of Critical state point subjected to pre-crushed sand

For investigating the direct effect of particle breakage on the locations of CSL, both the pre-crushed sand and original sand were employed in triaxial tests to reach critical state in comparison with the location of initial CSL on original sand.

Many CD and CU tests have been conducted on original sand and pre-crushed sand under 0.2 confining pressure as shown in Figure 5.4 and Figure 5.6, where most of the tests were sheared to reach critical state. In order to examine sole effect of particle breakage on soil behavior, the 0.2MPa confining pressure therein was adopted in triaxial tests for trying not to crush the sand any more with neglecting the effect of particle breakage occurred during shearing in assumption.

The critical state points from the tests in Figure 5.4 and Figure 5.6 with stress paths were appended to Figure 5.32 for investigating the effect of particle breakage on location of CSL as illustrated in Figure 5.33. As shown in Figure 5.33(a), in comparison with the stress paths to critical state on pre-crushed sand and original sand in e-logp′ in CD tests, particle breakage has a significant influence on the stress paths including the locations of critical state points. It can be concluded that the locations of critical state points moved downwards with the increase of particle breakage, which is consistent with the findings (Fourie and Papageorgiou, 2001; Murthy et al., 2007). Figure 5.33(a) shows that, in CU tests, the locations of critical state points under same void ratio moved to the direction of reduction of mean effective stress with increasing particle breakage. It is notable herein that under 0.2MPa confining pressure the mean effective stress in critical state in CU tests is larger than that in CD tests, which means that under 0.2MPa confining pressure the dilatancy has a more substantial contribution on critical stress in CU tests than that in CD tests. About the location of critical state point on original sand in CD test under 0.2MPa confining pressure, being far away from the CSL. It is caused by the initial state of each test on original sand (Been et al., 1991). As shown in Figure 5.33(b), the critical state points from CD tests in q-p′ plane are consistent with CSL with almost neglecting the effect of particle breakage on the locations of critical state points, which is consistent with the finding (Bandini and Coop, 2011). However, in CU tests the critical state points over the CSL moved towards the lower left in q-p′ plane to approach the CSL with increasing particle breakage. For being in correlation between critical state points in CD tests and CU tests at the same amount of particle breakage, CSL would be in translation and rotation in e-logp′ plane, which is consistent with the findings (Bandini and Coop, 2011).

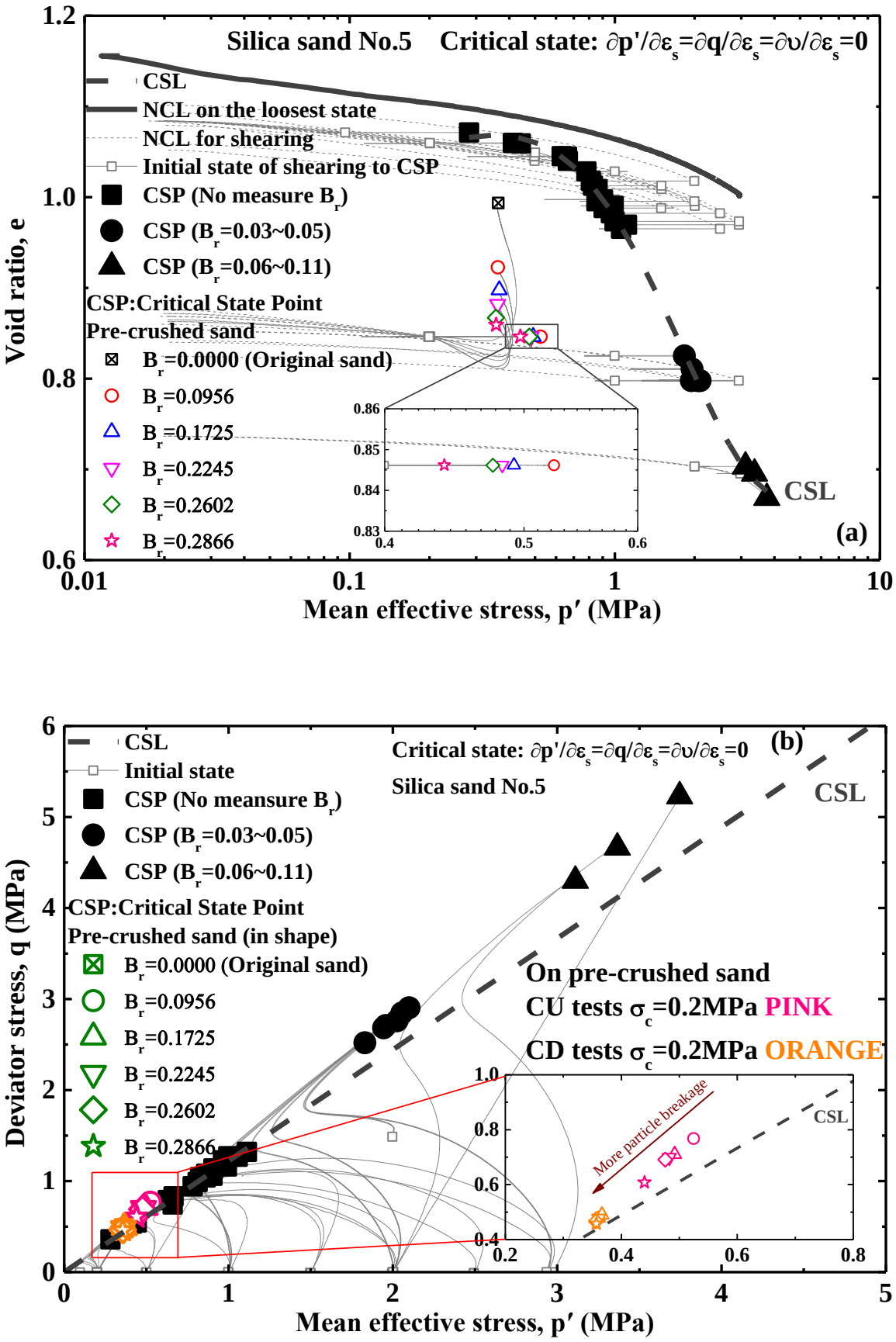

Figure 5.33 Critical state points on pre-crushed sand under 0.2MPa confining pressure

Another CD and CU tests have been conducted as well on original sand and pre-crushed sand under 0.5 confining pressure as shown in Figure 5.10 and Figure 5.12, where most of the tests were sheared to reach critical state as well.

The critical state points from the tests in Figure 5.10 and Figure 5.12 with stress paths were combined to Figure 5.32 for investigating the effect of particle breakage on location of CSL as illustrated in Figure 5.34, where the stress paths to critical state were completely influenced by particle breakage. It is notable in Figure 5.34(a) that the locations of critical state points in CD tests are found to move downwards with increasing particle breakage but in CU tests the locations of critical state points are seen clearly to move toward the direction of reduction of mean effective stress in same void ratio with increasing particle breakage, which are consistent with the findings of the tests under 0.2MPa confining pressure. About the location of critical state point on original sand in CD test under 0.5MPa confining pressure, being far away from the CSL, as mentioned above, it is caused by the initial state of each test on original sand (Been et al., 1991). It is shown in Figure 5.34(b) that the critical state points from CD tests in q-p′ plane are almost on CSL, which is consistent with the finding (Bandini and Coop, 2011). However, in CU tests the critical state points over the CSL moved towards the lower left in q-p′ plane to approach the CSL. Taking into account the correlation between critical state points in CD tests and CU tests at the same amount of particle breakage, it can be concluded that CSL would be in translation and rotation in e-logp′ plane, which is consistent with the findings (Bandini and Coop, 2011).

Many CU tests have been also performed on original sand and pre-crushed sand under 1MPa and 3MPa confining pressure as shown in Figure 5.16 and Figure 5.20, most of which were sheared to critical state as well.

The critical state points from the tests in Figure 5.16 and Figure 5.20 with stress paths were also combined to Figure 5.32 for investigating the effect of particle breakage on location of CSL subjected to high pressure as illustrated in Figure 5.35. It is notable in Figure 5.35(a) that the locations of critical state points in CU tests are seen clearly to move towards the direction of reduction of mean effective stress in same void ratio with increasing particle breakage but with increasing confining pressure from the locations of critical state points approaches the original CSL. It is illustrated in Figure 5.35(b) that the critical state points in CU tests the critical state points over the CSL moved towards the lower left in q-p′ plane to approach the CSL. Taking into account the correlation between critical state points in CU tests under 1MPa and 3MPa confining pressures at the same amount of particle breakage, it can be concluded herein that CSL would be in translation and rotation in e-logp′ plane, which is consistent with the finding from Bandini and Coop (2011).

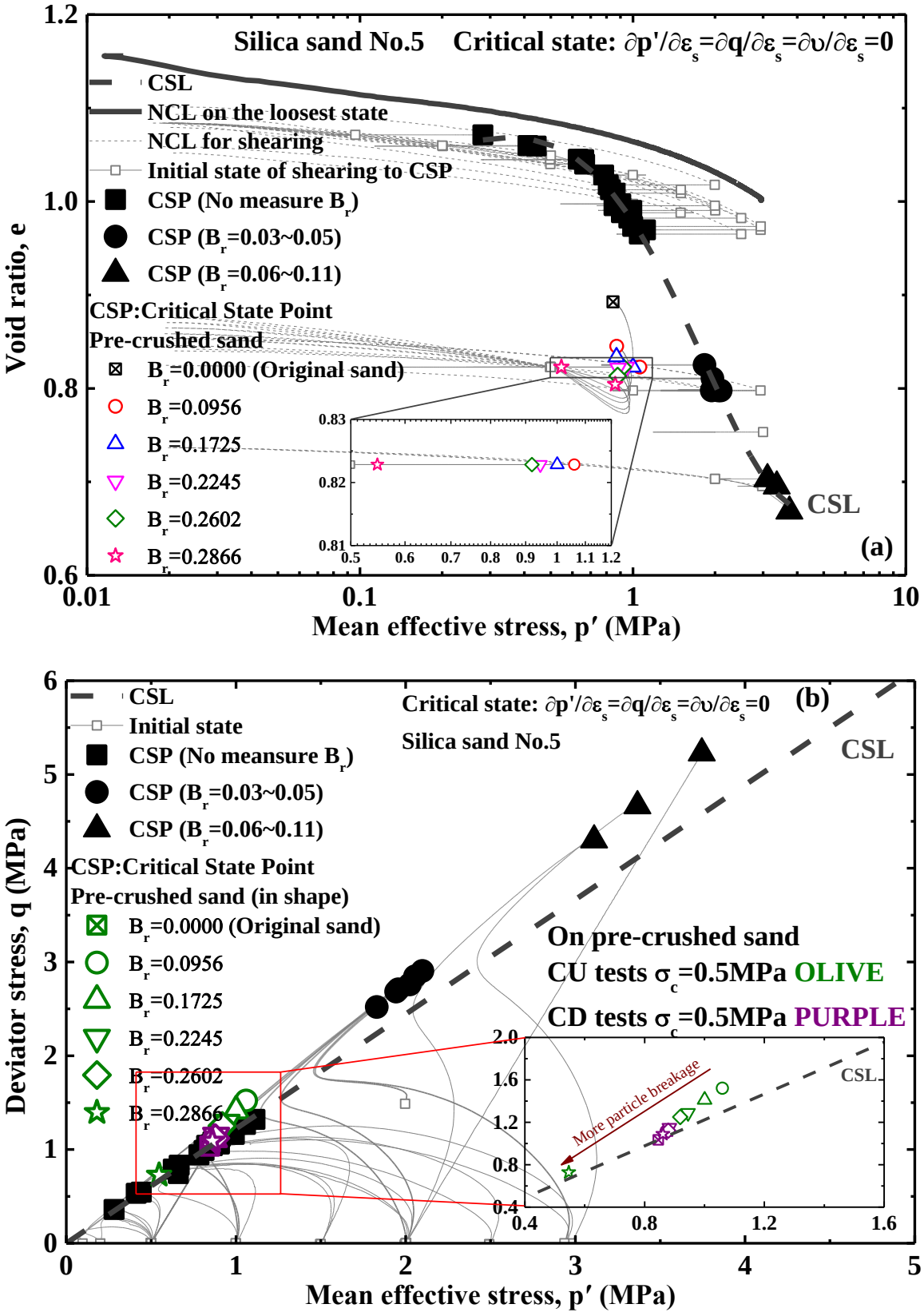

Figure 5.34 Critical state points on pre-crushed sand under 0.5MPa confining pressure

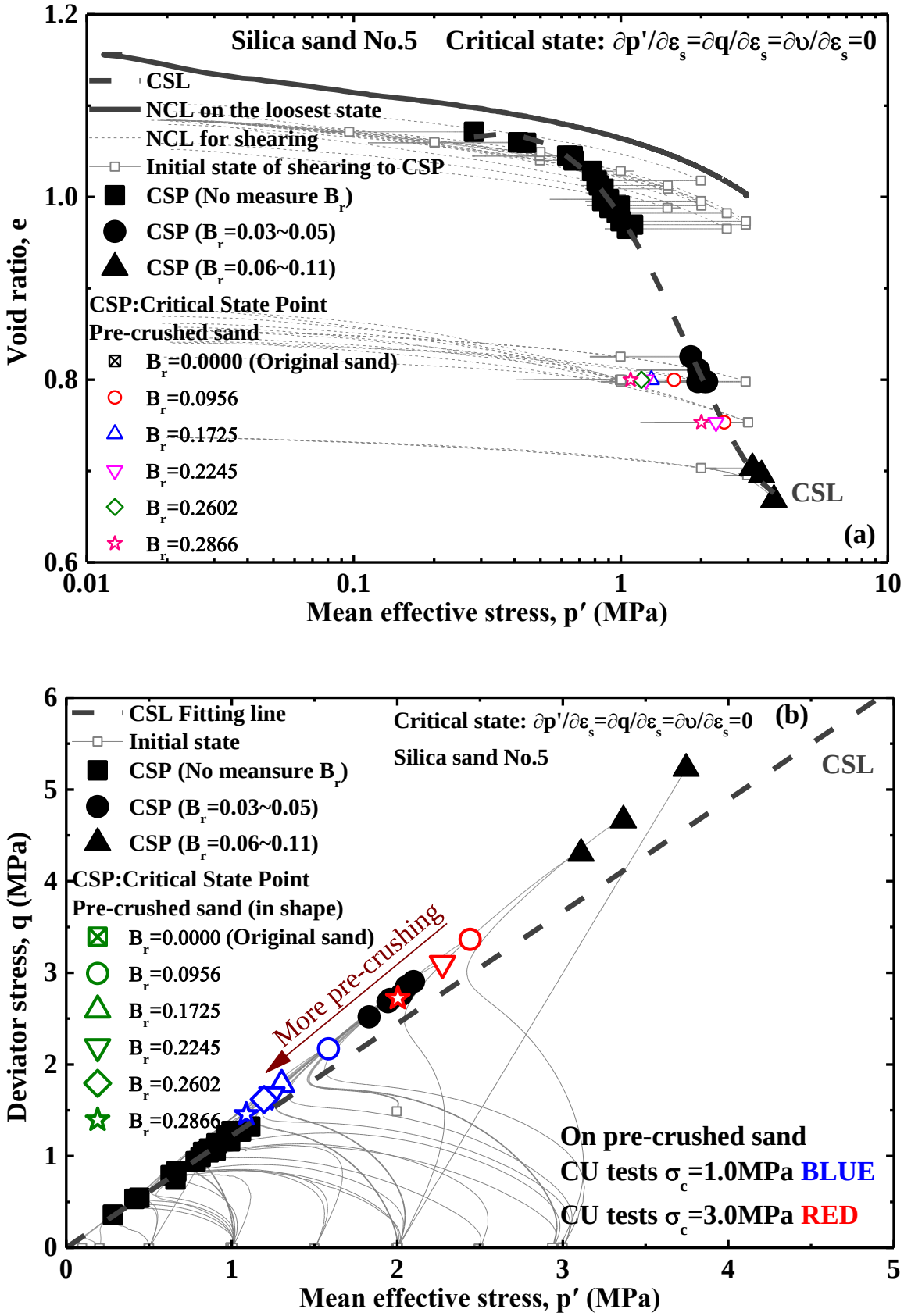

Figure 5.35 Critical state points on pre-crushed sand under 1MPa & 3MPa confining pressures

All critical state points were combined into Figure 5.36 for investigating the influence of particle breakage on the location of CSL subjected to various confining pressure. Considering the stress paths to critical state subjected to particle breakage, it is concluded in Figure 5.36 that particle breakage has a significant influence on the stress paths including the locations of critical state points especially in CD tests.

It is found in CD tests in Figure 5.36(a) that the locations of critical state points moved downwards in e-logp′ plane with the increasing particle breakage, which is consistent with the findings from Fourie and Papageorgiou (2001) and Murthy et al. (2007). However with the further increase of particle breakage, the CSL was found to may move back to upwards in e-logp′ plane (Thevanayagam et al. 2002; Carrera et al., 2011). Figure 5.36(a) shows that, in CU tests, the locations of critical state points under same void ratio moved to the direction of reduction of mean effective stress with the increase of particle breakage. It is notable herein that the locations of critical state points are getting close to original CSL in e-logp′ plane with increasing mean effective stress which may be caused by the combined effects of high pressure and particle breakage including the pre-crushed particle breakage and additional particle breakage induced during shearing. About the locations of critical state points are far away from the CSL, it is caused by the initial state of each test on original sand (Been et al., 1991). It is shown in Figure 5.36(b) that the critical state points from CD tests under relatively low pressure in q-p′ plane are almost on CSL with almost neglecting the effect of particle breakage on the locations of critical state points which is consistent with the finding from Bandini and Coop (2011), but in CU tests the critical state points over the CSL moved towards the lower left in q-p′ plane to approach the CSL with increasing particle breakage. With increasing mean effective stress in q-p′ plane, the critical state points in q-p′ plane become further and further from the linear CSL, which may be caused by the combined effects of high pressure and particle breakage including the pre-crushed breakage and additional breakage during shearing under high pressure. Considering the comprehensive influences of particle breakage and high pressure on locations of critical state points, it can be concluded simply that both high pressure and particle breakage have an important effect on CSL. For being in correlation between critical state points in CD tests and CU tests at the same amount of particle breakage, CSL would be in complex translation and rotation in e-logp′ plane, which is consistent with the finding from Bandini and Coop (2011). However, in q-p′ plane both high pressure and particle breakage result in nonlinearity of CSL in increase of M=q/ p′.

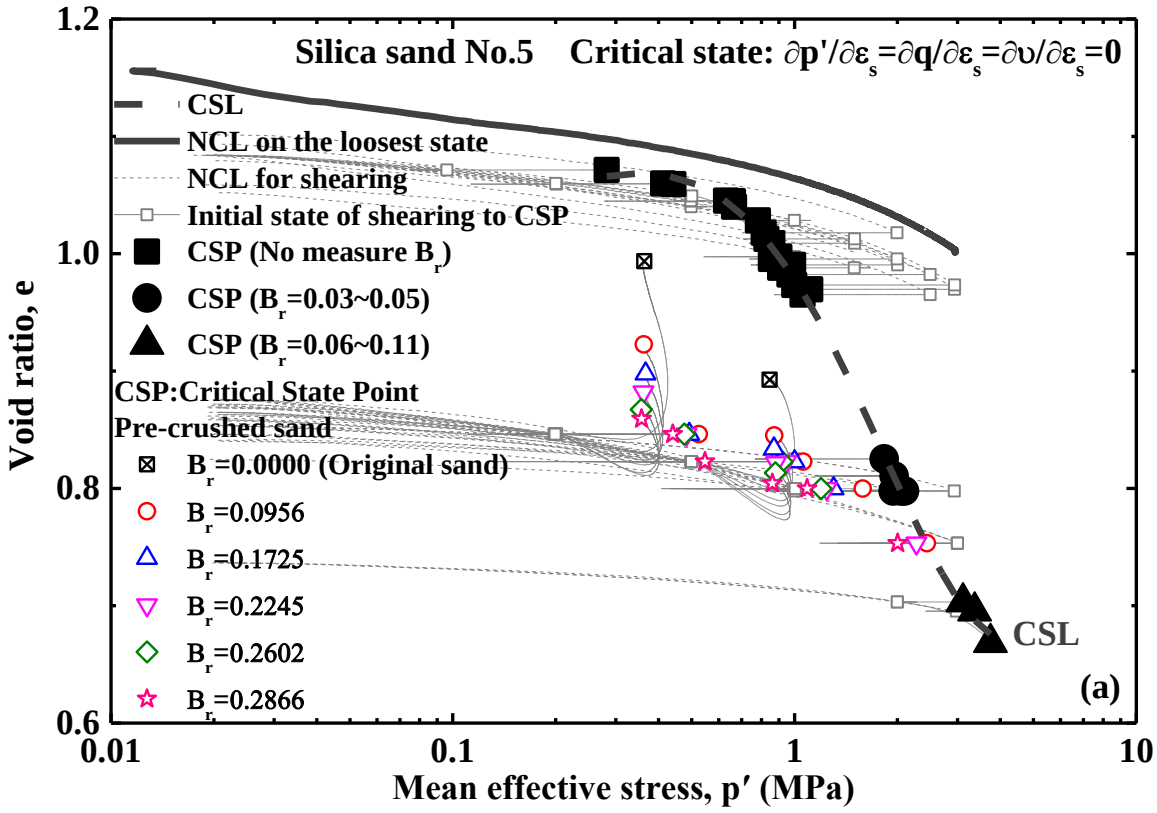

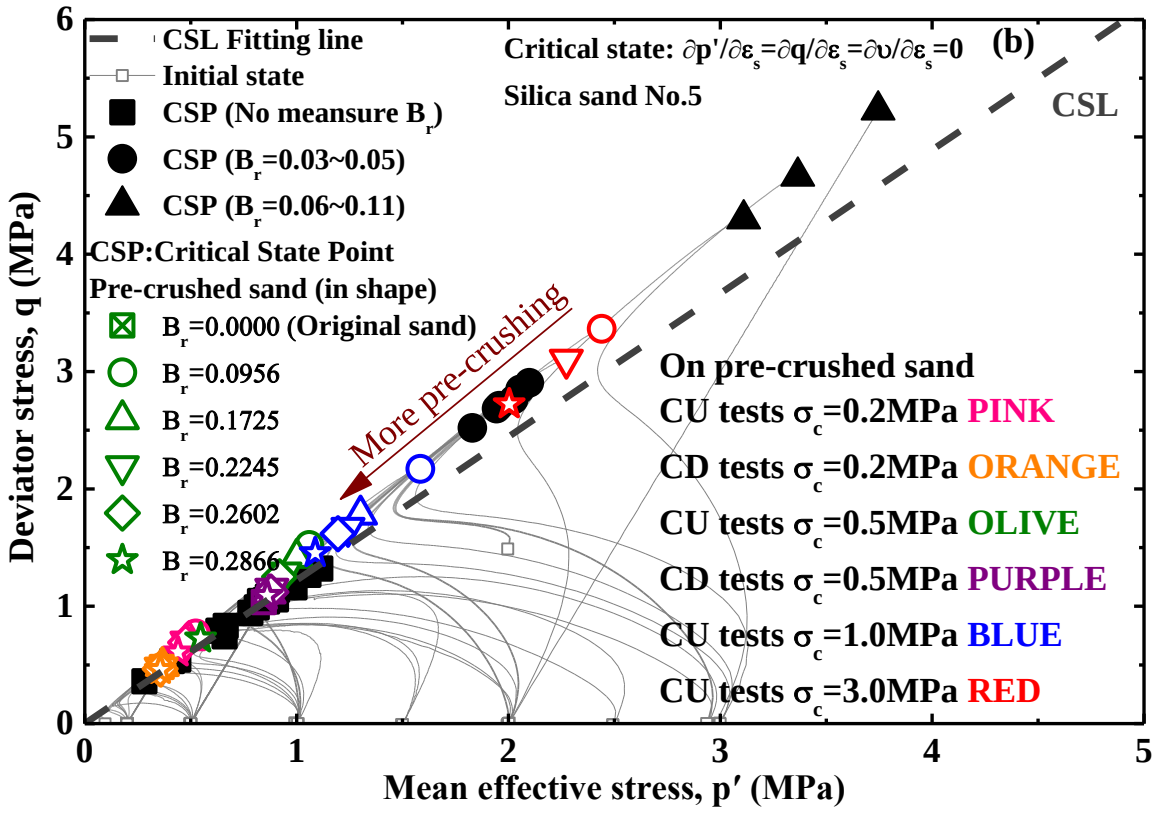

Figure 5.36 Critical state points subjected to pre-crushed sand

5.4 EXPERIMENTAL RESULTS ON CORAL SAND NO.3

5.4.1 Generation of Pre-crushed Sand

Many CD tests were conducted on original sand under 3MPa confining pressure after isotropic consolidation and terminated to designated axial strain such as from 10% to 40% by a 10% increment to generate pre-crushed materials in various extents of particle breakage, which would be kept after shearing to reuse in triaxial tests for investigating the influence of particle breakage on soil behavior in comparison with the results of original sand.

Figure 5.37 shows the triaxial tests results on original sand for producing pre-crushed sands, where the deviator stresses are found to increase gradually in down-concavity to converge at a value levelly but the volume changes during whole stage of shearing are seen clearly to be in contractancy, which is related to particle breakage induced during shearing. The stress path of the triaxial tests is given in Figure 5.37(c).

All material of each test after shearing was kept in an oven to dry and then the grain size distribution curve of each test was obtained by sieve analysis. According to all grain size distribution curves, herein relative breakage was calculated to quantify the amount of particle breakage of each test. The grain size distribution curves of the triaxial tests during shearing are shown in Figure 5.38(a), where it is concluded that particle breakage increases with increasing axial strain and the particle breakage occurred as well during isotropic consolidation even in vary few amount. Shear band in specimen was formed as the axial strain reached 40%. Consequently the extent of particle breakage in shear band and outside shear band was herein expected to investigate. The specimen was divided into three parts of top, middle and bottom uniformly as shown in Figure 5.38(b), where the 200g along the center axis of top or bottom parts of specimens was picked up to sieve to get the grain size distribution curves outside shear band but 200g was picked up along the shear band in the middle part of specimen to sieve to get the grain size distribution curve in shear band. The grain size distribution curves in shear ban and at top & bottom parts of specimen are shown in Figure 5.38(b), where particle breakage is found to be slightly more substantial in shear band than that at top or bottom part of specimen but there is no big difference about the particle breakage between top and bottom parts of specimen.

The shearing on original sand to produce pre-crushed sand was employed in simulating the mechanical process during construction of high dam and high-rise building, and the pre-crushed sand represents the crushed soil particles with various extent of pre-crushed particle breakage existed in different area in dam or around the tip of group pile. The soil behavior of the pre-crushed materials should be investigated to clarify the effect of particle breakage on soil behavior.

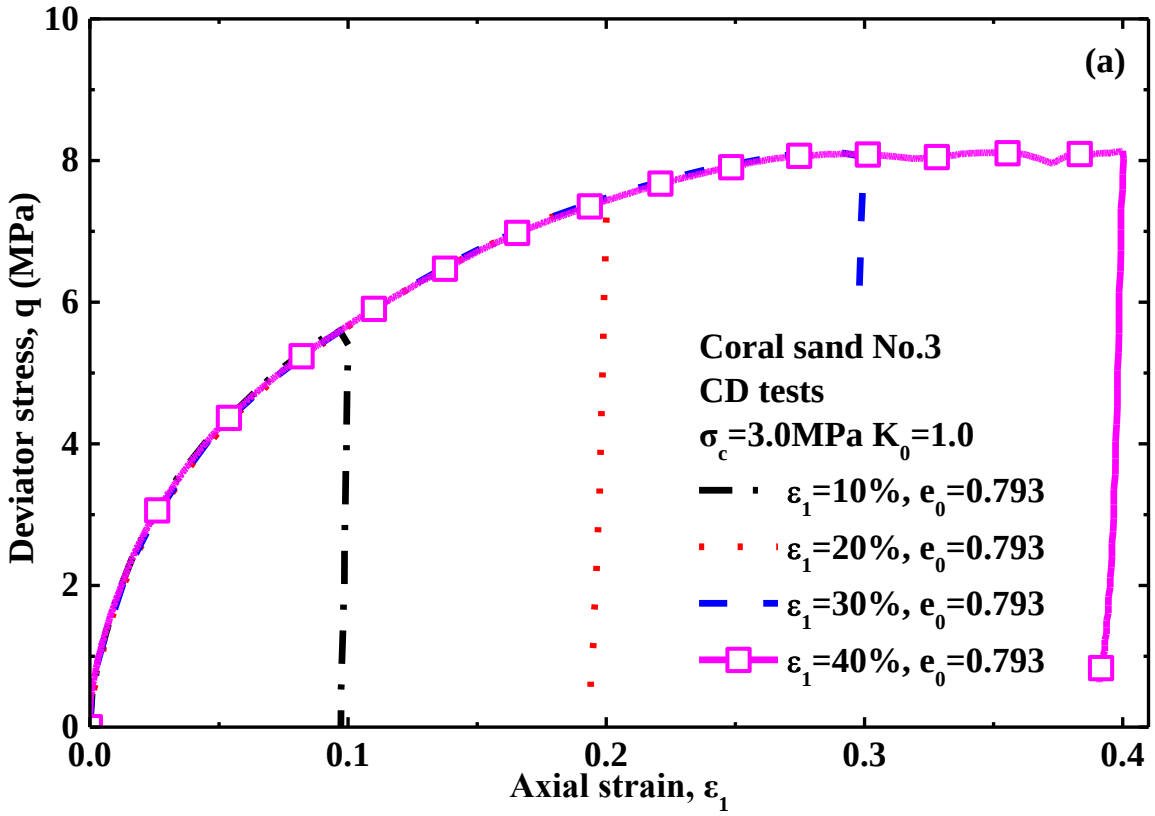
(a)
Deviator stress, q (MPa)
Axial strain, ε1
Coral sand No.3
CD tests
σc=3.0MPa K0=1.0
ε1=10%, e0=0.793
ε1=20%, e0=0.793
ε1=30%, e0=0.793
ε1=40%, e0=0.793

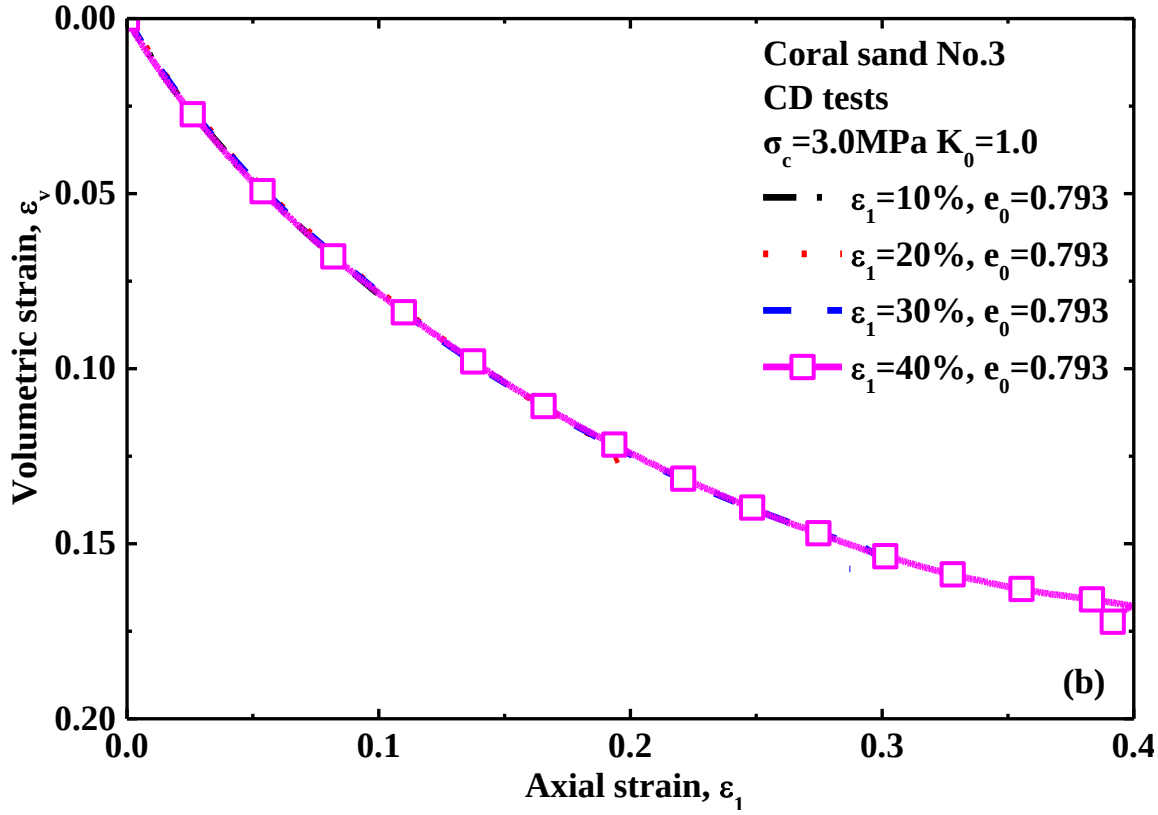
(b)
Volumetric strain, εv
Axial strain, ε1
Coral sand No.3
CD tests
σc=3.0MPa K0=1.0
ε1=10%, e0=0.793
ε1=20%, e0=0.793
ε1=30%, e0=0.793
ε1=40%, e0=0.793

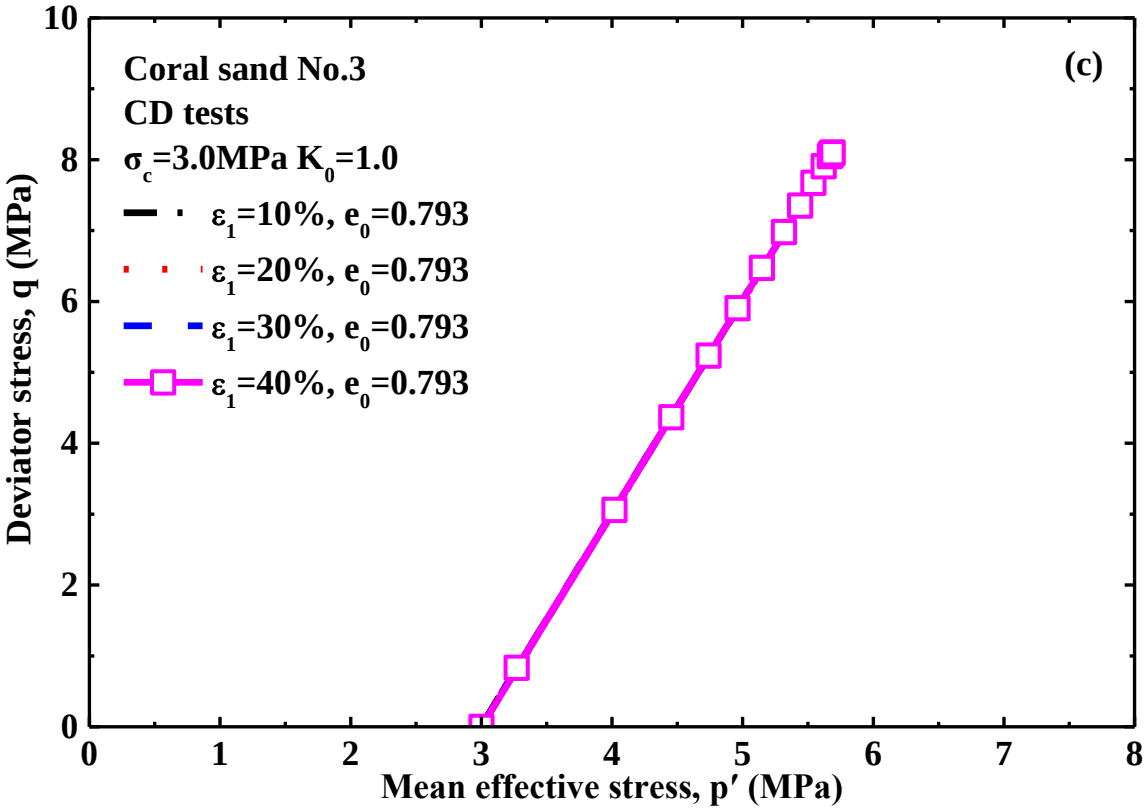

Figure 5.37 Triaxial test results on original sand for producing pre-crushed sands

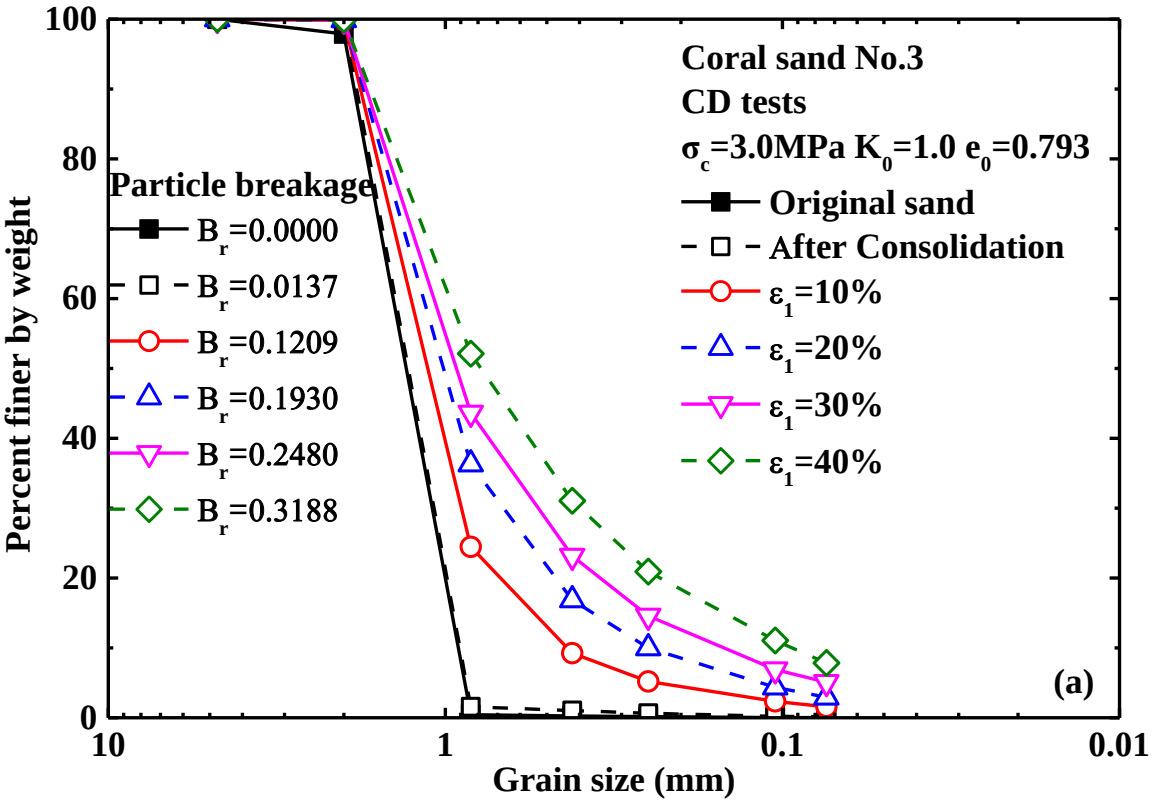

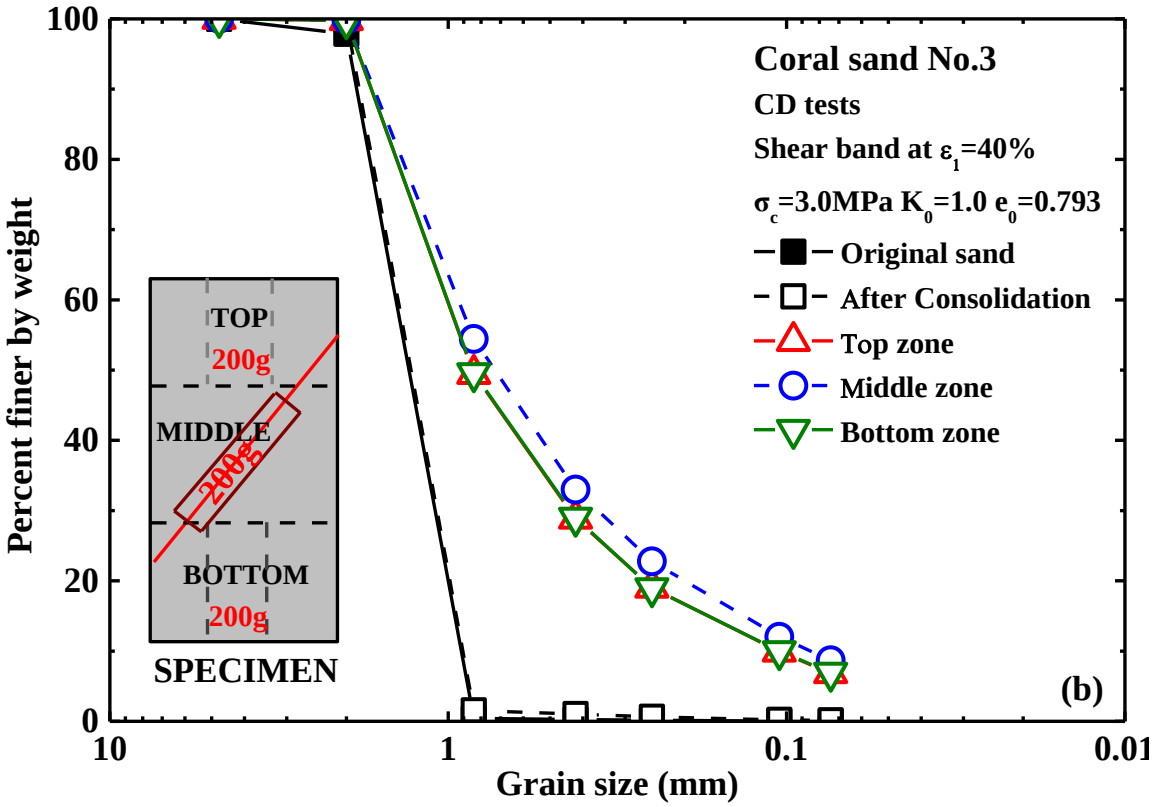

Figure 5.38 Grain size distribution curves during shearing and in shear band

Table 5.3 Physical properties of pre-crushed sand from Coral sand No.3

Item	Relative breakage B_r	D_{50} (mm)	$C_u=D_{60}/D_{10}$	$C_c=(D_{30})^2/(D_{10}*D_{60})$
Original sand	0.0000	1.306	1.561	0.916
After consolidation	0.0137	1.288	1.551	0.915
ε_1=0.10	0.1209	1.128	2.924	1.461
ε_1=0.20	0.1930	1.013	4.640	1.553
ε_1=0.30	0.2480	0.927	7.275	1.733
ε_1=0.40	0.3188	0.784	10.309	1.739

Note: D_i is the grain diameter at i% passing.

The physical properties of pre-crushed sand from Coral sand No.3 are shown in Table 5.3, which particle breakage is shown clearly to reduce $D_{50,}$ but to result in increase of coefficient of uniformity and coefficient of curvature, namely the coefficient of uniformity and coefficient of curvature in gradation of soil are found to increase with increasing particle breakage. For a sand to be classified as well graded, the $C_u \geq 6$ & $1<C_c<3$ should be met. The gradation of soil is herein found to be changed with increasing particle breakage and to become well graded with further increasing particle breakage such as B_r from 0.2480 to 0.3188.

5.4.2 The Influence of Particle Breakage on Soil Behavior

5.4.2.1 Isotropic consolidation behavior subjected to particle breakage

Isotropic consolidation on original sand and pre-crushed sand was conducted to 3MPa confining pressure to investigate the isotropic consolidation behavior in e-logp′ plane subjected to particle breakage. Figure 5.39 shows the isotropic consolidation in e-logp′ plane subjected to original sand and pre-crushed sand, where more contractive volume change is induced in pre-crushed sand, namely particle breakage leads to increase of being contractive. More volume contractancy or subsidence is caused by particle breakage in reality, where the particle breakage should be considered in practice. It is seen in Figure 5.39 as well that the e-logp′ curves are getting nonlinear with increase mean effective stress and the more substantial residual volume change after unloading was caused in pre-crushed sands in comparison with the residual volume change of original sand. It can be concluded herein that particle breakage has very important influence on the compression characteristics in being more contractive especially under high pressure. Consequently it is indispensable to consider permanent subsidence or deformation induced by particle breakage in reality.

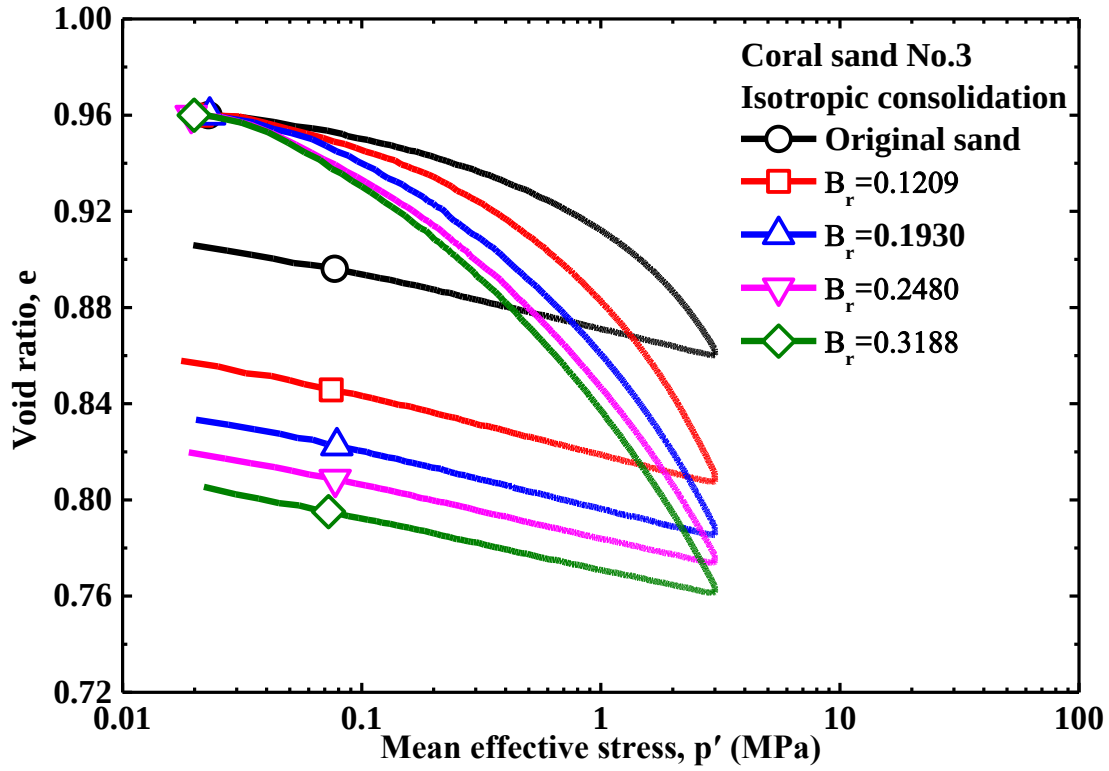

Figure 5.39 Isotropic consolidation subjected to original sand and pre-crushed sand

5.4.2.2 Shearing behavior subjected to particle breakage under 0.2MPa confining pressure

New specimens were prepared by original sand and pre-crushed sand separately in air

pluviation into a mould with a membrane in eight layers. Many triaxial tests were performed on original sand and pre-crushed sand after isotropic consolidated under CD and CU conditions for investigating the influence of particle breakage on shear behavior under 0.2MPa confining pressure, which as a relatively low confining pressure was used herein in triaxial tests for trying not to crush the sand any more so as to find out shear behavior subjected to pre-crushed breakage.

Figure 5.40 shows the CD tests results of original sand and pre-crushed sand under 0.2MPa confining pressure, where the particle breakage is found to deteriorate the deviator stresses in reduction of peak strength with the highest peak strength and residual strength in original sand as shown in Figure 5.40(a) and volume change of original sand shows the most dilative behavior in tending quickly to dilatancy after a very short stage of contractancy at the beginning of shearing of original sand but the pre-crushed sand is revealed to get more contractive as shown in Figure 5.40(b). It is seen clearly that particle breakage has a significant influence on residual strength simply in reduction but existing exception as shown in Figure 5.40(a).

In order to investigate directly the influence of particle breakage on dilatancy behavior, Figure 5.41 shows the void ratio against dilatancy factor subjected to particle breakage, where the original sand is seen to be most dilatant under the same void ratio of original sand & pre-crushed sand and particle breakage is concluded to result in being more contractive in pre-crushed sands in depression of dilatancy, which are consistent with findings from Lee and Seed (1967) and Miura and Ohara (1979).

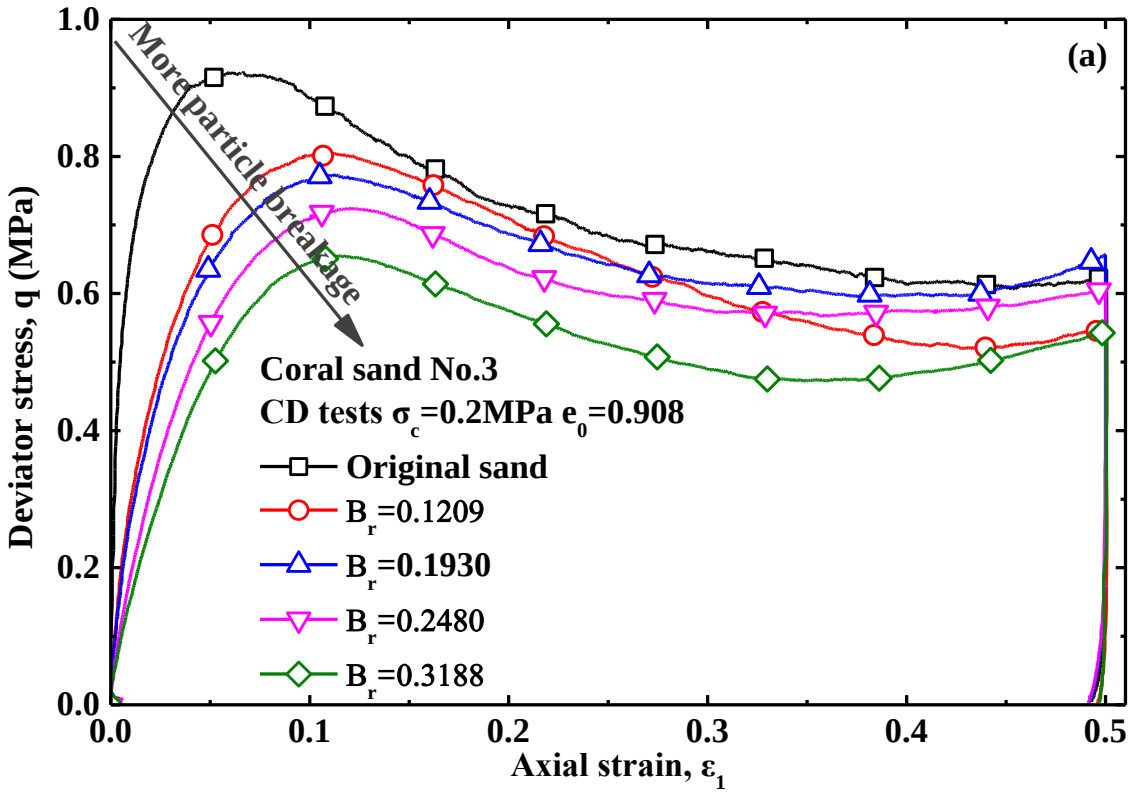

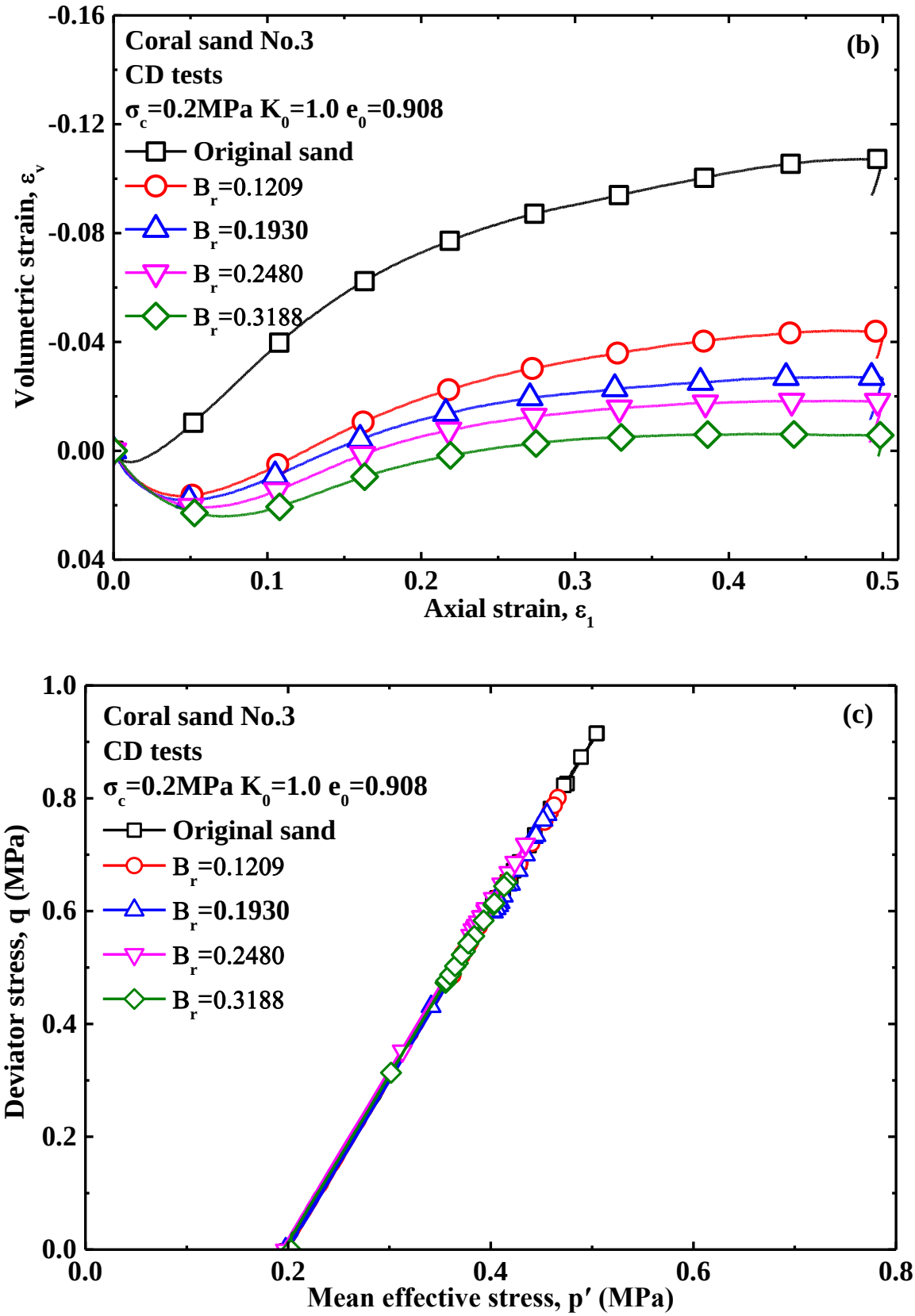

Figure 5.40 CD test results of original sand and pre-crushed sand under 0.2MPa confining pressure

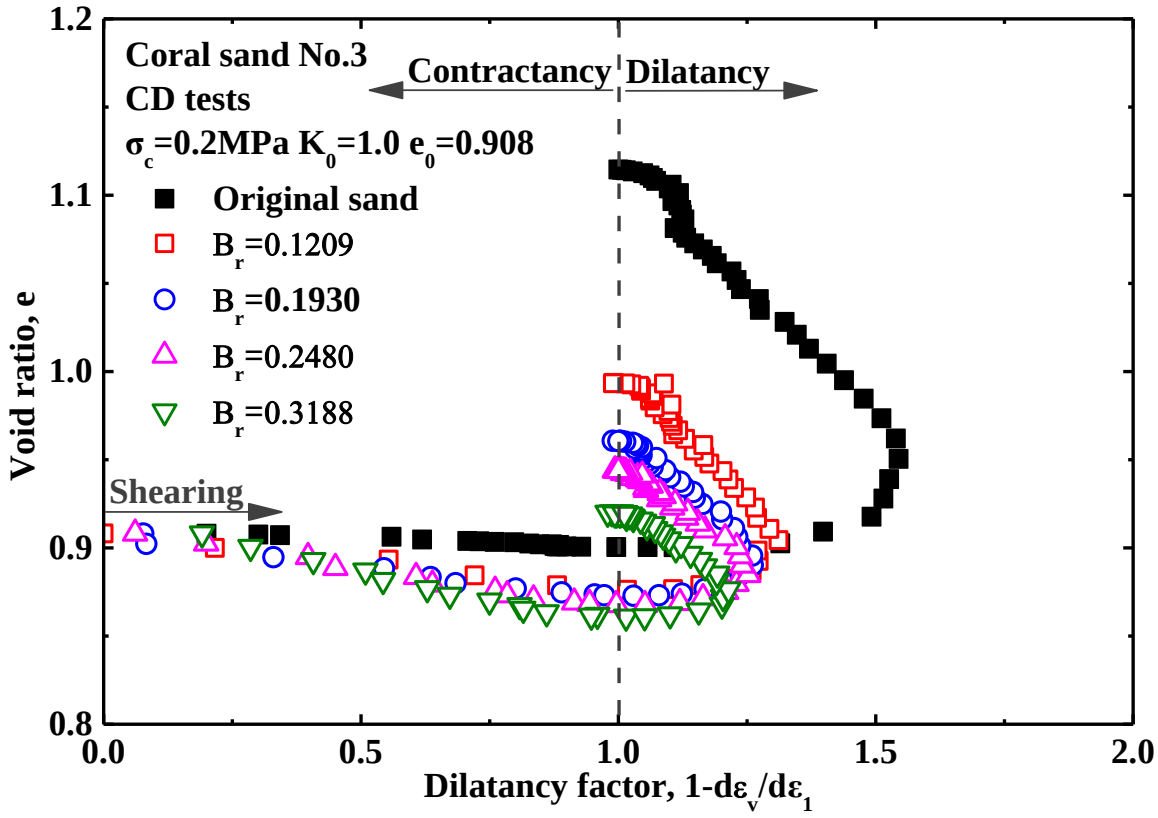

Figure 5.41 Void ratio against dilatancy factor subjected to particle breakage

CU tests were also carried out on original sand and pre-crushed sand under 0.2MPa confining pressure to investigate the influence of particle breakage on shear behavior including the evolution of excess pore water pressure. The CU test results of original sand and pre-crushed sand under 0.2MPa confining pressure are shown in Figure 5.42. It is seen clearly that particle breakage deteriorates the deviator stresses in reduction of peak strength as shown in Figure 5.42(a) and the excess pore water pressure has a more substantial development and slower dissipation with higher residual excess pore water pressure with increasing particle breakage as shown in Figure 5.42(b), which are caused by the depression of dilatancy and increase of contractibility in pre-crushed sands with particle breakage. However it has the highest peak strength and the lowest development of excess pore water pressure in original sand, which is related to the most dilative behavior existed in original sand. In addition, as shown in Figure 5.42(a), the axial strain at peak strength is revealed to increase to reach lower peak strength with increasing particle breakage, which means that particle breakage results in increased ductility of soil to reach reduced peak strength, namely particle breakage may cause more subsidence and lateral deformation. Stress paths of CU tests under 0.2MPa confining pressure are shown in Figure 5.42(c) in which particle breakage is revealed to affect the whole stress path in reduction of strength.

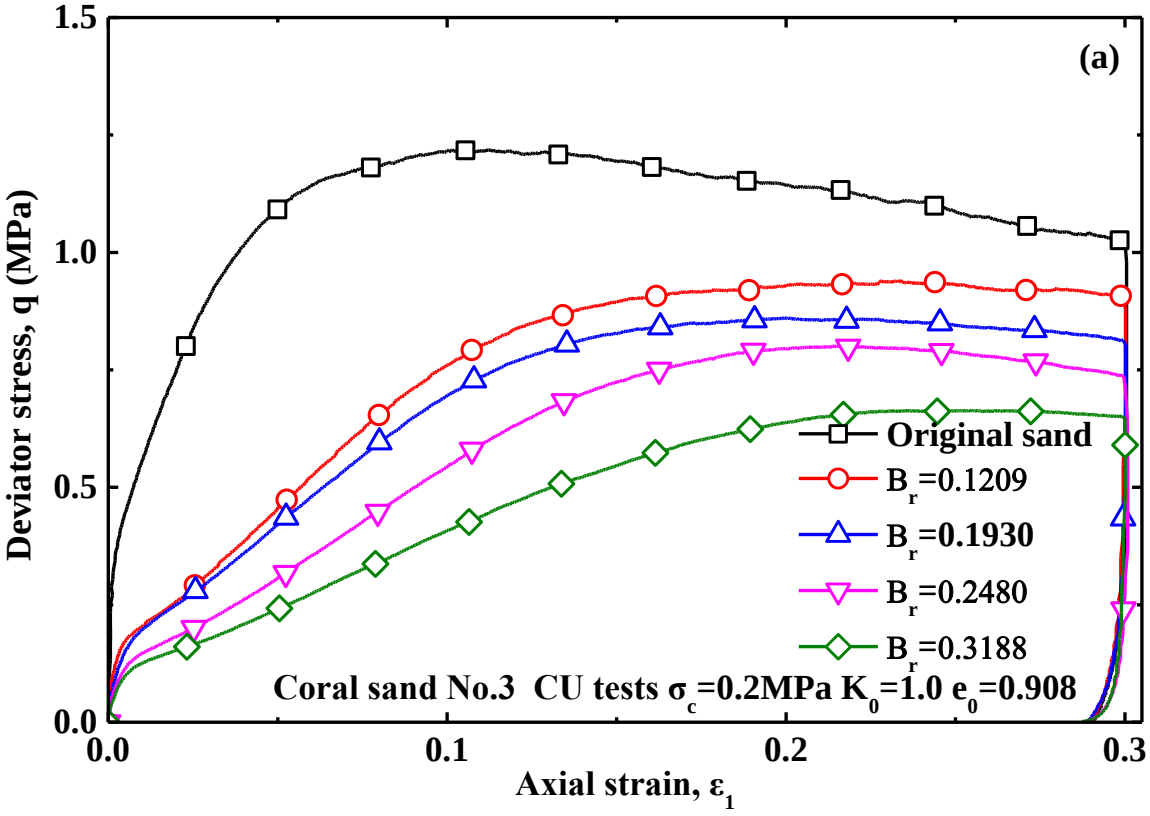
(a)
Deviator stress, q (MPa)
Axial strain, ε1
Original sand
Br=0.1209
Br=0.1930
Br=0.2480
Br=0.3188
Coral sand No.3 CU tests σc=0.2MPa K0=1.0 e0=0.908

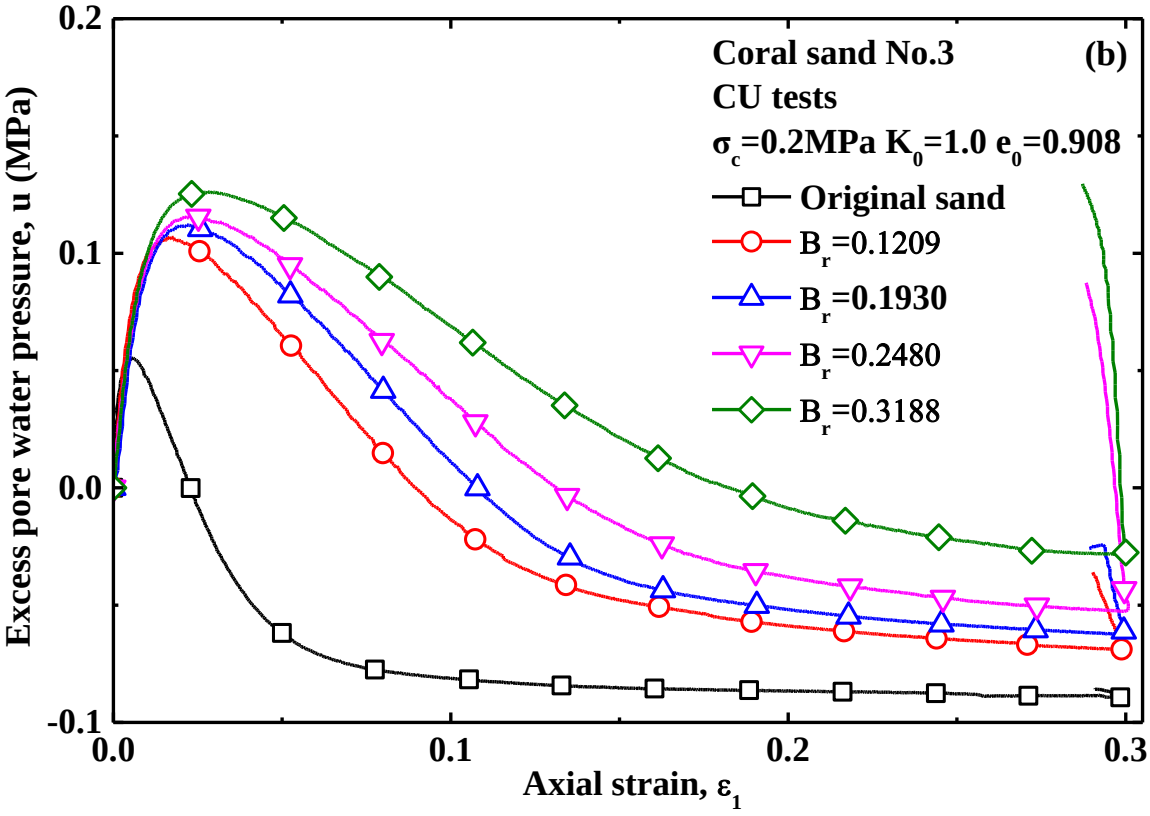
(b)
Coral sand No.3
CU tests
σc=0.2MPa K0=1.0 e0=0.908
Original sand
Br=0.1209
Br=0.1930
Br=0.2480
Br=0.3188
Excess pore water pressure, u (MPa)
Axial strain, ε1

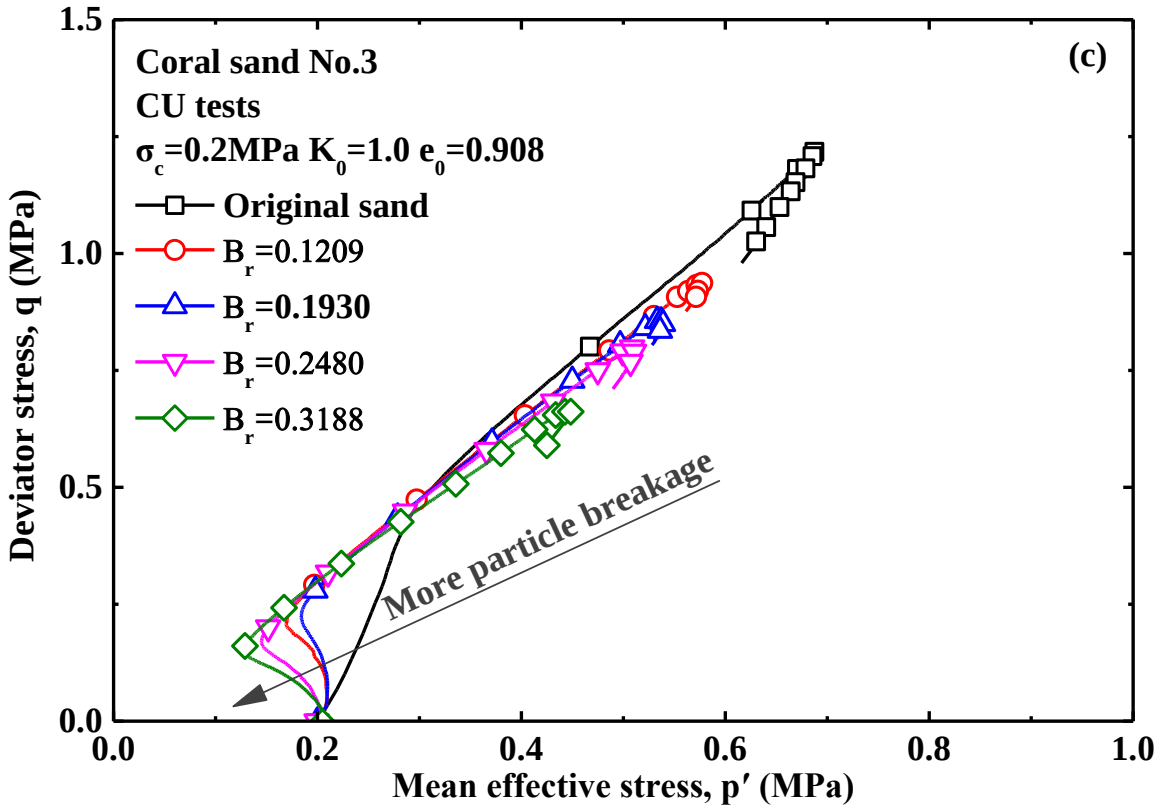

Figure 5.42 CU test results of original sand and pre-crushed sand under 0.2MPa confining pressure

As shown in Figure 5.40 and Figure 5.42, peak strengths and residual strengths were reached except a residual strength of original sand in CU test. Herein the peak strengths and residual strengths were picked out and investigated considering the influence of particle breakage. Figure 5.43 shows the peak strengths and residual strengths subjected to particle breakage in relative breakage. It is found in Figure 5.43(a) that peak strengths decrease monotonically with increasing particle breakage but residual strengths from CD tests decrease in fluctuation which means that the monotonically increased particle breakage has a non-monotonic complex influence on critical state in residual stage. In addition, as shown in Figure 5.43(a), the peak strengths from CU tests is found to be larger than that from CD tests but with increasing particle breakage they tend to intercept at a same value, which means that under low confining pressure (0.2MPa) the dilatancy of soil in CU condition has more substantial contribution on peak strength than that in CD condition but with increasing particle breakage in depression of dilatancy, this influence would be impaired. The deviator stresses curves in CD tests have a softening stage to reach the residual strength after peak strength, consequently it is reasonable to understand that the residual strengths are lower than the peak strengths as shown in Figure 5.43(a) but the difference between peak strengths and residual strengths are found to decrease approximately with increasing particle breakage, which means that particle breakage results in reduction of variation of peak strength and residual strength. The peak strengths or residual strengths were normalized by the relevant strength of original sand as shown in Figure 5.43(b), where peak strengths are found to reduce to 71% of peak

strength of original sand in CD test and 55% of peak strength of original sand in CU test in maximum but residual strengths in CD tests reduce to 77% of residual strength of original sand in maximum, which shown be considered in practice.

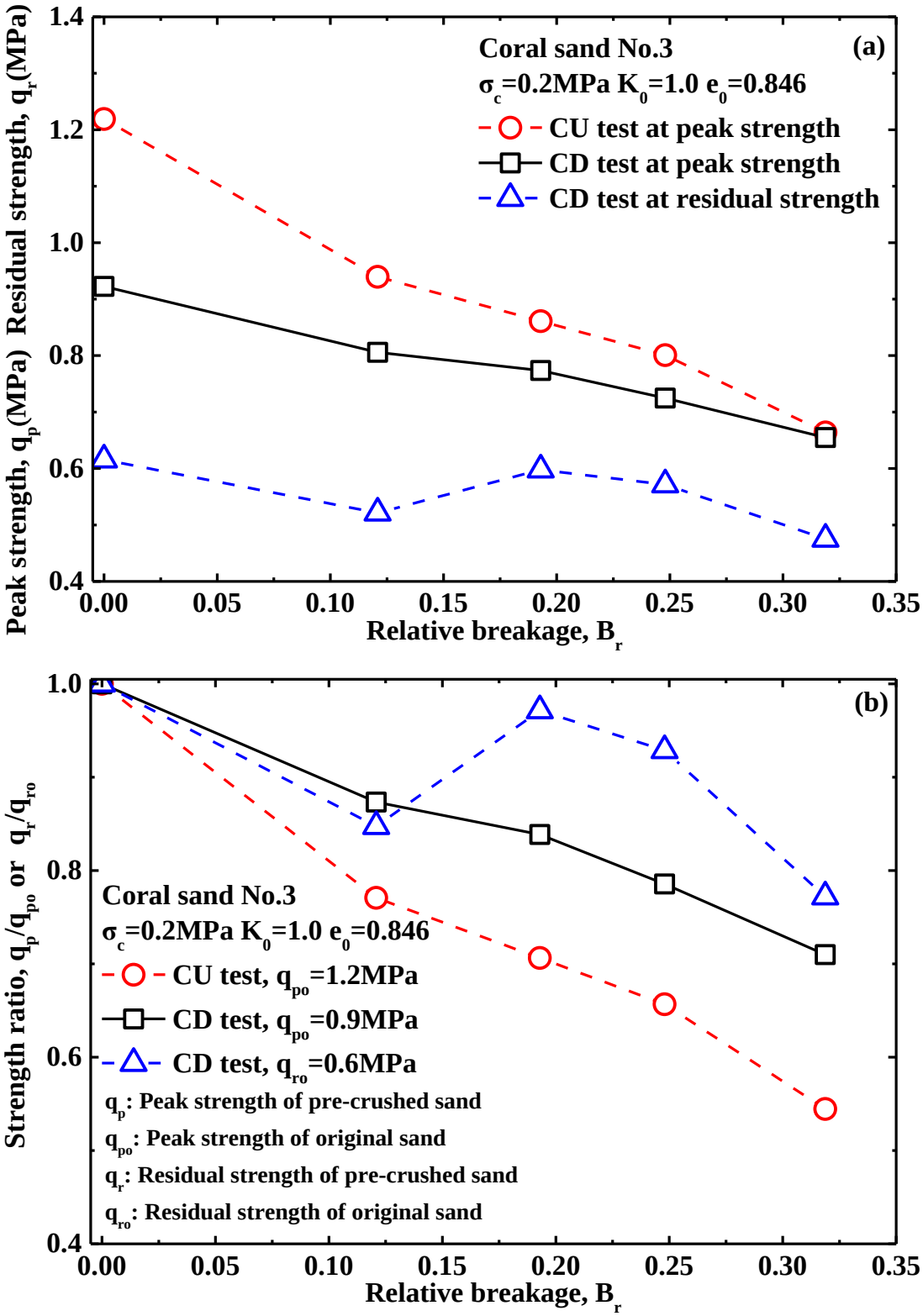

Figure 5.43 Peak strength and residual strength subjected to particle breakage

Friction angles at peak strengths and residual strengths of the tests under 0.2MPa confining pressure were calculated by Mohr-Coulomb theory to investigate the evolution of friction angles subjected to particle breakage. Figure 5.44 shows the friction angles subjected to particle breakage. It is herein that the friction angles at peak strengths in CD tests and CU tests decrease with increasing particle breakage, which is consistent with the finding (Ghanbari et al., 2013) but the friction angles in CD tests is a little larger than that in CU tests. The friction angles at residual strengths (critical state) in CD tests are found to decrease in fluctuation with increasing particle breakage as shown in Figure 5.44(a), which is consistent with trend of evolution of residual strengths as shown in Figure 5.43(a). The opposite finding is that particle breakage induced in the ring shear tests resulted in increase of the critical state friction angle (Sadrekarimi and Olson, 2011). In addition, Been et al. (1991) concluded that the critical state friction angle may be a function of critical state void ratio. As mentioned above, the current state has a significant effect on the evolution of critical state friction angle subjected to particle breakage. It is notable herein that the difference between friction angle at peak strengths and friction angle at residual strengths in CD tests are seen to approximately decrease with increasing particle breakage. The fiction angles were normalized by that of original sand at peak strength or residual strength as shown in Figure 5.44(b), where the friction angle ratios under 0.2MPa confining pressure are found to decrease monotonically with increasing particle breakage in exception of friction angle ratio at residual strength, being in maximum reduction to 87% of friction angle of original sand at peak strength in CD test, 85% of friction angle of original sand at peak strength in CU test and 88% of friction angle of original sand at residual strength in CD test.

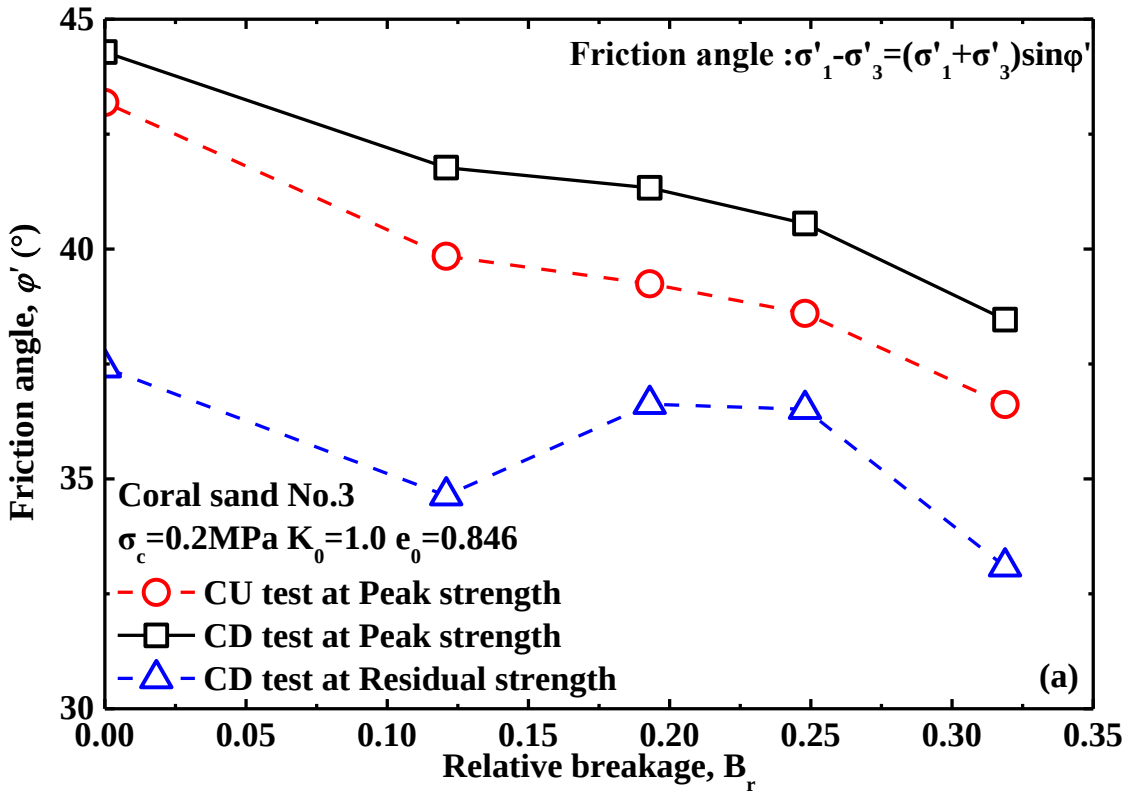

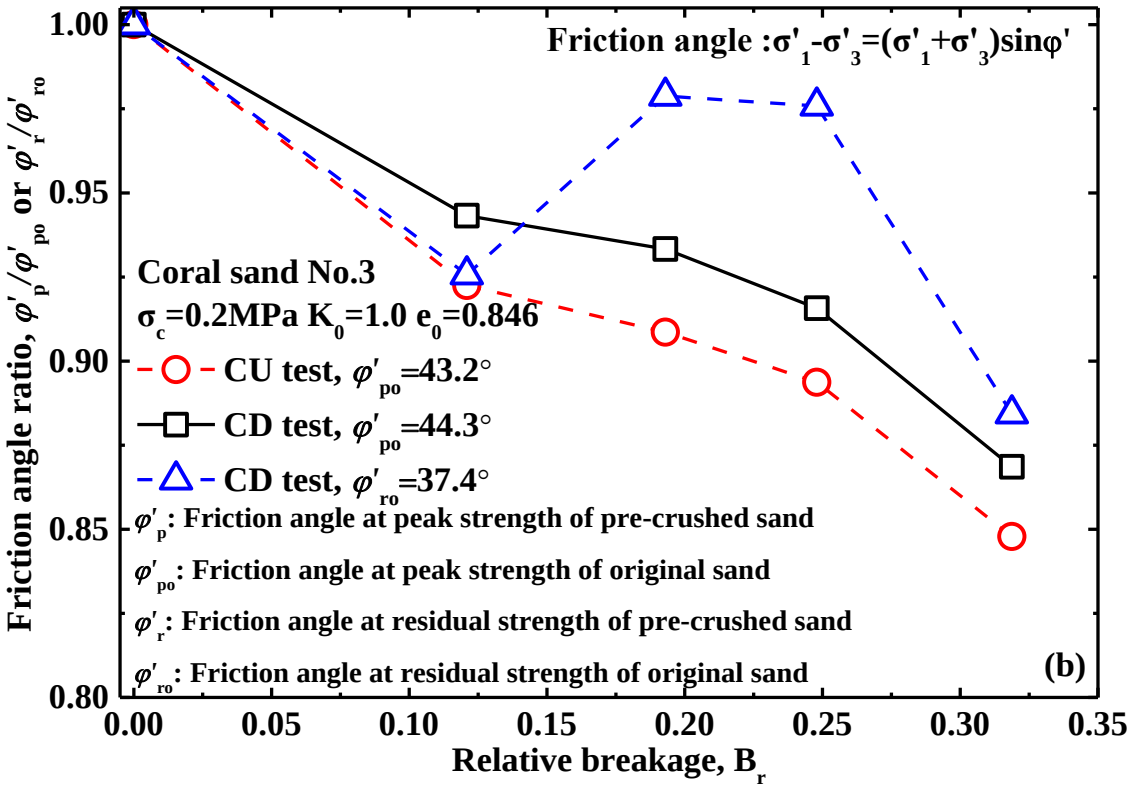

Figure 5.44 Friction angle subjected to particle breakage

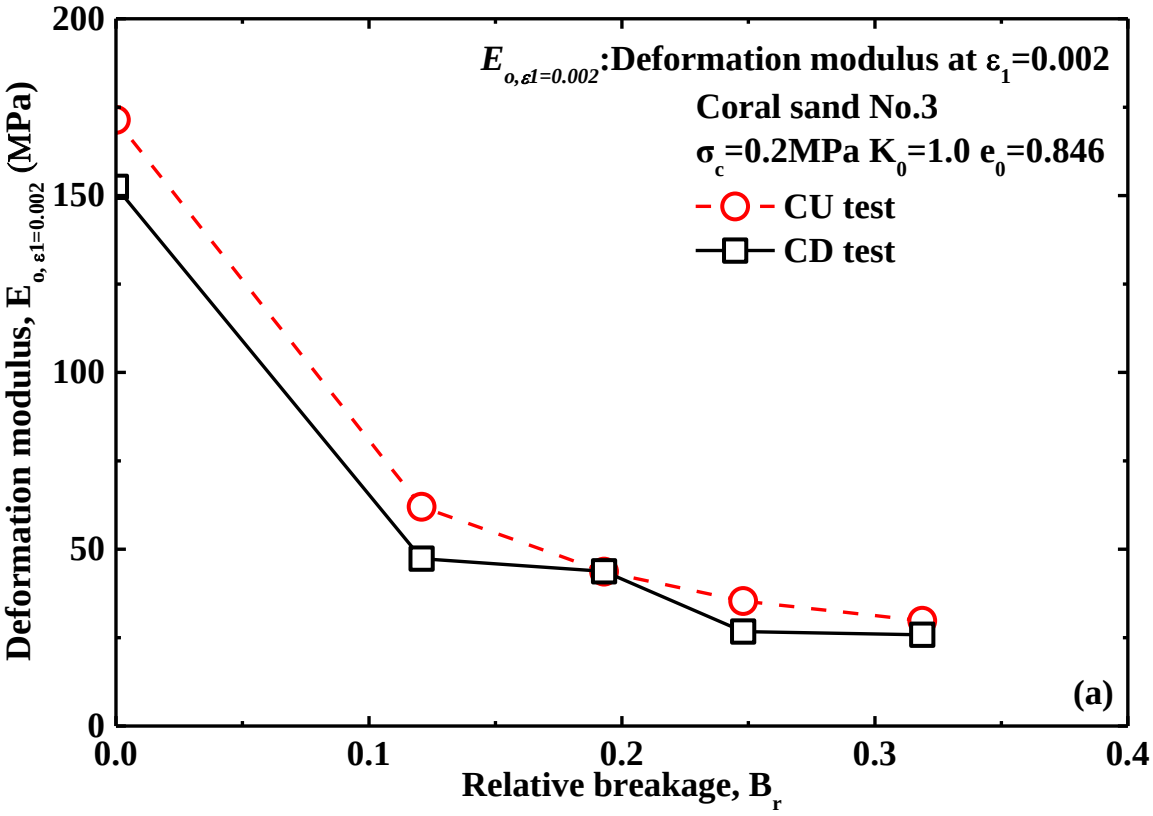

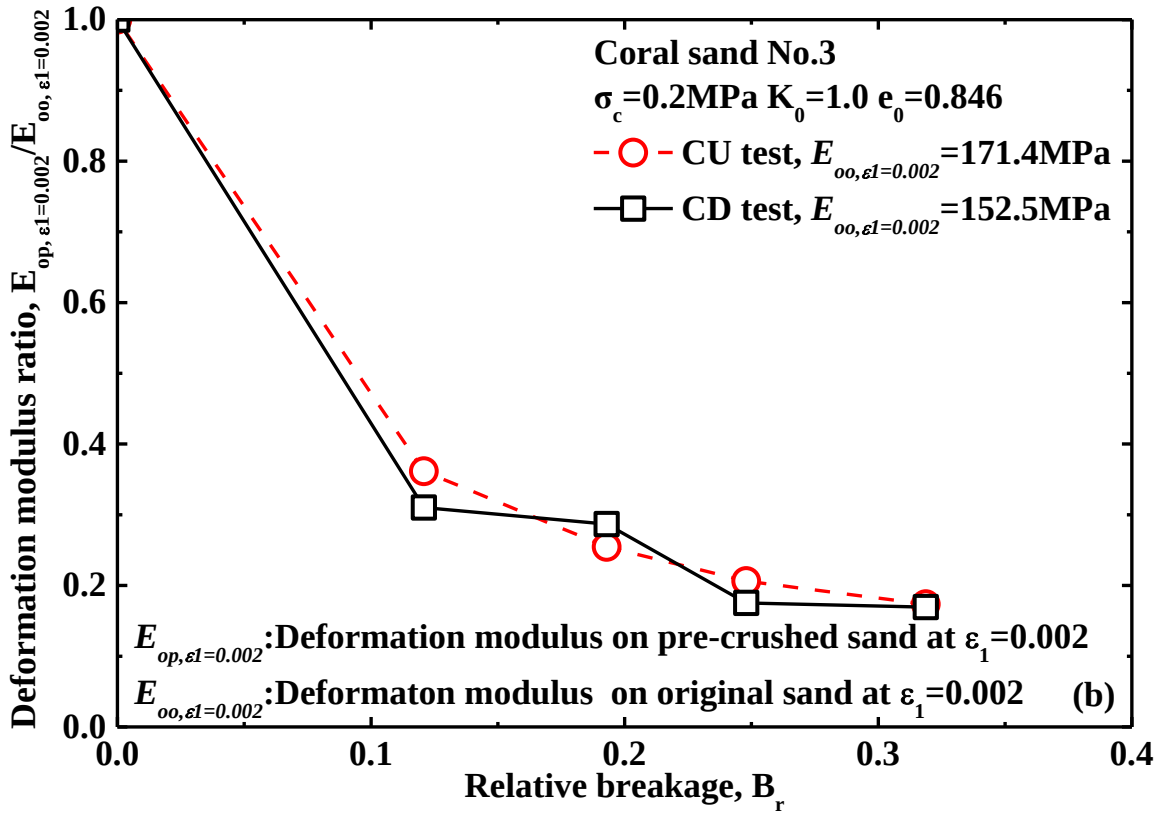

Figure 5.45 Deformation modulus subjected to particle breakage

Deformation modulus was calculated at 0.002 axial strain of each test under 0.2MPa confining pressure with an aim to investigate the influence of particle breakage on deformation modulus. Figure 5.45 shows the deformation modulus subjected to particle breakage, where deformation moduli in CD and CU tests are found to decrease in up-concavity with increasing particle breakage in relative breakage, which means that particle breakage results in impairment of deformation modulus. It is seen clearly in Figure 5.45 that the deformation moduli are larger in CU tests than that in CD tests but the difference of initial moduli between CD tests and CU tests is found to decrease to be consistent finally with increasing particle breakage. The deformation moduli of pre-crushed sands were normalized by that of the original sand as shown in Figure 5.45(b) where the deformation modulus ratios are found to decrease to around 17% of deformation modulus of original sand in CD and CU tests in maximum.

5.5 SUMMARY

Silica sand No.5 and Coral sand No.3 were employed in this research. The pre-crushed sands were produced by triaxial tests on original sand under 3MPa confining pressure. The relevant grain size distribution curves were obtained by sieve analysis and quantified by relative breakage as a single parameter. The pre-crushed sand and original sand were employed in triaxial tests to investigate the influence of particle breakage on soil behavior. The major findings are shown as what follows:

(a) Particle breakage was found to increase with the increase of axial strain and the

particle breakage still can be caused during isotropic consolidation.

(b) Particle breakage was found to be slightly more substantial in shear band than that outside shear band and there is no big difference about particle crushing between top and bottom parts of the specimen.

(c) Under isotropic consolidation, particle breakage was found to result in more volumetric contractancy and residual volumetric change after unloading, which can be regarded as a plastic deformation or subsidence at ground surface in reality.

(d) By triaxial test on pre-crushed and original sand under various confining pressures, particle breakage was found to deteriorate stress-stress curve in reduction of peak strength. Particle breakage resulted in loss of dilatancy behavior of soil to become more contractive. Particle breakage resulted in more substantial development and slower dissipation of excess pore water pressure with higher residual excess pore water pressure in pre-crushed sands. Particle breakage was found to change the stress path in reduction of strength.

(e) Particle breakage resulted in reduction of the friction angle at peak strength and the deformation modulus substantially. The critical state friction angle was influced by the current critical state.

(f) The initial CSL and NCL (on the loosest state) from original sand were found to have nonlinear characteristics with a marked yield stress around 0.7MPa and CSL before yield stress can be regarded as a linear line being parallel with the NCL on the loosest state. After yield stress, both high pressure and particle breakage have a complex influence effect on CSL during first shearing on original sand.

(g) The locations of the critical state points on original sand in CD test under 0.2MPa and 0.5MPa confining pressures were found to be far away from the CSL which was caused by effect of initial state of the test. In comparison with the locations of critical state points on pre-crushed sands and original sand in CD tests, critical state points moved downwards in e-logp′ plane with the increase of particle breakage but in q-p′ plane they are almost on the CSL linear fitting line. The locations of critical state points on pre-crushed sands in CU tests were found to move to left away in reduction of mean effective stress in e-logp′ plane but in q-p′ plane the critical state points over CSL moved towards the lower left to approach the CSL. With increasing mean effective stress, critical state points at same amount of pre-crushed particle breakage moved towards CSL in e-logp′ plane.

(h) Considering the locations of all critical state points from original sand and pre-crushed sand, it can be concluded that the locations of critical state points moved to lower left in e-logp′ plane in complex translation and rotation and developed to be nonlinear in increase of M=q/p′ in q-p′ plane with increasing particle breakage.

---

a-e: Findings on Silica sand No.5 and Coral sand No.3

f-h: Findings on Silica sand No.5

CHAPTER 6

MICROSCOPIC VIEW ON PARTICLE BREAKAGE

6.1 INTRODUCTION

For getting fundamental understanding of particle breakage induced by triaxial shearing under high pressure, sieve analysis should be done to obtain grain size distribution curves before and after loading to identify the particle breakage. In addition, microscopic view on particles before and after shearing was herein conducted to distinguish the extent of particle breakage in intuitionistic observation.

6.2 METHODOLOGY

Microscopic view on particle breakage were conducted just on Coral sand No.3 as a result of that Coral sand No.3 has a little larger particle size with being prone to crush as well in comparison with Silica sand No.5. Around 50g sand at middle-centric part of specimens after shearing was picked up into a plastic round box with a cap covered in natural air, which would be detected under microscopic lens in 25 times. Figure 6.1 show the microscope equipment with 175-time lens in maximum.

6.3 MICROSCOPIC VIEW ON PARTICLE BREAKAGE

Microscopic view on original Coral sand No.3, as shown in Figure 6.2, was conducted by microscope equipment for being in comparison with the microscopic views on particles subjected to shear under high pressure. As shown in Figure 6.2, it is seen clearly that coral sand has the characteristics of irregularity in particle shape with sharp edges, particle fragility and porosity inside particle, being in composition of bio-erosion of limestone skeletal material of marine organisms which are prone to crush during shearing under high pressure.

Figure 6.1 Microscope equipment with 186-time lens in maximum

Figure 6.2 Microscopic view on original Coral sand No.3

Many triaxial tests have been performed to investigate the characteristics of particle breakage subjected to various influence factors as shown in Chapter 4. Microscopic views on particle breakage would be herein investigated in proving the findings of characteristics of particle breakage.

According to the grain size distribution curves obtained by sieve analysis after shearing, the B_r and D_{50} were herein calculated for determining the extent of particle breakage incorporating microscopic view on crushed particles.

Figure 6.3 shows the microscopic view on particle breakage from triaxial tests with initial void ratio e_0=0.798 under 2MPa confining pressure, where microscopic views herein show progressive evolution of particle breakage with increasing axial strain. More particle breakage can be seen approximately on the microscopic views in CD tests and that in CU tests. The change of Br and D_{50} against the axial strain would be helpful to judge the evolution of particle breakage on the microscopic views. Figure 6.4 shows the microscopic view on particle breakage from triaxial tests with initial void ratio e_0=0.798 under 3MPa confining pressure. It is seen evidently in Figure 6.4 that particle breakage increases with increasing axial strain and more particle breakage was induced in CD tests than that in CU tests, which are consistent with the findings concluded by evolution of grain size distribution curves. Cyclic loading on specimen was performed in designated cycle numbers as triaxial tests were sheared to 20% axial strain. Microscopic views on particle breakage were taken after each test for investigating evolution of particle breakage subjected to cyclic loading. Figure 6.5 shows microscopic view on particle breakage from CD tests subjected to cyclic loading. According to the evolution of particle breakage in microscopic views, it is found that particle breakage increases with increasing cyclic numbers of cyclic loading. For investigating the influence of confining pressure on particle breakage, in comparison with the microscopic views on particle breakage under 2MPa & 3MPa confining pressure, it can be concluded that higher confining pressure results in more substantial particle breakage.

According to the evolution of particle breakage in microscopic view incorporating the B_r and D_{50}, particle breakage during shearing can be simply depicted in experiencing (1) sharp edges & corners and weak cave inside particles were first crushed by stress concentration at beginning stage of shearing as shown in Figure 6.3 (ε_1= 5%). D_{50} doesn't almost change at this stage. (2) the attrition and break-off of particles was predominant in contribution of particle breakage as shown in Figure 6.4 (ε_1=10% & 15%). D_{50} changes a little at this stage. (3) total smash & split of partial particles and severe abrasion of most particles as shown in Figure 6.4 (ε_1=20%) and Figure 6.5. D_{50} changes a little much at this stage (4) total smash of most of particles. D_{50} changes much. This stage doesn't appear in this research.

Considering the microscopic view just on very few scope of materials, the grain size distribution curve based on statistics is much more reliable and acceptable to determine the extent of particle breakage.

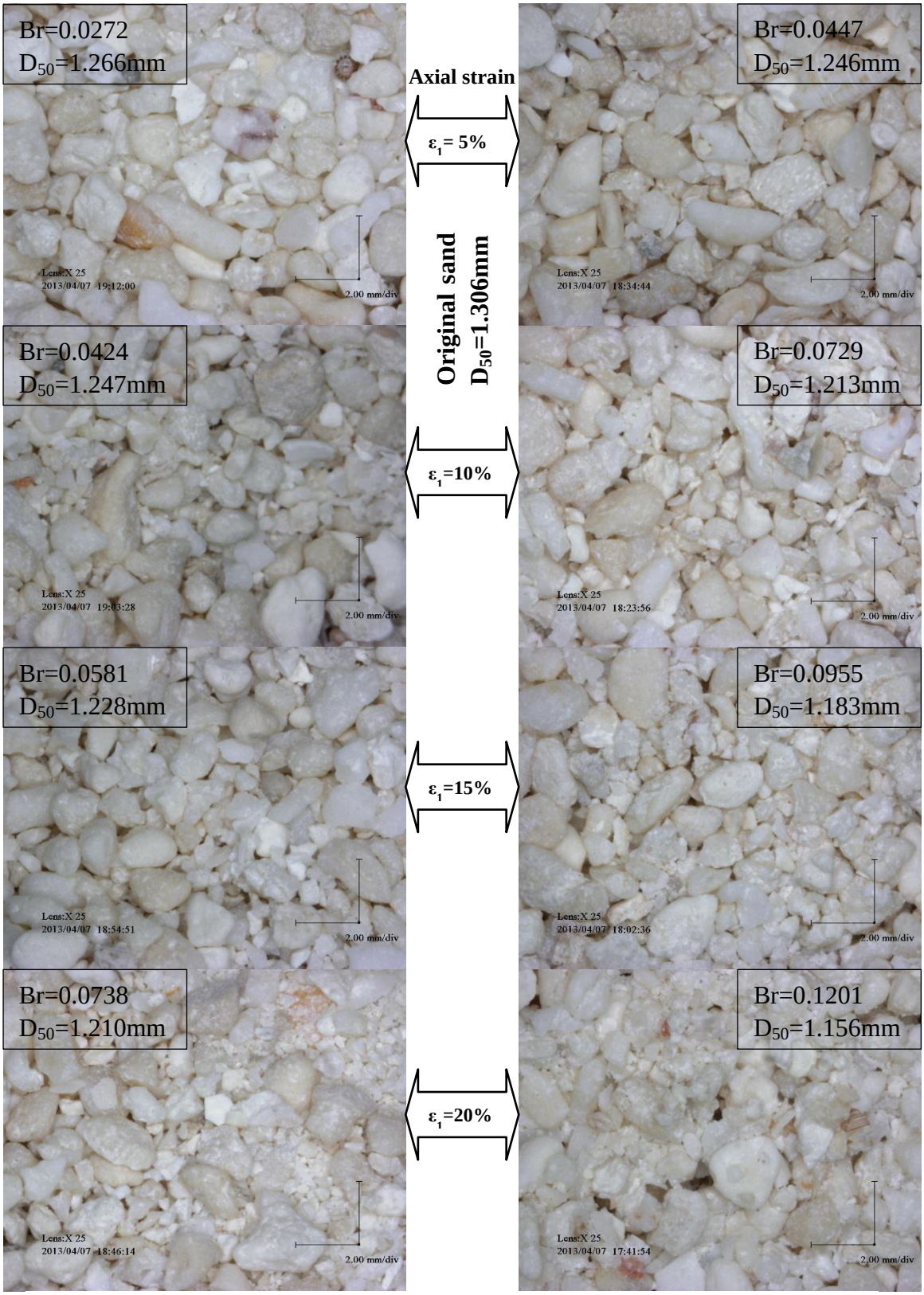

(a) CU tests (b) CD tests

Figure 6.3 Microscopic view on particle breakage from triaxial tests (σ_c=2MPa K_0=1.0 e_0=0.798)

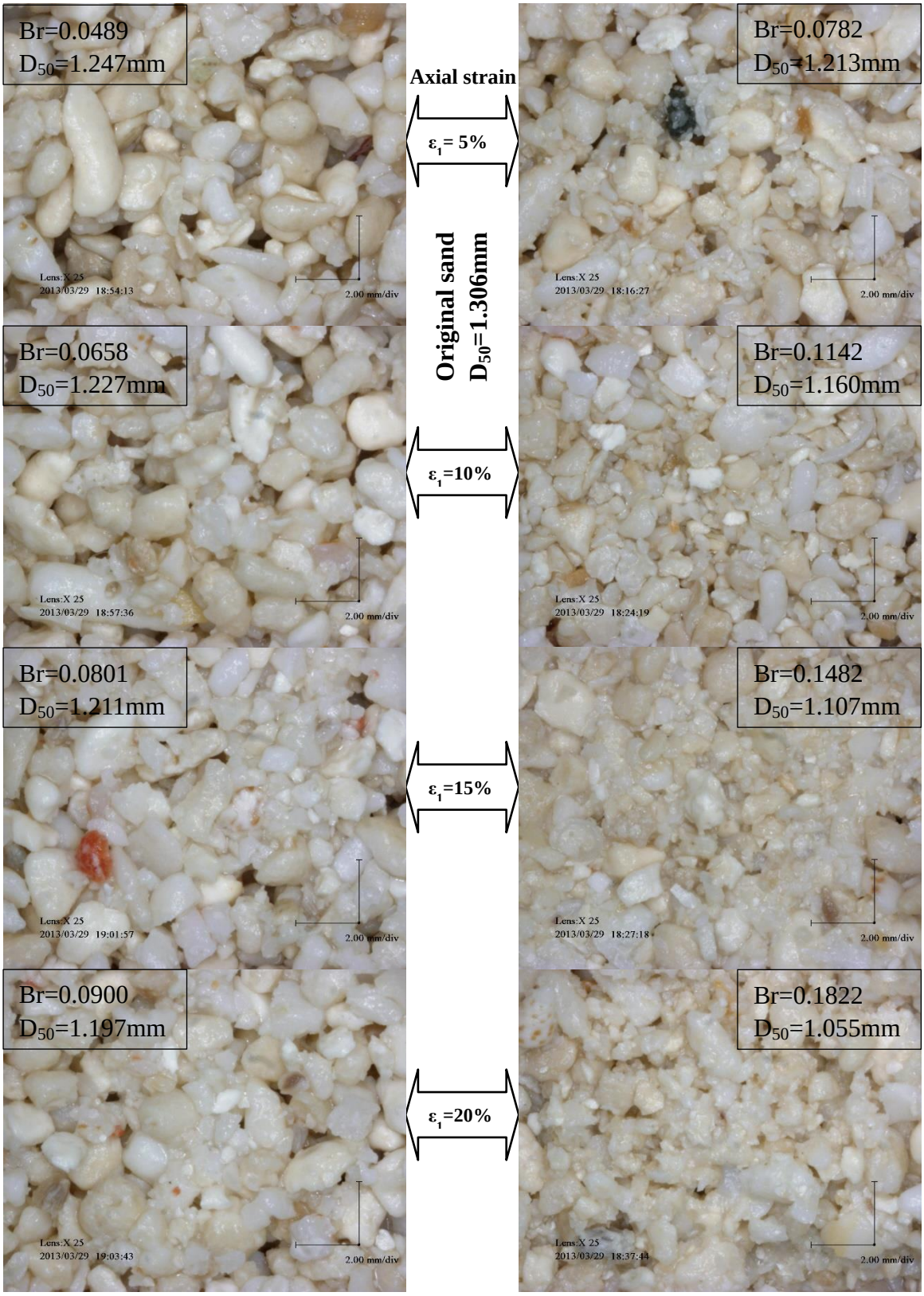

(a) CU tests (b) CD tests

Figure 6.4 Microscopic view on particle breakage from triaxial tests (σ_c=3MPa K_0=1.0 e_0=0.798)

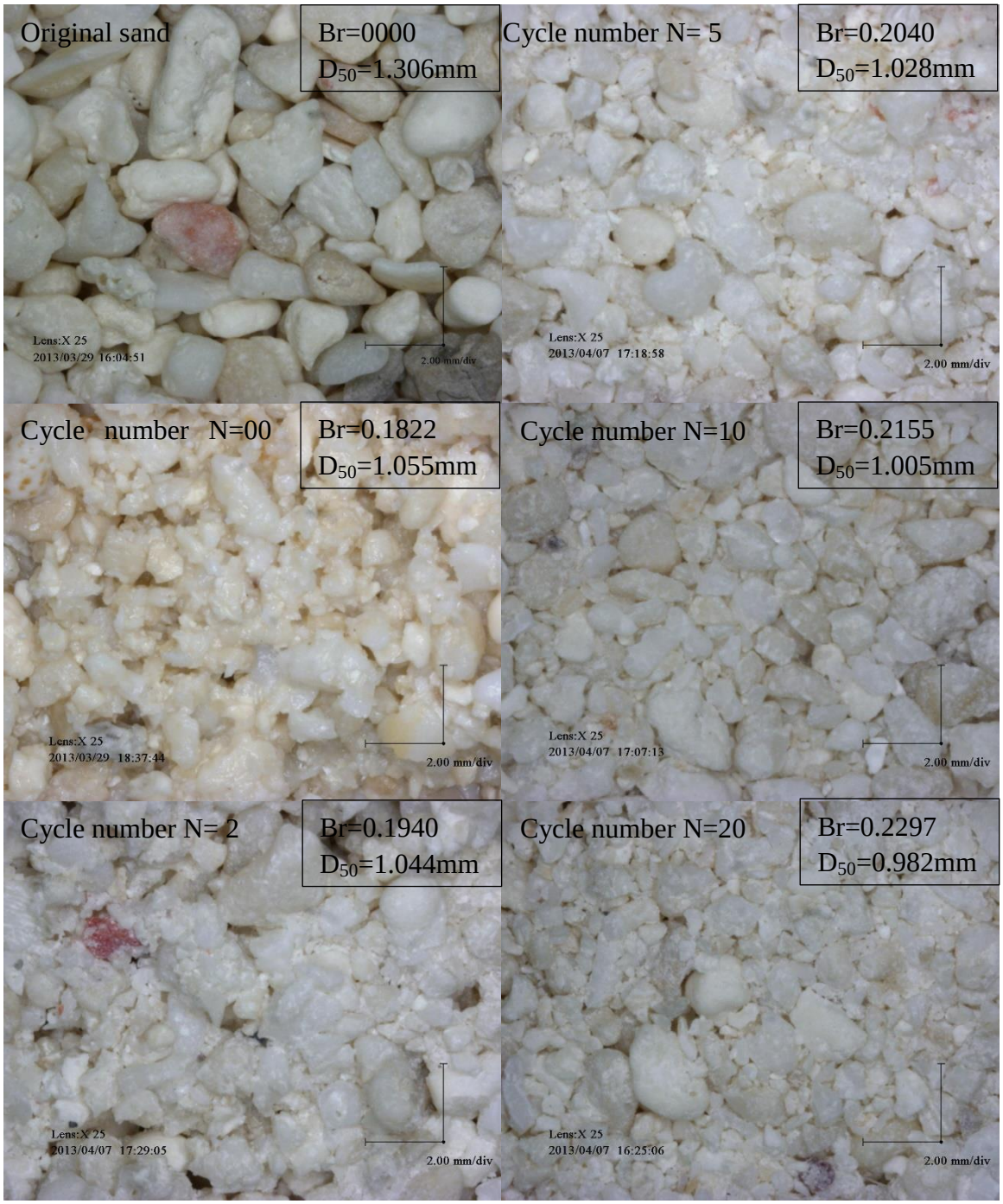

Figure 6.5 Microscopic view on particle breakage from CD tests subjected to cyclic loading (σ_c=3MPa K_0=1.0 e_0=0.798)

6.4 SUMMARY

Many microscopic views were taken on materials from several typical triaxial tests for identifying the extent of particle breakage in intuitionistic observation incorporating the change of B_r and D_{50} against particle breakage. The major findings are shown as what follows:

(a) Microscopic view on particle breakage is very effective in intuitionistic observation

of evolution of particle breakage.

(b) Microscopic views proved that particle breakage was found to increase with increasing axial strain and more substantial particle breakage was caused in CD tests than that in CU tests.

(c) Microscopic views proved that higher confining pressure results in more particle breakage and particle breakage increases with increasing cycle numbers of cyclic loading.

CHAPTER 7

CONCLUSIONS AND RECOMMENDATIONS

7.1 INTRODUCTION

Granular materials are comprised of particles which would be crushed under the pressure as the energy imposed on soil particle exceeds its strength. Particle breakage changes the natural grading of soil which has a significant influence on soil behavior.

Nowadays the stresses imposed on soil particles in geotechnical engineering tend to increase in falling into the range of high pressure with increasing the height of dams and high-rise buildings. Particle breakage is getting more and more significant in influencing soil behavior by the change of original grain size distribution of soil. Consequently Particle breakage induced by high pressure in the field of Geotechnical Engineering should be paid more attention on its effects on soil behavior in this research.

High-pressure triaxial apparatus was used in this research in simulating the engineering mechanical process for investigating the characteristics of particle breakage and its influence on soil behavior. Silica sand No.5 and Coral sand No.3 were employed as two kinds of common and uncommon sands in comparison.

7.2 CONCLUSIONS

Many triaxial tests were conducted by strain-controlled high-pressure triaxial apparatus on Silica sand No.5 and Coral sand No.3 for investigating the characteristics of particle breakage and its influence on soil behavior. Major conclusions can be drawn as follows:

(a) Particle breakage was found to increase with increasing axial strain.
(b) Particle breakage was caused as well during consolidation.
(c) Higher confining pressure was found to result in more substantial particle breakage.
(d) More particle breakage was caused in denser samples. Particle breakage should be a function of void ratio.
(e) More particle breakage was induced in CD tests than that in CU tests.
(f) Initial stress anisotropy was found newly to result in more particle breakage during

anisotropic consolidation than that during isotropic consolidation but during shearing higher confining pressure (σ_c=2.0MPa K_0=1.0) has more influence on particle breakage than initial stress anisotropy with a relatively lower confining pressure (σ_c=1.5MPa K_0=0.5).

(g) Unloading-reloading process during shearing was found newly to lead to particle breakage. More particle breakage was caused by unloading-reloading process at larger axial strain. More times unloading-reloading process resulted in more particle breakage.

(h) Particle breakage was found to increase with increasing cycle number of cyclic loading.

(i) A hyperbolic model was established to assess Relative Breakage by plastic work per unit volume. Different loading modes (monotonic loading and cyclic loading) were found newly to result in different evolution and mechanism of particle breakage.

(j) Particle breakage on Silica sand No.5 was compared newly with that on Coral sand No.3. More particle breakage was revealed in Coral sand No.3 than that in Silica sand No.5 as a result of more crushability of Coral sand No.3.

(k) Microscopic view is an effective way in identifying particle breakage in intuitionistic observation.

(l) Particle breakage was found to be slightly more substantial in shear band than that outside shear band and there is no big difference about particle crushing between top and bottom parts of the specimen.

(m) Pre-crushed sands were newly employed to investigate the influence of particle breakage on soil behavior in quantity.

(n) Under isotropic consolidation, particle breakage was found to result in more volumetric contractancy and residual volumetric change after unloading, which can be regarded as a plastic deformation or subsidence at ground surface in reality.

(o) By triaxial test on pre-crushed and original sand under various confining pressures, particle breakage was found to deteriorate stress-stress curve in reduction of peak strength. Particle breakage resulted in loss of dilatancy behavior of soil to become more contractive. Particle breakage resulted in more substantial development and slower dissipation of excess pore water pressure with higher residual excess pore water pressure in pre-crushed sands. Particle breakage was found to change the stress path in reduction of strength.

(p) Particle breakage resulted in reduction of friction angle at failure. Particle breakage was found newly to give rise to the reduction of the deformation modulus substantially. However the critical state friction angle was influenced by confining pressure, which may be related to current state.

(q) The initial CSL and NCL (on the loosest state) from original sand were found to have nonlinear characteristics with a marked yield stress around 0.7MPa and CSL before yield stress can be regarded as a linear line being parallel with the NCL on the loosest state. After yield stress, both high pressure and particle breakage have a complex influence effect on CSL during first shearing on original sand.

(r) The locations of the critical state points on original sand in CD test under 0.2MPa and 0.5MPa confining pressures were found to be far away from the CSL which was

caused by effect of initial state of the test. In comparison with the locations of critical state points on pre-crushed sands and original sand in CD tests, critical state points were newly found to move downwards in e-logp′ plane with increasing particle breakage but in q-p′ plane critical state points were almost on the CSL. The locations of critical state points on pre-crushed sands in CU tests were found newly to move to left away in reduction of mean effective stress in e-logp′ plane but in q-p′ plane the critical state points over CSL moved toward the lower left to approach the CSL. With increasing mean effective stress, critical state points at same amount of pre-crushed particle breakage were found newly to move towards CSL in e-logp′ plane.

(s) Considering the locations of all critical state points from original sand and pre-crushed sand, it can be concluded newly that the locations of critical state points moved to lower left in e-logp′ plane in complex translation and rotation and developed to be nonlinear in increase of M=q/p′ in q-p′ plane with increasing particle breakage.

7.3 RECOMMENDATIONS

According to the findings about particle breakage, the traditional classic soil mechanics should be improved during high pressure in considering particle breakage which influences soil behavior comprehensively. In addition, during construction and operating stage of high dam and high-rise building especially on crushable soil, particle breakage should be investigated on the case-by-case basis and considered in design and construction code to guarantee the utility functionality and engineering safety, for instance, a compensation coefficient in safety factor could be selected in engineering design to pre-consider the reduction of strength, stiffness and stability induced by particle breakage for ensuring the engineering safety.

Due to the limitations of time & apparatus and diversity of materials used, the findings of this research were acquired conditionally and may not be applicable unconditionally in practice. Further research about particle breakage should be done in the future as follows:

(a) Due to the limitation of particle breakage factor B_r which just focuses on the area change of gradation curve of soil before and after loading. More particle breakage factors can be developed or adopted to consider more comprehensive soil gradation information such as coefficient of uniformity C_u, D_{50}, fine content and so on.

(b) The type of particle breakage should be investigated by testing on color-dyed soil particle, which can be observed in microscope to identify the micro-mechanism of particle breakage.

(c) The additional particle breakage induced during progressive shearing should be measured as well to investigate the progressive influence of particle breakage on soil behavior.

(d) In improving the theory of traditional classic soil mechanics, particle breakage can be introduced to the mechanical constitutive model.

(e) As a results of that particle breakage changes the original grading of soil, consequently the influence of particle breakage on liquefaction potential can be

investigated under dynamic loading including the development of excess pore water pressure subjected to particle breakage.

(f) In the field of unsaturated soil mechanics, the matrix suction would be influenced by particle breakage, consequently the influence of particle breakage on soil water characteristics curve should be investigated in further research in being introduced to perfect the traditional unsaturated soil mechanics considering particle breakage.

(g) Particle breakage has a significant influence on soil behavior. Consequently the influence of particle breakage at sliding shear zone on stability of slope can be investigated as well.

(h) Acoustic emission technique can be introduced as well to identify the particle breakage qualitatively during pile penetration in model test or during shearing in triaxial test.

APPENDIX Ⅰ

CALCULATION OF PLASTIC WORK PER UNIT VOLUME FROM TRIAXIAL TESTS

Incremental strain parameters are shown as below.

$$d\varepsilon_{ij} = d\varepsilon_{ij}^{e} + d\varepsilon_{ij}^{p} \quad \text{(A1)}$$

$$d\varepsilon_{s} = d\varepsilon_{s}^{e} + d\varepsilon_{s}^{p} \quad \text{(A2)}$$

$$d\varepsilon_{v} = d\varepsilon_{v}^{e} + d\varepsilon_{v}^{p} \quad \text{(A3)}$$

For the special case of an axisymmetric triaxial specimen, the stress and strain invariants can be simplified as bellow:

$$q = \sigma_1' + \sigma_3' \quad \text{(A4)}$$

$$p' = \frac{(\sigma_1' + 2\sigma_3')}{3} \quad \text{(A5)}$$

$$\varepsilon_v = \varepsilon_1 + 2\varepsilon_3 \quad \text{(A6)}$$

$$\varepsilon_s = \frac{2(\varepsilon_1 - \varepsilon_3)}{3} = \varepsilon_1 - \frac{\varepsilon_v}{3} \quad \text{(A7)}$$

Plastic work per unit volume can be calculated as below:

$$E = w^e + w^p = \int q d\varepsilon_s + p' d\varepsilon_v \tag{A8}$$

$$w^e = \int q d\varepsilon_s^e + p' d\varepsilon_v^e \tag{A9}$$

$$w^p = \int q d\varepsilon_s^p + p' d\varepsilon_v^p \tag{A10}$$

$$w^p = E - w^e = \int q d\varepsilon_s^p + p' d\varepsilon_v^p = \int q d\varepsilon_s + p' d\varepsilon_v - \int q d\varepsilon_s^e + p' d\varepsilon_v^e \tag{A11}$$

For triaxial results, every test conducted up to specific axial strain was unloaded to initial consolidation state in order to acquire plastic work per unit volume by removing the elastic work per unit volume from total work per unit volume as shown in Figure A.

According to the Figure A, the plastic work per unit volume in monotonic shearing can be calculated as blows:

$$w^p = AREA\_A1 + AREA\_A2 + AREA\_B1 \tag{A12}$$

where the *AREA_B*1 is equal to zero in CU test.

According to the Figure A, the plastic work per unit volume in cyclic loading shearing can be calculated as below:

$$w^p = AREA\_A1 + AREA\_A2 + AREA\_B1 + AREA\_A2 + AREA\_A3 + AREA\_B2 \tag{A13}$$

where the *AREA_B*1 and *AREA_B*2 are equal to zero in CU test.

Note: Figure A just shows one-time cyclic loading. For more cycle number of cyclic loading, the plastic work per unit volume should be calculated according to each cycle of cyclic loading.

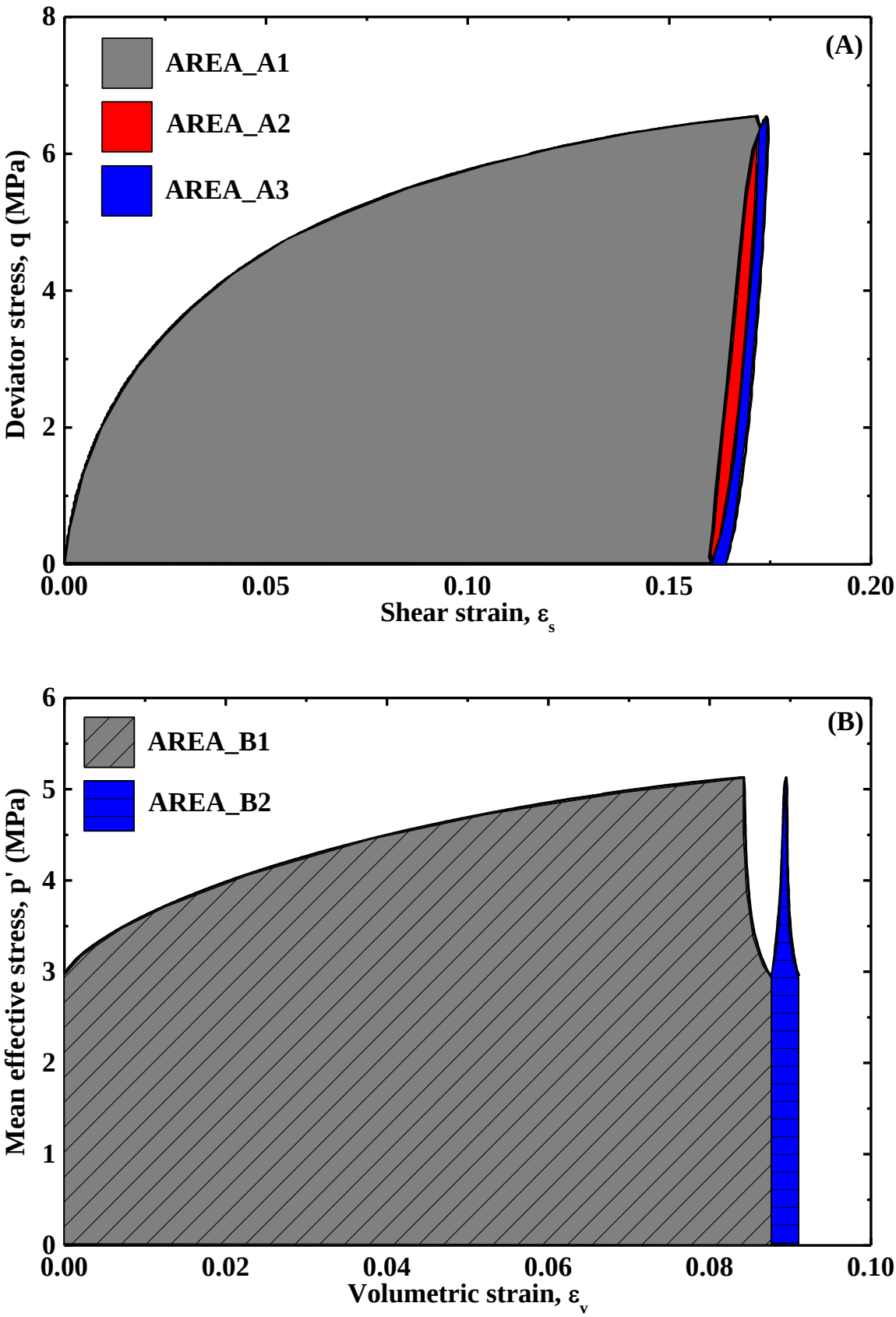

Figure A Schematic illustration of calculation of plastic work per unit volume

BIBLIOGRAPHY

Altuhafi, F.N. and Coop, M.R. (2011). Changes to particle characterisitcs associated with the compression of sands. *Geotechnique*, No.6, 459-471.

Andrawes, K.Z. and EI-Sohboy, M.A. (1973). Factors affecting coefficient of earth pressure K_0. J. Soil Mech. And Found. Div., ASCE, 99(7):527-539

Bandini, V. and Coop, M.R. (2011). The influence of particle breakage on the location of the critical state line of sands. *Soils and Foundations*, 51(4):591-600.

Been, K. and Jefferies, M.G. (1985). A state parameter for sands. *Geotechnique*, 35(2):99-112.

Been, K., Jefferies, M.G. and Hachey, J. (1991). The critical state of sands. *Geotechnique*, 41(3):365-381.

Bishop, A.W. (1958). Test requirements for measuring the coefficient of earth pressure at rest. *Proc. Brussels Conf. on Earth Pressure Problems, Brussels, Belgium*, Vol. 1, 2-14.

Bishop, A.W. (1966). The strength of soils as engineering materials. *Geotechnique*, 16(2):89-130.

Carrera, A.W., Coop, M.R. and Lancellotta, R. (2011). The influence of grading on the mechanical behaviour of stava tailings. *Geotechnique*, 61(11):935-946.

Casagrande, A. (1932). The structure of clay and its importance in foundation engineering. *J. Boston Soc. Civil Engrs.*, 19(4):168-209.

Casagrande, A. (1936). Characteristics of cohesionless soils affecting the stability of earth fills. *J. Boston Soc. Civ. Engrs. Reprinted in Contributions to Soil Mechanics 1925-1940. Boston Society of Civil Engineers.*

Coop, M.R. and Lee, I.K. (1993). The behavior of granular soils at elevated stresses. *Predictive Soil Mechanics, Thomas Telford, London*, 186-198.

Coop, M.R., Sorensen, K.K., Bodas freitas, T. and Georgoutsos, G. (2004). Particle

breakage during shearing of a carbonate sand. *Geotechnique*, 54(3):157-163.

Donohue, S., O'Sullivan, C. and Long, M. (2009). Particle breakage during cyclic triaxial loading of a carbonate sand. *Geotechnique*, 59(5):477-482.

Duncan, J.M., Witherspoon, P.A., Mithchell, J.K., Watkins, D.J., Hardcastle, J.H., and Chen, J.C. (1972). Seepage and ground water effects associated with explosive cratering. *Rep. No. TE-72-2, Univ. of California, Berkeley, California.*

Einav, I. (2007a). Breakage mechanics-Part Ⅰ: theory. *Journal of the Mechanics and Physics of Solids*, 55(6):1274-1297.

Einav, I. (2007b). Breakage mechanics-Part Ⅱ: modeling granular materials. *Journal of the Mechanics and Physics of Solids*, 55(6):1298-1320.

Feda, J. (2002). Notes on the effect of grain crushing on the granular soil behavior. *Engineering Geology*, 63(1-2):93-98

Fourie, A.B. and Papageorgiou, G. (2001). Defining an appropriate steady state line for Merriespruit gold tailings. *Canadian Geotechnical Journal*, 38(4): 695-706.

Fragaszy, R.J. and Voss, M.E. (1986). Undrained compression behavior of sand. *Journal of Geotechnical Engineering*, 112(3):334-347.

Ghanbari, A.,Hamidi, A and Abdolahzadeh,N. (2013). A study of the rockfill material behavior in large-scale tests. *Civil Engineering infrastructures Journal*, 46(2):125-143

Griffith, A.A. (1920). The phenomenon of rupture and flow in soilds. *Philosophical Transactions of the Royal Society of London*, V221:163-198.

Hagerty, M.M., Hite, D.R., Ullrich, C.R. and Hagerty, D.J. (1993). One dimensional high pressure compression of granular media. *Journal of Geotechnical Engineering*, 113(1):1-18.

Hardin, B.O. (1985). Crushing of soil particles. *Journal of geotechnical engineering*, 111(10):1177-1192.

Hendron, A.J. (1963). *The behavior of sand in one-dimensional compression.* Ph.D. disseration, Univ. of Illinois, Ill.

Hiramatsu, Y. and Oka, Y. (1966). Determination of the tensile strength of rock by a compression test of an irregular test piece. *Int. J. Rock Mech. Min. Sci.*, 3:89-99.

Hyodo, M., Hyde Adrian, F.L., Aramaki, N. and Nakata, Y. (2002). Undrained monotonic and cyclic shear behavior of sand under low and high confining stresses. *Soils and Foundations*, 42(3):63-76.

Indraratna, B. and Salim, W. (2002). Modelling of particle breakage of coarse aggregates incorporating strength and dilatancy. *Proceedings of the Institution of Civil Engineers, London*, 155(4):243-252

Ishihara, K. (1993). Liquefaction and flow failure during earthquakes. *The 33th Rankine Lecture, Geotechnique*, 43(3):351-415

Jaeger, J.C. (1967). Failure of rocks under tensile conditions. *Int. J. Rock Min. Sci.*, 4:219-227.

Jaky, J. (1948). Pressure in silos. *Proc. 2nd Int. Conf. on Soil Mech. and Found. Engrg., ASCE*, Vol. 1, 103-107.

Karimpour, H. and Lade, P.V. (2010). Time effects relate to crushing in sand. *Journal of Geotechnical and Geoenvironmental Engineering*, 136(9):1209-1219.

Kikumoto, M., Wood, D.M. and Russell, A. (2010). Particle crushing and deformation behavior. *Soils and Foundations*, 50(4):547-563.

Konrad, J.M. (1998). Sand state from cone penetrometer tests:a framework considering grain crushing stress. *Geotechnique*, 48(2):201-215.

Lade, P.V. and Karimpour, H. (2010). Static fatigue controls particle crushing and time effects in granular materials. *Soils and Foundations*, 50(5):573-583.

Lade, P.V. and Yamamuro, J.A. (1996). Undrained Sand Behaviour in Axisymmetric Tests at High Pressures. *Journal of Geotechnical Engineering*, 122(2): 120-129.

Lade, P.V., Yamamuro, J.A. and Bopp, P. A. (1996). Significance of particle crushing in granular materials. *Journal of Geotechnical Engineering*, 122(4):309-316.

Lee, D.M. (1992). *The angles of friction of granular fills.* Ph.D dissertation, University of Cambridge.

Lee, K.L. (1965). *Triaxial compressive strength of saturated sand under seismic loading conditions.* Ph.D thesis, University of California, Berkeley.

Lee, K.L. and Farhoomand, I. (1967). Compressibility and Crushing of Granular Soil in anisotropic triaxial compression. *Canadian Geotechnical Journal*, 4(1):68-86.

Lee, K.L. and Seed, H.B. (1967). Drained strength characteristics of sands. *Journal of the Soil Mechanics and Foundation Division*, 93(6):117-141.

Luzzani, L. and Coop, M.R. (2002). On the relationship between particle breakage and the critical state of sands. *Soils and Foundations*, 42(2):71-82.

Marsal, R. J. (1967). Large scale testing of rockfill materials. *Journal of the Soil Mechanics and Foundations Division*, 93(2):27-43.

McDowell, G.R. and Bolton, M.D. (1998). On the micromechanics of crushable aggregates. *Geotechnique*, 48(5):667-679.

McDowell, G.R., Bolton, M.D. and Robertson, D. (1996). The fractal crushing of granular materials. *Journal of the mechanics and physics of solids*, 44(12):2079-2101.

Miura, N. and Ohara, S. (1979). Particle-crushing of a decomposed granite soil under shear stresses. *Soils and Foundations*, 19(3):1-14.

Miura, N. and Yamanouchi, T. (1977). Effect of particle-crushing on the shear characteristics of a sand. *Proc. of JSCE*, (260), 109-118 (in Japanese).

Miura, S. and Yagi, K. (1997). Particle breakage of volcanic coarse-grained soils and its evaluation. *Journal of Geotechnical engineering, JSCE*, (561/3-38), 257-269 (in Japanese).

Miura, S., Yagi K. and Asonuma, T. (2003). Deformation-strength evaluation of crushable volcanic soils by laboratory and in-situ testing. *Soils and Foundations*, 43(4):47-57.

Murthy, T.G., Loukidis, D., Carraro, J.A.H., Prezzi, M. and Salgado, R. (2007). Undrained monotonic response of clean and silty sands. *Geotechnique*, 57(3):273-288.

Nakata, Y., Hyde, A.F.L., Hyodo, M. and Murata, H. (1999a). A probabilistic approach to sand particle crushing in the triaxial test. *Geotechnique*, 49(5):567-583.

Nakata, Y., Hyde, A.F.L., Kato Y., Hyodo, M. and Murata, H. (1999b). Single particle crushing and the mechanical behaviour of sand. *Proc. of 2nd Int. Symp. on Pre-Failure Deformation of Geomaterials*, IS Torino 99, 221-228.

Nakata, Y., Hyodo, M., Hyde, A.F.L., Kato, Y. and Murata H. (2001a). Microscopic particle crushing of sand subjected to high pressure one-dimensional compression. *Soils and Foundations*, 41(1):69-82.

Nakata, Y., Kato Y., Hyodo, M., Hyde, A.F.L. and Murata, H. (2001b). One-dimensional compression behavior of uniformly graded sand related to single particle crushing strength. *Soils and Foundations*, 41(2):39-51.

Pestana, J.M. and Whittle, A.J. (1995). Compression model of cohesionless soils. *Geotechnique*, 45(4):611-631.

Ramamurthy, T. (1969). Crushing Phenomena in Granular Soils. *Soil Mech & Fdn Eng Inst /India*, 8(1):67-86.

Robert, W.D. (1997). One-dimensional compression of sands at high pressures:

Discussion. *Journal of Geotechnical and Geoenvironmental Engineering*, 123(5):491-492.

Roberts, J.E. and De Souza, J.M. (1958). The compressibility of sand. *Proc. Am. Soc. for Testing Mat.*, Vol. 58, ASTM, Philadelphia, Pa., 1269-1277.

Roscoe, K.H., Schofield, A.N. and Worth, C.P. (1958). On the yielding of soils. *Geotechnique*, 8(1):22-53.

Rowe, P.W. (1962). The stress-dilatancy relation for static equilibrium of an assembly of particles in contact. *Proceedings of the Royal Society of London. Series A, Mathematical and Physical Sciences*, 269, 500-527.

Sadrekarimi, A. and Olson, S.M. (2010). Particle damage observed in ring shear tests on sands. *Canadian Geotechnical Journal*, 47(5): 497-515.

Sadrekarimi, A. and Olson, S.M. (2011). Critical state friction angle of sands. *Geotechnique*, 61(9):771-783.

Salim, W. and Indraratna, B. (2004). A new elastoplastic constitutive model for coarse granular aggregates incorporating partice breakage. *Canadian Geotechnical Journal*, 41(4): 657-671.

Shipway, P.H. and Hutchings, I.M. (1993a). Fracture of brittle spheres under compression and impact loading. I. Elastic stress distributions. *Philosophical Magazine A*, 67(6):1389-1404.

Shipway, P.H. and Hutchings, I.M. (1993b). Fracture of brittle spheres under compression and impact loading. II. Results for lead-glass and sapphire spheres. *Philosophical Magazine A*, 67(6):1405-1421.

Skempton, A.W. (1954). The pore-pressre coefficient A and B. *Geotechnique*, 4(4):143-147.

Tatsuoka, F. and Haibara, O. (1985). Shear resistance between sand and smooth or lubricated surfaces. *Soils and Foundations*, 25(1):89-98.

Tatsuoka, F., Molenkamp, F., Torii, T. and Hino, T. (1984). Behavior of lubrication layers of platens in element tests. *Soils and Foundations*, 24(1):113-128.

Taylor, D.W. (1948). *Fundamentals of soil mechanics.* John Wiley & Sons, Inc., New York, NY.

Terzaghi, K. (1920). Old earth pressure theories and new test results. *Engrg. News Record*, Vol.85, 632.

Terzaghi, K. (1925). Structure and volume of voids of soils. *Erdbaumechanik auf Bodenphysikalisher Grundlage, pp.10-13*, Translated by A. Casagrande in From

Theory to Practice in Soil Mechanics, New York, John Wiley & Sons, INC., (1960), pp.146-148.

Terzaghi, K. and Peck, R.B. (1948). Soil mechanics in engineering practice. *John Wiley & Sons, Inc., New York, N.Y.*, 65-67.

Thevanayagam, S., Shenthem, T., Mohan, S. and Liang, J. (2002). Undrained fragility of clean sand silty sands and sandy silts. *J. Geotechnical and Geoenvir, Engrg*, 128(10):849-859.

Towhata, I. (2008). *Geotechnical earthquake engineering.* Springer Berlin Heidelberg.

Ueng, Tzou-shin and Chen, Tse-jen. (2000). Energy aspects of particle breakage in drained shear of sands. *Geotechnique*, 50(1):65-72.

Verdugo, R. and Ishihala, K. (1996). The steady state of sandy soils. *Soils and Foundations*, 36(2):81-91.

Vesic, A.S. and Clough, G.W. (1968). Behavior of granular materials under high stresses. *Journal of the Soil Mechanics and Foundations Division*, 94(3):661-688.

Weibull, W. (1951). A statistical distribution function of wide applicability. *Journal of Applied Mechanics*, 18:293-297.

Wood, D.M. (2008). Critical states and soil modeling. *Deformational Characteristics of Geomaterials*, 1, ISO Amsterdam, 51-57.

Yamamuro, J.A. and Lade, P.V. (1996). Drained sand behavior in axisymmetric tests at high pressures. *Journal of Geotechnical Engineering*, 122(2):109-119.

Yamamuro, J.A., Bopp, P.A. and Lade, P.V. (1996). One-dimensional compression of sands at high pressures. *J. of Geotech. Engrg., ASCE*, 122(2):147-154.

Yao, Y.P., Yamamoto, H. and Wang, N.D. (2008). Constitutive model considering sand crushing. *Soils and Foundations*, 48(4):603-608.

Yasufuku, N. and Hype, A.F.L. (1995). Pile end-bearing capacity in crushable sands. *Geotechnical*, 45(4):663-676